Proceedings

of the

Estes Park Advanced Propulsion Workshop

19 —22 September 2016

Estes Park, Colorado, USA

edited by

H. Fearn

CSU Fullerton - Physics

L. L. Williams

Konfluence Research Institute

Proceedings of the Estes Park Advanced Propulsion Workshop

edited by H. Fearn & L. L. Williams

Space Studies Institute, Inc. Press
Mojave, California.

Dedicated to

JAMES F. WOODWARD

on the occasion of his seventy-fifth birthday

ESTES PARK ADVANCED PROPULSION WORKSHOP

Held at the YMCA of the Rockies
Estes Park, Colorado USA
19 –22 September 2016

Organizing and Technical Committee:

H. FEARN (Cal. State Univ. Fullerton – Physics)
L.L. WILLIAMS (Konfluence Research Institute)
J.F. WOODWARD (Cal. State Univ. Fullerton – Physics)

Workshop Production:

R. SMITH (audio)
R. SNELSON (video)
H. FEARN (moderator)
L.L. WILLIAMS (moderator)
&
YMCA of the ROCKIES staff

Workshop Sponsorship:

The Space Studies Institute

TABLE OF CONTENTS

Participants

John Brandenburg
Michelle Broyles
Nembo Buldrini
Dennis Bushnell
Bill Christie
John Cole
Todd Desiato
Heidi Fearn
Jeremiah Hansen
Jan Harzen
George Hathaway
Gary C. Hudson
Eric Jansson
Peter M. Jansson
David Jenkins
Wes Kelly
Eric Laursen
Anthony Longman
Paul March
David Mathes
Greg Meholic
Jean–Philippe Montillet (via Skype)
Glen Robertson
José J. A. Rodal
Martin Tajmar
Ron Turner
Lance Williams
Jim Woodward

Group Photo: Participants of the Estes Park Breakthrough Propulsion Workshop.
Seated at the front, left to right James F. Woodward and Heidi Fearn. From the left standing, Lance Williams, Jeremiah Hansen, Jan Harzen, Nembo Buldrini. Front row, Greg Meholic, John Cole, Tony (Glen) Robertson, Martin Tajmar, Anne Hudson, Gary Hudson, José Rodal and Michelle Broyles. Back row from the left, Peter Jansson, David Jenkins, Ron Turner, Eric Laursen, David Mathes, Anthony Longman, Eric Jansson (Obscured), Bill Christie. On the right behind Michelle is, Dennis Bushnell, Paul March, Todd Desiato and Wes Kelly.

Estes Park Advanced Propulsion Workshop

19-22 September 2016

Technical Agenda

Topic area in italics, **specific concept** in bold, presenter named.
Four blocks per day up to 100 min each.

 Coffee break between blocks.

Evening of Arrival Day – 19^{th} September

- **(Gravito-Electromagnetism) GEM theory mixer** .... John Brandenburg

Day 1– 20^{th} September

☐ Block 1 & 2: *General*

- **Ethos of Meeting** .... Lance Williams
- **Introduction to SSI** .... Gary Hudson
- **Facets of a Valid Extension to the Laws of Physics** .... Lance Williams
- **Facets of Valid Experiments** .... George Hathaway

☐ Block 3: *Mach Effect Theory*

- **Hoyle–Narlikar Theory & the Mach Effect** – (50min) .... Heidi Fearn
- **Mach Effect Electroelasticity Solution** – (50 min) .... José Rodal

☐ Block 4: *Group Discussion of Mach effects*

Day 2 – 21^{st} September

☐ Block 1 & 2: *Electromagnetic Approaches*

- **Experiments with RF Resonant Cavity Thrusters** .... Paul March
- **Experiments at Dresden** .... Martin Tajmar

☐ Block 3 :*Scalar Field approaches*

- **Kaluza Unification of Gravity and EM** .... Lance Williams

☐ Block 4 :*Additional Talks*

☐ **Reception at Windcliff**

Day 3 – 22^{nd} September

☐ Block 1: *Scalar Field Approaches*

- **Experimental Application of Chameleon Theory** .... Tony Robertson

☐ Block 2: *Alternative Conceptions*

- **Tri–Space View of the Universe** .... Greg Meholic

☐ Block 3: *Machian Approaches*

- **Mach Effects: Concepts and Experiment** .... Jim Woodward

☐ Block 4: *Additional Talks*

- **Workshop wrap and finalize Proceedings** .... L. Williams & H. Fearn

Unscheduled Talks

Day 2 – 21^{st} September

- **EM Drive explained with Mach Effects** .... Jean-Philippe Monitellet (via Skype)

Day 3 – 22^{nd} September

- **Mach effect experiments from Austria** – *invited* .... Nembo Buldrini
- **Arrays of Mach effect drives, computation** – *invited* .... Jeremiah Hansen
- **Engineering the Quantum Vacuum** .... Todd Desiato
- **Rotating Wave theory** .... Bill Christie
- **Evening Session: Introduction to MUFON** .... Jan Harzen

INTRODUCTION

OPENING REMARKS BY JAMES F. WOODWARD

JFW in 1988, a year before he figured out how inertia figures into advanced exotic propulsion and two years before he quit smoking. Photo, D. Woolum.

Early in the winter of 2015 I was approached by my colleague at CSU Fullerton, Heidi Fearn, with an unusual request. But first, some background. Back in 2011, the Department (Physics) had decided to create a NSF- supported Gravitational Wave Physics and Astronomy Center, and the real estate they wanted for this operation was the space that I had squatted on for years with my lab (doing off beat gravity experiments of very low public visibility). I happily assented to being moved, for GWPAC was exactly the sort of thing I hoped would one day occupy the space I was holding for the Department. Of the various new locations on offer, one was a large interior lab prep room that adjoined Heidi's office, the best option from my point of view. Heidi was not happy about the new occupant of what she regarded as her space (notwithstanding that it was obviously unused).

After a year or two of walking through the new digs, a shortcut to the Department office, Heidi expressed interest in working with me on the Mach effects project. The five sigma signal to noise ratio of the effects produced in some devices was just too large to ignore. The past five years have had their ups and downs, but Heidi is adding serious experimental skills to her already first-rate theoretical repertoire.

The request Heidi brought to me, she also brought on behalf of Lance Williams. We had gotten to know Lance in 2013 when, as a theoretician, he was a member of an Aerospace Corporation evaluation team headed by Greg Meholic. In that capacity he had convinced himself that Mach effects do follow from general relativity, and thus do not constitute "new" physics. I had the pleasure of spending time with Lance at STAIF II in 2014, and consider(ed) him a friend. Heidi and Lance shared experiences as presenters and interested audience members at several meetings where "advanced" propulsion was a section topic: Short talks of 15 to 20 minutes, to mostly indifferent audiences, followed by a question or two on some technical detail. Little or no interaction with others at the meeting, for others' interests rarely overlapped with theirs. A veteran of many years in this business, I was not surprised, and commiserated with them about their experiences at conferences.

Then came the pitch. How about if we create a conference/meeting constructed to avoid all of the negatives of regular conferences? Well, most of them anyway. A conference call ensued. (Lance lives in Manitou Springs, Colorado). The only topic of the proposed meeting would be advanced/exotic propulsion, so there would be no competing sections on other topics – and all of the participants would be in the same room sharing the same experiences. Presenters would be given up to 4 hours to address their topic. And they would be expected to address both theory AND experiment. Only a half dozen or so topics would be addressed at the meeting. Topics hopefully covering the range of proposals on offer for futuristic propulsion. Those invited to the event would be encouraged to interject questions in the course of the presentations, rather than waiting until the end of the formal presentations. White boards would be provided for spur of the moment calculations and illustrations. The event would be video recorded for posterity, and proceedings would be produced. I said it sounded good to me; but I thought they were underestimating the amount of work involved. I also volunteered to seek sponsorship of the meeting by the Space Studies Institute and the Tau Zero Foundation as I knew the folks in both outfits.

Then the matter of where and when to have the meeting came up. Initially, Lance suggested having it in Estes Park, since he knew I spent summers there. I immediately suggested the YMCA as a possibility to him. Meanwhile, Anthony Longman had put me in touch with David Hyland (of Texas A and M University), and David had asked me if I knew of any meetings seeking a venue – for they had a new building to put to use. I suggested TAMU, or a section at STAIF II, or UCCS, or CSUF. Site selection was put off while more important issues were dealt with. Like creating an invitee list and sending out invitations to see if anyone else were interested. And picking a name. Should we call the meeting a "workshop" or a "symposium" ? Or something else – I suggested that "symposium" would be a bad choice (notwithstanding its snooty overtones). The name came from the Greeks, for whom a symposium was a gathering in the afternoon of a bunch of old geezers who would discuss politics while imbibing wine and appetizers and get lightly snockered. Let others call their events symposia. We should call our meeting what it was intended to be: a workshop.

Planning the meeting was conducted with conference calls on Friday afternoons. When I asked Dave Hyland how much the TAMU facilities would cost, he stopped returning my emails. When I asked Tau Zero if they were interested in sponsorship, they thought about it for a week or so, and declined the invitation. The SSI said yes – as long as they didn't have to do the logistics. But they would do the audio and video recording, and take care of the coffee and donuts. By late winter, tentative invitations had gone out. This brought two problems to our attention. One was that a number of people had other ideas about how the meeting should be organized, and who should be invited. The other was what had become the tentative site: Estes Park. Greg Meholic, for example, wanted the meeting to take place in Aerospace Corporation facilities in El Segundo. But Lance had already settled the issue a week or two earlier when I again tried to get the meeting site be TAMU instead of Estes Park. He and Heidi were unmovable on the issue. Lance's reasoning was, should only the three of us show up, he wanted us to be in Estes Park, which is a nice place to be no matter how the meeting turns out. The timing of the meeting was easier. The week of September 19th was chosen because fall colors would be on display. Several suggested invitees got added to the original list.

Early in the planning process for the meeting, it was easy to believe that it might be possible to get the chief advocates for the major approaches to advanced propulsion to come and make the case for their preferred scheme. With past propulsion battles in mind, I concocted a motto for the meeting: "bury the hatchet". I even suggested a lapel pin design to Heidi for this theme: a crossed hatchet and shovel. Heidi, with her usual enthusiasm, went off and got a lapel pin maker to make up both silver and bronze versions of the pins. These were eventually distributed at the workshop, a distinctive, memento of attendance at the workshop. The hatchet has not in all cases been buried. But all of the major schools of propulsion physics were represented. And the proceedings were at all times congenial.

Invitations were sent out before Lance, Heidi, and I had a chance to figure out a specific agenda. We invited George Hathaway because of his decades of experience doing experiments related to advanced propulsion. Dave Hyland was also invited to present on his recently funded propulsion work involving the dynamic Casimir effect. Paul March was asked to talk about his work on EM Drives. But after the invitations went out, before we could do any more planning, we had several volunteer presenters, enough to more than fill out the schedule for a three day meeting. This plethora of potential presenters finally set off alarm bells for me. As a grad student, I had had a number of once weekly evening classes that ran for about three hours. And for pretty much all of my teaching career, I taught once weekly evening classes that ran for about three hours. Having not taught for more than a decade, I had forgotten the nature of that experience. When decisions about presenters were actually to be made, my memories flooded back. While allotting four hours to a group of two or more presenters might make some sense, my intuition told me that, as general rule, giving four hours to individuals did not. Even with breaks and careful planning by the presenter, avoiding burnout before three hours (much less four) is a serious task. The individual presentation time was reduced to two hours. At once this solved our problems. All of those who wanted to present could be accommodated, and presenter and audience burnout could be forestalled.

The remaining issue to which we devoted time in our conference calls was the production of the proceedings. The SSI had committed to producing videos and making them available on their website. Heidi and Lance agreed to be co-editors of a proceedings. It was agreed that the proceedings of the Dirac 70th birthday volume should be a model, especially regarding the inclusion of transcriptions of the comments after the presentations. If the meeting worked as the sort of workshop we hoped for, this material could rival the presentations themselves in importance. The following pages are the written results of all of these considerations. We hope that it measures up to your expectations for work on the interstellar propulsion problem.

INTRODUCTION TO THE SPACE STUDIES INSTITUTE

Gary C. Hudson
Space Studies Institute
16922 Airport Blvd. #24
Mojave, CA 93501

Welcome everyone, and my thanks for taking the trouble to attend this Workshop, SSI is very pleased to be able to act as the host, so as some of you may remember SSI and know what it's about, I am going to show only two or three slides, as an introduction.

Next year SSI will be 40 years old, which is a little hard to believe. It was started by Prof. Gerard K. O'Neill, a physicist from Princeton University back in 1977, and his goal was to open the space frontier to all humanity, and to utilize the resources and energy therein to support our future evolution and expansion into the cosmos. Our approach is not as to be advocacy organization, we are not interested in lobbying for bigger budgets for NASA or anyone for that matter, our approach is to engage with researchers in the field, to produce technological innovations that make this expansion into the cosmos feasible. It's obviously a huge challenge and we have some particular ideas about the approach that we want to take.

Our legacy is that we have done work with the lunar polar orbiter, the lunar prospector concepts in the 1980's and before that with MIT and Princeton University on the Mass driver approach to moving asteroids, and taking resources off the surface of the moon and using them for purpose build human settlements in space. To this end we have sponsored 14 conferences to date, typically on about 2 or 3 years centers. We published the proceedings in cooperation with the AIAA (The American Institute of Aeronautics and Astronautics) just like these proceedings will ultimately reach the public as well.

SSI has at the moment three initiatives, the first is ambitious beyond any dreams that I have to actually be able to fund and build, but it's hugely important, and that's the G-Lab. The second is E-Lab which is a closed loop environmental system, that's going to be necessary for human space settlements and also for starships. The third, where we really didn't take leave of our senses, was we wanted to move into the "exotic" propulsion arena. That was challenging, because in the past our work has been very solidly grounded in engineering and physics, and of course exotic propulsion is a pretty controversial subject.

(1) I wanted to mention our G-Lab Project even though it doesn't have any direct relation to this workshop – because you can never tell if someone in the audience knows a rich billionare who wants to put their name on it. It's going to be a very expensive project to do, but its also critical to our future survival in space.

Last night, during the invited early talk, someone mentioned the issues of going to Mars and landing on the Martian surface, we completely agree with this, our fear is that humans might not be able to survive at low g levels, below the g-level that we evolved at, we maybe able to fix everything else about living on a planetary surface, radiation and even the perchlorates on Mars but can we fix the low-g effects, that's the critical issue as far as we are concerned. What's appalling is after half a trillion dollars of expenditures and fifty years of activities of the space agencies of the world in space we have no clue to this answer.

So, the question is, is it a linear relationship between astronaut health and the strength of gravity, could there be a positive effect or a negative effect? By default we have to think there has to be a negative relationship, because we look at microgravity and we see the horrific effects on astronauts and cosmonauts. So the dream of living on planets or moons with less than 1g is potentially just a dream. We might explore them, but we may not be able to live on them. So to answer that question, we need to build a rotating artificial gravity centrifuge in space and raise generations of animals in this facility. This is probably a human tended facility, in conjunction with ISS (International Space Station).

This has been proposed in the past, actually attached to ISS. Since we are going to be talking a lot about momentum at this meeting, you can probably appreciate that people who wish to do microgravity research on ISS don't really like the notion of the largest momentum wheel in orbit physically attached to their structure. Because where ever that momentum wheel wants to go is where the ISS is going to follow, and not the other way around. So the two have to be separated, and NASA and the ESA (European space agency) and the Russians have never come to grips with that problem. So we would like to build it, and we would like to put some billionare's name on it, just like you can buy a building at Stanford, we can do the same thing.

(2) The E-lab initiative is tied to this because closed life support is obviously necessary for such facilities, but I won't go into any detail on it. It's a much less ambitious project because a lot more people are working on that issue than on gravity.

(3) So here is where I want to conclude, on the "exotic" propulsion initiative. (*or rather Breakthrough Propulsion Initiative*). I admit this is a personal interest of mine, and I'll tell you how that interest began. When I was 10 years old I read Arthur C. Clarke's ‡ "*Profiles of the Future*", and there's a chapter in that book titled*Space the Unconquerable*, and the last paragraph of that chapter says that *no man will ever turn homeward from beyond Vega, to greet those he knew and loved on Earth.* That's because Vega is 26 light years away, and a human lifetime doesn't really permit a round trip, traveling at less than light speed. So, of course, when you're 10 years old you don't want to be told you can't do something. Twelve years later, I had the opportunity to sit with Arthur for an evening at "The Arts Club" in London, and I talked to him about this and other subjects. I remember that conversation pretty distinctly, and the one thing I did say to him is that I wanted to prove him wrong on that point.

Instead of him patting me on the head, as a 22 year old, wet behind the ears kid, I am eternally grateful that he said to me, *you may have a chance* and encouraged me. Then he told me something else, which he has written as well in some of his commentaries, and that was:

"To be successful you need to find a physicist who will give you a straight answer to the question, what is inertia ? "

Now I'm only a simple minded rocket plumber – liquid rocket engines and launch vehicles are my specialty - physics and I never got along. So I'm only going to understand one in every three words that's said at this workshop. But I remember Arthur's words, and without denigrating anyone else's work, of EM drives or any other propulsion systems, I want to say that the first physicist that I encountered who gave me a straight answer to the question "what is inertia" was Jim Woodward, in about 2005. When Freeman Dyson asked me to take over the presidency of the SSI, and I said yes, Jim's Mach Effect propulsion device was one project I really wanted to study. I visited Jim's lab a few weeks ago and saw his chirped pulses in action. So to conclude, I'll borrow a remark from Galileo Galilei, **"Nevertheless it does move."**

One last note, not only are we celebrating 75 years with James Woodward, and his dream to get across space-time quickly, but Jim's anniversary is coincident with the *50th Anniversary of Star Trek.* Happy birthday to both Jim and Star Trek! It truly is time for a space drive. Have a fantastic workshop.

Ad Astra.

Clarke's 3 laws‡

1. When a distinguished but elderly scientist states that something is possible, he is almost certainly right. When he states that something is impossible, he is very probably wrong.
2. The only way of discovering the limits of the possible is to venture a little way past them into the impossible.
3. Any sufficiently advanced technology is indistinguishable from magic.

Ethos Of the Meeting

L. L. Williams, H. Fearn & J. F. Woodward

– WHAT WE HOPE TO DO DIFFERENTLY HERE, AND WHY –

The technical committee welcomes everyone to the workshop. At this workshop, we hope to do something a little different than other science meetings. Please allow us to challenge you – and challenge us! At typical meetings, someone presents a 20 minute paper, with 5 minutes for questions. Then they go home, and repeat next year.

The scope of our ambition demands more time for technical interchange. The format of typical science meetings just does not allow the necessary in-depth scrutiny of an idea among technical peers. This scrutiny is necessary for the community to identify plausible candidate ideas, and also for someone with an idea to explain it to peers and win converts.

As we contemplate this workshop, we take as axiomatic that no one gets to the stars alone. The dream of interstellar travel, if it is to be realized, will entail people working together. We can imagine an industrial enterprise of some sort, built on an engineering discipline. It will entail a broader mainstream science than we know today – a breakthrough will have occurred.

The first step along this road is for the discoverer to convince the second person. If someone has a potential discovery, the first step to bringing in society and mainstream science, is to convince the second person.

If someone has made a discovery, but has not convinced anyone or shared it with anyone, then no contribution is made to society. It might be due to poor people skills – or perhaps someone was delusional all along. The test of sanity is on the anvil of peer review.

Therefore, this workshop is your chance to convince the second person. This is your chance to convince educated peers and move the ball forward for society. And we are providing sufficient time to do it.

As we pursue this common objective, we also take it as axiomatic that we must abide the norms of science, something history shows us is necessary for technical progress of any sort. Some of the propulsion conferences these days degenerate into performance artists and sci-fi author panels. We want to inject a dose of scientific method back into this business.

We want to treat this endeavor with the same rigor and detachment that we would in trying to find a cure for polio, for example: no one looks to UFOs for a cure for polio; no one looks to YouTube for a cure; no one looks to cable news talking heads; no one convenes medical fiction authors to ask what they think. On the contrary, our road to a breakthrough in propulsion proceeds through the ground of repeatable experiment and peer review. Come as a scientist and as an engineer to Estes Park!

We must accord with the pillars of science so far. Concepts like conservation of energy are not easily forfeited. For example, in the 1930s, beta decay seemed to indicated a violation of conservation of energy. Pauli suggested an unseen particle – the neutrino – carried the energy away. If you are invoking the tooth fairy or otherwise turning centuries of science on its head, be prepared to climb a steep hill.

For our conduct, we want to stay respectful and constructive. We will investigte the concepts on grounds of theory and experiment, in an orderly way, moderated as necessary to stay on topic. All discussion should pertain to the concept at hand, and its technical aspects. And of course, we want to stay impersonal, since we are seeking the objective reality.

It is honorable to help one's colleagues find the flaws in their concepts, and it is equally honorable to seek the flaws in one's own concepts. Help yourself to understand if a breakthrough could finally be at hand!

As an editorial aside, my own opinion (Williams) is that it's too early to worry about funding. I know everyone has to eat. But funding must necessarily come after a believer has been made of the second person. So we will need day jobs til then, but that is not unlike any visionary who ever went before.

Today's space industry is different than the government-directed concepts for space exploration that have been nurtured since Apollo. Instead, it seems that a good idea will find a tech entrepreneur or venture capital firm. The big changes being made in the space industry today stem from that model, so perhaps breakthrough propulsion will as well.

Enough philosophizing. Let's get on to the workshop!

ASPECTS OF PLAUSIBLE EXTENSIONS TO PHYSICAL LAW

L. L. Williams
Konfluence Research Institute
Manitou Springs, Colorado, USA

We discuss some of the profound constraints on any viable extension to the known laws of physics.

1. THEORY WITHOUT EXPERIMENT

We can anticipate two basic situations in our search for a propulsion breakthrough. One is a compelling experiment with no theory. If someone can reliably produce an effect to levitate a cannonball, then the discovery is at hand and the theory can be developed from observation of the effect. More likely is the second case, in which we seek experimental confirmation for proposed modifications to physical law. It is for this second situation that we consider some aspects of allowable extensions to the laws of physics.

As we are likely considering extensions to the laws of gravity, we adopt the framework that Robert Dicke used in the 1950s to consider theories of gravity alternative to general relativity. These alternatives could be parameterized against observation to verify general relativity against other plausible theories.

2. COVARIANCE AND LORENTZ INVARIANCE

The first constraint is that the theory must be covariant: it must keep its form under coordinate transformations. Furthermore, the space and time coordinates must satisfy the Lorentz transformation. In practical mathematical terms, this means the equations must be written in terms of 4-vectors or tensors with 4 degrees of freedom per index. All current laws of physics, classical and quantum, are covariant.

Here are some examples of covariant or Lorentz-invariant equations:

$$R_{\mu\nu} - \frac{1}{2}g_{\mu\nu}R = \frac{8\pi G}{c^4}T_{\mu\nu} \qquad , \qquad \frac{dU^\mu}{d\tau} + \Gamma^\mu_{\alpha\beta}U^\alpha U^\beta = 0$$

$$\partial_\nu F^{\nu\mu} = \frac{4\pi}{c}J^\mu \qquad , \qquad \frac{dU^\mu}{d\tau} = \frac{q}{mc}F^{\mu\nu}U_\nu$$

By way of comparison, here are some equations that are generally not covariant or Lorentz invariant:

$$\mathbf{F} = \mathbf{E} \times \mathbf{B} \qquad , \qquad \nabla^2\phi = 4\pi\rho \qquad , \qquad \mathbf{F} = m\frac{d\mathbf{v}}{dt}$$

The non-covariant forms above are encountered in specific coordinate systems, and physicists work with them every day. But they cannot be the starting point. Forms like those above must follow by writing a covariant equation in a specific coordinate system.

3. LAGRANGIAN

A second important constraint from the Dicke framework is that the theory have a Lagrangian. All known laws of physics, classical and quantum, are derivable from a Lagrangian. The Lagrangian generates the field equations and equations of motion according to a fixed operation. There is no method for finding a Lagrangian; it must be guessed, its equations derived, and its predictions checked against experiment. Weinberg won the Nobel Prize for a 2-page paper guessing the correct electroweak Lagrangian (PRL, 19, 1264, 1967).

The Lagrangian for the known classical fields of gravity and electromagnetism is:

$$\mathscr{L} = A_\mu J^\mu - \frac{1}{4\mu_0} g^{\alpha\mu} g^{\beta\nu} F_{\alpha\beta} F_{\mu\nu} + \frac{c^4}{16\pi G} g^{\alpha\beta} R_{\alpha\beta} + T_{\mu\nu} g^{\mu\nu}$$

where A^μ is the electromagnetic vector potential 4-vector, J^μ is the electric current 4-vector, $g_{\mu\nu}$ is the gravitational metric tensor, $F_{\mu\nu}$ is the electromagnetic field strenth tensor, and $R_{\mu\nu}$ is the Ricci tensor.

It is remarkable that all the complexity of gravity and electromagnetism, with their tensor field equations, is captured by a scalar entity. An enormous amount of information is unpacked from the simple package of the Lagrangian.

I have not bothered with the quantum Lagrangian of the strong and electroweak forces. My own view is that reaching the stars is a classical, not quantum, problem.

Rodal: I agree the Lagrangian is important, but the Second Law of Thermodynamics cannot be written in terms of a Lagrangian. Some of the laws and effects we are dealing with involve dissipation, which cannot be written in terms of a Lagrangian. More than a Lagrangian may be needed for our case.

Williams: I take your point. The laws of thermodynamics are important and have no Lagrangian. However, we are focusing here on particles and fields, and the laws of thermodynamics are not specific to any particles or fields. They are general properties of natural processes.

4. FALSIFIABLE PREDICTION

A third constraint is to demand a concrete prediction. After all, there is no point to the theory if it makes no prediction. Closely related to this is that an experiment exists to prove or disprove (falsify) the theory.

A new viewpoint, but without a new prediction, is not a new theory. Feynman famously developed several alternate viewpoints to help him understand the particular theory under development.

And that concludes my short summary of some aspects of legitimate extensions to the laws of physics.

5. DISCUSSION

Robertson: Give me an example of a new prediction.

Williams: One example which I will give later is a tunable coupling of gravity. If there is a coupling between gravity and electromagnetism, and I can do some electrical experiment that changes the weight of a cannonball – that's not in existing physics. So a new prediction is an effect not known to physics and not contained in current physical law. Another example is Planck's evaluation of the blackbody spectrum and its resolution of the ultraviolet catastrophe. That was something new to physics at that time. It should generally manifest ultimately as a new experiment not explainable in existing physics. However, Jim's work is an example of a case in which the new effect is in existing physics.

P. Jansson: You agree that string theory is not falsifiable. So we have a higher standard on theories here than is demanded of mainline string theory.

Williams: That's a good point.

Turner: Doesn't a new theory need to fit into the old theory in certain limits? For example, Newtonian theory is found in general relativity in the limit of small velocities, etc. I thought that is what Tony was saying.

Williams: Yes that's a good point. Perhaps I should have listed it as another constraint, that it fit into the broader framework of known physics, and not violate or contradict anything there.

Tajmar: String theory can actually predict a violation of the equivalence principle. A space mission is being prepared to test that effect. So string theory is falsifiable.

Hathaway: Last night after dinner, we heard Brandenburg's prediction, or calculation, of the mass of the proton. Would you consider that a new prediction? In that case, there is no experiment, yet it is a new prediction.

Williams: That's a good point. An example of that type might be Bohr's calculation of the Rydberg constant.

Christie: I have a sort of foundational question. Why are space and time connected? Is anyone working on why that is?

Williams: It's essentially built into general relativity. The connection between space and time is what we call gravity. But it has a sound empirical basis going back to the Maxwell equations.

group discussion of the constancy of the speed of light...see video

Robertson: I want to make an argument against Einstein's general relativity. If general relativity had come after quantum physics, then general relativity would be consistent with quantum physics and we wouldn't be having this discussion. Isn't our obeisance to general relativity in part an accident of history?

Brandenburg: It has proven impossible to reconcile general relativity and quantum theory

Hansen: We should be careful to not disregard quantum mechanics. It may hold something important for the breakthrough propulsion problem.

EXPERIMENTING WITH NOVEL PROPULSION IDEAS

George Hathaway
Hathaway Consulting Services
Toronto, Canada

ABOUT MYSELF

I am a professional engineer, graduated EE in 1974 from the University of Toronto. I own a little company called Hathaway Consulting Services (HCS) near Toronto, Canada. HCS was established in 1979 and has an international clientele: foundations, private investors, institutions & agencies. The focus is on exotic technology: primary areas being propulsion, gravity, energy, and materials. The primary mandate of HCS is fundamental experimental research. I appreciate being invited to this workshop; it's an honor and I'm looking forward to all the talks.

1. INTRODUCTION: HCS CAPABILITIES

The bulk of my talk is going to be about measurement pitfalls and prosaic explanations for what is seen in the lab. However, I will give you a little overview to begin with about what we do. HCS has been established since 1979. It is a private organization. We are not associated with any government agency. We are not funded by any agency or institution. It is primarily private investors, private clientele, private foundations in North America and Europe.

Our operation is basically twofold. We provide a service for inventors: people who have what is considered a crazy enough idea that it might just be worthwhile looking into and funding. So, I will try to attract funding for inventors. We also, on the other hand, have a service that we provide for investors. Often a venture capitalist for instance, as they do quite often, has some group or person come up to them saying, "I've got the answer to space propulsion," or, "I've got the answer to free energy," or something like that and they don't know where to go. These are the areas in which I particularly specialize. A university typically won't touch it. It's not within the paradigm of what Lance has so adequately described just before my talk. Even the DoD or DARPA might say, "That's a little too flaky even for us." Then, if the investor knows about me, I will look at the invention and we will provide that service, primarily from an experimental standpoint, but also we have theorists that we can call on; for instance, the Institute for Advanced Studies in Austin, Texas.

Our capabilities have grown substantially since our inception and I won't go through all of them. But the reason I'm listing some items is in case some of you folks need a particular experimental capability that would be useful to you in one of your experiments. The list of lab capabilities below is a small subset of what is available. The lab is about 11,000 square feet of space with all sorts of wonderful and bizarre things. We not only can stimulate the experiment but we can measure the response with analytical instruments. We have been privileged also to produce some of the piezoelectric transducer crystals that Jim has used or was going to use in one of his experiments. We have a material science lab too where we produce magneto- and electro-active ceramics as well as other specialized materials. Here is a partial list of HCS capabilities:

1. cryogenic liquids and gases (to liquid He temperatures)
2. high magnetic fields, both pulsed and DC
3. microwave hardware, waveguide & cavity design
4. ultrahigh pressures and temperatures for novel materials processing

5. high voltage (up to 600 kV) ultrafast (sub–nS) pulsers and radiators
6. electric arc–induced shockwave studies in liquids
7. sensitive vacuum balances for gravity modulation & manipulation studies
8. RF anechoic chamber; large & small high vacuum chambers
9. unique apparatus for materials fabrication and testing
10. high–temperature ceramic superconductor manufacture
11. development of novel ultra–wideband ferrite, piezoelectric & dielectric materials
12. high–power RF designs both solid state and vacuum tube
13. test beds for gyroscopic and other mechanical and electrical thrusters
14. design and testing of apparatus to investigate energy production from quantum vacuum
15. wet lab for bio-communication research
16. SEM/EDAX, TEM, Confocal, RAMAN, XRD, Mass Spec, EPR/NMR, materials testing, high-speed cameras, gravimeter

Rodal: Do you have a sintering press?

Hathaway: Yes, we have various vacuum and controlled-atmosphere sintering furnaces and Cold and Hot Isostatic Presses. We have a 600 ton uni-axial press with a large die we made for the Podkletnov spinning disk experiment the results of which I published in Physica C in 2003. There we made 6 inch high temperature multi-layer YBCO superconductors.

Rodal: Did you grow the crystals? How large did they get?

Hathaway: Yes, probably on the order several centimeter but growing crystals is something we haven't done for a while but, let us know if you need some crystals.

Cole: What are the gravity meters you used, are any of them commercial gravity meters?

Hathaway: Yes, the one I'm listing here is not automated. It's sensitivity is about one part in 10^8g.

Cole: We used one before and the resolution was about an hour, not even seconds. So, it was basically worthless.

Hathaway: For high-speed studies, no. Ours uses a quartz gravimeter with a few seconds time constant. It has a tiny quartz lever with a little platinum weight on one end and you peer into it. It's primarily a commercial device used for geophysical surveying. But, it's available so if you have a long duration experiment that isn't a pulsed experiment, it can still be very useful. And we have balances that do react faster but don't have the sensitivity.

2. HCS PROPULSION EXPERIMENTS

Some of the propulsion experiments that we've been involved with, either designing or testing for various clients, are listed here. This is only a subset of some of the general studies we do in the lab which, as I mentioned are generally propulsion and energy. We've had a long history of involvement with people who have come to us with new energy devices. The list regarding energy is much longer than what is shown below. This is a propulsion workshop so I've emphasized the propulsion side of things.

Below is a partial list of HCS propulsion experiments. We have investigated Biefeld–Brown HV capacitors, John Brandenburg's GEM theory-based rotating currents and Barrett/Froning SU(2) coils, all with null results. These will not be further discussed here. A few that I will highlight in this talk are:

1. Graneau water-arc discharge thruster
2. gyroscopic force rectification

3. Williams div(J) & gravity

4. Podkletnov rotating superconductors & gravity beam

5. Zinsser HF force accumulation

6. spin-polarized nuclei/gravity interaction

7. Hutchison Effect

8. Woodward, Mach Effect drives

There are many individual experiments we've done on rectification of rotational motion to linear force, which is an old standby, and a lot of these particular experiments deal with purely mechanical devices. An inventor might say, "I've got a gyroscope and I put it on a string and it sort of swings over this way a couple of times and its average looks like it has a thrust in a certain direction". But, when you actually do the proper experiment, the average thrust is zero.

Cole: I don't want to criticize any experiments that anyone is doing in here, but I will criticize how it's being publicized. The publications a lot of these experiments I read and the impression I get from reading them is that what that person said would happen is untrue, when really what the experiment has actually done is a subset of what the person did, not the true experiment of what the person did. Yet, the article reads, "What that person did is wrong." And so you need to bring up when you're writing these papers is that you're in some kind of limit of the original experiment and not doing the original experiment, but that doesn't seem to be brought out in these papers. It's almost like you're saying we did the original experiment and it didn't work when you really did not replicate the original experiment.

Hathaway: Yes, for instance my Podkletnov reproduction was criticized by saying that I had not done the actual experiment. I had not said this is not a true representation. There are gradations as you pointed out. It is not always possible to perform an exact replication of an experiment which has already been designed or carried out or for a theory that has been developed and tested. Unfortunately people don't have a long enough attention span, or the ability to read. Anyway, we can come back to that.

FIG. 1: Peter Graneau shown with his high current discharge into water experiment. Fast fog from a cannon shot a projectile up to a catcher box above.

1. Graneau – energy from water by H–bond breaking

Some of you might have heard about Peter Graneau and his son Neil. We spent many years with the Graneaus, specifically in their energy experiments. They were suggesting that if you introduce a high current discharge from a capacitor bank very quickly into water, the water would produce around the arc a huge quantity of "fast fog" they called it. The fog would shoot up through the water into the air above and if you calculate the momentum and the energy in the fog in the air, it would be greater than the energy introduced by the capacitor bank in the first place [1]. Hence, there was some weird over-unity energy activity going on which they ascribed to something called hydrogen bond breaking in the water. That was an energy experiment, but it wasn't generally known that we also considered using this idea, whether it was over unity or not, as a propulsion system. So, we did some experiments. Here you can see (see Fig. 1) a high voltage pulsed power supply. There's an arc discharge device, a little water cannon down there, that is going to shoot fast fog which certainly is fast when it's coming out of the barrel and we're timing it as it pushes a light projectile up into this little catcher above.

This would have been a very interesting propulsion system even though it was classical. We would push pulsed fog out the back to provide forward momentum. But it would have been much more exciting if there was an over-unity component to it. Unfortunately, there was not.

2. Gyroscopic motion levitation experiment

Here is an example of what would be considered the grand-daddy of gyroscopic precession propulsion systems. This device stands almost a foot tall. (see Fig. 2) The rotor is on the order of 7 or 8 inches in diameter. The hoped-for outcome was that if we precess a spinning gyro at the correct ratio of the nutation frequency compared to the rotor spin frequency, we might get this thing to lift off, or at least lose weight. That's an old thought that has not proven itself in any experiment that I've ever known or been involved with. But I was involved with this one and these guys really went to town with the force gauges underneath and all sorts of instrumentation all over the place and they were just getting a whole bunch of noise (see Fig. 3). The investors put millions of dollars of high tech into this experiment.

FIG. 2: Gyroscope being testing for weight loss

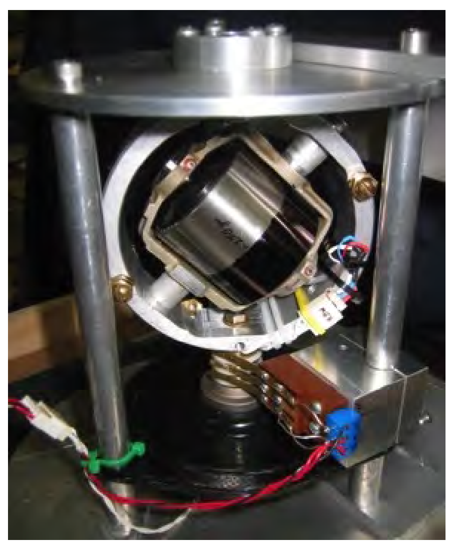

FIG. 3: Gyro being tested at HCS.

So, I made my own little reproduction (Fig. 3.) with a rate gyro from a WWII aircraft, doing basically the same as that experiment. But theirs was tightly instrumented, and it was not actually allowed to move much. So we experimented with several ways of seeing whether there was a force generated. One was on the end of an optical table with the device on the end of a simple swivel arm, and it would only oscillate back and forth. (see Fig.4) It never progressed its oscillation forward. Another simple way of testing for constant thrusts is a ball table (see Fig. 5). A lot of people denigrate this method but it's actually quite sensitive.

The grey area in Fig. 5 is a granite machinist's table which is ground flat within tenths of a mil. There's a thick glass plate on which the experiment sits and there are plastic (or steel) balls underneath. On the glass plate is a little white card with a cross in the center. A machinist's height gauge with pointed tip on an arm is placed on the table with the pointed tip aimed down onto the center of the cross. If there is a net thrust, the cross should move away from under the tip. My experiment just vibrated and jiggled around but the cross on the card under the pin showed no progressive motion.

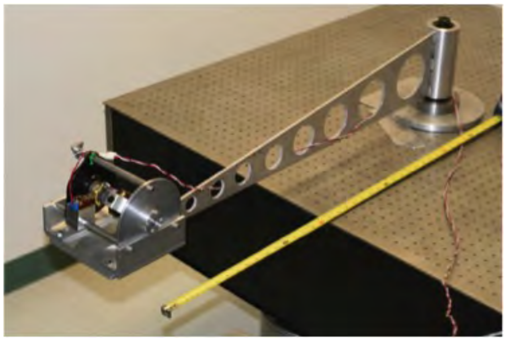

FIG. 4: Gyro tested at HCS, using pivot arm.

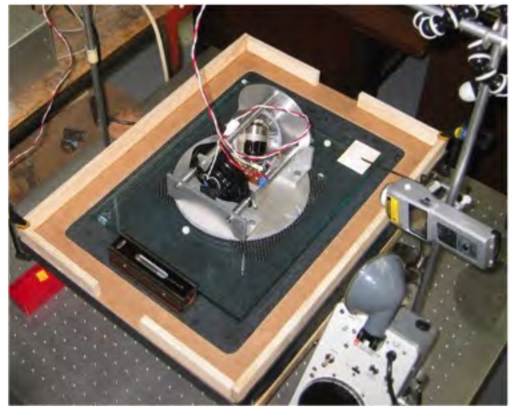

FIG. 5: Gyro tested at HCS, using ball table.

3. Williams' 5–Dimensional Theory

Pharis Williams's 5-dimensional theory suggests you can produce a region of reduced gravity between two conducting plates on which high current is respectively diverging and converging from the periphery to the center (div J). In the experiment, you produce a strong divergent current, which diverges from a point on one conducting plate and on a second plate nearby, the current is converging to a point. Then, according to his theoretical calculations, there should be a change in gravity between the plates. We devised an experiment for Williams where we had a high-current conducting rod attached to the center of the flat end of 4" copper plumbing end cap and another rod attached to the center of a second end cap which was facing the first and very close to it. A thin dielectric disk was suspended between them whose weight was measured during current conduction. (see Fig. 6). The 2 rods were attached via welding cable to a battery bank of several thousand amps through a high-current contactor. The circuit was closed by the O-shaped copper plumbing.

Unfortunately the dielectric disk didn't change weight even though we were able to measure the weight between the diverging and converging plates down to a factor much better than he was expecting.

Meholic: How did you measure the weight of the central dielectric plate?

Hathaway: The whole copper O-shaped apparatus was placed in a frame as shown but what you cannot see is a hole in the top left elbow. A thread supporting the dielectric disk passed through this hole and was attached to a sensitive analytical chemical balance above the apparatus. The top high-current rod was hollow to allow the thread to pass through.

Our experiment did not say that there is no anomalous force or a gravitational interaction because of diverging and converging currents according to Williams's theory. It just means that we were not able to detect it down to level that he wanted.

4. Podkletnov Spinning Superconducting Disks

In Fig. 7, there is Eugene Podkletnov (lower right) on one of his two visits to our lab in 1996. We are looking at an experiment that we reproduced from an experiment that had been done at the University of Turin in 1992 I think. There, a small Yttrium Barium Copper Oxide (YBCO) superconductor was spinning

FIG. 6: Williams' 5–Dimensional Theory Test Apparatus.

in the vapors of liquid nitrogen. It was in the Meissner state, but their method of looking at weight loss was not very sophisticated. The Turin setup was at the undergraduate level to see if any anomalous effect was present but our version had quite a bit more precision. We did not see the weight change. There were some strange transient effects when you start the spin up or you slow down suddenly a superconductor, but we could never ascribe them to anything other than instrumentation noise and spurious thermal effects.

We went on to make the larger experiment, the reproduction of Podkletnov's spinning superconductor experiment. The guts of it are shown in Fig. 8, which is an insert for a large liquid helium cryostat. There are 3 solenoidal levitation coils, two of which you see prominently at the bottom, copper colored. In this experiment there are also 3 high-frequency (5 MHz) coils which loop through the central hole in the superconductor. These are seen just above the levitation coils. And on top, the 2 plates of aluminum which hold the gearing mechanism I used to spin the superconductor even though, topologically, it also had these loops of wire running around it. So that was a nice little design challenge.

FIG. 7: Podkletnov, small table–top spinning superconducting disks.

FIG. 8: Podkletnov large disks setup.

Our paper was published in Physica C in 2003, [2]. I'm convinced Podkletnov never actually went to all this trouble.

Williams: So those were all null results?

Hathaway: It was null to within the measurement resolution of our equipment. Once again, I cannot say there is no effect. All I can say is that to the best of our ability, which was approximately fifty times better than what he had claimed, we saw a null result.

I suppose most people in the room have also heard about his so-called gravity beam experiment [3]. Podkletnov claimed that at high enough DC impulse voltage applied to a high-temperature superconductor, a flash of something magical will boil off the superconductor and head towards a target, in this case a grounded copper ring. Some magical beam of gravitational force will emanate from the other side of this ring and travel through space to impart a ponderable force on objects in its path.

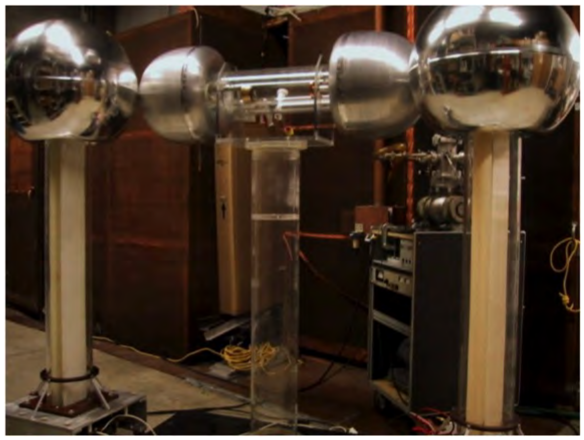

FIG. 9: Podkletnov gravity beam experiment.

I learned about that experiment when I went over to Europe to attend a lecture that he gave on the results of his initial beam experiments using a van de Graaff machine. I don't think anyone in this room was at that lecture back in the 90's when he first announced he had done that experiment. A few years later we had built two 600 kV van de Graaff machines for a different experiment. Using these, I put together a Podkletnov gravity beam experiment, where the superconductor is the black thing you see inside the horizontal glass vacuum tube. It's glued thermally to a little liquid nitrogen holder, and there's a little liquid nitrogen dewar inside the left inner dome here. The target is a grounded copper disk. The whole thing is pumped down using a turbo pump vacuum system.

We "aimed" this into the Faraday cage or screen room shown behind the apparatus, and we used a very sensitive force detector in that cage, and that was a wire "clothes hanger" with strips of toilet paper hanging from it. It turns out, that is extremely sensitive to small forces, much smaller than the forces claimed by Podkletnov to, for instance, knock over objects on a desk. So we were video taping the hanging toilet paper and operating this gravity beam rig. We got a null result.

Brandenburg: Is the superconductor actually a dual–layered superconductor?

Hathaway: This was actually a Murakami-style melt-textured (polycrystalline) superconductor we made in-house, because Podkletnov had used melt-textured in one of his very first gravity beam experiments. This is a three inch diameter melt-textured YBCO superconductor.

Brandenburg: But when he did his experiment he used a double–layer superconductor.

Hathaway: He did also use a double layer in some experiments.

Brandenburg: The rotating ones, were basically I think just crushed superconductor...

Hathaway: He actually did use three-layer disks, too. Note for some spinning disk experiments he specified sintering YBCO, then crushing and sieving, then sintering again to get the desired grain size distribution. We did make a three-layer to his specifications, which was two superconductors sandwiched with a praseodymium layer to kill the superconductor as the middle layer. He had all sorts of different kinds of materials he suggested would work.

Brandenburg: I have a little aside comment here. There was one particular expedition to the Livermore Lab, where we were tasked to try to reproduce a Russian result and actually got it work. In this case it was an experiment done by some very reputable Russian scientists. They published, as usual this is the Cold War, a very terse article describing vaguely how they got these marvelous results. And we actually got the thing to work to their amazement. We concluded later that the whole thing was a wild goose chase. We were doing laser pellets in one dimension, you know, everything converges absolutely spherically in one dimension. If you throw in two-dimensional effects everything goes all over the place, it's like scrambled eggs. But in one dimension we could get their stuff to work, and they had left out so much stuff that we kind of just put in my guesswork. I'm just saying that the Russians do send people on wild goose chases and part of it is to knock the system over here. They want to see what the reaction is, and also, it's to sop up money, any money that is actually going to worthy causes so – pardon me.

Hathaway: They're also interested in knowing what our technical and analytical capabilities are. How far are we advanced in the ability to measure these things?

5. Zinsser impulse accumulator based experiments

Probably not many people know a German experimenter named Rudolph Zinsser [4] who had a theory and an experiment where he claimed that if you produce 40 MHz saw-tooth waves, and introduce them into water in a certain way, and weigh the water, you will get an accumulation of force impulses. We experimented with this idea. Zinsser had explained this experiment and demonstrated this effect at a conference I held in 1981 at the University of Toronto. He had shown that on his balance that he brought over from Germany, he was able to have this container full of water and 2 electrodes actually lose weight as these force impulses accumulated in the water.

FIG. 10: Zinsser Experiment: water plus electrodes in acrylic container.

FIG. 11: Zinsser experimental vacuum chamber..

So, many years later, in 2003, I got around to finally doing the experiment properly. And properly means having water in a vacuum vessel. Zinsser did all his experimentation in air. The water has to be contained in a water-tight, vacuum-tight vessel. For the RF sawtooth energy to flow into the water, it has to go through the vertical capacitor plates shown on top of the water container which allow the vertical movement of this vessel on a balance beam without wire connections. That balance beam is inside a tube exiting the far side of the large vacuum chamber shown in Fig. 11. I used one of Jim Woodward's optical displacement sensors which he kindly provided to me some time ago. Thank you very much Jim, I appreciate it. Sadly, null results ensued.

6. Nuclear spins and Gravity

We were also involved with experiments to determine relationships between nuclear spin polarization and gravity. Here's an experiment that involves electron parametric resonance (EPR) which aligns electron spins which will then, by the Overhauser Effect (also called DNP - Dynamic Nuclear Polarization) align the nuclear spins in a much more effective way than simply by nuclear magnetic resonance (NMR) alignment. When the electron spin system is in thermal equilibrium, the polarization transfer from electrons to nuclei requires continuous microwave irradiation at a frequency close to the corresponding EPR frequency. So we require a microwave cavity and associated hardware and a very sensitive vacuum balance and vacuum system and a sample which is cryogenically cooled. So far this experiment is still underway and there are no results yet.

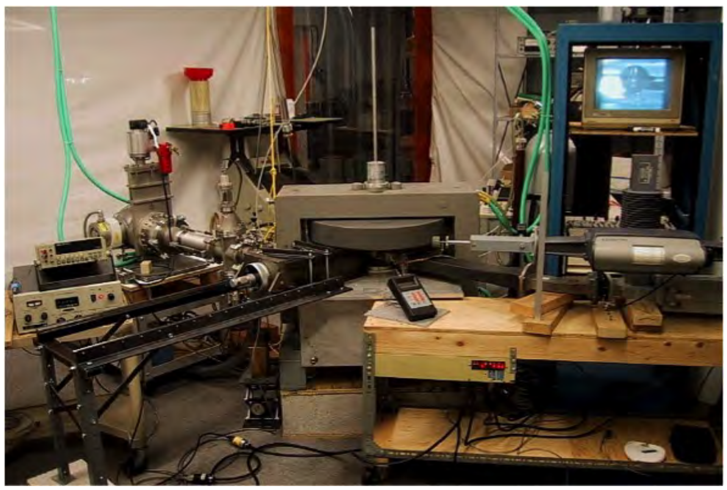

FIG. 12: Nuclear spin and gravity connection.

7. John Hutchinson

We also tested something called "The Hutchinson Effect". John Hutchison had a famous video of a cannon ball levitation, amongst many other bizarre occurrences.

I bring up John Hutchison because of what Lance had mentioned earlier, namely you can have experiments and no theory. There's no theory to explain this guy or any of the stuff associated with him. I've had lots of questions before the talk started here, like what do you think? Is Hutchison for real? All I can say, in the very brief time that I have, Hutchison was real at the time of the events that are described in my book [5]. Hutchison is not real now.

Mathes: What do you mean? He has moved onto the complex plane or what?

....audience laughter....

Hathaway: Not yet! Hutchison was able to levitate and break apart material and cause all sorts of other weird things to happen, which are described in my book, at the time that we were researching him. We had a contract to find out what was going on with this guy, and we tried our best but we were never able to discover what was going on. But, we witnessed and experienced the most unusual things that I have ever experienced in all my years being at this game.

Mathes: So you couldn't replicate it?

Hathaway: We couldn't but we set up the experiment ourselves, and we can go into this offline, but we set up the experiment ourselves just the way he did in a different location and we got some electrostatic effects. But only when he came and performed the experiments was there actual levitation, things like that.

Meholic: So on an independently constructed apparatus, he was able to operate it and get the results?

Hathaway: Yes, yes. The reason I'm bringing this up is that we are all talking about the technical aspects of advanced propulsion. You know, we've got theories and we've got quantum mechanics and we've got relativity and we've got experiments and all the stuff that I'm testing and that you guys have gone through. I just want to put in the very back of your mind the fact that consciousness might play a role.

FIG. 13: John Hutchison in 1997 in Vancouver.

8. Jim Woodward's Mach Effect Drive

Finally, we get to Jim's device [6]. I've seen very small effects that I believe are just above the noise in my thrust balance [7] using one of Jim's older first or second generation devices, a small PZT 19mm device. Fig 14 shows a picture of the vacuum chamber I built for the test and the associated electronics. What I saw was at 200V AC in magnetic shield in vacuum.

Woodward: It's a device that's the same as the one that Nembo tested and it's similar to the one in the setup we have now. Of course that device has been changed as you know, the brass reaction mass was changed as it produced much better effects. Did you get the new brass mass George?

Hathaway: Yes it's sitting there on the table.

Woodward: Aha! No you're fine. We're distributing new reaction masses to George and Nembo. We've produced a new device, and those are the reaction masses that should make it possible to see some slightly bigger effects.

A lot of our experiments have to be done on anti-seismic tables. The balance that we're testing Jim's and other thrusters on (and I'm sure Nembo will talk about as well) have to be free of seismic influences from the environment. It can never be totally free because the absorbing nature of, say, pneumatic bladders and such things do not get rid of all noise. But at least you have to know the frequency spectrum of the seismic vibration absorbing material so you can say ok, I'm working within this band of the noise spectrum which is outside the natural frequency of the absorber and you can then justify a little better than in fact you have removed that prosaic influence to a large extent from your experiments.

FIG. 14: Vacuum chamber for Jim's test article HCS.

FIG. 15: Balance beam with Jim's test article inside.

And it becomes a problem because anti-vibration damping does have frequency response. You can hit a resonance with some of the experiments and you'll get a false output. A lot of vibrations especially from vacuum systems become a real problem. If you are lucky, you can design a vacuum system that does not need hoses. The best way that we have found to get rid of tubing is ion pumps. Then, instead of having tubes or pipes that come from the vacuum system to your experimental chamber you now put these little ion pumps on. First, you still have to rough down the vacuum system but then you physically turn a valve off, and take off the hose, and connect the ion pump, which just has these little high voltage wires which are much less problematic coming down to your chamber than these big hoses.

3. TESTING ISSUES UNDER THE ASSUMPTION OF A COMPLETELY NOVEL INVENTION

When we consider a test campaign, several general issues need to be addressed prior to designing the experiments when the assumption is that the invention is completely novel. Some are listed below. Somewhat different issues arise when contemplating a series of validation tests on an invention that has already been built, e.g., in areas of hypothesis testing.

- who is the test for: inventor or investor?
- design of suitable test bed for each project;
  costs of new equipment vs re-use of existing equipment
- cost/benefit of simple "look–see" experiments without full testing
- hypothesis generation (observed physical phenomenon without prior theory) vs hypothesis testing (confirmation/denial of prior theory)
- test protocol development: replication vs reproduction
- enumeration of likely prosaic/artifactual explanations
- control experiments

- statistical & error analysis
- instrument calibration
- minimum resolvable thrust required to prove claims

4. INTRODUCTION TO TESTING NIGHTMARES

By way of introductory examples, an area in the list below is the effect of local gravitational variations where you have really sensitive experimental instruments. In fact, down in the low nano-Newton range that starts to have a significant effect. This one we ran into at Hal Putoff's lab in Austin. They were doing an experiment with a sensitive Cavendish balance and couldn't quite figure out why they could never zero it. One week they would be able to zero it at a particular rotation position of the torsion fiber and the next week they would have to turn it around and it turned out that somebody had moved a storage cabinet from one area to the other. It was about 20 feet away and it affected the zero position of their Cavendish balance. You would not think that would have any effect, but actually when they calculated it, the sensitivity of the balance was such that it did have this slight effect, this slight movement that was certainly enough to affect their final result.

Another example: Virtually all sensitive experiments that I know of have to be done under a vacuum of some degree depending on how you want to characterize them. A lot of stuff happens if you're not careful with how your vacuum system is constructed: where the ports are compared to your movable apparatus, the pumping rates, molecular drift within the chamber during the experiment, etc. You say, well, we pumped our chamber down and it was stable, at least from the gauge we put on the side of it. Either a thermal couple gauge or an ion gauge might have been attached to the side of the chamber and it has a steady reading so there are no transient pressure effects measured. In fact, you really don't know what's going on inside the chamber. The gases could be stratifying over time, causing an unstable, anisotropic situation versus what you think is a stable situation according to your gauge. All you have to look at is a gauge: a meter here or an ion gauge there saying we're down at 3×10^{-6} torr and it's been that way for half an hour. Well, in fact, inside there might be a whole bunch of other stuff going on gas wise, molecular flow-wise, that will take a longer time to settle down. That's just one component of the vacuum-related pitfalls.

Yet another example that comes up a lot is when you have a horizontal teeter-totter balance arm that is measuring something on one end, and you have a counterweight on the other end. A lot of "backyard" experimenters, at least those that are performing propulsion or thrust measurements, may have their thrust-producing device and/or counterweight rigidly fixed to and hanging at, let's say, 90 degrees from the balance arm. So, they see maybe an anomalous thrust happening with their balance but they forget that in fact the lever arm length is changing because the thruster or counterweight is a fixed angle. So, what they should be doing is pivoting the thruster so that you don't change the lever arm length.

Now we will overview the general experimental nightmares in the art of measuring: Are we seeing a real force, or is it some artifact of the experimental method? What follows is a list of effects which must be considered before claiming a new and game-changing result. A wise experimenter will make a check list and check off (and publish) each artifact as they are systematically eliminated from their experiment.

Question: Are you proposing, George, that everyone itemize and make sure that none of these artifacts are effecting their experiments?

Hathaway: No, I'm not proposing that they do anything. It's up to them to accept, or least be knowledgeable, about the fact that there are a myriad of effects that will interfere with their results. I'd be delighted if that was the case, but that will make an experimental report in some peer review journal excessively long. Usually, when someone really wants to get in and reproduce the experiment, they will go to the experimenter and say did you do this and this and run that test? So I'm not suggesting that one has to go through ALL of these items. Some items on this list are clearly not relevant to a particular experiment and can be ignored.

Woodward: I agree. You can't publish every test you did, but you have to be prepared when someone comes to criticize your work, to be able to answer their criticism that you did run though the needed precautionary tests and the result you are reporting is real and not some artifact.

Hathaway: If I were to write a check list of possible artifacts, then this is a subset of that list. It is by no means comprehensive, but covers a good subset of artifacts an experimenter should be aware of in this business.

NIGHTMARES IN THE ART OF MEASURING

I. Mechanical Effects

II. Temporal Effects

III. Electromagnetic Effects

IV. Electrostatic and Related Effects

V. Instrumentation Issues

VI. Signal Analysis

VII. Use of Controls

I. Mechanical Effects:

A. Thermal

1. Thermally-driven convective air or gas movements causing test masses connected to balances to move. Also, results from condensation of water vapor onto test mass or suspension during cryogenic experiments.

2. Radiometer effects on a test mass (in a radiometer, blade movement is caused by pressure of thin gas layers near blades due to absorption of solar energy).

3. Change of heat transfer conditions between test mass surface and liquid. This depends on i) delta-T between them which can change substantially over time, ii) thermal diffusivity of test mass.

4. Thermally-driven convective movement in liquid (usually cryogens) causing weight artifacts in submerged test masses connected to balances.

5. Change in length of lever arms or period of torsion balance due to thermal contraction/expansion.

6. Change in response of balances due to differential thermal expansion coefficients.

7. Short- or long-term temperature-induced drift of electronics in recording devices, amplifiers/signal conditioners.

8. Thermal noise in balance structures, eg, torsion fibre and masses in a Cavendish balance.

9. Thermal gradients, and their time excursions, induced in test masses, especially superconductors (with corresponding distributions of superconducting or non-superconducting phases), resulting in only partial conditioning (e.g., only part of the superconductor is in superconducting state) due to insufficient or inefficient cool-down or warm-up. Effect exacerbated by non-uniform test mass composition, density and thermal diffusivity.

10. Altered buoyancy of test masses, especially superconductors, in liquids (usually cryogens) due to free convection or 2-phase flow (gas bubble/liquid) in thin liquid layers close to the mass surface causing variations in liquid/solid friction.

B. Buoyancy

1. Different-shaped test, counterweight and dummy masses exhibit different buoyancy effects even in low-pressure gas.

2. Expected or calculated buoyancy of test mass or counterweight mass is enhanced or decreased by horizontal thermal stratification of still gas/air.

3. Account for buoyancy differences due to temperature differences even in low pressure gas.

4. Thermal shrinkage of test masses and supporting structures during cool-down causing reduction of buoyancy, e.g.,in sample holders with large thermal expansion coefficients.

5. Absorption of water vapor, oxygen or other gasses from the air by and into the cryogen causing density variations and corresponding variations in buoyancy.

6. Thermal expansion during warm-up of test mass causing increase in buoyancy in gas or liquid.

C. Seismic/Vibration

1. Local seismic noise effecting one part of a balance preferentially.

2. Subtle seismic or structural vibrations serendipitously synchronized to the expected experimental effect being measured interpreted as signal of real effect. This is especially true for condenser and other sensitive microphones due to high sensitivity over wide frequency response, which are clamped to a laboratory structure.

3. Vibrations from local rotating machines, e.g.,roughing and turbomechanical pumps.

D. Diurnal & Gravitational

1. Effect of motion of moon on sensitive balances.

2. Tidal motions of earth's crust altering orientation or periodicity of observations.

3. Cautions regarding use of sealed gravimeters for force detection (placement with respect to experiment, size of internal detection mass, handling, temperature, etc)

4. Avoidance of moving masses in laboratory (e.g., people and equipment) during sensitive gravity experiments.

5. . Calculation of effect of large nearby stationary masses.

E. Vacuum

1. Outgassing of materials in vacuum interacting with movable masses.

2. Outgassing of fastening/joining methods, e.g., gas from blind bold holes interacting with movable masses.

3. Mechanical strains on structural/electrical/measuring components during pump–down.

4. Slow leaks resulting in air stream impacting test mass.

5. Internal "wind" during pump–down or gas back fill.

F. Coriolis/ Earth Rotation, Torques

1. Correction for Coriolis acceleration/earth rotation effects in extremely sensitive moving-mass force–detection systems.

2. For test masses firmly fixed to a balance arm without provision for pivoting or gimbaling, the mass can exert a torque on the arm masquerading as a weight change. Especially true if mass has a magnetic moment (conductor or non-conductor, magnetic or non-magnetic) either induced or permanent, then stray fields can induce a "magnetic" torque in the test mass.

G. Liquid

1. Noise induced in weight/force measuring instruments due to separation of tests mass from liquid (usually cryogen) bath while lifting mass out of bath.

2. Noise induced in weight/force measuring instruments due to evaporation of liquid (usually cryogen) from surface of test mass.

3. Weight artifacts induced in suspended test masses approaching cryogenic temperatures due to condensation of residual water vapor on test mass and suspension not removed by vacuum system. This effect can appear as an increasing weight over time as more water vapor condenses.

4. Artifactual and fluctuating weight changes due to de–wetting of suspension (usually wire or filament) of submerged test mass while surrounding liquid evaporates and level decreases. This effect increases with surface tension, test mass circumference, and decreases with increasing contact angle. Surface roughness also important.

5. Surface tension can exert undesirable forces on a test mass when it passes through the surface of a liquid.

II. Temporal Effects:

A. Signal Duration

1. Mismatch between time scale/time constants of measuring device vs experimental variable.

2. Long-duration signals lost in long-term natural drift of experimental parameters.

B. Test Mass Conditioning

Allowance of sufficient time for sample to reach required temperature (e.g., cooling a superconductor to below transition temperature) between measurements if direct temperature determination is difficult or impossible.

III. Electromagnetic Effects:

A. Magnetic Coupling

1. Influence of time–varying fields on non–magnetic but conducting bodies, inducing local magnetic fields in conducting bodies which may be attracted or repelled from the field or other nearby bodies.

2. Simple magnetic coupling between magnetizable bodies considered unmagnetized before the experiment.

3. Over–reliance on magnetic shielding material which needs special handling and re–annealing after machining/forming/bending etc.

4. Improper reliance on magnetic shielding material for exclusion of DC or quasi–static magnetic fields.

5. Influence of earth's static magnetic field strength, gradient, and dip on magnetic bodies.

6. Stray artificial magnetic fields causing spurious electron beam deflection on oscilloscopes.

7. Sudden release of trapped magnetic fields in superconductors raised above transition temperature affecting & affected by nearby magnetic or conductive structures.

8. Coupling between magnetic moment of superconducting test mass and external magnetic fields including earth's field.

B. Electric/Magnetic Screening

1. Leaking/improperly sealed Faraday Cage/electrostatic screens.

2. Improper reliance on Faraday Cage for complete exclusion of DC or quasi-static electric fields.

3. Frequency dependence of Faraday Cage

4. Inability of screen-type Faraday Cage to screen magnetic fields

C. Electromagnetic Coupling

1. "Lorentz–Air" effect: the coupling of time varying EM fields in air on the local air molecules. (added by J. Woodward)

2. Avoidance of switching transients especially in high–power circuits, especially sudden stopping of current though inductive loads or conductors producing EMP inducing large spurious signals even through shielded coax or aluminum instrument boxes/cases.

3. High frequency RF radiation from nearby transmission lines or conductors interfering with electronic weigh scales.

4. Lack of RF suppression on instrument power lines and instrument lines, e.g., ferrites, shunting caps, proper RF connectors & cables, unless disallowed for frequency response reasons.

5. Avoidance of capacitive coupling between signal cables and grounds/ground leads carrying transient/fault currents.

6. When a source is incorrectly matched to a load, a greatly increased level of EMI across a broad frequency range may be generated as the reflected power interferes with the correct operation of the source (an amplifier usually). This in turn may cause spurious measurements to occur, and this is particularly troublesome when using an electronic balance.

7. Casimir force between test mass and measuring system at nano-scale dimensions.

D. Grounding/Earthing

1. Avoidance of contact potentials developing across multiple ground connections. In some cases contact potentials must be compensated by a deliberately applied counter potential.

2. Strive for single–point RF ground system for all instruments.

3. Correction of ground loops and ground faults both internal to the experiment and between experiment and measuring system.

4. Understanding the difference between independent earth ground (e.g., copper stake in virgin earth) vs mains "ground" vs mains neutral, and potentials between these.

5. Poor/loose ground connections: preventing complete charge draining, allow transient voltage artifacts on recording & display devices, allow small signals to be amplified by amplifiers along with the signal of interest, etc.
6. Use of large cross-section circular wire or flat ribbon strip from experiment and/or instrumentation to earth especially for pulsed high–power experiments.

IV. Electrostatic and Related Effects:

A. Gradient

Gradient of electrostatic field caused induced motion in nearby free bodies.

B. Charge Pooling & Induced Charges

1. Accumulation of pools of surface charges on invisible insulating patches on conductors. Especially problematic for metal enclosures/surfaces which have unavoidable insulating metal oxide layer formed on surface, eg. aluminum.
2. Accumulation of surface charges on water patches on inner surfaces of vacuum chambers and components.
3. Accumulation of charge on insulating or non-conductive surfaces, e.g.,wire insulation, after exposure to electrostatic and sometimes time-varying electric fields.
4. Reaction against image charges created on conductor

C. Ion & Molecular

1. "Ion wind" due to ionized surrounding gas causing artificial force on conductors especially in high-voltage DC or AC experiments.
2. High-voltage ablation/sputtering of molecules or ions from conductors or insulators.

D. Charge Leakage

1. Unaccounted–for corona or other uncontrolled charge leakage, usually in bursts ("Tricel Pulses") in high-voltage experiments, which can create time–varying charge on nearby conductors. Especially problematic at sharp corners.
2. Ions from leakage current interacting with gas molecules and imparting thrust to the leakage ion source body.
3. High voltage creation of weak conduction paths between device under test and ground. Depends on humidity, vacuum.

V. Instrumentation Issues

1. Measurement outside specifications of instruments, including sensing/measuring instruments, signal processors/amplifiers/conditioners, and recording/display/acquisition devices.
2. Lock–in amplifier response to high-amplitude transients riding on input lines, causing artifacts even when not phase locked to the reference signal.
3. Voltage sags/surges resulting in poor mains power quality, e.g.,startup of nearby large rotating equipment.

4. Ensuring correct vertical/plumb orientation of torsion balances, especially while on pneumatic anti–vibration tables.
5. Operation of bearings & pivots outside specifications
6. Operation of bearings & gears in vacuum using proper vacuum grease

VI. Signal Analysis

1. Averaging: to tease out buried signals and suppress noise
2. Statistical Analysis: use of χ^2, calc. of correlation coefficients, sigmas, etc.
3. Noise: is noise floor burying signals of interest?
4. Error Analysis: how confident that signal is inside measuring instrument range and is real – requires full specs. of instrumentation, error propagation.
5. Exploiting Adjustable Parameters
   - Adjusting phase of various parameters to detect artifacts
   - Suppression of common–mode noise.
   - Alternate mechanical orientation of experiment with respect to possible local forces or gravity.

VII. Use of dummy test mass/controls

1. Replacement of test mass by known null-effect mass.
2. Use of null-effect dummy mass of identical thermal characteristics to test mass, especially in superconductor/cryogen experiments.
3. Reversing sense of one experimental variable to determine if observed effect goes away.
4. Shorting one component or use of dummy electrical component with same electrical characteristics.
5. When using superconductors as test mass, check for correlations with test mass being in Meissner state.
6. Investigate all properties of test mass before and after experiment, including volume properties (phases, crystal or amorphous structure, chemical composition, absorbed species, density, thermal diffusivity) and surface properties (morphology, interfacial energy, wettability, depositions/adsorption, corrosion and erosion).

Finally, since this is very important to people at this workshop, here are some issues relevant to Roger Shawyer's testing of the recently-announced "EM Drive", taken from the list above .

- Self-contained power supply, or wires to lab frame?
- Absolutely vertical thrust bearing shaft?
- Rigidity of support frame?
- Off-center center-of-mass at any time during the test? changes in COM?
- Evidence of ratcheting? ("Dean Drive" effect)
- Serious thermal issues including waste heat flow, differential thermal expansion causing variations in lever arm

And some control experiment suggestions:

- Replacing thruster with cylindrical cavity and/or back-to-back tapered cavities

- De-Q the cavity tapered walls
- Re-arrange placement of radiator & piping vs cavity
- Re-arrangement of wires

References

[1] Peter Graneau PhD., "Extracting Intermolecular Bond Energy from water", `http://www.infinite-energy.com/images/pdfs/GraneauIE13-14.pdf`

[2] G. Hathaway & B. Cleveland, "Gravity modification experiment using a rotating superconducting disk and radio frequency fields" , Physica C Superconductivity **385**(4):488-500 April (2003)

[3] Dr. Evgeny Podkletnov on the Impulse Gravity-Generator, on `http://energia.moebius.com.br/oo/Energia/ENERG4L-antigravity/EugenePodkletnov-RussianScientist/PodkletnovInterview(EN).pdf` see also Evgeny Podkletnov and Giovanni Modanese, *Gravity-Superconductors Interactions: Theory and Experiment* Bentham science books/9781608053995.

[4] Rudolph G. Zinsser, "Mechanical Energy from Anistropic Gravitational Fields", `http://www.rexresearch.com/zinsser/zinsser.htm` US Patent 4,085,384.

[5] G. Hathaway, *Mindbending - The Hutchison Files: 1981 to 1995* , Paperback –July 25, (2014).

[6] J. F. Woodward, "*Making Starships and stargates*", (Springer press Dec 2012).

[7] G. Hathaway, "Sub-micro-Newton resolution thrust balance", Rev. of Sci. Instr. **86**, 105116 (2015).

On a most serious note, George was not wearing shoes during his presentation, and I have photographs of his festive socks. Although we do not endorse wearing no shoes while presenting, if you must, then at least wear really cool socks like these!

George wore these socks while giving his talk!

Later George was seen wearing these socks...

EXPERIMENTS WITH RF CAVITY THRUSTERS

Paul March
Friendswood, Texas, USA

This talk is about experimental tests of advanced, or breakthrough, propulsion systems that I was involved in at NASA Johnson Space Center. As you know, Johnson is devoted to the manned space program. We all share the ultimate goal of manned missions to the stars, by whatever propulsion system is available to us.

1. THE LONG-TERM VISION

Let me start with the goal, and then return to the current state of experiment. At NASA, we have dreams of manned missions to the stars. An artist by the name of Mark Rademaker [1] came up with a fantastic design for an exploration solar-system or poor-man's star-ship, called the IXS Clarke, based on Q-thrusters for propulsion, see Fig. 1.

[Editor: Q-thruster stands for "quantum vacuum thruster", a hypothetical propulsion device that would somehow extract energy from the quantum vacuum. The idea is controversial and its physical plausibility undemonstrated.]

The Q-thrusters in this concept design are powered by a ~ 2.5 MW nuclear reactor and work via a quantum vacuum based plasma system that Harold "Sonny" White came up with [2,3]. Roger Shawyer was the first to propose such a space drive, which he calls the "EM drive", see his EM-drive web page [4]. That is what we would like to build.

[Editor: the quantum vacuum plasma concept is controversial and its plausibility undemonstrated. The EM-drive stands for "electromagnetic" drive. Shawyer's device does not rely on any quantum concept in its design or construction, and its operation depends only on classical electromagnetic effects of RF radiation. It is essentially a microwave cavity resonator. Since any thrust should be impossible due to to electromagnetism alone, the influence of the quantum vacuum is invoked, and so March considers the EM-drive to be a Q-thruster.]

These twenty, Q-thruster "engines" on the IXS Clarke concept vehicle are projected to produce about 30,000 N total of thrust, with up to 1,500 N and up to 100 KW RF power per engine.

Rodal: How big are those Q-thrusters, how long are they and what diameter?

March: Those Q-thrusters are based on our current design dimensions that are being tested in the lab, at lower power. They are truncated copper cone radio frequency (RF) cavities, with a large diameter of 11 inches, small diameter of 6.5 inches, and 9 inches long. For the concept vehicle, we would pump 100 kW of RF power into these cavities at at frequency of 919 MHz. There are 20 engines, so that will require a 2.0 to 2.5 MW nuclear reactor. This ship would be constructed in space and the engines would be space-drives, meaning that they only work in space. With that in mind, given the total-thrust-to-spaceship-weight ratio of approximately 1.5×10^{-3}, we estimated the starship to weigh about 100 metric tons.

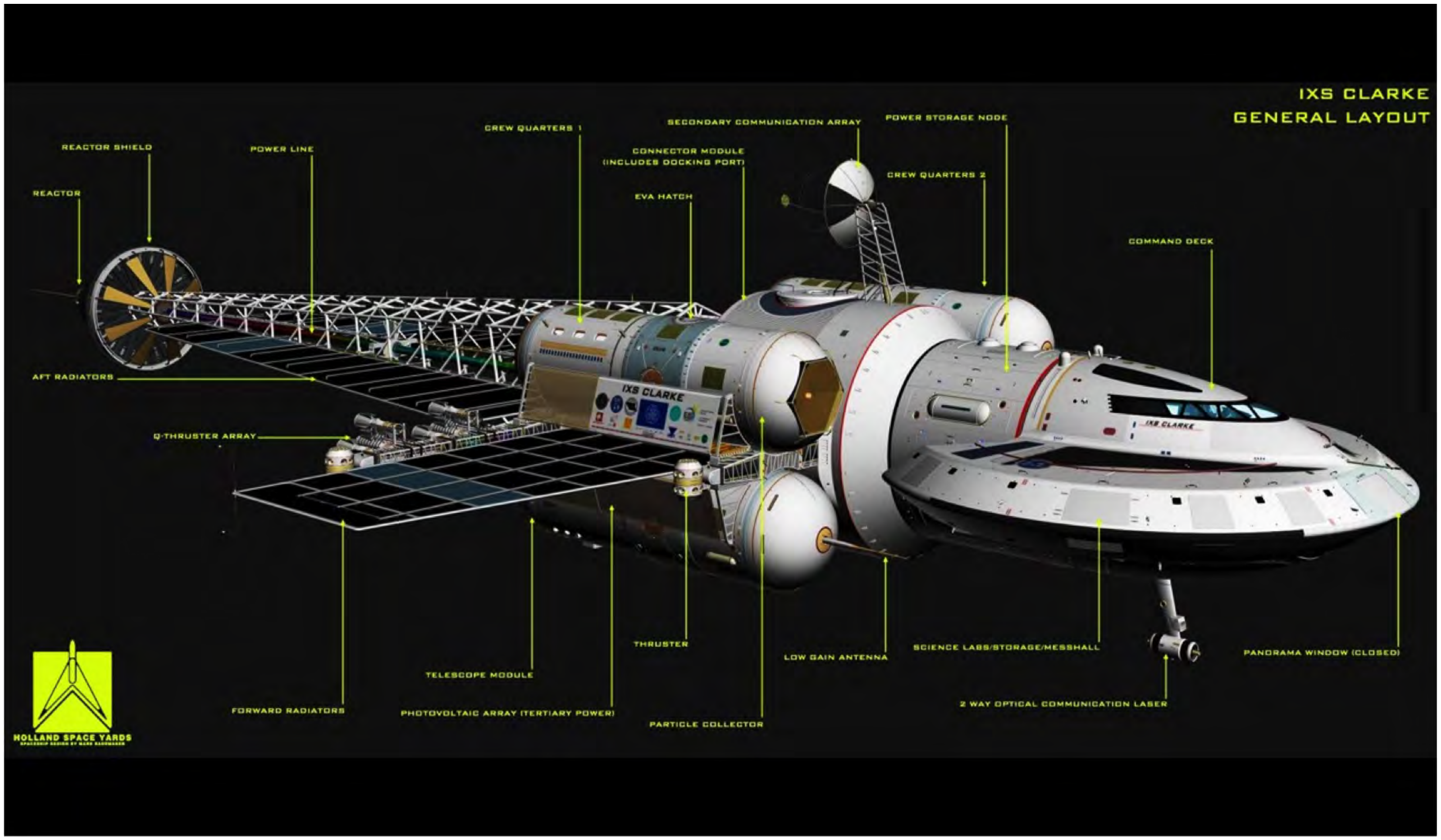

FIG. 1: Nuclear powered Q-Thruster Concept Exploration Ship called the IXS Clarke, artists impression [1].

Woodward: Do these cavities have polymer discs inside them? and how do you cool them?

March: Yes the cavities may have thermoplastics discs in them and cooling, well, that's the main trick, isn't it? I think Gary Hudson has an idea how that would work - basically very much like liquid fuel rocket engine cooling. These EM drives are truncated copper cones (called "frustrums"), which basically have the shape of a rocket nozzle. You can cool them like a rocket nozzle. Instead of liquid propellant you are dealing with either a quantum vacuum mechanism [3] or a gravitational field effect [5] to produce the thrust. This of course depends on whose theory you want to use to explain the force.

FIG. 2: Copper truncated Cone Cavity, of the type used by Shawyer. Tested at Eagleworks by Paul March 2013. This shows construction of the copper cavity. The large diameter is 11 inches, the small diameter is 6.26 inches and the cavity is 9 inches long. To complete the build 2 type-N RF feeds must be inserted into the cavity. This cavity shows PCB end plates in use. There were 36 # 6-32 nut and bolts used in construction.

Hansen: Would it make a difference to the thrust if you were to use a superconducting material for the cavity rather than the copper?

March: From what we have found to date experimentally, the thrust appears to scale with the input RF power times the quality factor of resonance Q, so if the Q is 100 to 2000 times larger, than what you can obtain for a room temperature version of the device, the thrust should scale up accordingly. Let's see, the level of thrust is currently at tens to hundreds of micro Newton. We hope the next generation of device will improve the thrust to tens of milli-Newtons. Now if you go to a superconductor, the Q jumps from 5×10^4 (depending on the mode you are in) currently to perhaps 5×10^6 (which is a hundred times improved) or to 100×10^6 which is 2000 times bigger. You would expect the thrust to scale with those Q factors. So if we started with a copper cavity device producing 1mN then went to a superconducting device with 2000 times bigger Q, all else being equal, we should have an improved thrust of 2N for that device. So your thrust per power input will go up accordingly. The problem you have, is that now you have to deal with cryogenics. For liquid nitrogen cooled superconductors the temperature is 77 Kelvin. If you have to use a liquid helium then you are down to 4 Kelvin. The liquid helium refrigeration is nasty. So there is the extra weight of the cryogenic equipment you need to carry along. But, there is quite a good increase in efficiency, so you reduce your power level for a given thrust level.

[Editor: Q-factor parameterizes the damping of a resonator, and the EM-drive is an RF resonator. Q-factor can be defined as the ratio of energy stored to energy dissipated per cycle; higher Q-factors correspond to lower dissipation.]

Rodal: The efficiency goes up with Q, and we have known for a long time that the Q increases with the size of the cavity, so why is your cavity so small? Dr. Luis W. Alvarez (Nobel prize winner) was at Massachusetts Institute of Technology during the war, in the 1940's, developing radar technology for early warning systems. He built a huge 40 foot long cavity using spare WWII equipment. Why is it, that looking into the future, you are using these small cavities, when a bigger one would be so much more efficient?

March: The resonant frequency of the cavity goes with inverse length squared. You can think of an oscillating parcel of air, of mass m, oscillating like a mass on a spring. The longer the length of the cavity the lower the frequency. The thrust increases with the frequency and the Q. That is all part of the optimization process, we would need to do a case study to find the optimal length of cavity and frequency, for a high Q and the maximum possible thrust. That particular unit was based on a 929MHz magnetron, at 200 kW power and running at 88% efficiency. You go with what you've got!. I'm sure if you had enough money you could develop a better more efficient system.

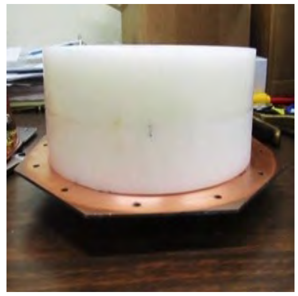

FIG. 3: High density Polyethylene (HDPE) discs. Outer disc diameter 6.13 inches and thickness 1.063 inches. Two discs are mounted on the small end of the truncated cone cavity.

Woodward: Assuming that the thrust is real, and that it is being produced inside the cavity by an interaction between the RF field you are injecting and the walls of the cavity, that should give you a means of testing which theory is correct. (Either the Mach effect gravitational interaction theory or Sonny's vacuum plasma theory.) Considering that there are RF photons, that can interact with the skin depth of copper and any polymer disc inside the cavity, that is all you have. So either the force is produced between the interaction between these photons and the walls of the cavity and polymer disc (if there is one) or the force is somehow produced by the electromagnetic field (the photons) independently, without any interaction between the cavity walls or the disc being present. You don't have anywhere near the Schwinger electric field strengths (10^{18} V/m), needed to induce vacuum breakdown and electron-positron pair creation!

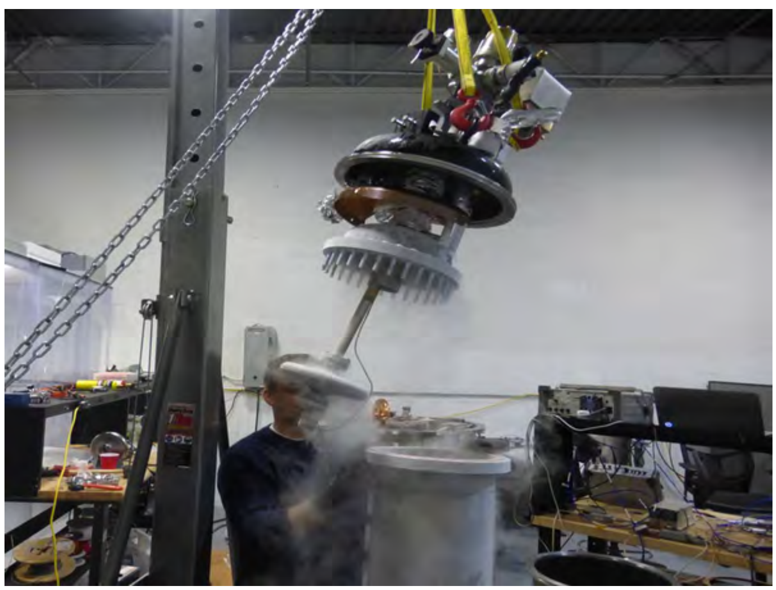

FIG. 4: Superconducting Niobium Cavity by Guido Fetta, from the Cannae website 2011 [6].

Woodward: Do you or Sonny have any plans to convert your copper cavity into a superconductor?

March: I don't have any plans for a superconducting cavity because I don't have the funds, I'm retiring. You would have to ask Sonny what his plans are.

Rodal: What would be the best experimental test to check on which theory is correct?

Woodward: Making a superconducting cavity, because the skin depth of a superconductor is a minute fraction for what it is for a non-superconductor like copper. So a theory depending on the interaction of the photons with the metal material would not predict as large an increase in thrust with the change to a superconducting material, even though the Q of the cavity does increase. The thrust may not go up at all.

Fearn - note added in proof: The gravitational interaction theory also predicts an increase of thrust with Q. All the Mach effect details have not been worked out yet for the EM drive. Any induced currents in the wall of the metal would increase for superconducting cavities. This could lead to additional Lorentz-type forces, due to both electric and magnetic fields being present inside the cavity. However, the EM fields would have difficulty penetrating the supercondctor. Overall, there would probably not be as big an increase as expected, with the superconducting material, if the gravitational Mach effect is responsible for the force.

Woodward: Have the Cannae people [6] built a superconducting cavity yet?

March: Guido Fetta built his first niobium superconducting cavity back in 2011, that may have produced up to 10 milli-Newton of thrust with a cavity Q of 11 million. Over the last two years (2015-thru-2016) Guido's team has produced three more niobium cavities, based on the same pill-box beam pipe resonant cavity geometry we tested in the Eagleworks Lab in August 2013 and January 2014, but made from Niobium instead of copper. That has now been tested in the up, down, and sideways configurations relative to the Earth's gravitational field. Guido indicated that these new niobium superconductive cavities that have *NO* dielectric inserts, were now operating with a cavity Q of >60 million and producing thrust with an efficiency of greater than $\sim$50 N/kW, with 4 watts of $\sim$930 MHz RF input. Martin Tajmar mentioned that Shawyer has built a superconducting cavity and this was published in Acta Astronomica [7].

Rodal : It is interesting to note that Fetta has published his superconducting cavity result in the AIAA JPC in 2014 [6] and he was not seeing the efficiency he expected from the use of the superconductor, using helium temperatures around 3 Kelvin. Neither Fetta nor Shawyer are seeing an effect of increase of force proportional to their Q.

Fearn - note added in proof: Rodal can show that Q scales like $\sqrt{L}$. Reference the Appendix

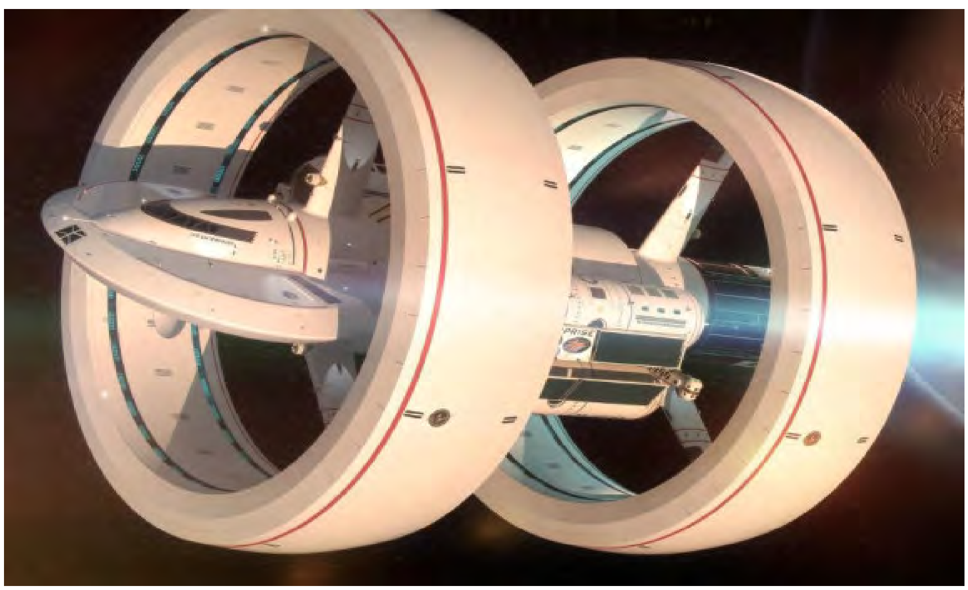

FIG. 5: The IXS Enterprise concept design [8], for deep space missions with a FTL, Warp drive engine rings.

Before we move on, let us address the use of warp drives as a possible mode of interstellar space transportation. Sonny White has been pushing this research for some time, in order to promote study in this area. A physicist needs to believe his/her work will be taken seriously by their peers. Many scientists (both physicists and engineers) at this meeting would like to congratulate Dr White for doing an excellent public relations job on their behalf, and for making an attempt to establish gravitational warp theory, as a legitimate field of study. Thank you Dr White!

The Mark Rademaker IXS Clarke concept drawing above is just the interplanetary (solar system) exploration ship since it does not have faster than light (FTL) engines on board. The IXS Enterprise [8] on the

FIG. 6: Pill-box beam pipe design cavity by Guido Fetta. [2]

FIG. 7: Three generations of device by Roger Shawyer. The photos can be found on the EMDrive website or in the youtube presentations referenced there, *http://EMDrive.com* [9]

other hand, has both the EM-drives and warp drive rings. The YouTube video [8] was meant to promote Science, Technology, Engineering and Mathematics (STEM) study in young adults.

2. TWO DIFFERENT DESIGNS; MANY EXPERIMENTERS

It is important to note that we have been discussing two very different designs of cavity which have different geometry and different electromagnetic modes of operation. We have mentioned the pill-box beam-pipe design by Guido Fetta [6], and a truncated cone [7,9] by Shawyer, both are illustrated below. There have been attempts to compare the thrust to power input of these devices online. They should not be compared directly, since they are very different in geometry and it would be like comparing apples to oranges.

Both of these models have been tested at the NASA Eagleworks facility. The cavities are seen in the Eagleworks vacuum chamber below. There is a photo of both Guido Fetta and Roger Shawyer with their respective devices.

I wanted to give fair credit to others working in the field of EM-drive propulsion. Here is a list of active scientists that I know of who are currently running their own experimental tests. I give the resonant frequency of their device, name, and location.

- 2.45 & 3.85 GHz, Roger Shawyer ...UK
- 1.937 GHz, Dr. Harold White & Paul March ... JSC/Eagleworks Lab, Texas, USA

- 2.45 GHz, Prof. Dr. Martin Tajmar ... Technische Universität Dresden, Germany
- 24.0 GHz, Paul Kocyla and Jo Hinchcliffe ... Aachen, Germany
- 2.45 GHz, Michelle Broyles ... Colorado, USA
- 2.45 GHz, Phil Wilson ... Australia
- 2.45 GHz, Dave Distler ... Ohio, USA
- 2.45 GHz, Jamie Ciomperlik ... Georgia, USA

FIG. 8: Pill-box beam pipe cavity in the vacuum chamber at Eagleworks.

FIG. 9: Shawyer's truncated cone undergoing testing in the Eagleworks vacuum chamber.

You make the EM-drive out of a highly conductive materials to reduce power losses (i^2R) in the material. The shape is usually a truncated cone of the Shawyer type. These are all AC driven systems, you cannot make a propulsion system with DC power no matter how high the voltage. We have an injection antenna, either a ring shaped one or a small cylinder, which injects RF electromagnetic radiation into the cavity. A variety of modes can be set up inside the cavity, due to the radiation bouncing back and forth between the end plates. You can scale these things to be any size, the resonant frequency would decrease with size, but as Rodal mentioned earlier, the Q increases with size. You can think of these cavities like an acoustic cavity (of a wind instrument), different lengths give you different resonant modes (different frequencies). These cavities are closed, not open ended like an instrument. They must be closed so that the electromagnetic waves can reflect back and forth. The greater the number of bounces, the higher the Q and the greater the electromagnetic field strength within the cavity. The electromagnetic waves will eventually die down due to power (heating) losses, once the RF input is shut off. The higher the cavity Q, the higher the field strength you can achieve inside the cavity and when the RF is shut off, the longer it takes for the electromagnetic field to die down inside the cavity and dissipate as heat.

NASA/JSC Eagleworks Laboratory has a large Stainless Steel & Aluminum vacuum chamber with inner diameter 30" $\times$ 38" long . Our RF sources range from 9 kHz up to 2.5 GHz. See AIAA 2014 JPC paper for details [2]. Below in Fig. 10, is a picture of our vacuum chamber, you can also see the rack mount with our data acquisition systems. The vacuum chamber has a sliding tray inside. Fig. 11 shows a photograph of the first generation magnetic damper, using 3 neodymium magnets and an aluminum bar.

The vacuum chamber has a micro-Newton force resolution-capable torque pendulum (see Fig 12.) The displacement of the pendulum is measured by a Philtec optical sensor, similar to the one Jim is using. The power to the test article is directed through Galinstan contacts (liquid metal) to avoid the weight of the cables producing an unwanted torque on the test device. The procured roughing and turbo-vacuum pumps can pump a clean chamber down to $\sim 5.0 \times 10^{-6}$ torr in about 4 hours, dependent on outgassing. The calibration of the force is done using electrostatic calibration fins, giving a known attractive force (see Fig. 13). A detailed theory of calibration using interlacing fins can be found here [10]. The force from the fins is constant over a small range and has a linear drop-off with distance. The constant force over

FIG. 10: Eagleworks stainless steel and aluminum vacuum chamber, 30” diameter, 38” long. [2]

FIG. 11: Magnetic damper on the pendulum balance. [2]

a small range makes it very convenient for calibration. We used a National Institute for Standards and Technology traceable 1mg mass to calibrate our chemical scale, which then weighed all the test masses for all our calibration runs. We used 200V, 300V, and 400V test pulses for calibration with 3 and 5 kg loads.

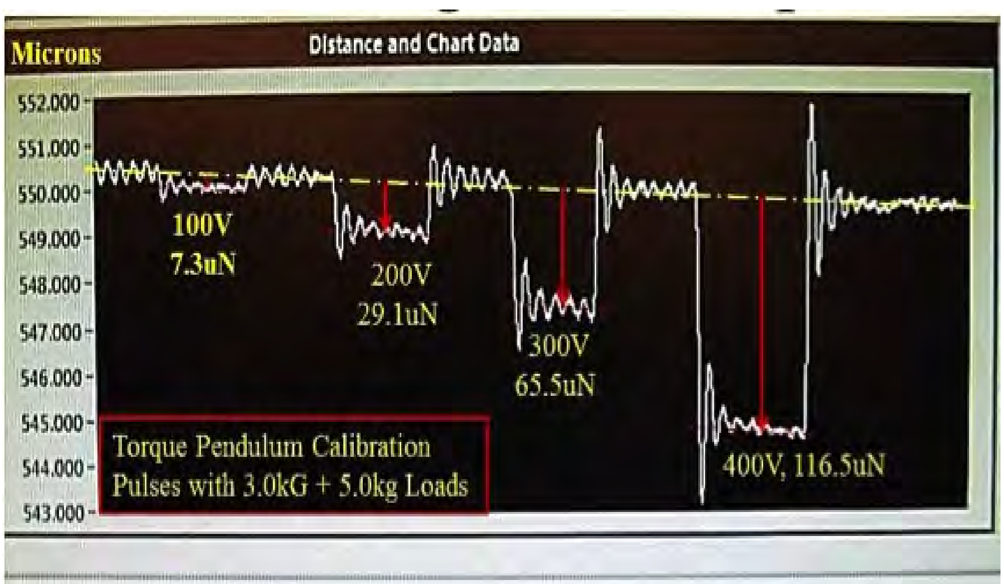

FIG. 12: Magnetic damping of the calibration pulses, showing the oscillation of the pendulum. We used 100-400V pulses to calibrate the thrust with loads of 3-5 kg.

You will be reading a great deal about electromagnetic field modes. For example transverse electric (TE) modes inside a truncated cone cavity would look something like Fig. 15. The TE boundary condition is that the electric field at each cavity wall must be perpendicular to the wall or zero there. If the electric field did have a component parallel to the wall, electrons in the conducting wall would flow inside the wall until they produced their own cancelling electric field. The magnetic field cannot have components perpendicular to the wall. The magnetic field must be zero or lie parallel to the wall. So in TE mode the electric field circulates around the z-axis (symmetry axis) of the cone, [11]. In the figures below, the z-axis is vertical, at the center of the truncated cone.

For the TM mode, the situation is reversed. The magnetic field is circulating around the symmetry axis (symmetry z-axis), and the electric field is perpendicular to the wall. See Figs. 16 and 17. The electric field is shown in red, the magnetic field is blue.

The electromagnetic mode plots were calculated by Frank Davies [12] using COMSOL [13] analysis to make

FIG. 13: The Eagleworks torsional balance [2].

FIG. 14: Calibration fins exert a known electrostatic non-contact force on the torsion balance [2].

the first map of the truncated cavities RF response from 900 MHz up to 2.5 GHz, see Fig. 18. Then we used the Eaglework Lab's Agilent FieldFox N9923A Vector Network Analyzer, to experimentally verify the COMSOL predictions using either its S11 one-port or S21 two-port analysis modes. Frank Davies conducted several finite element analyses of electromagnetically resonant cavities: Cannae's, Shawyer's, Yang's, and Eagleworks' truncated cone, including parametric analysis of different EM-drive geometries. He showed the eigenmodes, eigenfrequencies and S parameters with different graphs, including surface contour plots in 2 and 3-D, and 3-D vector field plots. Davies produced voluminous amounts of data, we don't have room to discuss them here.

[Editor: COMSOL is a commercial finite-element analysis and simulation software. It has a "multiphysics" capability to simulate different physical phenomena, including electromagnetic radiation.]

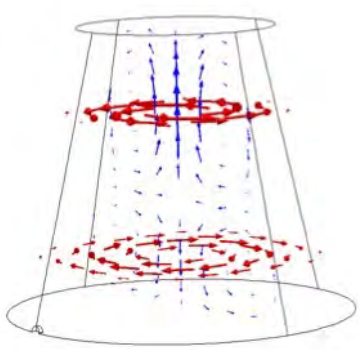

FIG. 15: The transverse electric mode, (TE012) electric field is red, magnetic field is blue. Frequency 2.1794 GHz, [12].

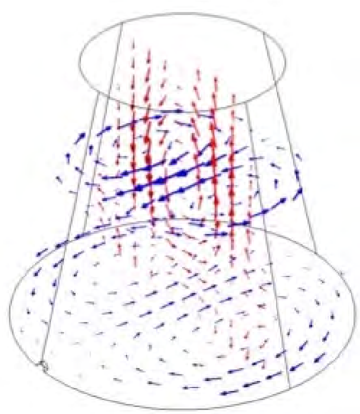

FIG. 16: Transverse magnetic mode (TM112), electric field in red, magnetic field in blue. Frequency 1.9355 GHz, [12].

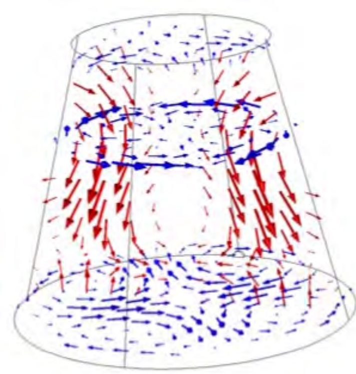

FIG. 17: Transverse magnetic mode (TM212), electric field in red, magnetic field in blue. Frequency 2.4575 GHz, [12].

Bushnell: Where are the Chinese on your list? There was one group headed by Yang Juan, Professor of Propulsion Theory and Engineering of Aeronautics and Astronautics at the Northwestern Polytechnic University in Xi'an. They published a paper in February 2016 [14] where they found their previous positive thrust results to be in error. The university is no longer conducting research into Shawyer's EM-drive. The abstract explains it briefly so I quote: *"In order to explore the thrust performance of microwave thruster,*

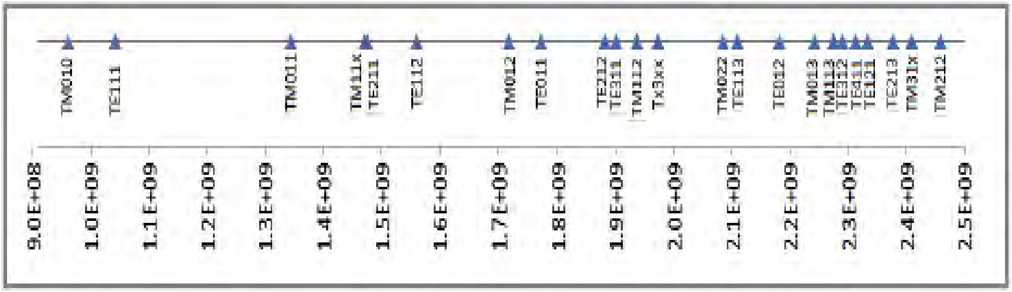

FIG. 18: Spectrum of electromagnetic field modes in the truncated cone cavity from 900 MHz to 2.5GHz, [12].

the thrust produced by microwave thruster system was measured with three-wire torsion pendulum thrust measurement system and the measurement uncertainty was also studied thereby judging the credibility of the experimental measurements. The results show that three-wire torsion pendulum thrust measurement system can measure thrust not less than 3 mN under the existing experimental conditions with the relative uncertainty of 14%. Within the measuring range of three-wire torsion pendulum thrust measurement system the independent microwave thruster propulsion device did not detect significant thrust". It appears the power leads to the cavity were heating up and thermal expansion of the leads was responsible for giving a force which was mistaken for thrust from the cavity. She had about 30 Amperes of current flowing through these power leads, which causes significant heating. Prof. Yang's stance on the EM-drive is that the thrust she published in previous papers were experimental artifacts due to the power cables. When she used a battery she measured no thrust. Her official bio-sketch at her new University no longer features her research on Shawyer's EM-drive among her "selected publications". Instead, her research is now on the conventional, classic Microwave Plasma Thruster, which uses a propellant for thrust.

Continuing now, there are a few others who have published their findings that I am aware of:

- Kurt Zeller and Brian Kraft, California Polytechnic State University, San Luis Obispo, [15]. `https://www.linkedin.com/in/kurtwadezeller`
- Iulian Berca, Romania. The first citizen scientist to report an independent test `http://www.masinaelectrica.com/emdrive-independent-test/`
- Eugene Samsonov, obtained no thrust, but the only citizen scientist to use a battery to conduct his tests, and hence his test was not subject to power cords issues, (thermal or electrical). `http://vixra.org/abs/1603.0153` & `http://vixra.org/pdf/1603.0153v1.pdf`
- Sorry if you have been missed out... there are many of you out there!

Samsonov's truncated cone had a loaded Q-factor of approximately 3100. With his TE012 resonance mode, with an input power ∼30 W, it was very unlikely he would see anything to begin with due to the thrust scaling as the electric field strength to the 3rd or 4th power. It took 30 W with a loaded Q-factor of ∼23000 in the Eagleworks' copper frustum's TE012 mode, plus the High Density PolyEthylene (HDPE) discs, to get a thrust signature of $\sim 65\ \mu N$ towards the small diameter end of the cavity.
Let's compare these two experiments. In terms of power P in watts, Samsonov had a $P \times Q$ product of $30 \times 3100 = 93000$, whereas the Eagleworks lab's TE012 experiment had a $P \times Q = 30 \times 23000 = 6.9 \times 10^5$.

So Samsonov's thrust levels should have been approximately factors of $(93/690)^3 = 2.4 \times 10^{-3}$ or $(93/690)^4 = 3.3 \times 10^{-4}$ less than the Eagleworks 65 μN TE012 test. Or, it should have been between 0.16 μN < thrust < 0.02 μN, assuming the Eagleworks' HDPE discs played no factor in the size of the thrust. (Jim's Mach-Effect conjecture would argue otherwise).

Now take into consideration that the battery powered Eagleworks Cavendish Balance free-flyer tests using the same copper frustum with HDPE discs demonstrated that the DC power source for the RF amplifier makes no difference in the thrust production in these devices. This indicates to me at least that the Samsonov test was a nice try, but it did not get the test article up into the proper $P \times Q$ power product range to see the effect using Samsonov's force detector with an as-built noise platform of 13 μN per micron of displacement while in a 1 atmosphere air environment.

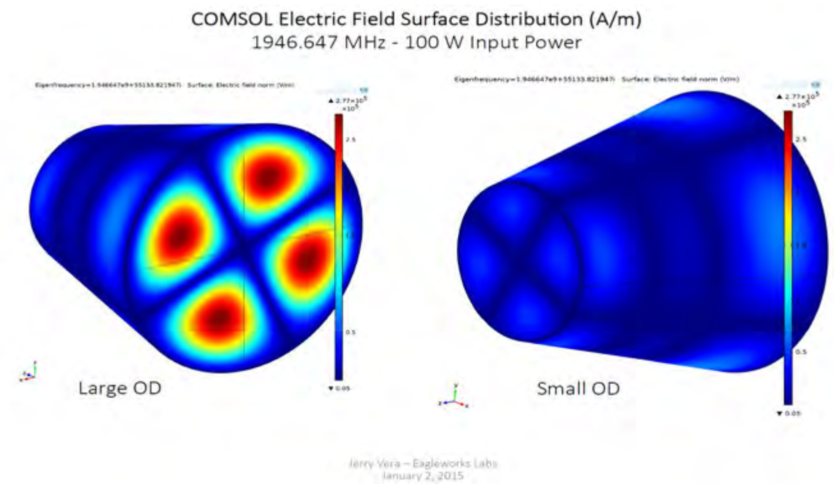

FIG. 19: COMSOL simulation of the TM212 mode, showing the electric field strength on the surface of the truncated cone cavity. Frequency 1.946 GHz, at 100 W power[12].

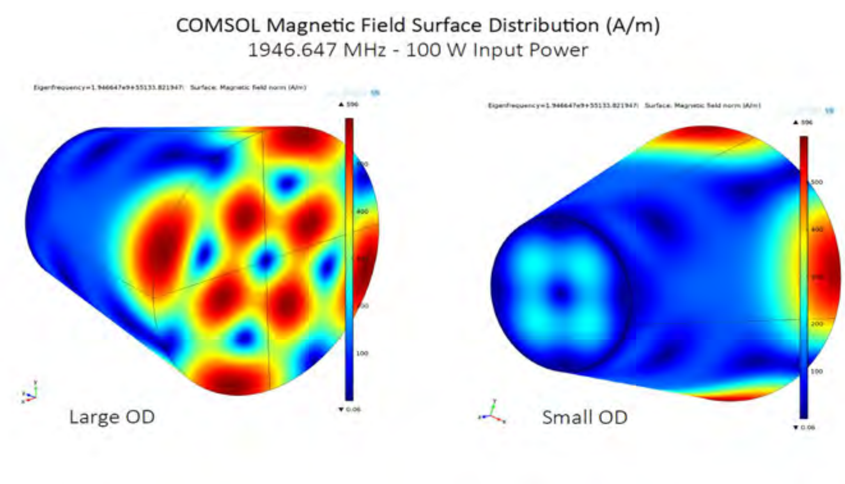

FIG. 20: COMSOL simulation of the TM212 mode, showing magnetic field strength on the surface of the truncated cone cavity. Frequency 1.946 GHz, at 100W power. Compare with the thermal image in Fig. 21.

Regarding the electromagnetic modes, Fig. 19 shows a contour plot of the electric field strength at the surface of the truncated cone for mode TM212. Fig. 20 shows a similar contour plot over the surface of the cavity but this represents the magnetic field strength. Fig. 21 shows a calculated energy-dissipation (temperature) plot, made using COMSOL. Over the large diameter end of the cavity and next to it, is an infra red camera photograph of the large diameter end of the cavity. There is a striking similarity between these two images in Fig. 21. It is important to know exactly what mode you have excited, inside the cavity, in order to predict the thrust values you can achieve. This is *the first time* an experiment using an IR camera has verified the exact mode of electromagnetic excitation within the cavity. Eagleworks was the first group to verify experimentally exactly what mode they had excited in the truncated cone.

The eigenfrequencies that were derived in the COMSOL study, by Frank Davies, were verified by the impedance resonances for the cavity detected at various frequencies (between 900 MHz and 2.6 GHz) using a Fieldfox, Vector Network Analyser. The agreement was very good between the theory and the experimental observations. The Agilent Technologies VNA model N9923A is seen in a photograph Fig. 22, the screen shows multiple impedance resonances. In Fig. 23. we show the comparison between the VNA measured spectrum and the calculated results from the COMSOL study.

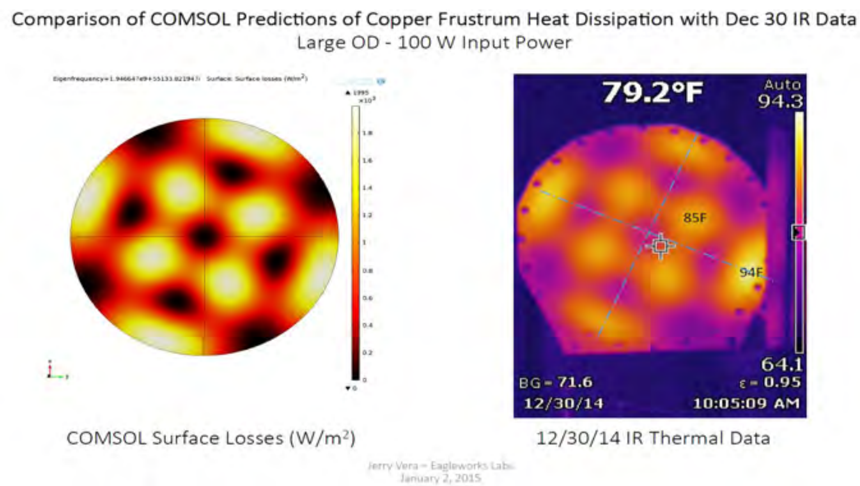

FIG. 21: The figure on the left is a COMSOL energy loss plot (heating) showing the large diameter disc of the cavity. The right figure shows an infra red image of the large diameter disc of the cavity. Note how the hot spots match the high energy loss regions in the simulated image on the left.

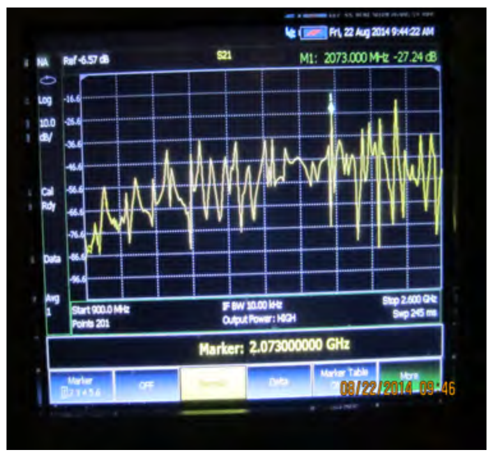

FIG. 22: Agilent Technologies Fieldfox Vector Network Analyser, model N9923A, showing impedance resonances in the truncated cone cavity at Eagleworks. Note the frequencies are between 900 MHz and 2.6 GHz, which corresponds to the frequency range studied by Frank Davies using COMSOL.

Fearn: Is the shape critical? Why don't you use something simple, like a cylinder or an ellipsoid, something you can solve for the cavity modes analytically? Why this weird, chopped-off cone shape?

March: First off, the cavity has to be an asymmetrical shape to give a force in one direction or another. A symmetric shape would not work. Otherwise you would have equal forces on the end caps and they would cancel and so no net force.

Rodal: Some of the theories have a polymer insert at one end, so if you put a HDPE disc at one end of the cylinder, that would act as the asymmetry and then the forces would not cancel, and so the cylinder should work. Other theories have a paramagnetic material at one end which acts as the asymmetry, or a different form of dielectric, all these are different forms of asymmetries.

March: Yes, when you put in an insert (polymer disc, dielectric, or paramagnetic material) that would cause an asymmetry and that may well open up the use of cylinders and ellipsoids and other shapes. I personally have not done any experiments using a cylinder with dielectric disc at the end, so I have no direct experience with it.

Broyles: There was a group of college students in California [15], who tried to use a cylinder with a

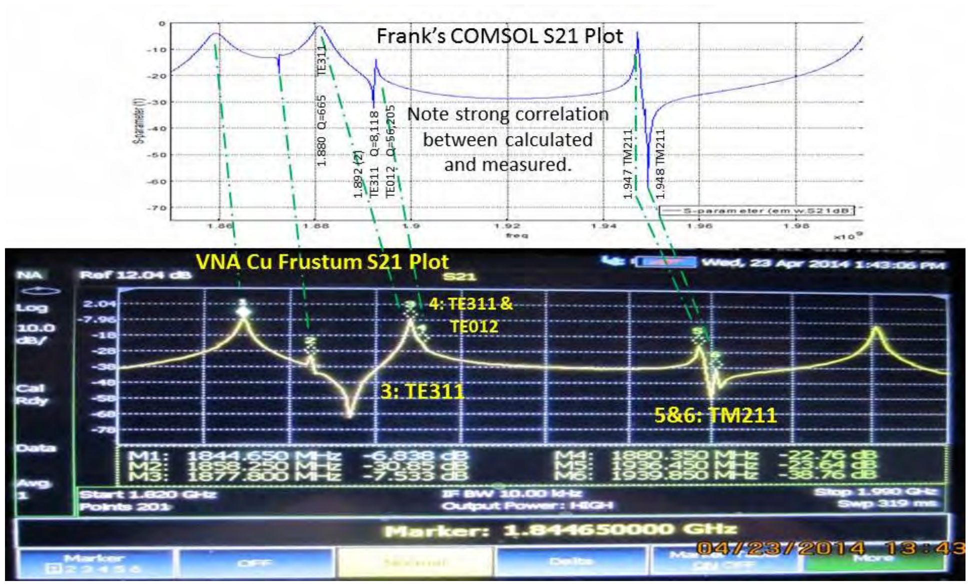

FIG. 23: This is a comparison between the eigenfrequencies calculated by Frank Davies using the COMSOL simulation software and the measured response of the truncated cavity using the Fieldfox VNA.

dielectric insert, but they were having some problems with their test setup so, at the moment, their results are inconclusive. What we are doing now is going with a slightly different cylindrical shape and repeating the experiment and trying variations of the truncated cone shape, with a polymer disc insert towards the smaller end.

Cole: Is the acceleration always toward the small end of the truncated cone?

March: It can be in either direction depending on the mode that is excited within the cavity.

Christie: Is the length of the cavity half the wavelength of the resonance frequency?

March: The length of the cavity is either half the resonant wavelength or a quarter wavelength, depending on how you set it up.

Christie: So if you are heating the side walls, they are not exactly at 1/2 or 1/4 wavelength spacing, is that going to effect the Q or the dissipation?

March: Yes the wall angle is part of the optimization process. I would like to have made a whole family of cones with different angles and done a systematic test of all of them to see which gave the most thrust, but we never had the time or rather budget for that.

Meholic: Did Shawyer ever give any indication that he did any of those types of studies?

Rodal: Shawyer had a patent from 1988 for a cylindrical cavity with a dielectric cone inside. He went from that to a truncated cone cavity with and without a polymer disc at the small end. There is no patent for a cylindrical cavity with asymmetric ends. Shawyers explanation for the acceleration makes no sense. He is only using Maxwell's equations and special relativity, we know from conservation of momentum, in that case, that there should be no thrust. Shawyer claims that there is no pressure on the side walls, he claims that the only pressure is on the flat end plates, which is not physically possible.

Meholic: He gives no proof, just states there is no pressure on the side walls?

March: Yes. I think we all agree that Shawyer's theory makes no sense, but we also agree there is an acceleration, so we need to find a better theory.

3. PROPELLANT-LESS PROPULSION TESTING, BEFORE AND AT EAGLEWORKS

I got into this business because of Dr. Woodward. I ran across a paper of his back in 1988 and started pursuing propellant-less propulsion from that point. My first build was in 2004, it was a Mach Lorentz thruster. (See Fig 24 & 25). The thruster consisted of a small ring of capacitors that had a toroidal magnetic winding around it. It was driven with an open wire transmission line system that drove something like 800 V peak across the capacitor ring and across the inductor (they were wired in series). There was a $\lambda/4$ phase shift between the capacitors and the inductor. With a 2 MHz frequency voltage, I saw some interesting results. I measured about 2 to 4 mN of force generated. This result was reported at "The Space Technology & Applications International Forum" (STAIF) in 2006. I never could replicate that, when I went to a co-axial version of it, but I never got to the same peak voltages either. When I went to a totally enclosed system with Faraday shields and all the rest, I could only drive up to, with the same RF frequency, about 160 Volts, and I didn't seen any significant force at those voltage levels.

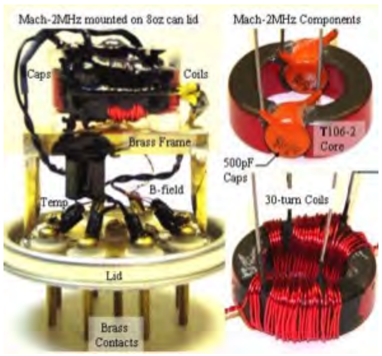

FIG. 24: Shown is the 2004 test Mach Lorentz Thruster (MLT). It consists of a small ring of capacitors with a toroidal magnetic winding.

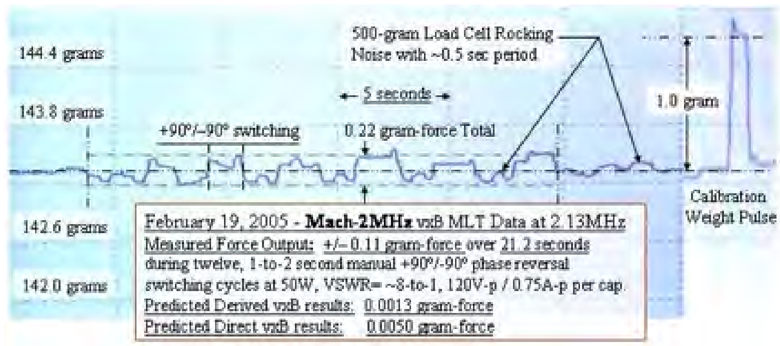

FIG. 25: The 2004 test results for the MLT, using 2 MHz frequency and 800 volts. The force was about 2160 μN.

The second test article was actually Jim's device, that he asked me to test for him. It was ∼1 mN at most. This is also reported in the STAIF 2006 report.

I had been laid off from the Orion program at JSC and Sonny White brought me out of premature retirement to help develop his new EagleWorks lab. This was back in May 2011. The objective was to test primarily EM-drives. So we got the vacuum chamber sitting on a floating optical isolation table to minimize vibration. We got the vacuum pumps and the usual lab equipment which took about 18 months total. Our torsion pendulum uses two flexural bearing blocks, which can support up to 100 pounds [16]. This is the same bearing as used by Nembo and Martin Tajmar.

Sonny White tested his resonant cavity on November 20 2012. (See Fig 26 & 27.) At a resonant frequency of 4.14 MHz , we applied a power of 150 W of radio-frequency The straight thrust prediction, for this applied capacitor-ring voltage level, was about 1.5 μN. We observed a force of 2.6 μN. I'm fairly sure I messed that up.

FIG. 26: Sonny White's resonant cavity "Q-thruster"

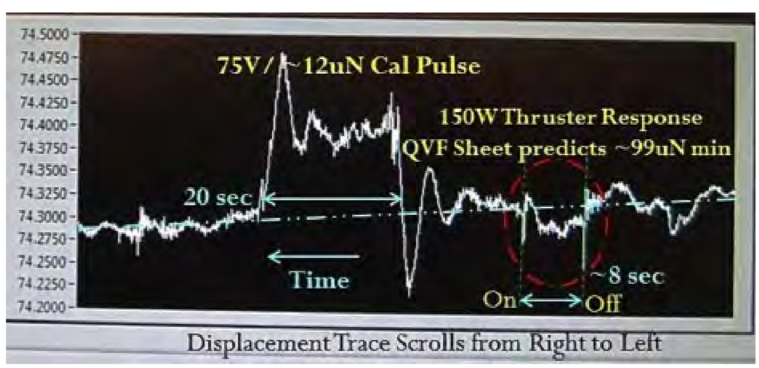

FIG. 27: The Q-thruster at frequency 4.14 MHz and power input 150 W. Driving at 22.9 volts per capacitor gives a force of 2.6 μN.

Eaglework's first outside test was for a DARPA customer, during the January 2013 to June 2013 time period, testing an electrostatic device (Scorpion Thruster) from Gravitec (founded by Hector Serrano). See

FIG. 28: DARPA test article 2013. From Gravitec, work of Hector Serrano.

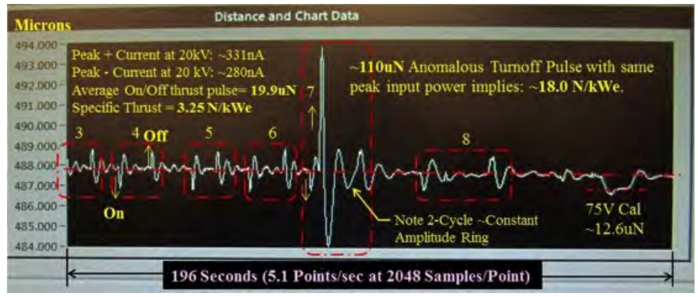

FIG. 29: Test results for the DARPA article, showing an anomalous transient thrust pulse with high voltage power switching.

Fig 28 & 29. We primarily observed electrostatic interactions with the vacuum chamber, but did find transient thrust pulses ~ 110 μN with a switching, high voltage power supply (30 kV). This was after an extensive shielding campaign was accomplished.

Eagleworks second customer test series was for Cannae LLC (Guido Fetta) and his 937 MHz, TM010 pillbox resonant cavity thruster in August 2013 and January 2014.

Mr. Fetta brought two kinds of pillbox, or "pancake", test articles, one with machined radial slots on the interior of one wall in the cavity, and a "null" test article that had no machined slots. However both test articles used a 1.0 inch outer diameter by 1.63 inch long Teflon (PTFE) cylinder in their RF power input section. The input RF power section was just over 5 inches long. There was a 0.115 semi-rigid coaxial cable with SMA attachment used for the input power. The main cavity was just less than 11 inches in diameter and about 1.5 inches wide. The RF signal stub antenna was in the opposite pipe from the input RF (about 3 inches long) and that section was used as the output to the spectrum analyzer.

A reversible thrust signature in the 35-to-65 μN range was observed during the August 2013, ten day test period when its Z-matching Teflon cylinder was mounted in the throat of the pillbox cavity's RF feed line. The loaded Q factor for the slotted cavity was 8500, the cavity without the slots had a loaded Q of 9500, which makes sense because the slots just give more surface area for i^2R losses.

During the Cannae test setup, it was determined that the Eagleworks' liquid metal contact array used for passing RF or DC power, control, and signal lines from the test article to the outside world severely attenuated RF signals above ~ 4 MHz, which made them unusable for passing UHF and above RF power signals through them. Above 50 MHz we couldn't get anything more than a couple of watts through the liquid metal contacts, so for UHF the Galinstan contacts were only used for DC voltage.

The solution to this problem was to mount Fetta's 937 MHz, 30W RF amplifier in the vacuum chamber and use it, and its heatsink, as a counter mass for the torque pendulum's test article. The Eagleworks lab then used this approach for all future testing. Later, we built an integrated copper frustum test article that we had to marry to its RF amplifier, needed to get a symmetrical forward and reverse thrust response from the torque pendulum. The amplifier had electrolytic capacitors inside it that were not vacuum rated, so we could not run this device in a vacuum. (You need ceramic capacitors for a vacuum so we ran those tests later with a different amplifier).

Tajmar: What happened to your liquid metal contacts as you went to UHF ?

March: The liquid metal heated up a little with DC, we measured it with an IR sensor. For RF they got warm. There was too much cross talk between all 10 liquid metal contacts, I should have had a co-axial arrangement of contacts, there was no coaxial shielding.... lessons learned. That's why we ended up making them all DC.

We can measure what the electric field strengths are inside the cavity using a small ring antenna probe. Thus we can confirm the fundamental transverse magnetic mode, TM010 mode structure. The magnetic field circulates around the perimeter of the saucer shape whereas the electric field is axial. The RF is injected in from the right side beam pipe and is taken out to the spectrum analyzer from the left side pipe, see Fig. 8.

Mr. Fetta brought two more TM010 test articles to the Eagleworks lab for testing in January 2014. One of these "pancake" test articles had internal radial slots and the other one did not, however unlike the previous two "pancake" resonant cavities, neither of these two new test articles had Teflon cylinders in their RF input impedance matching section. No detectable thrust signatures were observed with these two new pancake test articles without the PolyTetraFluoroEthylene (PTFE or "Telflon") inserts for "impedance matching".

The third Eagleworks customer test series was for Roger Shawyer's EM-drive. Shawyer likes to use the TE modes. This replication effort used a truncated copper cone, fabricated in-house, loosely based on Shawyer's 2nd generation dynamic thruster design. Sample data is shown below in Fig. 30.

During this time period, approximately a six month long program of COMSOL simulations, examined this frustum's various resonant modes. This work was done by the Eagleworks COMSOL analysts, Frank Davies and Jerry Vera. See the detailed plot of the resonant frequencies and the electromagnetic modes that can be excited at those frequencies in Fig. 31.

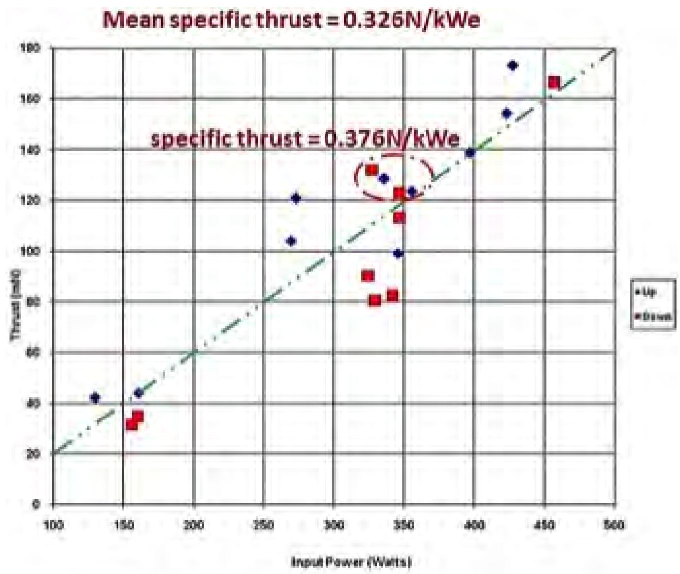

FIG. 30: The data for Shawyer's 2nd generation device. The triangles are for upward motion, the squares are for downward motion. The vertical axis is thrust in mN, the horizontal axis is input power in watts.

Magnetrons are notoriously wide bandwidth, about 3 MHz or so. Shawyer went from wide bandwidth to narrow using a travelling wave tube, which has a bandwidth of 10 kHz or so. Shawyer built three types of test article (see Fig. 7). The first cavity had flat end caps and produced about 16 mN of thrust. The 2nd generation and everything after used spherical end caps, like mirrors in reflecting telescope, Fig. 32. When you use the spherical end caps the electric fields increased by a factor of 5-10. If the thrust goes like the electric field cubed, that is a huge improvement. We are seeing microNewtons and he is getting milliNewtons. We should point out that Shawyer has never reported in-vacuum testing, all his tests are in air so there is a thermal component to it. Shawyer knows about buoyancy and has corrected for it. You can rotate your cavity 180 degrees and subtract one thrust from the other, since the buoyancy will remain the same, it subtracts out. Also the buoyancy effect is small, $\sim$3 mN with respect to the expected thrust signature $\sim$20mN.

Fearn: This may be a dumb question but does it make any difference where the RF input feed is, in the middle of the cavity or at the end?

March: Oh yes, it makes a difference. The optimum place to put the feed is in the middle. So it echoes. You want equal distance from the antenna to the end plates, otherwise there can be destructive interference between the wavefronts.

The third generation device was paid for by Boeing. It weighed 2.92 kg, was 265 mm diameter at the base plate and a height of 164 mm. This also had spherical end caps. The mean specific trust claimed by Shawyer was 0.326 N/kW. He used a 1/2 loop antenna tuner in this 3.85 GHz room temperature EM-drive. Further details can be found here `http://emdrive.com/flightprogramme.html`. The Boeing guys said they got nothing, they could not get the cavity to resonate.

The Eagleworks copper truncated cone (frustrum) build-up project was started in the October 2013 time frame, with the fabrication of our current copper frustum that was loosely based on Shawyer's 2nd generation

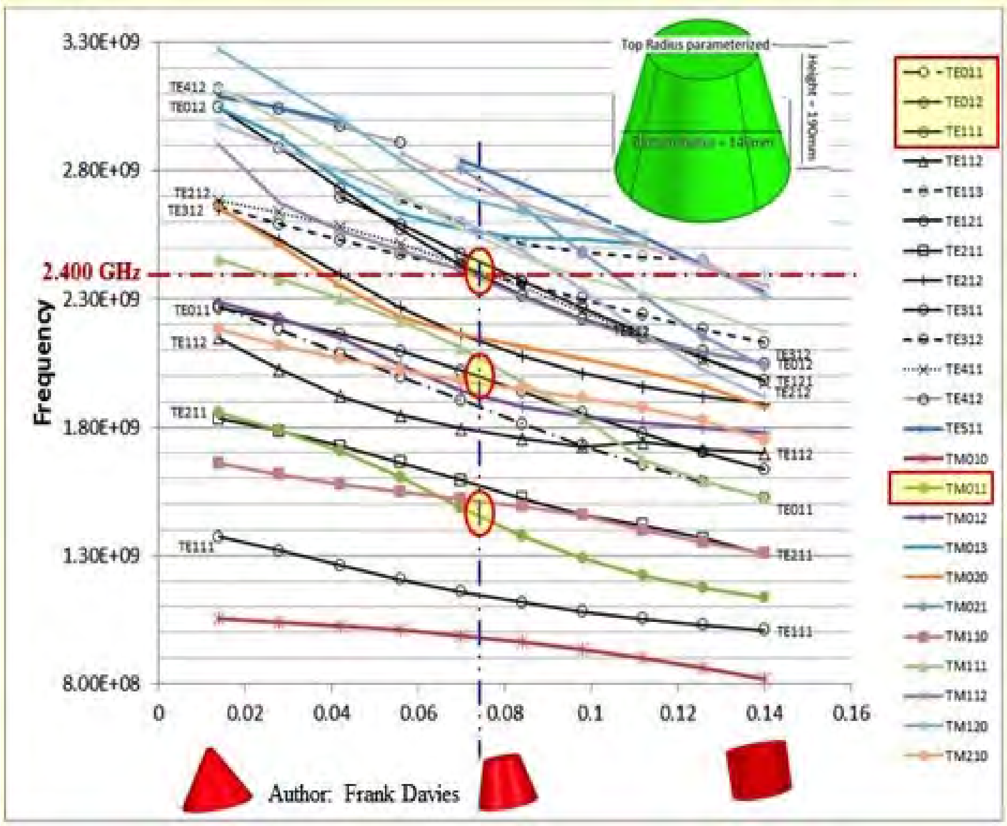

FIG. 31: COMSOL data provided by Frank Davies. Modes for a given frequency are plotted. Using an empty cavity, the geometry was changed from a cone on the left to a cylinder on the right. All the modes were noted on the right side. Eagleworks decided to test a geometry in the middle. The effect of the HDPE disc was to downshift the resonant frequency of the cavity by a certain percentage.

dynamic test copper cavity. (Eagleworks prefers to use the TM modes). The COMSOL code was used (summer 2013) to verify that according to Maxwell's equations alone there is no thrust on the cavity due to internal radiation pressure, as expected. So in order to account for the force on the cavity, new physics would need to be applied, not just Maxwell's equations.

It was decided to build a fixed-geometry frustum configuration and then electronically tune the solid state, narrow band RF signal frequency source to the *now* resonant frequency in question using a hand tuned and then a phase locked loop frequency tracking method. Construction was completed in December 2013.

During the spring and summer of 2014 we explored a number of this copper frustum's RF resonant modes from its fundamental TM010 mode through its other TE and TM modes up to 2.50 GHz. The affect of the HDPE discs was that the Q went down from 40,000 with no dielectric disc to 25,000 with the disc present. Also, the resonance frequency of the cavity would decrease by a certain percentage with the HDPE disc present; in the case of one cavity we built, from 2167 MHz down to 1880 MHz.

During the spring and summer of 2014, March explored a number of this copper frustum's RF resonant modes with and without dielectric disks from its fundamental TM010 mode at 957 MHz up through its other TE and TM modes up to 2.5 GHz.

In this frequency range we found that the TE012 mode at 2167.14 MHz had the narrowest -3dB bandwidth and thus became our first resonant mode to be used for thrust production. See Figs. 33 & 34. During our initial test at 2167.14 MHz, we found that with $\sim$ 20 W of RF input power, the average thrust signature was -77.0 μN after correcting for the actual calibration magnitude and the 28V dc offset bias of 34.8 μN. Thus the TE012 thrust efficiency = -3.85 μN/W. The TE012 copper frustum test without dielectric yielded an average - 77 μN negative going signal with $\sim$ 20 W of RF (- 3.85μN/W), in the direction of the large end of the Frustum.

Williams: I thought you had said in your 2014 paper, that when you had no HDPE discs present there

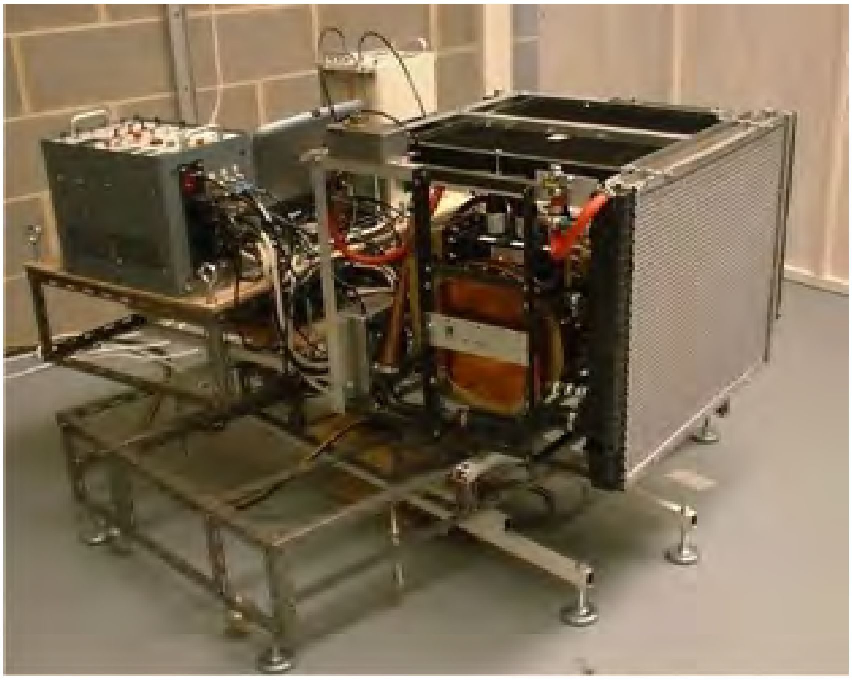

FIG. 32: Shawyer's 2nd generation device on a rotating test bed. This cavity used spherical end caps. For the Dynamic test, a thrust of 96 mN was recorded for an RF input power of 334 W or 0.287 N/kW.

FIG. 33: First run of the Eagleworks EM-drive, based on Shawyer's 2nd generation model. No disc present. Thrust to the right as shown by the red arrow.

FIG. 34: First data plot for our EM-drive. Note the rather large test pulse of 500 V. The loaded Q was 40900.

was no thrust?

March: Yes, I had misinterpreted the size of a calibration pulse, I thought it was 29 μN and it was actually 187 μN. That changed my analysis of the data and the value of the recorded thrust. So yes we did see a -77μN thrust with no discs present.

Rodal: I thought that Shawyer had claimed that the thrust he saw, with the same configuration (no HDPE discs), was in the direction of the small diameter end?

March: Yes he did claim that, and I cannot reconcile that discrepancy.

Thinking of Dr. Woodward's Mach-Effect electrostrictive work, I also tried the same copper frustum cavity with two, 6.13 inch by 1.06 inch thick polyethylene (HDPE) disks mounted at the small end of the frustum. I noted that its TE012 resonant frequency was now down at 1880.62 MHz with a loaded -3dB Q-factor of about 25000 and -3dB bandwidth of 88.0 kHz, which made for easier manual tuning. See Figs. 35 & 36.

Measured thrust level at this new TE012 resonant frequency with the same 18.7 W of RF was now a positive going 37.3 μN, or a thruster efficiency of 2 μ N/W.

FIG. 35: Eagleworks EM-drive, using 2 HDPE discs at the narrow end. Thrust to the left as shown by the red arrow.

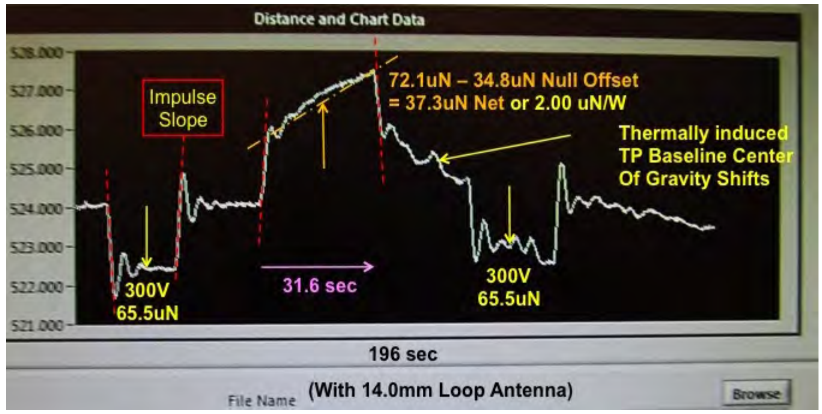

FIG. 36: Plot for our EM-drive using 2 HDPE discs at the narrow end.

Copper oxidizes in air, especially in Houston with all the humidity, so after the copper is rolled out we polished it. Here are the details: The process for finishing the interior of the copper frustum was that David Fletcher polished the interior surfaces of the copper cone and 1.0 oz copper (∼35 micron thick), single layer PCB end-plates with buffing compound with a power drill buffing wheel, then a warm soapy water wash, followed by distilled water rinse and dry cycle. He did not indicate to me that he used any finishing polish afterward. I then spray coated all the copper frustum's polished surfaces with one coat of MG-422B silicone conformal coating [17]. This silicone conformal layer was probably around 1.0 mil (0.0254mm or 25.4 microns) thick that was then cured in an oven set at 150 Fahrenheit for 90 minutes. That works very well to prevent oxidation.

I used PC boards for the end plates of the cavity, these had 1 ounce of copper on the board. This allowed me to use thermal imaging at the ends and verify the electromagnetic mode structure inside the cavity, which would show up as heat. The cavity had a 14.8 degree cone slope. The total weight of the cavity without the HDPE discs was 1.6 kg, and with the 2 discs was 2.57 kg. I had 6.125 inch diameter by 1.0626 inch thick discs of HDPE. I tried 1, 2, and 3 discs, in the cavity. The optimum seemed to be 2 discs for thrust production. The discs were held in place by teflon or polypropylene bolts. Nylon bolts tend to melt in RF fields. We did try Teflon tape around the nylon screws, it didn't work so well. I drilled and tapped the discs and used cap screws.

Our 2014 and early 2015 work was all in air, since we did not have an amplifier that could go inside the vacuum chamber. We got a vacuum ready amplifier in the summer of 2015.

We used magnetic loop antennas to excite the modes in the cavity. One half a millimeter made all the difference with these loops. See Fig. 37. I have not yet tried a loop at the dead center of the cavity. Ours was mounted about 15% up from the bottom. This small loop would not have been deep enough into the cavity to be along the symmetry axis. Deciding on where is the best placement of the antenna, depends on what mode you are trying to excite. Having a loop antenna horizontal in the center of the cavity would work for the TE01X modes, that have E-field donuts wrapped around with magnetic toroids. Then you would raise and lower the loop for impedance matching.

I was manually tuning the system throughout most of this work. At the TE012 mode, the loaded Q-factor was approximately 25000. The bandwidth was less than 100KHz. I was trying to hand tune the resonant frequency 1.88 GHz with a low 100KHz bandwidth and I just couldn't dial it in and track it. As the cavity heated up and expanded I couldn't keep the cavity in tune. The TE012, TE013 modes that Shawyer used have a higher Q but that also means that they have a narrow bandwidth and they are hard to excite initially, and harder to maintain as the cavity heats up, especially if you are manually tuning the cavity.

The TM212, at 1937.6 MHz, was easier for me to dial in by hand. It also seemed to produce a little more thrust with the HDPE discs in there. The quality factor went from 25000 to a -3dB loaded Q-factor of around 7000 and that means the bandwidth opened up to about 314 KHz. It was much easier for me to keep track of the resonant frequency and keep the cavity in tune with the RF input. We tried a phase locked loop for the frequency stabilization, designed by the NASA/JSC/EV electronics group on a volunteer basis, but that was not optimum since the mode structure could change. Typical thruster output was 90.4 μN with an thruster efficiency of 4.54 μ N/W, utilizing the Class-A, ZHL-32W-252 Mini-Circuit RF amplifier.

FIG. 37: Magnetic loop antenna, the difference of 1/2 mm made all the difference.

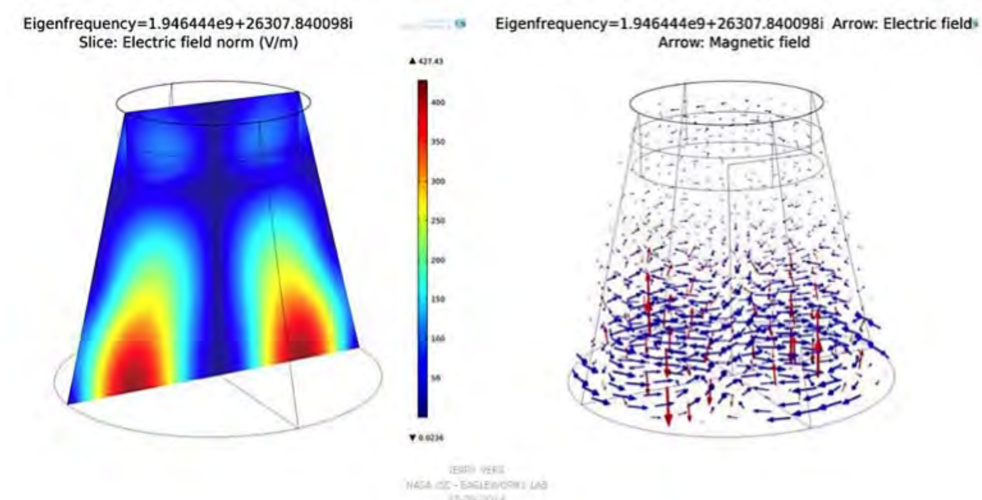

FIG. 38: Eagleworks copper cavity, TM212 mode E&M field distribution and strength. On the left you see a contour plot X-section of electric field strength in the center of the cavity. On the right is a vector field distribution, electric field is in red arrows, magnetic field is in blue. *By Jerry Vera, 28th Oct. 2014.*

The best way to go, by far, with automatic tuning is with a VSWR minimum tracker, which tracks how much power is reflected back from the cavity at the input. You want the power reflected back to be a minimum always.

Williams: What do these mode numbers stand for?

Rodal: There is no convention for mode shape numbering for a truncated cone cavity. The numbers are based on a cylindrical cavity. The TE and TM refer to transverse electric and transverse magnetic modes, which we have explained earlier. The first number has to do with the azimuthal direction, the second number represents a radial direction (normally perpendicular to the surface of the cylinder), and the last number is along the z-axis of symmetry, along the center of the cylinder.

Tuning the cavity is a multi-staged affair. The following descriptions are somewhat verbose, but I hope you find them useful:

- At the EW-Lab we had Frank Davies or Jerry Vera run a eigen value COMSOL analysis of the frustum

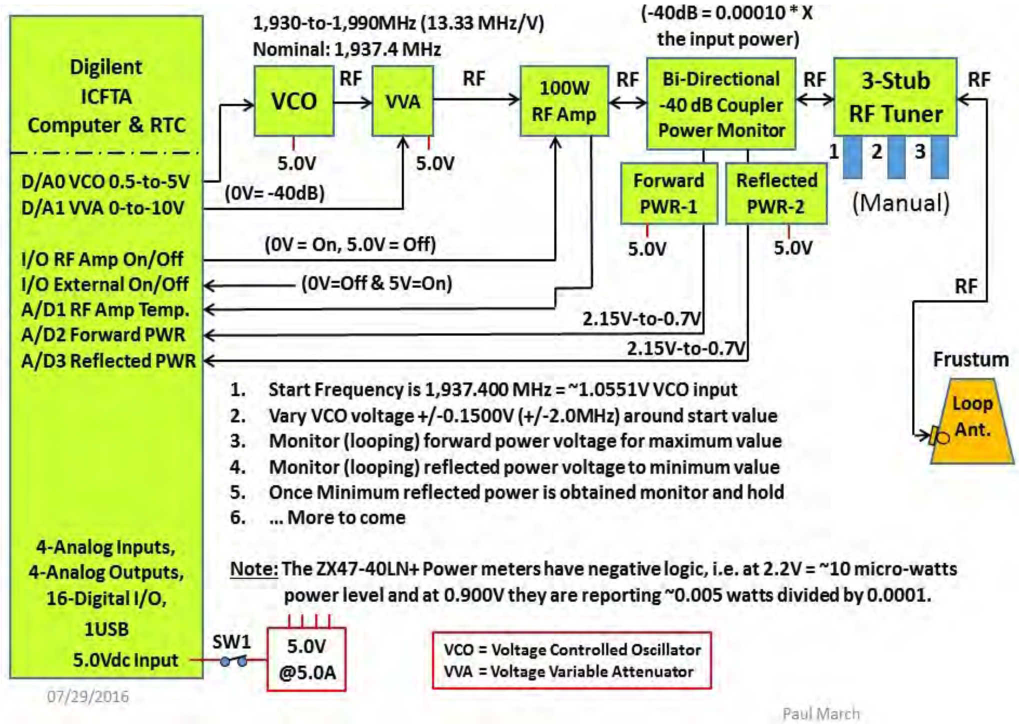

FIG. 39: ICFTA tuning subsystem block diagram.

in question that provided the frequencies for the resonant modes over the selected frequency range from the cavity's fundamental or lowest frequency TM010 resonant frequency. See the attached plot.

- After picking the resonance mode we want to excite, say the TE012 mode, I would then use the lab's Agilent FieldFox Vector Network analyzer in its S21 two-port configuration using the frustum's main RF input port antenna. I use its field sense port antenna to acquire the actual resonant frequencies for the modes of interest. I would then compare the VNA plot over the specified frequency range to the COMSOL analysis and validate what the actual resonant frequency is per the VNA S21 plot.

- Next I would insert the FieldFox VNA at the output of the RF amplifier going to the frustum to tune the RF amplifier's 50 Ω impedance matching network utilizing the narrowest frequency sweep bandwidth for the resonance in question. The 50 Ω impedance matching network consisted of the copper frustum's main RF input rotatable loop antenna, the transmission line 3-stub tuner and all the coaxial cable and connectors in between the frustum and the RF amplifier. That would entail recording the VNA S11 response plot, Smith Chart, and phase responses by first using the rotation of the frustum loop antenna. I would then repeat this process utilizing the 3-Stub tuner and then iterate between the loop antenna and 3-Stub tuner until I obtained the lowest overall S11 minima for the frustum resonance of interest. See attached two summary VNA slides with the frustum loop antenna and RF amp's 3-Stub tuning solutions for the TM212 mode.

- Lastly I would then vary the Phase Locked Loop Voltage Controlled Oscillator input control voltage to vary the RF amp's frequency, (control pot on the Frustum control panel), to first match the previously recorded VNA resonant frequency. I would then monitor the forward and reflected RF power meters attached to the RF amp's 50 Ω -30 or -40 dB dual directional coupler's forward and reflected output ports via our LabView control panel, to continuously minimize the reflected RF power coming back from the frustum, which at the same time maximizes the forward RF power.

- In our latest version of this tuning business, needed for the Cavendish Balance test, my semi-continuous tuning inputs were replaced with a micro-controller programmed by Sonny, that would automatically keep the RF reflected power at a minimum value by dithering the VCO output frequency around the frustum resonant frequency.

- The next step in automating this Frustum tuning procedure is to add a rotary actuator to the frustum loop antenna and three linear actuators to the 3-stub tuner, so all these tuning steps can be controlled by the micro-controller while is strives to maximize the forward RF power while minimizing the RF reflected power. However, we have noticed that due to the resonant phase shift requirements of the Mach-Effect wave equation, we will have to provide a frequency offset to the above max/min RF power solution that will maximize the thrust production utilizing an onboard the frustum or MEGA drive accelerometer signal as this algorithm's main input.

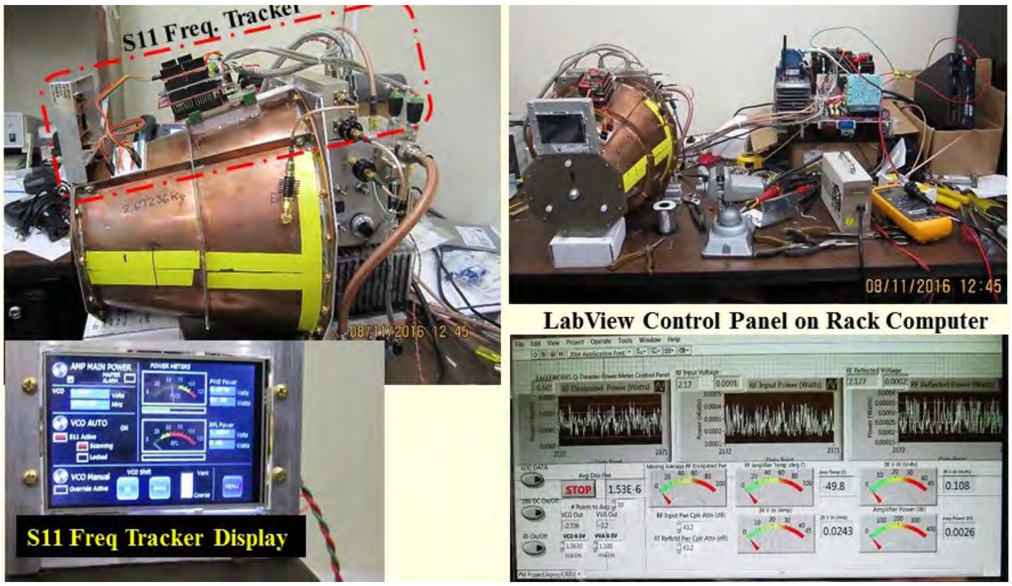

FIG. 40: Eagleworks Lab. ICFTA with S11 frequency tracker photo.

The first outside Eagleworks Lab Report paper was published and presented at the the 50^{th} AIAA Joint Propulsion Conference (JPC) in late July 2014 [2]. In July 2014, NASA called a Blue-Ribbon panel of eight PhDs that were asked to evaluate Dr. White's Quantum Vacuum Conjecture (QVC) and its associated experimental test program. Their conclusions were that they thought that the QVC was either "profound" or just a "mathematical coincidence". They were less critical of our experimental program. In August of 2014 DARPA had the JASON Group interview Dr. White in CA on his QVC conjecture. They did not like it. The first group *Dynamics of the Vacuum* theory paper was published in November of 2014, demonstrating that the QVC was NOT a mathematical coincidence, with a follow-on *Characteristics of the Vacuum* paper in 2015 by Dr. White [3]. Whether the QVC is "profound" or not, is yet to be determined.

During the winter and spring of 2014-2015, Eagleworks lab performed a set of in-vacuum test runs, with a split copper frustum, with PE disks and RF amplifier system that generated very clean thrust pulses in one direction, but almost non-existence thrust pulses in the other direction when the copper frustum was physically reversed in its torque pendulum mount. The problem appeared to be centered on having to change the system's physical mass configuration when doing so. Solution was to integrate the copper frustum with its RF amp and RF plumbing into one package, so RF cabling would not change when the test article was reversed. See Fig. 41.

The drawback to this integrated test article approach was that it doubled the sprung mass "flying" on the torque pendulum because in the original split configuration, the RF amplifier was being used as the counterbalance mass for the frustum test article. The results of doubling the sprung mass was a major increase in the torque pendulum's force resolution noise platform and a slowing of its dynamic response. However during the fall of 2015 Eagleworks performed an integrated copper frustum test article (ICFTA) in-vacuum ($\sim 8 \times 10^{-6}$ torr) test series in the forward, reverse, and null thrust test orientations. See Fig. 42. Thrust levels in the 40-to-120 μN levels with up to 80 W of RF input were observed, but the thrust traces were contaminated with thermally-induced center-of-gravity shift artifacts in the torque pendulum [18].

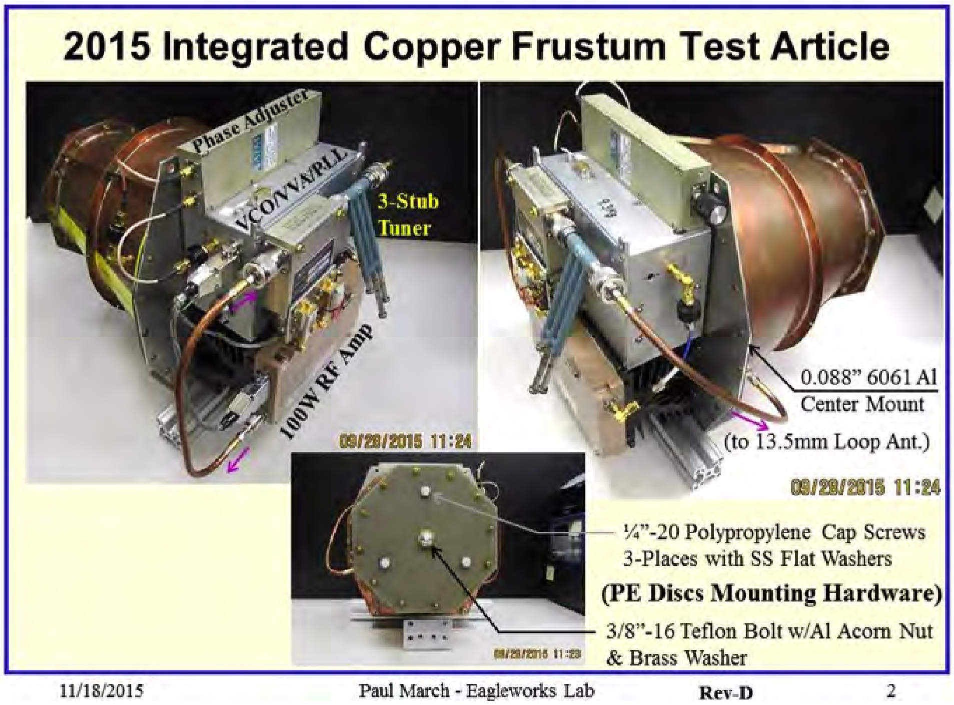

FIG. 41: Eagleworks copper cavity, with the power system onboard.

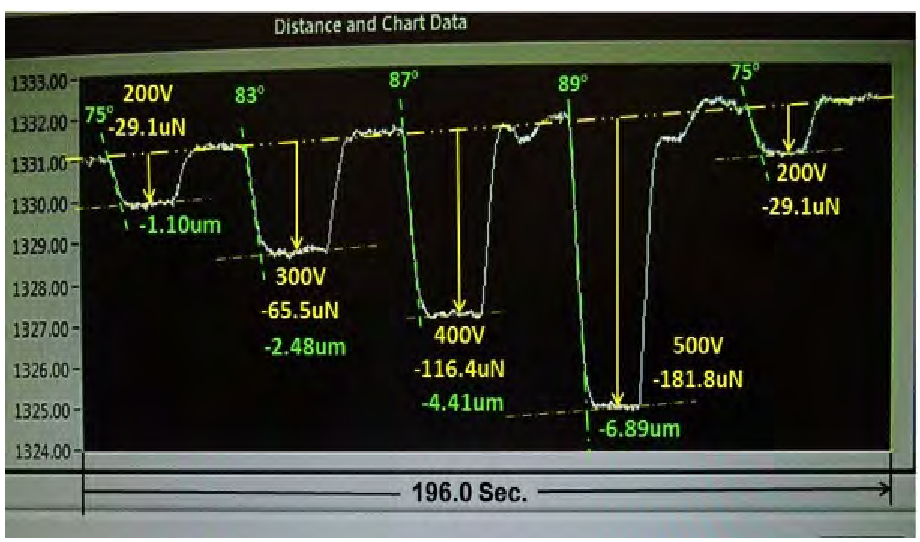

FIG. 42: Integrated copper "Frustrum" (9.3 kg) Force calibration pulses. (The uN stands for μN.)

Tajmar: Can you elaborate a little on the Lorentz force you get from the wires going to the test article?

March: Yes Martin. We've got a twisted pair wire coming from the liquid metal contacts going over to the RF amplifier. For this amplifier it was about 5.5 Amps and 28 Volts DC. If you had a single wire, going through ground return you would have a huge area in the loop which could interact with the Earth's magnetic field and give a Lorentz force. All the wires I have on the cavity are either twisted pair or twisted with shielding. So most of that area was reduced to a very small value, but I still ended up having RF ground loops going through the structure to ground. The only way I could really account for that was to do a dummy test, for a given power and DC current and evaluate the offset.

Williams: When the cavity heats up, how much can the cavity change in length?

March: The cavity can change by as much as 10-20 μm, both in length and diameter, which is enough to change the resonant frequency by 1-2 MHz. This is significant when the loaded Q-factor gives a bandwidth of 300 kHz.

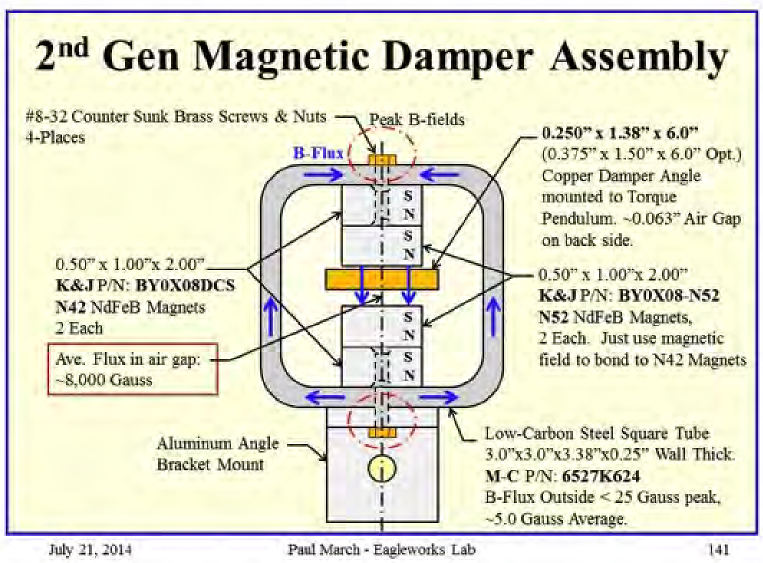

FIG. 43: The 2nd generation magnetic damper schematic drawing.

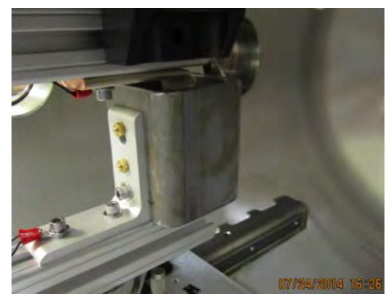

FIG. 44: The 2nd generation magnetic damper encased in a 1/4 inch thick iron tube, for shielding.

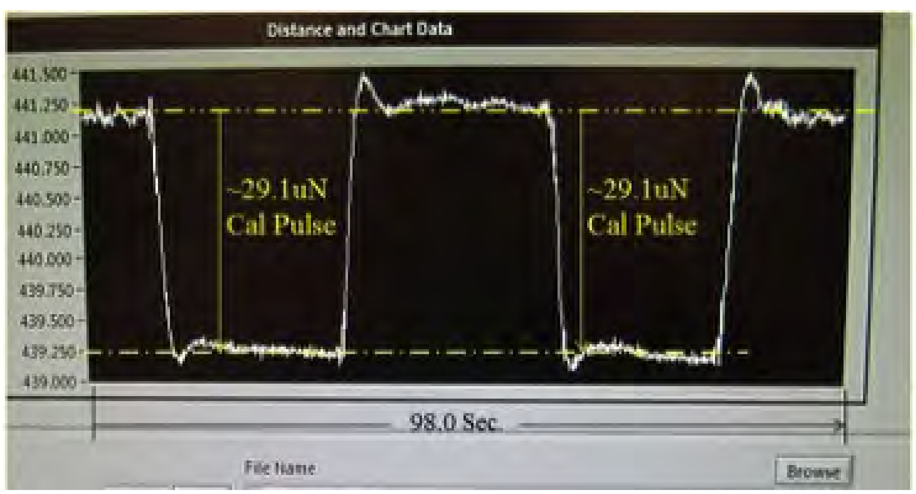

FIG. 45: The 2nd generation magnetic damper wth 1.38 x 0.25 inch copper blade, using a 200 V calibration pulses. (The uN stands for μN.)

I was never happy with the calibration of baseline noise of the vibration environment. I changed the magnetic damper design by enclosing the magnetic damper in a 1/4 inch thick iron tube, to shield any nearby wires from its magnetic field. See Fig. 43 & 44. I added one more neodymium magnet and substituted a copper metal plate for the aluminum plate used previously. That greatly enhanced the damping so that I almost got rid of the baseline noise. See Fig 45. (For comparison see Figs. 11 & 12 for the first generation damper.)

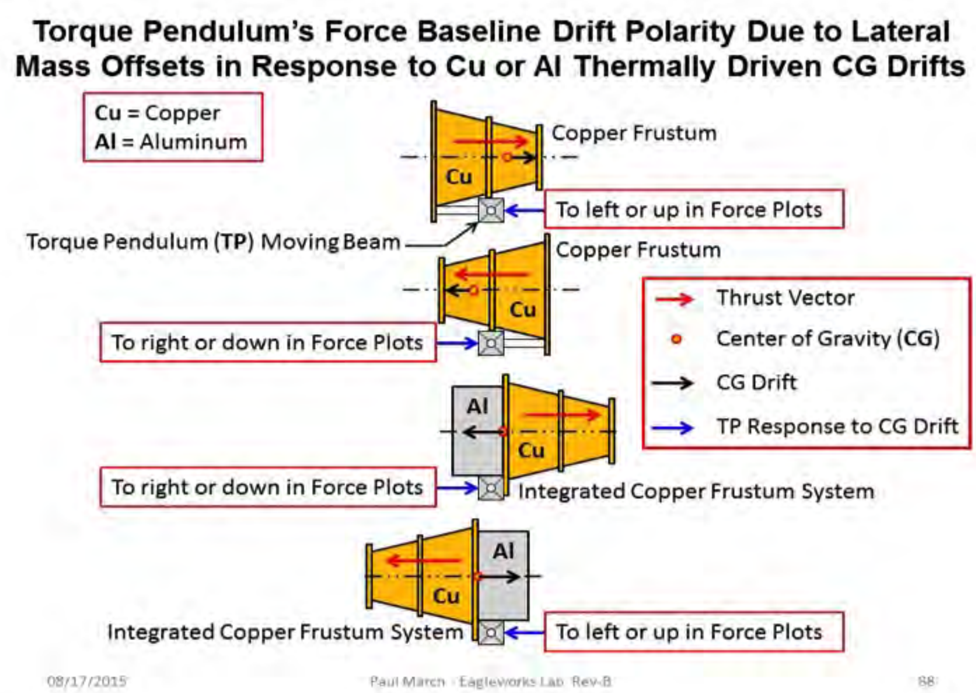

FIG. 46: Torque pendulum's Force Baseline Drift due to lateral mass offset. Thermally driven center of gravity drifts.

Someone suggested that a small (center of mass) COM tilt along the X axis of the balance arm would explain the apparent drift in the baseline seen in some of the thrust waveforms. When the cavity has the orientation shown below its COM shifts to the left. This would reduce the tilt, resulting in an increase in brightness of the reflected light the linear displacement sensor measures; due to the mirror position being closer to an optimal perpendicular position with respect to the light beam. The increase in brightness corresponds to a decrease in distance; hence the negative slope. With the device mounted the other way the shift in COM increases the tilt. This reduces the reflected light and is registered as an increase in distance. No actual motion of the beam occurs. This apparent motion is an optical artifact. This assumes the Philtec linear displacement sensor is used on the far side. If it is used on the near side a small counter-clockwise tilt along the X axis of the beam would produce the same effect; except requiring much less rotation from the change in COM. See Fig. 47.

There is a tilt in the torque pendulum's (TP) axis of rotation with the RF power supply lower than the test article, as shown in Fig. 47. Using my 24 inch long level, I use about a 1/4 bubble of tilt. From that point on its a matter of fine tuning the TP response by adding or removing small weights around the test article and/or adjusting the tilt angle with a micrometer adjusting the length of the TP support under the test article.

As the cavity expands you get center-of-gravity shifts which can torque the pendulum and cause it to move. So we had to spend quite some time quantifying exactly how much the pendulum moves due to small shifts in the center of gravity of the EM-drive. See Fig 46. Then we had to separate that out from the force calculations. We went into the details in our Dec 2016 paper so I won't dwell on the details here [18].

4. CONCLUSIONS

During this Sept. 2016 Estes Park Advanced Propulsion Workshop, I had the opportunity to exchange ideas and information on propellantless propulsion (P-P) and its current state of maturity. We reviewed various ways to build P-P effect devices based on either the Mach-Effect or quantum-vacuum conjectures that both rely on the cosmological gravitation field to convey momentum to and from the P-P thrusters in question.

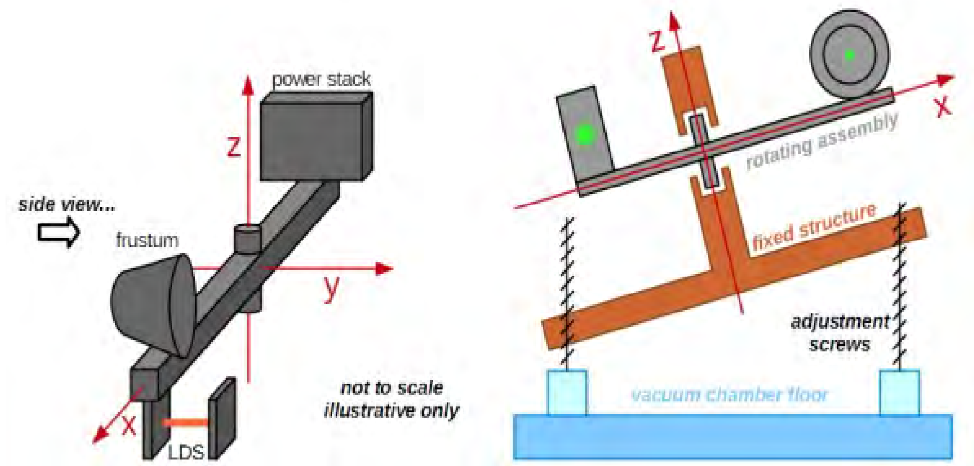

FIG. 47: Torque pendulum's, very exaggerated tilt. Diagram care of "Frobnicat" from NASA Spaceflight forum.

The Mach-Effect Gravity Assist (MEGA) P-P thrusters can utilize both low frequency (35 kHz) driven, high permittivity ($e-r=1500$), piezoelectric and electrostrictive dielectric capacitor discs used in vibrating stacks to generate these P-P effects. We also examined P-P EM-drive like thrusters that utilized microwave frequencies ($\sim$2.0 GHz) driven asymmetrical (frustum) resonant cavities, named by its inventor Roger Shawyer. These EM-drive microwave thrusters utilized either amorphous low-permittivity ($e-r=2.3$), but high electrostrictive dielectrics like polyethylene (P-E) or Teflon for their active media, or just the copper metal down to 5× its AC skin depth, that makes up these frustum resonant cavities as the active P-P agent. Both approaches are currently able to produce in-vacuum vetted thrust levels in the micro-Newton to tens or even low hundreds of micro-Newtons, at-this-time. Ways to increase these current thrust levels into the milli-Newton level and above were reviewed and discussed.

In regards to the theory of operation, we primarily talked about Jim Woodward's M-E conjecture and how that can be applied to both his Mach-Effect Gravity Assist (MEGA) drives and Roger Shawyer's microwave powered EM-drives. When Woodward disclosed that three other labs outside the USA had replicated the testing of his PZT stack based MEGA drives in their own facilities, it dawned on me that the P-P thruster community may have finally reached their "Chigago Pile Moment" where enough experimental data validating the P-P data in question comes together to form a body of knowledge that can then be used to build bigger and better P-P thrusters needed to build vehicles like IXS Clarke solar system cruiser [1] displayed at the front of this presentation. As to what is the best way to build these P-P drives has yet to be determined and may take many roads forward, but there is now at least two ways to build viable P-P thrusters that can be utilized in deep space transport design [8].

REFERENCES

[1] Mark Rademaker, http://mark-rademaker.blogspot.com/

[2] David Brady, Harold White, Paul March, James Lawrence, and Frank Davies. "Anomalous Thrust Production from an RF Test Device Measured on a Low-Thrust Torsion Pendulum", 50th AIAA/ASME/SAE/ASEE Joint Propulsion Conference, Propulsion and Energy Forum, July 28-30, 2014, Cleveland, OH (AIAA 2014-4029) http://dx.doi.org/10.2514/6.2014-4029, http://arc.aiaa.org/doi/abs/10.2514/6.2014-4029

[3] H. White and P. March, "Advanced Propulsion Physics: Harnessing the Quantum Vacuum", 2015 Website only: http://www.lpi.usra.edu/meetings/nets2012/pdf/3082.pdf

[4] Roger Shawyer, see the EM-drive website at http://www.emdrive.com.

[5] J. F. Woodward, "*Making Starships and Stargates*", (Springer press Dec 2012).

[6] Guido Fetta, "Numerical and Experimental Results for a Novel Propulsion Technology Requiring no On-Board Propellant" , http://arc.aiaa.org/doi/abs/10.2514/6.2014-3853, presented at the 50^{th} AIAA/ASME/SAE/ASEE Joint Propulsion Conference, Propulsion and Energy Forum, July 28 -30, Cleveland OH (2014). The Cannae website is at: http://cannae.com. See also http://cannae.com/cannaes-superconducting-test-lab-is-up-and-running/

[7] Roger Shawyer, "Second generation EM-drive propulsion applied to SSTO launcher and interstellar probe". Acta Astronautica **116**, 166-174 (2015). This paper has a YCBO superconducting cavity in it. Can be downloaded here, www.emdrive.com/IAC14publishedpaper.pdf

[8] Harold "Sonny" White, Warp drive space ships of the future: https://www.youtube.com/watch?v=4zPOxm6r_A

[9] Roger Shawyer, "A Theory of Microwave Propulsion for Spacecraft", http://www.rexresearch.com/shawyer/shawyer.htm\#gb233, New Scientist 2572, p24, 7 October (2006).

[10] Allen H. Yan, B. C. Appel & J. G. Gedrimas, "MilliNewton Thrust Stand Calibration Using Electrostatic fins", 47^{th} AIAA Aerospace Sciences Meeting, Including the New Horizons Forum and Aerospace Exposition, 5^{th}-8^{th} Jan. Orlando FL (2009). AIAA2009-212.

[11] Greg Egan, "Resonant Modes of a Conical Cavity", http://www.gregegan.net/SCIENCE/Cavity/Cavity.html

[12] Frank Davies, did a preliminary analysis of the truncated cone cavity using COMSOL. He supplied pictures of the electromagnetic modes from 900 MHz to 2.5 GHz. These were later verified experimentally.

[13] COMSOL Multi-physics is a finite-element general-purpose software package, for solving and modeling various engineering and physics-based problems, especially coupled-problems. http://www.comsol.com.

[14] Yang, Juan et al., "Thrust Measurement of an Independent Microwave Thruster Propulsion Device with Three-Wire Torsion Pendulum Thrust Measurement System", Journal of Propulsion Technology, Vol.37, (2) Feb. 2016.

[15] College students conducted an experiment on a cylinder with a HDPE disc at one end. They were having trouble with their setup and their results were inconclusive. California Polytechnic State University, San Luis Obispo. https://www.linkedin.com/in/kurtwadezeller

[16] c-flex flexural bearings, https://c-flex.com/ D-30 model has a load capacity of 100 pounds.

[17] Silicone spray used to prevent oxidation of the copper, http://www.tri-m.com/products/trim/spec-sheets/422B_TDS_Silicon.pdf

[18] H. White et al. “Measurement of Impulsive Thrust from a Closed Radio-Frequency Cavity in Vacuum”, AIAA Journal of Propulsion & Power (JPP) Nov. 17th 2016. http://arc.aiaa.org/doi/full/10.2514/1.B36120

REVOLUTIONARY PROPULSION RESEARCH AT TU DRESDEN

M. Tajmar
Institute of Aerospace Engineering,
Technische Universität Dresden,
01062 Dresden, Germany

Since 2012, a dedicated breakthrough propulsion physics group was founded at the Institute of Aerospace Engineering at TU Dresden to investigate revolutionary propulsion. Most of these schemes that have been proposed rely on modifying the inertial mass, which in turn could lead to a new propellantless propulsion method. Here, we summarize our recent efforts targeting four areas which may provide such a mass modification/propellantless propulsion option: Asymmetric charges, Weber electrodynamics, Mach's principle, and asymmetric cavities. The present status is outlined as well as next steps that are necessary to further advance each area.

1. INTRODUCTION

Present-day propulsion enables robotic exploration of our solar system and manned missions limited to the Earth-Moon distance. With political will and enough resources, there is no doubt that we can develop propulsion technologies that will enable the manned exploration of our solar system.

Unfortunately, present physical limitations and available natural resources do in fact limit human exploration to just that scale. Interstellar travel, even to the next star system Alpha Centauri, is some 4.3 light-years away which is presently inaccessible – on the scale of a human lifetime. For example, one of the fastest manmade objects ever made is the Voyager 1 spacecraft that is presently traveling at a velocity of 0.006% of the speed of light [1]. It will take some 75,000 years for the spacecraft to reach Alpha Centauri.

Although not physically impossible, all interstellar propulsion options are rather mathematical exercises than concepts that could be put into reality in a straightforward manner. For example, from all feasible propulsion systems ever proposed the highest performance is expected from nuclear bombs which are detonated behind the spacecraft (this concept was originally developed under the name Project Orion) [2]. Even such a system would require an order of magnitude more warheads than presently available just to achieve a fly-by mission to our nearest star within a human lifetime.

Even if we could achieve a good fraction of the speed of light, our practical action radius for human-return missions would still be limited to about 10 light-years which includes a maximum of 10 stars around us where no planets have been detected so far. According to the "Maccone Distribution" [3], the next civilization would be most probably some 2000 light-years away which would be inaccessible even with hypothetical light-speed propulsion systems. It is quite clear that we need some sort of breakthrough in propulsion physics to circumvent these limits and enable practical – and affordable – human exploration well beyond our solar system.

Following the spirit of past programs such as NASA's breakthrough propulsion physics and BAE Systems Project Greenglow, we started our own breakthrough propulsion physics program [4] investigating:

1. Theory: Explore theoretical concepts that can lead to a practical Space/Warp drive, new approach to gravity that can be experimentally tested, etc.

2. Mass Modification: Investigate experimentally if mass is influenced by temperature, rotation, charge/polarization, etc.

3. New Gravitational-Like Fields: Carry out experiments to investigate if gravitational/ frame-dragging fields can be enhanced in the lab e.g. by strong discharges through superconductors

4. Testing other Claims: Critically assess claims by others on revolutionary propulsion concepts of new physical effects that may lead to a breakthrough in propulsion and/or power.

Recent work by our group include a critical evaluation of the EMDrive [5], a replication of the Wallace gravitational generator [6], a superconducting gravitational impulse generator [7], [8], the evaluation of error sources when testing weight changes of mechanical gyroscopes [9], an evaluation of the claimed electrostatic torque effect [10] as well as a possible space drive concept [11], [12] and theoretical work on a connection between electromagnetism, mass and quantum theory [13].

As classical propulsion (force and Tsiolkovsky rocket equation, etc.) is based on Newton's mechanics, which in turn relies on inertia, it is quite straightforward to think that any new type of propulsion will probably involve a change in the inertial mass. Two main approaches have appeared so far:

1. Negative mass: If we find or create a substance with negative inertial mass, put it next to a normal positive inertial mass and allow for a force between them (e.g. by charging them up with opposite polarity), this so-called gravitational dipole will start to self-accelerate. That is a consequence of Newton's mechanics extended to negative inertia, which does not violate energy or momentum conservation as negative inertia also represents negative energy/momentum. The self-accelerating system therefore produces no net energy/momentum itself. This concept was first proposed by Forward [14] and recently even experimentally verified in an optical analog experiment with self-accelerating photons [15].

2. Variable/Oscillating mass: It may not be necessary for a revolutionary propulsion device to have negative inertial mass, it could be sufficient to have an inertial mass that is oscillating. If we imagine such a mass that we push when it is heavy and pull back when it is lighter, such a system could indeed produce a net momentum without spending propellant. As recently explicitly shown by Wanser [16], momentum conservation does only apply to a system with constant mass. Our oscillating mass system clearly violates this condition providing a method of producing real propellant-less thrust. Of course energy must be spent in order to modify mass and to push/pull it back and forth. Properly written down, also this approach does not violate any physical conservation principle.

Of course, the real challenge here is to produce macroscopic quantities of negative or oscillating inertial mass. So far, the properties of negative inertial mass have been mimicked in experiments using effective mass inside certain boundaries only (e.g. neutrons inside a crystal [17], or photons inside fibers [15]). How shall real negative mass exist outside such special boundaries? Oscillating inertial masses are much simpler to imagine. For example, charging and discharging a capacitor will change its mass by simply following $E = mc^2$. Unfortunately, c^2 is a large number so the resulting mass fluctuation will be very small. Of course the availability of high-frequency technology up to the THz range may compensate some of that if properly done.

The approach currently pursued at TU Dresden is to investigate four different possibilities to achieve negative/oscillating inertial mass as shown in Fig. 1. This paper will give an overview of the present status for each of the research lines.

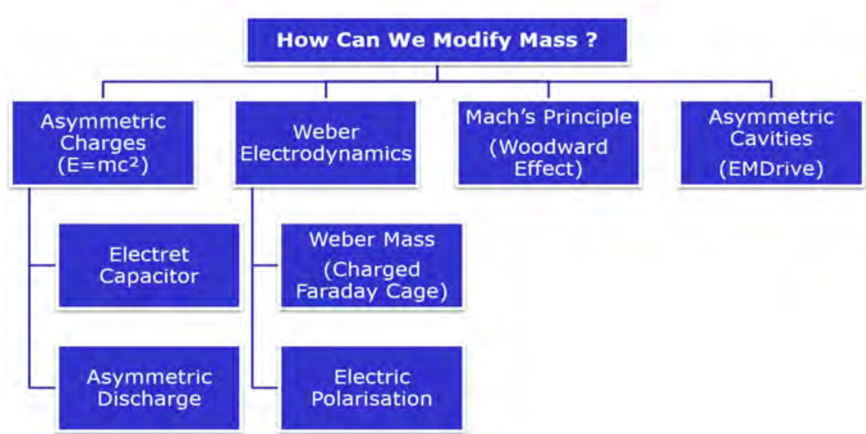

FIG. 1: Mass Modification Approach

2. ASYMMETRIC CHARGES

According to Einstein's famous equation $E = mc^2$, all non-gravitational sources of energy contribute to mass (the energy of the gravitational field cannot be localized according to the equivalence principle [18]).

Boyer [19] showed that two opposite charges should lose weight as the electrostatic potential energy between dissimilar charges is always negative. Considering two charges, the energy of the whole system is given as:

$$U = m_1c^2 + m_2c^2 + \frac{1}{4\pi\epsilon_0}\frac{q_1q_2}{r} \tag{1}$$

where r is the separation distance between the charges, and m and q is the respective mass and amount of charge. It is now straightforward to see that if the two charges have opposite signs, the electrostatic potential energy is reducing the total mass of the system by

$$\Delta m = \frac{1}{4\pi\epsilon_0}\frac{q_1q_2}{rc^2} \tag{2}$$

Of course the main question here is where this change in mass is actually localized. Is the delta-mass equally split between the charges involved, or is this delta mass only visible for the system of charges as a whole? If the actual mass of a charge would be modified, then this could open up the possibility to use this effect for our propellantless-propulsion scheme.

The contribution of electrostatic energy to mass is actually a century-old question. The simplest configuration is the one of a single electron acting on itself (self-energy). Initially J.J. Thompson derived the so-called electromagnetic mass (1881) and at the beginning of the 20th century it was thought that this electromagnetic contribution actually is responsible the whole mass of the electron. That changed of course with the development of relativity and quantum theory. Still, self-energy contributions to mass and the resulting perturbations to the classical motion of particles is an active field of research (e.g. [20]). However, self-energy contributions and contributions to each charge from multiple charge interactions are very different scenarios.

Brillouin [21] studied this question and argued that as almost all energy associated with the electric field is localized within the classical electron radius, the mass change should localize at the individual particles as well. If we consider a point-particle with charge Q, the energy of the electric field from infinity towards a radius R is defined as

$$U = \frac{1}{8\pi\epsilon_0}\frac{Q^2}{R} \tag{3}$$

Accordingly, the mass associated with that energy can be expressed as

$$M_q = \frac{U}{c^2} = \frac{Q^2}{8\pi\epsilon_0 c^2}\frac{1}{R} = \frac{Q\phi}{2c^2} \tag{4}$$

where ϕ is the electric potential. From these equations, it's clear that the mass diverges as R approaches zero and therefore a finite radius is required for the charged particle. That was how the classical electron radius was introduced. Still, the introduction of an arbitrary radius to justify that the energy of the field materializes as a mass change for every particle involved is not fully convincing.

Contrary to this classical approach that summarizes the energy from infinity towards an arbitrary radius (outside view), a more modern approach is given by the Reissner-Nordström metric which describes the field equations of a mass M with charge Q as

$$\begin{aligned} ds^2 = {} & \left(1 - \frac{2GM}{rc^2} + \frac{GQ^2}{4\pi\epsilon_0 r^2 c^4}\right)c^2dt^2 - \left(1 - \frac{2GM}{rc^2} + \frac{GQ^2}{4\pi\epsilon_0 r^2 c^4}\right)^{-1}dr^2 \\ & - r^2\left(d\theta^2 + \sin^2\theta d\phi^2\right) \end{aligned}$$

where the line element is approximated using

$$g_{00} \cong 1 + 2\frac{\Delta U}{c^2}\,, \quad \Delta U = -\frac{GM}{r} + \frac{GM_q}{r} = -\frac{GM}{r} + \frac{GQ^2}{8\pi\epsilon_0 c^2}\frac{1}{r^2} \tag{5}$$

This can be considered the length element inside the mass, as here we are really dealing with the equations of motion of the charged mass itself. As the gravitational potential energy is negative (mass attracts mass) but the electrostatic potential energy is positive, this charge-energy correction here acts as a negative mass component (Reissner-Nordström repulsion) at $r < R$, where R is the event horizon. We see that this is exactly opposite to the electromagnetic mass view that assigned a positive mass due to the electrostatic self-energy of the field. Bringing both views together, one may even say that indeed the motion of charged particles will be affected by the electrostatic field, but there is no net mass gain at the location of the particle as the negative contribution there is balanced out by the positive contribution due to the energy density of the field towards infinity.

Still, this question has not been experimentally assessed thoroughly. The contribution of an electrostatic potential to mass (electrostatic redshift) was experimentally investigated with a null result by Kennedy et al and Drill in the 1930s [22], [23]. Woodward and Crowley [24] pointed out that this result was to be expected using the Reissner-Nordström metric to predict the effect and the instrumentation resolution at that time. New experiments will be necessary to probe such an effect.

On the promise that electrostatic fields may influence a particle's rest mass, we recently published a configuration called the electret capacitor which could enable the utilization of this effect for propulsion purposes [11]. A capacitor typically consists of two sheets of metal with a dielectric in between. If the capacitor is charged, a certain amount of charge leaves one surface to go to the second one. Therefore, the charge density on both plates is equal but with different polarities. For the electret capacitor, two electrets (sheets of dielectrics with permanent electric charges on them) with different charge densities are opposite to each other, creating a new electrostatic situation where the positive self-energy from the interaction of charges with the same polarity can be outbalanced by the negative interaction energy between the charges with different polarities. In certain geometrical and charge density configurations, a negative energy larger than the positive rest mass energy of the charges from one side of this electret capacitor may be created, which could be used as a negative inertial mass source for propellantless propulsion.

Apart from the electric configuration, discharges in a highly asymmetric electric field may also provide the necessary boundary for charges to behave as negative inertial masses which may result in a novel propulsion scheme.

3. WEBER ELECTRODYNAMICS

In parallel to the development of Maxwell's equations, Wilhelm Weber proposed a force that also covered all known aspects of electromagnetism (Ampere, Coulomb, Faraday and Gauss's laws) and incorporated Newton's third law in the strong form, that is that the force is always along the straight line joining two charges [25] (which also implies the conservation of linear and angular momentum). However, Weber's electrodynamics also gives rise to new effects such as the change of the effective inertial mass of a charge inside a charged spherical shell which we could exploit for negative matter propulsion. Assis proposed an extension to Weber's electrodynamics that allows the derivation of a gravitation-type force [26], [27]. This extended model may be used to actually modify mass itself. Here we will give a short overview of both approaches.

A. Weber Mass (Charged Faraday Cage)

Weber's force expression and the related potential energy is given by

$$\boldsymbol{F} = \frac{q_1 q_2}{4\pi\epsilon_0} \frac{\hat{\boldsymbol{r}}}{r^2} \left(1 - \frac{\dot{r}^2}{2c^2} + \frac{r\ddot{r}}{c^2}\right), \quad U = \frac{q_1 q_2}{4\pi\epsilon_0} \frac{1}{r} \left(1 - \frac{\dot{r}^2}{2c^2}\right), \tag{6}$$

where q_1 and q_2 are the respective charges and r is the distance between them. If we now consider a single charge inside a charged spherical dielectric shell (in order to ignore eddy currents or mirror charges), we must integrate the force and sum up all the interaction between the single charge inside the shell and all other charges along the shell. Surprisingly, a net force remains that acts on the single charge when it accelerates inside the shell [28] given by

$$\boldsymbol{F} = \frac{qQ}{12\pi\epsilon_0 c^2 R} \cdot \boldsymbol{a} = \frac{q\phi}{3c^2} \cdot \boldsymbol{a}, \tag{7}$$

where Q is the charge on the shell, R the shell's radius and ϕ the electrostatic potential inside the shell. Classically, no force is expected on a charge inside a charged shell as the electric potential is constant and therefore no electric and no force acts on charges inside. According to Weber's electrodynamics, this force is proportional to acceleration of the charge and therefore influences the charge's inertial mass. If the total inertial mass is now the sum of the unaffected mass and the Weber mass, we may express the effective mass of the charge as

$$m^* = m - \frac{qQ}{12\pi\epsilon_0 c^2 R} = m - \frac{q\phi}{3c^2} \tag{8}$$

The equation predicts that a change in mass should be quite observable in a dedicated laboratory experiment. Considering a dielectric shell with a radius of 0.5 m charged up to 1.5 MV, we could expect to double an electron's mass – or reduce it to zero depending on the shell's charge polarity. In fact, up to a numerical factor, that result is very close to the one for the electromagnetic mass (see Eq. (4)).

Mikhailov published a number of experiments where such an effect was indeed observed. First, he put a neon glow lamp inside a glass shell that was coated by a thin layer of GaIn and an RC-oscillator inside a Faraday shield below [29]. The coated glass shell imitates the charged dielectric shell as originally proposed by Assis. Mikhailov assumed that the frequency of the lamp is directly proportional to the electron's mass. Indeed, he observed that the lamp's frequency changed if he charged the sphere as predicted by Equ. (9) within a factor 3/2. In a second experiment, the neon lamp was replaced by a Barkhausen-Kurz generator leading to similar results [30]. Finally, the neon-lamp experiment was repeated with two charged concentric shells showing that the frequency/mass effect from charging up the first shell can be counterbalanced by oppositely charging the outer shell [31].

Junginger and Popovich [32] repeated the neon glow lamp experiment and implemented an optical counter instead of electrically measuring the frequency of the lamp – and observed a null result. Also Little et al [33] performed a similar replication and observed a null result with optical counters and observed that the electric measurement of the lamp's frequency may be influenced by the Faraday's shield potential depending on the coupling capacitor used (however the signature of the effect was a parabola instead of the linear relationship as obtained by Mikhailov). At TU Dresden, we tried to replicate Mikhailov's setup and implemented an optical counter in parallel. Indeed, we could also verify the variation that Mikhailov has seen and traced it back to influence of the coupling capacitor. Running the experiment with an optical counter also produced a null effect.

However, we then asked ourselves how representative a neon discharge is with respect to the single electron prediction from Weber/Assis. A plasma discharge produces a significant current and a number of ions in close proximity to the electrons. This setup may therefore not be representative at all in order to test this prediction. Mikhailov's second setup used a Barkhausen-Kurz generator where an electron cloud is oscillating around a grid with high frequency. This frequency f should be closely linked to the mass of the electron as given by:

$$f \approx \sqrt{\frac{e\phi}{2m}} \cdot \frac{1}{\ell} \tag{9}$$

where ℓ is the distance from the cathode to the anode. Mikhailov did not measure the frequency directly in his setup but only qualitatively. We decided to make a replication using both the same tube as well as others that are known to produce Barkhausen-Kurz oscillations. We then put the tube inside a 3D printed shell with a metallic layer that could be biased. Using an Advantest R3261A signal analyzer, the actual frequency of the tube during biasing the spherical shell could be monitored as shown in Fig. 2.
The following observations were made (a detailed description of the experiment will be presented elsewhere):

- The original Mikhailov setup did not produce Barkhausen-type oscillations as the frequency did not scale with the square-root of the applied voltage to the grid.
- We replaced the tube and electronics successfully to observe Barkhausen-type oscillations with the correct characteristics.
- The frequency of the maximum signal peak emitted signal was tracked while varying the potential applied to the metallic sphere. The result is shown in Fig. 3. As it can be seen, our resolution was more than an order of magnitude better to see the predicted effect but no variation with the applied potential could be seen. However, it must be noted that the width of the signal was about 5 MHz which is in the range of the expected variation (8 MHz at 12 kV).

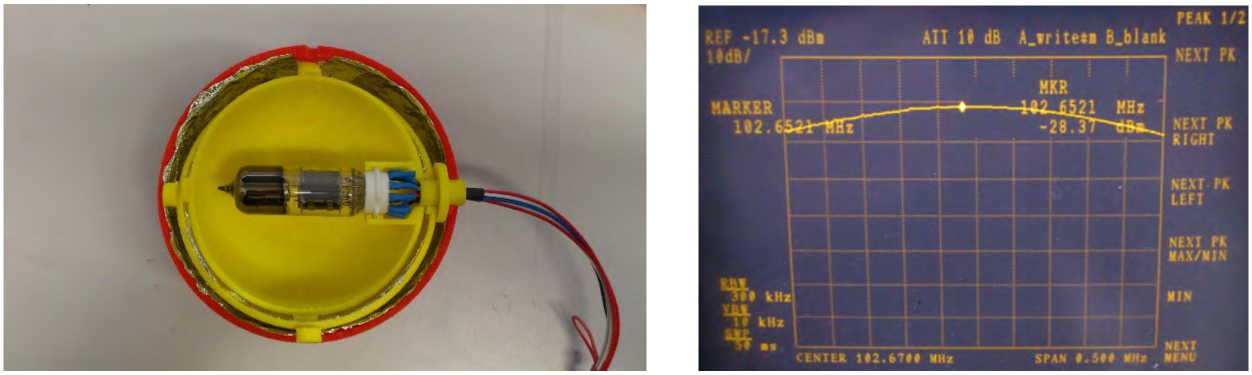

(a) Inside Charged Sphere (b) Frequency Measurement

FIG. 2: Barkhausen-Kurz Generator Setup.

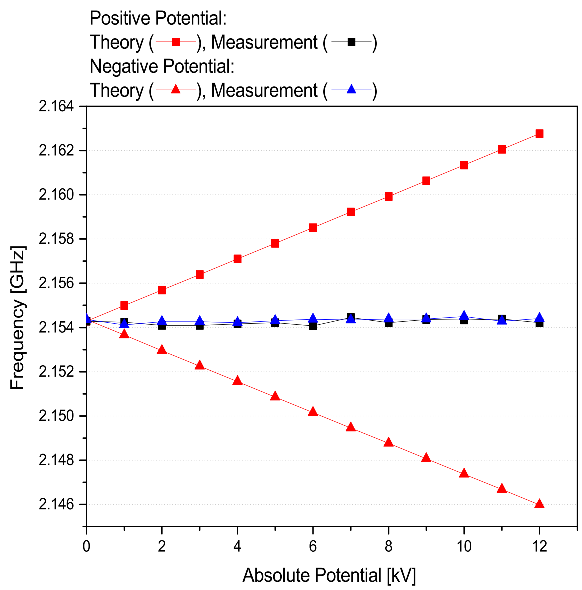

FIG. 3: Observed Frequency Variation of Maximum Signal Peak (Average of Three Test Runs) with Respect to the Expected Variation according to Weber/Assis

Of course, also here we have to ask if the experimental setup correctly represents the case predicted by Weber/Assis. For example, here we have an electron cloud instead of a single electron and the approximation of the Barkhausen oscillation in Equ. (10) also leaves room for correction factors that could possibly change our expected variation. Further experiments with different setups are necessary to look for an electrostatic influence on mass to find a definite answer.

B. Electric Polarization

Assis [26], [27] proposed an extension to Weber's electrodynamics that allowed him to derive gravitational and inertial-type forces from electrodynamics. His model is based on two assumptions:

1. Mass is composed of two opposite charges that vibrate with a certain amplitude and frequency. This can be considered a string-type approach.

2. Weber's potential Equ. (7) is actually a first order approximation valid for Maxwellian electromagnetism. Assis generalizes this equation with high-order terms as follows:

$$U = \frac{q_1 q_2}{4\pi\epsilon_0 r}\left(1 - \alpha\left(\frac{\dot{r}}{c}\right)^2 - \beta\left(\frac{\dot{r}}{c}\right)^4 - \gamma\left(\frac{\dot{r}}{c}\right)^6 \cdots\right), \tag{10}$$

where α is known as 0.5 and the other coefficients are assumed on the order of unity without knowing their precise value. Then he calculates the force between two oscillating dipoles with charge q, amplitude A and angular frequency ω by averaging over time and the three possible orientations (x, y, z) of the oscillating strings to arrive at

$$F = -\frac{7\beta}{18}\left(\frac{q_{1+}q_{2+}}{4\pi\epsilon_0 r^2}\right)\frac{A_{1-}^2\omega_1^2 A_{2-}^2\omega_2^2}{c^4}\left(1 + \frac{\gamma}{\beta}\frac{45\dot{r}^2 - 18r\ddot{r}}{7c^2}\right) \tag{11}$$

This looks like an always attractive force between the oscillators comparable with a similar $1/r^2$ dependence like gravity. The second-order correction term in the equation is identified with inertia. Of course, there are a number of free parameters (q, A, ω and the coefficients β and γ) that make it difficult to predict actual masses. However, recently we could show that this model allows the correct prediction of the maximum possible point mass which is equal to the Planck mass allowing to derive Planck's constant and the fine-structure constant with only one free coefficient [13]:

$$\hbar = \frac{h}{2\pi} = \frac{7\pi^3 e^2 \beta}{72 c\epsilon_0} = 2.92 \times 10^{-35}\beta \tag{12}$$

which matches the known value exactly for $\beta = 3.62$ (it is on the order of unity as Assis assumed). This is a remarkable result as it is the first derivation of the core assumption of quantum theory from an electromagnetic and gravitational model, providing a possible link between these cornerstones of modern physics and possibly an alternative to the Higgs model approach to explain mass.

If the Assis mass model is correct, then it may be possible to influence mass, e.g., due to electric polarization which is then influencing the orientation of the oscillating dipoles and therefore the average force between them. Apart from theoretical models to study such scenarios, we are currently testing the influence of highly polarized wax-electrets on their weight as a function of polarization and time. Similar tests were recently reported in a patent from Kita [34] where he claimed changes as high as 140 mg for samples with a weight of 278 g. We started our own wax-based electret production (45% carnauba wax, 45% resin and 10% bee wax) that were electrically polarized inside a capacitor with up to 10 kV during their cooling down phase. We used glass containers in order to limit any gas exchange with the environment which turned out to be very critical. That limited the observed weight changes in our experiments for samples with up to 200 g (including the container) to a few milli-grams only (see Fig. 4) [35]. We are presently further improving the setup in order to trace temperature and humidity changes in order to find an explanation for the observed drifts. Then we will proceed with measurements of different type of electrets or capacitors in order to investigate this mass change possibility.

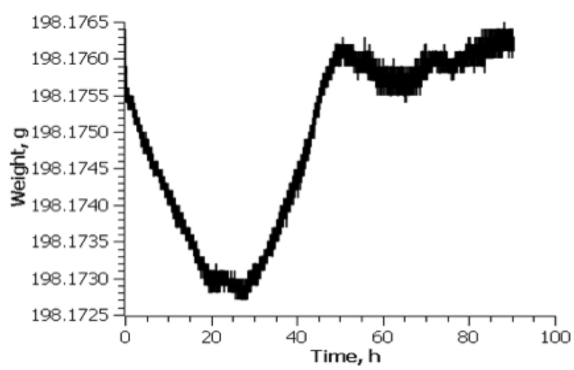

FIG. 4: Weight Change of Polarized Electrets over Time [35]

4. MACH'S PRINCIPLE (WOODWARD EFFECT)

Mach's principle is a concept in physics that tries to explain inertia [36]. It had been a guiding principle for A. Einstein in the development of his general relativity theory. Although there are many different interpretations, a simple explanation would be: "mass out there influences inertia here". It means that every mass is connected to all the masses of the whole universe by gravitational forces, which in turn is the cause for inertia. Some consequences of Einstein's theory can be indeed viewed as Machian, like the dragging of space-time by rotating objects which then influences objects in their close vicinity.

Over many years, J.F. Woodward used Mach's principle to propose a scheme that he calls transient mass fluctuations [37], which suggests that measureable changes in the inertial mass of a body can be created due to high-frequency oscillations which are caused by a back-reaction of the universe on the oscillating test mass. His derivation is based on a flat-space, low-velocity relativistic evaluation of the four-divergence of the back-reaction field that arises from the gravitation of the universe. Here we will present a simple analysis using linearized general relativity theory that arrives at similar conclusions without any necessary assumptions.

Linearizing general relativity is an approximation scheme valid for test masses at slow velocities (with respect to the speed of light), in an environment that is not dominated by large gravitational fields (e.g. black holes), which is a good representation of our laboratory boundaries. The starting point is the Einstein field equation, where the metric tensor $g_{\mu\nu}$ is treated as flat spacetime $\eta_{\mu\nu}$ with a perturbation component $h_{\mu\nu}$:

$$R_{\mu\nu} - \frac{1}{2} g_{\mu\nu} R = \frac{8\pi G}{c^4} T_{\mu\nu} \, , \quad g_{\mu\nu} \cong \eta_{\mu\nu} + h_{\mu\nu} \, . \tag{13}$$

By using the definitions

$$\bar{h}_{\mu\nu} = h_{\mu\nu} - \frac{1}{2}\eta_{\mu\nu} h \, , \quad \bar{h}_{00} = \frac{4\phi_g}{c^2} \, , \quad T_{00} = \rho c^2 \, , \tag{14}$$

it is possible to simplify Einstein's equation to

$$\frac{1}{c^2}\frac{\partial^2}{\partial t^2}\bar{h}_{\mu\nu} - \nabla^2 \bar{h}_{\mu\nu} = -\frac{16\pi G}{c^4} T_{\mu\nu} \tag{15}$$

Now, one usually takes as a first order only static solutions, which ignores the first term on the left side, that immediately leads to Newton's gravitational force law:

$$\nabla \cdot \boldsymbol{g} = -\nabla^2 \phi_g = -\frac{4\pi G}{c^2} T_{00} = -4\pi G \rho_0 \tag{16}$$

where $\boldsymbol{g} = -\nabla \phi_g$ is the gravitational force per unit mass. As we are looking for transient solutions, we will now relax the approximation for the static solution and keep the first term in Equ. (15). This then leads to a deviation from Newton's law that is given as:

$$\frac{1}{c^2}\frac{\partial^2 \phi_g}{\partial t^2} - \nabla^2 \phi_g = -\frac{4\pi G}{c^2} T_{00} = -4\pi G \rho_0 \tag{17}$$

and therefore

$$\begin{aligned} \nabla \cdot \boldsymbol{g} = -\nabla^2 \phi_g &= -4\pi G \rho - \frac{1}{c^2}\frac{\partial^2 \phi_g}{\partial t^2} \\ &= -4\pi G \left(\rho_0 + \frac{1}{4\pi G c^2}\frac{\partial^2 \phi_g}{\partial t^2} \right) \end{aligned} \tag{18}$$

By comparing Eqs. (16) and (18), we see that time-varying terms lead to a change in the body's density (or mass by integration over its volume) that is independent of the gravitational constant G, which make such terms very large compared to "static" density (mass). This structure looks similar to displacement currents in Maxwell's equations. In the introduction, we discussed the example of a capacitor that is being charged and discharged and therefore varies its mass due to $E = mc^2$, making the mass changes too small to be observed. However, Eq. (18) tells us that fast mass changes are coupling much stronger to the gravitational field (by the factor $1/G \approx 1.5 \times 10^{10}$) than static masses do, which should make this effect indeed observable.

The change in density can be expressed as

$$\begin{aligned}\delta\rho_0 &= \frac{1}{4\pi G c^2}\frac{\partial^2 \phi_g}{\partial t^2} = -\frac{\phi_g}{4\pi G c^2 m_0}\frac{\partial^2 m_0}{\partial t^2} \\ &= -\frac{\phi_g}{4\pi G c^2 \rho_0}\frac{\partial^2 \rho_0}{\partial t^2} = \frac{1}{4\pi G \rho_0}\frac{\partial^2 \rho_0}{\partial t^2}\end{aligned} \tag{19}$$

where we used $\phi_g = -Gm_0/r$ for the gravitational potential and $\phi_g/c^2 = -1$ which was derived by Sciama [38] due to the interaction of the gravitational potential throughout the whole universe, which is of course the concept of Mach's principle. This equation is similar to the one from Woodward (first order term) and clearly shows that indeed transient Mach-type fluctuations are predicted by general relativity theory without the introduction of new physics.

So far, over the years many tests have been published by Woodward's lab [37,39,40] and others [41,42]. His design is based on piezo crystals that act both as capacitors that trigger mass changes due to rapid charging/discharging, as well as accelerators to push and pull the crystals in order to get a directional thrust as outlined in the introduction. After the implementation of a torsion balance, the observed thrusts were in the sub-μN range for the models and electronics used. Many error sources were addressed such as thermal drifts or vibration artefacts.

Still, a number of shortcomings are present that we need to tackle in order to claim an experimental effect without any doubts. Most importantly, no tests were carried out up to now with the electronics (signal generator and amplifier) on the balance in order to completely rule out interactions between them. So far, all tests used electronics outside the vacuum chamber and liquid-metal contacts that connected to the thruster on the balance. We therefore decided to build vacuum-compatible electronics that can be mounted on a thrust balance to carry out thrust measurements with a fully integrated thruster-electronics package. Our test thruster is a model that was given to us in 1999 by J. Woodward which looks similar in design, however, it contains old piezo elements with non-optimal specifications so that we expect somewhat lower thrusts compared to his present models.

Our thrust balance uses flexural bearings and is similar in its design to many other low-thrust balances with several distinct differences [43], see Fig. 5:

- Up to 25 kg of thruster and electronics weight is possible, which enables the possibility of heavy shielding if necessary.
- On-board electronics and data acquisition system with infrared wireless communication, 24 V supply through the bearings, liquid-metal contacts if needed.
- Vibration damping of the whole vacuum chamber and inside the vacuum chamber
- Calibration with electrostatic combs or voice-coil
- Use of the attocube IPS laser interferometer which enables a thrust noise down to the sub-nN regime

The electronics on the balance as well as the Mach-Effect thruster can be seen in Fig. 6 and the whole thrust balance inside our large vacuum chamber is shown in Fig. 7. First tests show thrust values in the sub-μN range, however, balance calibration, thermal drifts and power feeding line interactions are still under investigation before our first test campaign will be finalized.

5. ASYMMETRIC CAVITIES (EM-DRIVE)

The EM-Drive has been proposed as a revolutionary propellantless thruster using a resonating microwave cavity [44-46]. The inventor R. Shawyer claims that it works on the difference in radiation pressure due to the geometry of its tapered resonance cavity. This may also be interpreted as a change in the effective photon mass at each side of the cavity, which somehow resembles Woodward's transient Mach-fluctuation thruster

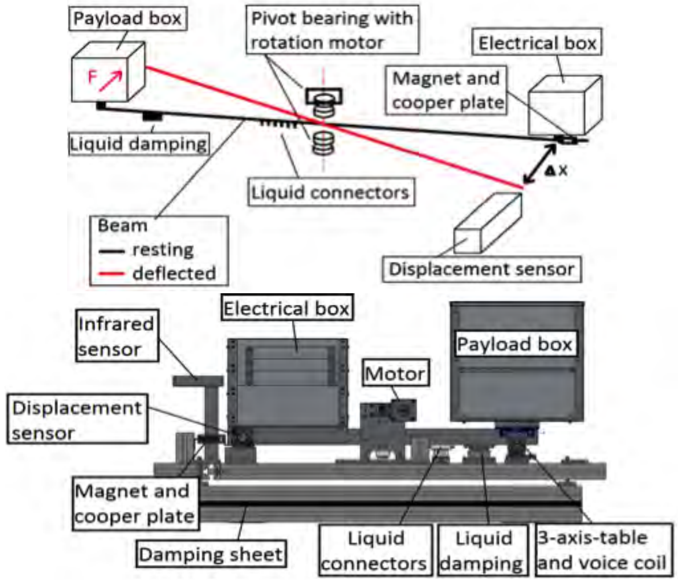

FIG. 5: Thrust Balance Setup [43]

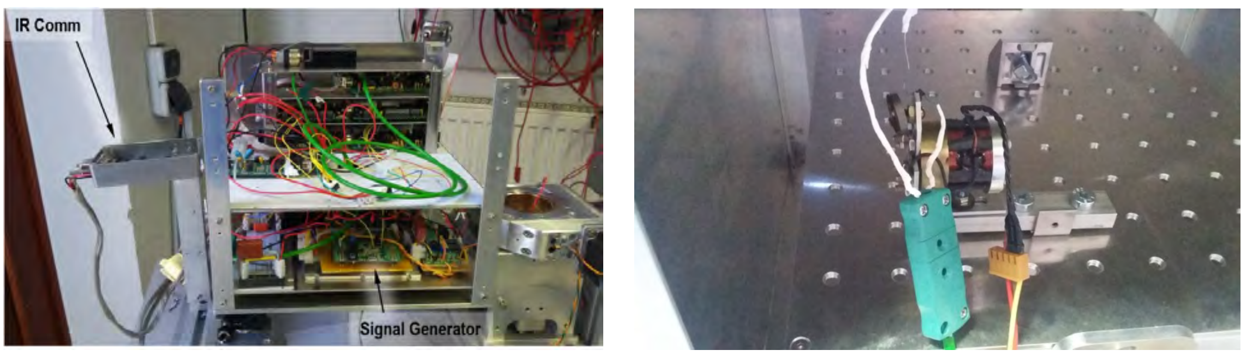

FIG. 6: Mach-Effect Thruster: Setup of Electronics and Thruster Model

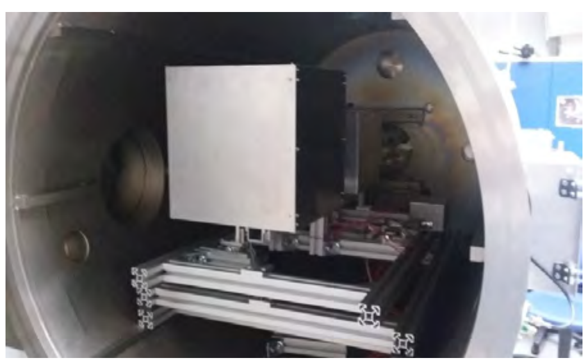

FIG. 7: Mach-Effect Thruster: Setup of Thrust Balance

with photons instead of piezo crystals, that may ultimately lead to higher efficiencies and thrust-to-power ratios.

We attempted to replicate an EM Drive and tested it on both a knife-edge balance as well as on a torsion balance inside a vacuum chamber, similar to previous setups, in order to investigate possible side-effects through proper thermal and electromagnetic shielding. After developing a numerical model to properly design our cavity for high efficiencies in close cooperation with the EM Drive's inventor, we built a breadboard

out of copper with the possibility to tune the resonance frequency in order to match the resonance frequency of the magnetron which was attached on the side of the cavity. After measuring the Q-factor of our assembly, we connected the EMDrive to a commercial 700 W microwave magnetron.
An overview of the different setups can be seen in Fig. 8.

Thruster Model with Magnetron | Setup with Box on Knife-Edge Balance | Setup on Thrust Balance inside Vacuum Chamber

FIG. 8: EMDrive Setups

Our measurements revealed thrusts as expected from previous claims (due to a low Q factor of < 50, we observed thrusts of $\pm 20 \mu$N), however also in directions that should produce no thrust. We therefore achieved a null measurement within our resolution which is on the order of the claimed thrusts. Details of the measurement can be seen found in [5].

The purpose of the test program was to investigate the EMDrive claims using improved apparatus and methods. To this end it was successful in that we identified experimental areas needing additional attention before any firm conclusions concerning the EMDrive claims could be made. Our test campaign therefore cannot confirm or refute the claims of the EMDrive but intends to independently assess possible side-effects in the measurement methods used so far. We identified the magnetic interaction of the power feeding lines going to and from the liquid metal contacts as the most important possible side-effect that is not fully characterized yet and which needs to be evaluated in the future in order to improve the resolution.

6. CONCLUSION

This paper summarizes the current activities towards revolutionary propulsion activities at TU Dresden. We believe this is an excellent educational topic which a great learning experience for students due to its theoretical and experimental challenges. Even an experimental null result leads to a better understanding of measurement artefacts or setup limitations which are very valuable for other similar investigations (e.g. low-thrust measurements for space thrusters). Of course, research towards totally new propulsion schemes can be very valuable to ultimately push the technological limit of our present limitations in space exploration.

ACKNOWLEDGEMENTS

I would like to thank the students involved in the activities that were summarized in this paper: Matthias Kössling (Thrust Balance and Mach Effect Thruster), Marcel Weikert (Weber Electrodynamics), Willy Stark (Mach Effect Thruster), Istvan Lörincz (Weber Electrodynamics), Tom Schreiber (Electret Measurements) and Georg Fiedler (EMDrive). Continued discussions with G. Hathaway were also greatly appreciated. In addition, I would like to thank the Estes Park organizers for their great efforts.

REFERENCES

[1] R. H. Frisbee, “Advanced Propulsion for the 21st Century,” J. Propuls. Power, Vol. 19, No. 6, pp. 1129-1154, 2003.

[2] M. Tajmar, Advanced Space Propulsion Systems. Vienna: Springer Vienna, 2003.

[3] C. Maccone, "The Statistical Drake Equation," in 59th International Astronautical Congress, Glasgow, Scotland, GB, Paper IAC-08-A4.1.4, 2008.

[4] M. Tajmar, "Breakthrough Propulsion Physics," 2016. [Online]. Available: `http://www.tu-dresden.de/ilr/rfs/bpp` . [Accessed: 09-Dec-2016].

[5] M. Tajmar and G. Fiedler, "Direct Thrust Measurements of an EMDrive and Evaluation of Possible Side-Effects," in 51st AIAA/SAE/ASEE Joint Propulsion Conference, 2015, AIAA 2015-4083.

[6] M. Tajmar, I. Lörincz, and C. Boy, "Replication and Experimental Characterization of the Wallace Dynamic Force Field Generator," in 51st AIAA/SAE/ASEE Joint Propulsion Conference, 2015, AIAA 2015-4081.

[7] I. Lörincz and M. Tajmar, "Null-Results of a Superconducting Gravity-Impulse-Generator," 52nd AIAA/SAE/ASEE Joint Propulsion Conference, AIAA 2016-4988, 2016.

[8] I. Lörincz and M. Tajmar, "Design and First Measurements of a Superconducting Gravity-Impulse-Generator," in 51st AIAA/SAE/ASEE Joint Propulsion Conference, 2015, AIAA 2015-4080.

[9] I. Lörincz and M. Tajmar, "Identification of error sources in high precision weight measurements of gyroscopes," Measurement, Vol. 73, pp. 453-461, 2015.

[10] D. Bojiloff and M. Tajmar, "Experimental evaluation of the claimed coulomb rotation (electrostatic torque)," J. Electrostat., Vol. 76, pp. 268-273, 2015.

[11] M. Tajmar, "Propellantless Propulsion with Negative Matter Generated by High Electrostatic Potentials," in 49th AIAA/ASME/SAE/ASEE Joint Propulsion Conference, 2013, AIAA 2013-3913.

[12] M. Tajmar and A. K. T. Assis, "Particles with Negative Mass: Production, Properties and Applications for Nuclear Fusion and Self-Acceleration,"' J. Adv. Phys., Vol. 4, No. 1, pp. 77-82, Mar. 2015.

[13] M. Tajmar, "Derivation of the Planck and Fine-Structure Constant from Assis's Gravity Model," J. Adv. Phys., Vol. 4, No. 3, pp. 219-221, Sep. 2015.

[14] R. L. Forward, "Negative matter propulsion," J. Propuls. Power, Vol. 6, No. 1, pp. 28-37, Jan. 1990.

[15] M. Wimmer et al., "Optical diametric drive acceleration through action-reaction symmetry breaking," Nat. Phys., Vol. 9, No. 12, pp. 780-784, 2013.

[16] K. H. Wanser, "Center of mass acceleration of an isolated system of two particles with time variable masses interacting with each other via Newton's third law internal forces: Mach effect thrust," J. Sp. Explor., Vol. 2, No. 2, pp. 122-130, 2013.

[17] K. Raum, M. Koellner, A. Zeilinger, M. Arif, and R. Gähler, "Effective-mass enhanced deflection of neutrons in noninertial frames," Phys. Rev. Lett., Vol. 74, No. 15, pp. 2859-2862, 1995.

[18] C. W. Misner, K. S. Thorne, and J. A. Wheeler, Gravitation. W. H. Freeman and Comp. Ltd., 1973.

[19] T. H. Boyer, "Electrostatic potential energy leading to an inertial mass change for a system of two point charges," Am. J. Phys., Vol. 46, No. 4, p. 383, 1978.

[20] S. E. Gralla, A. I. Harte, and R. M. Wald, "Rigorous derivation of electromagnetic self-force," Phys. Rev. D, Vol. 80, No. 2, p. 24031, Jul. 2009.

[21] L. Brillouin, "The Actual Mass of Potential Energy, a Correction to Classical Relativity," Proc. Nat. Acad. Sci, Vol. 53, No. 3, p. 475, 1965.

[22] R. J. Kennedy and E. M. Thorndike, "A Search for an Electrostatic Analog to the Gravitational Red Shift Author A Search for an Electrostatic Analog to the Gravitational Red Shift," Proc. Natl. Acad. Sci. U. S. A., Vol. 17, No. 11, pp. 620-622, 1931.

[23] H. T. Drill, "A Search for an Electrostatic Analog to the Gravitational Red Shift," Phys. Rev., Vol. 56, No. 2, pp. 184-185, Jul. 1939.

[24] J. F. Woodward and R. J. Crowley, “Electrostatic Redshift,” Nat. Phys. Sci., Vol. 246, No. 151, pp. 41, Nov. 1973.

[25] A. K. T. Assis, Weber’s Electrodynamics. Dordrecht: Springer Netherlands, 1994.

[26] A. K. T. Assis, “Deriving gravitation from electromagnetism,” Can. J. Phys., Vol. 70, No. 5, pp. 330-340, May 1992.

[27] A. K. T. Assis, “Gravitation as a Fourth Order Electromagnetic Effect,”’ in Advanced Electromagnetism –Foundations, Theory and Applications, T. W. Barrett and D. Grimes, Eds. Singapore: World Scientific, 1995, pp. 314-331.

[28] A. K. T. Assis, “Changing the Inertial Mass of a Charged Particle,” J. Phys. Soc. Japan, Vol. 62, No. 5, pp. 1418-1422, May 1993.

[29] V. F. Mikhailov, “The Action of an Electrostatic Potential on the Electron Mass,” Ann. la Fond. Louis Broglie, Vol. 24, pp. 161-169, 1999.

[30] V. F. Mikhailov, “The Action of an Electrostatic Potential on the inertial electron mass,”’ Ann. la Fond. Louis Broglie, Vol. 26, No. 1, pp. 33-38, 2001.

[31] V. F. Mikhailov, “Influence of a Field-Less Electrostatic Potential on the inertial Electron Mass,” Ann. la Fond. Louis Broglie, Vol. 28, No. 2, pp. 231-236, 2003.

[32] J. E. Junginger and Z. D. Popovic, “An experimental investigation of the influence of an electrostatic potential on electron mass as predicted by Weber’s force law,” Can. J. Phys., Vol. 82, No. 9, pp. 731-735, 2004.

[33] S. Little, H. Puthoff, and M. Ibison, “Investigation of Weber’s Electrodynamics,” 2001, [Online]. Available: `http://exvacuo.free.fr/div/Sciences/Dossiers/EM/Charges`.

[34] R. J. Kita, “Gravitational Attenuating Material,” US 8901943, 2014.

[35] T. Schreiber and M. Tajmar, “Testing the Possibility of Weight Changes in Highly-Polarized Electrets,” in 52nd AIAA/SAE/ASEE Joint Propulsion Conference, 2016, AIAA 2016-4919.

[36] J. Barbour and H. Pfister, Eds., Mach’s principle: from Newton’s bucket to quantum gravity. Boston: Birkhäuser, 1995.

[37] J. F. Woodward, *Making Starships and Stargates.* New York, NY: Springer New York, 2013.

[38] D. W. Sciama, “On the Origin of Inertia,” Mon. Not. R. Astron. Soc., Vol. 113, No. 1, pp. 34-42, Feb. 1953.

[39] H. Fearn and K. Wanser, “Experimental tests of the Mach effect thruster,” J. Sp. Explor., Vol. 3, No. 3, pp. 197-205, 2014.

[40] H. Fearn and J. F. Woodward, “Experimental Null test of a Mach Effect Thruster,’ arXiv, 25-Jan-2013. [Online]. Available: `http://arxiv.org/abs/1301.6178`.

[41] N. Buldrini, M. Tajmar, K. Marhold, and B. Seifert, “Experimental Results of the Woodward Effect on a μN Thrust Balance,” in 42nd AIAA/ASME/SAE/ASEE Joint Propulsion Conference, 2006, AIAA 2006-4911.

[42] P. March, “Woodward Effect Experimental Verifications,” in AIP Conference Proceedings, 2004, Vol. 699, pp. 1138-1145.

[43] D. Bock, C. Drobny, P. Laufer, M. Kössling, and M. Tajmar, “Development and Testing of Electric Propulsion Systems at TU Dresden,” in 52nd AIAA/SAE/ASEE Joint Propulsion Conference, 2016, AIAA 2016-4848.

[44] R. Shawyer, “Second generation EmDrive propulsion applied to SSTO launcher and interstellar probe” Acta Astronaut., Vol. 116, pp. 166-174, 2015.

[45] D. Brady, H. White, P. March, J. Lawrence, and F. Davies, "Anomalous Thrust Production from an RF Test Device Measured on a Low-Thrust Torsion Pendulum," in 50th AIAA/ASME/SAE/ASEE Joint Propulsion Conference, 2014, AIAA 2014-4029.

[46] H. White et al., "Measurement of Impulsive Thrust from a Closed Radio-Frequency Cavity in Vacuum," J. Propuls. Power, Article in Advance, Nov. 2016.

DISCUSSION FROM TAJMAR'S SESSION

During Martin's first talk, he mention's an electret capacitor, with asymmetric charge, as a possible way of getting a negative mass

Meholic: What would happen if you discharge an electret capacitor?

Tajmar: Well, I can't exactly discharge it, because to discharge I would need to connect the capacitor to a conductive circuit, and the electret is made of an isolator. So I have an isolator, and I'm bombarding it with ions or electrons which just stick to the surface. There is no current flow.

Meholic: How are you going to extract the usefulness of the negative mass out of that electret construct?
Tajmar: That's coming up in the next slides. By the way, if I get this to work I'll have a negative mass I can walk around with and I can sell it by the negative kilogram!

... audience laughter....

Fearn: During the Weber Electrodynamics section of the 1st talk, Martin describes the Wilhelm E. Weber force law, which just depends on charges, their separation, and velocity. It was a good enough description to derive the speed of light. It appears that Weber's force law does not take into account radiation reaction, which is very tiny and may have been overlooked at the time. Weber may not have known about it.

Tajmar: Yes, I'm coming to that, there was a later extension by A. K. T. Assis `http://www.ifi.unicamp.br/~assis/Pramana-J-Phys-V55-p393-404(2000).pdf` which adds in additional terms. Also, it turns out that massless charged particles don't radiate, this is apparently a new research topic, for example `https://arxiv.org/abs/hep-th/0212286`.

Martin starts to talk about EM-drives...

March: You should treat this as an RF system, not an analog audio system. You need to have a dual directional coupler to your RF source and the test article. You need to look at the reflected power from the cavity and use the minimum of the SWR power tracker as a frequency tracker with an arbitrary $\pm$ offset.

Tajmar: That would be the ideal way to do it, and that's what we will try to implement next year. Certainly tracking the frequency is something that needs to be done and we have not set that up yet.

Martin starts to talk about Woodward's Mach Effect thruster work. Martin has an old thruster, Jim gave him from 1999, that he has started to run tests on. The new devices Jim runs only requires one frequency, the older devices needed two frequencies to be present, since they did not have electrostriction.

Rodal: The usual thing "now" is that Jim inputs an excitation frequency f, within f_{op}/Q_m bandwidth of the first natural frequency $f_{op} \sim 34$ KHz due to the piezoelectric effect, and that the electrostriction of the material naturally provides an excitation at $2f$, twice the excitation frequency f. However, note that the electrostiction resonance occurs at $(1/2)f_{op}$, at half the piezoelectric natural frequency f_{op} so that

$2f = f_{op}$ and that the electrostriction resonant amplitude is orders of magnitude lower amplitude than the piezoelectric resonance.

Woodward: It's more complicated in this case José, because the thruster that Martin is checking is not like the ones that Heidi and I are running now, or like the ones tested by Nembo and George (they have newer devices). We are all using devices based on the Steiner–Martins SM-111 material, which has electrostriction as well as exhibiting the piezoelectric effect. The stack that Martin has, is made of EDO corporation (an American company now acquired by ITT corporation in 2007) EC-65 material discs. I don't know if that has any electrostriction response so he has to input two frequencies. It's a soft PZT material with a high dielectric constant of around 5000, it has about 4% dissipation. I built the stacks out of this stuff back then (1999) because it was cheap, they were a gift...

...audience laughter...

Woodward: Martin has shown his preliminary results, that show a small thrust from the old 1999 device. This was the first measurement of a self sustained system, with power and amplifier on board the torsion balance, to show thrust, with a very high resolution.

...audience applause...

March: Jim, didn't one of your early papers have a prediction for the thrust level in these older devices?

Woodward: No, not a paper that I recall, but there may be a graph in my "Making stargates and starships" book, that plots a thrust curve against various input power levels. Usually these devices had a small thrust measured in μN.

Tajmar: We were expecting μN or sub-μN levels of thrust, and that is what we saw in this preliminary data.

Woodward: Your data clearly shows the switching transients, tomorrow I'll show you what happens when you switch DC power on/off ... that is to say the switching transients go away. Thank you Martin !

Tajmar: You're welcome.

Martin is talking about his first data sets for the EM drive that his students built...

Rodal: Why does the thrust increase from 15 to 40 seconds?

Tajmar: Well I believe in this case, it is simply a shift in the center of gravity as the copper cavity expands. So it is an artifact of the thermal expansion of the copper. When I turn off the power, the force stops, you see the displacement sensor shifting down slowly, as the copper cools off. But this cannot be a force, since the power is off.

Williams: You said at the end that you could not confirm the existence of thrust for the EM drive, why is that?

Tajmar: When my "null" measurement, (which is in a direction perpendicular to the forward and backward direction) gives me the same thrust reading as a forward (or +) force direction measurement, then I know I have reached the level of resolution of my experiment. I cannot then say for sure that what I have seen is real or some noise. I need to improve my experimental setup (next year) and try again with higher resolution.

Broyles: Are you planning to change the design of your EM drive in the test run next year? If so, what design are you planning to use?

Tajmar: That's partly why I am here at this workshop. I wanted to ask if this or that is a good idea to try... we need to learn from each other, to avoid repeating the same mistakes.

VERIFICATION OF THE THRUST SIGNATURE OF A MACH EFFECT DEVICE

Nembo Buldrini
FOTEC Forschungs und Technologietransfer GmbH
2700 Wiener Neustadt, Austria

A Mach Effect Thruster is an apparatus based on piezoelectric material, which is supposed to produce thrust via an interaction of its components with, chiefly, the distant mass of the universe. A device of this sort, built and tested by Woodward, has been tested on a thrust balance in high vacuum at FOTEC (Austria). The results confirm qualitatively the presence of the same effect observed by Woodward.

1. INTRODUCTION

Being able to reach another planetary system in a reasonable amount time would only be possible if some kind of propellantless propulsion were developed. Propellantless systems like laser sails are an option, but they come with the drawback of relying on an external and distant source of power. The alternative of a self-contained propellantless system, capable of producing movement with seemingly no interaction with its surroundings, is considered to be the ultimate space propulsion scheme.

Since 1990, James F. Woodward and collaborators have shown that it should be possible, via Mach's Principle, to achieve such a scheme [1,2]. If the theory developed by Woodward were verified and validated experimentally, it would not only have practical consequences for space flight, but would also tell us more about the structure of our universe, as it would shed light on the origin of a fundamental property of mass, inertia. The last experimental embodiment of this theory is a device named MET, Mach Effect Thruster. The same device is also known as MEGA, Mach Effect Gravity Assist, an acronym which better describes the underlying working principle.

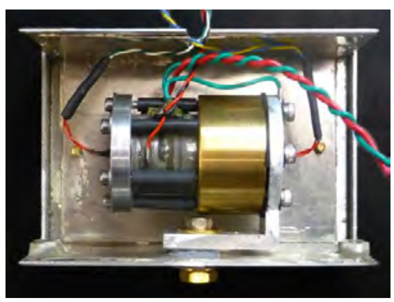

FIG. 1: The MET tested at FOTEC (lid of the Faraday cage removed)

A device of this sort has been sent to the author by Woodward in 2014. The device (Figure 1) is constituted by a stack of piezoelectric discs (material: lead zirconium titanate) clamped between an aluminium cap (left in the figure) and a brass reaction mass, and mounted inside an aluminium Faraday cage lined with mu-metal foil.

Applying a sinusoidal voltage to the piezoelectric stack causes it to change in size and shape, according to its piezoelectric and electrostrictive properties. The combined effect of these deformations is thought to produce thrust by an exchange of momentum via gravitational interactions with the distant cosmic masses [1,2].

What follows is a description of the tests this device underwent at FOTEC during the spring of 2014.

2. EXPERIMENTAL SETUP

The device has been installed on a thrust balance which has been developed to measure the thrust produced by liquid metal ion thrusters, usually ranging from some μN to more than 1 mN. The balance is of the torsion type, with vertical rotation axis, and the pivot consisting of two flexural bearings. The deflection of the balance is detected by a fiber optic displacement sensor. More details on the balance construction and verification can be found in [3].

The electrical connections to the device are implemented via a stack of liquid metal (Galinstan) contacts placed at the pivot: this method assures virtually no friction and no spurious forces produced when power is fed through the contacts (at reasonably low current/voltage values).

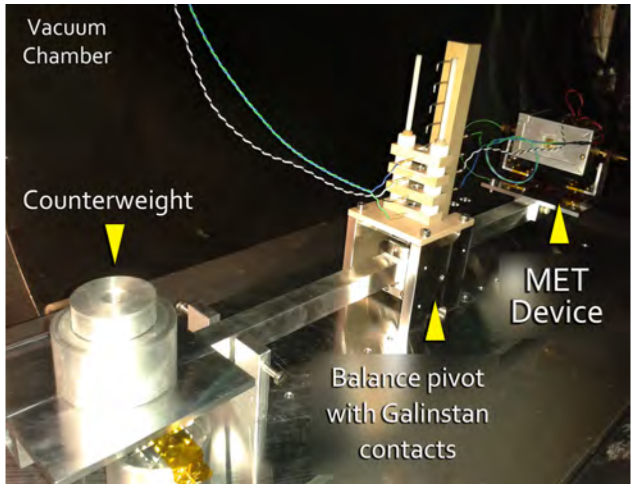

FIG. 2: The MET device mounted on the thrust balance inside the vacuum chamber

The device, mounted on the thrust balance, has been tested inside a vacuum chamber (Figure 2). The vacuum chamber is a cylindrical steel chamber of about 800 mm in diameter and 1750 mm in length; it is equipped with a roughing pump and a turbo pump, and pressures as low as $10^{-6} - 10^{-7}$ mbar ($10^{-4} - 10^{-5}$ Pa) can be customarily achieved.

Preliminary testing has been performed with only two electric lines to the device: the power line, which provided power to the stack of piezoelectric disks, and the temperature measurement line, for the measurement of the temperature on the aluminium cap end. Between the two available temperature measurement sensors, located respectively at the aluminium cap end and at brass reaction mass end, the first one has been chosen because of the faster response due to the lower thermal mass.

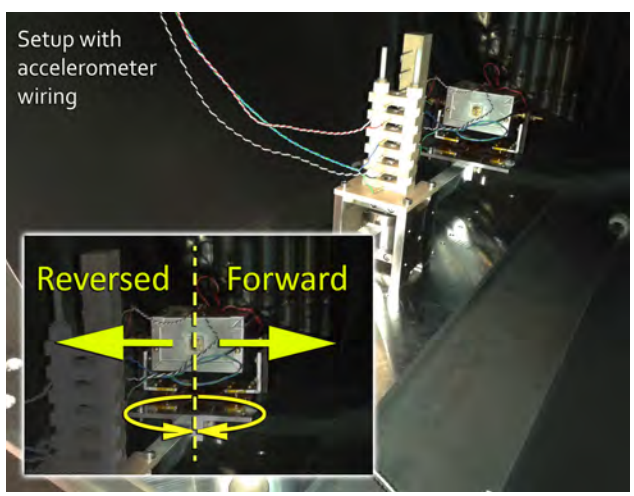

FIG. 3: Setup with added accelerometer wiring and explanation of the thrust vector direction. When going from forward to reversed thrust, the device is rotated around the axis represented by the dashed yellow line.

In subsequent testing, a third line has been added for measuring the voltage across a thin piezoelectric disk, part of the stack, which is passively used as an accelerometer (Figure 3). This enabled better monitoring of the operating conditions of the device. If fact, in order for Mach effects to be produced, both piezoelectric and electrostrictive force components must be present, and this can be confirmed by the presence of second harmonic content in the accelerometer signal (Figure 4).

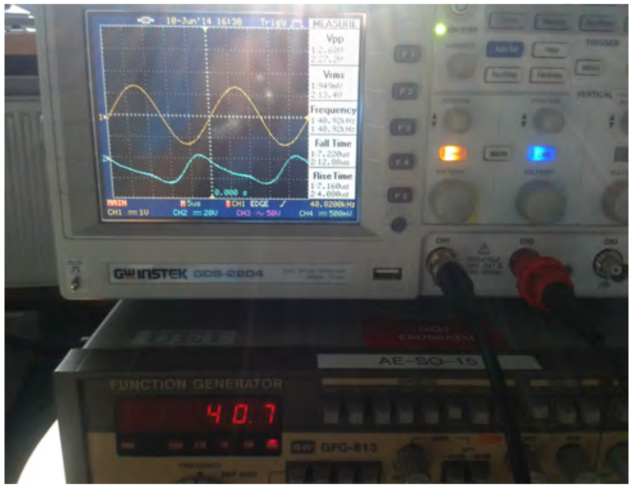

FIG. 4: Oscilloscope showing the driving signal (yellow) and the accelerometer signal (blue). The latter shows second harmonic content, indicative of the presence of electrostrictive force.

The power to the device has been supplied by a Carvin DCM 2500 amplifier, through a step-up transformer, capable of increasing the voltage of the amplifier to levels suitable for a proper operation of the piezoelectric device. Both the amplifier and the step-up transformer have the same specifications like the ones used by Woodward.

3. TEST RESULTS

All the tests have been run when the pressure in the vacuum chamber was 3×10^{-6} mbar (3×10^{-4} Pa) or lower. When a sinusoidal voltage of about 200 V peak to peak with a frequency of about 40 kHz is applied to the device, a thrust signal of about 0.15 μN is produced, with reliable repeatability, provided the temperature of the device was in the range between 30°C and 60°C. The chosen operating frequency of 40 kHz corresponds to the maximum thrust production, and it has been selected after testing the device at different frequency values.

The plots displayed in Figure 5 and Figure 8 show the direct response of the balance at the activation of the device. No further elaboration has been applied at the data. The gray bands indicate the time when power is supplied to the device.

Figure 6 compares the trace in Figure 5 with a trace obtained by Woodward when operating a twin device at approximately the same power level and frequency. Although the thrust magnitude is different, in both graphs a distinctive pattern can be identified, characterized by the presence of transitory effects occurring at the start and at the end of the operating time. Three phases can be recognized: (1) a starting transient constituted by a peak going in a direction opposite to the following steady thrust, (2) a steady thrust period of about 5 seconds, (3) at switch-off, a peak going in the same direction of the thrust. Figure 7 depicts an interpretation of the structure of the signal, where noise, drift and part of the overshooting are removed for sake of clarity.

Figure 8 shows a series of three runs in a row of the device after this has been rotated by 180° (direction reversal), as indicated in Fig. 3. Figure 8 serves also to point out the good repeatability of the thrust signal.

The fact that we have this distinctive common thrust pattern, which keeps its overall shape consistently across different devices of the same sort and different testing setups[**?**], and reverses with 180° rotation of the device, without changing in magnitude, is a strong indication that the effect is originating from the device itself and not from an interaction of the device with the close surroundings, nor from some interaction between different parts of the setup. In addition, if this signature is characteristic of the device, it may offer important clues on its actual operation, and could be compared with the results of models which try to characterize Mach effects in this kind of devices, like the one presented by J. Rodal in these workshop proceedings.

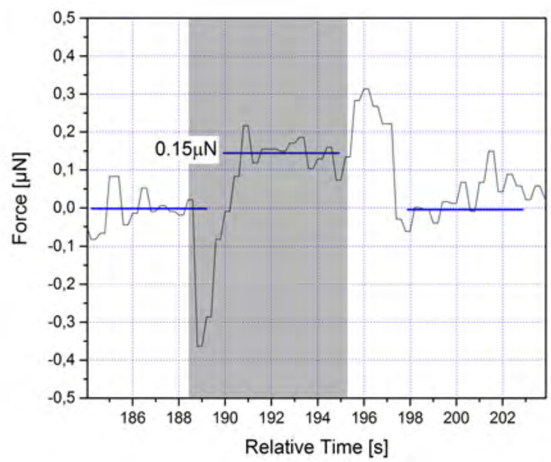

FIG. 5: Typical thrust plot. The area in gray indicates the time when the device is operating

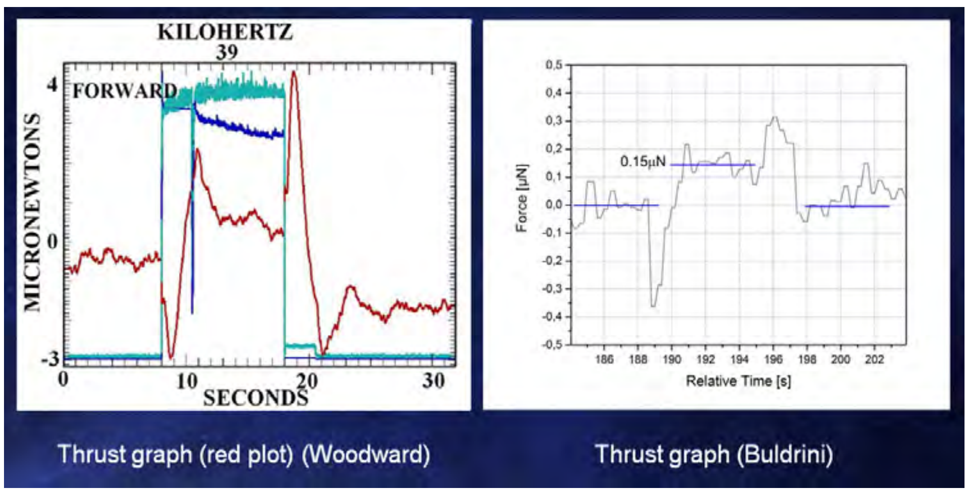

FIG. 6: Comparison with a typical MET thrust signature obtained by Woodward

Figure 9 makes a comparison of the plot in Figure 5 with a thrust plot obtained from the same device operated by Woodward at similar power level and frequency. It is interesting to note here that, while the transients are clearly visible and larger when compared with the measurement obtained at FOTEC, the steady thrust is difficult if not impossible to discern, due to what it seems a combination of noise, drift and zero-line offset.

In general, the different magnitude of the steady thrust value across otherwise similar and similarly operated devices could be ascribed to a sum of factors, these being, for example, degradation of device components (piezo stacks are sensitive to moisture), slight constructional differences between tested devices, different effective power delivered to the device and balance calibration issues. An additional factor, which would explain the mismatch in the magnitude of the transients, can be a different moment of inertia of the balances. Lighter balance beams, in fact, would react faster, showing larger transient peaks.

4. CONCLUSIONS

While previous replication efforts by the author on a different type of Mach effects device (Mach Lorenz Thruster) have produced inconclusive results [4], the kind of signal produced by the MET device here reported corroborates the results obtained by Woodward.

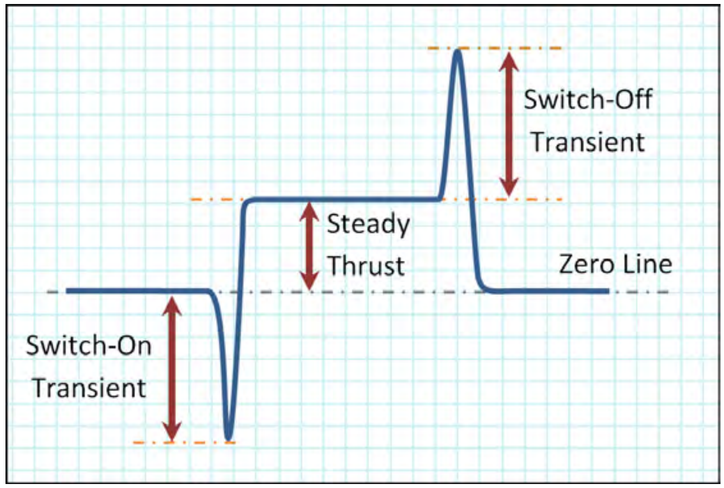

FIG. 7: Structure of the detected thrust signal.

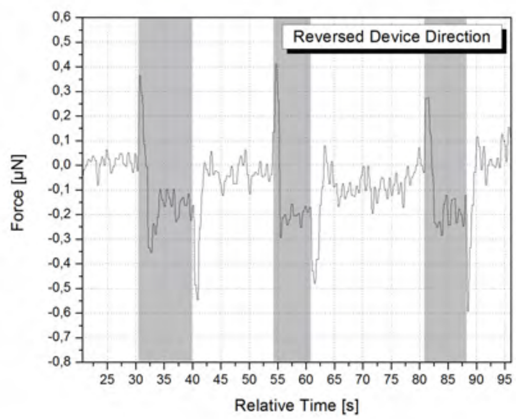

FIG. 8: Thrust plots with the device positioned in reversed direction.

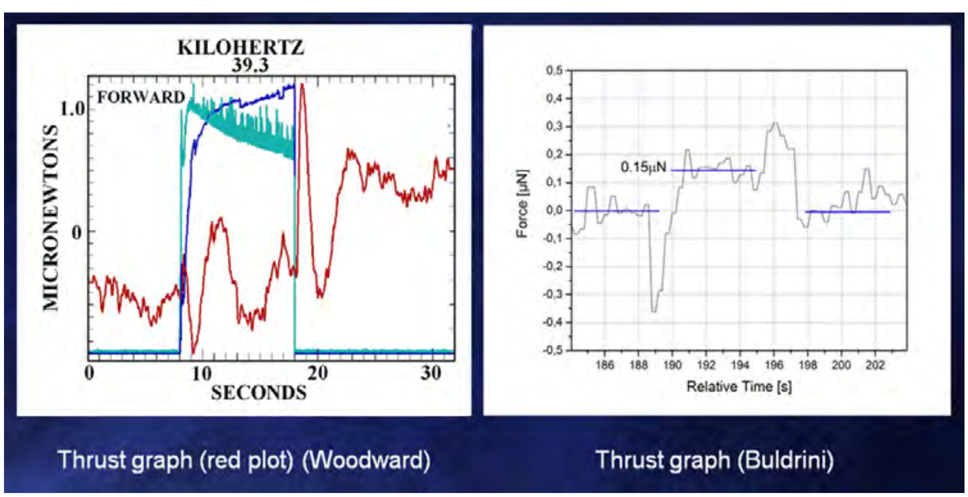

FIG. 9: Comparison of the thrust signature obtained from the same device by Woodward (left) and the author (right).

The distinctive shape of the thrust signal and its reversal with the rotation of the device allow to assert with high confidence that the effect is taking place inside the device itself, and it is not due to some sort of interaction between different parts of the experimental setup. Taking into account the small magnitude of the effect recorded to date, the possibility that other not yet considered complex (yet mundane) effects may be in play originating the signal seen cannot be totally excluded. However, the results obtained until now, together with several null tests performed (for example [5]), permit to reduce a lot the number of possible false positives and allow to focus on the device itself and its operation.

Considering the implications that the reality of Mach effects would have in many theoretical fields, for example in cosmology, and the immense benefits that propellantless propulsion would bring to space flight, further and extensive testing and characterization of this sort of devices is highly recommended.

5. ACKNOWLEDGEMENTS

The author would like to thank Prof. Jim Woodward for providing the tested device and continued support. Thanks go also to friends and colleagues, in particular to Paul March, Bruce Long, Duncan Cumming, David Mathes and Heidi Fearn for the first insights on the preliminary results of this work, and to Alexander Reissner, Bernhard Seifert, Florin Plesescu and Thomas Hörbe for supporting the experimental activity at FOTEC.

REFERENCES

[1] H. Fearn, N. van Rossum, K. Wanser and J. F. Woodward, "Theory of a Mach Effect Thruster II", Journal of Modern Physics, Volume 6, 2015, pp. 1868-1880

[2] H. Fearn, J. F. Woodward and N. van Rossum, "New Theoretical Results for the Mach Effect Thruster", 51st AIAA/SAE/ASEE Joint Propulsion Conference, AIAA Propulsion and Energy Forum, (AIAA 2015-4082)

[3] B. Seifert, A. Reissner, N. Buldrini, F. Plesescu and C. Scharlemann, "Development and Verification of a μN Thrust Balance for High Voltage Electric Propulsion Systems", The 33rd International Electric Propulsion Conference, The George Washington University, USA, October 6 –10, 2013

[4] N. Buldrini, M. Tajmar, K. Marhold and B. Seifert, "Experimental Results of the Woodward Effect on a μN Thrust Balance", AIAA-2006-4911

[5] H. Fearn, and J. Woodward, "Experimental Null Test of a Mach Effect Thruster", Journal of Space Exploration, Volume 2, Issue 2, 2013, pp. 98-105

GRAVITATIONAL ABSORBER THEORY & THE MACH EFFECT

H. Fearn
Physics Dept. CSU Fullerton,
800 N. State College Blvd.
Fullerton CA 92834, USA

The origins of mass can be described in terms of Mach's principle, which states that the mass of a body is determined by its interaction with the rest of the mass-energy in the universe. However, if a body undergoes a sudden acceleration, you may ask, "How can the universe respond immediately in a way to conserve momentum?" In order to explain this, we introduce the concept of advanced waves, which have been used successfully in both classical and quantum physics for the last 70+ years.

1. INTRODUCTION

The work of Hoyle and Narlikar (HN) is a "masterpiece" in general relativity (GR) theory because it is fully covariant and incorporates fully the idea of Mach's principle. It is what Einstein dearly wanted to do, but didn't think he quite managed with standard general relativity. But perhaps he did? This paper shows that the results of HN, or what I would prefer to call *gravitational absorber theory* (GAT) can be obtained from Einstein's GR with the addition of a mass fluctuation in time. In Section 2, I show that adding $m(t)$ is all that is needed. I have renamed the theory to emphasise that I am not interested in the static universe model; I do not include the HN mass creation (C)-field. I am only interested in the Machian development of the theory through the use of retarded and advanced waves.

The local field around a mass particle can still be thought of as the overlapping of the many retarded and advaced waves, which themselves carry energy and momentum. This field will have a potential anywhere in space-time and constitutes the background vacuum. The mass particle transfers energy and momentum with the "field" here and now, which is basically th vacuum. However, when the particle accelerates the universe as a whole reacts to the acceleration, causing changes in the local field, which can be transmitted to the particle conserving mometum on a universal scale.

Einstein began his work on general relativity by seeking a concordance with Mach's principle. That is, to explain inertia of a test mass in terms of other masses in the universe. Sciama, Nordtvedt, and others have shown that masses in motion exert non-radial gravitational forces on nearby masses (frame dragging). In particular, Sciama showed that just this frame-dragging effect from the rest of the universe can account for inertia. Woodward has exploited the result of Sciama to design a propellantless propulsion device that depends on such forces.

In spite of its prediction of frame-dragging, and apparent ability to account for inertia, some researchers feel that general ralativity does not provide a fully self-consistent Machian picture. While Sciama and Nordtvedt can calculate the inertial force on an accelerated object due to the rest of the mass in the universe, we feel that general relativity does not account for the effect of the accelerated mass back on the rest of the universe.

To properly account for the effect of the accelerated mass back on the rest of the universe, we employ the concept of advanced waves, made famous by Wheeler and Feynman. Hoyle and Narlikar developed a theory of general relativity that incorporated advanced waves. While Hoyle and Narlikar are well-known for their steady-state cosmology work, and they use HN theory in that work, we feel their theory stands as a fine extension to general relativity, ignoring the parts regarding mass creation.

The beauty of gravitational absorber theory (GAT) is that it allows one to think of a mass, here and now, being influenced by the rest of the matter in the universe via gravitational signals travelling at speed c and does not rely on some (old fashioned Newtonian) notion of "action-at-a-distance" or faster than light propagation of signals. Real gravitational signals travelling at speed c carry information from every part of the universe to a mass here and now. The only trick is, to have mass react instantaneously, you must invoke the advanced wave solution to the relativistic wave equation. This advanced wave travels backward in time from the distant reaches of the universe, to convey momentum to the here and now, allowing back reaction to appear instantaneous.

The reason that HN theory did not catch on in the 1960's is twofold.

1. Hoyle was looking for a static universe cosmology theory. He introduced the "C" field as a creation field to keep the mass density constant as the universe expanded. This C field can be removed without loss of the underlying theory.

2. Hawking raised an objection to the HN theory in 1965 which basically put the last nail on the coffin. He suggested that by integrating out into the distant future, the advanced wave integrals would diverge. That is correct. However, since the universe is not only expanding but accelerating in that expansion, there is a cosmic horizon beyond which you cannot integrate. That cutoff prevents the advanced wave integrals from diverging and therefore re-establishes the HN theory as a good working theory.

3. Now is the time to look at gravitational absorber theory in a new light. Forget the static cosmology and move forward.

Standard GR has the problem that masses are treated as static. That is in general not the case. The background gravitational potential can be nonzero even in a flat spacetime. The GAT allows for a dynamic communication of signals from every part of the universe to the here and now to conserve momentum. *Furthermore, and this is conjecture, the superposition of retarded and advanced waves throughout the universe could be a mechanism to understand dark energy and matter. For example, dark matter might just be the manifestation of the gravitational potential at a location in space where the retarded and advanced waves do not perfectly overlap. For example at the location of an accelerating mass. As an electromagnetic analogy, consider photons appearing near an accelerating mirror in the dynamic Casimir effect or equivalently Unruh radiation.*

There is sufficient reason to reconsider the gravitational absorber theory of Hoyle and Narlikar. In section 2, we allow for a mass fluctation in the Einstein equation of motion (geodesic) and obtain the HN equation of motion, which is a new result. In section 3, we give a very brief history of the HN paper sequence and rewrite their notation to assist the reader. In section 4, we compare the Einstein action and field equation with the HN field equation. In section 5, we show that the mass fluctuation frmula calculated by Woodward from the precepts of general relativity can also be obtained from HN theory. This is the main result of the paper.

Advanced waves were introduced by Dirac in 1938 to describe radiation reaction. His radiation reaction force equation is still in use today and can be found in most standard electrodynamics text books. The advanced wave concept was given a physical interpretation by Wheeler and Feynman in 1945 [1]. The idea has since been used successfully in quantum mechanics by John Cramer and later in the theory of gravitation by Hogarth 1962 [2] and Hoyle and Narlikar 1964 [3,4] whose work we will summarize for convenience below.

1.1 Electron Radiation Reaction in Electrodynamics

Dirac [5] first introduced the idea of advanced waves in electromagnetism in order to derive the radiation reaction of an accelerating electron.

The idea is as follows. Consider a single electron undergoing acceleration. The field surrounding the electron can be thought of in two parts, the outgoing and incoming. The actual field surrounding the electron is the usual retarded Lienard-Wiechert potentials and any incident field on the electron.

$$F^{\mu\nu}_{\text{act}} = F^{\mu\nu}_{\text{ret}} + F^{\mu\nu}_{\text{in}} \tag{1}$$

Furthermore, the Maxwell 4-potential wave equation allows for advanced solutions, which are the same form as retarded, only they go backward in time. The advanced solutions also satisfy the wave equation in Lorentz gauge (below, with $c = 1$):

$$\Box A_\mu = 4\pi j_\mu \tag{2}$$

$$\frac{\partial A_\mu}{\partial x_\mu} = 0 \tag{3}$$

We could equally well describe the actual field surrounding the electron by

$$F^{\mu\nu}_{\text{act}} = F^{\mu\nu}_{\text{adv}} + F^{\mu\nu}_{\text{out}} \tag{4}$$

where the $F^{\mu\nu}_{\text{out}}$ is the total field leaving the electron. The difference between the outgoing waves and the incoming waves is the radiation produced by the electron due to its acceleration.

$$F^{\mu\nu}_{\text{rad}} = F^{\mu\nu}_{\text{out}} - F^{\mu\nu}_{\text{in}} = F^{\mu\nu}_{\text{ret}} - F^{\mu\nu}_{\text{adv}} \tag{5}$$

In the appendix of Dirac's paper, it is shown that this equation gives exactly the well known relativistic result for radiation reaction which can be found in standard text books on electromagnetism, for example Jackson [6].

1.2 Wheeler & Feynman: Absorber Theory

Wheeler and Feynman [1] accept Dirac's result but wish to give a physical explanation as to where the advanced electromagnetic field comes from. They resort to a suggestion made by Tetrode [7] and later by Lewis [8] which was to abandon the concept of electromagnetic radiation as a self interaction and instead interpret it as a consequence of an interaction between the source accelerating charge and a distant absorber. The absorber idea has the four following basic assumptions, which we quote directly from Wheeler-Feynman [1],

> (1) An accelerated point charge in otherwise charge-free space does not radiate electromagnetic energy.
> (2) The fields which act on a given particle arise only from other particles.
> (3) These fields are represented by 1/2 the retarded plus 1/2 the advanced Lienard-Wiechert solutions of Maxwell's equations. This force is symmetric with respect to past and future.
> (4) Sufficiently many particles are present to absorb completely the radiation given off by the source.

Now, Wheeler-Feynman considered an accelerated charge located within the absorbing medium. A *disturbance* travels outward from the source. The absorber particles react to this disturbance and themselves generate a field half advanced and half retarded waves. The sum of the advanced and retarded effects of all the charged particles of the absorber, evaluated near the source charge, give an electromagnetic field with the following properties [1]:

> (1) It is independent of the properties of the absorbing medium.
> (2) It is completely determined by the motion of the source.
> (3) It exerts on the source a force which is finite, is simultaneous with the moment of acceleration, and is just sufficient in magnitude and direction to take away from the source the energy which later shows up in the surrounding particles.
> (4) It is equal in magnitude to 1/2 the retarded field minus 1/2 the advanced field generated by the accelerated charge. In other words, the absorber is the physical origin of Dirac's radiation field
> (5) This field combines with the 1/2 retarded, 1/2 advanced field of the source to give for the total disturbance the full retarded field which accords with experience.

The Wheeler-Feynman paper presents four derivations of the relativistic radiation reaction of an accelerated charge, each successive derivation increasing in generality. The first three derivations proceed by adding up all the electromagnetic fields due to the absorber particles. The fourth is the most general derivation, which only assumes that the medium is a complete absorber and so outside the medium the sum of all the retarded and advanced waves is zero. Each yields the well-known relativistic radiation reaction as given in text books [6].

So far, we have shown that the advanced wave idea has been used successfully in classical physics. Now we proceed to show that it can also be advantageously used within quantum mechanics. The transactional interpretation of quantum mechanics was written by John Cramer [9,10] in the 1980's. It is a way to view quantum mechanics which is very intuitive and easily accounts for all the well known paradoxes, EPR, which-way detection and quantum eraser experiments. We refer the reader to his paper, which is a very interesting read. All the usual quantum results hold, and it is simply an alternative point of view from the Copenhagen interpretation and collapsing-wave-function way of thinking.

Hoyle-Narlikar (HN) theory is a kind of absorber theory (with advanced waves) for gravitation rather than electrodynamics. HN theory agrees with Einstein's theory of gravitation in the limit of a smooth fluid mass density distribution in the rest frame of the fluid. All of the tests of Einstein's gravitation still apply to HN theory.

2. DERIVATION OF THE EINSTEIN GEODESIC EQUATION

One method used to derive the geodesic equation, also known as the equation of motion of a particle, is extremizing (minimizing) the line element. This will give us the shortest distance between two points. Taking the general line-element,

$$ds^2 = g_{\mu\nu} dx^\mu dx^\nu \tag{6}$$

varying both sides (a similar derivation can be found in Dirac [11] p16), we get

$$\begin{aligned}
2ds\delta(ds) &= dx^\mu dx^\nu \delta(g_{\mu\nu}) + g_{\mu\nu} dx^\mu \delta(dx^\nu) + g_{\mu\nu} dx^\nu \delta(dx^\mu) \\
&= dx^\mu dx^\nu g_{\mu\nu,\lambda}(\delta x^\lambda) + 2g_{\mu\lambda} dx^\mu \delta(dx^\lambda) \\
\delta(dx^\lambda) &= d(\delta x^\lambda) \\
dx^\mu &= \left(\frac{dx^\mu}{ds}\right) ds = v^\mu ds
\end{aligned} \tag{7}$$

In order to extremize the action $\int \delta(mds)$, treat mass as a constant. Then we consider the following,

$$\begin{aligned}
\int \delta(ds) &= \int \left[\frac{1}{2}\frac{dx^\mu}{ds}\frac{dx^\nu}{ds} g_{\mu\nu,\lambda}\delta x^\lambda + g_{\mu\lambda}\frac{dx^\mu}{ds}\frac{d}{ds}(\delta x^\lambda)\right] ds \\
&= \int \left[\frac{1}{2} g_{\mu\nu,\lambda} v^\mu v^\nu (\delta x^\lambda) + g_{\mu\nu} v^\mu \frac{d}{ds}(\delta x^\lambda)\right] ds
\end{aligned} \tag{8}$$

Integrating the second term by parts we find

$$\int \delta(ds) = \int \left[\frac{1}{2} g_{\mu\nu,\lambda} v^\mu v^\nu - \frac{d}{ds}(g_{\mu\lambda} v^\mu)\right] (\delta x^\lambda) ds = 0 \tag{9}$$

For this to be true for any variation δx^λ we find that the term inside the square bracket must be zero hence,

$$\frac{d}{ds}(g_{\mu\lambda} v^\mu) - \frac{1}{2} g_{\mu\nu,\lambda} v^\mu v^\nu = 0 \tag{10}$$

Furthermore

$$\begin{aligned}
\frac{d}{ds}(g_{\mu\lambda} v^\mu) &= g_{\mu\lambda}\frac{dv^\mu}{ds} + g_{\mu\lambda,\nu} v^\mu v^\nu \\
&= g_{\mu\lambda}\frac{dv^\mu}{ds} + \frac{1}{2}(g_{\mu\lambda,\nu} + g_{\lambda\nu,\mu}) v^\mu v^\nu
\end{aligned} \tag{11}$$

By substitution of Eq. (11) into Eq. (10) we find

$$\begin{aligned}
g_{\mu\lambda}\frac{dv^\mu}{ds} + \frac{1}{2}(g_{\lambda\mu,\nu} + g_{\lambda\nu,\mu} - g_{\mu\nu,\lambda}) v^\mu v^\nu &= 0 \\
\frac{1}{2}(g_{\lambda\mu,\nu} + g_{\lambda\nu,\mu} - g_{\mu\nu,\lambda}) &= \Gamma_{\lambda\mu,\nu} \\
\frac{dv^\sigma}{ds} + \Gamma^\sigma_{\mu\nu} v^\mu v^\nu &= 0
\end{aligned} \tag{12}$$

where the last equation, which is the usual geodesic equation, follows when you multiply throughout by $g^{\lambda\sigma}$. We did not start with a true particle Lagrangian, only a line element. The Lagrangian includes a mass of the particle. Note that we have left the mass entirely out of the variation since at present it is treated as a constant.

Let us compare this with what happens when you vary the rest mass of the particle.

2.1 Allow the Mass to change in Equation of Motion derivation

To see how similar the HN equation of motion is to the Einstein Geodesic, simply repeat the above calculation but allow the mass to change. The result is the Equation of Motion for the HN-theory. It is a little unclear as to why the usual Einstein geodesic does not contain the same mass variation. Is it because the mass is held constant in the Einstein case? If so **why** is the mass held constant?

Starting from the line element,

$$\begin{aligned} ds^2 &= g_{\mu\nu} dx^\mu dx^\nu \\ 2ds\delta(ds) &= \delta g_{\mu\nu} dx^\mu dx^\nu + 2g_{\mu\nu} dx^\mu \delta(dx^\nu) \\ \delta(ds) &= \left[\frac{1}{2}\delta g_{\mu\nu}\dot{x}^\mu \dot{x}^\nu + g_{\mu\nu}\dot{x}^\mu \frac{d}{ds}(\delta x^\nu)\right] ds \end{aligned} \tag{13}$$

Now, the action for mass m at position x can be simply written as,

$$\begin{aligned} I &= -\int m ds \\ \delta I &= -\int [\delta(m)ds + m\delta(ds)] \\ &= -\int \left[\frac{\partial m}{\partial x^\lambda}\delta x^\lambda + \frac{m}{2}\delta g_{\mu\nu}\dot{x}^\mu\dot{x}^\nu + m g_{\mu\nu}\dot{x}^\mu \frac{d}{ds}(\delta x^\nu)\right] ds \end{aligned} \tag{14}$$

Integrate the last term by parts and switch dummy variable $\nu \to \lambda$ we get,

$$\begin{aligned} \delta I &= -\int \left[\frac{\partial m}{\partial x^\lambda}\delta x^\lambda + \frac{m}{2}\frac{\partial g_{\mu\nu}}{\partial x^\lambda}\dot{x}^\mu\dot{x}^\nu\delta x^\lambda - \frac{d}{ds}(m g_{\mu\lambda}\dot{x}^\mu)\delta x^\lambda\right] ds \\ &= -\int \left[\frac{\partial m}{\partial x^\lambda} + \frac{m}{2}\frac{\partial g_{\mu\nu}}{\partial x^\lambda}\dot{x}^\mu\dot{x}^\nu - \frac{d}{ds}(m g_{\mu\lambda}\dot{x}^\mu)\right] \delta x^\lambda ds = 0 \end{aligned} \tag{15}$$

For this integral to be zero for any arbitrary δx^λ then the term in the square brackets must be zero, hence

$$\begin{aligned} \frac{d}{ds}(m g_{\mu\lambda}\dot{x}^\mu) &= \frac{m}{2}\frac{\partial g_{\mu\nu}}{\partial x^\lambda}\dot{x}^\mu\dot{x}^\nu + \frac{\partial m}{\partial x^\lambda} \\ \frac{dm}{ds} g_{\mu\lambda}\dot{x}^\mu + m\left(g_{\mu\lambda}\frac{d\dot{x}^\mu}{ds} + g_{\mu\lambda,\nu}\dot{x}^\mu\dot{x}^\nu\right) &= \frac{m}{2} g_{\mu\nu,\lambda}\dot{x}^\mu\dot{x}^\nu + \frac{\partial m}{\partial x^\lambda} \end{aligned} \tag{16}$$

where we may make the $g_{\mu\lambda,\nu}$ term symmetric in μ, ν as follows,

$$g_{\mu\lambda}\frac{d}{ds}(m\dot{x}^\mu) = \frac{m}{2}(g_{\mu\nu,\lambda} - g_{\mu\lambda,\nu} - g_{\nu\lambda,\mu})\dot{x}^\mu\dot{x}^\nu + \frac{\partial m}{\partial x^\lambda} \tag{17}$$

Then using the definition for the Christoffel symbol $\Gamma_{\lambda\mu,\nu}$ and multiplying throughout by $g^{\sigma\lambda}$ we get,

$$\begin{aligned} \frac{d}{ds}(m\dot{x}^\sigma) + m(g^{\sigma\lambda}\Gamma_{\lambda\mu,\nu})\dot{x}^\mu\dot{x}^\nu - g^{\sigma\lambda}\frac{\partial m}{\partial x^\lambda} &= 0 \\ \frac{d}{ds}(m\dot{x}^\sigma) + m\Gamma^\sigma_{\mu\nu}\dot{x}^\mu\dot{x}^\nu - g^{\sigma\lambda}\frac{\partial m}{\partial x^\lambda} &= 0 \end{aligned} \tag{18}$$

Written for mass m_a at position x_a the equation of motion becomes,

$$\frac{d}{d\tau}\left(m_a\frac{dx^\mu_a}{d\tau}\right) + m_a\Gamma^\mu_{\nu\lambda}\frac{dx^\nu_a}{d\tau}\frac{dx^\lambda_a}{d\tau} - g^{\mu\nu}\frac{\partial m_a}{\partial x^\nu_a} = e_a\sum_{b\neq a} F^{(\mathrm{b})\mu}_{\nu}\frac{dx^\nu_a}{d\tau} \tag{19}$$

where the Lorentz force has been included on the right for completeness. The world-lines of particles are not in general geodesics in the new theory. This equation agrees with the HN result in their book [12] p125 Eq.(138). In the HN book this equation of motion was derived directly from the gravitational field equation.

3. HOYLE-NARLIKAR THEORY DEVELOPMENT

There is some motivation for looking into the HN-theory in detail. We begin from the first of the Hoyle-Narlikar papers, through to the writing of their book. The notation they use is very unfortunate and difficult to read. There are too many similar letters being used for different parameters. Here we attempt to rewrite the theory in a more familiar notation, using Greek letters for 0,1,2,3 and Roman letters only to distinguish particle "a" from particle "b". We do not use their European style of 4-vector 1,2,3,4. Rather we use the 0,1,2,3 numbering which has become fairly standard throughout the world. The flat metric will be taken as $\eta_{\mu\nu} = \mathrm{diag}(1, -1, -1, -1)$. Where ever possible we leave c not equal to unity which helps with dimensional analysis. We tackle the papers in order starting with the first published.

Paper 1: The first paper in the sequence, in 1962, [13] was entitled "Mach's Principle and the creation of matter". The main point of the paper was to argue that although Einstein was very much influenced by Mach's ideas, he did not quite manage to get the full spirit of Mach's main idea embedded into the field equations... *mass depends on interaction with the rest of the mass-energy in the universe.*

We would argue that Mach's principle has several definitions and several of those are in fact already contained in Einstein's general relativity theory.

According to HN, they take the Einstein field equations, written as,

$$R^{\mu\nu} - \frac{1}{2}g^{\mu\nu}R + \lambda g^{\mu\nu} = -\kappa T^{\mu\nu} \tag{20}$$

and plug in the well known Robertson Walker line element,

$$ds^2 = c^2dt^2 - S^2(t)\left[\frac{dr^2}{1-kr^2} + r^2(d\theta^2 + \sin^2\theta d\phi^2)\right] \tag{21}$$

where $k = 0, \pm 1$ and where r can be chosen for an observer attached to any particular particle. For the stress-energy tensor, they assume

$$T^{\mu\nu} = \left(\rho + P + \frac{4}{3}u\right)\frac{dx^\mu}{ds}\frac{dx^\nu}{ds} - \left(P + \frac{u}{3}\right)g^{\mu\nu} \tag{22}$$

where ρ is the matter density, P is the gas pressure and u is the radiation density. Hoyle and Narlikar set out, in a series of papers, to formulate a gravitational theory (which encompasses Einstein's equations) which included Mach's principle from the start. This theory would have both retarded and advanced waves. Essentially this would be the gravitational equivalent of Wheeler-Feynman absorber theory for electrodynamics.

Paper 2: In 1963 [14], we see HN play around with the Einstein action and add in their C-field, to add matter to the universe in an attempt to preserve the density as the universe expands. This is not really of interest for our work. Sciama [15] publishes work in the same journal on Wheeler-Feynman absorber theory and mentions Hogarth's work [2].

Paper 3: In January 1964 we see the first attempt at something new. The paper is entitled, "Time symmetric electrodynamics and the arrow of time in cosmology", [16]. Here we see the first introduction of the Fokker-Schwarzschild-Tetrode action (FST action) [17,18,7], a discussion of the Wheeler–Feynman absorber theory [1], and reworking time-symmetric electrodynamics in a flat and Riemannian space-time. Here we rewrite these familiar equations for convenience since it will set up the new notation for their later work.

We start with a summary of the first few HN equations which we then "translate" into better notation below. We quote directly from the paper [16]:

.. we consider space-time to be given by the co-ordinates x^i and by the line-element

$$ds^2 = \eta_{ik}dx^i dx^k \tag{23}$$

where $\eta_{ik} = \mathrm{diag}(-1, -1, -1, +1)$. *The charges are labelled by letters $a, b, c\ldots$. The a^{th} particle has co-ordinates a^i, mass m_a, charge e_a and proper time a given by*

$$da^2 = \eta_{ik}da^i da^k \tag{24}$$

We have chosen the velocity of light to be unity so that the time units are the same as the space units. The Schwarzschild-Tetrode-Fokker action function is then defined by

$$J = -\sum_a m_a \int da - \sum_a \sum_{b\neq a} \frac{1}{2}e_a e_b \int\int \delta(ab_i ab^i)\eta_{lm} da^l da^m \tag{25}$$

where

$$\delta(ab_i ab^i) = \eta_{ik}(a^i - b^i)(a^k - b^k) \tag{26}$$

The equations of motion can be obtained from (25) by requiring that J be stationary with respect to variations of the world lines of particles. If we define the 4-potential of b at a point x by the function

$$A_m^{(b)}(x) = \int e_b \delta(xb_i xb^i)\eta_{mk} db^k \tag{27}$$

the equations of motion take the form

$$m_a \frac{d^2 a^k}{da^2} = e_a \sum_{b \neq a} F_l^{k(b)} \frac{da^l}{da} \tag{28}$$

where

$$F_{kl}^{(b)} = \frac{\partial A_l^{(b)}(x)}{\partial x^k} - \frac{\partial A_k^{(b)}(x)}{\partial x^l} \tag{29}$$

represents the 'field' of charge b at point x.

Note that a better notation of the FST action and derivations for the potential and Maxwell's equations, can be found at the very end of the book by Barut on electrodynamics [19]. Our notation is similar to Barut's only we use x instead of z. Also we use a and b to distinguish particles rather than α and β since these could easily be mistaken for summation variables. We start by rewriting the above notation as follows:
For flat space-time.

Define the metric as $\eta_{\mu\nu} = \mathrm{diag}(+1, -1, -1, -1)$. The charges are labelled by a, b, c as before. The a^{th} particle has coordinates x_a^μ , mass m_a, charge e_a, and proper time τ given by the line element as

$$ds^2 = c^2 d\tau^2 = dx_a^\mu dx_{a\mu} \ \ , \tag{30}$$

with $c = 1$ we get,

$$\begin{aligned} d\tau^2 &= \eta_{\mu\nu} dx_a^\mu dx_a^\nu \\ d\tau &\rightarrow \eta_{\mu\nu} \dot{x}_a^\mu \dot{x}_a^\nu d\tau \ \ . \end{aligned} \tag{31}$$

where differentiation w.r.t τ is represented by the dot above the symbol. The action can be written as,

$$I = -\sum_a \int \frac{1}{2} m_a (\dot{x}_a^\nu)^2 d\tau - \sum_a \sum_{b \neq a} e_a \int A_\mu^{(b)}(x_a^\nu) \dot{x}_a^\mu d\tau \tag{32}$$

$$A_\mu^{(b)}(x_a^\nu) = \int e_b D(x_a - x_b) \eta_{\mu\nu} dx_b^\nu \equiv \int e_b D(x_a - x_b) \eta_{\mu\nu} \dot{x}_b^\nu d\tau' \tag{33}$$

$$D(x_a - x_b) = \left[\eta_{\alpha\beta}(x_a^\alpha - x_b^\alpha)(x_a^\beta - x_b^\beta)\right]$$

Note that the 4-potential of particle b ($A_\mu^{(b)}$) is evaluated at the location of particle a. The proper time for particle b is given by τ' and $\dot{x}_b = dx_b/d\tau'$. The Lagrangian can be written as

$$I = \sum_a \int L(x_a^\nu, \dot{x}_a^\nu) d\tau \tag{34}$$

$$L(x_a^\nu, \dot{x}_a^\nu) = -\frac{1}{2} m_a (\dot{x}_a^\nu)^2 - e_a \sum_{b \neq a} A_\mu^{(b)}(x_a^\nu) \dot{x}_a^\mu \tag{35}$$

with equation of motion given by

$$\frac{\partial L}{\partial x_a^\nu} - \frac{d}{d\tau}\left(\frac{\partial L}{\partial \dot{x}_a^\nu}\right) = 0 \ \ . \tag{36}$$

Differentiating the Lagrangian we get

$$\begin{aligned}
\frac{\partial L}{\partial x_a^\nu} &= -\sum_{b\neq a} e_a \frac{\partial A_\mu^{(b)}}{\partial x_a^\nu}\dot{x}_a^\mu \\
\frac{\partial L}{\partial \dot{x}_a^\nu} &= -m_a\dot{x}_a^\nu - \sum_{b\neq a} e_a A_\nu^{(b)} \\
\frac{d}{d\tau}\left(\frac{\partial L}{\partial \dot{x}_a^\nu}\right) &= -\frac{d}{d\tau}(m_a\dot{x}_a^\nu) - e_a\frac{\partial A_\nu^{(b)}}{\partial x_a^\mu}\frac{dx_a^\mu}{d\tau} \\
m_a\ddot{x}_a^\nu &= e_a\dot{x}_a^\mu \sum_{b\neq a} F_{\nu\mu}^{(\mathrm{b})}(x_a^\nu) \qquad (37)
\end{aligned}$$

where the last equation is the equation of motion of particle a. The mass m_a is taken to be constant. Finally we define the electromagnetic field tensor as

$$\begin{aligned}
F_{\nu\mu}^{(\mathrm{b})}(x_a^\nu) &= \left(\frac{\partial A_\mu^{(b)}}{\partial x_a^\nu} - \frac{\partial A_\nu^{(b)}}{\partial x_a^\mu}\right) \\
F_{\nu\mu}^{(\mathrm{b})} &= \frac{1}{2}\left(F_{\nu\mu}^{(\mathrm{b})\mathrm{ret}} + F_{\nu\mu}^{(\mathrm{b})\mathrm{adv}}\right) \quad . \qquad (38)
\end{aligned}$$

Now we follow the paper but write only in the new notation. Using Dirac's identity,

$$\begin{aligned}
\eta^{\mu\nu}\frac{\partial^2}{\partial x^\mu \partial x^\nu}D(x-x_b) &= -4\pi\delta(x^0-x_b^0)(x^1-x_b^1)(x^2-x_b^2)(x^3-x_b^3) \\
&= -4\pi\delta^4(x-x_b) \quad . \qquad (39)
\end{aligned}$$

The 4-potential satisfies [19],

$$\begin{aligned}
\Box^2 A^{(\mathrm{b})\mu}(x) &= \sum_{b\neq a} e_b \int \dot{x}_b^\mu(\tau')\Box^2 D(x-x_b)d\tau' \\
&= -4\pi\sum_{b\neq a} e_b \int \dot{x}_b^\mu \delta^4(x-x_b)d\tau' \qquad (40)
\end{aligned}$$

which is the same as writing,

$$\Box^2 A^{(\mathrm{b})\mu}(x) = \eta^{\mu\nu}\frac{\partial^2}{\partial x^\mu \partial x^\nu}A_\sigma^{(b)}(x) = -4\pi j_\sigma^{(b)}(x) \qquad (41)$$

where the current density $j_\sigma^{(b)}(x)$ is given by

$$j_\sigma^{(b)}(x) = e_b\int_{-\infty}^{\infty}\eta_{\sigma\lambda}\dot{x}_b^\lambda\delta^4(x-x_b)d\tau' \qquad (42)$$

It can be shown that [19], the 4-potential satisfies the gauge condition

$$\begin{aligned}
\frac{\partial A^{(b)\mu}}{\partial x^\mu} &= \sum_{b\neq a} e_b \int \dot{x}_b^\mu \frac{\partial}{\partial x^\mu}D(x-x_b)d\tau' \\
&= -D(x-x_b)\,|_{\tau'=-\infty}^{+\infty} = 0 \quad . \qquad (43)
\end{aligned}$$

We may derive the following:

$$\frac{\partial F_\nu^{(b)\mu}}{\partial x^\mu} = -4\pi j_\nu^{(b)}(x) \quad , \qquad (44)$$

which are Maxwell's inhomogeneous equations.

Formally, all Maxwell's equations and the Lorentz force equation are derivable from the action principle, except radiation reaction terms (self force terms). The radiation reaction becomes a force due to advanced waves coming from the absorbing universe mass-energy. The time symmetry is emphasized by rewriting the 4-potential as a sum of retarded and advanced parts.

$$
\begin{aligned}
A_\mu^{(b)} &= \frac{1}{2}\left(A_\mu^{(\mathrm{b})\mathrm{Ret}} + A_\mu^{(\mathrm{b})\mathrm{Adv}}\right) \\
A_\mu^{(\mathrm{b})\mathrm{Ret}} &= e_b \frac{\eta_{\mu\nu}\dot{x}_b^\nu}{\eta_{\alpha\beta}(x^\alpha - x_b^\alpha)\dot{x}^\beta}
\end{aligned}
\tag{45}
$$

An alternative approach to the first term in the Lagrangian is to is to vary it directly and derive the equations of motion from scratch rather than using the Euler-Lagrange formula. The notation has now been introduced so we will not continue with the Riemannian Space-time summary.

Paper 4 & 5: These two papers [20,21] are referring entirely to the C-field, which was an addition of matter in order that the mass-density of the universe ρ remain constant as the universe expands. We are not interested in the C-field, since we do not require a static universe, and wish to treat the universe as not only expanding but accelerating in that expansion. We skip these two papers.

Paper 6, 7, & 8: Now we jump ahead to the full HN-theory and the fully Machian action, or in their words, the *full action.* The first of these [222] is a short paper including the C-field. This is not of so much interest. The next two papers [3,4] are the main papers with the theory we wish to use. These two papers should be read together. The HN-theory is given in *A new theory of gravitation* 1964 [3] with extra details in the 1966 paper [4] entitled *A conformal theory of gravitation.*

A summary of the new theory [3] follows with reference also to the extra detail in [4]. Particle interactions are propagated along null geodesics (at no distance in a 4 dimensional or light-like sense). According to HN the action developed thus far is of the form

$$
I = \frac{1}{16\pi G}\int R\sqrt{(-g)}d^4x - \sum_a m_a \int d\tau - \sum_a\sum_{b\neq a} 4\pi e_a e_b \int\int G_{\alpha\beta}dx_a^\alpha dx_b^\beta \tag{46}
$$

the first two terms looking very different that the direct particle interaction representing the electromagnetic last term. The term in m_a is derived from Galileo's concept of inertia and has been present since before Newton. Einstein retained this traditional term. Neither of the first two terms is correct, the first being a field or energy density the second being attributed to matter only. Only terms of the form using a double integral should be present. The first two terms have been artificially separated by traditional thinking. In what follows we construct a purely gravitational theory with the first and second terms combined into a single mass-energy term. It may also be possible to combine the electromagnetic term into the same term but we leave that for a later discussion. In order to convert the line integral $\int m_a d\tau$ into a sum of double line integrals we make the following assumptions:

(1) The mass $m_a = m(x_a)$ (mass at position x_a) must become a direct particle field, it must arise from all the other mass in the universe.

(2) Since mass is scalar we expect it to arise through a scalar Greens function.

(3) The action must be symmetric between any pairs of particles, [3].

Let each particle b give rise to a mass-field (*spherical monopole type g-waves*). Denote this field at a general point x by $m^{(\mathrm{b})}(x)$. At any point x_a on the path of particle a, we have $m^{(\mathrm{b})}(x_a)$ as the contribution of particle b to the mass of particle a at the position x_a. Summing for all b particles ,

$$
m(x_a) = m_a = \sum_b m^{(\mathrm{b})}(x_a) \tag{47}
$$

this gives the mass at point x_a due to all particles including those at position x_a. For electromagnetism we avoided positions where $x_a = x_b$ but for gravity we need not do this, [12] p109 Eq(46). The non-electromagnetic part of the action I_{mat} for many particles a,b... can be written in the form,

$$
I_{\mathrm{mat}} = -\frac{1}{2}\sum_a \int m(x_a)d\tau = -\sum_a\sum_b \int m^{(\mathrm{b})}(x_a)d\tau \tag{48}
$$

In order that (48) be symmetric for any particle pair a,b we must have $m^{(\mathrm{b})}(x_a)$ in the form

$$
m^{(\mathrm{b})}(x_a) = \int G(x_a, x_b)d\tau' \tag{49}
$$

so that

$$\int m^{(\mathrm{b})}(x_a)d\tau = \int\int G(x_a, x_b)d\tau d\tau' \tag{50}$$

where $G(x_a, x_b) = G(x_b, x_a)$ is a scalar Greens function. The mass function at a point x due to the world-line of particle a, at position x_a, is defined by

$$m^{(\mathrm{a})}(x) = \int G(x, x_a)d\tau \quad . \tag{51}$$

The mass function varies from point to point. *Before we plunge into the depths of HN-theory, let us first have a brief aside on the development of the field equations for the Einstein action, which is considerably easier!*

4. COMPARISON OF THE ACTIONS AND FIELD EQUATIONS.

4.1 The Einstein Action

For comparison we write down the basic Einstein Action, without the electromagnetic field,

$$I_{\mathrm{Einstein}} = \frac{1}{16\pi G}\int R[-g]^{1/2}d^4x - \sum_a m_a \int d\tau \quad . \tag{52}$$

The field equations are derived by varying the action and setting the variation equal to zero, [12] p112. The metric tensor will be varied according to $g_{\mu\nu} \to g_{\mu\nu} + \delta g_{\mu\nu}$ in a volume V with $\delta g_{\mu\nu} = 0$ at the boundaries. Varying the above action yields,

$$\begin{aligned}\delta I_{\mathrm{Einstein}} &= \frac{1}{16\pi G}\int \delta(R[-g]^{1/2})d^4x - \sum_a m_a \int \delta(d\tau) \\ &= \frac{1}{16\pi G}\int \delta(g^{\mu\nu}R_{\mu\nu}[-g]^{1/2})d^4x - \sum_a m_a \int \delta(d\tau) \quad .\end{aligned} \tag{53}$$

Using

$$\begin{aligned}-\sum_a m_a \int \delta(d\tau) &= \frac{1}{2}\int T_{\mu\nu}\delta g^{\mu\nu}[-g]^{1/2}d^4x \\ \delta\left([-g]^{1/2}\right) &= -\frac{1}{2}g_{\mu\nu}\delta g^{\mu\nu}[-g]^{1/2}\end{aligned} \tag{54}$$

Next we expand out the first term with the Ricci tensor,

$$\begin{aligned}\delta I_{\mathrm{Einstein}} = &\frac{1}{16\pi G}\int \delta(g^{\mu\nu}R_{\mu\nu})[-g]^{1/2}d^4x - \frac{1}{16\pi G}\int \frac{1}{2}Rg_{\mu\nu}\delta g^{\mu\nu}[-g]^{1/2}d^4x \\ &+\frac{1}{2}\int T_{\mu\nu}\delta g^{\mu\nu}[-g]^{1/2}d^4x \\ = &\frac{1}{16\pi G}\int \left[R_{\mu\nu} - \frac{1}{2}Rg_{\mu\nu} + 8\pi G T_{\mu\nu}\right]\delta g^{\mu\nu}[-g]^{1/2}d^4x \\ &+\frac{1}{16\pi G}\int g^{\mu\nu}\delta R_{\mu\nu}[-g]^{1/2}d^4x\end{aligned} \tag{55}$$

the last term is zero since the variation vanishes on the boundary. Hence by setting $\delta I_{\mathrm{Einstein}} = 0$ for any arbitrary variation $\delta g_{\mu\nu}$ we obtain the Einstein's field equations,

$$R_{\mu\nu} - \frac{1}{2}Rg_{\mu\nu} = -8\pi G T_{\mu\nu} \tag{56}$$

The familiar energy momentum tensor is easily derived, see Hoyle and Narlikar's book [12] p112. This follows from using $d\tau^2 = g_{\mu\nu}dx^\mu dx^\nu$ and thus $\delta(d\tau) = \delta g_{\mu\nu}\dot{x}^\mu \dot{x}^\nu d\tau$ which leads to

$$\begin{aligned} -\sum_a \int m(x_a)\delta(d\tau) &= -\sum_a \int m(x)\delta g_{\mu\nu}\dot{x}^\mu \dot{x}^\nu \delta^4(x-x_a)d\tau \\ &= -\int_V T^{\mu\nu}\delta g_{\mu\nu}[-g]^{1/2}d^4x = +\int_V T_{\mu\nu}\delta g^{\mu\nu}[-g]^{1/2}d^4x \\ \text{where } \ T^{\mu\nu} &= \sum_a \delta^4(x-x_a)[-g]^{-1/2}m(x)\dot{x}^\mu \dot{x}^\nu d\tau \ . \end{aligned} \tag{57}$$

The energy-stress tensor $T^{\mu\nu}$ is a sum over all the mass-energy in the universe, excluding the electromagnetic field which is treated separately. This is exactly the same calculation that will appear in the HN-theory later.

4.2 Quick note on scalar densities

Using J as the Jacobian (see Dirac's book on gravitation [11] p37),

$$\begin{aligned} dx^{\mu'} &= dx^\mu J \quad \text{or} \quad d^4x' = Jd^4x \\ J &= \frac{\partial x^{\mu'}}{\partial x^\alpha} \\ g_{\alpha\beta} &= \frac{\partial x^{\mu'}}{\partial x^\alpha} g_{\mu'\nu'} \frac{\partial x^{\nu'}}{\partial x^\beta} \ . \end{aligned} \tag{58}$$

The determinants satisfy,

$$\begin{aligned} g &= Jg'J \\ g &= J^2 g' \\ \Rightarrow \sqrt{-g} &= J\sqrt{-g'} \end{aligned} \tag{59}$$

since $g = \|g_{\alpha\beta}\|$ is negative. That makes $\sqrt{-g}$ a positive quantity. Hence we may define the following invariant quantity for any scalar density, for example $H \to T_{\mu\nu}\delta g^{\mu\nu}$,

$$\begin{aligned} \int_V H\sqrt{-g}d^4x &= \int_V H\sqrt{-g'}Jd^4x = \int_V H'\sqrt{-g'}d^4x' \\ \text{hence } \ \int_V T_{\mu\nu}\delta g^{\mu\nu}\sqrt{-g}d^4x &= \quad \text{invariant} \ . \end{aligned} \tag{60}$$

4.3 The HN-Theory Action

Omitting the electromagnetic field for now, using the definitions (47) and (50), the action can be written, following Hoyle-Narlikar "A New Theory of Gravitation", [3], as:

$$I = -\sum_a \frac{1}{2}\int m(x_a)d\tau = -\sum_a \sum_b \int\int G(x_a, x_b)d\tau d\tau' \tag{61}$$

There is just one term, a sum over all the masses in the universe. The energy is not separated out, because of mass-energy equivalence. This requires that a "universe" consist of at least two particles for them to interact and create a space-time between them. The factor 1/2 comes in because each $G(x_a, x_b)$ is shared by two particles a and b. This makes no difference to the equations of motion. The paper has no factor of 1/2 in front of the double sum, whereas the HN book does have the factor of 1/2. The most general wave equation is

$$g^{\mu\nu}G(x, x_a)_{;\mu\nu} + \mu R G(x, x_a) = -[-g]^{-1/2}\delta^4(x - x_a) \tag{62}$$

in which R is the Ricci scalar and μ is a constant taken later to be 1/6 since the wave equation is then conformally invariant [23]. The next step is to vary the geometry in a finite volume V, $g_{\mu\nu} \to g_{\mu\nu} + \delta g_{\mu\nu}$ with $\delta g_{\mu\nu} = 0$ on the boundary. It will be shown that

$$\delta I = \int P_{\mu\nu} \delta g^{\mu\nu} [-g]^{1/2} d^4x \tag{63}$$

where $P_{\mu\nu}$ is a symmetric tensor. The formalism becomes a theory when we assert that $\delta I = 0$ which requires

$$P_{\mu\nu} = 0 \tag{64}$$

which are the field equations of the new theory.

4.4 Field equation for HN-theory

Now for the field equations, [3]. Consider the change in $G(x_a, x_b)$ due to an infinitesimal change $\delta g_{\mu\nu}$ in $g_{\mu\nu}$ over a finite volume V, with $\delta g_{\mu\nu} = 0$ on the boundary of V. By dividing throughout by $[-g]^{-1/2}$, the equation for the Greens function $G(x, x_a)$ can be written as,

$$\frac{\partial}{\partial x^\mu}\left[[-g]^{1/2} g^{\mu\nu} \frac{\partial G(x, x_a)}{\partial x^\nu}\right] + \mu R [-g]^{1/2} G(x, x_a) = -\delta^4(x - x_a) \tag{65}$$

The variation can be made by setting $G \to G + \delta G$ and $g^{\mu\nu} \to g^{\mu\nu} + \delta g^{\mu\nu}$, and this becomes,

$$\frac{\partial}{\partial x^\mu}\left[[-g]^{1/2} g^{\mu\nu} \frac{\partial \delta G}{\partial x^\nu}\right] + \mu R [-g]^{1/2} \delta G = -\frac{\partial}{\partial x^\mu}\left[\delta([-g]^{1/2} g^{\mu\nu}) \frac{\partial G}{\partial x^\nu}\right] - \mu \delta(R[-g]^{1/2}) G \tag{66}$$

This agrees with Eq (71) in the HN book, [12] p113-114. It appears that δG satisfies the same differential operator as $G(x, x_a)$ itself, but with a distributed source term, not a δ-function at point x_a. The solution for δG can be written down as follows, (see [26] for first use of this solution on the scalar Greens function p186)

$$\begin{aligned}
\delta G(x_a, x_b) &= \int_V \frac{\partial}{\partial x^\mu}\left[\delta([-g]^{1/2} g^{\mu\nu}) \frac{\partial G(x_a, x)}{\partial x^\nu}\right] G(x_b, x) d^4x \\
&\quad + \mu \int_V \delta(R[-g]^{1/2}) G(x_a, x) G(x_b, x) d^4x \\
&= -\int_V \delta([-g]^{1/2} g^{\mu\nu}) \frac{\partial G(x_a, x)}{\partial x^\nu} \frac{\partial G(x_b, x)}{\partial x^\mu} d^4x \\
&\quad + \mu \int_V \delta(R[-g]^{1/2}) G(x_a, x) G(x_b, x) d^4x
\end{aligned} \tag{67}$$

where we have integrated the first term by parts and set $\delta g^{\mu\nu} = 0$ at the boundary of the volume. This agrees with Eq (12) in [3] (and Eq (72) in the HN book). The variation of the action then becomes

$$\begin{aligned}
\delta I &= -\frac{1}{2} \sum_a \int m(x_a) \delta(d\tau) - \frac{1}{2} \sum_a \int \delta m(x_a) d\tau \\
&= -\frac{1}{2} \sum_a \int m(x_a) \delta(d\tau) - \sum_a \sum_b \int \int \delta G(x_a, x_b) d\tau d\tau' \\
&= -\frac{1}{2} \sum_a \int m(x_a) \delta(d\tau) - \sum_a \sum_b \int_V \int \int \delta([-g]^{1/2} g^{\mu\nu}) \frac{\partial G(x_a, x)}{\partial x^\nu} \frac{\partial G(x_b, x)}{\partial x^\mu} d^4x d\tau d\tau' \\
&\quad + \mu \sum_a \sum_b \int_V \int \int \delta(R[-g]^{1/2}) G(x_a, x) G(x_b, x) d^4x d\tau d\tau'
\end{aligned} \tag{68}$$

Using the earlier definitions of mass at point x due to the world-lines of particle a and particle b, Eq.(236),

$$m^{(a)}(x) = \int G(x_a, x) d\tau$$
$$m^{(b)}(x) = \int G(x_b, x) d\tau'$$

we arrive at

$$\delta I = -\frac{1}{2}\sum_a \int m(x_a)\delta(d\tau) - \sum_a\sum_b \int_V \delta([-g]^{1/2} g^{\mu\nu}) \frac{\partial m^{(a)}(x)}{\partial x^\nu}\frac{\partial m^{(b)}(x)}{\partial x^\mu} d^4x$$
$$+ \mu \sum_a\sum_b \int_V \delta(R[-g]^{1/2}) m^{(a)}(x) m^{(b)}(x) d^4x \tag{69}$$

This agrees with Eq (13) in [3]. There are typos in the papers making these look like covariant derivatives when they are only partial derivatives.

The first term in the variation of the action, Eq. (69) is the familiar energy momentum tensor for mass-energy. This follows from using $d\tau^2 = g_{\mu\nu} dx^\mu dx^\nu$:

$$-\sum_a \int m(x_a)\delta(d\tau) = -\sum_a \int m(x)\delta g_{\mu\nu}\dot{x}^\mu \dot{x}^\nu \delta^4(x - x_a) d\tau$$
$$= -\int_V T^{\mu\nu}\delta g_{\mu\nu}[-g]^{1/2} d^4x = \int_V T_{\mu\nu}\delta g^{\mu\nu}[-g]^{1/2} d^4x$$
$$\text{where } T^{\mu\nu} = \sum_a \delta^4(x - x_a)[-g]^{-1/2} m(x)\dot{x}^\mu \dot{x}^\nu d\tau \tag{70}$$

This is exactly the same as for the Einstein action treated earlier. This does not include the electromagnetic fields which are treated separately.

At this point rather than follow the paper [3], it appeared quicker to follow the book [12]. We take up the derivation there. In order to compare the older paper [3] with the more recent text book [12] we return to the variation of the Greens function Eq (66). The book uses $\mu = 1/6$ and has a factor of 1/2 in front of the double sum, so the following terms will have a multiplicative factor 1/2 throughout. We may split the Green function into advanced and retarded parts, [12] p114 Eq (73),

$$G(x, x_b) = \frac{1}{2}\left[G^{\text{ret}}(x, x_b) + G^{\text{adv}}(x, x_b)\right] . \tag{71}$$

The retarded part gives the following contribution to $\delta G(x_a, x_b)$, see earlier Eq (67),

$$\delta G^{\text{ret}}(x_a, x_b) = -\frac{1}{2}\int_V G^{\text{ret}}(x_a, x)\frac{\partial}{\partial x^\mu}\left[\delta([-g]^{1/2} g^{\mu\nu})\frac{\partial G^{\text{ret}}(x, x_b)}{\partial x^\nu}\right] d^4x$$
$$-\frac{1}{12}\int_V \delta(R[-g]^{1/2}) G^{\text{ret}}(x_a, x) G^{\text{ret}}(x, x_b) d^4x \tag{72}$$

where $G^{\text{ret}}(x_a, x) = G^{\text{adv}}(x, x_a)$.

The equation for δG^{ret} above, can be written more symmetrically by integrating the first term by parts,

$$\delta G^{\text{ret}} = \frac{1}{2}\int_V \delta([-g]^{1/2} g^{\mu\nu})\frac{\partial G^{\text{adv}}(x, x_a)}{\partial x^\mu}\frac{\partial G^{\text{ret}}(x, x_b)}{\partial x^\nu} d^4x$$
$$-\frac{1}{12}\int_V \delta(R[-g]^{1/2}) G^{\text{adv}}(x, x_a) G^{\text{ret}}(x, x_b) d^4x \tag{73}$$

This agrees with the book [12] p115, Eq. (77). The advanced part of δG is similar with the advanced and retarded G's switched

$$\delta G^{\text{adv}} = \frac{1}{2}\int_V \delta([-g]^{1/2} g^{\mu\nu})\frac{\partial G^{\text{ret}}(x, x_a)}{\partial x^\mu}\frac{\partial G^{\text{adv}}(x, x_b)}{\partial x^\nu} d^4x$$
$$-\frac{1}{12}\int_V \delta(R[-g]^{1/2}) G^{\text{ret}}(x, x_a) G^{\text{adv}}(x, x_b) d^4x \tag{74}$$

The full expression for $\delta G(x_a, x_b)$ is the sum of the advanced and retarded parts. The next step is to find the variation of the action,

$$\sum_a \sum_b \int \int \delta G(x_a, x_b) d\tau d\tau' \ . \tag{75}$$

Here we introduce the mass field from p115 [112],

$$\begin{aligned} m(x) &= \frac{1}{2}\left[m^{(\mathrm{ret})}(x) + m^{(\mathrm{adv})}(x)\right] \\ m^{(\mathrm{ret})}(x) &= \sum_a \int G^{(\mathrm{ret})}(x, x_a) d\tau \\ m^{(\mathrm{adv})}(x) &= \sum_a \int G^{(\mathrm{adv})}(x, x_a) d\tau \end{aligned} \tag{76}$$

The variation of G becomes,

$$\begin{aligned} \sum_a \sum_b \int \int \delta G(x_a, x_b) d\tau d\tau' = &\frac{1}{2} \sum_a \sum_b \int_V \int \int \delta([-g]^{1/2} g^{\mu\nu}) \left[\frac{\partial G^{\mathrm{adv}}(x, x_a)}{\partial x^\mu} \frac{\partial G^{\mathrm{ret}}(x, x_b)}{\partial x^\nu}\right. \\ &+ \left.\frac{\partial G^{\mathrm{ret}}(x, x_a)}{\partial x^\mu} \frac{\partial G^{\mathrm{adv}}(x, x_b)}{\partial x^\nu}\right] d^4x d\tau d\tau' \\ &- \frac{1}{12} \sum_a \sum_b \int_V \int \int \delta(R[-g]^{1/2}) \left[G^{\mathrm{adv}}(x, x_a) G^{\mathrm{ret}}(x, x_b)\right. \\ &+ \left.G^{\mathrm{ret}}(x, x_a) G^{\mathrm{adv}}(x, x_b)\right] d^4x d\tau d\tau' \end{aligned} \tag{77}$$

Note that each term has one sum over a and one over b, so when we substitute in the mass fields all the summations are used.

$$\begin{aligned} \sum_a \sum_b \int \int \delta G(x_a, x_b) d\tau d\tau' = &\frac{1}{2} \int_V \delta([-g]^{1/2} g^{\mu\nu}) \left[\frac{\partial m^{\mathrm{adv}}}{\partial x^\mu} \frac{\partial m^{\mathrm{ret}}}{\partial x^\nu} + \frac{\partial m^{\mathrm{ret}}}{\partial x^\mu} \frac{\partial m^{\mathrm{adv}}}{\partial x^\nu}\right] d^4x \\ &- \frac{1}{12} \int_V \delta(R[-g]^{1/2}) \left[m^{\mathrm{adv}} m^{\mathrm{ret}} + m^{\mathrm{ret}} m^{\mathrm{adv}}\right] d^4x \end{aligned} \tag{78}$$

We may therefore simplify the δI to remove the summations. Here is a full summary so far:

$$\begin{aligned} \delta I &= -\frac{1}{2} \delta \left[\sum_a \int m(x_a) d\tau\right] \\ &= -\frac{1}{2} \sum_a m(x_a) \delta(d\tau) - \frac{1}{2} \sum_a \int \delta m(x_a) d\tau \\ &= -\frac{1}{2} \int_V T^{\mu\nu} \delta g_{\mu\nu} [-g]^{1/2} d^4x - \frac{1}{2} \sum_a \sum_b \int \int \delta G(x_a, x_b) d\tau d\tau' \\ &= +\frac{1}{2} \int_V T_{\mu\nu} \delta g^{\mu\nu} [-g]^{1/2} d^4x - \frac{1}{2} \int_V \delta([-g]^{1/2} g^{\mu\nu}) \left[\frac{\partial m^{\mathrm{adv}}}{\partial x^\mu} \frac{\partial m^{\mathrm{ret}}}{\partial x^\nu}\right] d^4x \\ &\quad + \frac{1}{12} \int_V \delta(R[-g]^{1/2}) \left[m^{\mathrm{adv}} m^{\mathrm{ret}}\right] d^4x \end{aligned} \tag{79}$$

where we have replaced the first term with the familiar energy-stress tensor expression and flipped from contravariant to covariant notation with a minus sign change. The second term in the above equation can be expanded to give;

$$
\begin{aligned}
\delta([\frac{1}{2}g]^{1/2}g^{\mu\nu})\frac{\partial m^{\mathrm{adv}}}{\partial x^{\mu}}\frac{\partial m^{\mathrm{ret}}}{\partial x^{\nu}} &= \\
-\frac{1}{2}\left[\delta[-g]^{1/2}g^{\alpha\beta}\frac{\partial m^{\mathrm{adv}}}{\partial x^{\alpha}}\frac{\partial m^{\mathrm{ret}}}{\partial x^{\beta}} + [-g]^{1/2}\delta g^{\mu\nu}\frac{\partial m^{\mathrm{adv}}}{\partial x^{\mu}}\frac{\partial m^{\mathrm{ret}}}{\partial x^{\nu}}\right] \\
= \frac{1}{2}\left[\left(\frac{1}{2}g_{\mu\nu}\delta g^{\mu\nu}[-g]^{1/2}\right)g^{\alpha\beta}\frac{\partial m^{\mathrm{adv}}}{\partial x^{\alpha}}\frac{\partial m^{\mathrm{ret}}}{\partial x^{\beta}}\right] \\
-[-g]^{1/2}\delta g^{\mu\nu}\frac{1}{2}\left[\frac{\partial m^{\mathrm{adv}}}{\partial x^{\mu}}\frac{\partial m^{\mathrm{ret}}}{\partial x^{\nu}} + \frac{\partial m^{\mathrm{adv}}}{\partial x^{\nu}}\frac{\partial m^{\mathrm{ret}}}{\partial x^{\mu}}\right] \qquad (80)
\end{aligned}
$$

where we have used the following useful identity [12] p 113, in the last step

$$
\delta[-g]^{1/2} = -\frac{1}{2}g_{\mu\nu}\delta g^{\mu\nu}[-g]^{1/2} \qquad (81)
$$

The $\delta(R[-g]^{1/2})$ term in δI can be expanded also as follows;

$$
\begin{aligned}
\frac{1}{6}\delta(R[-g]^{1/2}) &= \frac{1}{6}\delta(R_{\mu\nu}g^{\mu\nu}[-g]^{1/2}) \\
&= \frac{1}{6}\left[\delta(g^{\mu\nu}R_{\mu\nu})[-g]^{1/2} + R\delta([-g]^{1/2})\right] \qquad (82)
\end{aligned}
$$

using the Eq (81) again for the last term we find,

$$
\begin{aligned}
\frac{1}{6}\delta(R[-g]^{1/2}) &= \frac{1}{6}\left[R_{\mu\nu}[-g]^{1/2}\delta g^{\mu\nu} + g^{\mu\nu}\delta R_{\mu\nu}[-g]^{1/2} - \frac{1}{2}Rg_{\mu\nu}[-g]^{1/2}\delta g^{\mu\nu}\right] \\
&= \frac{1}{6}\left[\left(R_{\mu\nu} - \frac{1}{2}Rg_{\mu\nu}\right)\delta g^{\mu\nu}[-g]^{1/2} + g^{\mu\nu}\delta R_{\mu\nu}[-g]^{1/2}\right] \qquad (83)
\end{aligned}
$$

hence the contribution to δI becomes

$$
\begin{aligned}
\frac{1}{6}\int_V \delta(R[-g]^{1/2})\left[m^{\mathrm{adv}}m^{\mathrm{ret}}\right]d^4x &= \frac{1}{6}\int_V\left(R_{\mu\nu} - \frac{1}{2}Rg_{\mu\nu}\right)\delta g^{\mu\nu}[-g]^{1/2}\left[m^{\mathrm{adv}}m^{\mathrm{ret}}\right] \\
&+ \frac{1}{6}\int_V g^{\mu\nu}\delta R_{\mu\nu}[-g]^{1/2}\left[m^{\mathrm{adv}}m^{\mathrm{ret}}\right]d^4x \qquad (84)
\end{aligned}
$$

We will treat the $\delta R_{\mu\nu}$ term separately, it does not go to zero as in the Einstein case *unfortunately!*.

$$
\begin{aligned}
\frac{1}{12}\int_V g^{\mu\nu}\delta R_{\mu\nu}[-g]^{1/2}\left[m^{\mathrm{adv}}m^{\mathrm{ret}}\right]d^4x &= \frac{1}{2}\int \theta_{\mu\nu}\delta g^{\mu\nu}[-g]^{1/2}d^4x \\
\theta_{\mu\nu} &= \frac{1}{6}\frac{g^{\mu\nu}}{\delta g^{\mu\nu}}\delta R_{\mu\nu}m^{\mathrm{adv}}m^{\mathrm{ret}} \qquad (85)
\end{aligned}
$$

The shorthand for δI then becomes,

$$
\begin{aligned}
\delta I = &+\frac{1}{2}\int_V T_{\mu\nu}\delta g^{\mu\nu}[-g]^{1/2}d^4x \\
&+\frac{1}{2}\left[\left(\frac{1}{2}g_{\mu\nu}\delta g^{\mu\nu}[-g]^{1/2}\right)g^{\alpha\beta}\frac{\partial m^{\mathrm{adv}}}{\partial x^{\alpha}}\frac{\partial m^{\mathrm{ret}}}{\partial x^{\beta}}\right] \\
&\quad -[-g]^{1/2}\delta g^{\mu\nu}\frac{1}{2}\left[\frac{\partial m^{\mathrm{adv}}}{\partial x^{\mu}}\frac{\partial m^{\mathrm{ret}}}{\partial x^{\nu}} + \frac{\partial m^{\mathrm{adv}}}{\partial x^{\nu}}\frac{\partial m^{\mathrm{ret}}}{\partial x^{\mu}}\right] \\
&+\frac{1}{6}\int_V\left(R_{\mu\nu} - \frac{1}{2}Rg_{\mu\nu}\right)\delta g^{\mu\nu}[-g]^{1/2}\left[m^{\mathrm{adv}}m^{\mathrm{ret}}\right] \\
&+\frac{1}{2}\int \theta_{\mu\nu}\delta g^{\mu\nu}[-g]^{1/2}d^4x = 0\,. \qquad (86)
\end{aligned}
$$

The field equations are then seen to be,

$$T_{\mu\nu} + \theta_{\mu\nu} + \frac{1}{6}(R_{\mu\nu} - \frac{1}{2}g_{\mu\nu}R)m^{\text{adv}}m^{\text{ret}}$$
$$-\frac{1}{2}\left[\frac{\partial m^{\text{adv}}}{\partial x^{\mu}}\frac{\partial m^{\text{ret}}}{\partial x^{\nu}} + \frac{\partial m^{\text{adv}}}{\partial x^{\nu}}\frac{\partial m^{\text{ret}}}{\partial x^{\mu}} - g_{\mu\nu}g^{\alpha\beta}\frac{\partial m^{\text{adv}}}{\partial x^{\alpha}}\frac{\partial m^{\text{ret}}}{\partial x^{\beta}}\right] = 0 \tag{87}$$

What remains is to expand $\theta_{\mu\nu}$ in its full glory. See the Addendum for details.
After some trivial algebra, which is obvious to the most casual observer, and only takes a couple of pages of calculation we get...

$$\theta_{\mu\nu} = -\frac{1}{6}\left[g_{\mu\nu}\Box^2(m^{\text{adv}}m^{\text{ret}}) - (m^{\text{adv}}m^{\text{ret}})_{,\mu\nu}\right] \tag{88}$$

where $\Box^2$ is the wave equation $\partial_{\mu}\partial^{\mu}$.

5. DERIVATION OF WOODWARD'S MASS CHANGE FORMULA

5.1 Woodward's Power Equation → mass change formula

From Woodward's book [24], page 73 Eq(3.5), we find;

$$\delta m = \frac{1}{4\pi G}\left[\frac{1}{\rho_0 c^2}\frac{\partial P}{\partial t} - \left(\frac{1}{\rho_0 c^2}\right)^2\frac{P^2}{V}\right]$$
$$\delta m = \frac{1}{4\pi G}\left[\frac{V}{m_0 c^2}\frac{\partial^2 \varepsilon}{\partial t^2} - \left(\frac{V}{m_0 c^2}\right)^2\frac{1}{V}\left(\frac{\partial \varepsilon}{\partial t}\right)^2\right]$$
$$= \frac{1}{4\pi G}\left[\frac{V}{m_0}\frac{\partial^2 m}{\partial t^2} - V\left(\frac{1}{m_0}\right)^2\left(\frac{\partial m}{\partial t}\right)^2\right]$$
$$\frac{\delta m}{V} = \frac{1}{4\pi G}\left[\frac{1}{m_0}\frac{\partial^2 m}{\partial t^2} - \left(\frac{1}{m_0}\right)^2\left(\frac{\partial m}{\partial t}\right)^2\right] \tag{89}$$

where V is volume over the device, P is power to the device, and $P = d\varepsilon/dt$. Energy is $\varepsilon = mc^2$ and mass density $\rho_0 = m_0/V$. This agrees with the dimensions of $[G] = [FL^2/M^2]$.

5.2 HN-theory field equation → mass change formula

Let's define the HN-field equation (in a smooth fluid) as follows (which agrees with Eq.(16) in reference [4]) by grouping terms together;

$$R_{\alpha\beta} - \frac{1}{2}g_{\alpha\beta}R = -8\pi G(T_{\alpha\beta} + \delta T_{\alpha\beta}) \quad \text{where}$$
$$-(8\pi G)\delta T_{\alpha\beta} = \frac{2}{m}(g_{\alpha\beta}g^{\mu\nu}m_{;\mu\nu} - m_{;\alpha\beta}) + \frac{4}{m^2}(m_{;\alpha}m_{;\beta} - \frac{1}{4}m_{;\gamma}m^{;\gamma}g_{\alpha\beta}) \tag{90}$$

Now we expand the terms out. Let us put back in c and not set it equal to one, which can be confusing. The terms in μ, ν mix the time and spatial derivatives in an unexpected way.

Consider first the T_{00} and T_{jj} terms separately, using flat metric (+1,-1,-1,-1),

$$
\begin{aligned}
-\frac{8\pi G}{c^4}\delta T_{00} &= \frac{2}{m}\left[g_{00}\left(\frac{g^{00}}{c^2}\frac{\partial^2 m}{\partial t^2} + g^{jj}\frac{\partial^2 m}{\partial x_j^2}\right) - \frac{1}{c^2}\frac{\partial^2 m}{\partial t^2}\right] \\
&+\frac{4}{m^2}\left[\frac{1}{c^2}\left(\frac{\partial m}{\partial t}\right)^2 - \frac{g_{00}}{4}\left(\frac{1}{c^2}\left(\frac{\partial m}{\partial t}\right)^2 - \left(\frac{\partial m}{\partial x_j}\right)^2\right)\right] \\
&= \frac{2}{m}\left[\cancel{\frac{1}{c^2}\frac{\partial^2 m}{\partial t^2}} - \frac{\partial^2 m}{\partial x_j^2} - \cancel{\frac{1}{c^2}\frac{\partial^2 m}{\partial t^2}}\right] \\
&+\frac{1}{m^2}\left[\frac{4}{c^2}\left(\frac{\partial m}{\partial t}\right)^2 - \frac{1}{c^2}\left(\frac{\partial m}{\partial t}\right)^2 + \left(\frac{\partial m}{\partial x_j}\right)^2\right] \\
&= -\frac{2}{m}\frac{\partial^2 m}{\partial x_j^2} + \frac{1}{m^2}\left(\frac{\partial m}{\partial x_j}\right)^2 + \frac{3}{m^2c^2}\left(\frac{\partial m}{\partial t}\right)^2
\end{aligned}
\tag{91}
$$

where we treat the derivatives with respect to $\partial/\partial x_j$ as a 3 component gradient-like term.

$$
\begin{aligned}
-\frac{8\pi G}{c^4}\delta T_{jj} &= \frac{2}{m}\left[g_{jj}\left(\frac{g^{00}}{c^2}\frac{\partial^2 m}{\partial t^2} + g^{jj}\frac{\partial^2 m}{\partial x_j^2}\right) - \frac{\partial^2 m}{\partial x_j^2}\right] \\
&+\frac{4}{m^2}\left[\left(\frac{\partial m}{\partial x_j}\right)^2 - \frac{g_{jj}}{4}\left(\frac{1}{c^2}\left(\frac{\partial m}{\partial t}\right)^2 - \left(\frac{\partial m}{\partial x_j}\right)^2\right)\right] \\
&= \frac{2}{m}\left[-\frac{1}{c^2}\frac{\partial^2 m}{\partial t^2} + \cancel{\frac{\partial^2 m}{\partial x_j^2}} - \cancel{\frac{\partial^2 m}{\partial x_j^2}}\right] \\
&+\frac{1}{m^2}\left[4\left(\frac{\partial m}{\partial x_j}\right)^2 + \frac{1}{c^2}\left(\frac{\partial m}{\partial t}\right)^2 - \left(\frac{\partial m}{\partial x_j}\right)^2\right] \\
&= -\frac{2}{mc^2}\frac{\partial^2 m}{\partial t^2} + \frac{3}{m^2}\left(\frac{\partial m}{\partial x_j}\right)^2 + \frac{1}{m^2c^2}\left(\frac{\partial m}{\partial t}\right)^2
\end{aligned}
\tag{92}
$$

where $j = 1, 2$ or 3. Now take the trace of $T_{\alpha\alpha}$ where $\alpha = 0, 1, 2, 3$ by adding the last two equations.

$$
\begin{aligned}
-\frac{8\pi G}{c^4}\,\mathrm{Tr}(\delta T_{\alpha\alpha}) &= -\frac{2}{m}\frac{\partial^2 m}{\partial x_j^2} + \frac{4}{m^2}\left(\frac{\partial m}{\partial x_j}\right)^2 + \frac{4}{m^2c^2}\left(\frac{\partial m}{\partial t}\right)^2 - \frac{2}{mc}\frac{\partial^2 m}{\partial t^2} \\
\frac{1}{c^2}\,\mathrm{Tr}(\delta T_{\alpha\alpha}) &= \frac{1}{4\pi G}\left[\left\{\frac{1}{m}\frac{\partial^2 m}{\partial t^2} - \frac{2}{m^2}\left(\frac{\partial m}{\partial t}\right)^2\right\}\right. \\
&\left.+\left\{\frac{c^2}{m}\frac{\partial^2 m}{\partial x_j^2} - \frac{2c^2}{m^2}\left(\frac{\partial m}{\partial x_j}\right)^2\right\}\right]
\end{aligned}
\tag{93}
$$

where we assume we are summing over α and j. This last expression should be compared with the previous result Eq. (89) above. Note that there are also spatial terms here, which in previous papers I incorporated into the time derivatives [28]. I now think that was a mistake and have written them out explicitly here. This is the main result of the paper. Quoting from a paper [29] by R. Medina:

> "Unlike the inertia of energy, which is well known, many physicists are not aware of the inertia of pressure (stress). In many cases such an effect is negligible, but for the case of the stress produced by electrostatic interactions, it is comparable to the inertial effects of the electromagnetic fields. If the inertia of stress is neglected the calculations are inconsistent."

The spatial and temporal terms may be related, in the sense that in The Mach effect drive (or MEGA drive), PZT (lead zirconate titanate) expands and contracts. In a different device, that may not be the case.

6. CONCLUSIONS

The main result we wish to emphasize is the mass fluctuation, Eq. (93). Compare this with Woodward's result Eq. (89) from his book [24] p73, Eq. (3.5). The consequences of this mass fluctuation are *astounding* as related to the Woodward effect and propellant-less propulsion methods. A following paper in this chapter, by Rodal, will describe how to calculate a force using the mass fluctuation calculated here. The calculated force and resonant frequency predictions will be compared to experimental data.

Hoyle-Narlikar gravitation , or gravitational absorber theory (GAT), is a valid theory that is fully consistent with Einstein's GR. It is a fully Machian theory of gravitation, which means that the mass of a body depends on its gravitational interaction with all the other masses in the universe. Text books on Einstein's GR rarely if ever mention advanced waves, yet the are necessary if interactions with distant matter are to be thought of as instantaneous.
Around 1965 Hawking voiced an objection to HN-theory [27], but that objection is no longer valid due to the accelerating expansion of the universe [28]. Hoyle-Narlikar theory is to gravitation what Wheeler-Feynman absorber theory is to electromagnetism. Einstein's General Relativity (GR) remains valid and all the tests of Einstein's GR also remain valid and carry over to the HN theory presented here. The real difference is in the highly symmetric and simplified Lagrangian, which treats a mass as being influenced by all the other masses in the universe, and that is all. A real universe must therefore be made up of at least two masses.

ACKNOWLEDGEMENTS

HF thanks Lance Williams for helpful suggestions and for clarification of the introduction section. HF also thanks José Rodal for the suggestion of using the name *gravitational absorber theory* (GAT) as opposed to HN theory, to try and distance the basic theory from the ideas of static universe cosmology. Rodal also points out that GAT could stand for *gravitationally assisted trajectory* and I noticed it also could stand for *glorious awe-inspiring theory.*

Addendum

For those of you who just can't get enough algebra, here is the rest of the glorious details for the derivation of $\theta_{\mu\nu}$.

We need to expand out Eq. (85) and find the equation for $\theta_{\mu\nu}$;

$$\frac{1}{2}\int_V \theta_{\mu\nu}\delta g^{\mu\nu}[-g]^{1/2}d^4x = \frac{1}{12}\int_V (\delta R_{\mu\nu}g^{\mu\nu})m^{\mathrm{adv}}m^{\mathrm{ret}}[-g]^{1/2}d^4x$$

The term in the round bracket on the RHS of the equation can be written as, [12], p118 Eqs (98,99).

$$\begin{aligned}(g^{\mu\nu}\delta R_{\mu\nu}) &= \frac{1}{[-g]^{1/2}}\frac{\partial}{\partial x^\lambda}\left[[-g]^{1/2}w^\lambda\right] \\ w^\lambda &= (g^{\mu\nu}\delta\Gamma^\lambda_{\mu\nu} - g^{\mu\nu}\delta\Gamma^\nu_{\mu\nu})\end{aligned} \tag{94}$$

Hence we may write,

$$\begin{aligned}\frac{1}{12}\int_V (\delta R_{\mu\nu}g^{\mu\nu})m^{\mathrm{adv}}m^{\mathrm{ret}}[-g]^{1/2}d^4x &= \frac{1}{12}\int_V \frac{\partial}{\partial x^\lambda}\left[[-g]^{1/2}w^\lambda\right](m^{\mathrm{adv}}m^{\mathrm{ret}})d^4x \\ &= \frac{1}{12}\int_V w^\lambda\frac{\partial}{\partial x^\lambda}(m^{\mathrm{adv}}m^{\mathrm{ret}})[-g]^{1/2}d^4x\end{aligned} \tag{95}$$

where we have integrated by parts. This agrees with Eq (100) in Hoyle and Narlikar's book [12]. Using the following identities, from their book p118, w^λ can be expanded.

$$
\begin{aligned}
\Gamma^\nu_{\mu\nu} &= \frac{1}{[-g]^{1/2}}\frac{\partial}{\partial x^\mu}\left([-g]^{1/2}\right) \\
g^{\mu\nu}\Gamma^\lambda_{\mu\nu} &= -\frac{1}{[-g]^{1/2}}\frac{\partial}{\partial x^\nu}\left([-g]^{1/2}g^{\lambda\nu}\right) \\
\delta([-g]^{-1/2}) &= +\frac{1}{2}g_{\mu\nu}\delta g^{\mu\nu}[-g]^{-1/2} \\
\frac{\partial}{\partial x^\alpha}[-g]^{1/2} &= [-g]^{1/2}\Gamma^\beta_{\alpha\beta}
\end{aligned}
\tag{96}
$$

we will also be reusing the identity in Eq (81), which is also in reference [11] p50, Eq. (26.10).

Consider the following,

$$
\begin{aligned}
\delta(g^{\mu\nu}\Gamma^\lambda_{\mu\nu}) &= \delta g^{\mu\nu}\Gamma^\lambda_{\mu\nu} + g^{\mu\nu}\delta\Gamma^\lambda_{\mu\nu} \\
\Rightarrow w^\lambda &= (g^{\mu\nu}\delta\Gamma^\lambda_{\mu\nu} - g^{\mu\nu}\delta\Gamma^\nu_{\mu\nu}) \\
&= \delta(g^{\mu\nu}\Gamma^\lambda_{\mu\nu}) - \delta g^{\mu\nu}\Gamma^\lambda_{\mu\nu} - g^{\mu\nu}\delta\Gamma^\nu_{\mu\nu}
\end{aligned}
\tag{97}
$$

Now we need to consider the separate parts of the equation for w^λ and rewrite it;

$$
\begin{aligned}
\delta\Gamma^\nu_{\mu\nu} &= \delta([-g]^{-1/2})\frac{\partial}{\partial x^\mu}([-g]^{1/2}) + ([-g]^{-1/2})\frac{\partial}{\partial x^\mu}(\delta[-g]^{1/2}) \\
\delta(g^{\mu\nu}\Gamma^\lambda_{\mu\nu}) &= -\delta([-g]^{-1/2})\frac{\partial}{\partial x^\nu}([-g]^{1/2}g^{\lambda\nu}) - [-g]^{-1/2}\frac{\partial}{\partial x^\nu}[\delta([-g]^{1/2}g^{\lambda\nu})]
\end{aligned}
\tag{98}
$$

where we have differentiated the identities (96) above. Now we substitute these expression into the equation for w^λ to obtain,

$$
\begin{aligned}
w^\lambda = &-\delta g^{\mu\nu}\Gamma^\lambda_{\mu\nu} - \frac{1}{[-g]^{1/2}}\frac{\partial}{\partial x^\nu}[\delta([-g]^{1/2}g^{\lambda\nu})] - \frac{1}{[-g]^{1/2}}g^{\mu\lambda}\frac{\partial}{\partial x^\mu}[\delta[-g]^{1/2}] \\
&-g^{\alpha\lambda}\delta([-g]^{-1/2})\left[\frac{\partial}{\partial x^\alpha}[-g]^{1/2}\right] + \delta([-g]^{-1/2})[-g]^{1/2}g^{\alpha\beta}\Gamma^\lambda_{\alpha\beta}
\end{aligned}
\tag{99}
$$

Now we only need to substitute the following identities,

$$
\begin{aligned}
\delta([-g]^{1/2}) &= -\frac{1}{2}g_{\mu\nu}\delta g^{\mu\nu}[-g]^{1/2} \\
\delta([-g]^{-1/2}) &= +\frac{1}{2}g_{\mu\nu}\delta g^{\mu\nu}[-g]^{-1/2} \\
\frac{\partial}{\partial x^\alpha}[-g]^{1/2} &= [-g]^{1/2}\Gamma^\beta_{\alpha\beta}
\end{aligned}
\tag{100}
$$

to obtain the needed result for w^λ,

$$
\begin{aligned}
w^\lambda = &-\delta g^{\mu\nu}\Gamma^\lambda_{\mu\nu} - \frac{1}{[-g]^{1/2}}\frac{\partial}{\partial x^\nu}\left[\delta([-g]^{1/2}g^{\lambda\nu})\right] - \frac{1}{[-g]^{1/2}}g^{\mu\lambda}\frac{\partial}{\partial x^\mu}\left[\delta[-g]^{1/2}\right] \\
&-\frac{1}{2}g^{\alpha\lambda}\Gamma^\beta_{\alpha\beta}g_{\mu\nu}\delta g^{\mu\nu} + \frac{1}{2}\delta g^{\mu\nu}g_{\mu\nu}g^{\alpha\beta}\Gamma^\lambda_{\alpha\beta}
\end{aligned}
\tag{101}
$$

which agrees with Eq (102) p118 [12]. Now at this point, this wonderful expression for w^λ must be placed back inside the integral (276), because we need to find the result for $\theta_{\mu\nu}$. The three terms involving Christoffel symbols cancel out. You can integrate by parts and use the divergence theorem. The only remaining terms involve differentiations on the mass functions only.

$$\frac{1}{2}\int \theta_{\mu\nu}\delta g^{\mu\nu}[-g]^{1/2}d^4x = -\frac{1}{6}\int\left(-\frac{1}{[-g]^{1/2}}\frac{\partial}{\partial x^{\alpha}}\left[\delta([-g]^{1/2}g^{\lambda\alpha})\right] - \frac{1}{[-g]^{1/2}}g^{\alpha\lambda}\frac{\partial}{\partial x^{\alpha}}\left[\delta[-g]^{1/2}\right]\right) \times \frac{\partial}{\partial x^{\lambda}}(m^{\text{adv}}m^{\text{ret}})[-g]^{1/2}d^4x \tag{102}$$

Expand out the first term and substitute for the $\delta[-g]^{1/2} = -\frac{1}{2}g_{\mu\nu}\delta g^{\mu\nu}[-g]^{1/2}$, then the $[-g]^{1/2}$ terms cancel out.

$$\Rightarrow \theta_{\mu\nu}\delta g^{\mu\nu} = \left(-\frac{1}{12}g^{\lambda\alpha}g_{\mu\nu}\delta g^{\mu\nu}\frac{\partial}{\partial x^{\alpha}} - \frac{1}{12}g^{\alpha\lambda}g_{\mu\nu}\delta g^{\mu\nu}\frac{\partial}{\partial x^{\alpha}}\right)\frac{\partial}{\partial x^{\lambda}}(m^{\text{adv}}m^{\text{ret}}) + \frac{1}{6}\delta g^{\lambda\alpha}\frac{\partial}{\partial x^{\alpha}}\frac{\partial}{\partial x^{\lambda}}(m^{\text{adv}}m^{\text{ret}}) \tag{103}$$

Now we must substitute $\delta g^{\lambda\alpha} \rightarrow \delta g^{\mu\nu}$ to match the LHS of the equation in the last term. Performing contractions over α on the first two terms, leads to,

$$\begin{aligned} \theta_{\mu\nu} &= -\frac{1}{6}\left(g_{\mu\nu}\frac{\partial^2}{\partial x^{\lambda}\partial x_{\lambda}}(m^{\text{adv}}m^{\text{ret}}) - \frac{\partial^2}{\partial x^{\mu}\partial x^{\nu}}(m^{\text{adv}}m^{\text{ret}})\right) \\ \text{thus } \theta_{\mu\nu} &= -\frac{1}{6}\left(g_{\mu\nu}\Box^2(m^{\text{adv}}m^{\text{ret}}) - (m^{\text{adv}}m^{\text{ret}})_{,\mu\nu}\right)\ . \end{aligned} \tag{104}$$

REFERENCES

[1] J. A. Wheeler and R. P., Feynman, "Interaction with the absorber as a mechanism of radiation", Rev. Mod. Phys. **17** 157 (1945).

[2] J. E. Hogarth, " Considerations of the Absorber Theory of Radiation", Proc. Roy. Soc. **A267**, pp365-383 (1962).

[3] F. Hoyle and J. V. Narlikar, "A new theory of gravitation", Proc. Roy. Soc. Lon. **A282**, 191 (1964).

[4] F. Hoyle and J. V. Narlikar, "A Conformal theory of gravitation", Proc. Roy. Soc. Lon. **A294**, 138 (1966).

[5] P. A. M. Dirac, "Classical theory of radiating electrons", Proc. Roy. Soc. Lon. **A167**, 148 (1938).

[6] J. D. Jackson, "*Classical Electrodynamics*", 3rd edition, John Wiley and Sons, Inc. p771, (1999).

[7] H. Tetrode, Zeits. fur Physik, **10**, 317 (1922).

[8] G. N. Lewis, Nat. Acad. Sci. Proc. **12**, 22 (1926).

[9] Cramer, J. G. "The transactional Interpretation of quantum mechanics." Rev. Mod. Phys. **58**, 647 (1986)

[10] Cramer, J. G. *The Quantum Handshake, Entanglement, Nonlocality and Transactions.* Springer, Berlin (2015)

[11] P. A. M. Dirac, *"General Theory of Relativity"*, Princeton Landmarks in Physics, (Princeton Univ. Press 1996.) p 16 for geodesic derivation.

[12] F. Hoyle and J. V. Narlikar, "*Action at a distance in Physics and Cosmology*" W. H. Freeman and Company, San Francisco, 1974.

[13] F. Hoyle and J. V. Narlikar, "Mach's Principle and the Creation of Matter", Proc. Roy. Soc. Lon. **A270**, pp334-341 (1962).

[14] F. Hoyle and J. V. Narlikar, "Mach's principle and the creation of matter", Proc. Roy. Soc. Lon. **A273**, pp1-11 (1963).

[15] Sciama, D. W. , "Retarded potentials and the expansion of the universe", Proc. Roy. Soc. Lond. **A273**, pp484-495 (1963).

[16] F. Hoyle and J. V. Narlikar, "Time Symmetric Electrodynamics and the Arrow of Time in Cosmology", Proc. Roy. Soc. Lon. **A277**, pp 1-23 (1964).

[17] Fokker, A. D. Zeit. fur Physik, **58**, 386 (1929).

[18] Schwarzschild K., Nachr. Ges. Wiss. Gottingen **128**, 132 (1903).

[19] A.O. Barut, *" Electrodynamics and classical ttheory of fields and particles"*, pp213-220 (Dover Publications Inc. New York 1964).

[20] F. Hoyle and J. V. Narlikar, "On the Avoidance of Singularities in C-field Cosmology", Proc. Roy. Socv. Lon. **A278**, pp465-478 (1964).

[21] F. Hoyle and J. V. Narlikar, "The C-field as a Direct Particle Field", Proc. Roy. Soc. Lon. **A282**, pp 178-183 (1964).

[22] F. Hoyle and J. V. Narlikar, "On the gravitational influence of direct particle fields", Proc. Roy. Soc. Lon. **A282**, 184 (1964). See also "A conformal theory of gravitation", Proc. Roy. Soc. Lon. **A294**, 138 (1966).

[23] B. S. deWitt and R. W. Brehme, Annals of Physis **9**, 220 (1960).

[24] J. F. Woodward, *Making Starships and Stargates*, Springer Press , December 2012.

[25] H. Fearn et al. 'Theory of a Mach Effect Thruster II", Journal of Modern Physics, **6**, pp1868–1880 (2015).

[26] Rodrigo Medina, "The inertia of Stress", Am. J. Phys. **74** 1031 (2006).
`https://arxiv.org/pdf/physics/0609144.pdf`

[27] S. W. Hawking, "On the Hoyl-Narlikar Theory of Gravitation", Proc. Roy. Soc. Lon. **A 286**, 313 (1965).

[28] H. Fearn, "Mach's Principle, Action at a Distance and Cosmology", Journal of Modern Physics, **6**, pp260–272 (2015).

THEORY OF THE EM DRIVE IN TM MODE BASED ON MACH-LORENTZ THEORY

Jean–Philippe Montillet
Ecole Polytechnique Fédérale
Lausanne, Switzerland

Various theories have recently emerged to explain the anomalous thrust generated by the controversial EM Drive [1,2]. This work proposes a model based on the theory of the Mach-Lorentz thruster [3]. The thrust is generated by the combination between the Lorentz force and the Woodward effect [4]. The development has been facilitated due the discussions with Dr. José Rodal and Prof. Heidi Fearn. In addition, our approach is only based on the results from the experiments in TM mode released by the NASA Eagleworks group [5,6]. The purpose of this communication is to improve our model using feedback from scientists and to some extends with the EM Drive community in order to point out weaknesses on some of our assumptions and to plan future campaigns of experimental tests.

1. OVERVIEW

Since the first experiment at the beginning of this new millennium, the EM Drive has been the focus of many critics from scientists and engineers. In addition, public debates have also contributed in casting doubts on this possible technology. However, the latest tests and measurements by various academics [7] and government agencies [5], which should have dismissed this technology once and for all, have confirmed the anomalous thrust generated by this device. This latest development has sparked new interests for this device, which could play a critical role in space exploration of our solar system [8]. Nevertheless, the ultimate goal remains the creation of a model of the EM Drive supporting the experiments.

In the last two decades, various theories have emerged to understand the thrust generated by the EM Drive. The author in [1] or [2] developed a theory based on the difference of radiation pressure forces on the end plates of the cavity. More recently, an explanation of the anomalous thrust has been supported by the introduction of the Unruh radiation [9]. Another theory [10] attempts to model this exotic propulsion engine based on the emission of paired photons expulsed through the cavity end walls and generating the recorded thrust. In [11], the thrust is the result of a man-made gravitational field gradient taking place inside the cavity. Other emerging theories can be found online. Among all those theories, we are here only interested in the application of the theory of the Mach-Lorentz thruster (MLT) [3] to the EM Drive. Note that the MLT is also called Mach Effect Gravitational Assist-drive (MEGA-drive). This theory is based on the Lorentz force coupled to the Woodward effect [12] in order to explain the anomalous thrust. The Woodward effect relies on the Mach's principle, which defines inertia within general relativity theory [13], and demonstrates that inertia is caused by the gravitational interaction between an object and massive bodies in the distant universe. The Woodward effect describes a way to extract a linear force from an accelerating object which is undergoing internal deformation and mass-energy fluctuations. Momentum is conserved via the gravitational field. Experiments with capacitors and piezoelectric materials have reproduced the Woodward effect in laboratory environment [4].

Our model assumes that each element constituting the EM cavity (frustum), namely the two end plates and the conical wall, responds independently to the EM waves propagating inside the cavity and reflected on the walls. Each element is modelled with a capacitor in series with a resistance and in parallel with an inductor. The capacitor models the EM excitation phenomenon from the waves reflecting on the end plates in TM modes. Thus, the assumptions are from the EM excitation: creating surface currents on the surface of the walls; generating an EM energy density "stored" in the skin layer of the copper end plates (e.g., evanescent waves [14]). The capacitor charges and discharges instantaneously due to the creation and dissipation of the charges. If the capacitor is related to the EM excitation mostly due to the electric field, the inductor is then modelling the EM excitation with the magnetic field via the Eddy (Foucault) currents phenomenon [15]. The Eddy currents are loops of electrical currents induced within conductors by a changing magnetic field in the conductor, hence generated when the vector field and the cavity walls are intersecting. While the capacitor and inductor model two different phenomena, the additional strong assumption is that the capacitor should be the dominant effect when the electric field is perpendicular to the wall. However, if the electric field is parallel to the wall or if something prevents the EM excitation on the wall, the inductor should then be the dominant model. For example, when inserting some dielectric (e.g., High-density polyethylene (HDPE)) to one end (e.g., small end plate), it could prevent (partially) the creation of electric charges on this particular wall. The electric field is more attenuated than the magnetic field when passing through the dielectric field (i.e. electrical insulator properties [16]). Thus, we model this phenomenon by increasing the resistance in series with the capacitor.

Now, the current propagating at the interior surface of the conical wall (between the two end plates) is also going through the magnetic field generated inside the cavity, hence resulting in a Lorentz force. This force is the result of the integration on the whole interior surface. However, this force alone cannot be responsible for any movement of the cavity due to the conservation of momentum as explained further in this document.

Secondly, the MLT model is based on the assumption that the Woodward effect is generating the thrust and it is triggered by the Lorentz force. The variation of mass described in [4] is driven by the variation of EM energy density in the skin layer of the copper wall. Thus, the assumption is that the Woodward effect mostly relies on the capacitor model of the cavity wall.

The next sections describe the various steps of this model based on the TM010 simulations and experiments [6, 22, 27]. It is worth emphasizing that for TM010 we use the cylinder terminology for this mode shape since there is no universal convention for mode shape terminology for a truncated cone. Notice that for a truncated cone the electromagnetic field in the axial direction is not constant.

In order to facilitate the understanding of the overall model, an analogy between electrical circuits and Newtonian mechanics is made. We must state clearly that there are two different mechanisms which can be modelled with an RLC circuit in this work. The first mechanism is the response to the EM excitation of each element composing the cavity which basically explains two phenomena described above: Eddy currents from the magnetic field, and the surface current from the electric field. The second analogy with the RLC circuit is used to explain the anomalous thrust by modelling the whole cavity. This model is fully developed in the following sections. However, our analogy does not relate to the well-known model of a specific EM cavity with an RLC circuit used in the analysis of the EM properties. Readers interested in this analogy can refer to [17].

2. SOME EQUATIONS AND DISCUSSIONS

2.1 Modelisation of the Three Steps: Electro-mechanics and Gravitational Coupling (EMG)

RC circuit

Let us first assume that there is no force or no thrust acting on the cavity. The electric field is exciting the end plates, and parallel to the conical wall (e.g., [18] or [19]). The capacitor models the EM excitation via the electric field on the end plates. Thus, the capacitor charges and discharges instantaneously due to the creation and dissipation of the charges by EM excitation on the surface of the end plates. The EM cavity can then be modelled as two capacitors in series charging/discharging instantaneously. Taking into account the dissipation intrinsic to the conductor properties, the cavity can be modelled such as a RC circuit. The equations read:

$$\begin{aligned} Ri + \frac{q}{C} &= 0 \\ R\partial_t q + \frac{q}{C} &= 0 \\ q(t) &\sim q_0 \exp\left(-\frac{t}{RC}\right) \end{aligned} \tag{1}$$

q_0 is the charge at $t = 0$. The equation of the charge $q(t)$ shows that the dissipation of the initial charge q_0 during the discharge time $\tau = RC$. That is why we can understand it such as a *switch on- switch off* of the capacitor. To evaluate the discharge time τ, one can write the conservation of charge equation at the surface of the plates.

Let us consider the density of the charge $\rho(t)$, the conductivity of the copper σ and its permittivity ϵ_r, then [14],

$$\begin{aligned}\partial_t\rho(t) + div\vec{j} = 0\\ \partial_t\epsilon_r\epsilon_0\vec{E} + div\sigma\vec{E} = 0\\ \epsilon_r\epsilon_0\partial_t\Delta V + \sigma\Delta V = 0\\ V(t) \sim V_0\exp\left(-\frac{\sigma}{\epsilon_r\epsilon_0}t\right)\end{aligned} \tag{2}$$

The discharge time τ equal $\frac{\epsilon_r\epsilon_0}{\sigma}$ or $6 * 8.85e-12/5.85e7 \sim 1e-18$s (values from [20]). Note that we assume at the surface of the plate $\vec{E} = -\vec{\nabla}V$ (no magnetic potential). V_0 is the potential at $t = 0$ before the discharge. Now in order to evaluate the potential over the whole copper end plate, we integrate on the whole surface S. The difference of potential between the two end plates (without dielectric or HDPE insert) is then $DV = (S_1 - S_2)V_0\exp\left(-\frac{\sigma}{\epsilon_r\epsilon_0}t\right)$. Within the frustum model, S is equal to πr^2 (r the radius of the end plate). With the insertion of the HDPE (or dielectric) on the end with surface S_2, the difference of potential is then equal to $DV \sim S_1V_0\exp\left(-\frac{\sigma}{\epsilon_r\epsilon_0}t\right)$. Now, the Eddy currents generated on the conical wall due to the perpendicular magnetic field, compete with the current propagating from the difference of electric potential between the end plates (from large to small end plate). The direction of the Eddy currents depends on $\vec{curl}\vec{B}$ (see the Maxwell equation $\vec{curl}\vec{B} = \mu_0\vec{j}$, with μ_0 the permeability of the vacuum and $\vec{j}$ the Eddy currents). The two currents propagate in opposite directions in the TM010 scenario. In addition, the Eddy currents may have a larger amplitude than the other current propagating on the conical wall.

In the first step, **the main assumption is the creation of charges at the surface of the end plates** in TM mode.

The acceleration of the cavity due to the Lorentz force

The second step is when a force is generated acting on the cavity. The current propagates inside the magnetic field, and thus triggering a Lorentz force F_{Lo}. As previously said, this current can be either the Eddy current or the current induced by the difference of electrical potential between the two end plates. Let us assume that an alternative current (AC) is propagating between the two end plates. In terms of circuit analogy, the cavity is now a RLC circuit with an induced electromotive force ε:

$$Ri + \frac{q}{C} + L\partial_t i - \varepsilon = 0 \tag{3}$$

$L\partial_t i$ is equivalent to the mechanical action of the cavity getting accelerated (or $m\partial_t v$ in classical mechanics (Newton's second law), m the mass of the cavity and v the speed). ε can be expressed such as $\varepsilon = -\partial_t\phi_B(t)$, with $\phi_B(t)$ the magnetic flux through the copper conical wall surface [14]. In classical mechanics (i.e. Newton second law), when projecting the forces on the Z-axis (see Figure 1), the equation (3) becomes:

$$m\partial_t^2 z = \alpha\partial_t z - Kz + F_{Lo} \tag{4}$$

where $\alpha\partial_t z$ is the dissipative force due to the resistivity of the copper when the current propagates. Note that the force due to the weight of the cavity is perpendicular to the axis onto we project the forces and the Z-axis direction is toward the small end plate.

Let us estimate the Lorentz force applied to one electron (with charge q_e and speed v_e) moving through the magnetic field $\vec{B}$ at the surface of the conical wall

$$\vec{F}_{Lo} = q_e\vec{v_e} \times \vec{B}$$

$\times$ is the vectorial product. Using the convention in [18] and [19], the magnetic field is parallel to the conical wall with only a component on the surface of the azimuth direction $\vec{B} = B_\phi u_\phi$. The apex angle of the frustum is defined as $2\theta_w$. The expression of the force on the Z-axis is then $\vec{F}_L o$:

$$\vec{F}_{Lo} = q_e v_e B_\phi \sin(\theta_w) u_z$$

The displacement of the electrons is collinear to the unit length $\vec{dl}$ of the conical wall. If we assume that the number density of electrons in copper is n_{Cu}, dS the unit surface, then we can estimate the force over dl

$$\vec{F}_{Lo} = n_{Cu} v_e dS dl B_\phi \sin(\theta_w) u_z$$

Let us assume the current with an amplitude $dI_0 = n_{Cu} v_e dS$. Then the Lorentz force per unit of length dl is:

$$\vec{F}_{Lo} = dI_0 dl B_\phi \sin(\theta_w) u_z \quad (5)$$

Using the axis as defined in Figure (and the same as in [19]), (5) becomes:

$$\vec{F}_{Lo} = dI_0 B_0 exp(j(\omega t - Kz)) \cos(\theta_w) \sin(\theta_w) dz u_z \quad (6)$$

Note that the amplitude of the magnetic field at the surface of the conical wall is not constant and depends on the TM mode. In TM010, the experiments carried out by the NASA Eagleworks group, B_0 is constant in azimuthal plane [6, 27], but not on the Z-axis. Thus, the Lorentz force can vary while the current propagates from one end to the other.

dI_0 can be integrated over the whole azimuth plane, but there is an assumption to be made: do we consider the current propagating over the whole thickness of the copper sheet, or just over an elementary part of it? It is important to underline that we are here using a simpel model of the Lorentz force applied to free charges in a conductor. However, because surface charges are distributed over some infinitesimal depth, and those charges at greater depths are shielded by the others and therefore see a smaller electric field $\vec{E}$. In other words, the electric field created by the displacment of those charges decreases in amplitude with the depth in the conductor. Moreover, we did not take into account the possible effect of Kelvin polarization forces [21]. Note that (4) is only stated for a pedagogical point of view, because a creation of thrust from this equation is prevented by the momentum conservation principle (i.e. special relativity).

In the second step, the main assumption is the **current propagating at the surface of the conical wall** inside the cavity, hence generating the Lorentz Force.

Generating the thrust

The last step is the triggering of the Woodward effect generating the thrust. Basically, it is the introduction of $\partial_t z \partial_t m$ into equation (4). As previously mentioned, the variation of mass of the cavity is due to the Woodward effect applied to the EM energy density *stored* in the skin layer of the copper end plate(s). Thus, the Woodward effect is mostly associated with the capacitor model and not the inductor for each element of the cavity, hence introducing a dielectric should reduce it. In TM010 mode, the effect should take place mostly on the end plates. Recalling the Woodward effect takes place only if the cavity is accelerated while the energy inside the cavity is fluctuating [4]. The variation of mass is translated into the equation [4],

$$\delta\rho_0(t) = \frac{1}{4\pi G}\left[\frac{1}{\rho_0 c^2}\partial_t^2 U_0 - \left(\frac{1}{\rho_0 c^2}\right)^2 (\partial_t U_0)^2\right] \quad (7)$$

U_0 is the energy of the system, ρ_0 is the transient mass source, and c speed of light. Considering a rest energy $\mathcal{E}$, energy of the frustum at rest, including all the particles within the frustum with no EM excitation, one can state the famous Einstein's relationship in special relativity between $\mathcal{E}$ and the rest mass ρ, $E = \rho c^2$. In Appendix III, we justify the assumption that the variation with time of $\mathcal{E}$ equal the variation of EM energy density with the capacitor model. The variation of EM energy in the copper end plate (skin layer) is expressed with du (see Appendix I,(19)). The Woodward effect in (7) can then be rewritten

$$\delta\rho(t) = \frac{1}{4\pi G}\left[\frac{1}{\rho c^2}\partial_t^2 u - \left(\frac{1}{\rho c^2}\right)^2 (\partial_t u)^2\right] \quad (8)$$

The author in [4] calls $\partial_t^2 U_0$ the impulse engine, and $(\partial_t U_0)^2$ the wormhole. In the next section, we discuss the quantities $\partial_t^2 u$ and $\partial_t u$ and possible explanations in terms of EM theory. Note that the reader can find the rigorous derivation of (8) (based on [4]) with the assumptions of replacing the input power with the electromagnetic energy density in the appendices.

Finally, we assume that the Woodward effect creates a variation of mass (mass density) independently for each end plate when considering $\mathcal{E}$ as the rest energy for one end plate in order to obtain (8). Let us then define:

- $\partial_t \rho L$: variation of mass at large end plate
- $\partial_t \rho S$: variation of mass at small end plate

with $\partial_t m = \partial_t \rho L - \partial_t \rho S$. (4) becomes

$$m\partial_t^2 z + \partial_t z(\partial_t \rho L - \partial_t \rho S) = \alpha \partial_t z - Kz + F_{Lo} \tag{9}$$

One needs to underline that the terms $\alpha\partial_t z$ and Kz are intrinsic to the cavity parameters (i.e. resistivity, dimension), whereas the thrust or acceleration of the cavity ($m\partial_t^2 z$) depends on the Lorentz force F_{Lo} and the relativistic terms coming from the Woodward effect $\partial_t z(\partial_t \rho L - \partial_t \rho S)$. One can underline that $\partial_t \rho L - \partial_t \rho S$ can be interpreted as the Woodward effect created independently on each end plate with opposite direction (towards the outside of the cavity). Finally, the measurable thrust in the MLT comes from (9) which results from the coupling between the Lorentz force and the Woodward effect. Note that (9) sums up our model of the MLT.

In the last step, we assume that the **Lorentz force triggers the Woodward effect in order to generate the anomalous thrust**.

2.2 Variation of electromagnetic energy density

This section looks at numerical estimation of the EM energy density in the skin layer of the copper end plates.

Evanescent Waves in Copper Walls and Numerical Estimation

As seen in the previous section, the surface surcharges disappeared as soon as they are created (with $\vec{j} = \sigma_{Cu}\vec{E}$ and charge conservation equation, we have $\tau_{relax} = \frac{\epsilon_0}{\sigma_{Cu}} \sim 10^{-18}\ s \sim 0$). Note that in the following $\epsilon = \epsilon_r\epsilon_0$ and $\mu = \mu_r\mu_0$ as previously defined. We can then state the Maxwell equations at the surface of the copper wall end plates,

$$\left.\begin{array}{l} div\vec{E}_{tot} \sim 0, \\ c\vec{url}\vec{E}_{tot} = -\partial_t \vec{B}_{tot}, \\ div\vec{B}_{tot} = 0, \\ c\vec{url}\vec{B}_{tot} = \mu\epsilon\partial_t\vec{E}_{tot} + \mu\sigma_{Cu}\vec{E}_{tot}, \end{array}\right\}$$

The wave equation is then [14]:

$$\Delta\vec{E}_{tot} = \mu\epsilon\partial_t^2\vec{E}_{tot} + \mu\sigma_{Cu}\partial_t\vec{E}_{tot} \tag{10}$$

Assuming that the solution is a planar wave of the type $\vec{E} = \vec{E_0}e^{i(\omega t - \vec{k}.\vec{r})}$ ($i = \sqrt{-1}$), and knowing that on the end plates the electric field is only a radial component in TM mode (see [19]), then $\vec{E_0} = E_0 e^{i(\omega t - krcos\theta)}\vec{u}_r$ in spherical coordinates. One should expect by replacing it in the wave equation (10), the equation for the wavelength [14]

$$\begin{aligned} k^2 &= \mu\epsilon\omega^2 - i\mu\sigma_{Cu}\omega \\ k^2 &= \mu\epsilon\omega^2(1 - i\frac{\sigma_{Cu}}{\omega\epsilon}) \end{aligned} \tag{11}$$

In the good conductors such as copper, one can make the assumtion [14] that $\frac{\sigma_{Cu}}{\omega\epsilon_0} >> 1$. Thus, (11) becomes

$$\begin{aligned} k^2 &= \mu\omega(-i\sigma_{Cu}) \\ k &= (1-i)\sqrt{\frac{\sigma_{Cu}\mu\omega}{2}} \end{aligned} \tag{12}$$

Which ends up in an evanescent wave taking into account the real (k_1) and imaginary part (k_2) of the wavelength, $\vec{E} = E_0 e^{-k_1 rcos\theta} e^{i(\omega t - k_2 rcos\theta)}\vec{u}_r$. Now, we can estimate the energy density of the EM field

$< w > = < u_E > + < u_B >$ with

$$
\begin{aligned}
< u_E > &= \frac{\epsilon_{Cu}}{2\pi} \int_0^{2\pi} Re\{E.E^*\}dt \\
< u_E > &= \frac{\epsilon_0}{2\pi} \int_0^{n\tau_r} Re\{E.E^*\}dt \\
< u_E > &= \frac{\epsilon_0}{2\pi} \int_0^{n\tau_r} E_0^2 e^{-2k_1 r} cos^2(\omega t - k_2 r cos\theta)dt \\
< u_E > &\sim \frac{n\tau_r \epsilon_0}{2\pi} E_0^2 e^{-2k_1 r cos\theta}
\end{aligned} \tag{13}
$$

we assume that the Evanescent waves are created by the surface charges only during the relaxation time as explained above. τ_r is part of relaxation time τ_{rel} when the charges create the surface current. In the 2π average interval, there is $n\tau_r$ $(n\tau_r << 1)$. In the remaining time we consider the integral null. The first derivative of the EM energy density for the electric field is

$$
\begin{aligned}
< \partial_t u_E > &= \frac{\epsilon_0}{2\pi} \int_0^{2\pi} Re\{2E.\partial_t E^*\}dt \\
< \partial_t u_E > &= \frac{\epsilon_0 2\omega}{2\pi} \int_0^{n\tau_{rel}} E_0^2 e^{-2k_1 r} sin(\omega t - k_2 r) cos(\omega t - k_2 r)dt \\
< \partial_t u_E > &\sim \frac{n\tau_{rel}\omega\epsilon_0}{2\pi} E_0^2 e^{-2k_1 r} \\
< \partial_t u_E > &\sim \omega < u_E >
\end{aligned} \tag{14}
$$

The same development can be applied to the second derivative

$$
\begin{aligned}
< \partial_t^2 u_E > &\sim 2\omega < \partial_t u_E > \\
< \partial_t^2 u_E > &\sim \frac{n\tau_{rel} 2\omega^2 \epsilon_0}{2\pi} E_0^2 e^{-2k_1 r}
\end{aligned} \tag{15}
$$

For the magnetic field, one can estimate with $\vec{curl}\vec{E} = -\partial_t \vec{B}$. Choosing a spherical coordinates referential (Figure),

$$
\begin{aligned}
\vec{curl}\vec{E} &= \frac{-1}{r} \partial_\theta E \vec{u}_\phi \\
&= -i\omega \vec{B} \\
\vec{B} &= (\frac{k_1 sin\theta}{\omega}(1-i)) E \vec{u}_\phi
\end{aligned} \tag{16}
$$

In the same way we estimated $< u_E >$, one can estimate the magnetic energy density

$$
\begin{aligned}
< u_B > &= \frac{1}{\mu 2\pi} \int_0^{n\tau_{rel}} Re\{B.B^*\}dt \\
< u_B > &\sim \frac{1}{\mu\pi} (\frac{k_1 sin\theta}{\omega})^2 E_0^2 e^{-2k_1 r cos\theta} n\tau_{rel} \\
< \partial_t u_B > &\sim \omega < u_B > \\
< \partial_t^2 u_B > &\sim 2\omega^2 < u_B >
\end{aligned} \tag{17}
$$

However,

$$
\begin{aligned}
\frac{< u_E >}{< u_B >} &\sim \frac{\epsilon}{\mu} \frac{\omega^2}{k_1^2 sin^2\theta} \\
&\sim \frac{2\epsilon\omega}{\mu^2 \sigma_{Cu}} >> 1
\end{aligned} \tag{18}
$$

Because $\frac{<u_E>}{<u_B>} >> 1$, the energy density of the EM field is mainly the contribution from the electric field. Finally, additional measurements on n can check the assumption on the order of magnitude of the EM energy density.

Simulations and Preliminary Results

In this section, simulations of the copper frustum in TM010 mode has been performed by Christian Ziep using FEKO software [28]. The frustum is model as described in [22] and [27] without a dielectric insert. It is orientated following the Z-axis with the direction pointing towards the small end plate. The dimension of the cavity follows: 228.6 mm (height), 158.75 mm (diameter small end plate), 279.65 mm (diameter big end plate). The antenna model is an electrical dipole placed in the middle of the cavity. The input power is equal to 1W (30 dBm) with central frequency 0.9598 GHz and quality factor Q equal to 20.38. The resonant frequency is then estimated at 1020 MHz. Figure 2(A) displays the magnetic field inside the cavity perpendicular to the conical wall and parallel to the end plates as described in [18] and [19]. Figure 2(B) displays the electric field perpendicular to the end plates.

Now, the surface currents on the cavity walls are simulated following the previous description. Figure 3 (A,B) display the amplitude of the electric (E) and magnetic fields (H) at the surface of the conical wall as a function of the height; Figure 3 (C,D) the amplitude of the E and H-field at the surface of the small end plate; and Figure 3 (E,F) the amplitude of the E and H fields at the surface of the large end plate. The results show that the amplitude of the currents at the surface of the conical wall follows a gradient decreasing with the increase of the height of the frustum. It is in agreement with the observations that both E and H fields are larger (on average) at the surface of the large end than at the small end. Thus, the gradient of the amplitude of the wall current accommodates with the amplitude of simulated E and H fields at the surface of the end plates.

One assumption in our MLT model is the current propagating from large to small end plate due to the difference of electrical potential. In the simulations, the current at the surface of the conical wall propagates towards the large end plate. Thus, it seems that those currents are Eddy currents generated by the H field. As previously underlined, the Eddy currents could have higher amplitude than the one due to difference of electrical potential. This result underlines this phenomenon. In addition, the electric field at the surface of the large end plate is higher than at the small end plate, which supports a greater EM excitation. Based on our assumption that the Woodward effect is directly related to the skin depth effect taking place on the cavity wall, this effect should then be greater on the large end than on the small end. It has been shown in [6] that, in this experiment, the anomalous thrust is towards the large end plate. This result is in agreement with (9), assuming that the Woodward effect displaces the cavity towards the large end due to $\delta\rho_L > \delta\rho_S$. However, further study is required to understand the role of the Lorentz force taking place on the conical wall in the amplitude of the anomalous thrust.

3. CONCLUDING REMARKS

This model was based on a few results on the TM010 mode (i.e. [5,6, 22, 27]) and preliminary simulations. The study takes into account the EM excitation of each element of the cavity resulting in modelling them with a capacitor with a resistance in series, and an inductor in parallel. Thus, two types of currents are then taking into account: Eddy currents from transverse magnetic field and surface currents from electric field excitation. It is then produced a surface currents (dI_0) on the conical wall, hence creating a Lorentz force. The last step of our model is the generation of thrust using the Woodward effect. However, the thrust is only produced by a coupling between the Lorentz force and the Woodward effect from (9) in order to guarantee momentum conservation principle. Only a careful analysis via simulations and experiments of the frustum for a specific mode can quantify the contribution of those currents to the proposed model of the thrust.

The proposed model is just at an early development stage where many assumptions must be validated. For example, the theory stands at the moment with those few points to check:

- Estimation of the currents on the cavity walls due to the electric and magnetic fields.
- On the need to estimate the AC current I_0 on the conical wall and the Lorentz force $\vec{F}_{Lo}$ through simulations and experiments with different scenarios (e.g., with and without HDPE).
- Better understanding of the coupling between the acceleration of the cavity due to $\vec{F}_{Lo}$ and the Woodward effect.
- The variation of mass $\delta\rho(t)$ in (8) with the first and second derivatives of the EM energy density.

Overall, our assumptions on this model have to be compared with the results from following experimentations. One can underline

- The model can be invalidated if there is still a non negligible thrust if we use superconductive materials for the frustum in order to eliminate (or reduce drastically) all skin depth effects on the cavity walls (suggested by Prof. J. Woodward).
- The first and second steps of this model rely on standard EM theory. One needs to estimate the average electric field at the surface of the end plates in order to get some measurements for the amplitude of the difference of electric potential (DV) and also to confirm the simulations.

Furthermore, at the time of writing this manuscript, NASA Eagleworks laboratory has released a full study supporting the EM Drive generating a thrust in TM mode [5,6]. New experiments are planned to test the TE mode, which can help supporting or not this model. We also acknowledge that some engineers have recently carried out tests involving various new designs of the EM Drive showing successfully an anomalous thrust. The TE mode is the next step in order to produce a complete MLT model of the EM Drive and its anomalous thrust. To conclude, this new engine can be an example of EMG coupling if the presented model is validated.

4. Acknowledgements

The author would like to acknowledge the great contribution to this article by Christian Ziep, who conducted several numerical analyses of the EM Drive truncated cone cavity using FEKO software; some of those results are reproduced in this article. Also acknowledged are the contributions of people involved in developing the presented model via discussions with the author, including Paul March (NASA, Eagleworks) and Todd J. Desiato (Warp Drive Tech.).

Addendum I: Possible Mathematical Frame Work - the Energy Space Theory

We can formulate the variation of energy density at a higher order with a Taylor series development such as:

$$du = \partial_t u\, dt + \partial_t^2 u\, \frac{dt^2}{2} + o(dt^2) \tag{19}$$

o is the Landau notation to omit higher order quantities. Note that at the first order $\frac{du}{dt} = \partial_t u$. Let us consider a mathematical frame work from [23]. The higher order orders term are based on the assumptions that the EM waves inside the skin layer of the copper end plate are functions in the Schwartz space $\mathbf{S}^-(\mathbb{R}^2)$ ($\mathbf{S}^-(\mathbb{R}^3)$in $2D$, in $\mathbf{S}^-(\mathbb{R}^4)$ $3D$ considering also the time variable - see [23]). In addition, they are finite energy function (i.e.following [23] and [24], $L(E(xo, yo, zo, T)) < \infty$ at some given point in the skin layer defined by the coordinates xo, yo, zo). Fortunately, these EM waves are evanescent waves [14]. In the last section of [23], it is shown why these waves can be function of the Schwartz space $\mathbf{S}^-(\mathbb{R}^2)(\mathbf{S}^-(\mathbb{R}^3)$ or $\mathbf{S}^-(\mathbb{R}^4)$ respectively). Now, using the **Lemma** 1 (e.g. [23]) and the model based on the energy space in [24], let us introduce the subspace $\mathbf{N}^i$ (i in $\mathbb{Z}^+$) defined as

$$\begin{aligned}\mathbf{N}^i = \{g \in \mathbf{S}^-(\mathbb{R}^3)|\ & g = \partial_t^i\big(f^n(x_0, z_0, t)\\ & = \alpha_n(\partial_t^{i-1} f^{n-2}(x_0, z_0, t)(\Psi_1^+(f(x_0, z_0, t)))\\ , f \in \mathbf{S}^-(\mathbb{R}^3),\ n \in \mathbb{Z}^+ - \{0\}, \quad & \alpha_n \in \mathbb{R},\ z_0 \in [0, L],\ x_0 \in [0, a]\}\end{aligned} \tag{20}$$

With the definition of the family of energy operator $(\Psi_k^+(.))_{k\in\mathbb{Z}}$ from [23]. Here f is either the electric or magnetic field. In [24], the energy subspace is at the basis of the multiplicity of the solutions (e.g., **Theorem** 2, [24]). If g is a general solution of some linear PDEs, then f^n can be identified as a special form of the solution (conditionally to its existence).
Now considering the wave equation, the electric field and magnetic field are solutions and belong to the subspace $\mathbf{N}^0$ and associated with the variation of energy density $\partial_t w$. Furthermore, we can consider the solutions in $\mathbf{N}^1$ associated with the variation of energy density $\partial_t^2 w$, which can be explained with the *multiplicity* of waves and solutions of the wave equation [24]. The solutions of interest in $\mathbf{N}^1$ are for the electric field $g = \partial_t E$ and the magnetic field $g = \partial_t B$.

Another way to see the contribution of the functions in $\mathbf{N}^1$, is [24] with the Taylor Series development of the energy of (for example) the electric field on a nominated position in space r_0 and in an increment of time dt:

$$
\begin{aligned}
L(E(r_0,T)) &= \int_0^T (R(r_0,u))^2 du < \infty \\
L(E(r_0,T+dt)) &= L(E(r_0,T)) + \sum_{k=0}^{\infty} \partial_t^k (E^2(r_0,T)) \frac{(dt)^k}{k!} < \infty \\
dL(E(r_0,T+dt)) &= \sum_{k=0}^{\infty} \partial_t^k (E^2(r_0,T)) \frac{(dt)^k}{k!} \\
dL(E(r_0,T+dt)) &= E^2(r_0,T)dt + \sum_{k=1}^{\infty} \partial_t^{k-1} \big(\Psi_1^{+,t}(E)(r_0,T)\big) \frac{(dt)^{k+1}}{k+1!} \\
dL(E(r_0,T+dt)) &\simeq E^2(r_0,T)dt + \Psi_1^{+,t}(E)(r_0,T)\frac{dt^2}{2} + \partial_t \Psi_1^{+,t}(E)(r_0,T)\frac{dt^3}{6}
\end{aligned} \tag{21}
$$

Finally one can write the relationship with the energy density following (19) and the previous Taylor series development for the electric and magnetic field:

$$
\begin{aligned}
0.5\big(\epsilon_0 \ \frac{dL(E(r_0,T+dt))}{dt} + \frac{1}{\mu_0} \ \frac{dL(B(r_0,T+dt))}{dt}\big) = 0.5\big(\epsilon_0 E^2(r_0,T) \\
+\frac{1}{\mu_0} B^2(r_0,T)) + \partial_t w \ \frac{dt}{2} + \partial_t^2 w \ \frac{dt^2}{6} + o(dt^2)
\end{aligned} \tag{22}
$$

Therefore, taking into account the second order term of the energy density $\partial_t^2 w$ means that additional solutions of the type $\partial_t E$ and $\partial_t B$ should also be considered in the EM modeling. That is an application of **Theorem** 2 and the multiplicity/duplication theory in [24].

ADDENDUM II: CONSEQUENCES IN TERMS OF EM THEORY

To recall Appendix I, the EM field is now including ($\vec{E}$, $\delta\vec{E}$) and ($\vec{B}$, $\delta\vec{B}$), contribution of the subspaces $\mathbf{N}^0$ and $\mathbf{N}^1$ respectively. We call the total EM field $\vec{E}_{tot}$ and $\vec{B}_{tot}$ inside the copper plate (skin layer) with associated permittivity ϵ_r and permeability μ_r. They are solutions of the Maxwell equations:

$$
\left.
\begin{array}{l}
div\vec{E}_{tot} = \frac{\rho_{tot}}{\epsilon_r}, \\
c\vec{url}\vec{E}_{tot} = -\partial_t \vec{B}_{tot}, \\
div\vec{B}_{tot} = 0, \\
c\vec{url}\vec{B}_{tot} = \mu_r \epsilon_r \partial_t \vec{E}_{tot} + \mu_r \vec{j},
\end{array}
\right\}
$$

with the principle of charge conservation:

$$
\partial_t \rho_{tot} + div\vec{j} = 0 \tag{23}
$$

Now, the variation of energy density (19) together with the equation of charge conservation is formulated such as:

$$
\frac{dw}{dt} + div\vec{P}_{tot} = \vec{j}.\vec{E}_{tot} \tag{24}
$$

$\vec{P}_{tot} = \frac{\vec{E}_{tot} \times \vec{B}_{tot}}{\mu_r}$ is the Poynting vector. Now, writing $\vec{E}_{tot} = \vec{E} + \delta\vec{E}$, $\vec{B}_{tot} = \vec{B} + \delta\vec{B}$ and δ is the first derivative in time (∂_t) (i.e. solutions in $\mathbf{N}^1$ - see Addendum I), then following [14]

$$
(\vec{E} + \partial_t\vec{E}).\vec{j} = (\vec{E} + \partial_t\vec{E}).[\frac{1}{\mu_r} c\vec{url} \ \ (\vec{B} + \partial_t\vec{B}) - \epsilon_r \partial_t(\vec{E} + \partial_t\vec{E})] \tag{25}
$$

using the equalities $div\ (\vec{E}\times\vec{B}) = \vec{B}.\vec{curl}\vec{E} - \vec{E}.\vec{curl}\vec{B}$ and the Maxwell equation $\vec{curl}\vec{E} = -\partial_t\vec{B}$, $\vec{curl}\partial_t\vec{E} = -\partial_t^2\vec{B}$ the previous equation reduces to:

$$\begin{aligned} \vec{E}.\vec{j} + div\ (\frac{\vec{E}\times\vec{B}}{\mu_r}) + \partial_t w + \\ \partial_t\vec{E}.\vec{j} + div\ (\frac{\partial_t\vec{E}\times\partial_t\vec{B}}{\mu_r}) + \partial_t^2 w + \\ div\ (\frac{\partial_t\vec{E}\times\vec{B}}{\mu_r}) + div\ (\frac{\vec{E}\times\partial_t\vec{B}}{\mu_r}) + \frac{\partial\vec{B}.\partial\vec{B}}{\mu_r} + \epsilon_r\partial_t\vec{E}.\partial_t\vec{E} = 0 \end{aligned} \tag{26}$$

We can separate in three groups,

$$\left.\begin{array}{l} \partial_t w + div\ (\frac{\vec{E}\times\vec{B}}{\mu_r}) = -\vec{j}.\vec{E} \\ \partial_t^2 w + div\ (\frac{\partial_t\vec{E}\times\vec{B}}{\mu_r}) + div\ (\frac{\vec{E}\times\partial_t\vec{B}}{\mu_r}) = -\vec{j}.\partial_t\vec{E} \\ div\ (\frac{\partial_t\vec{E}\times\partial_t\vec{B}}{\mu_r}) = -\frac{\partial_t\vec{B}.\partial_t\vec{B}}{\mu_r} - \epsilon_r\partial_t\vec{E}.\partial_t\vec{E} \end{array}\right\}$$

The Poynting vector is defined as $\vec{P} = \frac{\vec{E}\times\vec{B}}{\mu_r}$ and its derivative $\partial_t\vec{P} = \frac{\partial_t\vec{E}\times\vec{B}}{\mu_r} + \frac{\vec{E}\times\partial_t\vec{B}}{\mu_r}$. Thus, the second order term of the energy density is the contribution of the EM field generated by $\partial_t\vec{E}$ and $\partial_t\vec{B}$ is:

$$\left.\begin{array}{l} \partial_t w + div\vec{P} = -\vec{j}.\vec{E} \\ \partial_t^2 w + div\ (\partial_t\vec{P}) = -\vec{j}.\partial_t\vec{E} \\ div\ (\frac{\partial_t\vec{E}\times\partial_t\vec{B}}{\mu_r}) = -\frac{\partial_t\vec{B}.\partial_t\vec{B}}{\mu_r} - \epsilon_0\partial_t\vec{E}.\partial_t\vec{E} \end{array}\right\}$$

The last line is the contribution from only the fields $\partial_t\vec{E}$ and $\partial_t\vec{B}$.

Finally, the creation of the wave defined by the EM field $(\partial_t\vec{E},\ \partial_t\vec{B})$ means that some material properties may allow to create two type of EM waves namely $(\vec{E},\ \vec{B})$ and $(\partial_t\vec{E},\ \partial_t\vec{B})$.

ADDENDUM III: DERIVATION OF THE WOODWARD EFFECT USING THE ELECTROMAGNETIC ENERGY DENSITY

Assumptions with the energy momentum relationship

When the Woodward effect was established in [4], the authors implicitly assumed the rest mass of the piezoelectric material via the famous Einstein's relation in special relativity $\mathcal{E} = mc^2$ ($\mathcal{E}$ the rest energy associated with the rest mass m) and its variation via electrostrictive effect.

Here, the system is the frustum. The rest mass is all the particles within it at the time of the capacitor is discharged. It excludes the photons considered with a null mass. Thus, the main assumption is that the EM excitation on the end plates creates electric charges (i.e. electrons) which makes the rest mass varying with time. This assumption is the same as the mass variation of a capacitor between the charge and discharge times [25]. It allows us to state the variation of rest energy such as:

$$\begin{aligned} \Delta\mathcal{E} &= \mathcal{E}(t+dt) - \mathcal{E}(t) \\ &= (m(t+dt) - m(t))c^2 \\ &= \Delta mc^2 \end{aligned} \tag{27}$$

Finally, the variation of rest energy $\Delta\mathcal{E}$ is assumed to be equal to the variation of EM energy density (Δu_{EM}) resulting from the charges within the skin depth of the copper walls. We also cannot forget the electrostrictive effect (Δu_{El}) when inserting HDPE disk(s) inside the frustum, but we consider that $\Delta u_{EM} >> \Delta u_{El}$.

Note that at the particle level, the rest mass should satisfy the energy momentum relationship for a free body in special relativity [26]:

$$\begin{aligned} u_e^2 &= (pc)^2 + (m_e c^2)^2 \\ p &= v\frac{u_e}{c^2} \end{aligned} \tag{28}$$

with p the momentum and m_e the rest mass of the particle associated with the total energy u_e. The particle is accelerated via the Lorentz force applied to the whole cavity with obviously $v << c$. Thus, we have also the relationship $p^2 < (u_e/c)^2$.

Woodward effect

From [4], one can write the mass variation per unit of volume

$$
\begin{aligned}
dm &= \frac{\delta m}{V} \\
dm &= \frac{1}{4\pi G}\big[\frac{1}{m}\partial_t^2 m - \frac{1}{m^2}(\partial_t m)^2\big]
\end{aligned}
\tag{29}
$$

If we define the mass density such as $\rho = m/V$, then

$$
\begin{aligned}
\delta\rho &= \frac{\delta m}{V} \\
\delta\rho &= \frac{1}{4\pi G}\big[\frac{1}{\rho}\partial_t^2 \rho - \frac{1}{\rho^2}(\partial_t \rho)^2\big]
\end{aligned}
\tag{30}
$$

Let us define the the rest energy $\mathcal{E} = \rho c^2$, then

$$
\begin{aligned}
\delta\rho &= \frac{1}{4\pi G}\big[\frac{1}{\rho c^2}\partial_t^2 \mathcal{E} - \frac{1}{(\rho c^2)^2}(\partial_t \mathcal{E})^2\big] \\
\delta\rho &= \frac{1}{4\pi G}\big[\frac{1}{\mathcal{E}}\partial_t^2 \mathcal{E} - \frac{1}{(\mathcal{E})^2}(\partial_t \mathcal{E})^2\big]
\end{aligned}
\tag{31}
$$

Now, with the assumption that the variation in time of the rest energy is equal to the variation of EM energy density u

$$
\delta\rho = \frac{1}{4\pi G}\big[\frac{1}{\mathcal{E}}\partial_t^2 u - \frac{1}{(\mathcal{E})^2}(\partial_t u)^2\big] \tag{32}
$$

The EM energy density u follows the general definition of the sum of energy density from the electric (u_E) and magnetic (u_B)fields [14].

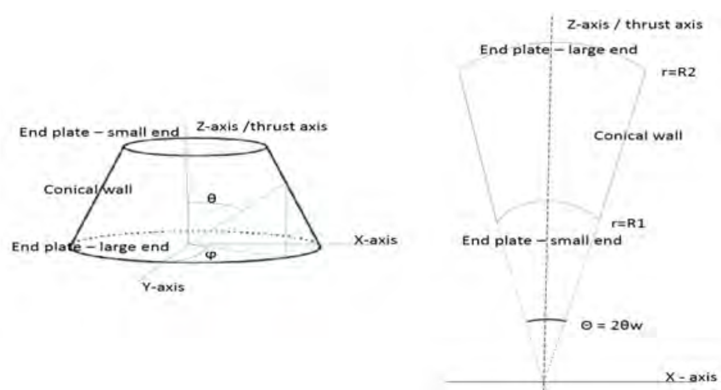

FIG. 1: Drawing of the EM Drive cavity

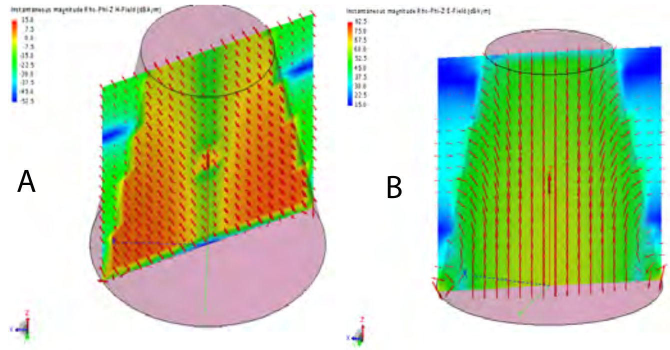

FIG. 2: Simulations of the EM field inside the frustum in TM010 mode: (A) magnetic field, (B) electric field

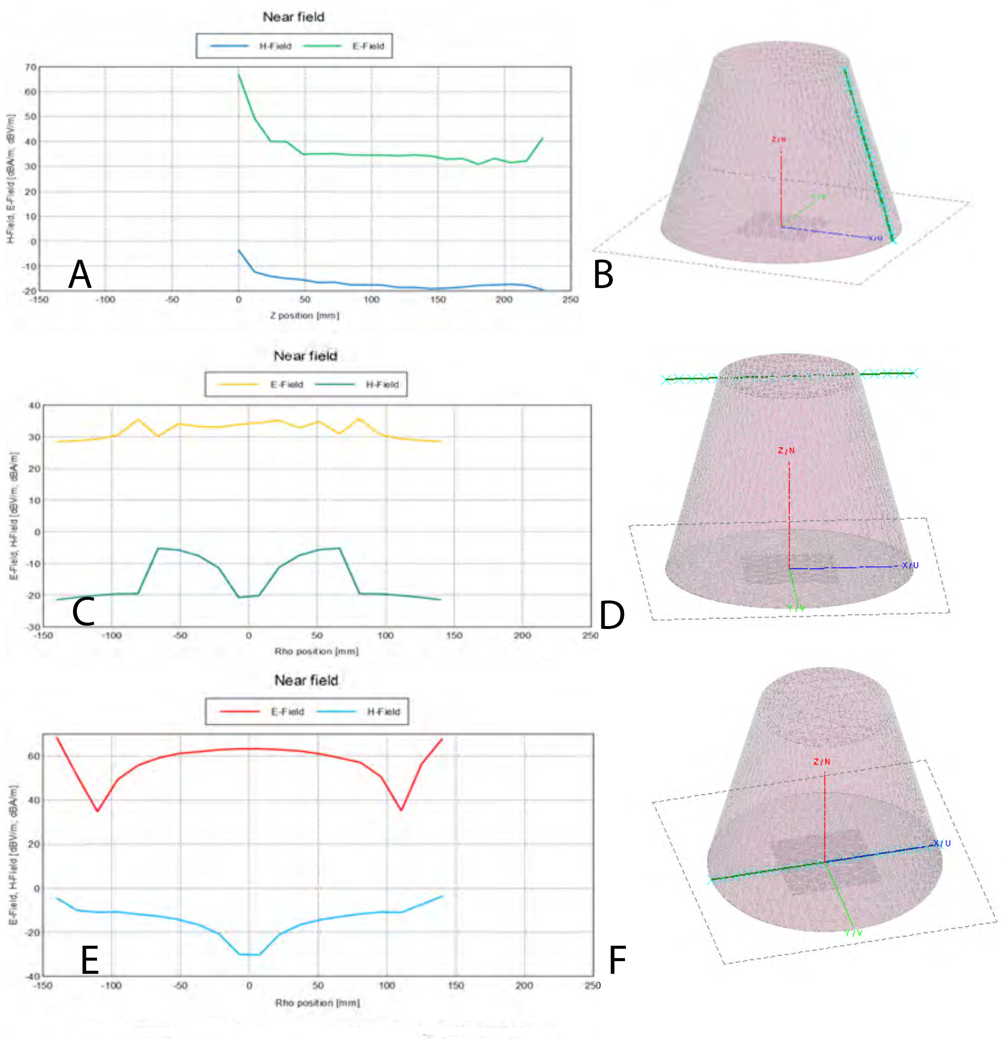

FIG. 3: Estimation of surface currents (A,B) conical wall, (C,D) small end, (E,F) large end. Note that rho is the x-axis (blue line), z-axis is the red line

REFERENCES

[1] R. Shawyer, *The EM Drive a New Satellite Propulsion Technology*, in Proc. of the 2nd Conference on Disruptive Technology in Space Activities, 2010.

[2] R. Shawyer, *Second generation EmDrive propulsion applied to SSTO launcher and interstellar probe*, Acta Astronautica, p. 166-174.
Doi:$http://dx.doi.org/10.1016/j.actaastro.2015.07.002$

[3] H. Fearn, A. Zachar, J. F. Woodward and K. Wanser, *Theory of a Mach Effect Thruster*, in Proc. of the AIAA Joint Propulsion Conference, Tech. Session: Nuclear and Future Flight Propulsion, $http://arc.aiaa.org/doi/abs/10.2514/6.2014-3821$.

[4] J. F. Woodward, *Life Imitating Art: Flux Capacitors, Mach Effects, and Our Future in Spacetime*, AIP Conference Proceedings. Space Technology Applications International Forum (STAIF 2004), Albuquerque, New Mexico. American Institute of Physics. p. 11271137, 2004. Doi: 10.1063/1.1649682.

[5] D.A. Brady, H.G. White, P. March, J.T. Lawrence, and F.J. Davies, *Anomalous Thrust Production from an RF Test Device Measured on a Low-Thrust Torsion Pendulum*, AIAA 2014-4029, 2014.

[6] H. White, P. March, J. Lawrence, J. Vera, A. Sylvester, D. Brady, P. Bailey, *Measurement of Impulsive Thrust from Closed Radio Frequency Cavity in Vacuum*, AIAA Journal of Propulsion and Power, December, 2016.

[7] M. Tajmar, and G. Fiedler, *Direct Thrust Measurements of an EM Drive and Evaluation of Possible Side-Effects*, in Proc. of the 51st AIAA/SAE/ASEE Joint Propulsion Conference, AIAA 2015-4083. Doi: $10.2514/6.2015-4083$

[8] J.F. Woodward, *Making Starships and Stargates*, Springer-Verlag New York, 2013. Doi: $10.1007/978-1-4614-5623-0$

[9] M. E. McCulloch, *Can the Emdrive Be Explained by Quantised Inertia ?*, Progress in Physics, vol. 11, 2015.

[10] P. Grahn, A. Annila, E. Kolehmainen, *On the Exhaust of Electromagnetic Drive*, AIP Advances, vol. 6 (6), 2016. Doi: 10.1063/1.4953807

[11] T. J. Desiato, *An Engineering Model of Quantum Gravity*, September, 2016.

[12] J.F. Woodward, *Gravity, Inertia, and Quantum Vacuum Zero Point Fields*, Foundations of Physics, 31 (5), p. 819835, 2001. Doi: 10.1023/A:1017500513005

[13] D. W. Sciama, *On the Origin of Inertia*, Monthly Notices of the Royal Astronomical Society, vol. 113 (1), p. 34-42, 1953. Doi: $10.1093/mnras/113.1.34$

[14] R. Petit, *Ondes Electromagnetiques en radioelectricite et en optique*, 2nd Edition, Masson, 1993.

[15] A. E. Fitzgerald, C. (Jr) Kingsley, S. D. Umans, Electric Machinery, 4th ed., Mc-Graw-Hill, Inc. p. 20, 1983. (ISBN 0-07-021145-0)

[16] G.G. Raju, *Dielectrics in Electric Fields*, CRC Press, 2003. (ISBN:9780824708641).

[17] MIT Web lecture, *Resonant Cavities and Waveguides*,
`http://web.mit.edu/22.09/ClassHandouts/ChargedParticleAccel/CHAP12.PDF`

[18] J. Rodal, *Resonant Cavity Space Propulsion*
`https://forum.nasaspaceflight.com/index.php?topic=39214.msg1546438#msg1546438`

[19] G. Egan, *Resonant Modes of a Conical Cavity.*
`http://gregegan.customer.netspace.net.au/SCIENCE/Cavity/Cavity.html`

[20] David R. Lide, *CRC Handbook of Chemistry and Physics*, CRC Press Inc, 2009, 90e Ed., 2804.(ISBN 978-1-420-09084-0)

[21] D. H. Staelin, *Electromagnetics and Applications*, Department of Electrical Engineering and Computer Science, Massachusetts Institute of Technology, Cambridge MA. Available at: https://ocw.mit.edu/courses/ or google
MIT6_013S09_notes.pdf

[22] F. J. Davies, *Copper Frustum Modes*, Personal Communication, NASA Johnson Space Center , NASA/JSC/EP5.

[23] J.P. Montillet, *The Generalization of the Decomposition of Functions by Energy Operators (Part II) and Some Applications*, Acta Applicandae Mathematicae. doi: 10.1007/s10440-014-9978-9, also available at: http://arxiv.org/abs/1308.0874.

[24] J.P. Montillet, *Multiplicity of Solutions for Linear Partial Differential Equations Using (Generalized) Energy Operators, available in:* http://arxiv.org/pdf/1509.02603v1.pdf

[25] E. B. Porcelli, V. S. Filho, *On the Anomalous Weight Losses of High Voltage Symmetrical Capacitors*, ArXiv. doi: 10.4006/0836-1398-29.1.002

[26] C. Möller, *The Theory of Relativity*, 2nd ed., Delhi: Oxford University Press. p. 220, 1952. ISBN 0-19-560539-X.

[27] P. March, *Examination of Eagleworks (EW) Labs Copper Frustums TM010 Resonant Mode Thrust Production with and without Dielectric Discs in the frustum at 90W RF*, 2016.

[28] FEKO, https://www.feko.info/references/publications-citing-feko

Introduction to "Mach Effect Propulsion, an Exact Electroelasticity Solution"

José J. A. Rodal[1]
Rodal Consulting
Research Triangle Park, North Carolina

[Editors' comment: Rodal's research article was considered too lengthy to fit well into the chapter, being the length of a small monograph, so here is just Rodal's introduction to his article which is located in Appendix D, at the end of the proceedings.]

This is a general introduction to my article in Appendix D, which presents a comprehensive analysis of a mathematical modeling of the experiments performed by Woodward and Fearn using piezoelectric stacks (known for over 100 years as Langevin stacks, since P. Langevin first invented and developed them). Up to now, Woodward and Fearn have analyzed these experiments without taking into account the effect of damping or stiffness (neither the quality factor of resonance nor any other form of damping measure, nor the modulus of elasticity nor any other form of stiffness measure appears in their equations) in the modeling of the response in their experiments. The Woodward and Fearn experiments are experiments conducted as closely as possible to the natural frequency. It is known that for zero damping, the response at the natural frequency would have infinite amplitude, which is physically impossible, which is why it is imperative to take damping into account. Similarly the vibration response is dependent on the stiffness of the system, and not just the masses involved, hence it is imperative to take into account the modulus of elasticity of the system components in the analysis of the response.

The Woodward and Fearn experiments are not quantum mechanics or particle physics experiments nor cosmological measurements dealing with verification of gravitational theories. Instead, they are dynamic measurements performed in a macroscopic man-made dynamic system, a Langevin stack of piezoelectric plates. Also, the Woodward and Fearn experiments have not been conducted for a Mach Effect Gravitational Assist (MEGA) drive floating freely in space, but instead for one attached at the back end to a bracket at the end of a torsional pendulum whose center of rotation is fixed to terra firma. Hence a mathematical analysis of these experiments has to concentrate on macroscopic aspects like materials science (phase transitions, crystallography), mechanics of materials (piezoelectricity, electrostriction, fracture mechanics, etc.), dynamic analysis, unsteady heat transfer and other aspects of continuum mechanics rather than aspects common to general relativity like cosmological measurements or aspects more familiar to fundamental physics experiments like quantum mechanics or particle physics. The mathematical analysis of the Woodward and Fearn experiments involves interdisciplinary aspects like mechanics of materials and structural dynamics that aerospace engineers are familiar with, but with (brittle anisotropic piezoelectric and electrostrictive) materials that may be familiar only to a segment of people interested in space propulsion.

Due to the fact that the disciplines involved in these experiments may not be familiar to people specializing in specific areas like general relativity or space propulsion, many things discussed in my article (in Appendix D) may at first glance perhaps appear insignificant or unimportant, for example, the reason why materials science (phase transitions, crystallography), and mechanics of materials (piezoelectricity, electrostriction, fracture mechanics, etc.) are discussed in some detail. A specific example is the discussion of the bolts that hold the stack. This is important because the materials involved in the experiment are very brittle materials that need to be pre-compressed (using bolts) to stop cracks from propagating and to therefore behave as structural materials able to take tension. The stiffness of the bolts used to pre-compress the sandwich stack of piezoelectric plates plays an important role in the stiffness of the stack of piezoelectric plates, and hence is necessary to take into account when modeling these experiments. The length of the paper is due to these numerous interdisciplinary aspects which are discussed.

Following is a short description of the sections covered in my article, which gives an overview of what is being discussed, and where, and allows the reader to jump to certain sections and skip other sections if she prefers. The figures, tables, references and pertinent details are in Appendix D.

---

[1] jrodal@alum.mit.edu

SECTION 1, PIEZOELECTRICITY, THE LANGEVIN TRANSDUCER AND PZT

In the first section, after a brief overview of the history of piezoelectricity, the role of the tail and front masses in achieving a desired natural frequency is discussed. Next is discussed the piezoelectric materials involved in the experiments of Woodward and Fearn, brittle materials that cannot function for transducer purposes without application of an initial compressive stress. The various physical behaviors of the materials used in these experiments are discussed: elastic, ferroelectric, piezoelectric, electrostrictive and pyroelectric. Most of the section is dedicated to a discussion of the material science issues associated with these experiments, including the phase diagram and associated crystallography in different phases, the transition temperature associated with a change from tetragonal or rhombohedral ferroelectric to a centrosymmetric cubic dielectric, the importance of proximity to the morphotropic phase boundary to favor enhancement of the piezoelectric coefficient, the poling process, the fact that the materials involved are doped, and that hard doping (involving acceptors) or soft doping (involving donors) can substantially impact the material properties exhibited by these materials.

SECTION 2, THE MEGA LANGEVIN STACK

Next, the second section deals with the specific construction of the Langevin stack used in the experiments of Woodward and Fearn. The MEGA Langevin stack has a tail mass made of brass and a front mass made of aluminum, with a stack of piezoelectric plates between the end masses, which is compressed by stainless steel bolts in tension. My analysis concludes that it would be better to use a copper tail mass, or optimally, a silver tail mass, because of thermal diffusivity considerations, due to the unsteady heat transfer that occurs as a result of internal heat generated inside the piezoelectric plates from the vibratory motion of the stack. The analysis and experimental results show that the passive piezoelectric plates used in the MEGA stack act as strain gauges, and not as accelerometers, due to the fact that the MEGA stack is purposely driven near the natural frequency resonance. The piezoelectric plates and brass electrodes in the stack are adhered with an epoxy adhesive in a sandwich sequence where the piezoelectric plates are connected mechanically (as springs) in series and electrically (as capacitors) in parallel. My analysis shows that it would be better to use a filled polymer adhesive to decrease the thermal expansion of the adhesive (in relation to the thermal expansion of the electrodes and the piezoelectric plates), increase the thermal diffusivity of the adhesive, and increase the strength of the adhesive. It also would be better to use an adhesive with a higher glass transition temperature than the one presently used, because the glass transition temperature of the present adhesive is much lower than the Curie temperature of the piezoelectric plates presently used in the MEGA stack and therefore acts as the weak link in the system. The piezoelectric plates presently used have a negative coefficient of thermal expansion, and therefore it would be better to replace the stainless steel bolts presently used to compress the stack with bolts having a much smaller coefficient of thermal expansion, like invar bolts, as the bolts result in compression being lost during heating of the stack which leads to damage and loss of functionality of the piezoelectric plates.

SECTION 3, VARIATION OF INERTIAL MASS FROM HOYLE-NARLIKAR COSMOLOGY

The third section takes off from the re-derivation by Fearn (using Hoyle-Narlikar's theory without the creation field) of the inertial mass fluctuation equation originally derived by Woodward. I derive the force differently from previous derivations by Woodward and Fearn, using the relativistic kinetic energy and purposely avoiding any use of the energy mass equivalence relation. I clearly identify the terms that are neglected. Only three assumptions are involved: 1. Hoyle-Narlikar's theory (dropping the creation field), 2. that the speed of material points is negligibly small compared to the speed of light and 3. that the second derivative with respect to time of the natural logarithm of the rest mass is negligibly small compared to the second derivative with respect to time of the kinetic energy per unit mass.

SECTION 4, THE MEGA DRIVE MODEL: 2 UNEQUAL MASSES CONNECTED BY A VISCOELASTIC PIEZOELECTRIC/ELECTROSTRICTIVE STACK

The fourth section discusses the MEGA drive mathematical model: 2 unequal masses connected by a stack of compressed viscoelastic piezoelectric/electrostrictive plates. The calculated natural frequency of the MEGA Langevin stack using book values for the material properties compares very well with the previously reported MEGA experiments.

SECTION 5, THE MACH EFFECT FORCE: ANALYSIS OF INPUT VARIABLES

Section five starts by discussing the exact analytical calculation of the Mach effect force on the center of mass as the product of the total mass times the acceleration of the center of mass. Most of this section is dedicated to a detailed discussion of the proper values of the input variables for the model. Although some of the input parameters have unquestionable values (like the gravitational constant or the speed of light) and other parameters are straightforward to measure (like the geometrical dimensions and the masses), other parameters are not, and therefore they deserve a thorough discussion. Prominent among these are the constitutive properties, since the materials involved in the MEGA drive experiments are anisotropic (different material properties in different directions), and their properties are a complex function of frequency, temperature, electric field, initial stress, fatigue life and electromechanical history, including polarization history. Material properties for which the material supplier gives book values still need to be carefully assessed. For example, in the rare case where the supplier gives the test conditions under which the material properties were measured, those test conditions may be unrepresentative of the MEGA stack testing conditions, and hence the input properties have to be carefully converted. Most importantly, previous derivations of the Mach effect force have not used the proper constitutive equations: they have used the voltage as the field variable. The proper field variable to use in electroelastic constitutive equations is the electric field (see Maxwell's equations) instead of the voltage. Previous Mach effect force derivations have used this improper constitutive equation and inconsistently used as an input the piezoelectric values based on the electric field (hence using different physical units, which has led to inconsistencies). Particular attention is dedicated to an examination of the value of the electrostrictive tensor physical component value, since this material property has such small value for the piezoelectric material used in MEGA experiments, paling in comparison to the piezoelectric effect, that it is not provided by the material supplier. The (fourth order) electrostriction tensor components can be properly defined in terms of the electric field or in terms of the polarization field. These constitutive properties are properly analyzed mathematically and the correct transformation is derived, which leads to a consistent value for the electrostrictive property to use in the analysis. Hysteresis in the strain vs. electric field or in the polarization vs. electric field domain are shown to be negligible for the MEGA experiments conducted up to now because of the low level of electric field applied in the experiments. For the MEGA drive experiments, much more important than nonlinearities like hysteresis, are the issues associated with the brittle nature of the piezoelectric materials employed. The electric field used for the MEGA experiments is ten times larger than the industry standard reliability limit for the electric field in piezoelectric ceramics. Furthermore, as previously discussed, due to thermal expansion mismatch between the piezoelectric stack and the stainless steel bolts, necessary pre-compression is progressively lost as the stack heats up due to internal heat generation, and therefore the piezoelectric stack becomes more prone to damage due to micro-crack propagation. I show that MEGA experiments should be conducted taking impedance vs. frequency spectra measurements of the MEGA drive stack immediately before and immediately after conducting the MEGA experiment, so that one knows the electromechanical fatigue state of the piezoelectric ceramic being tested ahead of the test, and can assess the level of damage suffered by the piezoelectric as a result of the test.

SECTION 6, THE MACH EFFECT FORCE: OUTPUT ANALYSIS

Section six analyzes the numerical results of different Mach effect force experiments. In addition to calculating the MEGA experiments conducted by Woodward and Fearn, the behavior of a MEGA drive floating freely in space is analyzed. A very small amplitude (a few nanoNewtons) subharmonic Mach effect force response due to the electrostrictive effect is calculated to take place at one half the first piezoelectric natural frequency. The magnitude of the Mach effect force at the first piezoelectric natural frequency is several thousands of times larger than the subharmonic electrostrictive resonance (as expected, since the value of the piezoelectric tensor component is 24 million times greater than the value of the electrostrictive tensor component and the applied electric field is not high enough to compensate for this difference). As the first fundamental frequency due to piezoelectricity is approached from lower or higher frequencies that are more than the (dimensionless) damping ratio (the ratio of the actual damping to the critical value of damping) away from the resonant frequency peak, the Mach effect force response is directed towards the tail (brass) big mass, in agreement with the experiments of Woodward and Fearn. Inside a bandwidth enveloped by the damping ratio, the Mach effect force response changes direction and is instead directed in the opposite direction, towards the front (aluminum) small mass, reaching a peak value at the piezoelectric natural frequency that is seven times greater than the peak value reached in the direction towards the tail mass. It is necessary to have equipment that can lock on this frequency with a bandwidth much smaller than the damping ratio to lock onto this peak Mach effect force. This is very difficult to do because as the MEGA Langevin stack vibrates, heat gets internally dissipated inside the piezoelectric plates, which raises the temperature, which changes the dimensions of the stack, as well as the piezoelectric and electrostrictive properties, hence the natural frequency changes during operation, and it needs to be chased within this small bandwidth. To achieve the highest Mach effect forces, it is better to have a material with a higher quality factor of resonance, but the higher the quality factor of resonance, the smaller this bandwidth around the natural frequency, hence the higher the quality factor of resonance, the more difficult it is to find and stay at the value of frequency at which Mach effect forces have larger values.

Fearn and Woodward tested the MEGA drive with several different tail (brass) masses while keeping everything else constant. They found that there was an optimal tail (brass) mass that maximized their measured Mach effect force. I show that this "optimal tail mass" is not a fixed characteristic of a piezoelectric Langevin stack, but it is an experimental artifact due to the restrained-end condition in the experiments run by Fearn and Woodward. A MEGA drive floating free in space will not exhibit an optimal tail mass, but the greater the tail mass the better, with diminishing returns as the tail mass gets larger, approaching an asymptotic value at infinite tail mass. For the experiments run by Fearn and Woodward, with a restrained-end, there is a different optimal tail mass that depends on how far the excitation frequency is from the natural frequency, and it depends on the stress and electrical history of the piezoelectric material.

SECTION 7, CONCLUSIONS

The final section states the conclusions of this study. I have selectively pointed out several of these conclusions in the previous synopsis of each section. The calculated direction of the Mach effect force and the optimal tail (brass) mass are shown to compare excellently with Woodward and Fearn's experimental data.

Section seven also discusses that in order for theoretical calculations to match experimental results (based on book values of material properties) it is necessary to introduce an ad-hoc factor. I show that Woodward and Fearn effectively used an ad-hoc factor of 0.2% multiplying the book value of the piezoelectric constant in their Mach effect force calculations of their MEGA drive experiments. In order to match the magnitude of the experimentally measured Mach effect force in Woodward and Fearn's MEGA experiments, it is also necessary in my analysis to introduce an ad-hoc factor of 0.4% multiplying the piezoelectric constant and the electrostrictive coefficient. This factor is about 100 times smaller than the coupling coefficient one would expect based on electromechanical coupling. Since the total Mach effect force is comprised of the multiplication of three excitation factors (two factors due to piezoelectricity and one factor due to electrostriction), the total ad-hoc coupling factor for the Mach effect force is quite small: of the order of one millionth ($10^{-2} \times 10^{-2} \times 10^{-2} = 10^{-6}$). The following explanations are considered to explain this ad-hoc coupling factor:

- Arguable reality (and magnitude) of the Mach effect propulsion hypothesis
- Neglected gradients of mass terms
- Neglected counterbalancing inertial mass fluctuations due to effects other than kinetic energy
- Material properties: modulus of elasticity and masses
- Material properties: piezoelectric and electrostrictive properties
- Material nonlinearity: strain vs. electric field hysteresis

- Material nonlinearity: polarization vs. electric field hysteresis
- Thermal effects
- Fracture mechanics and fatigue, including electromechanical history
- Mach effect inertial mass fluctuations may affect only a portion of the total mass

Upon examination of these possible explanations it is clear that several of the above explanations cannot be responsible for the coupling factor of 10^{-2} needed to match Woodward and Fearn's experimental results. Woodward stated in his book that it was not clear to him where exactly (within the affected masses) the mass fluctuations took place. I conclude that indeed, if the Woodward mass fluctuation propulsion hypothesis is real, the most plausible explanation for the small value of the coupling factor seems to be that the mass fluctuations most significantly take place over a small proportion of the total inertial mass. However, why the coupling factor on the piezoelectric and electrostrictive forces should be 10^{-2} or the coupling factor on the total Mach effect force should be 10^{-6} is unclear, as for example the electron-proton mass ratio is 5.446×10^{-4}.

DISCUSSION

During Rodal's talk, he gives a formula for a static solution to the displacement of the two masses in Jim's Mach Effect device, it has in it the electrostrictive parameter of the lead zirconate titanate, PZT (Steiner & Martins, Inc.'s SM–111, a modified form of PZT–4 or Navy Type I) material in it.

Fearn There are very few references that have the value of the electrostrictive parameter of PZT-4 in them, this equation shows how you can experimentally determine the value for electrostriction for a given stack at a certain temperature and frequency.

Rodal Yes, I only found 3 references that had enough data on experimentally measured values of electrostriction for PZT formulations to ascertain an estimate of the electrostrictive parameter of hard-doped PZT.

Meholic Does the natural frequency change with temperature, so as you run the device would it change natural frequency as it heats up?

Rodal Yes– the natural frequency will decrease with higher temperature (since the stiffness decreases with temperature) and will change with thermal, electrical, and stress-strain history. The PZT material is also very brittle, with very low value of fracture toughness. The scanning electron microscope image I showed reveals the presence of large voids between the grains. Those voids can coalesce and form cracks than can propagate and result first in softening (lower natural frequency), damage and eventual failure of the stack. Pre-compression has to be applied to the stack with bolts in tension, so that the PZT is not exposed to tension, to avoid the crack opening mode.

Hathaway Can you determine theoretically how much torque you need to put on the bolts for optimum thrust ?

Rodal We should not talk about the torque on the bolt but rather the bolt should be tightened based on the stress on the stack. The compression should be performed based on the magnitude of the compressive stress and not on torque level. You need to keep the stress constant, therefore you need to change the force (therefore change the torque) when you change the cross-sectional diameter of the stack. A smaller diameter stack made with the same material and having the same void volume, should use less force (and hence less torque) than a larger diameter stack. Once the optimal pre-compression stress is determined for a given piezoelectric material, all stacks made with the same material and having the same void volume content should be compressed to the same level of stress, which will often mean different levels of torque (depending on dimensions and depending on the void volume content). This is very important to maximize fatigue life. Insisting on blindly applying the same torque to all stacks without measuring the resulting compressive stress and ensuring the same stress is the wrong thing to do: it results in stacks having different stiffness, hence different natural frequencies, and also in shorter lifetimes of the stacks.

Buldrini *Nembo was not seated near a microphone and the question is hard to hear but the jist of it is the following...* Does the aluminum bracket have any effect on the natural frequency of the stack?

Rodal I took a good look at that. Either by luck or as a result of trial and error, the brackets in use are thin enough so that the stack behaves as a free-free resonant spring with lumped masses attached at its ends, at the resonant frequency, for stiffness purposes, disregarding damping. (However, the rubber pad at the end acts like a damper fixed at one end, and hence it impacts the force measurement). The support is not stiff enough (compared with the stiffness of the stack) to act as a stiff mechanical clamp. The bracket is able to flex and accommodate the natural frequencies of a free-free stack. We actually tested this, we used a piece of very thin aluminum as a bracket so thin it was easy to bend by hand and Heidi was worried it would not support the weight of the stack. Heidi ran one PZT stack with brass tail mass and aluminum head mass on Keith Wanser's SR-780 impedance analyzer with the ~ 0.72mm thick (2.7 g) aluminum bracket and ten separate runs of the regular ~ 3.21mm thick (6.8 g) aluminum bracket and all tests gave the same impedance spectrum (José shows a slide of the impedance spectrum with the different brackets showing the same results with both brackets). So we are quite sure that the bracket is effectively decoupling the device from the balance beam, for stiffness purposes, and is not significantly influencing the natural frequency of a free-free stack.

Broyles What were the bolts made of that hold the stack together?

Fearn There are 12 stainless steel bolts. Six 4:40 cap screws attach the brass to the mount bracket and six 2:56 cap screws run through the aluminum end cap on the outside of the PZT stack and enter the threaded brass mass. These hold the stack in place and have heat shrink around them for electrical insulation.

Broyles Stainless steel may not be the best material for the bolts. The heating effect comes from the stack I assume, and that is causing the shift in natural frequency?

Rodal The function of the bolts is to apply an initial compressive stress on the stack, its purpose being to avoid any tension during vibration, because the piezoelectric PZT material is very brittle and it will fail if tension is applied to it or if cracks can grow in crack opening mode. The coefficient of thermal expansion in the thickness direction of the plates of the piezoelectric material used in the MEGA stack PZT-4 (Navy Type I) is negative (the plate shrinks in the thickness direction due to an increase in temperature) during its first heating, particularly as the temperature gets near 100 $°C$ ($\alpha = -6\times10^{-6}$ per $°C$ at 100 $°C$). By comparison the coefficient of thermal expansion of metals like stainless steel is positive (it expands with temperature). The coefficient of thermal expansion of stainless steel has a magnitude about 3 times greater ($\alpha = +17\times10^{-6}$ per $°C$). During subsequent heating cycles, the magnitude of the coefficient of thermal expansion of PZT-4 substantially decreases ($\alpha = -1\times10^{-6}$ per $°C$ at 100 $°C$). This behavior (the fact that the PZT shrinks in the thickness direction, mainly during its first heating) is due to stress relaxation and softening of the PZT-4 material. So you are right, this entails a loss of compressive stress as the PZT-4 is heated. The problem is the thermal history dependence of the properties of PZT-4, particularly its stress relaxation behavior. To substantially ameliorate this behavior, all PZT stacks should be run through a first vibration run, and the compressive stress should be checked once again, and the torque should be re-applied if necessary, after that initial run to accommodate the stress relaxation of PZT-4. This will take care of the stress relaxation as well permanent shakedown (due to vibration) that takes place during initial heating, which is substantial. To accommodate further stress-relaxation, one can use, for example spring fasteners. Heidi has used Belleville springs to accommodate stress-relaxation of the stack. However, in practice, the use of Belleville springs did not result in any significant difference in the natural frequency or the forces measured with the MEGA stack.

Meholic It appears the only cooling, at the moment, is at the ends of the stack, by the brass mass and the aluminum end cap.

Rodal The heating is internally generated inside the volume. Cooling can only be provided through surfaces, hence a priority should be to maximize the amount of surface through which cooling is provided and to minimize the amount of internal volume generating the heat. The surface to volume ratio should be maximized, subject to other constraints (generating maximizing force). Passive cooling, using metal conductors as a heat sink is much more efficient than active cooling. Aside from changing the geometry (for example, instead of just providing heat sinks at the ends, to also provide metal heat sinks inside the stack and on its exterior cylindrical surface), the materials used need to be re-examined. The present choice of brass for the tail mass is a non-optimal choice. Copper would be a much better choice because copper has 3.5 times higher thermal conductivity and 3.4 times higher thermal diffusivity than brass, at practically the same density. The spot price for copper is about 50 cents per 100 grams (the typical mass of the tail mass in the MEGA drive) while brass sells for about 30 cents for 100 grams, so that the cost of copper (instead of brass) should not be an issue. Silver is even better: it has 3.7 times higher thermal conductivity than brass and 5 times higher thermal diffusivity than brass. What matters is thermal diffusivity because it is the material property governing transient heat transport: it measures the time rate of heat transfer from the hot side to the cold side. Silver sells for about \$60 per 100 grams. Is that unaffordable for the MEGA drive?

More questions were about to be asked ... coffee was being brought in....

Fearn Perhaps we should have a little break (we've just had two back-to-back theory talks) have some coffee and continue the discussion after we all calm down and relax a little ...

Audience laughter – coffee is up next –

MACH EFFECT GROUP DISCUSSION

Editor Note: The precedings sessions on various aspects of Mach effects produced such a zeal for further Mach-effect consensus building that the Block 4 scheduled session was cancelled, and Block 4 was devoted instead to the following stimulating follow-on discussion of Mach effects...

Bushnell: I just have a couple of observations. A few of us came here to really carve out the Mach effects and the EM drive details. We have a lot of people asking us about this stuff. It is incredibly important to get this right. First of all the retro-causation theory that we heard of, this is one of many interpretations of quantum mechanics. There is no canonical interpretation of quantum mechanics, there is no agreement on the correct version of quantum mechanics.

We heard this morning what I think is a superb presentation by George Hathaway. I asked the JSC (Johnson Space Center) people (namely Eagleworks), they have a chart we could go over, they had an experimental chart with some of the experimental artifacts and issues on their particular thing, (EM drive) I didn't see a similar chart, maybe George has one for Jim's (James Woodward's) Mach effect work.

So I asked Jim, have you been through all this, because you say the people at JSC have been beat up by the JASONS (an independent group of elite scientists which advises the United States government on matters of science and technology, mostly of a sensitive nature) and some external committees that JSC brought in, to look at all this. Jim replied he had not had time to go through them all. So the current state of play seems to be, that the amounts of force from the Mach effects are still fairly small, that all of the experimental artifacts and issues have not by any means been addressed and unless and until they are, and the importance of this is so massive, that I think we deserve to (for the scientific people as well as society) do our due objective diligence on this, just as well as we can, before we decide what is right and what's wrong, what's real and what's not OK.

The issue of the Mach effect. You know I've been an engineer I'm not a physicist, so I go read stuff. The vogues in physics are not particularly kind to the Mach business. So along with the retro causation, there's the whole issue of the viability of the Mach approach. So there's a lot of issues here that I think need to be discussed going forward and the people in this room, a great many of them, are probably the best in the country to do that.

This is why I prevailed and fussed at the organizers. They came to me and they said no no we got a schedule, we got to move forward and do this and so forth and I looked at them and I said this is supposed to be a technical meeting, we're not here to salute schedules as far as I am concerned. We're here to sort out what's really going on with all this stuff. Thank you for listening.

Fearn: Dennis Bushnell is correct, this is a technical meeting and a workshop. The schedule is not as important as the discussion we are here to promote. We were supposed to leave time after the talk (and during) for feedback and discussion. So in order to allow for Q&A we are going to postpone the rest of todays talks and continue right now with a Q&A session for both José, myself and earlier talks.

Woodward: Can I start off with a question to George? I think I may have missed something that was said about a replication [of the Mach effect] using a device that I sent you. I heard later on, near the end of your talk, you said you saw a 0.2μN thrust which is about the same thing that Nembo got with a similar device that I sent him. Did you see the transients as well?

Hathaway: Yes, I called them "pips" in my talk, they were not as pronounced as yours but they were in the right direction.

Woodward: Were you using the picoscope software? (a small device which hooks up to a computer via USB and generates an oscilloscope like screen on the computer monitor)

Hathaway: No, I was using a standard oscilloscope, a real analog type scope. You know, one of those old things with a funny looking small green screen...

Woodward: I remember storage oscilloscopes where you had to pull a handle down...

...laughter...

Hathaway: Well not quite that old, I used an analog scope and some digital ones too, but I like the analog scopes when there are fast transients. If I want to see a fast transient I throw the digital scope out of the window. But I did see the "pips", as I called them, the leading edge and the trailing edge on the thrust trace.

Woodward: Okay, and theoretically the reaction mass you have was the 5/8" brass mass and Heidi gave you the new 3/4" brass mass to use?

Hathaway: Yes, I presume take off the old brass mass and substitute this new one and everything else stays the same?

Woodward: Yes that's right.

Buldrini: I would recommend you let the device sit in the vacuum chamber for some time before making a new measurement because the PZT (lead zirconium titanate) tends to absorb water vapor which reduces the Mach effect force.

Hathaway: Yes and I'll make sure I re-torque the bolts to 4 inch pounds as Jim recommends.

Woodward: That's 4 inch pounds for the 2:56 bolts and 2.5 inch pounds for the 4:40 bolts. I just wanted to make sure I didn't miss anything important this morning.

Hathaway: What you did miss was my many concerns about prosaic effects and one of them was something you brought up. You mentioned the Lorentz air effect where there is a possibility that you can give enough momentum to enough air molecules that they collectively produce a force that is measurable. That was one of the issues I forgot to mention.

Woodward: The way that is taken care of is by simply running the device at different pressures because the Mach effect does not change with pressure. The Lorentz air force however, would be greater at higher pressure.

Rodal: It is extremely important to characterize what it is that you are going to measure before you run the test. Otherwise one is flying blind. That piezoelectric materials have history dependent properties has been known for 100 years. The PZT may lose its poling. Every time you conduct a test you are going through cycles where you may cause damage to PZT, which is a very brittle sintered ceramic, and you need to characterize its state of damage. I would run an impedance spectrum and I would look for the natural frequencies. It should be that the natural frequencies are staying the same. If those frequencies are getting lower every time, you know that you have damage. The mechanical natural frequency depends on the square root of the stiffness divided by the mass. The mass is not going to increase with cyclic life. The only reason the natural resonances would decrease is due to damage; it is caused by the stiffness going down with time. This happens because there are cracks emanating from voids in the sintered ceramic PZT and they cause a decrease in the resonant frequency. So when you run the device again and again and see the force decreasing every time it may be due to damage. These sintered ceramic materials are sensitive to fatigue damage. Conducting tests on a stack without immediately prior conducting impedance testing is like a physician conducting a stress test on a patient without prior measuring her blood pressure, pulse and other physical tests. Also this goes for any statistical analysis that plots variability without taking into account the initial state of damage. It is not right really to compare the results of healthy new stacks to old stacks. For example, let's suppose that that Jim measures a new, young vital stack and someone else [George or Nembo] measures an old decrepit stack, clearly the young one without all the damage is going to do much better.

Hathaway: To add to that comment, something that was glossed over, there is an accelerometer in the stack, that is also a good, subtle way, of looking at how the stack maybe deteriorating. The comparison between the input waveform and the waveform that is produced by that accelerometer at the beginning of your series of experiments versus say the the middle or the end of your data set because that accelerometer itself can change characteristics because it is inside the stack, it's the same material as the stack.

Woodward: Yes, the accelerometer is just a thinner PZT disc 0.3mm thick, rather than 1 or 2mm thick for the rest of the discs.

Hathaway: Right, so they are of the same material only thinner, so they are even more subject to change than the thicker discs.

Meholic: How do you get the signal out of the accelerometer?

Fearn: There are wires attached to the electrodes on either side of the accelerometer. The accelerometer is the only disc in the stack not receiving power. We take out the piezoelectric voltage, caused by contraction in the stack, and use that as an indication of stack acceleration.

Meholic: So you have electrodes inside the stack of PZT discs, made of brass, that must change the whole integrity of the stack. Jose drew the stack, in his model, as if it was a spring, now you have this different material in the stack which must change the properties?

Rodal: Right, not only do you have damage due to initial voids in the PZT that coalesce into cracks, but you have to consider the unequal stiffness of the segments in the stack, which translate into interface stresses: the PZT, the epoxy adhesive and the electrodes have different stiffness. Therefore you also have, due to cyclic fatigue, damage at the PZT/adhesive/electrode interfaces. You have a spring which does not have equal stiffness in each segment of the stack. That segmented nature of the stack makes the system more complex.

Meholic: So it sounds like, what you have been saying, that these stacks have a very limited life span, because the material breaks down that is key to producing the Mach effect.

Woodward: In test devices that is true, but when these things go into production, and you know the thing is working the way you think it is, you'll be able to cool them and keep them in running order much longer than it is possible when it's just an isolated device in a vacuum chamber with no real heat sink attached to it.

Meholic: But, independent of the cooling, you have high cycle fatigue that was mentioned to worry about.

Rodal: Wait, remember we have 100 years of transducer knowledge for sonar, and there is a lot of data on this. With a commercial device you can go through billions and billions of cycles. But look at what we have here. Here we have a stack where every piezoelectric disc has been bonded with epoxy adhesive by hand, with an unfilled epoxy mixed and cured at low temperature (120 degree Centigrade) for 1 hour, hence having a low Tg (Glass transition temperature).

Meholic: So my basic question was assuming those stacks show a real effect, then you can scale these up? Is the science of piezoelectric materials sufficient to allow you to have a long life thruster?

Woodward: Yes

Rodal: Yes, but you have to be skeptical like Dennis was saying. You cannot assume that every problem is going to automatically take care of itself. We know this fatigue is a well known problem, and it has been tackled before with success. How has it been dealt with? You can either co-sinter the electrodes directly to the piezoelectric ceramic so you don't have the bonding problem or use an adhesive with fillers (that raise the adhesive strength and stiffness as well as thermal conductivity and reduce the thermal expansion). Another approach is to have a single crystal so that you avoid the grain boundaries and voids that promote crack damage. Another concern has to do with the preload. At the moment, the preload is kind of empirical isn't it. [To Woodward] You have not run a finite element analysis to look at fracture mechanics parameters like KIc and KIIc (stress intensity factors, in crack opening mode and in-plane shear mode, respectively.) and determined what kind of preload they need to have. This kind of analysis can be done and has been done in the aerospace industry. If you do that, then the device can be taken to a very high number of fatigue cycles and if run below the fatigue endurance limit one can talk about infinite life. But this requires using a high level of technology to do the analysis and construct the stacks. [Rodal refers to self healing materials]

Meholic: Okay. Here's another weird question for you, Jim. Assume this is based on my primordial understanding of what you guys are doing. So this stack changes its energy content and so essentially changes its mass and the universe reacts accordingly. In the same vein, if it's changing its energy and this changing its mass, does the Earth react on it accordingly to give it a vertical component of displacement?

Woodward: Yes very slightly

Meholic: Why is it very slightly vertical and more horizontally?

Woodward: Because the Earth's gravitational field at the surface is only GM/R for potential energy. The universal potential is $\phi = c^2$ for flat space, which is a lot bigger.

Fearn: The property of inertia is due mainly to the distant matter in the universe. That is what Einstein believed, as did John Wheeler.

Hathaway: Can you guys summarize for me, I think we have at least 3 different methods of arriving at Jim's mass change formula for the Mach effect. We have Jim's, Heidi's, and José's is that a correct evaluation?

Woodward: There's a fourth, that is Lance [Williams] has another way, from linearized general relativity.

Fearn: Yes that's about right. I used Hoyle and Narlikar gravitation which is a fully Machian theory. It is fully covariant and reduces to Einstein's general relativity in the limit of a smooth fluid, in the rest frame of the fluid. I found Jim's mass change equation in the Hoyle Narlikar field equation for a smooth fluid mass density, together with some extra spatially changing mass terms.

Mathes: Heidi, can you write an executive summary, two pages that explain the Hoyle Narlikar theory simply, so a non specialist can understand the derivation?

Fearn: I have some typed up notes from reading the Hoyle Narlikar papers and book, but it's about 60 pages...

Meholic: That's brief for Heidi...

...laughter...

Rodal: There is a difference, because I was looking very skeptically at this at the beginning and I was able to reconcile this looking at kinetic energy, where I can see a clear path to get through it. I am not happy in the derivation where you put $E = mc^2$ and translate into a changing mass. Einstein's first $E = mc^2$ proof was shown to be a circular argument. Einstein himself was so dissatisfied by it that he had a number of improved derivations throughout his life. I can only see it when I consider kinetic energy, then I can see it step by step. I think it is very interesting that the experiment is showing a force in the same direction as the calculation. I can also calculate an optimal tail (brass) mass. This could be a coincidence, but I find it very interesting at this point. But I am not there yet because to match results I need to use a single coupling factor of unknown origin. I think that there are a lot of nonlinear terms that are being dropped and those need to be examined in more detail.

Hathaway: Is there any overlap between the derivations of Jim, Heidi and Lance or are the theories totally independent?

Woodward: They are three variants on making one or two assumptions. One assumption is that the rest mass is not a constant, the rest mass can change with time. The other is that inertia is a gravitational effect and those are the only two assumptions you need. In effect the three derivations you are talking about are three ways of getting to the same answer. Simply a choice of approximation.

Williams: But they come out somewhat different. I get something a bit different, but in essential aspects they are the same.

Hathaway: Looking at it from the view point of a physics journal editor, these three papers come in, and they are all essentially claiming the same bottom line. I'm thinking logically are they self consistent, are they saying the same thing from different viewpoints and so you should put them all together or state the individual assumptions that are similar or different than the other two.

Woodward: Let me give you an example, Lance versus mine. What Lance does, he derives the result from the geodesic equation and in order to get the result he makes an assumption about the time dependence of the field quantities in favor of the time dependence of the source quantities.

Williams: I just used standard linear general relativity, like in gravitational waves or the Newtonian limit.

Woodward: You can read Lance's version, it's in the prep kit he sent out and you'll see what I mean. You'll find there that he has a comment about how his version differs from mine because I insisted on keeping the time dependent quantities as field quantities so I would get the d'Alembertian of the potential is equal to the sources, he gets the Laplacian of the potential is equal to the sources. But the time dependent sources are basically the same thing. So it's a matter of his choice of approximation versus my choice. It's not a matter of fundamental elementary physics. He's not talking about anything fundamentally different than me. Would you say that's fair Lance?

Williams: Yes that's sounds fair.

Hudson: It sounds like some high level comparison between differences and assumptions

Woodward: No, it's just the difference between a theoretician and an experimentalist...

...laughter...

Hudson: That's okay but I still think it might be useful.

Rodal: Yes it would be nice to know what the assumptions are. You just said there is a difference in the assumptions being made, I would like to know.

Woodward: You can read Lance's paper too and you'll see what I mean.

Williams: Also, there is a quick study that summarizes Jim's derivation, and it has all the assumptions that Jim made, straight out of the stargates book [Referring to "Making starships and stargates", Springer

2012, by J. F. Woodward]. My version does not have any of the assumptions that Jim has, it's just mechanical linear general relativity.

Kelly: You said there were two assumptions. One was that inertia is a gravitational effect. Isn't there some kind of experimental test to show if the Mach principle is true? Since the universe is expanding wouldn't inertia (from Mach's principle) be different in the past from what it is now? Isn't there some distant object you could look at to show if inertia has changed?

Woodward: As it turns out Wes, that's not true in general relativistic cosmology. Because you are choosing one cosmological model, it's one that is spatially flat and borderline between open and closed universes and that has the odd property that the value of Ω, which is the measure of spatial flatness ($\Omega = 1$ in this case) is the same in all epochs. So all of this is automatically compensated for. Inertia in early epochs and inertia in much later epochs than ours, will be the same if $\Omega = 1$. You can do experiments to see if $\Omega = 1$ or not.

Kelly: The whole idea of inertia seems a bit slippery to me

Woodward: Yes I agree, it was slippery when I first came across it too.

Hathaway: Are there any other experiments other than force experiments that could validate Jim's theory? Anything that does not involve measuring small thrusts?

Woodward: Yes.... Big thrusts!!

...laughter...

Woodward: No seriously, what we really want to do now is find a way of scaling the thrust, with the merger resources we have, as quickly as possible. Indeed, I've already talked with Jose about this. I'm going to be ordering a bunch of Steiner-Martins crystals sometime in the next week or two and perhaps you could join in the conversation about what would be the ideal configuration for those....

Hudson: What bothered me about your talk [addressing Hathaway] this morning, was all these tiny effects you were trying to mitigate by proper experimental design. But if you put a rocket engine on a test stand you won't pay attention to the rotation of the earth or the angle of the sun, these are obviated completely by the scale of the thrust. A demonstration of an ambiguously larger thrust that would eliminate the concern about many of these small experimental error sources, that you described, would go a long long way to making the Mach effect look real to the public. This is why I have always encouraged more thrust. I know a lot of people in this room view rockets as the best way of getting into space, and I agree with this, but I think the problem of energy dissipation in these Mach devices, perhaps the problem of fabrication might actually be solved by the technologies we use in the liquid rocket industry. I would like to get the few of us with liquid rocket experience sitting down together with the physicists to engineer a new device that could incorporate some of these new technologies. We can do things today that were impossible ten years ago. Things like diffusion bonding, small channel laminar flow for cooling...

Hansen: These new technologies will change the resonant frequency of the device. There are more ways of cooling than with rocket technologies. A rocket engine runs at several thousand Kelvin, a PZT stack won't get anywhere near those temperatures, it would no longer function long before those temperatures are reached. So there are other ways to deal with it. My main job is working with radar. They are actively cooled, some are air cooled. We also look at duty cycle, which is the amount of time you transmit versus the time you don't. Some of that is based on heat, because you can't heat up the radar components more than a certain amount. We have to calculate how much heat we have to take out before we do any cooling because we don't want to spend too much money on a solution.

Turner: I would like to follow through with Gary's idea of where we could go with this. You mentioned to Jim that there were things you could do to increase the thrust level substantially. So if I look at tens of micro Newton of thrust requiring a 100W of power and assuming power is 10W per Kilogram I don't get a very big acceleration and I haven't put a payload in yet. So what are the thoughts on how to scale this to something that is practical?

...discussion about packaging of multiple wafers onto a sheet of silicon and discussion of possible arrays of devices that have not been tested yet...

Turner: But there was talk about even the current devices producing more thrust, how would that work?

Rodal: Yes, the first order of business is to improve the device we have working now. Correct me if I am wrong Jim, but you are using guitar amplifiers and set the frequency by hand with no automated control?

Woodward: Yes that's right.

Rodal: To me, the first order of business is to have automatic frequency control. This would allow you to track the resonant frequency with a very small bandwidth. The bandwidth you need to be at resonance has to be considerably smaller than 1/(2Q) where Q is the mechanical quality factor, with the value of Q about 1000. The people that are working on the EM drive, at much higher Q, are already using automatic frequency control. This may get you about 10 to 50 times more force. We want 1000 times more force, so how do we get it? That is where I see the nonlinear terms that were dropped out of the equation coming into play. The terms that have been dropped may play a very important role especially in the damping term (the speed term). Most people neglect damping altogether and just say it is very small. But assuming zero damping means an infinite amplitude response, which is absurd. There must be damping because of the second law of thermodynamics. What does neglecting these nonlinear terms do? Well it may result in a Mach effect force which is much smaller than it could be, not by 10 times, by 100 times, possibly by orders of magnitude. How could it be a million times? By parametric amplification and self excitation, considering nonlinear dynamics. Many types of rocket engines have exhibited self-excited vibration. They are called POGO vibrations, the Saturn V had a number of bad episodes due to POGO self excited vibrations. All this knowledge of self-excitation has not yet been applied [to the Mach effect drive]. I would like to explore how a Mach effect force can be amplified by nonlinear, self-excitation, and that's it.

Hudson: Do you have an idea how to take advantage of this nonlinear effect?

Rodal: Yes I do. The trouble is, to take into account all the nonlinear terms that have been dropped out, will result in an exponentially larger number of terms, that would demand very large computational resources in terms of memory and computing time. At the moment I am calculating 20 + 269 terms, where each term involves a large number of terms, this is no problem at the moment. However, to take into account the neglected nonlinear terms would result in an exponentially larger number of terms. Is anyone here using Mathematica? If you try to use Mathematica to analytically solve expressions with a larger number of terms you know what a hard time Mathematica has to deal with a large number of terms.

Mathes: We can rent time on a cluster or supercomputer to deal with whatever you can throw at us. We can buy a supercomputer off the shelf at Amazon these days. It's a big problem but one that money can solve.

Hathaway: How far will the nonlinear code go to suggesting new experimental approaches for increasing the Mach force?

Rodal: When you run your Mach effect experiment, what are you doing with the frequency? Can you assure me that you are right on resonance? And as the resonance frequency changes due to thermal and nonlinear effects are you changing the frequency to match?

Hathaway: I'm using the same manual method as Jim is using.

Rodal: Well that's no good.

Hathaway: Absolutely, I agree... Automatic frequency control is clearly the first thing to do, but parametric amplification can come in a number of different forms, and sometimes it comes with different materials. Materials can change in a way you can exploit to get your parametric amplification. Sometimes its a DC electrical signal superimposed on an AC signal. Would throwing a large amount of money at the computer problem allow the experimentalist to extract from that a way of conducting the experiment to achieve more force?

Rodal: Are you familiar with the Van der Pol equation, that is a good example. We need to consider the additional terms as nonlinear additions to the equation. Once they are taken into account we can say what the experimentalist should look out for.

Fearn – note added in proof: In dynamics, the Van der Pol equation represents an oscillator with a nonlinear damping term. It evolves according to the equation, $\ddot{x} - \mu(1 - x^2)\dot{x} + x = 0$, where x is position and μ is a scalar indicating the strength of the nonlinear damping. This equation has a simple representation in terms of a small circuit shown in the Figure below.

Hathaway: In the case of the Van der Pol equation, it could be interpreted as a little oscillator circuit and you could see the amplification going up like crazy.

Rodal: Exactly, if you can, and I don't know if you can, but if you can get self excitation in the mass fluctuation then it will proceed like in the Van der Pol equation and the force will increase dramatically.

Hathaway: In that case, you are taking known off the shelf components, putting them together in a particular way, and getting an unusual result...

Rodal: Yes that's right.

Hathaway: And the "unusual result" is perfectly calculable through the Van der Pol equation.

Rodal: In that case you know the exact equation, but in the Mach effect case we don't have the exact equation because a large number of nonlinear terms were dropped.

Hathaway: In these other systems, if you dope the piezoelectric material, like these PZT discs, you might enable parametric amplification that way.

Rodal: This is an excellent point, I completely agree with you. As far as I know, Jim has tried all kinds of devices before the piezoelectric one, you tried capacitors as well right?

Woodward: Yes...

Hathaway: Certainly, the first step is to introduce automatic frequency control, but perhaps you can focus in on exactly which nonlinear terms could produce an approach to an engineering solution for parametric amplification.

Rodal: I can certainly analyze this problem and perhaps come up with something in a few weeks. I have solved problems like this at MIT and also in my professional life. I worked for a company that made very large industrial machines which had all kinds of self excitation problems. It was a big headache for them that we were able to solve and gain a big advantage on our competition. The machines had polymer components that had nonlinear frequency-and-temperature-dependent damping characteristics that resulted in self excitation which increased the magnitude of vibration exponentially under certain operating conditions. Normally you need to eliminate mechanical self excitation problems. This is the first time, I have a problem, where I need to enhance the self excitation!

Hathaway: José mentions a good point, you need to be able to throttle this parametric amplification or you might "blow up" your device.

Rodal: Jim is presently running chirps instead of steady-state resonance. I don't want to self excite to the point that I destroy the stack. These self excitations grow exponentially, they follow a curve and you can stop it at a certain point. To stop them, all you have to do is to cut off the voltage to the stack.

Hathaway: The chirp and voltage cutoff would be part of the autotune system.

Rodal: Yes, as soon as you stop chasing the resonant frequency the self excitation will fall off. In industry, sometimes these big machines with rotational parts start vibrating strongly and the operator gets scared and slowly reduces the speed just a bit, which makes matters worse due to the nonlinear nature of the vibration backbone curve - which is of course the worst thing you can do - it usually makes the vibration worse - you should rapidly increase the speed to reduce the self excitation. But naturally, people are afraid to do this.

Tajmar: I would like to throw in a comment. You spoke a lot of electrostriction, there is also magnetostriction. This introduces a totally different material, there may be no cracks in this like in the piezoelectric you

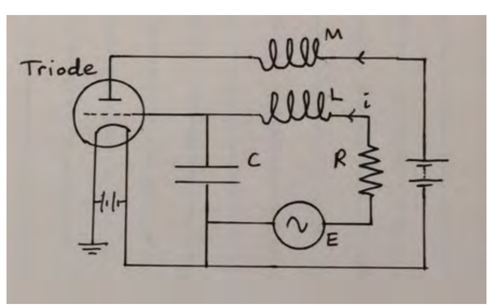

FIG. 1: This is a simple Van der Pol Oscillator using a Triode

are using.

Rodal: So Martin just reminded me of something here. The frequency dependence of the force. If we look at the equations we see a ω^6 and an ω^{10}, you think wow, our problems are solved, just go to higher frequency. But it is not so simple. You have damping and the equations are complex. Several parameters depend on frequency so really the frequency dependence for the force is more like $\omega^{5/2}$ or somewhere between the second and third power. This is what my solution shows when one calculates specific examples.

Fearn: Experimentally, we can show the increase of force cannot exceed ω^2 or ω^3 at most. The frequency range, that we have data for, is between 29KHz and 40 KHz and so we would have noticed a huge increase in force if the frequency dependence was something like ω^6, and we haven't seen that.

Rodal: So we are confident that the experiments show that the force should go up with something like the square of the frequency, so we should go to higher natural frequency devices. The quickest way to do that is to make shorter stacks.

Tajmar: Then we have a much higher dissipation rate, perhaps a higher voltage would also work.

Rodal: The voltage increase would work, the force goes like V^4 but that is not attractive from the point of view of power consumption... If you go to one or two discs there is another problem with the frequency. These discs are expanding not only in the longitudinal direction (the thickness direction of the PZT discs) but also in the perpendicular direction, the radial direction of the stack. The radial resonances are due to shear deformation and result in similar or lower natural frequencies than the longitudinal resonances for the very short stacks, so you may excite the wrong mode. For the Mach effect you need to excite the longitudinal mode. We haven't tried yet going from 8 discs to 4 discs which might be better. There are also many other piezoelectric materials that we could test, other than PZT, doped materials. A lot of things could be done if we have enough people and divide up the work.

Hathaway: Jim did you ever try using quartz crystals in any of these stacks?

Woodward: No. I inherited a collection of PZT 19mm discs from a nearby industry. They had a fabrication facility just to the south of campus. They were closing down and phoned up the university asking if anyone could use a batch of PZT discs - so I took them.

Hathaway: I'm wondering since the quartz crystals have a much higher mechanical quality factor than the PZT stacks. Quartz has a lower piezoelectric action than the PZT but it maybe that the higher quality factor trumps it.

Rodal: But we have historical experience from the piezoelectric transducers for Sonar. They started with quartz 100 years ago and they moved to PZT more than 60 years ago. However, for the transducer you also want higher displacement.

Hathaway: That's true, but we are not looking for high displacement for the Mach effect.

Rodal: That's right, it is not necessarily the case that what makes the best transducer will produce the largest Mach force.

Hudson: Have you looked at some of the latest sonar transducers? I'm not sure that the Navy is still using PZT's any more.

Woodward: They may well be using a PZT-PMN composite material that came out about 5 years ago. It used to be that you could buy pure PMN by itself and now you can't.

Hathaway: You have to make it yourself, like we did.

Woodward: Yes, but you can purchase PZT-PMN composite materials, it's just a lot more expensive than the Steiner Martins (SM-111) material I've been using.

Hathaway: Another question for Jim: what is the downside of making a boat, instead of your Faraday cage, and filling the boat with a dielectric fluid to put your stack into, for cooling purposes?

Woodward: Once you are satisfied that the stack is really producing thrust, and there are probably half a dozen people in this room that figure this is really a good bet - at that point talking about any kind of cooling process that doesn't mechanically disrupt the function of the device will do. Since you don't need to worry about Lorentz forces in the fluid that might be making something appear as a force of non Mach origin.

Hathaway: The next question is, can Jose's equations handle a fluid bath of a material of a specific density? So I'm suggesting we immerse the entire moving body in a bath of dielectric fluid.

Rodal: As a skeptical experimenter, if I take a powerful probe (like a scanning electron microscope) and take a close look at this material stack, I will see a lot of little voids, and eventually cracks that may be interconnected. Now I'm going to be putting this stack into a fluid and I know that when I do this, when the stack expands a crack will open and the liquid will flow inside. Now when the stack goes into compression I have that fluid there, that is going to expand the crack and cause damage at the crack tip, further expanding the crack. So the result is damage. Damage that results in lower natural frequency, lower stiffness and eventually failure. I need some way of keeping the fluid out of the cracks. You also need a low viscosity fluid because of the damping.

Hathaway: Yes, I was thinking of a low viscosity fluid with a high thermal conductivity. Can this be fit into your computational model? Can you show that it would not damp the stack too much?

Rodal: Yes it can be worked out. You have a nonslip boundary condition between the cylinder and the fluid. I don't think it would be a major problem to model. You would have to use a non-permeable material interface. Epoxy is not acceptable. Epoxy, like most polymers, is quite permeable to fluids.

Woodward: Instead of using a liquid you could use Helium gas at room temperature. Helium has fabulous thermal properties.

Woodward: The other thing is, given my slight knowledge of the PZT business, they have very elaborate encapsulation techniques for commercial PZT's. If you set a non-coated PZT disc out in a humid environment, the disc will absorb water vapor and that kills it. We have been keeping our PZT's in sealed containers with desiccant or inside the vacuum chamber to preserve it. When the discs absorb water vapor they do not function very well. I discovered this by accident a few years ago. In some cases you can reverse the damage just by putting the stack into the vacuum chamber and pumping on it for a month. It gets the water vapor out of the cracks.

Hudson: It would be better from the rocket engineer point of view, to have a solid state cooling solution. I wouldn't want to put a fluid on a rocket undergoing high g-forces.

Hathaway: Oh no, I'm talking about for laboratory experimental purposes. My basic question is whether Jose's equations are amenable to adding this kind of fluid bath and noting if it might cause too much damping to be an effective cooling method or not.

Rodal: Yes it is doable to model it.

MUSINGS ON MACH EFFECTS

J. F. Woodward[1]
Department of Physics
California State University Fullerton

1. INTRODUCTION

As you have already heard, tests of Mach effect thrusters (METs), or as they have recently been renamed, Mach effect gravity assist (MEGA) drives, in three labs other than ours at CSUF, have produced thrust signatures like those we have obtained over the past several years. These tests, Nembo Buldrini at FOTEC (Austria), George Hathaway in Toronto, and Martin Tajmar at Dresden Technical University, have all been conducted by experts with world class facilities at their disposal. Buldrini's corroboration was made public a year and a half ago. Hathaway's results have been known to me for more than a year, but only made public at this workshop. Heidi (Fearn) and I were alerted by Martin that he was working on a replication several months ago, but it has only been in the past few days that anyone, including Martin I gather, has learned the outcome of his work.

Remarks by each of these presenters relating to the observation of Mach effect thrusts are to be found in these published proceedings. Tajmar and Hathaway are somewhat more circumspect in their written version than they were at the workshop. Buldrini's remarks in writing are somewhat more complete. If this is an area of interest, you should view the videos of the workshop on their SSI YouTube channel. Buldrini's entire talk was devoted to this topic. Hathaway's comments are at 52:40 – 56:20 minutes in his presentation. Tajmar's remarks are found at 6:08 – 26:30 minutes in his presentation.

We will all tell you that much work remains to be done before the scientific test apparatus we have been working with can be transformed into practical devices, the space drives of popular lore. Nonetheless, over the past few years, we at CSUF have been working in the direction of a transition from science to engineering. This has been especially true in the past six months or so. So the focus of this talk will NOT be to defend the scientific integrity of the experimental work and the implications of its results. Rather, the focus will be on issues related to making the transition from science to engineering.

2. MACH EFFECTS

Mach effects are fluctuations in the rest masses of extended objects capable of storing internal energy as they are accelerated by external forces. This is a consequence of the action of the total (local and cosmic) gravitational field acting as the inertial reaction force that resists the acceleration, excited by the action of the accelerating external force. The predicted phenomena in question, in the relativistic Newtonian limit, arise from considering the effect of an "external" accelerating force on a massive, extended test particle. Instead of assuming that such an acceleration will lead to the launching of a (ridiculously minuscule) gravitational wave and asking about the propagation of that wave, one assumes that the inertial reaction force, acting through the accelerating test particle, experienced by the accelerating agent is caused by the action of, in Dennis Sciama's words, "the radiation field of the universe" [1]. Then, allowing that the inertial force is produced by the gravitational action of chiefly distant matter, one asks, given the field strength as the inertial reaction force per unit mass, what is the local source charge density at the test particle? Taking the direction of the accelerating force to be positive, the field strength at the test particle is just minus the derivative of the four momentum of the test particle with respect to proper time divided by the mass of the test particle.

---

[1] jwoodward@fullerton.edu

I should call attention here to an issue that can be the source of confusion. The time-like part of the four momentum is $mc = \gamma m_0 c$, where m_0 is the rest mass of the test particle. One sometimes hears it claimed that rest mass is a constant. This statement, as a general assertion, is simply false. It may be true for structureless elementary particles. But for systems as simple as colliding billiard balls, it is obviously wrong during the collision. This means that when the derivative of $\gamma m_0 c$ is taken, terms involving the derivative of m_0 cannot be set equal to zero. Life can be a lot more complicated when rest mass isn't treated as a constant. But that's our reality.

The answer to the local sources question is obtained by taking the four-divergence of the field strength at the test particle. The field equation that results from these operations is:

$$\nabla^2\phi - \frac{1}{\rho_0 c^2}\frac{\partial^2 E_0}{\partial t^2} + \left(\frac{1}{\rho_0 c^2}\right)^2\left(\frac{\partial E_0}{\partial t}\right)^2 = 4\pi G\rho_0 \tag{1}$$

In this equation ϕ is the scalar potential of the gravitational field, ρ_0 the local proper matter density, E_0 the local proper energy density, c the vacuum speed of light, and G Newton's constant of gravitation. This equation looks very much like a wave equation. However, the space-like part (the Laplacian) involves a scalar potential, whereas the time-like part (the time-derivatives) involves the rest energy density. (The complete derivation of these effects can be found in Chapter 3 of Making Starships and Stargates, Springer, 2013, [2]). Were we dealing with any other interaction than gravity and inertia, we would be stuck at this point, for there would be no way to extract a time-like term from the rest energy dependent terms to complete and isolate the d'Alembertian of ϕ on the left hand side of Equation (3.1). But we are not dealing with any old (or new) field. We are dealing with gravity understood, as Einstein did, to encompass inertia.

When inertial forces arise from the gravitational action of chiefly distant matter, one finds that the total gravitational potential everywhere/when must be locally measured to be equal to the square of the speed of light. [2] And you don't even have to fudge to get the dimensions to turn out right. The dimension of ϕ is velocity squared. If ϕ isn't equal to the square of the speed of light, then inertial forces are not equal and opposite to applied forces. That is, Newton's third law is violated.

Now, Equation (1) can be put into the form of a standard classical wave equation by using the gravitational origin of inertia to "separate variables", for the gravitational origin of inertia implies more than the statement above involving the origin of inertial reaction forces. Indeed, it actually implies that the origin of mass is the gravitational interaction. In particular, the inertial masses of material objects are a consequence of their potential energy that arises from their gravitational interaction with the rest of the matter in the causally connected part of the universe. That is, in terms of densities,

$$E_g = \rho\phi \tag{2}$$

where E_g is the local gravitational potential energy density, ρ the local "quantity of matter"' density, and ϕ the total gravitational potential at that point. (Note that it follows from Sciama's analysis that $\phi/c^2 = 1$, so Equation (2) is nothing more than the well-known relationship between mass and energy that follows from special relativity theory if E_g is taken to be the total local energy density.) Using this form of the gravitational origin of inertia, we can write:

$$E_0 = \rho_0\phi \tag{3}$$

and this expression can be used in Equation (1) to affect the separation of variables. After some straightforward algebra (recounted in [2]) we find that:

$$\nabla^2\phi - \frac{1}{c^2}\frac{\partial^2\phi}{\partial t^2} = 4\pi G\rho_0 + \frac{\phi}{\rho_0 c^2}\frac{\partial^2\rho_0}{\partial t^2} - \left(\frac{\phi}{\rho_0 c^2}\right)^2\left(\frac{\partial\rho_0}{\partial t}\right)^2 - \frac{1}{c^4}\left(\frac{\partial\phi}{\partial t}\right)^2 \tag{4}$$

or, equivalently,

---

[2] This is exactly true in the vector approximation to general relativity. When the calculation of inertial forces is done in the second rank tensor version of general relativity, a pesky factor of 4 appears that complicates things a bit.

$$\nabla^2\phi - \frac{1}{c^2}\frac{\partial^2\phi}{\partial t^2} = 4\pi G\rho_0 + \frac{\phi}{\rho_0 c^4}\frac{\partial^2 E_0}{\partial t^2} - \left(\frac{\phi}{\rho_0 c^4}\right)^2\left(\frac{\partial E_0}{\partial t}\right)^2 - \frac{1}{c^4}\left(\frac{\partial\phi}{\partial t}\right)^2 \quad . \tag{5}$$

This is a classical wave equation for the gravitational potential ϕ, and notwithstanding the special circumstances invoked in its creation, it is general and correct, for when all the time derivatives are set equal to zero, Poisson's equation for the potential results. That is, we get back Newton's law of gravity in differential form. You might think that general relativity is not involved in this calculation since we are working in the Newtonian approximation with flat spacetime. That would be a serious mistake. This calculation only works because inertial effects are gravitational, giving us Equation (3) to use to separate variables. Curvature and all that, by itself, is not the essential core of general relativity theory.

The transient source terms on the right hand sides of Equations (4) and (5) are those of interest to us, for if they encode real phenomena, a real prospect that we will eventually be able to get out of our gravity wells (terrestrial and solar) exists. Skeptics, when confronted by a scheme that holds out such promise usually respond with disbelief. Sidney Harris captured their view in a cartoon decades ago. Two guys in lab coats are standing in front of a black board filled with equations. In the middle of the board, separating steps one and three, "and then a miracle occurs" is written. One of the guys, pointing to the "miracle" statement, says to the other (who is holding a piece of chalk in his hand), "I think you should be more explicit here in step two." The natural reaction to anyone who proposes a scheme that appears to be incompatible with well-established principles invites the reaction that there must be a "miracle" step somewhere in the physics they are advancing. This is almost always right. And sometimes the "miracle" step is hidden or disguised, making it a thankless task to try to find it.

In the case of Mach effect rest mass fluctuations, the closest thing to the invocation of a miracle is the assumption that Einstein really understood his own theory of general relativity. That he was right about inertia being a gravitational effect built into his theory. That assumption is what dictates that $\phi = c^2$ and $E_0 = \rho_0 c^2$, the conditions that must be true for the calculation of rest mass fluctuations to be true. I suppose that should you think that "matter" (stuff that gravitates) at cosmic distances should have no effects locally, this may seem miraculous. But common sense suggests otherwise, for as the gravitational influence of matter at a distance R decreases with the inverse square of R (in the Newtonian approximation), the amount of stuff in a spherical shell (of thickness dR) at distance R increases with the square of R. So, generally, distant stuff is, gravitationally speaking, just as important as local stuff. And there is an utterly gigantic amount of distant stuff out there. Whether one chooses to take this fact as a miracle is arguably a matter of taste. But viewed as a miracle or not, it remains a fact of our reality. To transform the predicted rest mass fluctuations in the source terms of Equations (4) and (5) we note that they can be written:

$$\delta\rho_0(t) \sim \frac{1}{4\pi G}\left[\frac{\phi}{\rho_0 c^4}\frac{\partial^2 E_0}{\partial t^2} - \left(\frac{\phi}{\rho_0 c^4}\right)^2\left(\frac{\partial E_0}{\partial t}\right)^2\right] \tag{6}$$

or, taking account of the fact that $\phi/c^2 = 1$,

$$\delta\rho_0(t) \sim \frac{1}{4\pi G}\left[\frac{1}{\rho_0 c^2}\frac{\partial^2 E_0}{\partial t^2} - \left(\frac{1}{\rho_0 c^2}\right)^2\left(\frac{\partial E_0}{\partial t}\right)^2\right] \tag{7}$$

where the last term in Equations (4) and (5) has been dropped as it is always minuscule. It is in the transient proper matter density effects – the RHSs of Equations (6) and (7) – that we seek evidence to demonstrate that the origin of inertia, as conjectured by Mach, Einstein, Sciama, and others, is in fact the gravitational interaction between all of the causally connected parts of the universe.

The obvious way to test for the presence of proper matter density fluctuations of the sort predicted in Equations (6) and (7) is to subject capacitors to large, rapid voltage fluctuations. Since capacitors store energy in dielectric core lattice stresses as they are polarized, the condition that E_0 vary in time is met as the ions in the lattice are accelerated by the changing external electric field. If the amplitude of the proper energy density variation and its first and second time derivatives are large enough, a detectable mass fluctuation should ensue. That mass fluctuation, δm_0, is just the integral of $\delta\rho_0(t)$ over the volume of the capacitor, and the corresponding integral of the time derivatives of E_0, since $\delta E_0/\partial t$ is the proper power density, will be:

$$\delta m_0 = \frac{1}{4\pi G}\left[\frac{1}{\rho_0 c^2}\frac{\partial P}{\partial t} - \left(\frac{1}{\rho_0 c^2}\right)^2 \frac{P^2}{V}\right] \tag{8}$$

where P is the instantaneous power delivered to the capacitor and V the volume of the dielectric. Note that the assumption that all of the power delivered to the capacitors ends up as a proper energy density fluctuation is an optimistic, indeed, perhaps wildly optimistic, assumption. Nonetheless, it is arguably a reasonable place to start.

3. APPARATUS

Before turning to tests and results, we first review in broad terms what a MEGA drive is and how it works. MEGA drives, at least as tested so far, have several parts. The core part is a stack of lead-zirconium-titanate (PZT) disks of powdered crystalline material compressed and sintered into 19 mm diameter by 2 mm thick disks. Silver electrodes are deposited on the flat surfaces of the disks. PZT is a ferroelectric material with a dielectric constant typically of more than 1000 that, because of the asymmetry of the crystalline structure of the material, can be polarized by the application of electric fields. If the material is heated to a sufficiently high temperature (typically a few hundred degrees Celsius or less) and polarized by an external electric field, and then allowed to cool with the field applied, the resulting polarization of the material is frozen in. (This is the electrical analog of making a permanent magnet). If mechanical stresses are applied to polarized PZT, generally, an electric field is induced in the material and electric charge appears on the surfaces of the material. The inverse of this process is to apply an electric field to the material (by charging adjacent electrodes) and produce a mechanical deformation of the material. These "piezoelectric" effects are linear in the voltage applied. "Poled" PZT has many electromechanical applications.

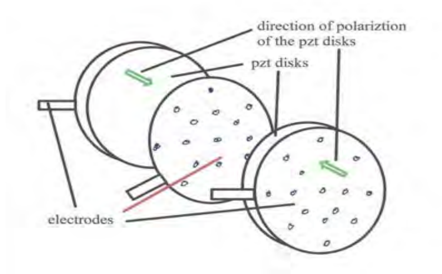

FIG. 1: Exploded view of the parts of an elementary section of a PZT stack. The electrodes that convey electric charge to the silvered surfaces of the disks are 0.002 inch thick brass foil. The assembly is glued together with special epoxy.

Assembly of a PZT stack consists of gluing together a sequence of pairs of disks arranged so that the direction of the disk polarization alternates from disk to disk, as shown in Figure 1. Electric charge is delivered to the silvered surfaces of the disks with electrodes. Since the behavior of the disks –expansion or contraction – depends on the relative directions of the crystal polarization and electric field. This pair-wise construction produces expansion or contraction throughout the stack when a voltage is applied to the external electrode tabs (which are alternately wired in parallel). A PZT stack of 8 disks (4 pairs of disks, typically about 19 mm long when the electrodes and an accelerometer are included) is mounted for testing on a cylindrical brass reaction mass 28.2 mm in diameter by 19 mm long. The stack is held in place by an aluminum cap of the same diameter and about 3 mm thick attached to the reaction mass by six 2 -56 stainless steel socket head cap screws (torqued to 4.0 inch pounds) as shown in Figure 2.

An accelerometer consisting of a pair of thin (0.3 mm) thick disks is included in the stack toward the end of the stack nearest the aluminum cap so that by monitoring the passive voltage of this pair of disks, the mechanical behavior of the stack during operation can be observed. This assembly is attached to an aluminum bracket that is, in turn, mounted on one surface of an aluminum and mu metal box – a Faraday cage – that is mounted on the end of a very sensitive thrust balance. An assembled device mounted in half of a Faraday cage is shown in Figure 3. Note that a thermistor is embedded in the aluminum cap so that the temperature of the device can be monitored.

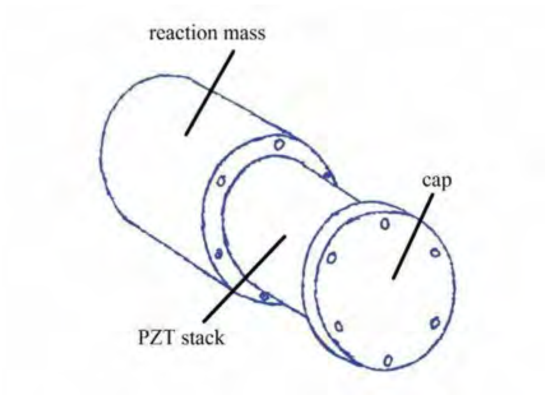

FIG. 2: Schematic view of the arrangement of the main parts of a Mach effect gravity assist (MEGA) drive device.The assembly is held together and the PZT stack preloaded with six 2-56 stainless steel socket head cap screws (not shown) torqued to 4.0 inch-pounds.

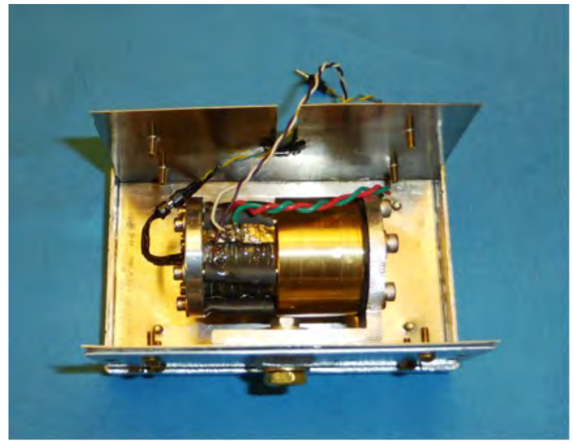

FIG. 3: A MEGA drive element mounted in part of an enclosing aluminum and mu metal Faraday cage.

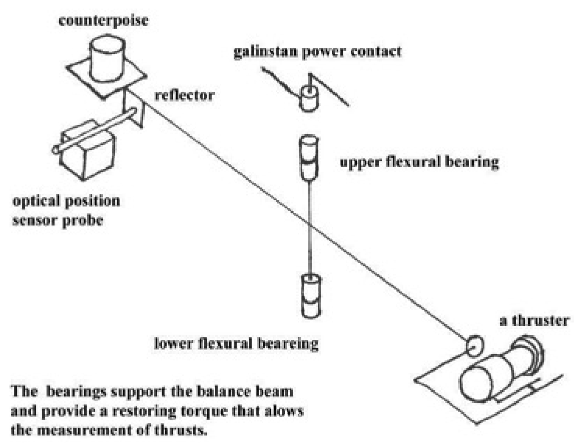

FIG. 4: A schematic diagram of the flexural bearing based horizontal torsion balance used to detect very small thrusts. Thrusts are measured as displacements of the balance beam by the optical position detector at the opposite end of the beam from the location of the test device. Galinstan (liquid metal) contacts mounted coaxially with the flexural bearings are used to minimize torques on the balance from the power circuit.

The thrust balance in use at CSUF is a third generation piece of equipment. (The first generation balance was built by Andrew Ketsdever when he was a grad student at USC, and the second by Martin Tajmar when he was at the Austrian Research Center [now Austrian Institute of Technology].) Ours was built by Tom Mahood and me about 10 years ago. At the time, it was the most sensitive thrust balance in the world. Nowadays, there are lots of balances as good or better. The core of the thrust balance is a pair of C-Flex flexural bearings and some liquid metal (galinstan) contacts for power transfer. (See Figures 4 through 6.) Once a device has been run, the surface encapsulation epoxy develops micro-fractures that, when exposed to everyday environmental conditions, leads to the degradation of the response of the stack. Moisture seems to be the chief culprit. That is why devices are stored in a vacuum when possible. (See Fig 8 below.)

The Faraday cage in which the device being tested runs is located on one end of the balance beam as shown in Figures 7 and 8. The beam of the thrust balance moves horizontally about the axis of the flexural bearings. The position of the beam is detected with the probe of a Philtech optical position sensor (see Figures 4 and 9). The position, because of the restoring torque provided by the flexural bearings, is linearly related to the thrust produced in the test device. The motion of the balance beam is damped by several magnets that produce a field in which aluminum blades affixed to the beam, at the opposite end from the

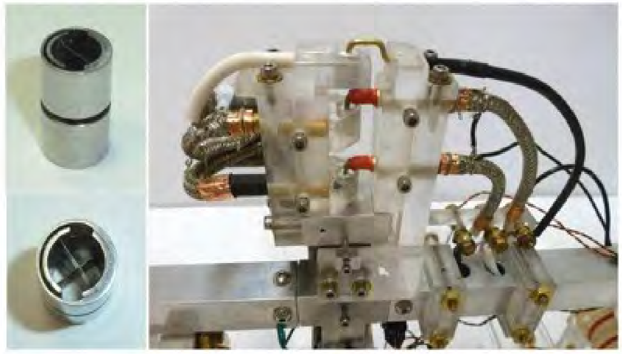

FIG. 5: On the left, two views of one of the flexural bearings used in the thrust balance. On the right, a close-up of the galinstan power feed contacts mounted above the flexural bearing assembly.

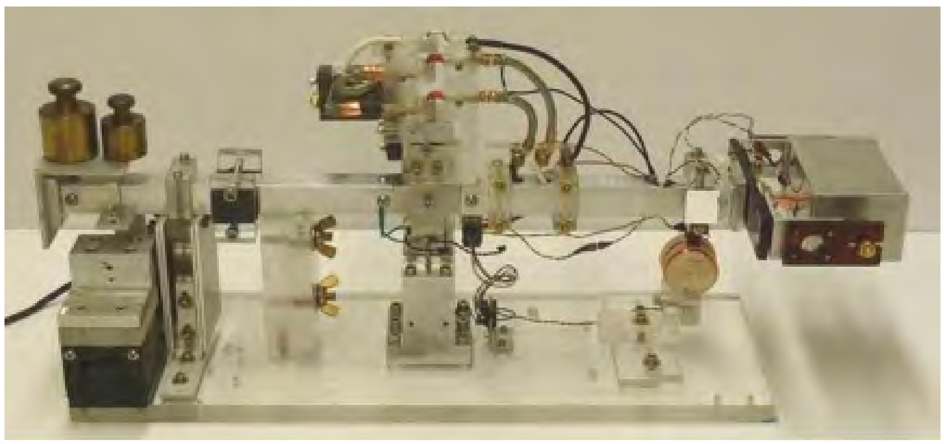

FIG. 6: The fully assembled thrust balance (minus some shielding added later). The test device is located in the metal box (Faraday cage) mounted on the right end of the balance beam. That box is mounted in a red plastic and aluminum yoke secured to the beam with a nut that enables the disposition of the device and box on the end of the beam to be changed with a simple rotation of the yoke.

test device, move (see Figure 10). Calibration of the system is accomplished with the help of coils mounted on the base plate of the balance and the beam (see Figure 11). This entire assembly is enclosed in the plastic vacuum chamber shown in Figure 12.

4. OPERATION

Operation of a device consists in applying a suitable electrical signal to the PZT stack and looking for a thrust effect manifested as a displacement in the position of the beam of the thrust balance. The applied signal is produced by a voltage controlled oscillator (VCO) that generates a sine wave at a selected frequency (typically in the 30 to 40 kHz range). The signal from the VCO, switched by a computer controlled relay, drives a power amplifier (Carvin DCML-1000, see Figure 3.13). The output of the power amplifier goes through a step-up/isolation transformer and a box with a resistor divider (capacitatively compensated) to monitor the voltage across the device. (See Figure 14.) A programmable frequency control voltage is used to generate frequency sweeps when desired.

The power feeds are carefully shielded. The basic protocol adopted for the early exploration of the response of a device was to select some frequency as the "center" frequency of some swept frequencies and activate a run. After several seconds of background data, the power amp was switched on at the center frequency for several seconds. This was followed by a sweep of typically 30 kHz, starting 15 kHz above the center frequency. And the sweep was followed by several seconds of operation on the center frequency. This

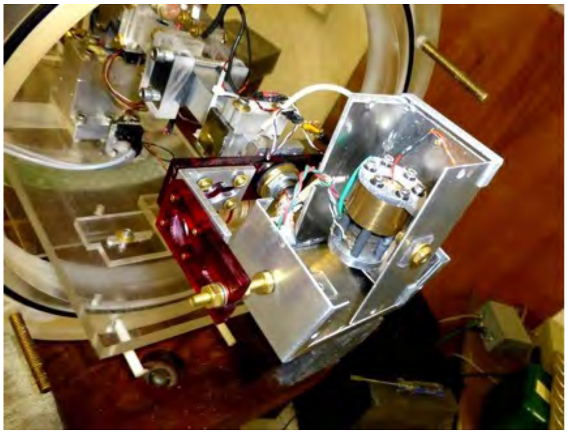

FIG. 7: Detailed view of the partially assembled device carrier (part of the Faraday cage) on the end of the balance beam. The locknut that enables rotation of the device/box assembly is visible near the center of the picture.

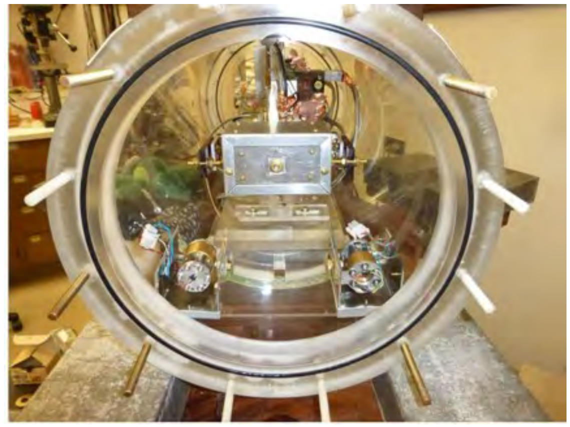

FIG. 8: End view of the thrust balance in the vacuum chamber (with the end plate removed). The yoke and Faraday cage are near the center of the picture. Below, to the right and left of the beam are two other devices mounted in Faraday cage half-shells.

FIG. 9: The opposing end of the thrust balance beam loaded with brass counterpoise masses. The probe of the optical position sensor (spiral jacketed) is clamped to a block on a stepper motor that is used to adjust the position of the probe with respect to a reflector attached to the balance beam.

FIG. 10: Detail of the opposite beam end. The damper – aluminum blades attached to the beam with neodymium-boron magnets in between attached to the base plate – is located next to the probe/stepper motor. To the right of the damper is a clear plastic beam rest used when working on the beam.

protocol is displayed in Figure 15. The sweep allows one to identify the resonant frequencies of the system and, when tuned to resonance, the center frequency pulses allow one to determine resonant behavior over an extended interval. After resonances are identified, this protocol can be modified in a variety of ways. A plot of a dozen runs averaged together with a typical device is shown in Figure 16.

If the only electromechanical response of the stack is piezoelectric (linear in the applied voltage), then a voltage signal comprised of two frequencies – one twice the frequency of the other – would have to be applied. The first harmonic part of the signal would drive a mechanical oscillation at that frequency and cause the internal energy of the stack to oscillate at that frequency too. The combination of the electromechanical acceleration and internal energy oscillation should produce a mass fluctuation at twice the frequency of the first harmonic signal. To transform that mass fluctuation into a thrust, a second electromechanical oscillation at the second harmonic frequency – with the right phase – must be supplied so that with respect to the reaction mass, the stack is accelerated in one direction as it is less massive, and the other direction as it is more massive. If this is done, the reaction mass will experience a time-averaged net force.

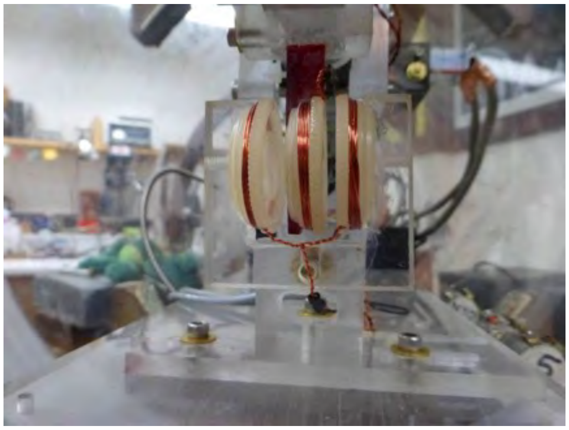

FIG. 11: The three coils used to calibrate the thrust balance. Each coil is ten turns of magnet wire wound on a 35 mm film canister cap. The left and right coils are attached to the base plate, and the center coil is attached to the balance beam. The coils are wired in series with the polarity of the center coil reversible. Currents on the order of a few tens of milliamps are sufficient to produce calibration forces on the order of micro Newtons.

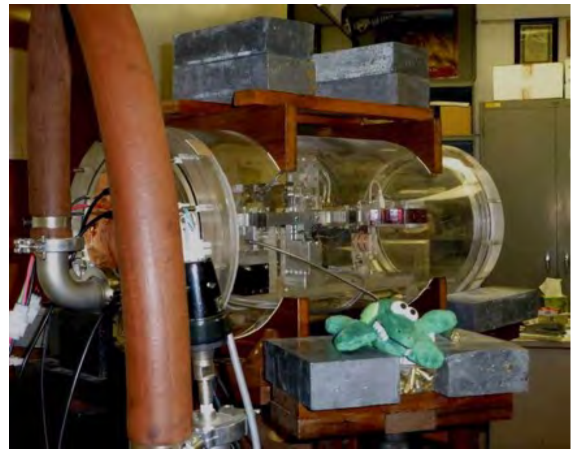

FIG. 12: The thrust balance in its clear plastic vacuum chamber. The vacuum chamber is located on a vibration isolation table. Lead bricks that are part of the vibration isolation system are visible in the lower right and at the top of the picture.

FIG. 13: The Carvin DCML –1000 power amplifiers used to energize the device being tested.

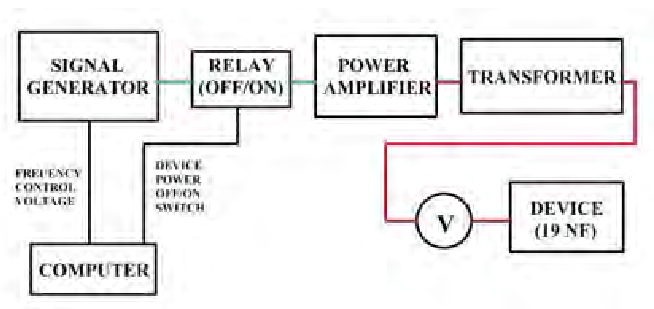

FIG. 14: A schematic diagram of the power circuit.

When the stack and reaction mass type devices were first tested more than 15 years ago, the PZT disks used were made by EDO Corp., their material EC-65. This is a very high dielectric constant ($\sim$ 5000), high loss (4%) material. The device that Martin tested is one of these. When I returned to this device design several years ago, I chose another material (and manufacturer) with about a tenth of the loss of the EC-65 disks and somewhat lower dielectric constant ($\sim$ 1800) to reduce the heating in the devices during operation. The material chosen was Steiner-Martins SM-111 [3]. This material has the unappreciated feature of a strong electrostrictive response to applied electric fields. Electrostriction is an electromechanical effect present in some measure in all materials, for unlike piezoelectric effects, it does not depend on the presence of an asymmetric crystal lattice structure. The effect, accordingly, is insensitive to the polarity of the applied voltage that excites it. As a result, the deformations that follow from the application of a periodic applied voltage occur at twice the frequency of the exciting voltage. If the relative phase of the electrostrictive deformations and the mass fluctuations excited by the piezoelectric response of the stack to a single frequency voltage signal is auspicious – since the mass fluctuations occur at twice the frequency of the voltage signal – net time-averaged thrust will be produced. In simple situations, the requisite phase relationship obtains. Reality can be more complicated; but at least one starts from the correct phase relationship. And often life is simple in practice. Tests with recent devices, as a result, have been done with single frequency voltage excitation. Relative phase first and second harmonic responses can be discerned by examining the waveforms

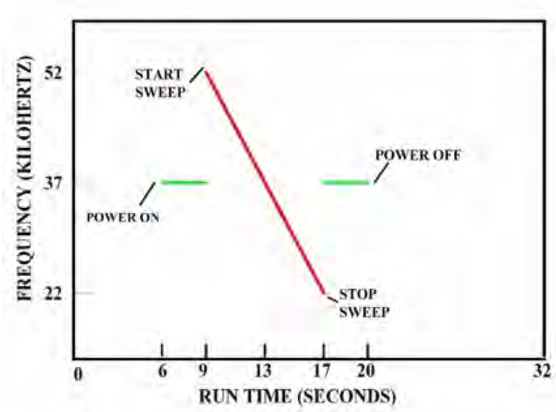

FIG. 15: A graphical display of a standard search protocol run. Several seconds of quiescent background data are acquired before the power is switched on at the "center" frequency of the run (left green line). After several seconds at the center frequency, a frequency sweep of (typically) 30 kHz is initiated (the red line). The sweep is followed by another several seconds operation at the center frequency (right green line). And that is followed by several seconds more quiescent background data.

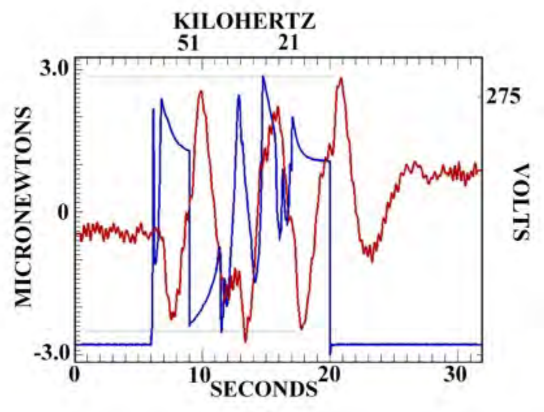

FIG. 16: The thrust (red) and voltage (blue) traces for the difference of the averages of a dozen runs done with the device in the"forward" and "reversed" directions on the balance beam using the protocol of Figure 15. The "center" frequency occurs half way between the two 3 second pulses that bracket the sweep.

of the voltage and accelerometer signals. Sample waveforms are displayed in Figure 17. The first of these plots was obtained with a device that produced serious thrust; the second was obtained with a device that produced essentially no thrust. The obvious difference between the waveforms in the two displays is the relative phase of the voltage (blue) and accelerometer (yellow) signals.

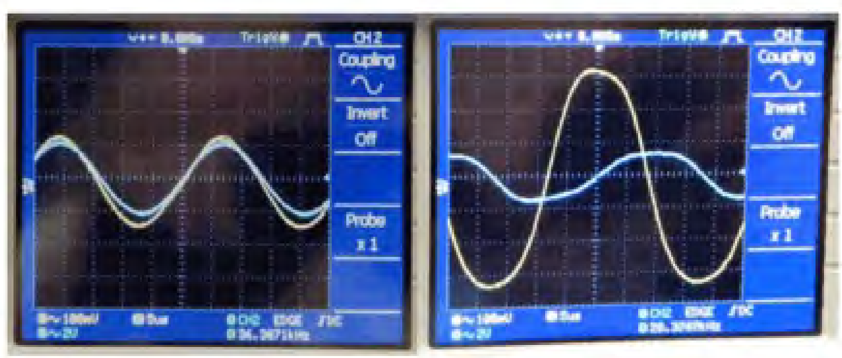

FIG. 17: The accelerometer (yellow) and voltage (blue) oscilloscope traces for on resonance operation for two different devices. The device that produced the traces on the left also produced significant thrust. The device that produced the traces on the right did not produce detectable thrust. Evidently, phase matters.

5. TRANSIENT AND STEADY THRUST

As mentioned at the outset, more recent results that were guided more by engineering than science concerns will be addressed first. The issue addressed has been evident in the results obtained at CSUF for a number of years now. In particular, a distinctive feature of the thrust traces produced by our system is pronounced switching transients when the device tested is switched on and then off. These transients are easily seen in the results plotted in Figures 18 and 19. The acquisition protocol for these averages was not that described in the previous section. The 3 second constant frequency pulses of that protocol were extended to 8 seconds duration, and the 8 second frequency sweep between the pulses was suppressed, leaving an unpowered 8 second interval between the pulses. Two plots are shown in Figure 18 because standard procedure included getting averaged data with the device pointing in two directions, "forward" and "reversed". These are displayed in Figure 18. Taking the difference of these averages yielded a net thrust that could only be attributed to the action of the device – as all other signals, since they do not reverse when the direction of the device on the beam is reversed – were cancelled by the subtraction process. The net thrust in Figure 19 shows clearly that a steady thrust is produced by the voltage driven at the resonance frequency of the device – this is the thrust offset toward the end of the eight second power pulses which is different from the thrust toward the end of the eight second unpowered interval between the power pulses.

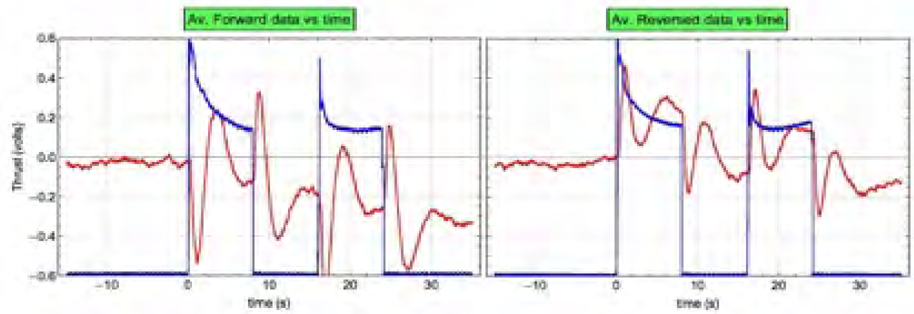

FIG. 18: Averages of a dozen runs for the device in the forward and reversed directions on the end of the balance beam. Were the thrust traces (red) entirely due to actions having nothing to do with the test device, they would be the same for both directions. While both thrust traces show signs of, for example, thermal drift, most of the signals reverse with the direction of the device.

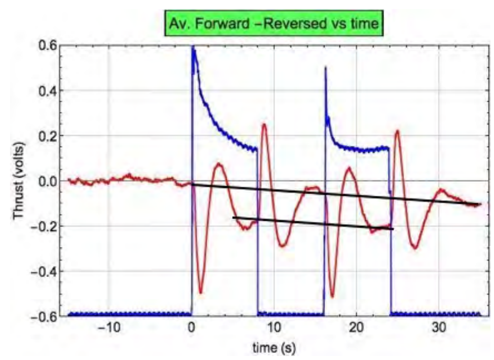

FIG. 19: The net, forward minus reversed, thrust trace for the run averages in Figure 18. The upper black line shows the thermal drifts in the two plots of Figure 18 were not exactly the same. The lower black line shows the steady thrust – about a micro Newton – present after the on switching transient has settled.

What's especially interesting about the thrust trace in Figure 19 is the large switching transients that occur when the power to the device is turned on and off. It is easy to believe that these transients are just electrical artifacts having nothing to do with any long-range gravitational interaction. However, this accounting for the transients is wanting for a couple of reasons. First, the signal that drives the power amplifier is switched at random phase of the AC signal. So the voltage at switching is just as likely to be negative as positive, and just as likely to be increasing as decreasing in magnitude. These considerations suggest that the switching transients in individual runs, if present, should have random magnitudes and be equally likely positive and negative. When transients of this sort are averaged over several runs, they should average to zero. The observed transients do NOT display this behavior. They are always in the same direction and do not average away.

Another way to address the switching transients is to ask if they are produced when a DC voltage is switched. In this case, one is no longer bothered by pesky random phase AC effects. But the DC voltage does produce a displacement of the center of mass of the device, and that should produce a displacement of the balance beam as the new center of mass moves to the equilibrium position of the old center of mass. Since the voltage polarities produce displacements in opposite directions, one might expect any such effect to be polarity dependent. Actually, this test was first carried out several years ago at the behest of evaluators from Aerospace Corp. The results are contained in Figure 20. Run averages for both positive and negative polarities and forward and reversed device orientation were obtained. When the negative polarity averages were subtracted from the positive polarity averages for the two orientations, and then the reversed polarity difference was subtracted from the forward polarity difference, the resulting net thrust showed a small transient (a few tenths of a uN) at switch-on, as is evident in the left panel of Figure 20. This is to be compared with the transients in Figures 19 (where the thrust scale is 0.15 volts = 1 μN).

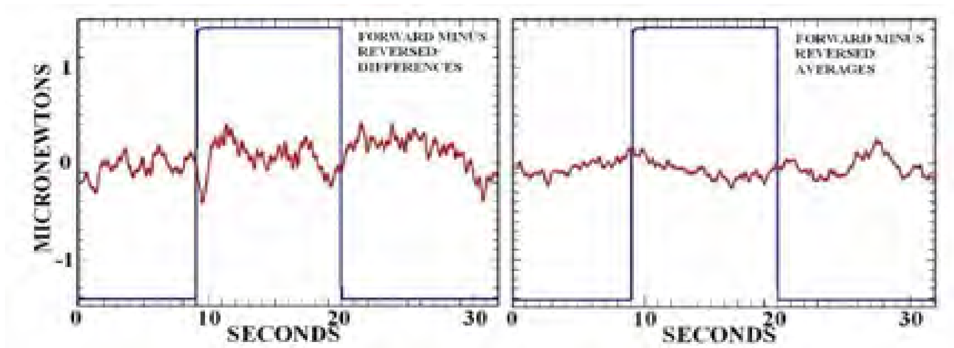

FIG. 20: The net thrusts – forward minus reversed – for the differences of the runs done with positive and negative polarity (left) and the averages of the two polarities (right). Neither protocol produces thrust transients like those in Figures 18 and 19.

The obvious questions are, are such thrust transients expected on the basis of Mach effects? And, why do you see the transients with AC voltage signals, and not with DC voltage signals? The answer to the first question is yes, switching transients of the sort observed are expected in appropriate circumstances. This follows immediately from the dP/dt term in the mass fluctuation equation (Equation (8)). You may be thinking, well, dP/dt isn't equal to zero when a DC voltage is switched, so why aren't transient mass fluctuations seen when they are switched?

Keep in mind that the power in the circuit with the device is just the product of the voltage, V and current, i. Or, $P = iV$. When a DC voltage is switched, both i and V are non-zero and changing, so dP/dt isn't equal to zero either. But as the voltage approaches the steady voltage of the DC circuit, the current, instead of rising as at the outset, decreases. And the same thing happens to dV/dt, for once the full voltage is achieved, the current stops, the voltage stops changing, and there is no power in the circuit. P is equal to zero before the switching takes place, and after too. So, dP/dt integrated over the complete event is roughly zero – and no mass fluctuation of significance is expected. The results of a switched DC voltage test are displayed in Figure 20. When the polarity of the applied DC voltage was preserved, and the averages for the polarities are ultimately differenced, one finds a minute transient at switch-on and none at switch-off. When the polarities are averaged together, all signs of a switching transient vanish. The simple fact of the matter is that the thrust signals seen with the device in normal operation cannot be attributed to switching of a DC voltage. And all explanations that depend on a prompt displacement of the center of mass of the stack are also excluded by this test.

The situation with an AC voltage signal of a Mach effect device is different. Before the signal is switched, both P and dP/dt are zero. When the signal is switched, the power rises from zero to some preselected, non-zero value, typically a few hundred watts or less. So, dP/dt may vary in magnitude during a switching event, but it's always the same sign. And it does not average to zero when integrated over the switching event. If the on and off switching events are pretty much alike, we should expect to see mass fluctuations that are also pretty much alike – with an important difference. Since the signs of dP/dt are different for on and off, the mass fluctuations should also have opposite signs. This is exactly what we see in Figure 19.

The at least qualitative agreement between expectation and observation contained in Figure 19 can only be called most remarkable. The fact that the switching transient is a factor of two or more larger than the steady thrust (and in some cases more than an order of magnitude larger with some devices) suggests that switching transient production of thrust pulses is likely to be the most efficient way to implement Mach effects for propellantless propulsion.

6. CHIRPING

Even casual inspection of Figure 19 is enough to identify a potential problem with using switching transients for propulsion. Since dP/dt has opposite signs for the on and off transients, the thrust transients have opposite signs too. If the magnitudes of the thrust impulses are the same, or nearly the same, the off transient will cancel the on transient and the net thrust over one cycle will be small or zero. If everything were simple and linear, it might well be the case that the on and off impulses were equal and opposite. But the devices tested here are not simple and linear, so there is a real prospect that one of the transients can be suppressed, leaving the other transient unbalanced. The simplest way to accomplish this is to turn on or off either the on or off transient slowly, leaving the other transient prompt. Since these devices run on an electro-mechanical resonance of the device, there is a simple way to affect slow turn-on or turn-off. Say we want to turn the device on slowly (and off promptly). We simply energize the device with a voltage signal several kHz away from the resonant frequency. Then, using the voltage control of the oscillator, we bring the operating frequency onto resonance slowly. Code was written to affect this procedure. The result is shown in Figure 21. The quality of the thrust resolution is good enough to show an at first negative, and then positive going thrust as the frequency is brought down to resonance (by raising the oscillator control voltage). The switching transient that follows the power being switched off is obvious and cannot be due to power considerations as the power is off.

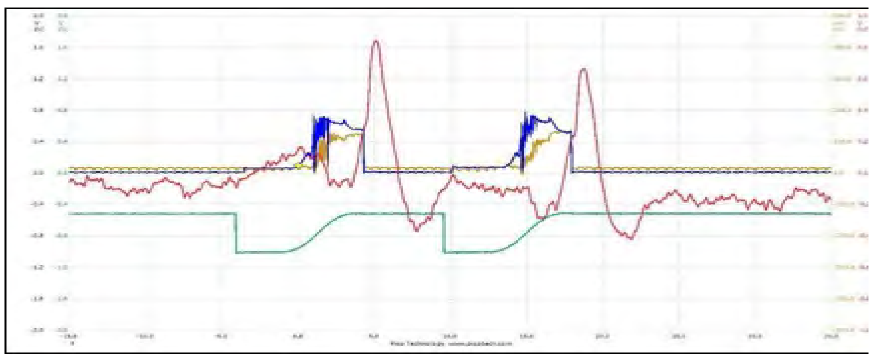

FIG. 21: The green trace shows the control voltage delivered to the voltage controlled oscillator that generate the voltage signal applied to the test device (via the power amplifier). When the control voltage is turned on after several seconds, it sets the frequency of the voltage signal to 5 kHz above the pre-tuned center frequency – off resonance that is. After a few seconds the control voltage slowly brings the frequency back to resonance, and then is shut off to produce the switching transients present in the thrust trace (red). The voltage (blue) and accelerometer (brown) traces show the sort of behavior expected in the circumstances.

The frequency chirping method used here is only one of several ways that either on or off switching transient suppression can be realized. In other circumstances some other method might be more advantageous. But whatever the particulars might be, pulsed power to induce auspicious switching transients seems a prudent path to follow. See further chirp tests in Figures 22 and 23.

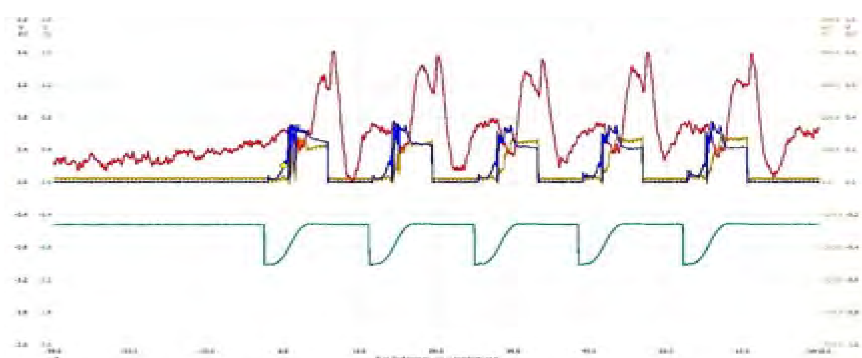

FIG. 22: A run showing a sequence of chirped voltage frequencies.

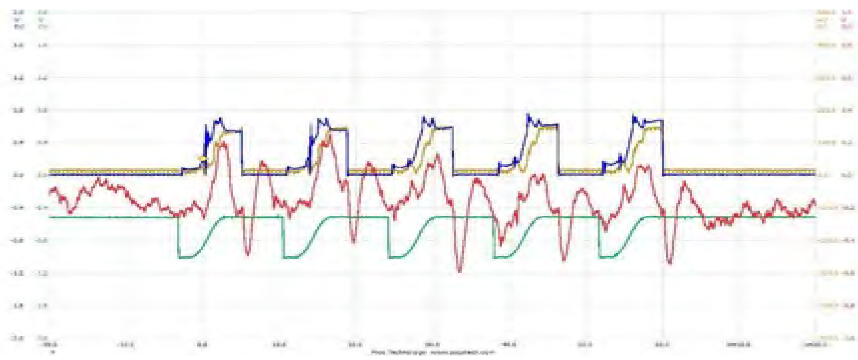

FIG. 23: The thrust (and other) trace(s) with the direction of the device reversed. The thrust trace is inverted, as expected.

7. VOLTAGE SCALING

In the spring of 2015, Nick Herbert, looking for tests that might shed light on the reality of Mach effect thrusts, noted a curious feature of the SM-111 devices being run: since they are activated by a single frequency voltage that excites both first and second harmonic responses in the stacks, and the expected thrust depends on the product of the first and second harmonic excitations, the predicted thrust should scale with the fourth power of the applied voltage. Crude power scaling tests had been done, but no systematic voltage scaling test had been carried out. Doing this test by going to higher voltages was ruled out but the fact that the devices were already being pushed about as hard as possible. But going to lower voltages was possible, though more signal averaging than usual was required to get a reliable thrust reading for the smallest voltage. The results of this test are displayed in Figures 24 and 25. They are consistent with the predicted quartic voltage scaling. Aside from the technical details of execution, there really isn't too much more to say about this; other than that there is no other basis for the prediction of quartic scaling [4].

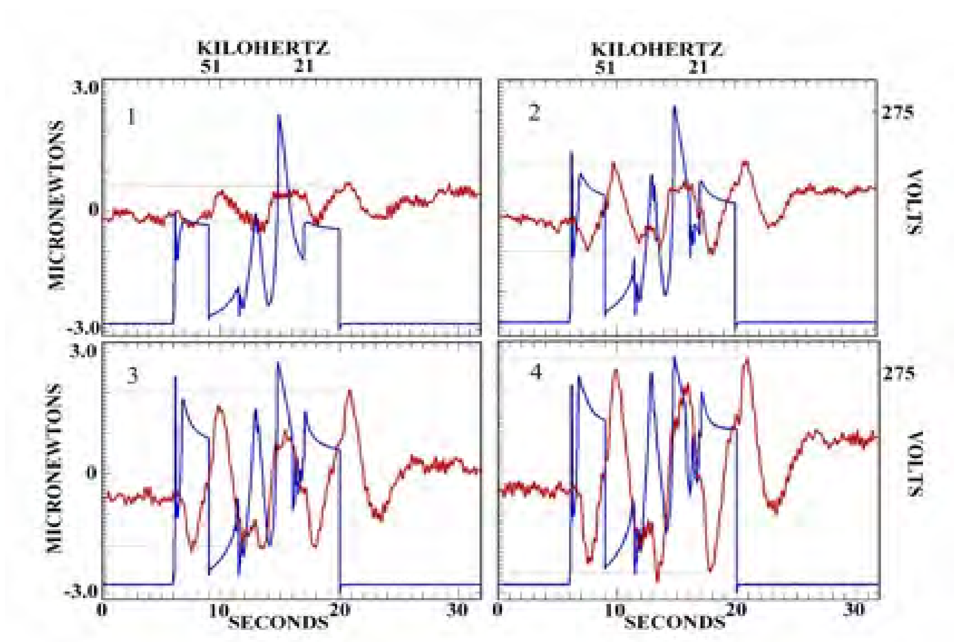

FIG. 24: Results for the differences of forward and reversed for a dozen runs of each averaged for several different voltages. The panel on the lower right (number 4) may be inspected in greater detail in Figure 16. The peak to peak thrust trace in the second center frequency pulse was used as the thrust measure, and the point on the voltage curve about a third of the way through the pulse was taken for the voltage. These results are displayed graphically in the next slide.

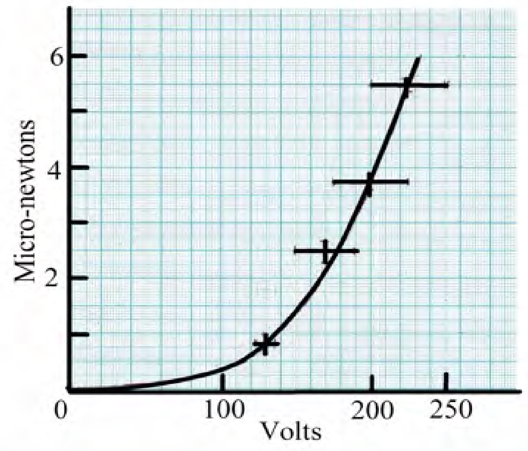

FIG. 25: The graphical display of the results shown in Figure 23. The bars at the data point locations show the range of thrusts and voltages in the averages – though the voltage range is dominated by the decay of the voltage in the second center frequency pulse, rather than a real variation of the center frequency from run to run.

8. WRAPPING UP

There isn't really much to say that has not already been said, once at least and sometimes more than that. What is new is that there are now three publicly declared replications done with care an professionalism that corroborate the work at CSUF. The thrust effect obeys quartic voltage scaling, as predicted. And chirping the frequency of the applied voltage signals looks to be a feasible way to use the observed switching transients as a primary propulsive strategy. But, realistically, we are only at the beginning of the path out of our gravity wells. And, grace of the Great Spirit, more workshops of this sort will grace the travels of those who pursue this path.

ACKNOWLEDGEMENTS

The Mach effect project, never very sexy (like, for example, the quantum vacuum schemes for breakthrough propulsion), has steadily over the years attracted a compliment of supporters willing to tolerate that no new physics is required and that inertia has to be understood as Einstein understood it in his general relativity theory. Their number is now too large for me to individually identify all of them. Many of them were attendees at this workshop. All of them are friends, some nearly family. You, dear reader, may be one of them. I trust you to understand that I intend no slight by singling out a few people for special mention. John Cramer [5,6] who first brought Mach effects to public notice through his Alternate View column in Analog back in 1996, and was involved with the project at a distance for many years thereafter. Nembo Buldrini and Paul March, both of whom have been with the project for more than 15 years. George Hathaway and Martin Tajmar, both of whom have invested their world class talents and skills in checking up on the project. No one will ever go to the stars without their type of contributions. Greg Meholic and Dennis Bushnell, each strong advocates in their own ways. Jim Peoples and David Mathes who have urged the project along at times when it could have gone astray. Gary Hudson and the staff of the SSI. Gary's advice has always been spot on, and SSI sponsorship through the Exotic Propulsion Initiative, including this workshop, has really helped. Lance Williams and Heidi Fearn, who did all of the real work to make this workshop a success. Especially Heidi, who has been a partner in the research effort now for five years, sharing the successes and the failures. And no acknowledgement would be complete without mention of my physicians, my CSUF Physics colleagues and Carole and the cats.

DISCUSSION

During Jim's talk, he shows a hand draw graph of force versus voltage V showing a V^4 dependence. There are some strange looking "errors bars" in the form of ovals drawn on the graph.

Hathaway: Why are the error bars larger for larger thrust levels?

Woodward: Those are not error bars in the usual sense (like RMS values); the width of those ovals represent the spread of voltages I used for that data point– there were several runs taken for each point and a corresponding small change in voltage for each run.

Williams: What would it take to get to Newtons of thrust, is the scaling practical?

Woodward: Yes the scaling is practical, but I wasn't thinking of going straight to heavy lift. We should increase the frequency to MHz rather than kHz, that would do the trick. For thousands of Newtons we would need GHz frequency. Right now we have $F_0 \sim 1\mu N$ of force say, that is at 35 kHz. We believe the force is dependent on frequency f between f^2 and f^3. It's difficult to say exactly how the force scales with frequency. There are a lot of parameters n our equations which change with frequency, so as the device heats up the natural frequency changes and all those parameters change too. If you go through all these terms and extract the frequency you get a force that appears to go like f^6– all you have to do is go up in frequency to GHz and I could move my house ...

...audience laughter ...

Woodward: It's not so simple I'm afraid. But running at higher frequency is clearly a desirable thing to do. Let's assume the force goes like f^2. So if we increase the frequency from 35 kHz to 35 MHz, with everything else remaining the same, then the new force is $F = F_0(35 \times 10^6/35 \times 10^3)^2 \rightarrow F = F_0 \times 10^6$ then the new force would be $F \sim 1\text{N}$. If instead I used 3.5 GHz then $F = 10KN$. Right now my equipment can only manage the kHz type frequencies, I don't know if these devices have resonances with that high a frequency. Whether the devices will end up looking like PZT stacks or some other solid state device or like an EM-drive is not obvious to me yet. I would not be surprised if they turn out to be solid state devices like the ones we are running. Cavities have a lot of extra baggage that is not present in solid state devices. The optimum running conditions for any device turns out to be $\sim$ 1 GHz. If you get too much above that frequency then the ionic response of the material cannot oscillate fast enough. You want the heavy ions moving not the electrons, they would decrease the magnitude of the effect by 3 orders of magnitude or so.

Williams: Are these devices only space drives in a sense they only work in space or are they capable of heavy lift on the ground?

Woodward: At the moment we are talking about space drives because of the low thrust levels. But eventually these drives could be developed so they can have heavy lift capability.

Williams: How big do you think these heavy lift drives will be ?

Woodward: I expect the size to be similar to what they are now, maybe a little smaller – but we would be using arrays of devices possibly with redundancy and plug – in replacement capability. We might cycle them on and off to reduce fatigue and failure and make them last longer. On a space mission we would carry 20% more devices than needed in an array to compensate for failures and have added redundancy array systems in place. Trying to scale any device to give a force bigger by a factor or 5 (or perhaps 10) is a fraught with difficulty and a bunch of unknowns. There is a lot of hard work ahead. We have only just started on a journey which could lead to heavy lift eventually. This is not going to happen overnight. At least we now know the physics which points us in the right direction and suggests what we should try next. We have a clear path forward, and I think it is fair to say that as short as 6 months to a year ago that was arguably not the case.

REFERENCES

[1] D. W. Sciama, "On the origin of Inertia", Mon. Not. R. Astron. Soc. 113 p34 (1953)

[2] J. F. Woodward, *Making Starships and Stargates*, Springer Press , December 2012

[3] Steiner Martins materials, STEMINC: `https://www.steminc.com/piezo/PZ_property.asp`

[4] H. Fearn et al. "Theory of a Mach Effect Thruster II", Journal of Modern Physics, **6**, pp1868–1880 (2015)

[5] Cramer, J. G. "The transactional Interpretation of quantum mechanics." Rev. Mod. Phys. **58**, 647 (1986)

[6] Cramer, J. G. *The Quantum Handshake, Entanglement, Nonlocality and Transactions.* Springer, Berlin (2015)

A CONVENTIONAL POST-NEWTONIAN MACH EFFECT

L.L. Williams
Konfluence Research Institute
Manitou Springs, Colorado, USA

Realizing that Jim has derived a post-Newtonian field equation (equation 5 of Estes Park Quick Study VI), and that standard GR provides a prescription for generating post-Newtonian field equations, I wanted to do a straightforward calculation in GR to see what the equation corresponding to (VI-5) would be. This approach does not require Jim's ansatzes 1, 2, or 3. It departs merely from textbook results in GR.

So let us start with the field equations. In the linear theory of GR, the metric $g_{\mu\nu}$ is decomposed into a Minkowski piece $\eta_{\mu\nu}$ and a small perturbation: $g_{\mu\nu} = \eta_{\mu\nu} + h_{\mu\nu}$, where $h_{\mu\nu} \ll 1$.

Standard texts give the field equations for the linear theory in a convenient gauge. Weinberg's expression (10.1.10) in harmonic gauge is:

$$\frac{\partial^2 h_{\mu\nu}}{c^2 \partial t^2} - \nabla^2 h_{\mu\nu} = \frac{16\pi G}{c^4}\left(T_{\mu\nu} - \frac{1}{2}\eta_{\mu\nu}T^\alpha_\alpha\right) \tag{1}$$

The Newtonian limit is recovered from the linear theory by considering the time-time (0-0) component, which relates h_{00} to $T_{00} \sim \rho c^2$. This would seem to be the reasonable departure point to connect to (VI-5). The difficulty is to recover the peculiar mass time derivatives in (VI-5). We see that the standard linear equation (1) has no time derivatives of mass, but instead time derivatives of the field.

The interaction between matter and fields is not solely described by the field equations, which describe how fields arise from matter. We also need to look at the equations of motion, which describe how fields influence matter. The equation of motion for GR is called the geodesic equation, and it describes how matter is influenced by gravity. It describes the precession of the perihelion of Mercury, for example. It is in terms of the 4-velocity $U^\mu \equiv dx^\mu/d\tau = p^\mu/m$:

$$U^\alpha \nabla_\alpha p^\mu = U^\alpha \left(\frac{\partial p^\mu}{\partial x^\alpha} + \Gamma^\mu_{\alpha\beta}p^\beta\right) = \frac{dp^\mu}{d\tau} + \Gamma^\mu_{\alpha\beta}U^\alpha p^\beta = 0 \tag{2}$$

Equation (2), along with the Einstein field equations, is the whole content of GR. The non-relativistic, post-Newtonian limits of (2) are given by Weinberg in section 3.4, and by Schutz in section 7.2. In this case, the spatial components of the 4-momentum p^μ are assumed much less than the time component. Then the non-relativistic limit of the geodesic equation (2) is:

$$\frac{dp^\mu}{d\tau} + \Gamma^\mu_{00}U^0 p^0 = Order(v/c) \tag{3}$$

The linear affine connection is given by

$$\Gamma^\mu_{00} \simeq \frac{1}{2}\eta^{\mu\nu}\left(2\frac{\partial h_{0\nu}}{c\partial t} - \frac{\partial h_{00}}{\partial x^\nu}\right) \tag{4}$$

Returning to the field equations, consider a simple stress-energy tensor, for a cold fluid or dust: $T_{\mu\nu} = \rho W_\mu W_\nu$, where $\int \rho W^\alpha dV \equiv \Sigma p^\alpha$ of the particles. Then

$$T^\alpha_\alpha \simeq \rho\left(\frac{cdt}{d\tau}\right)^2 = \rho W_0^2 \tag{5}$$

where again we ignore the spatial components of the 4-momentum relative to the time component, this time now for the bulk matter.

Let us put this together, setting $h_{00} \equiv -2\phi/c^2$, to accord with the usual identification of the Newtonian potential ϕ with the time-time component of the metric perturbation. Then the linear field equation (1) can be written:

$$\nabla^2\phi - \frac{\partial^2\phi}{c^2\partial t^2} = \frac{4\pi G}{c^2}\rho W_0^2 \tag{6}$$

Likewise, the linear equation of motion (3) for the time component p^0 of the 4-momentum is (cf. also Carroll 7.23):

$$\frac{U^0}{c}\frac{\partial p^0}{\partial t} = \frac{U^0}{c^3}\frac{\partial \phi}{\partial t}p^0 \tag{7}$$

Equation (7) is typically dropped in textbook treatments of linearized gravity, on the assumption that the Newtonian limit should be time-independent. Those treatments are typically interested in the spatial pieces of (3) that show trajectories under gravitational influence. Allowing this time dependence is a nice insight that Jim has brought to this discussion.

Equation (7) allows us to write the time derivative of the field in terms of particle energy:

$$\frac{\partial^2 \phi}{\partial t^2} = \frac{\partial}{\partial t}\left(\frac{c^2}{p^0}\frac{\partial p^0}{\partial t}\right) = \frac{c^2}{p^0}\frac{\partial^2 p^0}{\partial t^2} - \left(\frac{c}{p^0}\right)^2\left(\frac{\partial p^0}{\partial t}\right)^2 \tag{8}$$

so that the field equation (6) now becomes:

$$\nabla^2 \phi = \frac{4\pi G}{c^2}\rho W_0^2 + \frac{1}{p^0}\frac{\partial^2 p^0}{\partial t^2} - \left(\frac{1}{p^0}\right)^2\left(\frac{\partial p^0}{\partial t}\right)^2 \tag{9}$$

This is strikingly similar to (VI-5). To make the identification complete, put $p^0 = mc$ and $W^0 = c$, and convert the mass factors to mass density:

$$\nabla^2 \phi = \frac{4\pi G}{c^2}\rho W_0^2 + \frac{1}{\rho}\frac{\partial^2 \rho}{\partial t^2} - \left(\frac{1}{\rho}\right)^2\left(\frac{\partial \rho}{\partial t}\right)^2 \tag{10}$$

Furthermore, this recovers the 2nd and 3rd terms on the RHS of (VI-5) if Jim's original substitution is used in those terms to set ratios of $\phi/c^2 \to 1$. Missing from (10) relative to Jim's (VI-5) are the quadratic time derivatives of the field. Neither of those terms are important to Jim's Mach effect, so it appears they are dispensible parts of his theory. I like this simple derivation here because it reproduces the essential parts of (VI-5) without any assumptions or without the uncertainty of where to substitute for c^2.

Indeed, in hindsight we can recover equation (10) from Jim's equation (VI-4) if the 3rd ansatz is dropped. Taking straightforward derivatives of the first term on the LHS of (VI-4) yields exactly equation (10). This seems to imply that the 3rd ansatz is outside GR, and it accounts for the extra time derivative terms in Jim's derivation.

Jim feels the extra time derivatives are important, especially the piece of the d'Alembertian, to make the Mach equation look relativisitic. I am not so bothered by this because we know the Newtonian limit of GR is not covariant, and we know the linear limits of GR are not covariant. We can still get relativistic effects to a certain order, but without a covariant equation.

MACH THRUSTERS IN A PHASED ARRAY

Jeremiah Hansen[1]

Experimental research into Mach Effect thrusters has been limited to small thrusts at the edge of detectability. These thrusts have been slowly improving. The mathematics within the theories show greater thrust is possible. However, the material mechanics and electrical behavior will likely cause limitations in thrust levels. This work was done to explore a new direction in order to improve thrust levels through a unique method of employing the thrusters. The Mach thrusters utilize gravitational waves to interact with the distant matter in the universe. The mathematics behind wave mechanics is applicable to both gravitational and electromagnetic waves, with some distinctions related to phase. This preliminary modeling was developed to calculate the potential of a phased array based on the electromagnetic antenna array mathematics to calculate MEGA thruster behavior in an array. The modeling results are discussed with plotted results displaying the directionality of the array. Some explorations on the impact of array size are explored. A brief discussion follows relative to opportunities for future refinement.

1. INTRODUCTION

The current experimental Mach thrusters, termed MEGA (Mach Effect Gravitational Assist), are very low thrust devices. As experimentation continues, the near term likelihood is that thrusts will remain below a Newton force. There will likely be a physical limit to the capability of these devices, meaning alternate solutions might be necessary for useful thrusts. These MEGA solid state devices utilize gravity waves in its interaction with the distant mass. The wave physics of the array are the same between an electromagnetic array and a gravitational array. This provides an opportunity to explore the effect of multiple Mach Effect devices using the same algorithms used for electromagnetic arrays. Preliminary calculations within this report show a MEGA phased array shows improvement relative to the omnidirectional results.

2. PHASED ARRAY BACKGROUND

Phased arrays are used for radar and communications. A phased array allows for electronic steering of the beam and gains that rival standard dishes. The benefits are obvious, and the methods of control are pertinent to any emitter array using waves. Each one of the emitters is omnidirectional. The wave front is formed by timing of the emissions and control of the phase of the electronic waves. The timing of the emissions from each element is combined in 3-D space, with the emissions from each line of the 2-D array looking like Figure 1.

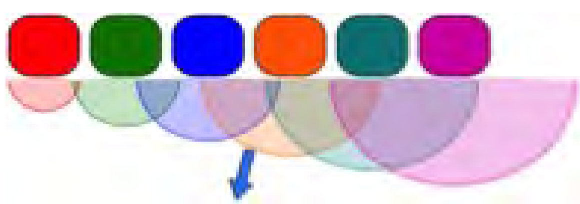

FIG. 1: Phased Array Emission Forming Wave Front

Phased array control for Mach Effect will be similar as gravitational waves propagate at the speed of light and spherically. However, there are no phases associated with MEGA thruster induced gravitational waves.

Normally phase is required to generate stable beams that are not directly perpendicular to the array through the use of constructive and destructive interference. This is referred to as an “off bore-sight” beam. Since gravitational waves lack of phase information, any off bore-sight beam has to be a rapidly pulsed operation for a phased-like operation and/or utilize the emission timing as the method of beam control.

---

[1] jeremiah.hansen@comcast.net

First, though, it is necessary to explore the interaction of the array without phase information as this is the primary mode of operation.

It is worth noting that this paper does not address other possible effects, such as the impact to the array when multiple, gravity wave generating emitters are broadcasting. Changes in the shape and timing within the array will need to be addressed at a later time.

3. OCTAVE SCRIPT OVERVIEW

The calculations of the wavefront and the following distribution of wave energy were accomplished via an Octave script. The script was written to provide an array in 3-D space, a method to time sample and distance sample to determine the response from an input function at a radial distance from the array center. The input function allows for any input signal to be created at each emitter with a specified time delay. Signal from an emitter is then determined based on the distance from the emitter to the calculation point. If the sample point is between input function sample points, simple linear fit is used. Calculation points are determined as the arc from the center of the array at the distance at a specific bearing and elevation relative to bore-sight. The algorithm uses the time sample to determine the amplitude at the selected position from each of the emitters. The sum of those values determines the overall value at that position. It is worth noting here that the phase information in a normal phased array would cause interference patterns in addition to basic intensity, modifying the intensity based on the interference pattern. However, the lack of phase information changes the result and reduces directionality.

The code uses the standard omnidirectional antenna power density equation, S, shown in Eq. 1, which is used from [1]. This equation is based on the expanding sphere surface of the omnidirectional antenna where the "surface" represents the wave front from a single element of the array. This is valid for all omnidirectional waves, including gravity waves. This calculation is run for every element at the current distance from the phased array center to determine the overall signal at that point. The result is then summed to determine the overall signal amplitude at the distance. The code assumes the amplitude is a normalized unitary value for each emitter for calculation purposes. This makes the code applicable regardless of the actual emitter power. This means the power radiated term, P_{rad}, is 1 for each element. Please note this ignores losses in power applied versus emitted and that will need to be determined in the future. The plotted results are in the next section showing the structure of the emitted waves. Equation 1 is the equation for the power density from an emitter at a given distance.

$$S = \frac{1}{4\pi}\frac{P_{\text{rad}}}{r^2} \quad . \tag{1}$$

Directivity, D, is normally defined as the distribution of power density on the spherical surface for a specific polarization. In the case of gravity waves, there are no polarizations. This means the effect is simply the power density distribution over the surface, which would be the equivalent of the combined value from all polarizations for an electromagnetic calculation. The relationship between directivity and emitted power is shown in Equation 2. The calculation is for all radial positions from the array center. This preliminary work didn't include directivity in the calculations due to time constraints. It is helpful to note the relationship to provide the context when comparing with electromagnetic phased arrays. The directivity will be included in the code in the future, as it is especially helpful in identifying the array gain (a product of the derivative) and the beam width, which is traditionally a 3 dB reduction from the peak gain.

$$D = \frac{4\pi S r^2}{P_{\text{rad}}} \tag{2}$$

4. RESULTS

The results are for a 16 element array at 1.5 cm center-to-center distance. The central point of the array is centered within the 4 inner most elements. Figure 2 displays the array for reference. The values shown are in meters. The input signal to each element is in Figure 3. The signal is intended as a method for both testing the algorithm and to provide some distinctions in the output for distance and time sampling. The x-axis is the time in seconds, and the y-axis the normalized amplitude. The output calculations are at a constant distance of 0.91 m from the array for the following images for azimuths from +/- 180 degrees and +/- 90 degrees elevation in 2 degree increments.

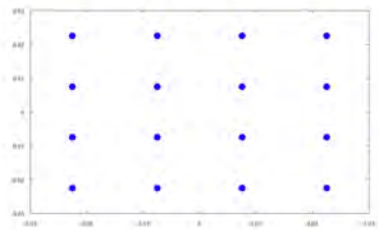

FIG. 2: Mach Thruster Array

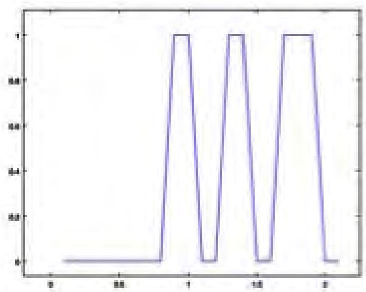

FIG. 3: Input Signal

Even though there is no phase information, the effective gravity wave "beam" has a "near field" and a "far field". The "near field" is where the wave fronts have not combined and are overall separate from each other. The "far field" is where the wave fronts have combined and results in the beam. It is the far field that most concerns MEGA thrusters, EM Drives, and other gravity wave associated thrusters. The beam at a distance of 0.91 meters from the center of the array looks like Figure 4. The extent of the plot is the full sphere around the central point of the array at (0,0). The maximum value at the center of the deep red is 1.5708 and the minimum (deep blue center) is 1.5033. This is a 4.5% difference in intensity between the maximum and minimum. The figure makes it clear that the gain will be minimal, but there is directivity present.

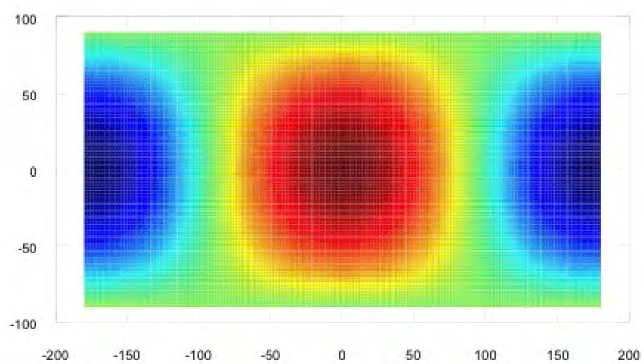

FIG. 4: Far Field Beam at 0.91 m

Adjusting the array by increasing or decreasing the array might adjust the beam intensity through aperture size. It is simple in the code to provide a multiple to the array. Multiplying the array by 0.5, making the separation 0.75 cm, results in Figure 5. The maximum value is 1.55 and the minimum is 1.52 resulting in a 2.22% percentage difference. This is a lower ratio, showing the negative impact on the output of the array. The maximum number is 1% lower from the original array. The overall beam distribution however isn't much different.

Changing the array multiple to 2, with spacing at 3.0 cm, results in a maximum signal 2% greater compared to the original array. The maximum is 1.603 and a minimum of 1.468 with a relative percentage of 9.2%. Figure 6 displays the results, which look very similar to the previous two figures.

The increase in the maximum signal amplitude by increasing the size of the array points to an improved result with array design. This result makes sense as aperture size in electromagnetic arrays increases sensitivity, or relative gain, of an electromagnetic array as it is proportional to square of the aperture area. There is likely a drop off for the array beyond a certain size in signal amplitude as elements move too far apart. The results are promising that the methods used with electromagnetic phased array communications systems look to be applicable to the use of gravitational wave based thruster concepts without phase content.

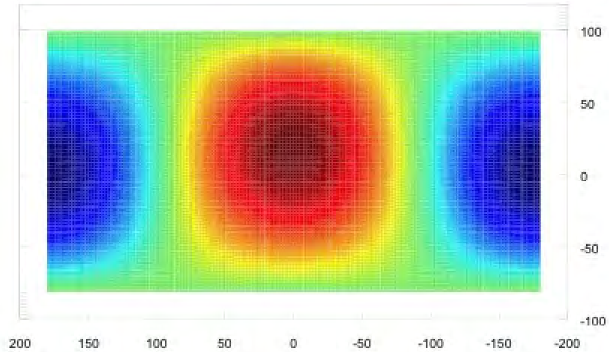

FIG. 5: Half Size Array Beam at 0.91 m

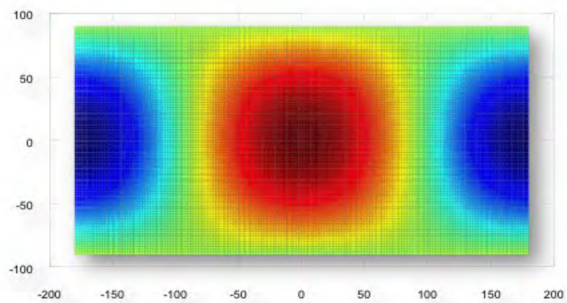

FIG. 6: Two Times Size Array at 0.91 m

5. FUTURE POSSIBILITIES

The modeling seems to provide a basic ability to evaluate the overall strength of the gravity wave beam. It doesn't provide clarity on the impact on directionality with the changes in the array size. It also isn't confirmed via experimentation. Experimentation with small arrays is possible and can provide confidence that this approach is viable when applied with the actual thrusters. Assuming that the approach is viable, it still doesn't inform on the potential of turning the modules on and off in a relatively rapid fashion to provide off bore-sight beams. That will have to come after consideration of the physical and electrical abilities of the modules and the confirmation that the forces produced scale as expected within a phased array.

The ability to control a pseudo-frequency content signal and optimizing the array can increase the gain, or improvement in directivity, of the beam. The impacts for this are not known relative to devices utilizing gravity waves. The benefits of doing so, however, are well worth the effort in directional beams, and real-time adjustment of the beam shape to generate different thrust profiles based on the array output. This includes constructive and destructive interference, and what that really means in a gravity wave propulsion device.

6. CONCLUSION

The experimentation within the EM drive and Mach Thruster community is yielding positive, but tiny, results. The groups might be able to make significant strides in thrust production, but there is always the real possibility the thrust will remain small due to physical limits. One method of dealing with low thrust in rockets is to add multiple engines. However, the gravity wave emission from the thruster provides a potential link to a much different method using the developed field of electromagnetic phased arrays. Preliminary results are promising, and need to be evaluated within a test environment. The potential of creating space drives without using mass ejection as the key thrust component can cause a revolution in space travel. Being able to do that sooner and potentially with more flexibility amplifies the impact such technology will have.

REFERENCES

[1] Mailloux, R.; “Phased Array Antenna Handbook” ; Artech House, 2005. Available in PDF form at: `http://www.omidi.iut.ac.ir/SDR/2007/WebPages/07_SmartAntenna/references/PhasedArrayAntennaHandbook(Maillou`
`.pdf`

RECEPTION AT WINDCLIFF.

Jim Woodward
Celebrating 45 years of trying to get around space-time quickly.

Transcribed by H. Fearn from iphone video taken at the reception by Greg Meholic.

Thank you all for coming this evening. I hope that all of you are as happy with what has transpired over the last few days as I am. Almost a year ago Lance Williams and Heidi Fearn, Heidi's over there, where's Lance, *David Mathes shouts for Lance to get in here... "you didn't train him very well"... audience laughing...* This has been a free–form operation by the three of us.

Almost a year ago Lance and Heidi approached me with the idea of having a workshop, initially it was a conference, but Lance's view that a typical conference has thousands of participants and you typically stand in front of a small fraction of them and give a 15 min talk and have questions for 5 mins and then go find the next section room where the presentation you want to see is being done. With lots of parallel sessions. So they are very efficient from the point of view of the managers that create the conferences, but from the point of view of the participants, they are something less than that. The idea was we would have a conference where there would only be one set of presenters, and the presenters would have an hour or two to talk so real communication could take place. That got kicked around by us for some time and eventually it got down to, well yes, let's try and do it. The question then was, where was the venue to be? One of the people who couldn't come was David Hyland, who offered Texas A&M. Lance and Heidi were both hesitant, and when I asked David how much would it cost, he disappeared. *... Audience laughing ...*

You see we don't have serious financial backing from a professional organization or anything like that. There isn't a professional organization for what those of us, who are the experimental types, in this propulsion field do. Because what we are trying to do is figure out how to get around spacetime quickly without throwing a lot of toxic stuff out of a tailpipe, or trying to solar sail or whatever. Anyway, we were discussing the location and Heidi said why not Estes Park? I said it's really out of the way, why would you want it there. Heidi said, well it's close to where you live, you wouldn't have to travel far and we'll be sure you will come to the workshop. *...Audience laughing....*

I said well we'll see, and the conversation went on and Lance said, well look if it's just the three of us and nobody else comes I would rather be in Estes Park, in a cabin in the mountains, than some hotel in a city anywhere else... *audience laughter again...*

 

So at that point I gave up, we decided on Estes Park. Heidi had already found the YMCA location and Lance drove up to check it out and booked the workshop room. How we ended up literally here, in this house, was that I called Lanier (*Our hosts were Wade and Lanier Whilden.*) for some advice about a reception at my house, and she asked how many people, and I said about 35, she said you're going to get 35 people in your place, you must be joking? We have a much smaller place on Windcliff, at about 400 feet lower elevation. And a day or two later I got an email from her saying why don't you have the reception over at our place. And of course seeing the eminent good sense in not trying to get 35 people into our place, I said yes, OK. That's why we're here tonight. The cake is emblazoned exactly the way I asked it to be, EPBPW, for Estes Park Breakthrough Propulsion Workshop 2016 and whether there will be a 2017, 18 and all that is yet to be seen. What I can say to all of you, the workshop to date has exceeded my most optimistic expectations, is going very very well. Real work is getting done, people are doing the right thing and we are all talking to each other, which is a first in many years. So without further ado, I need someone to cut the cake..

Joe Adair– in the brown jacket: Jim one quick word... In April 29,1962, in welcoming a group of Nobel Prize winners to a dinner, in their honor, at the White House, President John F. Kennedy said,

> "I think this is the most extraordinary collection of talent, of human knowledge, that has ever been gathered together at the White House – with the possible exception of when Thomas Jefferson dined alone." *... Audience Laughing....*

This is likely the largest gathering of intellect, on Windcliff mountain, at any time in history. *... Audience Laughter...*

Wade and Lanier Whilden, hosts You have honored us with having your workshop reception here at our house and we are very proud and happy to have you all here. Thank you *...Audience applause ...*

Let's eat cake! *cutting of the cake ...*
More photos of people at the reception.

There follows a couple of photos of the YMCA meeting center and surrounding area.

View over the lower part of the YMCA of the Rockies Park, away from the building.

Emerald Lodge Exterior. We saw several deer outside in the mornings and late evening.

Outside the Emerald Lodge, on the last day of the workshop 22^{nd} Sept 2016, we saw the most brilliant double rainbow I've ever seen.

CHAPTER 5 – SCALAR FIELD APPROACHES

EXPERIMENTAL VERIFICATION OF THE KALUZA THEORY OF GRAVITY AND ELECTROMAGNETISM

L. L. Williams[1]
Konfluence Research Institute
Manitou Springs, Colorado, USA

The Kaluza unified theory of general relativity and Maxwellian electrodynamics has intrigued researchers for a century. However, no new prediction of the theory, not already found in either existing general relativity or electrodynamics, has ever been proposed – until now.

ESTES PARK CATEGORIES

According to the categories established in the prep kit for this session, this is a mature theory that completely includes general relativity and classical electromagnetism. The theory is relevant to the time-distance problem, as summarized in the pre-workshop Prep Kit. No experiment to falsify the theory has been proposed until now.

1. MOTIVATION: A SYLLOGISM

We are driven by an irresistable logic to search for a solution to the time-distance problem within the framework of the Kaluza theory.

1. The time-distance problem is one of special and general relativity. (cf. Estes Park Quick Study II)
2. Electromagnetism is the only force of nature humans control. Our machinery, our communications, our power generation, even our chemistry and metallurgy – is all electromagnetic
3. The human solution to the time-distance problem may be found at the intersection of general relativity and electromagnetism.
4. The Kaluza unification of general relativity and electromagnetism is the only theory to sit at that intersection, and is the only unified theory ever found that encompasses general relativity

2. KALUZA, NOT KLEIN

The Kaluza theory under consideration here is purely classical. Kaluza submitted his paper to Einstein in 1919 [2], and Einstein forwarded it for publication in 1921 [1]. In 1925 came the quantum revolution of Schroedinger and Heisenberg. A search was soon undertaken to find quantum versions of the classical field theories. Electrodynamics was successfully quantized in the 1940s, but general relativity never was. In 1926, Klein entered the picture by translating Kaluza's purely classical picture into a quantum interpretation. [3] Klein hypothesized that Kaluza's fifth dimension was closed and microscopic. The term "Kaluza-Klein" has been used ever since, but I emphasize we consider only Kaluza here, not Klein. We presume Kaluza's fifth dimension to be macroscopic, as he originally understood it, not closed and microscopic, as Klein understood it. Also note that a series of researchers working independently [4] have worked on the field equations to be summarized below.

---

[1] lance@konfluence.org

3. THE POWER OF THE EINSTEIN EQUATIONS

The basic hypothesis of Kaluza is that the Einstein equations hold true in five dimensions, not just the familiar four of space and time. Why should we extend Einstein's framework to five dimensions? In fact, there are good reasons for doing so.

The Einstein equations are the most general covariant, second-order differential equations, that can be written. In effect, they generalize Newton's law of gravity $\nabla^2\phi = 4\pi G\rho$. They have a supreme mathematical power that is not particular to the number of dimensions in which they are written. In fact, after Kaluza, other workers began to pursue unified field theories by writing the Einstein equations in even higher numbers of dimensions.

The standard Einstein equations are typically written

$$R_{\mu\nu} - \frac{1}{2}g_{\mu\nu}R = \frac{8\pi G}{c^4}T_{\mu\nu} \tag{1}$$

The equivalent Lagrangian, discovered by Hilbert, is

$$\mathscr{L} = g^{1/2}\left(\frac{c^4}{16\pi G}g^{\alpha\beta}R_{\alpha\beta} + T_{\mu\nu}g^{\mu\nu}\right) \tag{2}$$

where the quantities are as described in my earlier talk on aspects of a valid extension to the laws of physics. But now, the factor $g^{1/2}$, necessary to preserve an invariant volume element, is shown explicitly. The action $S = \int \mathscr{L} d^4x$. Where Newton identified a scalar gravitational potential, Einstein identifies a symmetric metric tensor $g_{\mu\nu}$ with 10 components. Note also the unique coupling of the metric, in that it enters both terms of (2), even as $R_{\mu\nu}$ is composed of derivatives of the metric.

4. KALUZA HYPOTHESIS: VACUUM FIELD EQUATIONS

Although Kaluza originally considered a five-dimensional source for the equations, we consider here the five-dimensional (5D) field equations in vacuum.

The 5D vacuum field equations:

$$\widetilde{R}_{ab} - \frac{1}{2}\widetilde{g}_{ab}\widetilde{R} = 0 \tag{3}$$

where roman indices span the five dimensions, and a tilde is used to indicate 5D tensors.

The Lagrangian for these field equations was verified using tensor algebra software [5] to be the standard Hilbert Lagrangian:

$$\mathscr{L} = \widetilde{g}^{1/2}\widetilde{R} \tag{4}$$

In addition, Kaluza applied the constraint known as the cylinder condition. It is that no field variable depends on the fifth coordinate:

$$\frac{\partial \widetilde{g}_{ab}}{\partial x^5} = 0 \tag{5}$$

This is the mathematical expression of the fact that the fifth dimension is not detected: there is no variation in that coordinate. Klein alternatively "explained" why we don't detect a fifth dimension by hypothesizing the fifth coordinate was compact and microscopic.

If derivatives with respect to the fifth coordinate are included, the resulting field equations yield many more terms. Since standard general relativity and electromagnetism are recovered under the cylinder condition, some researchers have relaxed the cylinder condition, and identified the resulting extra terms with an effective stress-energy tensor; viz., matter arises from geometry.

The 15 components of the 5D metric $\widetilde{g}_{ab}$ are decomposed into the 10 components of the 4D metric $g_{\mu\nu}$, the 4 components of the electromagnetic vector potential A^μ (the constant k preserves units), and a scalar field ϕ.

$$\begin{aligned} &\widetilde{g}_{\mu\nu} = g_{\mu\nu} + \phi^2 k^2 A_\mu A_\nu, \quad \widetilde{g}_{\mu 5} = \phi^2 k A_\mu, \quad \widetilde{g}_{55} = \phi^2 \\ &\widetilde{g}^{\mu\nu} = g^{\mu\nu}, \quad \widetilde{g}^{5\mu} = -kA^\mu, \quad \widetilde{g}^{55} = A_\mu A^\mu + 1/\phi^2 \end{aligned} \tag{6}$$

Greek indices span the 4 dimensions of space and time. Kaluza originally set $\phi = 1$, and ignored its dynamics. Subsequent researchers such as Jordan, Thiry, Brans, and Dicke, have investigated this version of scalar field theories and others [4].

5. VACUUM FIELD EQUATIONS: COUPLING OF GRAVITY AND ELECTROMAGNETISM

In a recent work, using tensor algebra software, I was able to show [5] that the vacuum Lagrangian under the Kaluza hypothesis is

$$\mathscr{L} = g^{1/2}\left(\frac{c^4}{16\pi G}\phi g^{\alpha\beta}R_{\alpha\beta} - \frac{1}{4\mu_0}\phi^3 g^{\alpha\mu}g^{\beta\nu}F_{\alpha\beta}F_{\mu\nu}\right) \tag{7}$$

This is quite an unusual Lagrangian, because the scalar field enters only algebraically. Nearly all researchers have been tempted to insert by hand a term proportional to $\partial_\alpha\phi\partial^\alpha\phi$. Yet it is inescapable that the Hilbert Lagrangian (4) and the decomposition (6) lead to the Lagrangian (7).

To consider the field equations from this decomposition, we evaluate the components of $\widetilde{G}_{ab}$ as $G_{\mu\nu}$, $G_{5\mu}$, and G_{55}.

$$\widetilde{G}_{\mu\nu} = 0 \qquad \longrightarrow \qquad R_{\mu\nu} - \frac{1}{2}g_{\mu\nu}R = \frac{8\pi G}{c^4\mu_0}\phi^2 T^{EM}_{\mu\nu} + T^{\phi}_{\mu\nu} \tag{8}$$

where

$$T^{EM}_{\mu\nu} \equiv g^{\alpha\beta}F_{\mu\alpha}F_{\nu\beta} - \frac{1}{4}g_{\mu\nu}F_{\alpha\beta}F^{\alpha\beta} \qquad , \qquad T^{\phi}_{\mu\nu} \equiv \frac{1}{\phi}\left(\nabla_\mu\partial_\nu\phi - g_{\mu\nu}\Box\phi\right)$$

The result (8) is quite extraordinary. From a vacuum equation, we obtained sources to the 4D field equations. It is extraordinary how the correct form of the electromagnetic stress-energy tensor falls out, and this has been called the "Kaluza miracle" that makes the theory so attractive. It is also extraordinary that we get a conventional stress-energy tensor for the scalar field, even though the scalar field enters only algebraically in the Lagrangian (7). Also note that (8) allows the constant k to be fixed in terms of the gravitational constant and the permeability of free space.

Of particular interest for the propulsion problem is that the scalar field enters as a variable coupling between gravity and electromagnetic energy. It would effectively lead to a variable gravitational constant.

Moving on to another aspect of the Kaluza miracle,

$$\widetilde{G}_{5\nu} = 0 \qquad \longrightarrow \qquad \nabla^\mu(\phi^3 F_{\mu\nu}) = 0 \tag{9}$$

Here are the covariant vacuum Maxwell equations, but now with an effective displacement-current type source in the scalar field.

Finally,

$$\widetilde{G}_{55} = 0 \qquad \longrightarrow \qquad \frac{12\pi G}{c^4\mu_0}\phi^2 F_{\alpha\beta}F^{\alpha\beta} = R \tag{10}$$

Again, as can be verified trivially from the Lagrangian (7), the equation for the scalar field is algebraic with no dynamics.

Question: The expression for the metric (6) involves also the quantity A^2. Where is the equation for that?

Williams: It is accounted in the equations for $F_{\alpha\beta} \equiv \partial_\alpha A_\beta - \partial_\beta A_\alpha$. We do have 15 equations in 15 unknowns and everything is accounted for.

6. EQUATIONS OF MOTION: 5D GEODESIC EQUATION

While the field equations describe how the fields respond to sources, the equations of motion describe how matter responds to the fields. The geodesic equation in 5D is:

$$\frac{d\widetilde{U}^c}{d\theta} + \widetilde{\Gamma}^c_{ab}\widetilde{U}^a\widetilde{U}^b = 0 \qquad , \qquad \widetilde{U}^a \equiv \frac{dx^a}{d\theta} \tag{11}$$

Decomposing this into U^μ and U^5, we find

$$\frac{dU^\mu}{d\tau} + 2\widetilde{\Gamma}^\mu_{5\alpha}U^\alpha U^5 + \widetilde{\Gamma}^\mu_{55}(U^5)^2 + U^\mu \frac{d}{d\tau}\ln\left(\frac{d\tau}{d\theta}\right) = 0 \tag{12}$$

Now, the motion of a body under combined gravitational and electromagnetic forces is known to be

$$\frac{dU^\mu}{d\tau} + \Gamma^\mu_{\alpha\beta}U^\alpha U^\beta = \frac{Q}{m}F^\mu{}_\nu U^\nu \tag{13}$$

Another Kaluza miracle is that $\widetilde{\Gamma}^\mu_{5\nu} \propto F^\mu{}_\nu$, inviting us to identify U^5 with the charge-to-mass ratio Q/m. The term in U^5 caused some concern at first, because U^5 can be large for elementary particles, and then this term would dominate the equations of motion. However, $\widetilde{\Gamma}^\mu_{55} \propto \partial_\alpha\phi$, and so this term vanishes in regions of constant ϕ.

7. CHARGE = MOTION

Using the value for k in (6) fixed by (8), we can relate:

$$\frac{dx^5}{d\tau} \quad \to \quad c\frac{Q/m}{\sqrt{16\pi G\epsilon_0}} \tag{14}$$

Mathes: Are you saying the fifth dimension stores charge? Is it stored in the compact fifth dimension? Is this related to quantum theory or will it be reconciled with quantum theory?

Williams: First, this is a purely classical theory. There is to be no reconciliation with quantum theory, and Planck's constant does not enter. A century ago, researchers were not interested in this theory because there seemed to be no point at trying to unify gravity and electromagnetism at the classical level, since we know they are quantum fields. But since then, no quantum theory of gravity has been found. The century's greatest minds – Feynman, Schwinger, Paul, Dirac – were unable to solve that riddle. How long should we keep trying? As to your other question, the fifth dimension does not store charge. Rather, what we call charge is actually due to motion in the fifth dimension. When you see a charged particle at rest, it is actually traveling through the fifth dimension while its spatial coordinates remain unchanged.

We see that electric charge is a fifth component of an energy-momentum-charge 5-vector:

$$\widetilde{U}^a = \frac{\gamma_5}{m}(E/c, \mathbf{p}, Q/k) \tag{15}$$

As energy is due to motion in time, and momentum is due to motion in space, so electric charge is due to motion in the fifth dimension.

Buldrini: This seems to imply that the speed with which the electron moves in the fifth dimension is absolutely constant and unchanging.

Williams: Yes, that's right. In fact, speeds are astronomical for elementary particles, $\sim 10^{20}c$.

Hansen: Earlier you said the cylinder condition stipulated no change in the fifth dimension, so how can things be moving in the fifth dimension?

Williams: Those are two different things. The cylinder condition tells us no fields depend on the fifth coordinate, but that does not mean things are not moving (uniformly) through the fifth dimension.

Mathes: Can you remind us of the definition of proper time?

Williams: Yes, it is the invariant length element. In 4D, $d\tau^2 = c^2dt^2 - dx^2$. In 5D, we add in a piece such that $d\theta^2 = c^2dt^2 - dx^2 - d(x^5)^2$.

8. TIME DILATION OF CHARGED CLOCKS

Here we propose a way to verify or falsify the Kaluza hypothesis. As just mentioned, we can write the 5D invariant length element at a fixed position ($\Delta x = 0$):

$$d\theta^2 = c^2dt^2 + d(x^5)^2 = c^2dt^2(1+\beta_5^2) \qquad ; \qquad \beta_5^2 \equiv \frac{Q^2/m^2}{16\pi G\epsilon_0} \tag{16}$$

We see here the core features of a time dilation or time contraction effect. If there is a rest frame in the fifth dimension, then a clock could feasibly run faster or slower, depending on its motion in the fifth dimension. It is analogous to the time dilation exhibited by muons produced in the upper atmosphere. But instead of motion in space, we wish to consider motion in the fifth dimension. These considerations raise several questions.

Is there a rest frame in the fifth dimension?

A major distinction between space and time is that the former allows a rest frame for massive objects, whereas the latter does not. No massive object can be at rest in time, but one can be at rest in space. If the fifth dimension has no rest frame, then this effect may not be detectable. But if the fifth dimension is spacelike in that it does allow a rest frame, then time dilation or time contraction may be something we can find a way to detect.

What is the meaning of the mass of a clock?

The mapping of speed to charge (14) requires a mass. Considering clocks in spatial motion, we do not encounter this conceptual issue. But in this case, we wish to consider a rest frame characterized by a charge-to-mass ratio.

If there were a rest frame to the fifth dimension, and if the effect were detected, it would be a new effect unknown to physics.

10. PROPERTIES OF A CHARGED CLOCK

The first property of a charged clock is that it must be uniformly charged throughout its volume. Under the Kaluza hypothesis, only charged particles are moving through the fifth dimension. But if those particles merely surround a volume that is itself uncharged, then the interior volume is not moving in the fifth dimension, and is not charged in the sense implied here.

Volume charges are perhaps more difficult to realize than surface charges, so perhaps a two-dimensional clock, if it could be found, could be more easily charged.

Meholic: Perhaps the effect could be somehow realized with an atomic clock such as a cesium clock.

Williams: Yes, I had also thought of using the decays of nuclides somehow.

Cole: Could it be realized with a capacitor?

Meholic: It seems plausible because the discharge time might depend on the charges on the capacitor plate.

Buldrini: Perhaps an electret.

March: Are you familiar with Erwin Saxl's experiments with electrified pendulums in 1964? He found some strange time effects. It was in Nature, 1964. Earl Saxl.

Tajmar: Before you repeat that experiment you should know it was found out to be due to electrostatic charge on the chamber walls.

Another key property of a charged clock is that it must offer two different charge-to-mass states, but without affecting its timekeeping mechanism or principle. This is because we need to test how time varies depending on the charge state.

Broyles: Could you use a double slit experiment, using charged bucky balls? Do it charged and uncharged. Evaluate the time of flight to the detector.

Cole: I would come back to the capacitor. Except, use just one plate. The plate is charged and can be considered a 2D clock. The clock is the discharge time of the capacitor.

Tajmar: You must consider that if you use alternating currents, you can get accelerations and radiation, and makes it difficult to control. Ideally, you will have linear motion with no acceleration and no radiative losses. I would approach this with a mass spectrometer and time of flight considerations. You can control the charge state of the ions, and measure the time of flight very accurately.

Williams: I don't understand why time of flight would be a charged clock. I think it's motion in space is not really the motion we are trying to isolate in the fifth dimension.

Tajmar: Perhaps you could charge up a macroscopic quantity of something radioactive, and see if its decay rate changes. Perhaps a cesium plasma would constitute a 3D charge state.

Buldrini: Aren't any of these schemes just moving charges around? The charges don't change, whatever material they may be in. It is not clear what is decaying.

Moving along, let us consider the alternative case, where there is no rest frame to the fifth dimension. In that case, the time coordinate and the fifth coordinate are bound together for charged particles. This situation holds promise in that there may be an effective speed c' and an effective time t' such that $(c')^2(dt')^2 = c^2dt^2 + (dx^5)^2$. Since the coefficient of the time coordinate is what sets the limiting speed (speed of light – cf. Estes Park Quick Study II), perhaps this situation would promise an alternative, effective limiting speed that could be manipulated with electric charge.

11. TIME DILATION OR CONTRACTION FROM ELECTRIC CHARGE, IN EXISTING PHYSICS

The most famous example of time dilation about an electrically charged region is given by the Reissner-Nordstron metric. The time component is:

$$d\tau^2 = dt^2\left(1 - \frac{2GM}{rc^2} + \frac{Q^2G}{r^2 4\pi\epsilon_0 c^4}\right) \tag{17}$$

Although the mass M causes the familiar gravitational time dilation, the electric charge Q causes a counter-acting time contraction. Note that the variation in time is proportional to the gravitational constant, and independent of any mass.

However, the Reissner-Nordstrom metric applies to the vacuum surrounding a charged mass. We are interested in the interior, where the charge is. Let us turn to the interior solution result of Arnowitt et al [6]. They find the balance between mass-energy, gravitational energy, and electrostatic energy, is given by:

$$mc^2 = m_0c^2 + \frac{Q^2}{2r}\frac{1}{4\pi\epsilon_0} - \frac{GM^2}{2r} \tag{18}$$

In the limit that $r \to 0$, the mass does not vanish, but acquires a value

$$M = \pm Q/\sqrt{4\pi\epsilon_o G} \tag{19}$$

In this case, we have a scaling of $M^2 \sim Q^2/G$. This is the same scaling as (14). So we see that the scaling from the Kaluza result is consistent with expectations from existing classical theory.

12. SUMMARY OF BREAKTHROUGH POTENTIAL

Let us summarize the aspects of the Kaluza theory that hold promise for a breakthrough in propulsion.

- An electromagnetically-tuneable coupling of mass to gravity
- A hyperspace dimension with large characteristic speeds
- Electromagnetic control of the flow of time, if the fifth dimension has a rest frame
- A way to re-scale the time-distance problem, if the fifth dimension has no rest frame

Woodward: I am not sure you will be able to tune the coupling of gravity, because it is not clear what the charge-carriers are for the scalar field. To control electromagnetism we move charges and currents around. I am not sure this will be workable unless you have scalar charge carriers that you can manipulate.

Williams: Your point is well taken. Kaluza did write down the source terms for the scalar field, and it is something like "charge squared", the 5-5 component of the stress-energy tensor. But I don't know what that means physically, or how to isolate the scalar charges.

P. Jansson: What about an excited atom? Would the decay time depend on its energy?

References

[1] T. Kaluza, *Sitzungsberichte der K. Preussischen Akademie der Wissenschaften zu Berlin*, 966 (1921).
[2] A. Pais, *Subtle is the Lord: The Science and the Life of Albert Einstein*, Oxford University Press: Oxford (1982). (cf. section 17c)
[3] O. Klein, *Z. Phys.*, **37**, 76 (1926).
[4] H. Goenner, *Gen. Relativ. Gravit.*, **44**, 2077 (2012).
[5] L. Williams, *Journal of Gravity*, Article ID 908170 (2015), http://dx.doi.org/10.1155/2015/901870
[6] R. Arnowitt, S. Deser, & C. Misner, *Physical Review*, 120 (1960).

EXPERIMENTAL APPLICATIONS OF CHAMELEON COSMOLOGY

Glen A. Robertson
265 Ita Ann,
Madison, AL 35757

Space propulsion science has been progressing slowing over the last half century, partly due to the inconsistency between Einstein physics and quantum physics; and more so, to the incapability of propulsion engineers to understand both! The Modified Chameleon Model was developed in an attempt to bring non-classical propulsion concepts into better focus for engineers.

1. INTRODUCTION

Since indulging in the aspects of space propulsion science, I have had a hard time seeing how Einstein Relativity (ER) and its sub-theories could ever lead to the engineering of a real space drive. From my prospective, ER can only tell one that space drives are possible within the understanding of the Universe (i.e., things on a big scale) with little focus back to us mundane humans (i.e., things on a smaller scale). In recent years, there has been a focus to bring the large scale of Newtonian gravity (where today's propulsion lives) down to a smaller scale called quantum gravity (where future propulsion theories are arising). However, little (if any) engineering progress has been made.

In his paper, *"Copenhagen vs Everett, Teleportation, and ER=EPR,"* Susskind [1] provides a means to connect Quantum mechanics to Einstein Relativity and its sub-theories through a kind of non-locality called Einstein-Podolsky-Rosen (EPR) entanglement.

> *"EPR does not violate causality, but it is, nevertheless, a form of non-locality. It is most clearly seen if one imagines trying to simulate quantum mechanics on a system of classical computers. By assuming the computers are distributed throughout space and represent local degrees of freedom. The whole conglomeration is required to behave as if there were quantum systems inside the computers; systems that local observers can "observe" by pushing buttons and reading outputs. The computers will of course have to interact with each other, as they also would if we were simulating classical physics. But simulating classical physics only requires the computers to interact with their local neighbors." Susskind [1].*

Although Susskind's idea of entanglement represents a neat way to bridge Newtonian gravity to quantum gravity through ER, when dealing with space drive theories, it may be better to indulge in the concept of coupled entanglement.

Here coupled entanglement is defined as a measure of the degree in which a system is entangled to the neighboring environment. The measure is defined as a coupling factor, where full coupling is equal to one.

For example, space drive concepts dealing with the quantum theory known as zero point energy (ZPE) may better be presented with the ZPE propulsion theory including coupled entanglement by adding a coupling factor into the ZPE propulsion equations. That is, the coupling factor represents the amount of coupling a ZPE propulsion system has to the enormous amount of ZPE energy in the Universe by only considering the coupled entanglement amount in the local or neighboring environment about the ZPE propulsion system. In other words, ZPE propulsion theories and other space drive theories have not consider entanglement to the local environment, whereby they represent a coupling factor = 1 (i.e., entanglement to the entire Universe) when it may be much smaller (i.e., coupled entanglement to the local neighboring environment). Of course understanding the correct coupling factor for any space drive may not be mathematically attainable at this time, i.e., such insights may only be attainable through experimentation. From this, it is then easy to see that coupled entanglement could solve the disagreements between ER and quantum theory by allowing coupling factors related to the degree of local entanglement to solve mathematical discrepancies. For example, although the Universe contains an enormous amount of ZPE per cubic meter, the local amount of ZPE depends on the coupled entanglement to the local environment, where the coupled entanglement is a quantum mechanism. Now the hard part, "How can propulsion engineers use the concept of coupled entanglement to investigate new propulsion theories?" Although I suspect that many new theories will emerge over time, there is one today that represents a starting point. This theory is still in its infancy and needs much work, called the "Modified Chameleon Model ", [2–4] as it is an acceleration model derived from "Chameleon Cosmology " [5].

2. ENTANGLEMENT: CHAMELEON COSMOLOGY AND THE MODIFIED CHAMELEON MODEL

Chameleon Cosmology represents a small subtractive change to gravity related to the local or neighboring density environment, developed from a general Lagrangian where each matter field couples to a metric related to an Einstein-frame metric by a conformal transformation, where coupling factors are introduced as dimensionless constants. Unfortunately, in the papers on Chameleon Cosmology, the coupling factors are not well defined and are set to unity (=1). However, the local density environment defined in these papers provides a well-established local environment tied back to an Einstein metric, whereby the local density environment is a neighboring entanglement environment. Further, the coupling factors in Chameleon Cosmology provide a means for considering the amount of coupled entanglement to the local density environment. That is, although the Universe is large, the local density environment change across the Universe provides a local entanglement environment with coupled entanglement, where the value of a coupling factor is dependent on where you are in the Universe.

> *The universe is filed with subsystems, any one of which can play the role of observer. There is no place in the laws of quantum mechanics for wave function collapse; the only thing that happens is that the overall wave function evolves unitarily and becomes more and more entangled. The universe is an immensely complicated network of entangled subsystems, and only in some approximation can we single out a particular subsystem as THE OBSERVER.* Susskind [1].

In Chameleon Cosmology, the coupling across densities are mediated by a thin-shell mechanism (i.e., THE OBSERVER) that can be envisioned to exist about all objects to include any region defined in the Universe, where the region can include any of the states of matter, empty vacuum, or a combination of them. This observer (thin-shell) is in effect the quantum matter of the Universe, that is definable in a thin-shell medium about a defined density, where it is in entanglement to the densities on either side (internal and external to the defined density) and reacts to the changes in these densities by increasing or decreasing its thickness. The thin-shell thickness in Chameleon Cosmology effectively acts like the bridge between“folded space” in order to draw spatially distant points (densities) close to one another. The thin shell thickness in Chameleon Cosmology is basically the short black line in Susskind’s [1] figure 2 and the densities are the two red dots.

> *The two red dots are maximally entangled particles and I indicate their entanglement by linking them by a short black line. The black link has some structure; for example, it distinguishes between the various maximally entangled Bell states. Despite appearances the nonlocal features of entanglement cannot be used to transmit messages super-luminally (faster than light).* Susskind [1].

Note: The Bell states are a concept in quantum information science and represent the most simple examples of entanglement. An EPR pair is a pair of qubits (or quantum bits) which are in a Bell state together, that is, entangled with each other. Unlike classical phenomena such as the nuclear, electromagnetic, and gravitational fields, entanglement is invariant under distance of separation and is not subject to relativistic limitations such as the speed of light (though the no-communication theorem prevents this behavior being used to transmit information faster than light, which would violate causality). (from Wikipedia)

General Relativity also has its non-local features. In particular there are solutions to Einstein’s equations in which a pair of arbitrarily distant black holes are connected by a wormhole or Einstein-Rosen bridge (ERB). The thin-shell thickness in the Modified Chameleon Model (MCM) effectively acts like a wormhole or Einstein-Rosen bridge (ERB) (see [6]) connecting density fields. The thin-shell thickness is basically the ERB in Susskind’s [1] figure 3 and the “folded spaces” are density fields. Inside the ERB resides an object constituting the location of the two observer that have jumped in, to meet.

> *At first sight it would seem that ERBs can be used to super-luminally transmit signals. But this is not so; the wormhole solutions of general relativity are “non-traversible.” (Non-traversibility means that two observers just outside the black holes cannot communicate through the ERB. Non-traversibility does allow them to jump in and meet in the ERB.) The similarity between figures 2 and 3 is quite intentional. The punchline of the ER=EPR joke is that in some sense the phenomena of Einstein-Rosen bridges and Einstein-Podolsky- Rosen entanglement are really the same: ER=EPR. Susskind [1].*

Susskind further states:

This is a remarkable claim whose impact has yet to be appreciated. There are two views of what it means, one modest and one more ambitious. The ambitious view is that some future conception of quantum geometry will even allow us to think of two entangled spins (a Bell pair) as being connected by a Planckian wormhole. The modest view first of all says that black holes connected by ERBs are entangled and also the converse; entangled black holes are connected by ERBs. But there is more to it than that. The idea can be stated in terms of entanglement being a "fungible resource." Entanglement is a resource because it is useful for carrying out certain communication tasks such as teleportation. It is fungible because like energy, which comes in different forms (electrical, mechanical, chemical, etc.), entanglement also comes in many forms which can be transformed into one another. Energy is conserved but entanglement is not, except under special circumstances. If two systems are distantly separated so that they can't interact, then the entanglement between them is conserved under independent local unitary transformations. Thus if Alice and Bob, who are far from one another, are each in control of two halves of an entangled system, the unitary manipulations they do on their own shares cannot change the entanglement entropy. If Alice's system interacts with a nearby environment (a first density field), the entanglement with Bob's system can be transferred to the environment (a second density field), but as long as the environment stays on Alice's side (does not cross the thin-shell) and does not interact with Bob's system (acts only with the thin-shell) the entanglement will be conserved. Susskind [1].

That is, the thin-shell in Chameleon Cosmology (CC) and the Modified Chameleon Model (MCM) act as a mediator (i.e., ERB) to conserve energy and as a mediator (i.e., EPR) to conserve entanglement between density fields. This basically entails that all objects whether stationary (CC) or moving (MCM) reside within the fundamental constitutes (i.e., exotic energy = the thin-shell energy) of a "wormhole", as defined by the wormhole solutions of general relativity. Given this, as an object moves, the "wormhole" develops around it, never having to cross an event horizon as these would form in the aft and forward wakes of the thin-shell (see ref. [6]).

3. Chameleon Cosmology and The Modified Chameleon Model

The thickness of the thin-shell about an object m of density ρ_m and radius R_m was derived in more engineering (i.e., simple) terms during the development of the Modified Chameleon Model (MCM) as

$$\Delta R_m \approx \frac{\kappa_0}{\rho_m R_m} \quad , \tag{1}$$

where

$$\kappa_0 \approx \frac{1}{3} M_E^2 \left(\frac{2M_{PL}^4}{\rho_0} \right)^{1/3} \tag{2}$$

where ρ_0 is the external density (i.e. atmospheric density about the object m) and the parameters:
Where the Reduced Plank mass (m_p) is given by

$$M_{PL} = \frac{m_p}{\sqrt{8\pi}} \approx 4.34 \times 10^{-9}\text{Kg} \ ; \tag{3}$$

and Energy Scale Constant is

$$M_g \approx \left(\frac{\Lambda}{8\pi \ell_p^2} \right)^{1/4} \approx 11378\text{m}^{-1} \tag{4}$$

where Λ is the cosmological constant and ℓ_p is the Plank length. Then it follows from the MCM derivations of Chameleon Cosmology that the subtraction to the gravitational force or Chameleon Field force is given by,

$$-F_\phi = -6\, \beta_m \left(\frac{\Delta R_m}{R_m} \right) F_{\text{N}} \ \ , \tag{5}$$

where β_m is the object's internal density coupling factor, i.e., the internal density coupled entanglement moderator of the thin-shell, and $F_N = mg_N$ is the local Newtonian gravitational force of gravity with g_N being the gravity acceleration. Under Chameleon Cosmology with MCM derivations, the gravitational force on a small object near a larger object is given by

$$F_{\text{gravity}} = F_{\text{N}} - F_\phi = \left[1 - 6\beta_N\left(\frac{\Delta R_m}{R_m}\right)\right] F_{\text{N}} \ , \tag{6}$$

where in Eq.(6), the subscript N is used to denote that the larger object is also the primary Newtonian gravitation force producer. And since it can be easy seen from equations (1-4) that the thin-shell thickness for the earth would be very small, ($\sim 10^{-14}$m) and $\beta_N \approx 1$ under Chameleon Cosmology, whereby the Chameleon Field force $F_g \ll 1$, so that current Newtonian gravity is not violated.

It should be appreciated that the thin-shell thickness is a quantum mechanism defined by the Planck scale parameters m_p and ℓ_p , normalized to ER (the Universe) by the cosmological constant Λ , to the external local entanglement environment of an object by the local atmospheric density ρ_0 , and to the local internal entanglement environment of the object by the object's density ρ_m. Whereby, an object's thin-shell provides the Universe entanglement (quantum) mechanism for simulating classical physics interactions between the local entanglement environments (atmosphere and object or space and space drive system). Noting that this is similar to simulating classical physics between entangled computers which only requires the computers to interact with their local neighbors.

3.1 Coupling Factors

During the development of the Modified Chameleon Model (MCM) the problem in defining the coupling factor was resolved by noting that for the earth (denoted by the subscript $\oplus$)

$$\Delta R_\oplus \approx \sqrt{\ell_p R_\oplus} \Rightarrow \ell_p \approx \frac{\Delta R_\oplus^2}{R_\oplus} \ , \tag{7}$$

but for other objects in our solar system this is not true. To correct this, equation (7) was rewritten as

$$\Delta R_\oplus \approx \beta_{E_\oplus}^2 \sqrt{\ell_p R_\oplus} \Rightarrow \ell_p \approx \beta_{E_\oplus}^4 \frac{\Delta R_\oplus^2}{R_\oplus} \ , \tag{8}$$

where for $\beta_{E_\oplus} \approx 1$, or for any object

$$\Delta R_m \approx \beta_{E_m}^2 \sqrt{\ell_p R_m} \Rightarrow \ell_p \approx \beta_{E_m}^4 \frac{\Delta R_m^2}{R_m} \ , \tag{9}$$

where β_{E_m} is the object's external density coupling factor, i.e., the external density coupled entanglement moderator of the thin-shell.
Combing Eq.(9) back with Eq.(1) then gives,

$$\beta_{E_m}^2 \approx \frac{\kappa_0}{\rho_m R_m \sqrt{\ell_p R_m}} \ , \tag{10}$$

where we let all coupling factors of objects i have the same form

$$\beta_i \equiv \left(\frac{\kappa_0}{\rho_i R_i \sqrt{\ell_p R_i}}\right)^{1/2} \ , \tag{11}$$

as it can be shown that $\beta_\oplus \approx \beta_{E_\oplus} \approx 1$.
It should be appreciated that the external and the internal coupling factors are quantum factors in the same way that the thin-shell thickness is a quantum mechanism.

Now combining Eqs. (9) and (5) to the Chameleon Field force is given in terms of the coupling factors as

$$F_\phi = -\left(6\,\beta_m \beta_{E_m}^2 \sqrt{\frac{\ell_p}{R_m}}\right) F_{\mathrm{N}} \tag{12}$$

and since both coupling factors approach 1 for any object, it can be easy seen from equations (12) that the Chameleon Field force is dominated by the Planck length ($\ell_p \sim 10^{-35}$m), such that, Chameleon Cosmology does not violate Newtonian gravity theory for any gravitational object. That is, the subtraction of the Chameleon Field force does not change our view of Newtonian gravity.

4. THE MODIFIED CHAMELEON MODEL: AN ACCELERATION MODEL

Chameleon Cosmology looks at the Chameleon Field force from a gravitation source on a nearby smaller objects in an external density (i.e., atmosphere) environment, where all densities are considered static. In the Modified Chameleon Model (MCM) all objects have a scalar density field, where an object's density field is only equal to its actual density when the object is static, as covered by Chameleon Cosmology. That is, the density field of an object is allowed to be timevarying. Further, MCM treats the density of the object generating the Newtonian gravitation source as a secondary external density field to the object's internal density. These density fields are taken to have same local entanglement to the thin-shell as the density environment in Chameleon Cosmology. By allowing all density fields to change, produces changes to the thin-shell thickness about the object though coupled entanglement to these density fields. Whereby, MCM investigates the Chameleon Field "acceleration" force on an object due to changes in the thin-shell thickness about an object, due to internal and external changes to local density fields. The changing density fields in MCM forces the form of the coupling factors per Eq.(11) to change as

$$\delta\beta_i \equiv \left(\frac{\kappa_0}{\beta_a \partial\rho_i \bar{R}_i \sqrt{\ell_p \bar{R}_i}}\right)^{1/2} \quad , \tag{13}$$

where β_a is a motion coupling factor due to acceleration, $\partial\rho_i$ is the changing density field of an object i, and R_i is the changed radius called the radial factor. These will be discussed later.

4.1 The Time Varying Density Field Model

By treating the scalar density fields like scalar potential fields, a time varying density fields can be investigated through the concept of time dilation and retardation, which is shown to eliminate the need for coupling factors by using the acceleration mediators, i.e., the mediators that cause of the coupling factors to not equal 1.

Time dilation and retardation is taken into consideration by electrical engineers when there are interfering sinusoidal electric and magnetic field; producing a small retardation of the electron motion. Retardation is a relativity slow phonon mediated process that occurs when electric and magnetic fields are sinusoidal (time-varying) and overlap in a material by an average separation distance s as described by the Lienard-Wiechert potentials (i.e., scalar potential fields [7]). This induces a small reaction time or retardation time $\Delta t = s/c$ between earlier field interactions and corresponds to a phase shift $\omega\Delta t$ and infers a retardation time $t' = t - \Delta t$, which results in unidirectional forces "on the material" in the overlapping fields.

Note: Another way of looking at the time dilation and retardation (TDR) of the thin-shell thickness is by considering the thin-shell of be composed of subatomic particles. In particle physics, many subatomic particles exist for only a fixed fraction of a second in a lab relatively at rest, but some that travel close to the speed of light can be measured to travel farther and survive much longer than expected (a muon is one example). According to the special theory of relativity, in the high-speed particle's frame of reference, it exists, on the average, for a standard amount of time known as its mean lifetime, and the distance it travels in that time is zero, because its velocity is zero. Relative to a frame of reference at rest, time seems to slow down for the particle. Relative to the high-speed particle, distances seem to shorten. Einstein showed how both temporal and spatial dimensions can be altered (or "warped") by high speed motion. (from Wikipedia) .

That is, the thin-shell thickness on one side moves faster in time than the other (time retarded) side.

4.2 Time Dilation and Retardation Model

The following time dilation and retardation (TDR) derivation is shown in more detail in ref. [3]. Under the MCM, we let the cause of the TDR comes from the motion of particulate matter (i.e., the acceleration mediators) in an object due to an applied energy potential that causes the particulate matter to move at the speed of light (even when the parent mass is moving slower) and specifically only to a small group much less than the total matter in the object and such matter that can be easily modulated without distortion to the peripheral boundary of the object or vibration of the object. That is, no visible distortion or vibration of the object would be detected. Any distortion or vibration to the object would invoke a classical energy loss in the form of mechanical, thermal or etc. energy. Although, thermal heat loss would be expected if the subatomic particulate matter is an electron, proton or neutron. Therefore, the suspect subatomic particulate matter here is probably at the quantum scale, as at this scale, matter and energy behave very differently from what much of everyday experience would lead us to expect. Under this criteria, an object's density field $\partial\rho_m$ would be changing and is given in like to Eq.(65) in ref. [3] as

$$\partial\rho_m \approx \rho_m + |\frac{\vec{F}_{\phi_a}}{\vec{F}_{\mathrm{N}}}|\rho_i = \frac{3m}{4\pi\bar{R}_m^3} \quad , \tag{14}$$

where ρ_i is the density of the particulate matter and $\bar{R}_m$ is the radial factor, i.e., the change to the object's density field radius, given from Eq.(14) as

$$\bar{R}_m = R_m\left(1+|\frac{\vec{F}_{\phi_a}}{\vec{F}_{\mathrm{N}}}|\frac{m_i}{m}\right)^{-1/3} = R_m\left(1+\left[\frac{a_i}{g_{\mathrm{N}}}\right]\frac{m_i}{m}\right)^{-1/3} \quad , \tag{15}$$

where m is the mass of the object and m_i is the total mass of the accelerated particulate matter in the object with acceleration a_i.

4.3 Time Dilation

The acceleration field force equation is then given as

$$\bar{F}_{\phi_a} \approx 6\,\partial\beta_m\left(\frac{\partial\Delta R_m}{\bar{R}_m}\right)\vec{F}_{\mathrm{N}} \quad , \tag{16}$$

where $\partial\Delta R_m$ is the change in the thin-shell thickness that gives rise to the acceleration field force.

Now letting the ratio $\partial\Delta R_m/\bar{R}_m$ be a function of the number N of perturbations in the distribution of the particulate matter in the object over an effective time t with each perturbation occurring over the object's relaxation time $\tau \approx t/N$ corrected by a time dilation $\tau+\Delta\tau$ corresponding to a volume expansion $V_r+\Delta V_r$, which results in a dimensional translation that gives rise to the change $\partial\Delta R_m$ in the direction of any resulting motion. Such that, the acceleration field force can be given in terms of time dilation by

$$\bar{F}_{\phi_a} \approx 6\,\partial\beta_m\left(\frac{\tau}{\tau+\Delta\tau}\right)\vec{F}_{\mathrm{N}} = 6\,\partial\beta_m\left(\frac{t}{t+\Delta t}\right)\vec{F}_{\mathrm{N}} \quad , \tag{17}$$

where the retardation time Δt reflects an interaction with an earlier event from the current time t and corresponds to a phase shift

$$\Delta\omega_m \approx \omega\Delta t \quad . \tag{18}$$

4.4 Retardation

Retardation implies that there is a retarded or past density change $(\partial\rho_m)_R$ and a non- retarded or current density change $(\partial\rho_m)_{NR}$, which gives rise to a motion coupling factor between the object and the Newtonian gravitation object to not be identical. This difference implies that there exists both a retarded internal coupling factor $(\beta_m)_R$ and a retarded Newtonian internal coupling factor $(\beta_N)_R$, given by

$$(\beta_m)_R \approx \partial\beta_m \sin(\omega t + \phi - \Delta\phi_m) \ ; \tag{19}$$

$$(\beta_N)_R \approx \partial\beta_N \sin(\omega t - \Delta\phi_m) \ , \tag{20}$$

noindent where ωt is the phase between events and ϕ is the phase between the changing coupling factor $\partial\beta_m$ and the changing Newtonian mass to field coupling factor $\partial\beta_N$ relating to the non-retarded or current density change $\partial\rho_m$ of the object, given by

$$(\beta_m)_{NR} \approx \partial\beta_m \sin(\omega t + \phi) \ ; \tag{21}$$

$$(\beta_N)_{NR} \approx \partial\beta_N \sin(\omega t) \ , \tag{22}$$

where the subscript ($_R$) implies retarded and the subscript ($_{NR}$) implies non-retarded. Now let

$$\theta_m \approx 6 \ \partial\beta_m \left(\frac{t}{t+\Delta t}\right) \ , \tag{23}$$

defined as the local fifth force coefficient, where equations (20-23) provide a phasing of the local fifth force coefficients as

$$\theta_m \approx 6 \ \partial\beta_m \sin(\phi) \ . \tag{24}$$

Then noting that,

$$\sin(\phi) = \frac{t}{t+\Delta t} = \frac{\partial\Delta R_m}{\bar{R}_m} \ll 1 \tag{25}$$

and that when the $\sin(x) \ll 1$, $\sin(x) \approx x$, such that the phase

$$\phi \approx \frac{t}{t+\Delta t} \ . \tag{26}$$

Then using Eq.(17), the acceleration field force can be given in terms of a phase factor as

$$\vec{F}_{\phi_a} \approx 6 \ \partial\beta_m \phi \vec{F}_N \ , \tag{27}$$

where from equations (27) and (13), the internal coupling factor

$$\partial\beta_m \approx \frac{1}{6\phi}|\frac{\vec{F}_{\phi_a}}{\vec{F}_{\mathrm{N}}}| = \frac{1}{6\phi}\left(\frac{a_i}{g_{\mathrm{N}}}\right) \approx \left(\frac{\kappa_0}{\beta_a \partial\rho_m \bar{R}_m \sqrt{\ell_p \bar{R}_m}}\right)^{1/2} \ . \tag{28}$$

Whereby, the Eq.(28) gives the thin-shell change

$$\partial\Delta R_m \approx \phi\bar{R}_m \approx \frac{1}{6\phi}\left(\frac{a_i}{g_{\mathrm{N}}}\right)\left(\frac{\kappa_0}{\beta_a \partial\rho_m \bar{R}_m \sqrt{\ell_p \bar{R}_m}}\right)^{-1/2} \bar{R}_m \ , \tag{29}$$

by noting Eqs. (25) and (26) to give the phase factor

$$\phi \approx \frac{1}{6\phi}\left(\frac{a_i}{g_{\mathrm{N}}}\right)\left(\frac{\kappa_0}{\beta_a \partial\rho_m \bar{R}_m \sqrt{\ell_p \bar{R}_m}}\right)^{-1/2} = \frac{1}{6 \ \partial\beta_m}\left(\frac{a_i}{g_{\mathrm{N}}}\right) \ . \tag{30}$$

The main point of Eq. (30) is that the phase factor inherently carries the motion factor a β_a and the internal coupling factor $\partial\beta_m$. That is, once knowing the phase factor, the motion factor and the internal coupling factor can be derived. However as is shown in the following knowing the motion factor and the internal coupling factor is not required, once the phase factor is known.

4.5 MCM Rocket Model

A rocket is a two density field model, i.e., the changing propellant causes the rocket to have a changing density field and the gas flow through the nozzle induces a new changing density field, such that a two density field approach is required [3, 4].

For a rocket, the thrust can be given by

$$T \approx (m_i - m_{ex})a_r \quad , \tag{31}$$

where m_i is the initial mass of the rocket and m_{ex} is the exhausted mass.

In ref. [8], it was shown that the MCM model can be simplified to the rocket acceleration as

$$a_r \approx 6 \left[\frac{\phi^3 \ell_p^{-1/2}}{\left(\bar{R}_r^{-1/2} - \bar{R}_{gas}^{-1/2} \right)} \right]^{1/2} g_{\mathrm{N}} \quad , \tag{32}$$

Where the rocket radial factor $\bar{R}_r$ is the nozzle throat radius (the active interface between the rocket and nozzle) and the gas radial factor $\bar{R}_{gas}$ is $\sqrt{2}$ times the exhaust nozzle radius (the active interface between the nozzle and the external density field), and where the phase is given by

$$\phi \approx \left[1 + \left(\frac{v_{gas}}{\bar{R}_{gas}} \right) \left(\frac{m_{ex}}{\dot{m}} \right) \right]^{-1} \quad . \tag{33}$$

The active interfaces are the locations where mass is flowing out of one density field and into another.

For a rocket, the hot gas relaxation time

$$\tau \approx \frac{\bar{R}_{gas}}{v_{gas}} \quad , \tag{34}$$

where v_{gas} is the hot gas velocity, and the rocket's mass flow retardation time

$$\Delta\tau \approx \frac{m_{ex}}{\dot{m}} \quad , \tag{35}$$

where $\dot{m}$ is the propellant mass flow rate crossing the throat.

4.6 MCM Single Object Model

Extrapolating the case of a rocket to a single object with no active interfaces (i.e., no expelled mass), we let an object's acceleration

$$a_m \approx 6 \left[\frac{\phi^3 \ell_p^{-1/2}}{\left(\bar{R}_1^{-1/2} - \bar{R}_2^{-1/2} \right)} \right]^{1/2} g_{\mathrm{N}} \quad , \tag{36}$$

where $\bar{R}_1$ is the radial factor in the direction of motion produced by an accelerated particulate matter of total mass m_i and $\bar{R}_2$ is the radial factor in the opposition direction of motion cause back the relaxation accelerated particulate matter of total mass m_i , i.e., the particulate matter in the object is accelerated in one direction and allowed to relax (i.e., the acceleration force is turned off) back across the object in the opposite direction. Noting that $\bar{R}_1$ should be smaller than $\bar{R}_2$, so that the acceleration is positive.

The phase factor then becomes

$$\phi = \phi_1 - \phi_2 \approx \left[1 + \left(\frac{v_1}{\bar{R}_1} \right) \left(\frac{m_i}{\dot{m}_1} \right) \right]^{-1} - \left[1 + \left(\frac{v_2}{\bar{R}_2} \right) \left(\frac{m_i}{\dot{m}_2} \right) \right]^{-1} \quad . \tag{37}$$

Or noting acceleration $a = dv/dt$

$$\phi = \phi_1 - \phi_2 \approx \left[1 + \left(\frac{a_1 dt_1}{\bar{R}_1}\right)\left(\frac{m_i}{\dot{m}_1}\right)\right]^{-1} - \left[1 + \left(\frac{a_2 dt_2}{\bar{R}_2}\right)\left(\frac{m_i}{\dot{m}_2}\right)\right]^{-1} \quad . \tag{38}$$

Noting that ϕ_1 should be smaller than ϕ_2 , so that the acceleration is positive. Also note that when $a_1 = a_2$, $\bar{R}_1 = \bar{R}_2$ from Eq.(14), $dt_1 = dt_2$, and $\dot{m}_1 = \dot{m}_2$. Whereby the phase factor and the object's acceleration is zero.

4.6 Gravity and Phase Factor

Equation (38) can be reduced by looking at the relaxation phase factor ϕ_2 when it is a result of gravity ($a \equiv 1$, $g \equiv 2$), where the phased factor is given as

$$\phi = \phi_a - \phi_g \approx \left[1 + \left(\frac{a_m}{\bar{R}_a}\right)\left(\frac{m}{\dot{m}_a}\right) dt\right]^{-1} - \left[1 + \left(\frac{g_{\rm N}}{R_m}\right)\left(\frac{m}{\dot{m}_g}\right) dt\right]^{-1} \quad ; \tag{39}$$

note that $\bar{R}_2 = R_m$ from Eq.(14) as $\partial\rho_m = \rho_m$, and the time dt for the two phases are the same as the two accelerations a_m and g_N are acting on the object at the same time.

Now at some time $dt = t_h$, $\phi_g = \phi_a$ and the object falls back to earth with a phase factor

$$-\phi_g \approx -\left[1 + g_{\rm N}\left(\frac{t_h}{R_m}\right)\left(\frac{m}{\dot{m}_g}\right) dt\right]^{-1} \tag{40}$$

Now using Eq.(36) with the object's acceleration $a_m = g_{\rm N}$ and with $\bar{R}_1 = \bar{R}_a = 0$ as the acceleration stops, where

$$g_N \approx 6\left(-\phi_g^3\sqrt{\frac{R_m}{\ell_p}}\right)^{1/2} g_{\rm N} \quad \Rightarrow 6\left(-\phi_g^3\sqrt{\frac{R_m}{\ell_p}}\right)^{1/2} \approx 1 \ . \tag{41}$$

or

$$-\phi_g \approx \left(\frac{1}{36}\sqrt{\frac{\ell_p}{R_m}}\right)^{1/3} \quad . \tag{42}$$

Combining Eqs. (40) and (42) yields the acceleration of gravity at time t_h as

$$g_{\rm N} \approx \left(\frac{R_m}{t_h}\right)\left(\frac{\dot{m}_g}{m}\right) \quad , \tag{43}$$

which when combined back with Eq.(41) yields

$$\phi_g \approx \frac{1}{2} \quad , \tag{44}$$

which when combined with Eq.(40) (ignoring the directional - sign) yields

$$\dot{m}_g \approx m\left(\frac{t_h}{R_m}\right) g_{\rm N} \quad . \tag{45}$$

Now noting that $\dot{m}_g = m/t_h$, Eq.(45) (ignoring the directional - sign) yields

$$t_h \approx \sqrt{\frac{R_m}{g_{\rm N}}} \quad , \tag{46}$$

where when combined back with Eq.(45) (ignoring the directional - sign) yields

$$\dot{m}_g \approx m\sqrt{\frac{g_{\mathrm{N}}}{R_m}} \ . \tag{47}$$

As a check, from similarity, at time $dt = t_h$ with $\phi_g = \phi_a$,

$$\dot{m}_a \approx m\sqrt{\frac{a_m}{\bar{R}_a}} = \frac{m}{t_h} \ \Rightarrow t_h \approx \sqrt{\frac{\bar{R}_a}{a_m}} \ , \tag{48}$$

which when combined with the acceleration phase factor of Eq. (39) yields $\phi_a \approx 1/2$.

Now combining Eqs. (47) and (48) with Eq.(39) the phase factor is reduced to

$$\phi = \phi_a - \phi_g \approx \left(1 + dt\sqrt{\frac{a_m}{\bar{R}_a}}\right)^{-1} - \left(1 + dt\sqrt{\frac{g_{\mathrm{N}}}{\bar{R}_m}}\right)^{-1} \ , \tag{49}$$

or rewriting Eq.(49) in the form of Eq.(38), the phase factor of an object with internal matter acceleration is given by

$$\phi = \phi_1 - \phi_2 \approx \left(1 + dt_1\sqrt{\frac{a_1}{\bar{R}_1}}\right)^{-1} - \left(1 + dt_2\sqrt{\frac{a_2}{\bar{R}_2}}\right)^{-1} \ , \tag{50}$$

which can be combined with Eq.(34) to give the net acceleration of a non-classical (no ejected mass) thrusting system.

5. CONCLUSIONS

As mentioned in the introduction, the MCM [2-4, 6 and 8] is a work in progress, where the visual and math models are based on the thin-shell mechanism in Chameleon Cosmology [5, 6] converted to an acceleration model and further converted to a more engineering series of equations. Chameleon Cosmology has had much work given toward its application to quantum phenomena as the Casimir Force (e.g., see [9] and its references) and is a Planck scale model. Susskind?s [1] entanglement approach to link Einstein Relativity to quantum theory can easily be applied to the thin-shell mechanism as the thin-shell is in an entanglement to the density both internal and external to an object. Whereby, Chameleon Cosmology provide another link from Einstein Relativity to quantum theory for fixing ER toward investigating and understanding new propulsion models. The MCM equations in both the more science form having coupling factors and the more engineering form not including coupling factors have been applied to the same solid rocket motor problem [3, 4, and 8] with the correct acceleration derived in each case. Beyond this no other acceleration device has been analyzed. The engineering acceleration Eq.(36) and the phase factor of Eq.(50) derived in this paper will require validation by testing. Changes to the equations in general would not be unexpected at this point, but the equations presented provide a good start toward modeling and understanding new propulsion concepts that reside outside the classical model. It is noted that the MCM of propulsion, i.e., Eq.(48), requires the propulsion systems to be non-linear, i.e, the forward and reverse accelerations are non-equal. This may require metamaterials, a material engineered to have a property that is not found in nature, to be developed to fully utilized the MCM model to the fullest extent possible.

This paper takes a new look at the Modified Chameleon Model by drawing in entanglement through the work of Leonard Susskind, who lays the foundation that entanglement is the bridge between Einstein Physics and Quantum Physics. A discussion entailing the entanglement connection is presented followed by an overview of the Modified Chameleon Model. Lastly, the acceleration equation in the Modified Chameleon Model is revisited and a general form of the acceleration phase factor is developed for use with non-classical propulsion concepts that have no mass ejection.

6. DISCUSSION

Woodward: You showed inertia as a sort of offset due to an asymmetry in the expanding universe. Yet the expansion is isotropic in the universe. How do you get such an asymmetry?

Robertson: I am not showing the matter of the universe, but the product of density and acceleration.

Woodward: But the acceleration is isotropic, too.

Robertson: If you are at the edge of the universe, looking back, you don't see anything beyond you.

Woodward: No, you just see more universe. It is all isotropic about every point.

Robertson: My assumption is that if you go beyond the edge of the universe, there is nothing.

Woodward: The edge of the universe isn't defined that way. There is always more beyond it.

Robertson: I take your point, but right or wrong, this is how I am visualizing things in this model.

Hathaway: Can you remind me where the Planck length comes into this chameleon model?

Robertson: It came from me. I inserted it based on an assumption relating a parameter to the mass of the earth.

Hathaway: Can you explain how you were getting a force on a density field, and what that means? I don't understand the concept.

Robertson: From our standpoint, the density field is the space drive.

Rodal: I would like to comment on your coupling parameters. Remember the old model of planetary motion involving epicycles? There was a lot of data to feed the model of epicycles, and every new discovery involved more epicycles. But the epicycle model was quite good. I see your coupling parameters as like the epicycles. The test of a theory is not whether it can be made to match data – it always can with an appropriate choice of parameters. The real test of a theory is whether it can make new predictions outside the known field of data, that can be verified in data. Does your theory make a prediction outside known data?

Robertson: I have not done that. I am just an engineer that assumes the model. But I leave it to physicists to determine whether the model is valid. I like this model because I think it can be used as a common model. And I just don't have the time to look in detail at these things.

Williams: You mentioned to George that you want input to improve your model. I am still having trouble with the density field. We have various pictures and concepts we use to organize our understanding. It would be good if you could tie this back to something that is understood. It's hard when you simultaneously introduce a new concept and start doing calculations with it.

Robertson: I suggest you go back to the original paper to understand the density field. I have added the assumption that the density field depends on accelerations within the density field. Somebody needs to go back to the original paper and put in my changes to alter their theory.

Williams: But I just want to know what the concept is. What is a density field? Since it is the basis of your talk, can you offer a picture?

Robertson: I don't really understand the math. I would rely on people like you to help me understand the math. I am really asking for your help. But I have this simple picture of the density depending on acceleration. Maybe density is the wrong term? But I am taking it out of the chameleon cosmology. We can call it whatever you want.

Woodward: In an earlier slide, you were showing acceleration with no mass ejection, just density fields. I am curious how you get that and treat that?

Robertson: What you are operating on is the thin shell. The acceleration comes from that.

Woodward: That sounds like making your car move by pushing on the dashboard.

Robertson: I have claimed in the past you can do that. But I really want to show your theory and others can be cast in these terms.

Woodward: My theory is already within existing physics, I just have a new effect. Why would I want to introduce density fields and all these other parameters when I can simply use existing physics to describe my theory?

Robertson: It might not be so useful for your theory, but wouldn't it be a useful common framework for evaluating lesser-known theories than yours.

Woodward: Only theories that involve your density field.

Robertson: My impression from attending these conferences for years is that all these theories are talking about the same thing. My approach allows a way to express these in a common framework.

Woodward: What you have done is taken an outside cosmological model with questionable assumptions and suggested it as a framework that all models should be pushed into.

Robertson: I'm not sure this is the right model, we just need a common model so that funders can understand what we're doing. If this is not the right model, I challenge others to come up with a better one.

Williams: You would not want to use this to capture things like the Mach effect that purport to be within general relativity. It could only be for new physics.

Robertson: This is the sort of derivation that could get into an aerospace book, but the Mach effect could not. I have not seen anything today that you could not put into the thin-shell chameleon model. The equations may change but it would fit.

Laursen: Are you familiar with Kane's approach at Stanford? He developed a framework in which any dynamics problem could be formulated. It sounds similar.

Robertson: If you fit your parameters into this model, it will help improve your experiment, because the free parameter are experimentally determined. So I am not saying put your theory in this model, put your experiment in this model.

Meholic: Have you seen Richard Obussey's PhD thesis on the Alcubierre metric? He had a picture of expanding dimensions to propel an object. This sounds similar.

Robertson: The equations may change but the model stays the same.

Williams: In terms of parameterizing theories, if you have enough free parameters you can fit anything. If you make enough assumptions to get to an answer, why not just assume the answer and save a step?

Robertson: The parameters are not from the theory but from the experiment.

Williams: That's fine but if the space of parameterization is too big... How many parameters do you have?

Robertson: I couldn't answer that, but not too many. Perhaps 4. Coupling factor to internal field, coupling factor to external field, ... phase factor, radial factor... but it should come out of experiment. If you can't put your experiment derived from your theory into this model, then it is suspect.

Woodward: I don't understand how experiments can be suspect. If an experiment is done well, it can be taken as factual. Whereas, models can be suspect.

Robertson: Your experiment fits well in this model. Your experiment changes the density field of the PZT.

Woodward: I'm not changing the density field of the PZT. I am applying a voltage to a PZT stack, producing electro-mechanical motion of known physical elements. Your density fields are not known physical elements. Nobody has ever measured a density field. If it's a calculation of an assumption it does not have the same status as an observed fact.

Robertson: My main assumption is we need a common base to give to people who don't understand theoretical physics.

Woodward: That's a worthy goal. Why not try to do it without density fields and chameleon stuff?

Robertson: Nothing else has worked.

Woodward: That's not so. There is a parameterization of gravitational theories developed by Ken Nordtvedt and Cliff Will back around 1970. It is still in common use: Parameterized Post-Newtonian Theory. You could find the appropriate terms of those equations and map them to real effects. They have already done for gravity what you would like to do, without needing to introduce any new fields.

Robertson: I am presenting a common model for your evaluation but you must decide its utility for yourself.

Broyles: Do you have a simple, step-by-step block diagram to walk people into this model? Let's say I have a black box that produces some effect. How do I parameterize what I measure with it in your model? Your equations don't help us in that regard. You would need the detailed steps to present to an organization you hope would fund this.

Robertson: I will have to think about putting something like that together.

Turner: I work at NASA and have some experience with the issues of explaining proposals. I agree with Tony's assertion there is a need to compare alternative approaches at a level that could be easily understood by a wide range of people. Whether it's a common model or impartial review by competent scientists, that would be good.

Tajmar: One point is that PPN is the valid way to depart from general relativity, which is the accepted theory. A second point is that, in terms of propulsion, a proposal should give two numbers: power to thrust ratio and specific impulse. Those are the parameters to use to compare approaches. In general, these figures of merit already exist from an engineering perspective for thrusters, and from a theory perspective for gravity. There is nothing else.

Bushnell: There are probably more theories than theorists. I have tried to work through a lot of these exotic proposals. I have talked to the best scientists at Harvard, Princeton, Michigan, whatever. And they tell me the woods are full of this stuff. There aren't enough hours in a year to look through it all, and it probably wouldn't be of value. There is something here broken between conventional physics and this field, and conventional physics faces many big questions. So how do we parse which of any to go forward with? But conventional physicists won't touch this stuff. If this meeting does nothing, we should get the theory squared away. There are lots of issues in the experiments. But with unverified assumptions, how can you possibly believe anything?

Broyles: You look for specific, repeatable, verifiable experiments. The basics.

Meholic: It's also important to have people who understand the data. In the military world, they want to know what capability is promised. There is no clear mission for this in the NASA realm, but possibly in the military realm.

Fearn: As a theorist, I had to look up the meaning of specific impulse that Martin mentioned. It is a ratio of thrust to mass ejection. But our experiments don't eject anything. Why can't we have thrust over power in?

Meholic: Yes, specific impulse is meaningless in this application. It is related to expelled matter. But in the electrical propulsion world, they use just what you say. I have always defined specific impulse as the time to burn one unit mass of propellant to produce one unit of thrust. The higher the number, the more efficient.

Cole: The electric propulsion thrust to power ratio is sometimes called alpha. But the key parameter is how much energy the power supply can produce before you "run out of gas".

Broyles: It took decades to understand the physics of flight after the Wright brothers proved it experimentally. So I am not concerned if we are seeing new physical effects without a clear theory.

Tajmar: Or superconductivity. We use it all the time and haven't got a clue how it works!

References

[1] Susskind, Leonard, *Copenhagen vs Everett, Teleportation, and ER=EPR,* arXiv:1604.02589 v2 [hepth], 23 Apr. 2016.

[2] Robertson, Glen A., *Engineering Dynamics of a Scalar Universe, Part I: Theory & Static Density Models,* Lecture Series paper Proceedings of Space, Propulsion & Energy Sciences International Forum, edited by Glen A. Robertson, AIP Conference Proceedings, CP1103, Melville, New York, (2009).

[3] Robertson, Glen A., *Engineering Dynamics of a Scalar Universe, Part II: Time-Varying Density Model & Propulsion,* Lecture Series paper in Proceedings of Space, Propulsion & Energy Sciences International Forum (SPESIF-09), edited by Glen A. Robertson, AIP Conference Proceedings, CP1103, Melville, New York, (2009).

[4] Robertson, Glen A., *The Chameleon Solid Rocket Propulsion Model,* in these proceedings of Space, Propulsion & Energy Sciences International Forum (SPESIF-10), edited by Glen A. Robertson, AIP Conference Proceedings, Melville, New York, (2009).

[5] Khoury, Justin and Weltman, Amanda, *Chameleon Cosmology,* arXiv: 0309411v2 [astro-ph], 1 Dec. 2003 and *Chameleon Fields: Awaiting Surprises for Tests of Gravity in Space* arXiv: 0309300v3 [astro-ph], 9 Sept. 2004.

[6] Robertson Glen A. and Pinheiro, Mario J., *Vortex Formation in the Wake of Dark Matter Propulsion,* Physics Procedia, **20**, Elsevier Science, 2011.
[7] Lienard-Wiechert potentials, Wikipedia, 6 Sept. 2016.
[8] Robertson, Glen A., *Propulsion Physics under the Changing Density Field Model,* JANNAF, 2012 and presented at the Advanced Space Propulsion Workshop 2012.
[9] Almasi, A., Brax, Philippe, Iannuzzi, D. and Sedmik, R. I. P., *Force sensor for chameleon and Casimir force experiments with parallel-plate configuration,* arXiv:1505.01763v1 [physics.ins-det], 7 May 2015.

THE GEM THEORY OF ENERGY AND MOMENTUM EXCHANGE WITH SPACETIME, AND FORCES OBSERVED IN THE EAGLEWORKS Q-V THRUSTER

John E. Brandenburg[1]
Morningstar Applied Physics, LLC

The basic premises and results of the GEMS (Gravity-EM Super) Unification theory are presented as well as its application to EM or "Q-V" thruster results. The GEMS theory began as an attempt to unify the long-range forces of nature, gravity and EM. But it unexpectedly also yields the observed masses, spins and charges of the πmesons, which carry the Strong Force; as well as the W and Z boson of the Weak Force, thus unifying the four forces of nature in one theory for the first time. A new spin-zero, neutral particle, is predicted by the GEMS theory, of rest-mass 22 MeV. The GEMS theory is based on two postulates:

1. that gravity fields exist as arrays of $E \times B$ drift cells, or Poynting vectors
2. that gravity and EM forces separated in a correlated way with the separation of protons and electrons from the Planck scale after the deployment of a Kaluza-Klein compact 5^{th} dimension.

The theory, to first order, assumes transfer of particle momentum to a rigid spacetime structure from the $E \times B$ fields of the array. Likewise, in modeling the EM thruster, the reaction to the action of the thrust is considered, to first approximation, to be transferred to the nearby large masses via a rigid spacetime. A linear theory is found, approximately yielding the observed thrust to power relation observed experimentally in the Q-V thruster experiment. At higher powers, a nonlinear effect is seen theoretically, which yields the approximate thrust to power relation seen in higher power (kW) experiments of 0.2 N/kW. In the nonlinear limit, the thrust goes as the applied EM power squared, so large levels of thrust can be expected theoretically. A simple calculation shows that rapid trips to Mars can be effected by using this EM drive, powered by large, megawatt-scale solar panels.

1. INTRODUCTION

The Q-V Thruster [1] appears to create a force due to an interaction between applied RF power and the vacuum itself, within a specially shaped container. This result, confirming experimental results obtained elsewhere, may represent a breakthrough in space propulsion. A conceptual model has been proposed based on an interaction between the RF and virtual particles whose presence is required by quantum theory. This device was built to try to reproduce the results of experiments by Shawyer [2], where microwaves of much higher power were directed into a closed asymmetric vessel and generated thrust at a level of 0.1 N/kW. This result has been reproduced in the Q-V Thruster experiment, albeit at much lower power levels and much lower thrust per unit power (Figure 1). The thrust detected by the device is a reaction force to momentum that is transferred to the virtual particles. Two problems are present in the Q-V results: one is the global conservation of momentum, and the other is the problem of the divergence-free nature of the vacuum EM field that would seem to preclude transfer of momentum to the virtual particles.

However both of these problems can be solved by considering that the Q-V thruster and other similar devices are exchanging momentum directly between EM fields and space-time itself, which to first order acts like a rigid background. This effect occurs in the GEMS theory because, in that theory, the fabric of space-time itself is electromagnetic and EM fields can interfere constructively and destructively to change

[1] jeBrandenburg@madisoncollege.edu

the structure of space-time. In this brief manuscript, the basic GEM theory will be briefly presented and its application to the Q-V thruster, to explain the origin of the measured forces with their approximate magnitude and scaling with applied power.

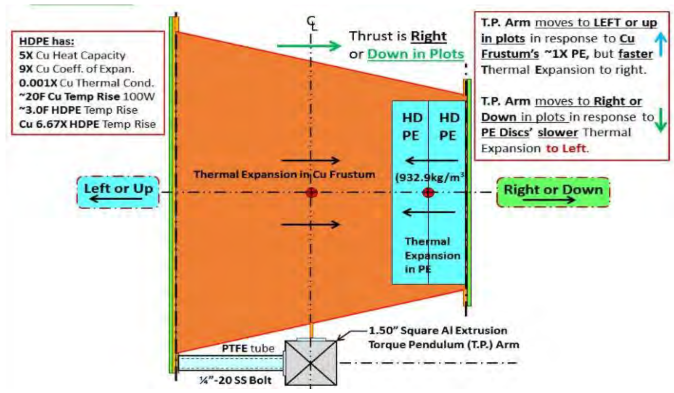

FIG. 1: The Frustum of the Q-V Thruster

Based on the positive result of the Q-V thruster at low power, and the support for this result seen in the GEM theory, plus the great promise of this possible new means of space propulsion, a simple calculation will also be performed to see how long a 50-metric-ton, 1 megawatt solar-powered craft will take to go from Earth to Mars.

2. MOMENTUM AND ENERGY BETWEEN VACUUM EM FIELDS AND SPACETIME

In the standard theory of General Relativity the EM energy density

$$u = \frac{1}{2}\left(\epsilon_0 E^2 + \frac{B^2}{\mu_0}\right) \tag{1}$$

Expressing the EM energy density in terms of a mass density:

$$\rho = \frac{u}{c^2}$$
$$\nabla \cdot \mathbf{g} = -4\pi G\rho \tag{2}$$

In a plasma, the charged particles of the plasma would move to create currents to generate a $J \times B$ force to counteract this gravity force. But in a vacuum this is not possible. What then counteracts the gravity pull on the magnetic lines of force? We can answer this by going to the covariant form of the problem in general relativity. By starting with the problem of a EM field in a vacuum we can write

$$R_{\mu\nu} - \frac{1}{2}g_{\mu\nu}R = \frac{8\pi G}{c^4}T^{EM}_{\mu\nu} \tag{3}$$

where $T^{EM}_{\mu\nu}$ is the EM Stress tensor.

In covariant formalism we take the divergence of both sides and obtain, because the divergence the left side must vanish mathematically due to the Bianchi identities,

$$0 = \frac{8\pi G}{c^4}T^{\mathrm{EM}\nu}_{\mu;\gamma} \tag{4}$$

Using covariant formalism, we have in expanded form

$$0 = T^{\mathrm{EM}\nu}_{\mu,\gamma} + \Gamma^{\nu}_{\beta\gamma}T^{\mathrm{EM}\beta}_{\mu} - \Gamma^{\beta}_{\mu\gamma}T^{\mathrm{EM}\nu}_{\beta} \tag{5}$$

where $\Gamma^{\eta}_{\mu\nu}$ is the Christoffel symbol. The Christoffel symbol provides the part of the divergence that is due to gradients in the metric of space time, that is, gravity. Therefore, we obtain

$$T^{\mathrm{EM}\nu}_{\mu,\gamma} = -\Gamma^{\nu}_{\beta\gamma}T^{\mathrm{EM}\beta}_{\mu} + \Gamma^{\beta}_{\mu\gamma}T^{\mathrm{EM}\nu}_{\beta} \tag{6}$$

This can be interpreted physically as spacetime, to first approximation, behaving as a rigid background. In the Newtonian limit for time constant gravity fields and using 3 vectors this becomes

$$-\frac{1}{c^2}\frac{\partial S}{\partial t} + \nabla \cdot T = \rho \tag{7}$$

where S is the Poynting vector. Careful summing of effects leads to the relation that $\rho = 2u/c^2$, or twice the expected mass density. It is for this reason that the angular deflection of starlight by the Sun is twice what would be expected from Newtonian theory.

Because we have a vacuum EM field with no charge,

$$\nabla \cdot T = 0 \tag{8}$$

Therefore we must have, to conserve momentum with $\rho = 2u/c^2$

$$-\frac{1}{2u}\frac{\partial S}{\partial t} = \mathbf{g} \tag{9}$$

This is the fundamental relation of the GEM theory, equating gravity to an $E \times B$ flow.

3. GEM THEORY AND THE VACUUM BERNOULLI EFFECT

The Poynting vector is a fundamental quantity in EM theory and transports momentum and energy in EM fields. For example: a beam of light travels through space-time as a transverse electromagnetic wave expressed as the Poynting vector $\mathbf{S}$ as:

$$S = \frac{1}{\mu} E \times B = E \times H \tag{10}$$

This operation propels fundamental information about the elementary perturbation of space-time across the universe. The E and B fields expressed above are shown through the fundamental Poynting vector equation to be coupled at the point where the Poynting vector exists and couples to particles and space-time (Figure 2).

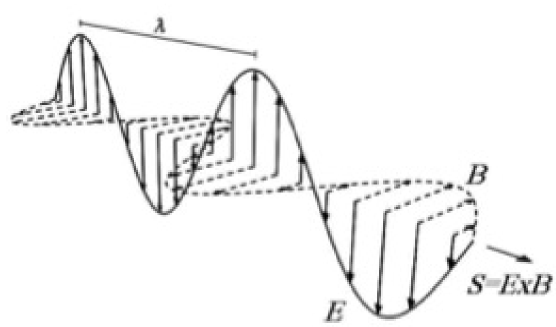

FIG. 2: Components of a transverse light wave noting the propagation due to the Poynting vector

The Poynting fields around the "Morningstar Energy Box" [3] device can be visualized as seen in Figure 3 and are in the form of generating an electromagnetic vortex. Following our fluid concept of space-time, we can imagine that since the fluid space-time is stationary far away from the center of the Poynting vortex, a velocity gradient must exist. Such velocity gradients lead to turbulence when they exceed a small threshold, as is seen in everyday fluid flows. Added to this effect is the nonlocal nature of the wave functions of the particles, which sample the Poynting field at many locations at once, and thus do not see the vortex as a coherent entity but as a collection of interactions. So we can assume that the quantum mechanical matter waves will experience the Poynting vortex as a source of turbulence.

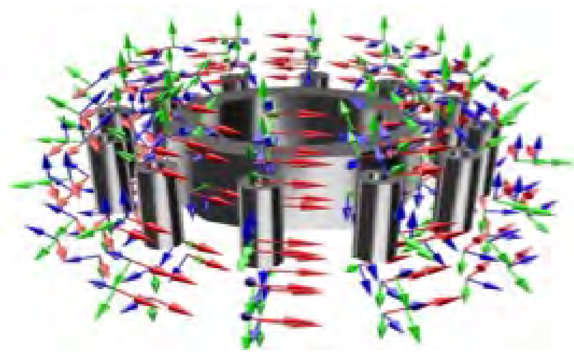

FIG. 3: The electromagnetic fields surrounding a rotating "energy box" array of magnets. Magnetic fields are shown in blue, electric fields are shown in green, and the Poynting vector is shown in red. Note that the Poynting vectors form a vortex pattern

This intersection of fields is expressed in the Murad-Brandenburg equation, a Poynting conservation equation, which treats the Poynting vector field as a wave field, and away from its sources can be written:

$$\mu_0 \left[\frac{1}{c^2} \frac{\partial^2 \mathbf{S}}{\partial t^2} - \nabla^2 \mathbf{S} \right] = 0 \tag{11}$$

When near field source terms are included we have:

$$\left[\frac{1}{c^2} \frac{\partial^2 \mathbf{S}}{\partial t^2} - \nabla^2 \mathbf{S} \right] = \nabla \cdot \left[\epsilon_0 EE + \frac{1}{\mu_0} BB \right] + \nabla \times \nabla \times \mathbf{S} \tag{12}$$

where it can be seen the vorticity of the Poynting vector, $\nabla \times \mathbf{S}$, is prominent.

Away from sources, Poynting fields can be considered as a chaotic sum of waves, moving through each other. The Murad-Brandenburg Equation is a result of standard EM theory, but we can move beyond this theory to extend this with the GEM (Gravity Electro-Magnetic) theory.

The GEM theory [2] is a combination of the Sakharov theory of gravity as consisting of radiation pressure (Figure 4). That is, gravity fields are an array of $E \times B$ drifts arising from the quantum ZPF (Zero Point Fluctuation), and from the Kaluza-Klein theory of EM gravity unification through a hidden 5th dimension.

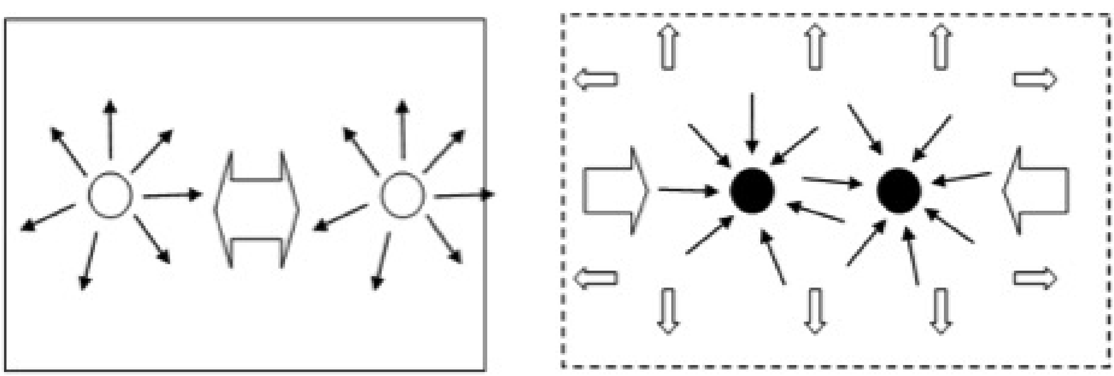

(a) Two bright objects in dark box repel each other

(b) Two dark objects in a bright box attract each other

FIG. 4: The Sakharov model of gravity

It provides the basic mathematical results:

$$\ln \left(\frac{m_0}{m_p} \right) \equiv -(\alpha^{-1/2} + 1) \ln \sigma \tag{13}$$

$$\ln\left(\frac{r_0}{r_p}\right) \equiv \sigma \tag{14}$$

where r_0 is the hidden dimension size, $m_0 = [m_p m_e]^{1/2}$, where m_p and me are the proton and electron masses respectively, $r_p = [G\hbar/c^3]^{1/2}$ is the Planck length, m_P is the Planck mass, and the square root of the mass ratio $(m_p/m_e)^{1/2} = \sigma = 42.8503$ is a parameter relating the electron and proton masses. This model has recently been refined to give corrected behavior near the Planck scale where all the quantities m_0/m_P, r_0/r_P, σ, and $\sigma \to 1$ leading to the corrected forms of Eq. 4a,b:

$$\ln\left(\frac{m_0}{m_p}\right) \equiv -(\alpha^{-1/2} + \alpha + 1)\ln\sigma \tag{15}$$

$$\ln\left(\frac{r_0}{r_p}\right) \equiv \sigma - \frac{1}{\sigma^2} \tag{16}$$

The expression can be inverted to yield the formula for the Newton gravitation constant:

$$G = \left(\frac{e^2}{m_p m_e}\right)\alpha \exp\left(-2\left[\sigma - \frac{1}{\sigma^2}\right]\right) = 6.6752 \times 10^{-8} \text{ dyne } cm^2 g^{-2} \tag{17}$$

Which is within 2 parts per ten thousand of the measured value for G. And we find the proton mass, m_p, from the vacuum:

$$m_p = \sigma^{-(\alpha^{-1/2}+\alpha)} = 1.667 \times 10^{-24}\ g \tag{18}$$

This result is within a 4 parts per thousand of the measured proton mass of 1.673×10^{-24} g. This demonstrates the importance and accuracy of the GEM theory in its developed form.

Recently, the GEM theory was able to predict the masses of the charged pion, W boson, and Higgs boson to high accuracy using the concept of quantum Mie scattering, or action integral, off of the structural resonances [2], of the classical EM radii, r_c. In a new analysis, which we briefly summarize here, this concept is generalized to include virtual paths of reduced probability of order α or $1/\sigma$:

$$\frac{E\ell}{c} = Nh \tag{19}$$

$$\ell = 2\pi r_c(1 + \alpha M) \tag{20}$$

where E is the particle rest energy, c, is the speed of light h is Planck?s constant, and ℓ is the path length. The previous derived masses were all for the case $N = 1$ $M = 0$. The most probable path is thus just simple circumference around a particle classical radii, but with a reduced probability, the path may divert to orbit the particle M times, this giving an effectively longer path. For the reduced probability cases of $M = 5$ and even $N = 5$, reflecting the dimensionality 5 of the GEM theory, we have the following particle masses, including a particle exclusively predicted by the GEM, the $M*$, (Morningstar) particle never before observed (see Table 1):

TABLE I: **Particle masses predicted by the GEM theory and observed masses including the new predicted $M*$ particle**

Particle	**Predicted Mass-Energy**	**Observed Mass-Energy**	**Error**
Neutral Pion	135.12 MeV	134.98 MeV	0.1 %
Z Boson	91.03 GeV	91.19 GeV	0.2 %
Muon	105.63 MeV	105.66 MeV	0.02 %
M* Particle	21.9 MeV	****	****

Returning to the problem at hand, how to explain the Q-V thruster results, we begin by looking at the Poynting vector:

$$S = \frac{1}{\mu} E \times B = E \times H \tag{21}$$

$$S = \frac{1}{\mu_0} E \times B \tag{22}$$

Now the $E \times B$ drift will move all charged particles at the same speed and can be written in terms of S. For a vacuum we have, with u_0 as a steady state magnetic field energy density, the $E \times B$ drift velocity:

$$V = \frac{E \times B}{B^2} = \frac{S\mu_0}{B^2} = \frac{S}{2\mu_0} \tag{23}$$

This $E \times B$ velocity depends only on the ratio E/B and not on the mass of the particles affected or their charge. As a practical matter, the particles only assume this $E \times B$ motion after a cyclotron period, but we assume they are all "up to speed". We can adopt the physical model that E/B is the speed of the quantum vacuum since it obeys the equivalence principle and effects all masses the same. This means we can assume all the quantum particles appearing and disappearing from Heisenberg Uncertainty move at this rate. We can keep the magnetic field constant and create a gradient in the E field by tilting the plates relative to each other while keeping the E field everywhere normal to the B field as seen in Figure 5. This model has been tested and verified with a particle simulation code for the curvature E and B field configuration and the results are shown in Figure 6.

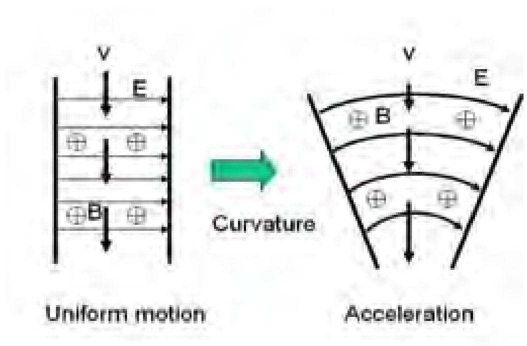

FIG. 5: Motion of charged particles in cross E and B fields, with E vector formed between charged plates and B vector coming out of the paper. In the second case using tilted plates the charged particles accelerate. Velocity for all particles is the same regardless of charge or mass.

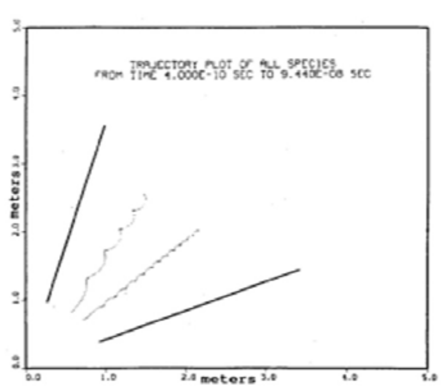

FIG. 6: A Particle code simulation of the $E \times B$ drift gravity model showing an electron and a 10x electron mass positron

When this model of EM gravity is combined with Poynting's theorem, the Kaluza-Klein action falls out as a conserved quantity and can be called the Vacuum Bernoulli Equation (VBE) [4]. A brief version of it derivation shown below. We assume B^2 is constant and vary E in time, then the charged particles will all accelerate at the same rate:

$$\dot{V} = \frac{\dot{E} \times B}{B^2} = \frac{\dot{S}}{2u} \tag{24}$$

We can also write form Newtonian gravity theory with gravity vector field g, where G is Newton's gravity constant

$$\nabla \cdot \mathbf{g} = -4\pi G\rho \tag{25}$$

where we assume $E = mc^2$ and so an EM energy density can form a mass density as a source for a gravity field. This density ρ becomes:

$$\begin{aligned} \rho &= \frac{u}{c^2} \\ u &= \frac{1}{2}\left(\epsilon_0 E^2 + \frac{B^2}{\mu_0}\right) \end{aligned} \tag{26}$$

This means when EM energy flows into a spherical region from all sides, gravity vectors pointing into the region increase in time so that, for the case of a spherically symmetric region, we have:

$$\nabla \cdot \dot{\mathbf{g}} = -4\pi G\dot{\rho} = -\frac{4\pi G}{c^2}\nabla \cdot \mathbf{S} \tag{27}$$

where both vectors can generate an additional vortex-like field $F = \nabla \times A$ that include curls of a vector potential.

For the simplest case of no "curl fields" we have,

$$\begin{aligned} \frac{\dot{\mathbf{g}}}{4\pi G} &= \frac{\mathbf{S}}{c^2} \\ \mathbf{g} \cdot \frac{\dot{\mathbf{g}}}{4\pi G} &= \mathbf{S} \cdot \frac{\dot{\mathbf{S}}}{2u_0 c^2} \\ \frac{g^2}{4\pi G} &= \frac{S^2}{2u_0 c^2} \\ \frac{g^2}{2\pi G} - \frac{S^2}{u_0 c^2} &= 0 \end{aligned} \tag{28}$$

This is the VBE expression we get from the Kaluza-Klein action in the Newtonian limit, with $\langle E \cdot B \rangle = 0$ in the vacuum, that is, a vacuum made of EM waves.

$$\text{Kaluza Klein Action } = \frac{R}{16\pi G} - \frac{F^{\mu\nu}F_{\mu\nu}}{4} \rightarrow \frac{g^2}{2\pi G} - \frac{S^2}{u_0 c^2} = 0 \tag{29}$$

Therefore, the same $E \times B$ drift theory of gravity, EM fields directly effecting spacetime rather than merely serving as a mass density source term, is also the basis for the coupled equations of General Relativity and Electromagnetism [5].

The Vacuum Bernoulli Equations says that gravity fields are associated with a net Poynting Flow in the vacuum. Therefore, we can change the local gravity field by changing the Poynting fields.

Now, we perturb the Poynting flow with a new an artificial Poynting flow, in the case of the Q-V thruster, created by the applied RF field. This perturbing flow is at right angles to the main Poynting flow and assumed of equal magnitude and is due to photon-photon scattering [6], a commonly observed phenomena, so the two flows can have a constructive interference term $dS \cdot S_\perp \approx |dS||S|$.

$$
\begin{aligned}
\frac{d\mathbf{g}\cdot\mathbf{g}}{2\pi G} &= \frac{d\mathbf{S}\cdot\mathbf{S}}{uc^2} \\
\frac{|dg|}{|g|}\frac{g^2}{2\pi G} &= \frac{d\mathbf{S}\cdot\mathbf{S}_\perp}{|S^2|}\frac{S^2}{u_0c^2} = \frac{|dS|}{|S|}\frac{S^2}{u_0c^2} \\
\frac{|dg|}{|g|} &\cong \frac{|dS|}{|S|}
\end{aligned} \tag{30}
$$

Now since we can assume each Poynting or $E \times B$ flow S is a "flow of the vacuum" and all it contains, and that it is a continuous flow field, we can perturb the flow fields as though they are of comparable underlying energy. We will assume the flow rate of the vacuum at the Earth's surface to be the escape velocity $V_{\rm esc} = 1.1 \times 10^4$m/sec, since that is the velocity of a particle falling from outer space. We will call this the assumption that "all vacuums are weightless", which is an extension of the equivalence principle to the vacuum itself, and says we can combine their $E \times B$ flows.

4. THE NEWTONIAN GRAVITY POTENTIAL

We have then a gravity potential in terms of an $E \times B$ drift model of gravity that is valid for both DC and oscillating E fields, where charged particles are accelerated into the strongest part of the perturbing E field. How then does the Newtonian gravity potential between charged particles come about? We begin with the expression for a gravity potential in terms of E and B fields in the vacuum, where V_D is the particle drift velocity in the crossed E and B fields. Here we use esu units for electromagnetic quantities:

$$
\begin{aligned}
\langle g_{00}\rangle &= -1 - \frac{2\phi}{c^2} = \frac{E^2}{E^2 - B^2} \\
E^2 &= E_0^2 \text{ or } E_1^2 \\
-1 - \frac{2\phi}{c^2} &= -1 - \frac{E_1^2}{B^2} \\
\frac{\partial V_D}{\partial t} &= V_D\frac{\partial V_D}{\partial x} = \frac{Ec^2}{B^2}\frac{\partial E}{\partial x}
\end{aligned} \tag{31}
$$

We now consider the mechanisms of how gravity arises from our $E \times B$ drift model and the interaction of charged particles with the quantum vacuum. We obtain the Newtonian potential as the perturbing E electric energy density divided by the powerful ZPF magnetic field:

$$
\phi = \frac{1}{2}\frac{\langle E_1^2\rangle}{B_0^2}c^2 \tag{32}
$$

Note that this is expression for the gravity potential.

We can now proceed approximately with the derivation of the Newtonian potential from the GEM model of gravity potential shown in Figure 5 as an array of $E \times B$ drifts. We can consider the bending of light by gravity to be photon-photon scattering (Figure 7).

According to the Standard Model all massive particles, electrons and quarks making up ordinary matter, are charged point particles. These charged particles all move freely in the presence of the ZPF fields of the quantum vacuum. It has been pointed out by Puthoff [7], that under the Standard Model even the quarks move freely because of the phenomenon of "Ultraviolet Freedom" and hence their interaction with the quantum vacuum can be considered in isolation. All these free charged particles are in constant motion, "Zitterbewegung", or quantum jitter, because of their accelerated motion must radiate as discussed by Puthoff. The radiation field is irregular, but statistically isotropic. The radiation E field is normal to the radiation direction coming from the particle and decays as $1/r$, where r is the distance from the particle. This radiation field constructively interferes with a portion of the ZPF that is isotropic and uniform, to surround the particle, resulting in an electric field energy density. It is this electric energy density that forms the numerator of the fraction. The magnetic energy density of the ZPF is the denominator of the fraction. Using our expressions for the classical radius of a charged particle, the Planck length and writing G as $G = c^4/(T_o r_p^2)$, we can write, using $B_o^2 = T_o$

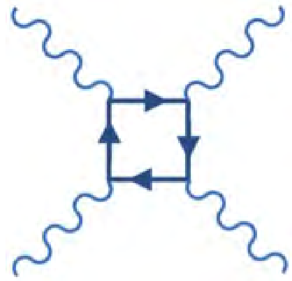

FIG. 7: A Feynman diagram of photon-photon scattering, a well known process in the quantum vacuum.

$$\frac{1}{2}\frac{E_1^2}{B_0^2}c^2 = \frac{Gr_p^2}{2c^4}E_1^2 \tag{33}$$

The particle radiating because of its motion in the ZPF creates an electric field stress on the surface of a sphere of radius r, centered on the particle, and is proportional to the radiated power of the particle, where a is the acceleration of the particle.

$$4\pi r^2 \frac{E_1^2}{8\pi}c = \frac{2}{3}\frac{e^2}{c^3}a^2 \tag{34}$$

This expression is limited to $a < c^2/r_c$, where $r_c = e^2/mc^2$ is the particle classical radius in esu units. We limit the acceleration to the value $a = c^2/r_c$, and obtain, upon simplification:

$$E_r^2 = \frac{4}{3}E_c^2\frac{r_c^2}{r^2} \tag{35}$$

Where $E_c = e/r_c^2$, the electric field at the classical particle surface. We then write the mean constructive interference term between the particle radiation and the background ZPF fields where $E_o = q_p/r_p^2$ takes into account the geometrical variations and time fluctuations, and obtain approximately:

$$\langle E_r \sin(2\pi\nu t)\rangle \sim \frac{1}{2\pi}E_r \tag{36}$$

where $\nu = 1$. From this expression we then obtain:

$$\langle E_r E_0\rangle \cong \frac{1}{2\pi}\left(\frac{4}{3}\right)^{1/2} E_c\frac{r_c}{r}\frac{q_p}{r_p^2} \tag{37}$$

Gravity fields arise in the GEM theory from the constructive interference of the action of the ZPF:

$$\frac{1}{2}\frac{\langle E_r E_0\rangle}{B_0^2}c^2 \cong \frac{c^2}{2\pi}\left(\frac{4}{3}\right)^{1/2}\frac{e}{rr_c}\frac{q_p}{r_p^2}\frac{Gr_p^2}{c^4} \tag{38}$$

Using the expression for the Planck charge $q_p = e\alpha{-}1/2$, where α is the fine structure constant, we simplify Eq. (29) and obtain:

$$\frac{1}{2}\frac{\langle E_r E_0\rangle}{B_0^2}c^2 \cong \frac{\alpha^{-1/2}}{4\pi}\left(\frac{4}{3}\right)^{1/2}\frac{Gm}{r}$$

$$\frac{\alpha^{-1/2}}{4\pi}\left(\frac{4}{3}\right)^{1/2} = 1.07$$

$$\frac{1}{2}\frac{E_1^2}{B_0^2} \cong \frac{Gm}{r} \tag{39}$$

Thus, the Newtonian gravity potential can be recovered, to within factors close to one, from a physical model of $E \times B$ drifts of particles in a combination of the fluctuating fields of the particles radiation in response to the ZPF, and fibrous magnetic flux and fluctuating E fields of the ZPF. The presence of the charged particle breaks the symmetry of the spacetime and causes a $1/r$ electric field energy density to form. The gravity force is thus not a steady force on an individual particle but an average acceleration in this model. The weakness of gravity, caused by the smallness of G, is due to the strong nature of the ZPF magnetic fields. The $1/r$ dependence of the potential stems from the $1/r$ dependence of the radiation fields of the jittering particle, constructively interfering with the uniform background of the ZPF electric field fluctuations. These effects are, of course very small. However, the radiation field interference terms are independent for each particle and can add, causing the gravity force to combine in large ensembles of particles in a way that the pure EM force cannot. The gravity force can thus be said to be the result of the statistical mechanics of the fields of charged particles interacting with the vacuum around them, and combining in large ensembles.

Let us assume in the frustum that the EM waves follow the pattern of the simulations and create a concentration of field near the large end of the frustum. We will assume here, as in our derivation from the principle of a massless vacuum, that the magnetic field need not be that of the EM waves but is a magnetic field from the ZPF.

$$\phi = \frac{1}{2}\frac{\langle E_1^2 \rangle}{B_0^2} c^2 \tag{40}$$

Using the model of the gravity potential as created by a gradient of E^2 in a uniform background B field we find that the inclusion of plastic disks in the small end of the frustum suppresses the E field in that region. Thus the region near the wide end of the frustum has much more E field than the small end even without plastic dielectric disks, but that the inclusion of the disks in the small end will amplify the E^2 gradient. In the GEM theory this will create a curvature of space-time creating a gravity field pulling on the large end of the frustum and thus pulling the frustum towards the small end (Figure 8).

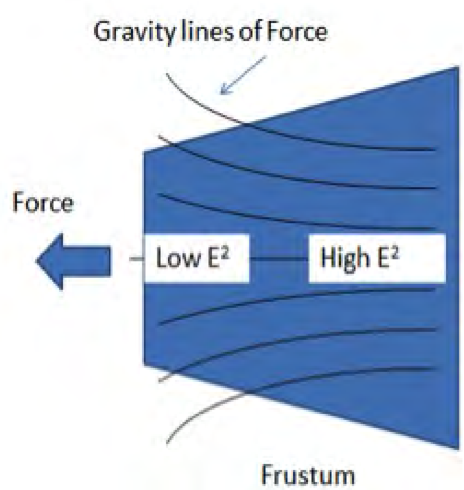

FIG. 8: The gradient of E^2 caused by the standing EM fields in the frustum create, via the GEM theory, a curved metric and thus a net gravity force on the frustrum.

We can estimate the magnitude of the force via the GEM theory by using the vaccum Bernoulli equation.

5. ACTION-REACTION AND MOMENTUM CONSERVATION IN THE GEM THEORY OF THE Q-V THRUSTER

In a normal plasma thruster, real particles are accelerated by EM fields to depart the thruster and this gives a reaction force in agreement with Newton's 3^{rd} law of motion. The reaction force accelerates the thruster, and the spacecraft it is attached to will give an equal and opposite momentum to the exhaust. If we did not use plasma but merely radiated microwaves out of an open metal vessel instead, this would also give a reaction force, albeit a small one per unit of power expended, because the EM waves carry momentum via the Poynting vector. However, by standard EM theory, if the metallic vessel is closed, the EM waves cannot escape and instead bounce around in the vessel, exchanging no net momentum with the walls, thus producing no net Poynting flow and thus no thrust. However, standard EM theory must be modified to include GEM effects, the fact that spacetime is electromagnetic, and thus can carry momentum itself. In the case of the frustum, the intense, and asymmetrically distributed, EM fields inside can modify spacetime, inducing a space-time curvature, and thus create gravity fields that create a net force on the Frustum.

Interpreting this thrust as a reaction force, where is the corresponding action? Stated differently: what then is this a reaction force to? The force on the frustum, that must exist to satisfy Newton's 3rd law? What if the device freely accelerated in space? Where would the momentum be that balanced its acceleration? The answer from the GEM theory is that the force on the frustrum occurs because of the GEM interaction with the gravity field (curved spacetime) of the Earth and thus the frustrum is pushing against the Earth via its gravity field. By this analysis, a spacecraft propelling itself by a Q-V thruster away from the Earth would cause the Earth to recoil. This is because gravity fields, even in the Newtonian limit, transfer momentum like EM fields.

A simple example of gravity fields exchanging momentum with EM fields is the bending of light by gravity fields (Figure 9). Obviously, the momentum carried by the light ray is changed, the global momentum flow is then to deposit the reaction to this exchange of momentum to the mass creating the spacetime curvature.

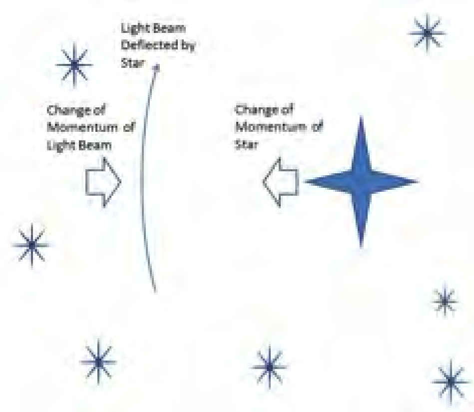

FIG. 9: The exchange of momentum between a light beam and a nearby star. The star must provide "reaction" required by Newton's 3^{rd} law in order for momentum to be conserved.

6. THE THRUST VERSUS POWER RELATION

To complete this calculation we need to estimate S in the gravity field at the Earth's surface. The GEM theory says that gravity is essentially an EM interaction at the subatomic scale, and so we can write the gravity force acting on each nucleon as a radiation pressure acting on an EM cross section that is proportional to mass. The GEM theory allows us to write for a nucleon in the Earth's gravity field:

$$P_{\text{EM}}\sigma_n \cong m_n g \tag{41}$$

Where $\sigma_n \approx 10^{-26} cm^2$ is the EM cross section of a nucleon, similar to the Thompson cross section of an electron, and m_n is a typical mass of 1 amu $= 1.7 \times 10^{-24}$ g. This model is aided by the fact that nuclear matter occupies a fixed volume per unit mass, so individual nucleons preserve their size in a nucleus:

$$P_{\text{EM}} \cong \frac{m_n}{\sigma_n} g \tag{42}$$

The mass per unit area is then $m_n/\sigma_n \approx 50\ g/cm^2$ or $500\ kg/m^2$, surprisingly similar to macroscopic matter. Using g at the Earth's surface we obtain $P_{\text{EM}} \approx 5 \times 10^3\ J/m^3$.

Outer space vacuum is thus arriving at $V_{\text{esc}} = 1.1 \times 10^4$m/sec and we can write:

$$S = V_{\text{esc}} V_{\text{esc}} \cong 6 \times 10^7\ W/m^2 \tag{43}$$

The perturbing Poynting flux, which we assume is asymmetrically absorbed in the wall nearest the field concentration, on the large end of the frustum (area approximately $0.1\ m^2$), is approximately $P/A = 500\ W/m^2$. Thus, we can write for the steady-state perturbation of space time curvature due to the asymmetric S field in the thruster:

$$F_{\text{QV}} \cong m_{\text{QV}} g \frac{dS}{S} \cong 1 \times 10^{-5} N = 10 \mu N \tag{44}$$

We can also write this force as a function of applied RF power.

$$\frac{F_{\text{QV}}}{W} \cong \frac{m_{\text{QV}} g}{AS} \cong 2 \times 10^{-7} N = 0.2 \mu N/W \tag{45}$$

in approximate agreement with the experimental results of $F_{\text{QV}}/W = 0.7\ \mu$N/W.

Therefore, the results of the Q-V thruster experiments and other similar experiments can be explained through the GEM theory. This GEM model is somewhat primitive, but can be refined with the help of more experimental data. This effect is inherently non-linear due to the presence of S^2 terms in the GEM equations, so the low thrust per unit power can be expected to improve at higher power densities such as employed in the Shawyer experiment.

The GEM interpretation of the Q-V data appears much different than the quantum virtual plasma model of the Q-V thruster but is actually very similar. Both models assume a reaction mass tied to the vacuum itself. In the case of the GEM theory, that vacuum is spacetime itself and is tied to the Earth and other nearby masses. In the case of the Q-V theory, it is the virtual particles that are part of the quantum vacuum, and must close the momentum transfer equation by transferring momentum through spacetime to nearby masses.

In the low power experiments Vacuum Bernoulli Equation is in effect in a linear perturbation model, being proportional to the applied power. However, at high powers we can expect the Vacuum Bernoulli Equation to enter into a fully nonlinear mode and the gravity force will be proportional the square of the power. This can be seen from the VBE with the assumption that he cavity will act like a high Q resonator, with high circulating power. Assuming an power of 1 kW and a Q =10,000 (typical for a copper resonator), we can assume a power flux of $10^8\ W/m^2$. In this case we have the equation

$$\begin{aligned} \frac{|dg|}{|g|} \frac{g^2}{2\pi G} &= \frac{S'^2}{|S^2|} \frac{S^2}{u_0 c^2} \\ \frac{|dg|}{|g|} &\cong \frac{S'^2}{|S^2|} \end{aligned} \tag{46}$$

where S' is the applied circulating power of $10^8 W/m^2$ and S is the Poynting flux due to the Earth's gravitational field. We obtain then at 1 kW input power, the approximate thrust force,

$$F_{\text{QV}} \cong m_{\text{QV}} g \frac{S'^2}{|S^2|} \cong 0.1 N \left[\frac{100MW}{60MW} \right]^2 = 0.27\ N\ \ . \tag{47}$$

with a thrust that should increase as the power squared.

7. APPLICATION TO SPACEFLIGHT: AN APPROXIMATE MARS MISSION CALCULATION

Using the 0.1 N/kW value from the high power Shawyer experiment [2], we can find a simple estimate for the total ΔV and trip time to Mars. Assume a 30 metric ton solar powered space craft with a power of 1 MW from a high performance solar array, which we will assume reconfigures itself to maintain constant power on the way to Mars. This gives a thrust of 100 N and an acceleration $T/M = 3.33 \times 10^{-3}$. Here we take advantage of the fact that a spiral out to Mars orbit at $R_M = 1.5$A.U. from $R_E = 1.0$A.U. (see Figure 10) involves a $\Delta R/R_E < 1$, and this trip can be expected to take place in much less than an Earth orbit period : $\Delta t/P_{\text{orbit}} \ll 1$. Thus, we can use the approximation that the trajectory spirals out through a series of orbits with the circular orbit condition,

$$\frac{GM_s}{R} = V_\theta^2 \tag{48}$$

where V_θ is the rotational velocity in the, R is the radius from the Sun, and M_S is the mass of the Sun. The total change in specific energy is approximately:

$$\Delta W = -\frac{GM_s}{2R_E} + \frac{GM_s}{2R_M} = 150\ km^2/sec^2 \tag{49}$$

However, because the the orbit will actually be a spiral outward and not a series of circles, part of the thrust will ineffective due to the thrust vector not being aligned with the rotational component of velocity. We can approximate this inefficiency by expression,

$$\Delta W \cong V_E \frac{T\Delta t}{M} < \langle \cos\phi \rangle \ \ . \tag{50}$$

The average projection of the thrust vector onto the rotational velocity on the spiral orbit is a function of $\Delta R/\ell$, where we have defined the parameter $\ell = 2\pi R_E(\Delta t/P_{\text{orbit}})$, where P_{orbit} is the period of the original orbit. We obtain in the limit of $\Delta R/\ell$ and $\Delta t/P_{\text{orbit}}$ both $\ll 1$:

$$\langle \cos\phi \rangle \cong \frac{\ell}{\sqrt{(\Delta R)^2 + \ell^2}} \tag{51}$$

This system gives a correct limit of $\langle \cos\phi \rangle = 1$ or zero gravity losses, in the limit of $\Delta R/\ell \ll 1$, a spiral out over many orbital periods for $\Delta R/R_E \ll 1$. Solving the system of Eqs. 46 and 47 by iterations, we obtain the estimate $\langle \cos\phi \rangle \approx 0.7$, for an average angle of the spiral of $\phi \cong 45°$. We then obtain by this analysis a $\Delta V \approx 7.2$ km/sec. This is roughly double the required $\Delta V \approx 3.5$ km/sec for a minimum energy Hohmann Transfer requiring a $\Delta t \approx 10$ months. This increase in ΔV for low thrust trajectories is due to gravity losses and is unavoidable [8]. However, despite the gravity loss inefficiency, the required for our Q-V thruster is $\Delta t \approx 4$ weeks or ~ 1 month, so we can take advantage of abundant solar power and the propellant-less character of the Q-V thruster to get to Mars in 1/10 the time required for more conventional chemical fuel approaches. Accordingly, assuming the Q-V thruster results at high power can be reproduced, this propulsion technology will be a true breakthrough in space propulsion.

8. CONCLUSIONS

Creating thrust by injecting microwaves into an isolated asymmetrical metal container may seem impossible at first glance, but if one accepts the concept that spacetime is fundamentally electromagnetic, then forces on the asymmetrical container are not only possible but expected. Creating an asymmetrical EM field, under the GEM theory, will directly create a curvature in spacetime and thus a gravity force. The gravity force, a curvature in local spacetime whose structure connects all large masses in the vicinity, creates a force on the metal container, and it also creates a reaction force that conserves momentum with the Earth and Sun, that anchor the local structure of spacetime.

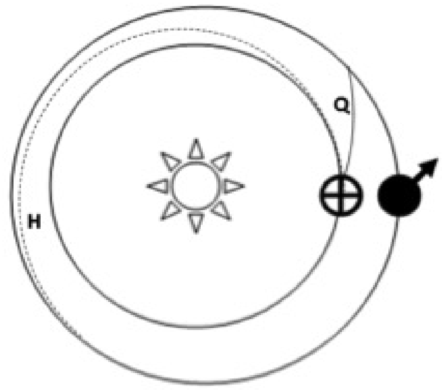

FIG. 10: The approximately 1 month trajectory of a Q-V Thruster propelled spacecraft (path Q) versus a 10 month minimum energy trajectory Hohmann transfer trajectory for a spacecraft (path H) journeying from Earth to Mars.

The GEM theory predicts that gravity fields are a distortion of the quantum ZPF fields and have a net Poynting flow. That is, the fabric of spacetime is electrodynamic, consisting of ZPF fields. This theory also predicts that we can change the Poynting flow associated with gravity by constructive and destructive inference between the ZPF and artificially applied Poynting flows. Thus, in the GEM theory Poynting flows can create artificial curvatures in the ZPF and by this curve spacetime creating local gravity fields that can create forces on a spacecraft or its components. The reaction force to this created force is felt by spacetime itself and transferred to the nearby astronomical masses such as the Earth. The medium for the transfer of momentum is the gravity field itself, as if it was a solid object. This is similar to the bending of light, an EM field, in a gravity field where EM momentum is exchanged with the gravity field. (Figure 10) Therefore, the application of EM Poynting field in carefully controlled geometries can, in the GEM theory, create gravity forces. This preliminary analysis suggests the frustum experiment at Eagleworks may be creating forces by bending spacetime, and the GEM theory allows the calculation of magnitude and scaling behavior to be made, and gives approximate agreement with what is observed.

In a very recent development, the GEM theory prediction of a neutral, spin 0, particle of mass-energy $M* = 21.9$MeV [9,10] that would decay into electron-positron pairs, has been partially confirmed with the discovery of a similar particle "X" at $M_x = 16.9$ MeV [11]. This newly discovered particle with a spin 0 and decaying into electron-positron pairs appears to be a perturbed state of the $M*$ particle, caused by the neighboring electron quantum mass state:

$$M_x \cong \frac{M*}{1+\alpha\sigma} = \frac{21.9\,MeV}{1.31} = 16.7\,MeV \tag{52}$$

In summary, it appears possible that a great breakthrough in space propulsion has been made at a NASA associated laboratory. This experimental breakthrough may be explained, both conceptually and quantitatively, by a theory of Gravity-EM unification that has been in development for decades, and which yields the value of G and the proton mass from quantum vacuum quantities to high accuracy [9,10]. Therefore, the road appears open to great advances and revolutionary changes in human spaceflight, to include the entire solar system. Let us proceed with all diligence and discuss and explore these possibilities further.

REFERENCES

[1] Brady, D., White, H. G., March, P., Lawrence, J., and Davies, F. J., ?Anomalous Thrust Production from an RF Test Device Measured on a Low-Thrust Torsion Pendulum?, presented at the 50th AIAA Propulsion Conf., July 2015.

[2] Shawyer R. (2008) "Microwave Propulsion-Progress in the EMDrive Programe", 2008 International Astronautics Conference IAC-08-C4.4.7

[3] J.E. Brandenburg (2012) "An Extension of the GEM Unification Theory to Include Strong and Weak Nuclear Forces and an Estimate of the Higgs Boson Mass", STAIF II Conference Albuquerque NM March 2012 now published as : `http://www.mehtapress.com/images/stories/journal_of_space_exploration/vol_1_issue_1_file_3.pdf`

[4] Murad, P. A., Boardman, M. J. and Brandenburg, J. E., "The Morningstar Energy Box- Part Redux", Journal of Space Exploration - STAIF II, 2012.

[5] Brandenburg, J.E. and Kline, J. K., "Application of the GEM theory of Gravity-Electro-Magnetism Unification to the problem of Controlled Gravity: Theory and Experiment". AIAA 98-3137, 1998.

[6] Witten, E., "Anomalous Cross-Section for Photon–Photon Scattering in Gauge Theories", Nucl. Phys. B120, (1977) 189.

[7] Puthoff, H.E., "Gravity as a zero-point fluctuation force", Phys. Rev. A 39, 2333, (1989).

[8] Goebel, M., Dan and Ira Katz. *Fundamentals of Electric Propulsion.* New York: Wiley, 2008.

[9] Brandenburg J.E. "The GEM Unification Theory ; Extending the Standard Model to Include Gravitation", Lambert Academic Publishing. June 2016.

[10] Brandenburg , J.E. , "The GEM (Gravity-EM)Theory : the Unification of the Strong, EM , Weak ,and Gravity Forces of Nature", Journal of Multidisciplinary Engineering Science Studies (JMESS) ISSN: 2458-925X Vol. 2 Issue 7, (2016)

[11] Feng, J. L. et. al., Particle Physics Models for the 17 MeV Anomaly in Beryllium Nuclear Decays, `http://arxiv.org/abs/1608.03591`

RECORD OF THE PROCEEDINGS:

a session on

THE TRI–SPACE MODEL OF SPACETIME AND THE UNIVERSE

led by Gregory V. Meholic

Greg provided a change of gears and change of perspective at the workshop by asking us to reconsider our conceptions of the propulsion problem. He has developed over time a conceptual, notional model that to tie together some underlying phenomena of nature. He brings an engineer's visual perspective to these considerations, but in a way that does not involve mathematical equations. So this is a presentation to allow him to share his visualization of some of the aspects of spacetime and the propulsion problem.

This picture was inspired when Greg stumbled upon an old report on tachyons by Edward Puscher of Rand Corporation. That report contained the relativistic equation for energy of a body of rest mass m moving with speed v:

$$E = \gamma mc^2 = \frac{mc^2}{\sqrt{1 - v^2/c^2}} \tag{1}$$

Any massive body accelerating from rest must have $v < c$, and so the denominator in the energy expression is always positive. The quantity γm is sometimes called the relativistic mass. When $v \ll c$, $E \simeq mc^2 + mv^2/2$, the non-relativistic kinetic energy plus rest mass energy.

When speeds $v > c$ are considered in (3), then the energy becomes imaginary. It is therefore hypothesized that such a particle must have an imaginary mass, so that the energy stays real. Therefore the range of energies (for positive speeds) is

$$\begin{aligned} E &= \frac{mc^2}{\sqrt{1 - v^2/c^2}} \quad , \quad v < c \\ E &= \frac{mc^2}{\sqrt{v^2/c^2 - 1}} \quad , \quad v > c \\ E &= \infty \quad , \quad v = c \end{aligned} \tag{2}$$

Therefore the entire domain of values of energy E for any v comprises two domains with finite values of energy: above and below the speed of light. A third domain consists of diverging energy values when approaching the speed of light from above or below. The figure below allows a negative energy region as well, in the spirit of Dirac. The negative velocity region accounts for particles moving left or right, and it is understood these speeds are projections of three-dimensional velocity vectors.

It is hypothesized that the laws of physics may be different in the 3 regions; 3 overlapping realms in the same space. We only have access to the $v < c$ region. Particles inhabiting the $v > c$ region are tachyons, although none have ever been observed.

The $v = c$ realm is inhabited by electromagnetic waves and gravity waves. The $v > c$ realm has the curious property that higher speeds correspond to lower energies. Energy would be required to slow down a tachyon to the speed of light.

The 3 realms are envisaged as mirroring their representation in velocity space: the subluminal and superluminal regions adjoin at a "luminal" sheet where $v = c$. The sheet can be deformed similar to how we picture deformation of spacetime under gravity. It is suggested that the sheet could be identified with quantum foam or the quantum vacuum.

Williams: Don't we also have quantum foam in the subluminal realm? What is the connection to moving at the speed of light?

Meholic: It should become clear later.

Williams: And aren't the 3 realms sharing the same space? I can have a particle moving

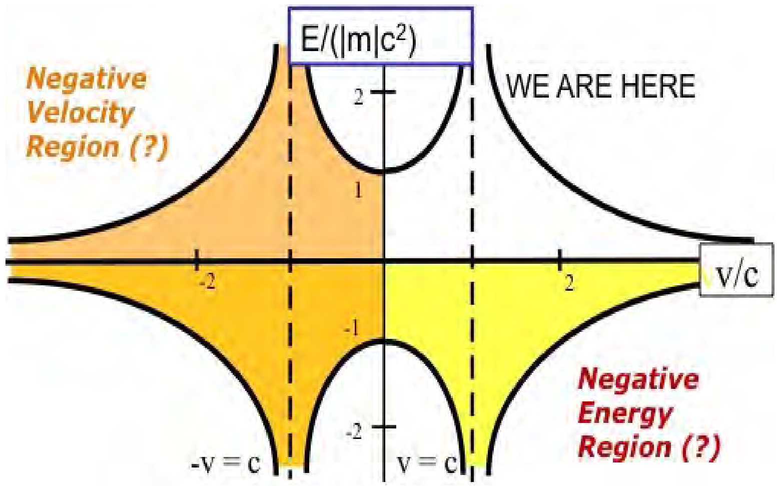

FIG. 1: Basis of the Tri–Space Universe.

submluminal and a hypothetical superluminal particle, and couldn't they meet in the same space?

Fearn: I think time stops for the luminal particles, and goes backward for the superluminal ones.

Meholic: Let me put that discussion off and we will come back to it.

Greg introduces a model of the electron developed by Richard Gautier. It hypothesizes that the electron is a manifestation of a sub-particle that executes spatial motion on a lengthscale similar to the size of the electron. This model is an alternative explanation for the zitterbewegung phenomena *[Ed: that Schroedinger showed to be implied by the Dirac equation: a relativistic interaction between an electron's translational motion and spin should lead to a violent oscillation of the particle at very high frequencies and over distances of roughly one Compton wavelength. So far, this has not yet been observed.]*

Williams: Are you treating the electron as a particle? As opposed to a wave?

Meholic: Yes, that is his model.

It is conjectured that perhaps the fundamental sub-particle that constitutes the electron in the Gauthier picture, called by Gauthier a "TEQ", could also be a constitutent of other types of matter, and Gauthier has made some investigations in this area. Since the Gauthier model involves the sub-particle moving alternatively faster and slower than light, Greg suspects this conjectured particle could provide a link to the superluminal realm. Perhaps all mass has a superluminal component in an analogous way.

Williams: What are the parameters of the TEQ that produce the other parameters of the electron like charge and mass?

Mathes: The parameters are in Gauthier's paper. We can send it to you. But there are about 6 parameters. But this particular model does not have charge in it yet.

Jansson: So you are saying this TEQ goes across the luminal boundary?

Meholic: Yes

Bushnell: The wavefunctions for tachyons are sub-luminal, so the wave function could provide the coupling between the superluminal and subluminal realms; through a sort of quantum entanglement.

Greg goes on to suggest the luminal boundary has a finite "thickness" and relates this to space and time in a sketch at the whiteboard. He emphasizes he is just brainstorming with this picture and does not present these as in any way complete results.

Fearn: This sounds very similar to Cerenkov radiation.

The history of fluid conceptions of spacetime, such as the aether, are reviewed. It is suggested that a fluidic picture may have relevance for today's physics. Moreover, the Tri-Space model invites some quasi-mechanical conceptions, "physical analog", of the phenomena underlying charge and mass.

Williams: The references shown on the slide for papers on fluidic spacetime are not really mainstream journals. So we are unsure if there is a renaissance of the aether, for example.

Meholic: These may be some dated references.

Rodal: What are the properties of the spacetime fluid?

Meholic: We are coming to that. Stay tuned.

Rodal: Also, you refer to the fluid properties of spacetime, and also to the aether, but the aether is a solid. Are you not distiguishing a solid and a fluid? The speed of light was related to its putative modulus of elasticity. The aether has a very high modulus of elasticity. There are mathematical distinctions between a solid and a fluid.

Meholic: The answer to your question is that it's a fluid in this model, because of the Gauthier assumptions.

Tajmar: Earlier you said the aether approach could resolve some questions that quantum mechanics cannot. What are those?

Meholic: I must admit I was just quoting that unverified and I cannot name any.

Greg goes on to describe fluidic interpretation to masses and fields, and a similarity is noticed to the quantum vacuum. Density, compressibility, viscosity, etc, are ascribed to spacetime.

Williams: When you talk about spacetime, do you mean the subluminal, luminal, what?

Meholic: The luminal.

Williams: So when you talk about compressibility, you aren't referring to subluminal or superluminal states? Aren't we in subluminal realm?

Meholic: We are experiencing subluminal speeds in luminal spacetime...Because we are receiving light from the lights...It's a convoluted way to think about this.

Williams: Which of the 3 realms corresponds to spacetime?

Meholic: All of them. It's the same space, but with 3 possible velocities at once. Depending on your energy state in that continuum, you would experience subluminal, luminal, or superluminal.

Bushnell: I question the validity of your continuum model. It implies a certain mean free path. The fundamental reality must be quantum.

Meholic: Point taken, I am just trying to keep things at the simplest meaningful level.

Fearn: I think Dennis is saying, for example, you can't define an index of refraction for two atoms. There is a limit to the continuum analogy. Is it an appropriate conception?

Meholic: There is no rarification. TEQs are everywhere and they are right next to each other.

Fearn: Perhaps you have a tight coupling due to short timescales?

Tajmar: You are saying the TEQ density is uniform everywhere?

Greg departs into some conjectures regarding the superluminal space. It is emphasized that the rest masses are presumed imaginary to keep the energy real.

Williams: I just want to point out that the imaginary mass is an artifact of extending the subluminal energy relation to superluminal speeds. The theory of relativity does not actually dictate whether the metric signature is $+ - --$ or $- + ++$. If you know you are going to allow superluminal speed, you can adopt a convenient normalization for the energy relation that keeps the energy positive. The point is I would not read too much into the notion of imaginary mass.

Greg then describes a picture of interaction at the boundary between the subluminal and superluminal spaces.

Williams: You describe this as a spatial boundary, but didn't you say the 3 realms share the same physical space? And you describe as a plane something moving at the speed of light. So I am having trouble with the concepts.

Meholic: I am not surprised, it took me 27 years to come up with this!

Greg goes on to describe an interpretation of gravity in terms of the membrane between the realms. He conjectures that the 3 realms could be tied to different phase states of the different states of motion. Could a phase change lead to superluminal velocities? Greg sees many phenomena of nature "explainable" in terms of the tri space model.

– *discussion of changing between the three states of motion* –

Greg suggests instead of thinking of acceleration and deceleration, to instead think of changing states of motion as if entering a different space.

Fearn: Perhaps you could think about it like changing the refractive index of space.

Greg showed some of his intuitive visualizations of gravity in these terms. He conjectures that spacetime provides a viscous resistance to the motion of bodies, that accounts for inertia. It is treated as something continuous on a subatomic scale, even. In Greg's vision, electric charge is related to the TEQs, and they are imagined to be corkscrewing through different realms. He visualizes that electromagnetic waves are also TEQs.

Greg concludes by thanking us for indulging his intuitive pictures, challenging us to keep open minds and defy convention to make progress.

Reported by L. Williams

References

[1] Puscher, E. A., "Faster-than-Light Particles: A Review of Tachyon Characteristics, Paper N-1530-AF, Rand Corporation, Santa Monica, CA, 1980. `http://www.rand.org/content/dam/rand/pubs/notes/2009/N1530.pdf`

CHAPTER 7 – UNSCHEDULED PRESENTATIONS

INTRODUCTION

H. Fearn & L.L. Williams

We were pleased that Workshop attendees had a high level of enthusiasm, both for the technical sessions and for the celebration of the life and career of Dr. Woodward. Attendees were prepared in advance for the technical sessions, including a Prep Kit sent out summarizing the sessions, and a set of Quick Studies that summarized key results relevant to the workshop. However, some attendees requested time to make unscheduled short presentations summarizing items of interest to them, so they could gather impromptu feedback from colleagues. So that this Proceedings properly captures the full transactions of the Workshop, those unscheduled presentations are summarized in this chapter.

On the eventing before the technical sessions, John Brandenburg provided an entertaining and provocative discussion of an alternative explanation for isotope anomalies on Mars. Todd Desiato presented his view of spacetime based on a refractive index. Bill Christie presented his model for the electron in terms of a concept he calls a rotating wave. Jan Harzen presented an after-dinner session on the attempts of MUFON to act in a scientifically rigorous manner on a topic that is so often susceptible to sensationalism.

AN ENGINEERING MODEL OF QUANTUM GRAVITY

Todd J. Desiato[1]
Vista, California, USA

It is proposed that gravitational fields may be interpreted as a variation in the relative available driving power (watts) of the Electromagnetic Zero-Point Field (ZPF). It is shown that variations in the relative available power are covariant with variations in the coordinate speed of light as measured by a distant observer in unaltered space-time. Gravitational time dilation and length contraction may then be interpreted as a loss of driving power from the ZPF. It is hypothesized that the loss of power is due to increased radiative damping of matter, resulting from an increase in the local relative energy density which promotes this process. The relative radiative damping factor affects the relative ground state energy of the quantum mechanical harmonic oscillator such that the mean-square fluctuations in matter reproduce the behavior attributed to, and resulting from, variations in the space-time metric of General Relativity (GR). From this principle, all of the variations observed by a distant observer that occur due to gravity, or space-time curvature, under GR may be reproduced from the variable relative damping function acting on the harmonic oscillator. What is presented herein, is an engineering model for quantum gravity that puts gravity in the hands of engineers, who will understand this process and will potentially advance artificial gravity and anti-gravity technology from pure speculation, to achievement in our lifetime.

Nomenclature

$g_{\mu\nu}$	= metric tensor where, μ and ν are indices
χ	= relative dielectric susceptibility, used as a control parameter
K	= relative refractive index of vacuum, measured from a dis. ref. frame
K	= $(-g_{11}/g_{00})^{1/2} = 1 + \chi$
c_0	= speed of light in vacuum, measured in a local, IRF (m/s)
$c_k = c_0/K$	= relative coordinate speed of light, measured from a dis. ref. frame (m/s)
Δx_0	= an interval along the x-axis, measured in a local, IRF (m)
$\Delta x = \Delta x_0/\lvert K\rvert$	= an interval along the x-axis, measured from a dis. ref. frame (m)
Δt_0	= an interval of time, measured in a local, IRF (s)
$\Delta t = \Delta t_0/\lvert K\rvert$	= an interval of time as measured from a dis. ref. frame (s)
q^2	= squared magnitude of the electrical charge quantum e (C)
$\hbar$	= reduced Planck's constant, $h/(2\pi)$ (Js/rad)
ϵ_0	= dielectric permittivity of vacuum, measured in a local, IRF (F/m)
μ_0	= dielectric permeability of vacuum, measured in a local, IRF (H/m)
G	= the gravitational constant (Nm^2/kg^2)

where ref. & dis. stand for reference & distant and IRF stands for inertial reference frame.

1. INTRODUCTION

Practically speaking, time is measured with a clock and space is measured with a ruler. Each is a device used to compare with other identical devices at different sets of coordinates. The distant observer uses his own devices to establish a coordinate system with which to compare his observations to identical devices at distant coordinates. He chooses for example, to observe the light emitted by distant supernovae and then compare them to the light of other similar events. From this data the distance to these events, and their motion relative to the observer is determined [1].

Of course there are other ways to achieve this. This was just one example to illustrate the point, that measurements are made using physical tools of our choosing which are composed of some form of matter,

[1] tdesiato@warpdrivetech.com

and all matter must react to the physical effects of gravity in the same way. There are no absolute rulers or absolute clocks that are impervious to the physical effects of gravity.

In the reference frame of the distant observer, space and time appear to be variables, or curved, when the local devices and the remote devices disagree. It is interpreted such that the remote devices are variables which undergo gravitational length contraction and time dilation in the presence of gravitational fields. This is not an illusion. Time dilation and length contraction are real, physical effects whose action can be described using elementary quantum mechanics, and the correct procedure to do so shall be shown here.

The Engineering Model of Quantum Gravity presented here uses the reference frame of the distant observer because it allows all observations to be consistently scaled without the need of complicated tensor coordinate transformations when working with gravitational fields. In this presentation, gravity is treated as a scalar field. However, due to the quantum mechanical basis of the model itself, the quantum to classical correspondence principle will apply. Whereby, individual quantum oscillators behave in such a way that, in large numbers, their averages should reproduce the behavior of classical test particles in a curved space-time.

That being said, it is necessary to drop any notion of doing quantum field theory on a curved space-time manifold. In this model, space-time is considered to be perfectly flat. As such, the typical equations of QED in flat space-time will be applied (See Milonni for example.) [2].

Engineers are clever, but aside from the calibration of the Global Positioning Satellite network, we really don't know what to do with space-time curvature as a means to manipulate gravity. The Gravitic Caliper is not a tool in our toolbox. Likewise, referring to gravitational fields as a variable refractive index, as is done in the Polarizable Vacuum (PV) Model of GR [3, 4, 5], adds some pedagogical value to gravitational fields but does not address the pressing issue of: "What to do to create or mimic gravity?" What engineers require is a more practical set of tools to work with when dealing with the effects of gravitational fields, so that they can acquire a deeper understanding of the "nuts and bolts" regarding how gravity and matter interact.

Space-time curvature is a useful mathematical description of the available data regarding gravity, but it is not the only useful interpretation of the data. The interpretation presented here describes gravitational time dilation and length contraction in the proximity of increased mass-energy densities as a physical effect acting on clocks and rulers at the quantum scale. This physical effect begins with a typical harmonic oscillator, something most engineers should be familiar with. For the practical purposes of discussion, matter may be usefully approximated as being comprised of such oscillators [2].

If there is dissipation occurring within the oscillator, eventually the oscillation will decay to its lowest energy state. In a passive electronic oscillator circuit for example, there may be a sinusoidal power supply (a.c. source) driving a resonant LC circuit [6]. In the circuit there may be a resistance, R which dissipates power and damps the oscillation. Eventually, the source of power and the dissipation reach an equilibrium condition.

In the case of matter, when it decays to its lowest energy state, it is in the ground-state where the minimum energy is not zero [2, 7]. The minimum energy is the equilibrium between a constant, uniform ZPF which drives the oscillators, and a variable damping function which damps them. The damping function is dependent on the local mass-energy density, which increases the radiative damping, resulting in the observed behavior of oscillators in a gravitational field, where they have a lower ground state energy than they would in an unperturbed ZPF. In other words, the damping function lowers the relative ground state energy below that which the ZPF establishes as the natural ground state. In GR, this is interpreted as the gravitational field possessing *negative energy density*.

In section 2, the physical effects of gravitation are derived from the space-time metric of GR and associated with the variable refractive index of the PV Model. In section 3, the quantum vacuum processes that determine the ground state equilibrium condition between matter and vacuum are discussed, in addition to the co-variant relationship between relative power and the relative coordinate velocity of light.

In section 4, the *relative radiative damping factor* is derived and the connection to gravity is established. It is shown that the variable metric coefficients result from variations in the radiative damping factor that reduces the relative available power of the ZPF, making it vary in a way which may be interpreted as curved space-time. In section 5, the expected relationship is established between the relative damping factor and the local energy density, in accordance with GR.

2. THE PHYSICAL EFFECTS OF GRAVITATION

It has been shown that a gravitational field may be interpreted as a variable refractive index that alters space-time and determines the relative scale of rulers and clocks in the altered region, as measured by a distant observer in an unaltered region of space-time [3, 4, 5]. A brief introduction to the physical effects that engineers will encounter when working with modified space-time and matter, in the context of GR and the PV Model, will be presented in this section.

One obvious disadvantage of working with GR from the perspective of a local observer is that the speed of light remains constant in the local inertial reference frame. Observers in the local frame cannot measure light moving faster than c_0, the speed of light in vacuum. Nor can they measure light moving slower than c_0 in the local vacuum using rulers and clocks immersed in the same local vacuum. Therefore, it is advantageous for engineers to understand what to expect, what to look for, and why there is a need to make observations from the perspective of a distant observer in an unaltered reference frame, outside of the effects to be measured.

In GR, the four-dimensional line element is given by the expression,

$$ds^2 = g_{\mu\nu} dx^\mu dx^\nu \tag{1}$$

where summation is assumed for repeated indices. In flat space-time, the line element reduces to the more familiar expression,

$$ds^2 = -c_0^2 dt^2 + dx^2 + dy^2 + dz^2 \tag{2}$$

The reader does not need to be well versed in GR to follow most of what is presented here. Think of this as calculating the length of the hypotenuse of a right-triangle in two dimensions. In two dimensions, $ds^2 = -c_0^2 dt^2 + dx^2$. The metric coefficients from equation (1) are, $g_{00} = -1$, $g_{11} = 1$, and $g_{\mu\nu} = 0$ for $\mu \neq \nu$, where, $dx^0 = c_0 dt$ and $dx^1 = dx$ in Cartesian coordinates. For any light ray, $ds^2 = 0$ and may be solved to discover $c_0^2 = c_k^2$, where, $c_k = dx/dt$ is the relative coordinate velocity of light. The refractive index of this metric is then simply defined by $K = |c_0/c_k|$.

Similarly, Eq. (2) may be written in terms of variable metric coefficients g_{00} and g_{11} in a curved space-time. Typically, they take on values that are determined by a solution of Einstein's field equations of GR, such as the Schwarzschild solution. For simplicity, in two dimensions the resulting line element becomes,

$$ds^2 = g_{00} c_0^2 dt^2 + g_{11} dx^2 \tag{3}$$

The refractive index can now be read off as,

$$K = |\sqrt{g_{11}/-g_{00}}| \tag{4}$$

The refractive index is accompanied by physical effects in the gravitationally altered region of space-time. The metric coefficients alter the scale of rulers and clocks in their region of influence, as compared to those of the observer in a distant unaltered region. For example; when $|\sqrt{-g_{00}}| < 1$ and $|\sqrt{g_{11}}| > 1$, then $|\sqrt{-g_{00}}|dt < dt$ and, $|\sqrt{-g_{11}}|dx < dx$. Clocks in the altered region, as well as atomic oscillations there, appear to have slowed down. $\Delta t = \Delta t_0/|\sqrt{-g_{00}}|$ and rulers in the altered region, as well as atomic spacing, appear to have contracted. $\Delta x = \Delta x_0/|\sqrt{g_{11}}|$, as compared to those rulers and clocks used by the distant observer [3]. This is simply gravitational time dilation and length contraction as described in GR.

In the special case where $-1/g_{00} = g_{11} = K$, the physical effects of altering the refractive index can be simplified and tabulated for engineering purposes in terms of K, as shown in Table 1. Power is measured in watts. Power P_k varies inversely with the refractive index and is therefore covariant with the relative coordinate velocity of light, c_k . Referring to Table 1, it can be shown that,

$$\begin{aligned} P_k &= \Delta E/\Delta t = P_0/K \\ c_k &= c_0/K \end{aligned} \tag{5}$$

Why this is true will become evident in section 4 where the effect on power will be derived from first principles.

From the perspective of the distant observer in an unaltered region of space-time, it is observed that in an altered region of space-time near a massive star clocks are running slower, rulers are contracted, and the speed of light has become slower. The conclusion drawn would be that matter in the region is running low on power. There is not enough power to *inflate* matter to its "proper" size, as was presented in [8]. Alternatively, from the same perspective, in a region of space-time where matter is moving Faster Than Light (FTL), matter is inflated, clocks are running faster, rulers are expanded, and the speed of light has increased. The conclusion would then be drawn that the scale of matter and the speed of light is regulated by the relative power of the ZPF available to do work to drive these physical processes, as will be shown in the following sections.

TABLE I: Physical effects of space-time acting on matter in a gravitationally altered region, as measured by a distant observer in an unaltered region of space-time. GS = Ground State, accel. = acceleration, FTL = faster than light

Variable Refractive Index $K = \lvert\sqrt{g_{11}/-g_{00}}\rvert$	**Gravity of a Massive Star** $K > 1$	**Anti-Gravity or FLT Effects** $K < 1$
$c_k = c_0/K$	c is slowed down	c speeds up
$\Delta x = \Delta x_0/\lvert K^{1/2}\rvert$	rulers contract	rulers expand
$\Delta t = \Delta t_0\lvert K^{1/2}\rvert$	clocks run slow	clocks run fast
$v = \Delta x/\Delta t = v_0/K$	velocity is slower	velocity is faster
$a = a_0/\lvert K^{3/2}\rvert$	accel. decreases	accel. increases
$m = F/a = m_0\lvert K^{3/2}\rvert$	force (mass) increased	force (mass) decreased
$\omega = 2\pi/\Delta t = \omega_0/\lvert K^{1/2}\rvert$	freq. decreased	freq. increased
$\Delta E = \hbar\omega = \Delta E_o/\lvert K^{1/2}\rvert$	GS. Energy decreases	GS. Energy increases

3. ZERO-POINT EQUILIBRIUM IN A GRAVITATIONAL FIELD

Although a charged particle is constantly undergoing accelerated motion due to interactions with the electromagnetic ZPF, it does not appear to radiate [2, 7]. The reason for this apparent lack of radiation is that the ground state of the particle is at steady-state equilibrium with the electromagnetic ZPF of the quantum vacuum.

In section 3.3 of The Quantum Vacuum, Milonni [2] writes,

> "The fact that an accelerating charge loses energy by radiating implies, according to classical ideas, that an electron should spiral into the nucleus and that atoms should not be stable. The balancing of the effects of radiation reaction and the vacuum field..., however, suggest that the stability of atoms might be attributable to the influence on the atom of the vacuum field.... We now know that the vacuum field is in fact formally necessary for the stability of atoms in quantum theory. As we saw..., radiation reaction will cause canonical commutators $[x, p_x]$ to decay to zero unless the fluctuating vacuum field is included, in which case commutators are consistently preserved."

In an inertial reference frame where a charged particle is in bounded, steady-state motion, such as in a harmonic oscillator, there is a non-zero ground state that is in equilibrium with the local ZPF. All fields, including the Dirac field (fermions) that makes up matter, and force carriers, (photons and gluons) have a ZPF where the ground state energy is, $E_{\rm GS} = \hbar\omega/2$, per frequency mode.

An intuitive way for engineers to look at this is that in the ground state, the mean power absorbed by the particle from the ZPF is equal in magnitude to the power radiated from the particle, due to acceleration.

$$\langle P_a^{\rm rad}\rangle = \langle P_{\rm ZP}^{\rm abs}\rangle \tag{6}$$

The works of Milonni [2, 9, 10] and also Puthoff [7] illustrate this clearly. Power absorbed from the ZPF by a charged particle in bounded, steady-state motion is given by,

$$\langle P_{\rm ZP}^{\rm abs}\rangle = \frac{1}{4\pi\epsilon_0}\frac{q^2\hbar\omega_0^3}{3m_0c_0^3} \tag{7}$$

where dimensionally $\hbar\omega_0^3/m_0 \sim a^2$ and ω_0 is the natural resonant frequency of oscillation. Power radiated from an accelerated charge to the vacuum is given by,

$$\langle P_{\text{ZP}}^{\text{rad}} \rangle = \frac{1}{4\pi\epsilon_0} \frac{2}{3} \frac{q^2 \langle a^2 \rangle}{c_0^3} \tag{8}$$

where, $\langle a^2 \rangle$ is the mean-square acceleration fluctuation given in Eq. (16). It may be inferred that when the symmetry of this equilibrium state is broken, the system accelerates.

Puthoff uses the Stochastic Electrodynamics (SED) Fourier composition of the ZPF as the proposed driving function [3]. The electric field is given by,

$$\mathbf{E}_{\text{ZP}} = \Re e \sum_{\sigma=1}^{2} \int d^3k \, \hat{\varepsilon} \left(\frac{\hbar\omega}{8\pi^3\epsilon_0} \right)^{1/2} \exp[i(\mathbf{k}\cdot\mathbf{r} - i\omega t + i\theta(\mathbf{k},\sigma)] \tag{9}$$

The exponential term is the wave part of the equation. A similar equation can be expressed for the magnetic field by replacing $\mathbf{E}_{\text{ZP}}$ with $\mathbf{H}_{\text{ZP}}$, the unit vector $\hat{\varepsilon}$ with $(\hat{\mathbf{k}} \times \hat{\varepsilon})$ and ϵ_0 with μ_0. However, this example is sufficient to describe the concepts to be conveyed.

The indefinite integral over the field modes, k in Eq. (9) may be tuned by utilizing matter in ways that alter the limits of the integration, as is done in the Casimir effect [2, 11]. These limits are referred to as the cut-off modes of the field. The frequency limits of the ZPF are formally infinite, but can be modified or limited by the presence of matter.

The electromagnetic ZPF is used to calculate the mean-square fluctuations in position, velocity and acceleration of a particle in bounded, steady-state motion. Utilizing the standard procedures from quantum mechanics, these fluctuations are determined by integrating over the modes and summing the various polarizations of $\mathbf{E}_{\text{ZP}}$. The derived equations of motion for a particle with charge to mass ratio, q/m are as follows, [2, 7].

$$\begin{aligned}
x &= \frac{q}{m} \Re e \sum_{\sigma=1}^{2} \int d^3k \, (\hat{\varepsilon}\cdot\hat{\mathbf{x}}) \left(\frac{\hbar\omega}{8\pi^3\epsilon_0} \right)^{1/2} \left(\frac{1}{D} \right) \exp[i(\mathbf{k}\cdot\mathbf{r} - i\omega t + i\theta(\mathbf{k},\sigma)] \\
\dot{x} = v &= \frac{q}{m} \Re e \sum_{\sigma=1}^{2} \int d^3k \, (\hat{\varepsilon}\cdot\hat{\mathbf{x}}) \left(\frac{\hbar\omega}{8\pi^3\epsilon_0} \right)^{1/2} \left(-i\frac{\omega}{D} \right) \exp[i(\mathbf{k}\cdot\mathbf{r} - i\omega t + i\theta(\mathbf{k},\sigma)] \\
\ddot{x} = a &= \frac{q}{m} \Re e \sum_{\sigma=1}^{2} \int d^3k \, (\hat{\varepsilon}\cdot\hat{\mathbf{x}}) \left(\frac{\hbar\omega}{8\pi^3\epsilon_0} \right)^{1/2} \left(-\frac{\omega^2}{D} \right) \exp[i(\mathbf{k}\cdot\mathbf{r} - i\omega t + i\theta(\mathbf{k},\sigma)]
\end{aligned} \tag{10}$$

where the denominator, D expresses a resonance condition at the natural frequency, ω_0 ,

$$D = \omega_0^2 - \omega^2 - i\Gamma\omega^3 \tag{11}$$

The natural radiative damping function, Γ is expressed as,

$$\Gamma = \frac{q^2}{6\pi\epsilon_0 m_0 c_0^3} = \left(\frac{2\alpha}{3} \right) \frac{\hbar}{m_0 c_0^2} \tag{12}$$

Equations (8) and (12), come from the Larmor radiation power formula [7, 12]. For an electron in the reference frame of the local observer, $\Gamma_0 = 6.336 \times 10^{-24}$s. Which is small in comparison to the natural frequency of the electron, such that, $\Gamma_0\omega_0 = 0.005$. If the natural frequency is taken to be, $\omega_0 = m_0 c_0^2/\hbar$. Then the natural damping function is just a proportionally scaled re-expression of the period of the natural frequency; an *odd* harmonic.

$$\Gamma_0 = \frac{2\alpha}{3\omega_0} \tag{13}$$

where α is the fine structure constant, $\alpha = q^2/(4\pi\epsilon_0\hbar c_0)$.

4. PARTICLE FLUCTUATIONS AND GRAVITY

From the equations of motion above, the mean-square fluctuations in the particle's motion are derived. For example, from equation (10), the mean-square position fluctuation is,

$$\langle x_0^2 \rangle = \frac{q^2 \hbar}{6\pi^2 \epsilon_0 m_0^2 c_0^3} \int_0^\infty \frac{\omega^3 d\omega}{[(\omega_0^2 - \omega^2)^2 + \Gamma_0^2 \omega^6]} \tag{14}$$

The derived integrand is almost precisely a Lorentzian line-shape, because, $\Gamma_0 \omega_0 = 1$ is small and the integrand in equation (14) is sharply peaked. Therefore, the standard resonance approximation for a harmonic oscillator may be used to high precision. Making the appropriate substitutions, simplifying and noting that the Lorentzian line-shape integral is unity, the resulting mean-square position fluctuation is,

$$\begin{aligned} \langle x_0^2 \rangle &= \frac{\hbar}{2m_0\omega_0} \int_{-\infty}^{\infty} \frac{1}{\pi} \frac{(\Gamma_0 \omega_0^2/2)}{(\omega_0 - \omega)^2 + (\Gamma_0 \omega_0^2/2)^2} d\omega \\ &= \frac{\hbar}{2m_0\omega_0} \end{aligned} \tag{15}$$

An easy to follow derivation of the mean-square fluctuations is found in [7]. These results are the standard quantum mechanical values for the mean-square fluctuations in position, velocity and acceleration, that will be referred to in what follows.

$$\begin{aligned} \langle x_0^2 \rangle &= \frac{\hbar}{2m_0\omega_0} \quad , \\ \langle v_0^2 \rangle &= \frac{\hbar\omega_0}{2m_0} \quad , \\ \langle a_0^2 \rangle &= \frac{\hbar\omega_0^3}{2m_0} \end{aligned} \tag{16}$$

The mean-square fluctuations in Eq. (16), provide the coupling to the oscillator and the gravitational effects. The mean-square power fluctuation of the oscillator is given by

$$\langle P_M^2 \rangle = m_0^2 \langle a_0^2 \rangle \langle v_0^2 \rangle = \left(\frac{\hbar \omega_0^2}{2} \right)^2 \tag{17}$$

The smallness of $\Gamma_0 \omega_0 = 1$ implies that the oscillator is extremely underdamped [6]. Once stimulated, it will continue to oscillate for a long time. This fact greatly simplifies what follows.

In an underdamped oscillator, the *relative damping factor*, ζ, may be defined in terms of the power lost from the mean power fluctuations at the natural frequency.

$$\frac{\hbar\omega_\zeta^2}{2} = \frac{\hbar\omega_0^2}{2} = -\frac{\hbar(\omega_0\zeta)^2}{2} \tag{18}$$

where the power term on the left is the difference between the initial mean power of the oscillator and the power lost to the local environment. They were radiated and absorbed back into the EM ZPF.

The value of ζ is a variable in the coordinate system of the distant observer. It may be thought of as a deficit in the equilibrium condition of Eq. (6). These are photons that were radiated and not reabsorbed by the oscillator, i.e., lost to the environment.

In agreement with the underdamped oscillator, a naturally variable frequency (energy) arises that is dependent on the relative damping factor [6].

$$\omega_\zeta = \omega_0 |\sqrt{1 - \zeta^2}| \tag{19}$$

Increased damping, such that $\zeta > 0$ will result in $\omega_\zeta < \omega_0$ and thereby, reduce the ground state energy of the oscillator below its natural value.

Similarly, substituting the new resonant frequency, ω_ζ into Eq. (17) yields a reduced power fluctuation.

$$P_0 = \frac{\hbar\omega_0^2}{2}$$
$$P_\zeta = P_0(1-\zeta^2) \tag{20}$$

The key new idea that permits this phenomenon to be interpreted as space-time curvature is as follows. Given equation (5) and the understanding that in the coordinates of the distant observer, the relative coordinate velocity of light varies with the relative available power. The coordinate velocity of light, c_k may be expressed anew as,

$$c_\zeta = c_0(1-\zeta^2) \tag{21}$$

From this, wavelength and mass may be determined from the dispersion relationship in the usual way,

$$\lambda + 2\pi\frac{c_\zeta}{\omega_\zeta} = 2\pi\frac{c_0}{\omega_0}|(1-\zeta^2)^{1/2}| \tag{22}$$

$$m = \frac{\hbar\omega_\zeta}{c_\zeta^2} = \frac{\hbar\omega_0}{c_0^2}|(1-\zeta^2)^{-3/2}| \tag{23}$$

In total, all of the references in Table 1 that apply to GR and the PV Model can be reproduced by substituting the metric components with the local relative damping factor, as shown in Table 2.

$$(1-\zeta^2)^{-1} = \left|\sqrt{g_{11}/-g_{00}}\right| \tag{24}$$

It may be inferred by inspection that for a spherical mass with a negligible net charge, such as the planet Earth with mass $M_{\mathrm{E}} = 5.972 \times 10^{24}$ kg and radius $R_{\mathrm{E}} = 6.371 \times 10^6$ m, the relative damping factor is,

$$\zeta = \sqrt{\frac{2GM_{\mathrm{E}}}{c_0^2 R_{\mathrm{E}}}} \tag{25}$$

The ratio, $2GM/(c_0^2 R)$ is the familiar gravitational potential found in the Schwarzschild solution of GR, [13] and in the PV Model [14, 15]. Where,

$$K = (1-\zeta^2)^{-1} \equiv \left(1 - \frac{2GM}{c_0^2 R}\right)^{-1} \tag{26}$$

The normalized frequency shift at the surface of the Earth may then be expressed as,

$$\frac{\omega - \omega_0}{\omega_0} = |\sqrt{1-\zeta^2}| - 1 = 6.961 \times 10^{-10} \tag{27}$$

The normalized value for the frequency shift of the oscillator appears to be very small, but it results in a gravitational acceleration of $g = 9.81\ ms^{-2}$. Notice that it does not take much of a frequency shift to generate significant results.

The mean-square fluctuations from Eq. (16) may be restated in terms of the relative damping factor,

$$\langle x_\zeta^2 \rangle = \frac{\hbar}{2m_0\omega_0}(1-\zeta^2) \ ,$$
$$\langle v_\zeta^2 \rangle = \frac{\hbar\omega_0}{2m_0}(1-\zeta^2)^2 \ ,$$
$$\langle a_\zeta^2 \rangle = \frac{\hbar\omega_0^3}{2m_0}(1-\zeta^2)^3 \tag{28}$$

TABLE II: General Comparison of Relative Damping Factor vs the PV Refractive Index

Variable Refractive Index $K = \|(g_{11}/-g_{00})^{1/2}\|$	**Variable Relative Damping** $(1-\zeta^2)^{-1}$	**Description**
$c_k = c_0/K$	$c_\zeta = c_0(1-\zeta^2)$	Speed of light
$\Delta x = \Delta x_0/\|K^{1/2}\|$	$\Delta x_\zeta = \Delta x_0\|(1-\zeta^2)^{1/2}\|$	Length
$\Delta t = \Delta t_0\|K^{1/2}\|$	$\Delta t_\zeta = \Delta t_0 \left\|(1-\zeta^2)^{-1/2}\right\|$	Time
$v = v_0/K$	$v_\zeta = v_0(1-\zeta^2)$	Velocity
$a = a_0/\|K^{3/2}\|$	$a_\zeta = a_0 \left\|(1-\zeta^2)^{3/2}\right\|$	Acceleration
$m = F/a = m_0\|K^{3/2}\|$	$m_\zeta = m_0 \left\|(1-\zeta^2)^{-3/2}\right\|$	Mass
$\omega = 2\pi/\Delta t = \omega_0/\|K^{1/2}\|$	$\omega_\zeta = \omega_0 \left\|(1-\zeta^2)^{1/2}\right\|$	Frequency
$\Delta E = \hbar\omega = \Delta E_o/\|K^{1/2}\|$	$\Delta E = \Delta E_0 \left\|(1-\zeta^2)^{1/2}\right\|$	Energy

This illustrates how the mean-square particle fluctuations transform according to the relative damping factor. Note that this is identical to how such variables behave in a gravitational field, under GR.

As a result of increased relative damping, a particle's frequency (clock) is slowed and its mean-square position fluctuation (length) contracts. There is less available power to inflate matter to its proper scale, as observed by a distant observer in an unaltered space-time.

There is less available power, because the power provided by the ZPF source is radiated away by the damping of the oscillation. This explains why gravity has negative energy density, i.e., an energy density less than the ZPF. Matter in a gravitational field is oscillating at energies less than the normal ground state energy in a region without a gravitational field. It is less than its ground state energy in a ZPF because the ZPF sets the baseline driving power (the a.c. source), and the radiative damping (loss) reduces the energy and the available power to a value below that baseline. This energy deficit is why it is required to do work to climb a hill.

5. ENERGY DENSITY

Equation (29) expresses the electrostatic force between two identical charges, q, separated by a distance r_0.

$$8\pi r_0^2 \rho_{\rm E} = \alpha\hbar\frac{c_0}{r_0^2} = N\frac{q^2}{4\pi\epsilon_0 r_0^2} \tag{29}$$

where $\alpha = q^2/(4\pi\epsilon_0\hbar c_0)$ is the fine structure constant and $\rho_{\rm E}$ is the local energy density of the electric field surrounding the charges.

$$\rho_{\rm E} = \frac{1}{2}\epsilon_0 E^2 = \frac{\epsilon_0}{2}\left(\frac{q}{4\pi\epsilon_0 r_0^2}\right)^2 \quad Jm^{-3}\ . \tag{30}$$

Equation (29) can be expressed as a function of the relative damping dependent variables presented in Table 2.

$$8\pi r_\zeta^2 \rho_\zeta = \alpha\hbar \frac{c_\zeta}{r_\zeta^2} N \tag{31}$$

The right hand side of this equality is invariant with respect to changes in the relative damping factor, therefore the left hand side must also be invariant to these changes. The individual variables, however, are not invariants. c_{zeta} is covariant with r_ζ^2 such that their ratio remains constant.

On the left hand side of the equation, the only two dependent variables are the area, r_ζ^2 and the energy density, ρ_ζ, which must be contravariant variables. This means that when r_ζ^2 contracts due to increased damping, ρ_ζ must increase by the same proportion such that their product remains invariant. Therefore, the energy density and the relative damping factor must have the following relationship.

$$\rho_\zeta = \rho_{\mathrm{E}}(1-\zeta^2)^{-1} \tag{32}$$

This result is perfectly consistent with GR and the PV Model.

In GR one would say that gravity resulting from the increased local energy density caused the gravitational length contraction. Then the relative refractive index and the relative damping factor may be defined in terms of the relative energy densities.

$$K = (1-\zeta^2)^{-1} \equiv \frac{\rho}{\rho_0} \tag{33}$$

where, ρ_0 would be the value of the vacuum energy density (any source, electrostatic or otherwise), in the reference frame local to the distant observer, and ρ is the energy density of the identical system being observed from a distance. In this context, this model of quantum gravity may be summarized as follows;

The increased energy density in the region local to the oscillator leads to increased radiative damping and a loss of power. This results in length contraction of the mean-square position fluctuations, along with a reduction in frequency, which is observable as relativistic time dilation effects. Length contraction does not occur independently from time dilation effects, because both result from the same root cause, i.e., a change in the relative damping factor, ζ .

Up until now, only cases where $\zeta = 1$ have been considered. In the case where $\zeta = 1$, the oscillator is said to be critically damped. From equation (26), this is understood to be the event horizon of a black hole in the Schwarzschild space-time. In cases where $\zeta > 1$, the oscillator is overdamped and will not oscillate, but rather decay exponentially. This gives engineers an intuitive understanding for what it means when it is said that "time stops" at the event horizon or when the speed of light is reached. Literally, it means that damping has increased to the point where the natural oscillation can no longer exist.

Sensibly, one can surmise that it is the very same process that results in time dilation and Lorentz contraction in special relativity (SR). The gravitational potential in equation (25) is a ratio of velocities squared. It is identical to the way the velocity potential arises in SR as v^2/c_0^2 . Therefore, it may be deduced that in SR, the relative damping factor is

$$\zeta^2 = \beta^2 \equiv \frac{v^2}{c_0^2} \tag{34}$$

Obviously, this does not change any of the physics associated with SR or Lorentz invariance. It is simply a reinterpretation of the physics in terms which are more appropriate for engineering purposes.

This equality between GR and SR provides a clue as to how the damping factor should be interpreted. The damping factor may be expressed as a damping ratio, relative to the natural frequency [6].

$$\zeta = \frac{\sigma}{\omega_0} \tag{35}$$

where, σ is a scattering parameter. It is also referred to as the Neper frequency. It may be interpreted as the rate at which collisions cause a stimulated emission from the oscillator, resulting in a loss of power.

Given the Compton frequency of an electron as its natural frequency,

$$\frac{\omega_0}{2\pi} = \frac{m_e c_0^2}{\hbar} = 1.222 \times 10^{20} \quad \text{Hz} \tag{36}$$

the change in energy at the surface of the Earth, relative to the distant observer is given by equation (37).

$$\Delta E = \hbar\omega_0 \left(\left| \sqrt{1-\zeta^2} \right| - 1 \right) = -5.637 \times 10^{-23} \text{ J} \tag{37}$$

This is a very small number, but given that Avogadro's number is 6.022×10^{23} particles per mole, it does not take many grams of matter before the energy requirement becomes enormous. Why it is so enormous has to do with the Neper frequency, which may be calculated from Eqs. (25) & (35).

$$\sigma = \frac{\omega_0 \zeta}{2\pi} = 4.56 \times 10^{15} \text{ Hz} \tag{38}$$

Note that this frequency is just beyond the range of visible light, in the near ultraviolet spectrum, 65.7 nm . It is reproducible and within the realm of modern technologies. Unfortunately, it only applies to electrons. For a proton, the frequency is more than 3 orders of magnitude higher at, $\sigma_{\text{proton}} = 8.4 \times 10^{18}$ Hz , with an energy of 35 KeV . This is in the hard X-ray/gamma-ray spectrum, where matter begins to become transparent.

If, by some means not yet devised, engineers can provide a way to reduce the relative Neper frequency and reduce the amount of relative damping within matter, such matter will inflate and become lighter.

In regards to an accelerating spaceship, a means by which to reduce the relative damping that is increasing throughout the ship as $v \to c_0$, will increase the maximum velocity and reduce the mass to be transported. The cosmic speed limit will be lifted and the dream of warp drives and starships become realistic endeavors.

On the other hand, if engineers were to increase the Neper frequency to increase relative damping, objects would gain weight, contract, and become denser. The possibility of a box that is bigger on the inside becomes not so unimaginable if objects shrink as they enter the box, and are then preserved by a reduced clock-rate.

Most importantly, applying gradients to the potential will allow the invention of devices which can control gravity.

6. DISCUSSION

It was shown that a correlation exists between the observations used in GR to determine space-time curvature and the relative radiative damping factor of the quantum mechanical harmonic oscillator, which affects our measuring devices. The relative frequency and energy varies as a function of the damping factor, in accordance with the metric coefficients. It was shown that the damping factor can take the form of the gravitational potential, by matching it to the Schwarzschild solution of GR and calculating the frequency shift of the Compton frequency of the electron, at the surface of the Earth.

Variations in frequency, and therefore in the energy of the oscillator, affects the mean-square fluctuations in length, velocity, acceleration, and power of the oscillator. This results in what is perceived and interpreted as space-time curvature in the classical theory.

Note that this model rules out certain geometries in GR. For example, shift-only space-times where length contraction occurs without time dilation, or vice versa. The two are linked by the same statistical processes that govern quantum mechanics and determine the mean-square fluctuations of matter.

In GR, a gravitational field has negative energy density. This means its energy density is less than that of the surrounding vacuum. In the Engineering Model of Quantum Gravity presented here, matter is inflated to its maximum relative ground state energy by the ZPF, only when it is in a vacuum far from other matter, i.e., in the local frame of the distant observer. As two objects are brought close together, their respective fields and power spectrums overlap, such that interference occurs that damps the resonant frequencies in both objects. Increased local vacuum energy density increases the radiative damping. This lowers the relative energy (frequency) of the composite oscillators below their normal value and allows them to attract each other gravitationally.

From a cosmological perspective here on Earth, if the relative damping in our solar system were increasing linearly with time, such that the length of 1 meter were contracting by just 6.935 nm/century relative to the distant galaxies and supernova, it would appear from our perspective that the universe is expanding. Light arriving from the distant past is redshifted, because our local measuring devices have contracted. When we measure the increasing velocity of expansion across great distances, far into the distant past, to when matter was in a hotter, more inflated state, we measure the Hubble constant [16].

Consider atoms and nuclei which are cooling from a hotter, less dense state in the distant past. This would be a natural thermodynamic process for matter to undergo. However, there would be no way to measure such a small effect locally, because there is nothing local that is unaffected by this. The only references to compare to are the distant stars. Therefore, the Hubble constant may be evidence that such a process is taking place and that the thermodynamic energy of the universe is actually running down as it should be. Matter absorbs higher frequency photons from the ZPF and emits lower frequency photons due to accelerations.

The opposite conclusion would be reached if matter were inflating rather than contracting. In such a scenario, the universe would appear to be getting smaller. This is how a warp drive would be described. Matter is inflated by a warp field which makes the distance from point A to point B in the universe literally shorter in scale, relative to the reference frame of the inflated ship.

7. CONCLUSION

This engineering model firmly establishes a viable solution to quantum gravity for engineers within the standard model of quantum electrodynamics. It opens the door to new innovations that might permit artificial gravity or anti-gravity technologies to be invented. This is through the use of stimulated emission, increased or reduced radiative damping, or by amplification of the resonant driving fields that inflate matter to higher ground state energies. Engineers now have a new set of old, familiar tools to work with when thinking about gravity and metric engineering [3].

REFERENCES

[1] Type 1A Supernovae, hubblesite.org. (Last Accessed 16, July 2016)

[2] P. W. Milonni, *The Quantum Vacuum –An Introduction to Quantum Electrodynamics*, Academic Press, Inc. 1994. Secs., 2.6 - 2.13, 3.1 - 3.3, 5.1 - 5.4, 11.8. (Book)

[3] H. E. Puthoff, "Advanced Space Propulsion Based on Vacuum (Spacetime Metric) Engineering", JBIS, **63**, pp. 82-89, `http://www.earthtech.org/pubs`, Nov. 2010.

[4] H. E. Puthoff, Polarizable-Vacuum (PV) Representation of General Relativity, `https://arxiv.org/abs/gr-qc/9909037`, Sept., 1999. (Last Accessed 16, July 2016)

[5] H. E. Puthoff, et. Al., Engineering the Zero-Point Field and Polarizable Vacuum for Interstellar Flight, JBIS, **55**, pp.137-144, `https://arxiv.org/abs/astro-ph/0107316`, Jul. 2001. (Last Accessed 16, July 2016)

[6] RLC Circuit, `en.wikipedia.org/wiki/RLC_circuit`, (Last Accessed 16, July 2016)

[7] H. E. Puthoff, "Quantum Ground States as Equilibrium Particle-Vacuum Interaction States", Quantum Stud.: Math. Found., **3**, No.1, pp.5-10, 2016.

[8] T. J. Desiato, "The Electromagnetic Quantum Vacuum Warp Drive", JBIS, Vol. **68**, pp. 347-353. Apr. 2016.

[9] P. W. Milonni, Quantum Mechanics of the Einstein-Hopf Model, Am. J. Phys. **49**, pg. 177 (1981a)

[10] P. W. Milonni, Radiation Reaction and the Nonrelativistic Theory of the Electron, Phys. Lett. **82A**, pg. 225. (1981b)

[11] H. E. Puthoff, Casimir Vacuum Energy and the Semiclassical Electron, International Journal of Theoretical Physics **46**, (12), pp 3005-3008, `http://www.earthtech.org/pubs`

[12] Larmor Formula, `en.wikipedia.org/wiki/Larmor_formula`, (Last Accessed, 16, July 2016)

[13] Schwarzschild Metric, `en.wikipedia.org/wiki/Schwarzschild_metric`, (Last Accessed 16, July 2016)

[14] T. J. Desiato, General Relativity and the Polarizable Vacuum, 12 March, 2006. (Last Accessed 16, July 2016). `vixra.org/pdf/1203.0100v1.pdf`

[15] J. G. Depp, Polarizable Vacuum and the Schwarzschild Solution, `researchgate.net/publication/265111294_Polarizable_Vacuum_and_the_Schwarzschild_Solution`, May 2005. (Last Accessed, 16, July 2016)

[16] Hubble's Law, `en.wikipedia.org/wiki/Hubbles_law`, (Last Accessed, 16, July 2016)

EVIDENCE OF THERMONUCLEAR EXPLOSIONS ON MARS

John E. Brandenburg
Morningstar Applied Physics, LLC

The concentration of ^{129}Xe in the Martian atmosphere, the evidence from ^{80}Kr abundance of intense particle flux over the northern young part of Mars, and the excess abundance of uranium and thorium on Mars surface relative to Mars meteorites, can be explained by two large thermonuclear explosions on Mars in the distant past. Based on the pattern of thorium and radioactive potassium gamma radiation, the explosions were centered in the northern plains in Mare Acidalium at approximately 50N, 30W, near Cydonia Mensa; and in Utopia Planum at approximately 50N 120W near Galaxias Chaos. The xenon isotope mass spectrum of the Mars atmosphere matches that from open air nuclear testing on Earth and is characteristic of fast neutron fission rather than that produced by a moderated nuclear reactor.

A signature feature of Mars atmosphere is the predominance of two noble gas isotopes, ^{129}Xe and ^{40}Ar, over their other respective isotopes relative to Earth and other inventories; see Figure 1. These isotopic features are unique to Mars, and allowed the identification of Mars as the parent body of the SNC meteorites. The high concentration of ^{129}Xe in the Martian atmosphere, the evidence from ^{80}Kr abundance of intense 10^{14} cm^{-2} neutron flux over the Northern young part of Mars, and the detected pattern of excess abundance of uranium and thorium on Mars surface, relative to Mars meteorites, first seen by the Russians and now confirmed by the Mars Odyssey Spacecraft Gamma Ray Spectrometer, mean that the surface of Mars was apparently the site of massive radiological events. They created large amounts of signature isotopes and covered the surface with a thin layer of radioactive debris enriched in certain elements relative to its subsurface rocks. This pattern of phenomenon can be explained as due to two large anomalous nuclear explosions on Mars in the past.

Xenon Isotope Abundance Normalized to ^{130} Xenon Abundance

Inventory	^{124}Xe	^{126}Xe	^{128}Xe	^{129}Xe	^{130}Xe	^{131}Xe	^{132}Xe	^{134}Xe	^{136}Xe
Earth	2.337	2.180	47.146	649.58	≡100	521.27	660.68	256.28	217.63
Earth w/o NT	2.337	2.180	47.146	605.3	≡100	518.73	651.8	247.0	207.5
Earth Δ	0.00	0.00	0.00	44.28	0	2.54	8.88	9.28	10.13
Mars	2.45	2.12	47.67	1640.0	≡100	514.7	646.0	258.7	229.4

FIG. 1: Xenon isotope abundance comparison between Earth and Mars

A predominance of ^{129}Xe is also present in a component of the Earths atmosphere that can be traced to fast neutron fission reactions from nuclear weapons testing and production. Moderated nuclear reactors, on the other hand, create little if any of this ^{129}Xe. Therefore, the signature ^{129}Xe predominance of Mars can be explained as due to fast neutron fission of ^{238}U and also ^{232}Th, which shares this same fission product property in fast neutron fission. The hyper-abundance of ^{40}Ar is consistent with neutron irradiation of ^{39}K over large areas of Mars surface, with transmutation to ^{40}K and subsequent decay.

The ^{129}Xe anomaly at Mars is profound. The ratio of ^{129}Xe to ^{130}Xe is around 1 most places in the solar system, including Earth. On Mars it is 2.5. The basement rocks of Mars show a ratio closer to 1. The Mars atmospheric Xe has evolved in time, with younger meteorites showing more ^{129}Xe.

The large amount of ^{15}N in the Mars atmosphere relative to Earth, while carbon and oxygen are nearly Earth-like, can be also explained by the intense neutron bombardment that would accompany any nuclear detonation that created such large amounts of ^{129}Xe. Evidence for this is seen in the correlation between ^{129}Xe and ^{15}N in rock samples from the primordial mars meteorite ALH84001. Enrichment in ^{15}N would occur since the predominate isotope, ^{14}N, has a much larger neutron absorption cross section than either O or C.

Some have proposed that ^{129}I, which decays into ^{129}Xe with a 15.7 million year half-life, was sequestered at planetary accretion and the resultant ^{129}Xe outgassed later after an early atmosphere was lost. These models require Mars to accrete itself and lose its early atmosphere quickly, in a few million years. Mars

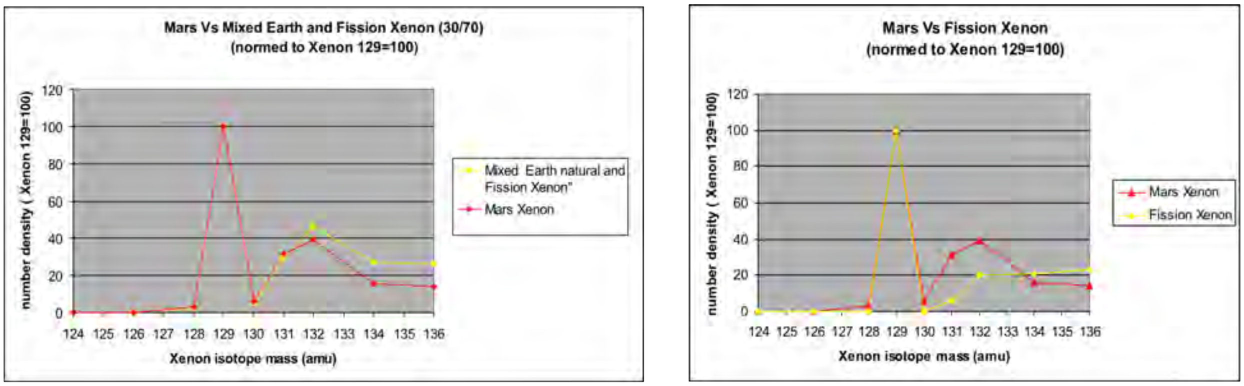

(a) Natural Xenon on Mars seems similar to Earth

(b) Fission Xenon on Mars seems much higher than normal.

FIG. 2: **Comparison of Xenon isotope levels on Earth and Mars**

accretion time is poorly constrained and may have lasted 30 million years. The same phenomena would have happened at Earth and yet Earth follows the same solar system pattern. Such sequestration models also require the Mars replacement atmosphere to have been thin, when overwhelming evidence, based on abundant water channels flowing into a liquid ocean and strong outgassing, show that whatever atmosphere replaced the Mars atmosphere at accretion was dense and would have reflected its basement rock gases. Other models suggest that a heavy bombardment of gas rich carbonaceous chondrite material or comets after accretion was the source of the ^{129}Xe anomaly.

The problem with either an intense carbonaceous chondrite or cometary source for the ^{129}Xe is these reservoirs display normal solar system ratios of Xe isotopes. The average carbonaceous chondrite Xe spectrum has xenon ratios similar to Earth. As for comets, the only Xe data for them, recently obtained from the Rosetta mission landing on comet Churyumov-Gerasimenko, showed its Xe isotope spectrum to follow the Solar system ratios. Even the ^{129}Xe anomaly seen in isolated well gases on Earth, believed to be due to ^{129}I sequestration, displays deviations from the Solar System norm of only 5%, whereas Mars is at 250%. Therefore, Mars ^{129}Xe levels are profoundly anomalous, and other explanations can only be admitted if the vast amount of other Mars and Solar system data is ignored, see Fig 2.

Mars xenon is found to match closely the component in the Earths atmosphere produced by nuclear weapons programs, both hydrogen bomb testing and plutonium production. It is found that Mars xenon can be approximated by a mixture of 70% nuclear-testing xenon and 30% natural Earth xenon.

Taken together, this suggests Mars was the site a massive nuclear event.

References

[1] Brandenburg, J.E., Evidence for a large, natural, paleo nuclear reactor on Mars, 42nd Lunar and Planetary Conference, 2011.

[2] Glasstone, S., and P.J. Dolan, The effects of nuclear weapons, 3rd ed., US Gov. Printing Office, 1977.

[3] Mahaffy, P., et al., Abundance and Isotopic Composition of Gases in the Martian Atmosphere from the Curiosity Rover, *Science*, **341**, 263, 19 July 2013.

[4] Mathew, K.J., et al., Martian atmospheric and indigenous components of xenon and nitrogen in the Shergotty, Nakhla, and Chassigny group meteorites, Meteoritics and Planetary Science, July 1998.

[5] Rao, M.N., et al., Isotopic evidence for a Martian regolith component in shergottite meteorites, J.G.R. Planets, 116, Issue E8, August 2011.

[6] Surkpov, Y.A., et al., Determination of the elemental composition of Martian rocks from Phobos 2, Nature, 341, 595, 1988.

[7] Swindle, T.D., et al., Xenon and other noble gases in Shergottites, Geochemica et Cosmochemica Acta, 50, 1001, 1986.

ELECTRON ROTATING WAVE THEORY AND THE EM PROPELLER

William H. F. Christie
AIBC
Port Coquitlam, British Columbia

I have reverted to classical concepts of space and time to develop a pure wave theory of the electron (or fermion) as a simple *Rotating Wave*. The essential postulate is that an electromagnetic wave is brought into classical rotation by a local binding energy. The spin model then yields the required phenomena of charge, relativity, mass, gravity, and quantum mechanics in a naturally derived and graphic fashion.

1. INTRODUCTION

While completing a degree in architecture after another degree in economics and studies in physics, I discovered a Rotating Wave Theory (RWT) of the Electron that appeared to explain relativity, mass, gravity, charge and quantum mechanics. Essentially, the Electron Rotating Wave is a **wave function in the form of a propeller transmitting itself through space**. Like a photon, **it thus has traction in space**. In order to test this theory, a model was thus devised in the shape of a propeller inside a glass vacuum ball, mounted on a rolling cart, and of course devoid of any outside electromagnetic fields. A more accurate test would of course be done in space, see Figs. 1 & 2.

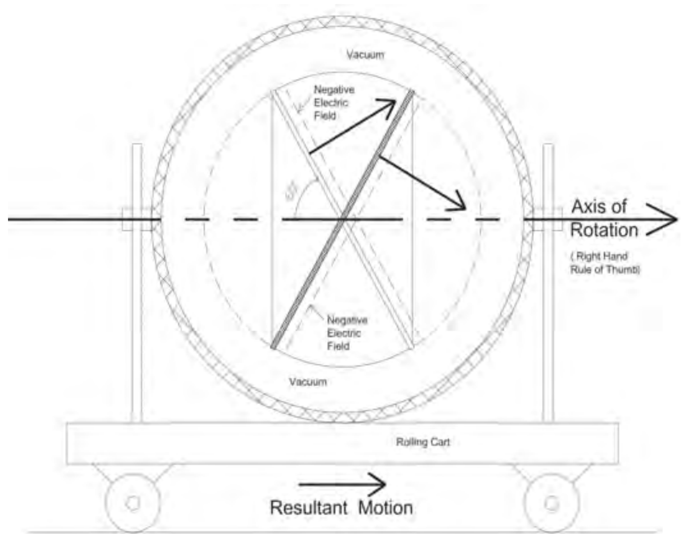

FIG. 1: Charged Vanes are rotated clockwise creating a helical field which propels the cart to the right

An experiment has not yet been done, but a brief overview of the RW Theory shows how compelling the Rotating Wave might be and thus the potential for the EM Propeller as a "massless rocket". The RW Theory is presented with respect to relativity, gravity and quantum mechanics and then the RW 5^{th} Vector v_T is related to Kaluza 5^{th} Dimension.

2. ELECTRON ROTATING WAVE AS A BASIC FORM OF MATTER AND THE SPECIAL THEORY OF RELATIVITY

RWT posits that the apparent space-time connection and quantum mechanics are due to the Rotating Wave function. Specifically, a **Rotating Wave** (RW) is formed by a photon brought into rotation by some kind of binding energy, creating an electron and positron. At a certain radius, the RW has a tangential velocity at the speed of light. At greater radii, the velocity is superluminal and lesser radii sub-luminal.

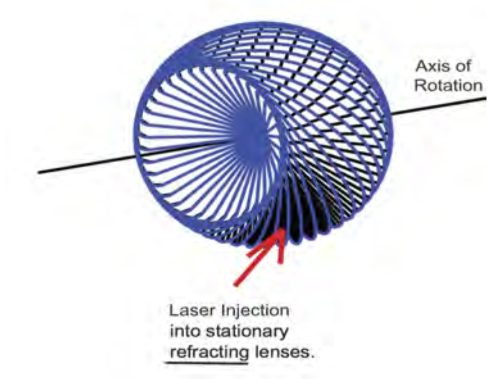

FIG. 2: Laser light is injected. Translational momentum and energy are redirected and transformed into Rotational energy and momentum.

Furthermore, the electromagnetic nodes of the photon are included in the RW, giving cause to Quantum Mechanics.

A stationary RW would induce an electric monopole and magnetic dipole. The only way an electron RW can move is along its axis of rotation (or spin). In accordance with Maxwell, the rotating wave fronts must be perpendicular to both the electric and magnetic fields and thus both length contraction and time dilation in the Special Theory of Relativity (STR) may be alternatively interpreted as due to angular realignment of the wave fronts as the RW traces out a helical path in space. Effective length contraction is obvious with the inclined wave front and time dilation is due to a longer helical path of rotation. See following Figs. 3, 4, and 5.

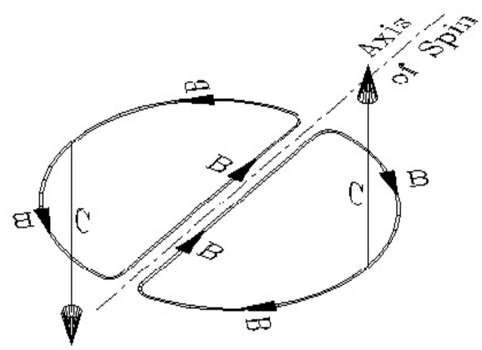

FIG. 3: Stationary RW $v_R = c$ Oblique Elevation of stationary electron wavicle with magnetic lines of force B (electric field not shown here for simplicity) and nodal wave front spinning with tangential velocity c.

Notice in Fig. 3., the arrayed vanes of the RW are compacted and mass energy is increased. Vectorially, the total energy is composed of kinematic rotation (plus binding energy) plus the added translational (linear) motion. The same can be derived for momentum. Just as a photon's electric and magnetic fields react with space in order for it to move forward, so does the RW thus creating magnetic moment plus rotational and linear inertia. This might enable new speculative insights into propulsion by injection of energy and conversion from rotational to translational motion in the form of an EM Propeller. *Newton's 3rd Law would be upheld with momentum conserved by rotation* as well as translational motion in the RW.

3. ROTATING WAVE THEORY OF GRAVITY

Albert Einstein predicted correctly by the "principle of equivalence" in his General Theory of Relativity that matter would gravitate or bend light and slow down time. He found a deeper significance than mere coincidence that a gravitational reference system could be made equivalent to a uniformly accelerated reference system because it enabled him to extend his Special Theory of Relativity to his all-encompassing

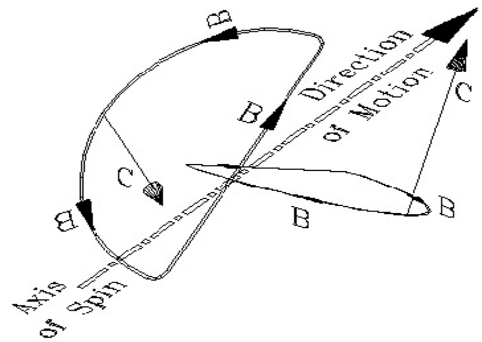

FIG. 4: Moving RW $v_R = (c^2 - v^2)^{1/2}$ Oblique Elevation of moving electron with magnetic lines of force B and nodal wave fronts reoriented at an angle as previously illustrated in Figure 6.

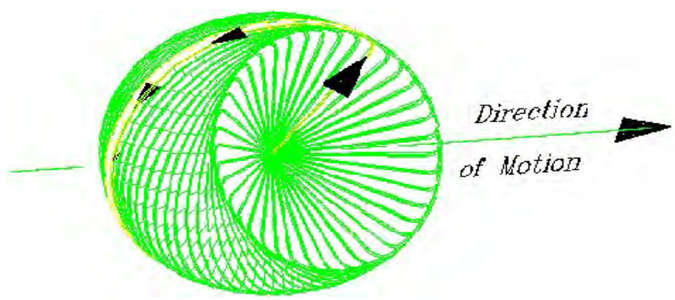

FIG. 5: Moving RW Creating a Right-handed Magnetic Field - Oblique Elevation of moving electron with wave fronts of lessor field strengths shown as well as the nodal wave front (highlighted lines with arrows). This figure clearly indicates a right-handed induced magnetic field.

General Theory.

According to the RW, free space or vacuum is defined as an electromagnetic field in which light and matter waves are able to propagate. The basic premise of this theory of gravity is that the binding energy (EB) holds the RW in rotation by affecting the permittivity and permeability of free space. Thus any other incidental wave will also be bent and slowed down by the binding energy of the RW, although to a lessor degree.

The second premise of this theory of gravity is that uniformity of gravitational acceleration at a constant distance about a spherical mass is simply due to the fact that such mass is composed of many RW's at various angles of spin and random motion. Therefore, while the electron has a gravitational field severely distorted by its magnetic poles, larger non-elementary particles and groups of matter would have more uniform gravitational fields at a given radius.

Furthermore, since the rotating wave is itself light, then the path of that rotating wave will also be bent and slowed down in the same manner by another RW. Hence, spin frequency of two RW?s in close proximity will be less than those separated at a greater distance. Any energy given up in the interaction between rotating waves will thus form background radiation and lead to the apparent expansion of the universe and slowing down of time.

In summary, the Electromagnetic Wave Theory of Gravity first predicts the gravitation and slowing down of light and thus second the gravitation and slowing down of the time cycle of matter. The "principle of equivalence" can be completely explained by the equivalence of light and matter according to the concept of the RW.

4. DERIVATION OF $G_{k\ell}$ IN ROTATING WAVE THEORY

The Rotating Wave also shows how tensor math allows for the calculation of intrinsic curvature of space-time. According to relativity, it must be just as valid in one reference frame to analyze the path of free falling light influenced by the gravitational field of a stationary mass in order to describe the curvature of space-time as it is to postulate in another reference frame the curvature of space-time by the mass energy density tensor of an attracting mass which is in motion.

Consider the dashed helical path of the Rotating Wave as illustrated in the previous Fig. 6. The helical path can be defined by a time derivative of the position vector $POS_c = POS_v + POS_T \cdot POS_v$ is the vector in the forward moving translational motion of the Rotating Wave and same direction of rotational axis. POS_T is a rotor and is the vector in the purely rotational motion. If the velocity vector v_T is greater than zero (or less than zero), then the velocity vector c of the Rotating Wave with constant speed of light will spiral outwards (or inwards):

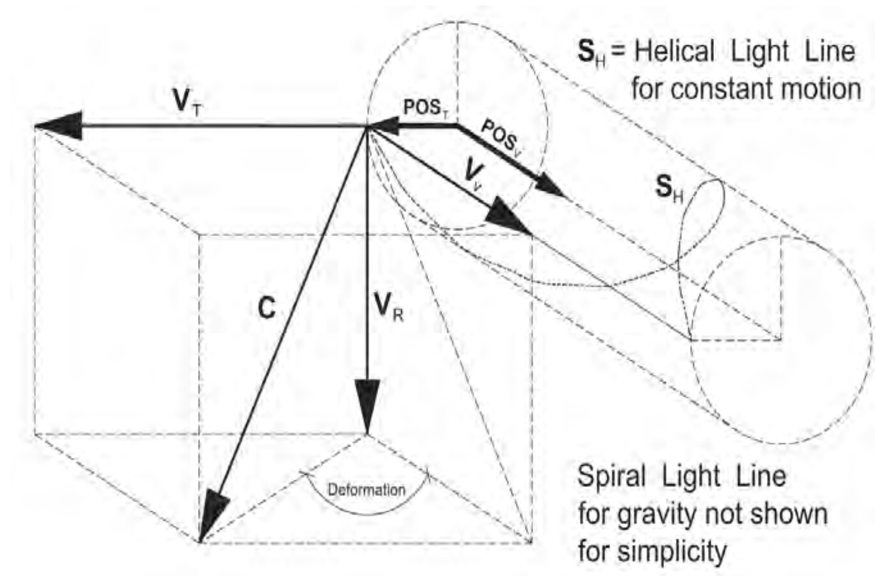

FIG. 6: Rotating wave of the Electron (fermion). Position vectors $POS_c = POS_v + POS_T$, where POS_T rotates. Velocity vectors, $c = v_v + v_R + v_T$.

$$
\begin{aligned}
c &= \frac{dPOS_C}{dt} = \frac{dPOS_v}{dt} + \frac{dPOS_T}{dt} = v_v + \frac{dE_T}{dt}POS_T + E_T\frac{dPOS_T}{dt} \\
c &= v_v + v_R + v_T
\end{aligned} \tag{1}
$$

Also the base vectors for the Riemannian space time located along the light line are defined by the partial derivative of the position vector:

$$
e_\ell = \partial POS_c/\partial x^\ell = \partial POS_v/\partial x^\ell + \partial POS_T/\partial x^\ell = POS_{c,\ell} = POS_{v,\ell} + POS_{T,\ell} \tag{2}
$$

Thus $e_c c = e_\ell u_\ell = (POS_{v,\ell})u^\ell + (POS_{T,\ell})u_\ell = dPOS_v/dt + dPOS_T/dt$. Thus the path of the Rotating Wave with constant speed of light is defined by five vectors in our familiar three dimensions of space by:

$$
c = v_v + v_R + v_T \tag{3}
$$

of which $v_v = v_X + v_Y + v_Z$.

The spiral helical path also lies within a generated surface that can be described in Riemannian five dimensional space-time with

$$
c = e_\ell u^\ell = e_v u^v + e_r u^r + e_t u^t \tag{4}
$$

of which again $e_v u^v = e_x u^x + e_y u^y + e_z u^z$ (with implied Einstein summation on ℓ).

Note that in the spiral condition: $c = v_v + v_R + v_T$ whereas before the simple helical (cylindrical) form of the Rotating Wave in accordance with the Special Theory of Relativity, $v_T = 0$ and thus $c = v_v + v_R$.

Note also that the $e_r u^r$ certainly corresponds to the rotational velocity v_R of the Rotating Wave while $c = e_c c$ corresponds exactly to $c = v_v + v_R + v_T$, so the $e_v u^v = e_1 u^1 + e_2 u^2 + e_3 u^3$ must as a result correspond to the forward (translational) velocity of the Rotating Wave.

When there is an attracting mass, gravity will accelerate a free falling Rotating Wave and also cause it to spiral outwards. The combination of spiral and helical path will create intrinsic curvature.

4.1 General Surfaces – Curvature Calculation – $R_{k\ell}$

The intrinsic curvature of the spiral helical surface can be calculated by the Riemannian curvature tensor $R^n_{ik\ell}$ and sufficiently by the Ricci tensor $R_{k\ell} = R^n_{k\ell n}$ which is the contraction of the curvature tensor. Note vectors are embolded,

$$R_{k\ell} = [T^n_{\ell n,k} + T^n_{sk}T^s_{\ell n}] - [T^n_{\ell k,n} + T^n_{sn}T^s_{\ell k}] \tag{5}$$

and with explicit notation of base vectors, rewritten as:

$$R_{k\ell} = (e_{\ell,nk} - e_{\ell,kn})e^n \quad . \tag{6}$$

Rotating Wave Position Vectors and Curvature Calculation – $R_{k\ell}$

Since e_c and e_ℓ lie within the surface $c = e_c c = e_\ell u^\ell$ the following can be found with use of partial derivatives, chain rule and commutation (not written here for brevity):

$$R_{k\ell} = R_c u_\ell c^{-4}(a_n u_k - a_k u_n)e^n \tag{7}$$

where R_c = curvature due to the rotational motion of the wave.

Note: $c = e_c c = e_n u^n$ is always perpendicular to $cR_c = de_c/dt$ and thus the scalar dot product between R_c and $c = 0$. Thus for a Spiral Rotating Wave:

$$R_{k\ell} = R_c a u_k u_\ell c^{-4} \tag{8}$$

while a= acceleration of the u_ℓ velocities and the Ricci scalar

$$R = g_{k\ell}R_{k\ell} = R_c a c^{-2} \tag{9}$$

and

$$G_{k\ell} = R_{k\ell} - \frac{1}{2}g_{k\ell}R = \frac{R_c a}{c^2}\left(u_k u_\ell c^{-2} - \frac{1}{2}g_{k\ell}\right) \tag{10}$$

which compares somewhat with the Einstein Tensor $G_{k\ell} = -8\pi k T_{k\ell}$ where the mass energy density tensor

$$T_{k\ell} = (\sigma + p)u_k u_\ell - g_{k\ell}\, p \tag{11}$$

has been written. Also, the scalar

$$G = g^{k\ell}G_{k\ell} = \frac{1}{2}R_c a c^{-2} \tag{12}$$

Note again, we are deriving the surface curvature where the light line follows the path of the wave which is going at velocity c at certain radii from the axis of spin. That light–line spirals out and the angular velocity thus decreases, slowing down the time cycle of the rotating wave. This is relevant to the apparent expansion of the universe and the apparent slowing down of time. Without this expansion and slowing of time, there can be no intrinsic surface curvature of the path of the rotating wave and thus no gravity.

Line Eq. (8) is very telling. If $a = 0$ or a is perpendicular to R_c, then there will be no intrinsic curvature. In order to get intrinsic curvature, we need spiral expansion of the helical light line plus the forward motion and use of Riemannian geometry.

Where the Rotating Wave had a rotational velocity v_R before at lessor radius of rotation, the time cycle of the Rotating Wave slows down in a gravitational field and v_r is now at a greater radius.

Thus the Rotating Wave of the Wavicle has a built-in function that manifests itself in the apparent slowing down of time and expansion of the universe. The Spiral Condition immediately obviates the need for the Cosmological Constant.

Note, according to the Rotating Wave, the Cosmoloical Constant is not required because the spiral helical Rotating Wave is already slowing down and expanding. In order to maintain the law of energy conservation, the

$$G_{k\ell} = R_{k\ell} - \frac{1}{2} g_{k\ell} R = \frac{8\pi G}{c^4} T_{k\ell} \tag{13}$$

is sufficient.

5. EXPLANATION OF QUANTUM MECHANICS

The concept of the rotating wave explains why Plank's constant h is intimately included and quantized in the characteristics of the electron and all cyclical functions. According to the Definition of Rest (Energy) Mass, h automatically enters any equation of matter. Also, since the two nodes of the RW rotate, the effect of their electromagnetic and gravitational field strengths on an adjacent particle must vary in a cyclical fashion. Therefore, an orbiting electron RW must have a distance from the nucleus which undulates in direct correspondence to the electron's spin. Relativistic effects of the orbiting electron and nuclear particles would of course further define the path of orbit. Furthermore, since the nuclear particles themselves spin and therefore must have cyclical variations in their effective field strengths, then the electron RW must make an integral number of spins for each orbit in order to stabilize in that orbit. Thus orbital energies must be quantized with respect to spin or rotational energies E_R.

Matrix quantum mechanics requires that the energy level of an electron orbiting in an atom be $h\nu(n+1/2)$ where ν is the frequency and n is the number of typical photons which are absorbed or emitted. According to Rotational Kinematics, the energy level should be equivalent to the total angular energy of the electron RW, which is equal to its orbital energy plus its innate rotational energy E_R . The rotational energy $E_R = h\nu/2$ explains why the ground state or "zero point" energy of the electron in an atom must be $h\nu(n+1/2)$ where $n = 0$ for an electron with no orbit.

Also, the concept of the RW simply explains why matter has a wave probability distribution. Since the RW is purely a rotating electromagnetic wave, then the probability of detecting the wavicle near some point in space should be described by a wave function. Given an arbitrary maximum amplitude N, wavelength λ, and spin angular velocity ω, the sinusoidal real wave function of the traveling RW must be defined as:

$$\psi = N \sin\left(\frac{2\pi}{\lambda} S - \omega t\right) \tag{14}$$

6. DIRAC MATRIX EQUATION & ROTATING WAVE VECTORS

In 1928 Paul A.M. Dirac used Pauli spin matrices to combine the Special Theory of Relativity with wave mechanics and naturally derived electron spin in his "Quantum Theory of the Electron" [1]. Dirac maintained that the time derivative operator for the relativistic Hamiltonian $W = ih\partial/\partial t$ should be linear in the first order (and likewise the momentum operator $p_r = -ih\partial/\partial x_r$), just as in the case of the non-relativistic wave equation. Thus Dirac got the idea to factorize the relativistic wave equation in order to get the first order derivative operators which then suggested a positive charge (positron later discovered) as well as the electron.

6.1 Derivation of Dirac's Matrix/Wave Equations:

Dirac first considers the case of no field present and and posits the form of the four dimensional wave equation

$$[p_0 + \rho_1(\boldsymbol{\sigma}, \boldsymbol{p}) + \rho_3 mc]\boldsymbol{\psi} = 0 \tag{15}$$

where $\boldsymbol{\sigma}$ denotes the vector $(\sigma_1,\ \sigma_2,\ \sigma_3)$. Then he adds in vector and scalar potentials to get his Eq. (D14) [**?**]:

$$[p_0 + \frac{e}{c}A_0 + \rho_1(\boldsymbol{\sigma}, \boldsymbol{p} + \frac{e}{c}\boldsymbol{A}) + \rho_3 mc]\boldsymbol{\psi} = 0 \tag{16}$$

and again multiplies the conjugate and non-conjugate to get:

$$\left(p_0 + \frac{e}{c}A_0\right)^2 \boldsymbol{\psi} = \left[\left(\boldsymbol{p} + \frac{e}{c}\boldsymbol{A}\right)^2 + \frac{e\hbar}{c}(\boldsymbol{\sigma}, \boldsymbol{H}) + i\frac{e\hbar}{c}\rho_1(\boldsymbol{\sigma}, \boldsymbol{E}) + m^2c^2\right]\boldsymbol{\psi} \ . \tag{17}$$

After squaring Dirac divides by $2m$ and finds:

$$\begin{aligned} \frac{e\hbar}{c}\frac{(\boldsymbol{\sigma}, \boldsymbol{H})}{2m} &= \frac{e\hbar}{mc} \cdot \boldsymbol{\sigma} = \text{ magnetic moment of 1 Bohr Magneton and} \\ i\frac{e\hbar}{c}\rho_1\frac{(\boldsymbol{\sigma}, \boldsymbol{E})}{2m} &= i\frac{e\hbar}{mc} \cdot \rho_1\boldsymbol{\sigma} = \text{ electric moment with imaginary number} \end{aligned} \tag{18}$$

6.2 Rotating Wave - Vectors and Derivative Operators:

Recall earlier that given an arbitrary maximum amplitude N, wavelength λ , and spin angular velocity ω, the sinusoidal real wave function of the Rotating Wave in motion can be defined as:

$$\psi = N \sin\left(\frac{2\pi S}{\lambda} - \omega t\right) \tag{19}$$

Since $P\lambda = P_c\lambda = h$, then $P^2\psi = (P_v^2 + P_R^2)\psi$ can be derived with $P_c,\ P_v$, and $P_R$as either simple variables or derivative operators as postulated by Erwin Schrödinger. Note, one can extend the Rotating Wave equation into the General Theory of Relativity:

$$P_c^2\boldsymbol{\psi} = (P_v^2 + P_R^2 + P_T^2)\boldsymbol{\psi} \tag{20}$$

Note Dirac terms which relate to the vectors of the Rotating Wave are: $p_0 = P_c,\ p = P_v$, and $m_c = m_0c = P_R$ for constant motion (where m_0 is the Rest Mass of the Rotating Wave). Thus when an electromagnetic field is introduced to the electron, the associated vector potentials can be added respectively:

$$(P_c + (e/c)\boldsymbol{A}_c)\boldsymbol{\psi} = (P_v + (e/c)\boldsymbol{A}_v)\boldsymbol{\psi} + (P_R + (e/c)\boldsymbol{A}_R)\boldsymbol{\psi} \tag{21}$$

which represents another (boosted) state of constant motion. The added potential $(e/c)\boldsymbol{A}_R$ is required in order to keep the RW rotational momentum at right angles to P_v.

7. KALUZA 5^{th} DIMENSION AND THE ROTATING WAVE.

In 1919 the German mathematician Theodor Kaluza developed a theory in 5 dimensional Reimannian geometry from which electromagnetism appeared to be a natural consequence of the 5th dimension. Finnish physicist Gunnar Nordstrom had proposed a similar idea earlier in 1914 but it was ignored. Kaluza immediately approached Einstein who became very interested and it was finally published in 1921 under Einstein's recommendation.

After rechecking the derivation of the $G_{k\ell}$ and becoming sure of the intuitive model of the Rotating Wave, I began to realize that its 5th vector v_T was most likely the same 5th dimension as suggested by Kaluza, [2].

Without the radial (outward or inward) v_T vector part of the Rotating Wave, one will not be able to derive intrinsic curvature of the surface on which the Light Line travels. In other words, the General Theory of Relativity GTR could not be explained by the Rotating Wave function, unless it is allowed to spiral outwards (slowing down) or inwards (speeding up).

The Lorentz Force in the usual 4 dimensional space can be derived from an arbitrary coordinate variation δx^γ of the invariant quantity:

$$I = -mc\int ds - q\int A_\alpha dx^\alpha \tag{22}$$

and carrying the variation out and setting it to zero yields the expression for the Lorentz Force:

$$\frac{d^2x^\gamma}{ds^2} + \Gamma^\gamma_{\alpha\beta}\frac{dx^\alpha}{ds}\frac{dx^\beta}{ds} = \frac{q}{mc}F^\gamma_\alpha\frac{dx^\alpha}{ds} \tag{23}$$

Now let $ds/dt = c$ (speed of light) as defined in the Rotating Wave Fig. 4. where

$$c^2 = g_{\alpha\beta}u^\alpha u^\beta \tag{24}$$

$$\frac{1}{c^2}\left[\frac{d^2x^\gamma}{dt^2} + \Gamma^\gamma_{\alpha\beta}\frac{dx^\alpha}{dt}\frac{dx^\beta}{dt}\right] = \frac{q}{mc^2}F^\gamma_\alpha\frac{dx^\alpha}{dt} \tag{25}$$

and thus:

$$a^\gamma + \Gamma^\gamma_{\alpha,\beta}u^\alpha u^\beta = \frac{q}{m}F^\gamma_\alpha u^\alpha \tag{26}$$

Now a vector can be constructed by pairing the contravariant components with covariant base vector components so:

$$\begin{aligned}(a^\gamma + \Gamma^\gamma_{\alpha\beta}u^\alpha u^\beta)e_\gamma &= (\frac{e}{m}F^\gamma_\alpha u^\alpha)e_\gamma \\ e_\gamma a^\gamma + \Gamma_{\alpha\beta}u^\alpha u^\beta &= \frac{q}{m}\boldsymbol{F}_\alpha u^\alpha\end{aligned} \tag{27}$$

where $\boldsymbol{F}_\alpha$ is now embolded because it acts like a base vector.

Also, as is common practice when analyzing Kaluza theory, Greek indices are again here used to denote 4 dimension quantities ($c_4 = e_\alpha u^\alpha$) while Latin indices are used to denote overall 5 dimensional quantities ($c_5 = e_\ell u^\ell = e_\alpha u^\alpha + v_T$). To be clear: $c_5 = c_4 + v_T$ Thus for 4 dimensions when $v_T = 0$ (Rotating Wave cylinder condition of constant translational motion):

$$\begin{aligned}\frac{dc_4}{dt} &= c\frac{de_c}{dt} = c^2R_4 = e_\alpha du^\alpha + \frac{de_\alpha}{dt}u^\alpha \\ &= e_\alpha a^\alpha + \Gamma_{\alpha\beta}u^\alpha u^\beta = \frac{q}{m}F_\alpha u^\alpha\end{aligned} \tag{28}$$

And for the Rotating Wave 5 vectors:

$$\begin{aligned}\frac{dc_5}{dt} &= c^2R_5 = e_\alpha du^\alpha + \frac{de_\alpha}{dt}u^\alpha + \frac{dv_T}{dt} \\ &= e_\alpha a^\alpha + \Gamma_{\alpha\beta}u^\alpha u^\beta + \frac{dv_T}{dt}\end{aligned} \tag{29}$$

Now, as per the standard model of General Relativity the Equation of Motion (EOM) is set to zero for the straightest geodesic and thus the rotation curvature R_5 is not considered nor observed. So for the moment let:

$$\begin{aligned}c^2R_5 = 0 &= e_\alpha a^\alpha + \Gamma_{\alpha\beta}u^\alpha u^\beta + \frac{dv_T}{dt} \\ e_\alpha a^\alpha + \Gamma_{\alpha\beta}u^\alpha u^\beta &= -\frac{dv_T}{dt}\end{aligned} \tag{30}$$

but from the variational principle,

$$c^2R_4 = e_\alpha a^\alpha + \Gamma_{\alpha\beta}u^\alpha u^\beta = \frac{q}{m}\boldsymbol{F}_\alpha u^\alpha = -\frac{dv_T}{dt} \tag{31}$$

Thus according to the Rotating Wave model, the extra term (E_T) generated by the Kaluza 5 dimensional model is clearly:

$$E_T = -\frac{dv_T}{dt} = \frac{q}{m}\boldsymbol{F}_\alpha u^\alpha \tag{32}$$

and hence,

$$E_T = \frac{e}{m}\boldsymbol{F}_\alpha u^\alpha = -\frac{v_R}{P_T}v_T - \boldsymbol{E}_T A_T \ . \tag{33}$$

So when a homogeneous electric field is present, there appears to be a boost in potential that is both rotational ($v_R P_T^{-1} v_T$) and radial ($\boldsymbol{E}_T A_T$).

8. DISCUSSION

One can imagine this intuitively when using the right hand rule of thumb: it is like tightening the fist while pushing the thumb forward. When the homogeneous electric field is attracting the negative field of the electron?s Rotating Wave, then the potential is positive and the rotation and forward translational motion is immediately amplified. In that case, the Light Line (radius at which Rotating Wave speed is c) spirals inwards (tightens) creating the bullet form of intrinsic curvature and the mass energy is increased. When the potential is negative, the rotation and translational motion are immediately decreased. In that negative case, the Light Line spirals outwards and mass energy is dissipated. In comparison to the gravitational theory and its slowing down of time and energy, this suggests some additional impact on the expansion of the universe by electromagnetic interactions.

Note that as per the Rotating Wave, the speed of light increases at greater radii, sub-luminal at lesser radii and super-luminal at greater radii. Perhaps it is possible to detect Rotating Waves like beacons of light at great distances, albeit with associated weak fields. With futuristic applied technological advances, that might permit communication across stellar distances and significantly further the potential of quantum entanglement.

In the more near term, perhaps we could just try to model the Rotating Wave and see what technological applications it might have. The Rotating Wave suggested to me long ago that we might be able to create an electromagnetic propeller that can transmit itself through space.

Certainly, if we are going into space for the long haul, we can't afford to pollute it with micro particles from propellant along the same trajectory. Also, a massless rocket (like an electromagnetic propeller) would certainly be much more efficient overall with much less fuel payload. This would afford constant acceleration and deceleration along trajectories which would also save time and have fewer moving parts, making space travel more comfortable and safe.

A neutron spins and during a beta minus decay it turns into a proton while ejecting an electron, an electron neutrino, and a photon. The electron appears to come out of the south pole of the neutron. Using the Rotating Wave model of the electron might provide another insight to these other particles and forces.

References

[1] Dirac, Paul.A.M. Dirac, The Quantum Theory of the Electron, Published 1 February 1928.DOI: 10.1098/rspa.1928.0023
`http://rspa.royalsocietypublishing.org/content/117/778/610`

[2] Williams, Lance L., The Nature of the 5th Dimension in Classical Relativity, Konfluence Research, Manitou Springs, Colorado 719-685-1163;
`http://www.konfluence.org/final_AIPv1103p243_1.pdf`

PERSONAL INTRODUCTION TO MUFON

by Jan Harzan

Jan Harzan made an enjoyable after-dinner presentations on a fun and entertaining topic.

Jan is a former IBM executive, and now the executive director of the Mutual UFO Network (MUFON). MUFON is a non-profit organization whose mission statement is "The Scientific Study of UFOs for the Benefit of Humanity". Jan presented a very personal introduction to the UFO phenomenon by way of his own encounter as a young boy. It was this encounter that led him to dedicate himself to a sound scientific characterization of the UFO phenomenon.

Jan spoke about how he and his brother had an encounter with a UFO in a Los Angeles suburb in the 1960s. One of them was awoken early one morning by a disturbance in the back yard of their home, and went to get his brother and investigate. Jan provided maps and sketches of the incident in his presentation. They saw something that looked like a flying barbecue grill: 4 feet long, cylindrical, with protruding legs. Jan and his brother reported a lapse of time, in which something that seemed to take minutes actually occurred over several hours.

The incident resonated deeply with Jan and his brother throughout their lives, and his brother experienced psychological difficulties in the aftermath of the encounter. The encounter may well have adversely affected the life of Jan's brother.

It is not surprising, then, that Jan would dedicate himself to pursuing an answer to the phenomenon that has so affected his life. After a career in information technology, Jan assumed leadership of the MUFON. He described the history of the organization, and its activities. Anyone can read more at MUFON.com.

Jan's organization is committed to a scientific processing of thousands of reports each year. They try to bin them into categories of explainable phenomena, hoaxes, and truly unidentified objects. The group filters the reports and attempts to pursue the most promising cases each year. They collect physical evidence and take onsite radiological measurements; they interrogate witnesses and corroborate reports.

Jan was drawn to follow the work of Dr. Woodward because Jan suspects that the UFO phenomenon is ultimately extraterrestrial, and therefore some propellantless propulsion must be involved. Woodward's work seemed to Jan to be a lead worth following.

Jan presented a particular incident that Jan felt was paradigmatic for the quality of the report. It involved several bear hunters in Ontario, Canada in 2013. This incident was recently featured in the March 2016 issue of the MUFON magazine. The bear hunters were technically savvy and made some sophisticated reports of a craft they saw flying silently. But unfortunately, there was electromagnetic interference and their video cameras did not record.

There was a lively and engaging discussion. When the issue of Roswell was raised in Jan's presentation, Robert Smith noted that Robert Goddard was undertaking rocketry experiments in Roswell for 15 years before the famous Roswell incident. Smith wondered why the Goddard rocket research facility in Roswell is not often mentioned when the incident is pondered.

In spite of enthusiasm, it seems the evidence to galvanize a definitive consensus on an extraterrestrial origin for any UFO sightings is still to come. In the age of widespread video cameras on smartphones, one hopes that the tools are now available to definitively document one of the many thousands of UFO sightings.

The discussion was engaging and the group enjoyed Jan's presentation.

Reported by L. Williams

CHAPTER 8 – OBSERVATIONS & SUMMING UP

L.L. Williams & H. Fearn

This was the first meeting of its kind devoted to the propulsion problem, and we are gratified that the unique format and approach proved to be a success as judged by the participants. Our focus was on the process of reviewing and assessing new ideas, and we threw a wide net to feed that process. We feel we provided the time and space necessary for promising new ideas to get a hearing, win adherents, and effect progress.

These Proceedings present papers on a range of topics. However, there was a focus at the meeting on propellantless propulsion experiments. There were several sessions devoted to this topic: see chapters 1, 2, and 3 of the Proceedings. A keen interest in this topic was shared by many participants, and the schedule was altered at the last minute to accommodate an extended group discussion on it. Other papers in the Proceedings stand on their own. Here, we draw together the combined implications of the Estes Park propellantless propulsion results. Perhaps the most significant outcome of the workshop was a tentative concordance among different research groups that a non-zero thrust signal may be present in one or the other of the two propellantless thrust device designs considered in Estes Park.

One design is the Mach effect device, which relies on an understanding of inertia as being due to the cumulative gravitational interaction of all the mass-energy in the universe. A putative propellantless thrust is produced with a clever electro-mechanical manipulation of the device. The Mach effect theory and first experiments were developed by Woodward. A host of other researchers have tested similar devices or other devices built by Woodward. That includes Hathaway, Tajmar, and Buldrini, who present detailed results in this volume.

Buldrini finds that the Mach effect devices exhibit a characteristic profile of thrust versus time. It is shown in Figure 1, taken from Buldrini's paper in this volume.

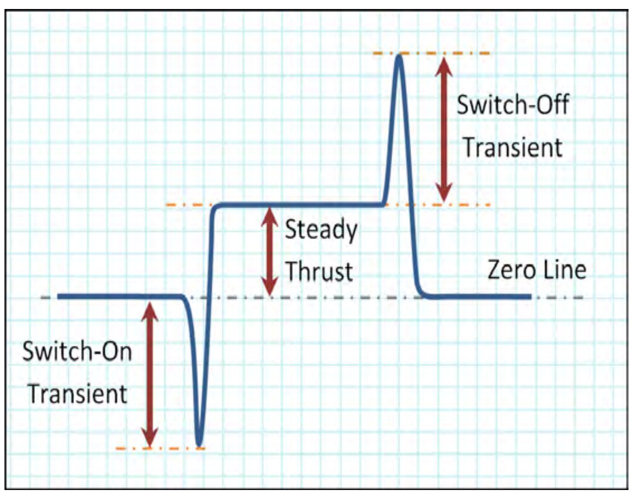

FIG. 1: Schematic diagram of the typical Mach-effect thrust signal.

The second design is an asymmetrically-shaped resonant RF cavity that is reported to produce thrust when microwaves are emitted inside. This is commonly called an EM-drive, for electromagnetic drive. March, who reports results in this volume, calls it a Q-thruster, for quantum-vacuum thruster. Here, March assumes the thrust produced by the device is due to an interaction with the quantum vacuum. This hypothesis has been questioned by other researchers, and all parties agree that it is impossible to produce such thrust from electromagnetic effects alone, no matter the shape of the cavity. The device was first proposed by Shawyer, and his theoretical understanding of electromagnetism is suspect. However, experimentalists seem to be seeing a repeatable effect. Woodward suspects that EM-drive devices are operating on a Mach effect principle, and Montillet attempts to provide such an explanation in this volume.

The typical thrust levels of the Mach effect devices reported by Estes Park participants was 0.1 to 1 μN. Thrust levels reported for the EM-drive were 10-100 μN. These results should be normalized to the power required to achieve the thrust for a photon rocket, which can set a lower limit from the thrust achievable by electric power.

The only conventional type rocket that does not involve rest mass ejection is the photon rocket. In that case, the momentum flux is p = E/c which is minute for a given amount of energy input (power). For a propellantless engine to be better than a photon rocket, the thrust produced for a given input power must exceed this value. The maximum photon momentum output per power input is just the ratio of momentum to energy of a single photon, $1/c$. Since a watt is 1 kg m^2 s^{-3}, and a newton is 1 kg m s^{-2}, then 1 second per meter $= 1/3 \times 10^8$ newton per watt, which equals 3.3 micronewton per kilowatt (μN/kW). The limiting momentum per input power of a photon rocket is therefore 3.3 μN/kW. As many of these tests are at power levels in the tens or hundreds of watts, the propellantless devices appear to compare well with the photon rocket limit, yielding performance in the range of mN/kW.

As seen in the results in these Proceedings, there are some tantalizing indications of a verifiable signal in the Mach experiments. The devices tested and reported at Estes Park were older devices with known lower levels of thrust. The newer devices tested by Woodward typically have steady thrust signals of 2 μN and much higher transient thrust signals. Even more important than the thrust levels seen (which are usually several μN in the switching transients) is the fact that the thrust signals are 3 to 5 sigma out of the noise in single runs, and more than 10 sigma when signal averaging is used to suppress the noise.

The EM-drive results remain somewhat more controversial among experimentalists. There is some concern among the community that all experimental artifacts have not been shown to be exhaustively eliminated, as would be necessary to establish confidence in a violation of momentum conservation in a closed, electromagnetic system. Soon after the Estes Park meeting, Hathaway undertook an assessment of the potential for experimental artifacts explaining EM-drive results by the Eagleworks group at Johnson Space Flight Center. The assessment did indeed find that insufficient control tests, of the kind Hathaway discusses in these Proceedings, were undertaken to establish confidence in the signals reported.

The workshop provided some opportunity to develop consensus on the theoretical underpinnings of the Mach effect proposed by Woodward. There is agreement that conventional general relativity would seem to predict an effect of the sort upon which Woodward predicates his design. Tajmar and Williams both present alternative derivations of a Mach effect from standard, linearized general relativity in the harmonic gauge. Fearn has presented similar linearized gravity work elsewhere. But where Woodward considered the inertial backreaction force from all mass in the universe, and explicitly introduced a mechanical acceleration to obtain the effect, the separate but similar calculations by Williams and Tajmar did not consider either acceleration or back-reaction. While we remain optimistic, work is still to be done to couch a Mach effect within the framework of textbook general relativity. Woodward's mass fluctuation has been shown to fit perfectly into the framework of gravitational absorber theory, of the type described by Fearn, based on Hoyle and Narlikar theory using advanced waves. This is a fully nonlinear theory which reduces to Einstein's gravitation in the limit of a smooth fluid, in the rest frame of the fluid.

Regarding the theoretical underpinnings of the EM-drive, there is consensus among experimentalists and theorists alike that no thrust should be possible from electromagnetic effects alone.

Appendix A

Estes Park Quick Studies

key concepts and results in space, time, and gravity
that bear on the interstellar propulsion problem
provided to participants in advance of the workshop

1. The Fuel Problem
2. The Time-Distance Problem
3. Warp Drives and Wormholes: Good News and Bad News
4. Maxwellian Gravity
5. Inertia from Gravity: Insights of Sciama
6. Woodward's Mach Equation

The Fuel Problem

one of two fundamental obstacles to interstellar travel

Travel between the stars, and even between planets around a star, requires propulsion to overcome the effects of gravity. A propulsion source drives motion of the spacecraft with respect to the nearby stars or planets, lifting it out of the local gravitational well.

Chemical rockets are the main propulsion source used in the interplanetary programs. They operate on the principle of throwing something out the back so that the spacecraft is thrown forward. To accelerate a chemical rocket at 1 g half way to the nearest star, and decelerate at 1 g the other half way, would require a fuel tank the size of the moon. Therefore, rockets achieve a speed limited by the fuel they can practically carry. The speed is so small as to require centuries to reach the nearest stars.

Other fuel options include ion beams, microwave sails, and reflecting the blast waves of nuclear explosives. These options do not seem to alter the basic feasibility of chemical rockets, because all these alternative methods yield velocities as small as those of chemical rockets.

To solve the fuel problem would be to provide a limitless source of fuel that could be used to power a spacecraft indefinitely. This would presumably be through some aspect of the universe that is everywhere existent.

It is understood that even with the fuel problem solved, the time-distance problem would remain. The fuel-problem would only allow the continuous acceleration of objects up to speeds approaching that of light, but a solution to the fuel problem alone would not be sufficient to achieve hyper-relativistic travel.

The Time-Distance Problem

one of two fundamental obstacles to interstellar travel

The Time-Distance Problem is the really profound problem of interstellar travel. Even if the fuel problem were solved, and we could accelerate freely in any gravitational field, accelerating even up to the speed of light, our civilization could still not explore the stars. This is because the severe effects of time dilation would isolate any emissary or probe in time, very much like a Planet-of-the-Apes scenario. Our astronauts could see the center of the galaxy, but they would return to the far future of their planet, and their civilation would be gone.

It is best to approach this problem mathematically, so that we can be awed by the fundamental simplicity of our obstacle. In essence, the time-distance problem is inherent to the structure of space and time.

We understand space and time to be joined together in a spacetime continuum. Moreover, "distance" between any two events in spacetime is invariant with respect to the state of motion.

$$c^2 d\tau^2 \equiv c^2 dt^2 - dx^2 - dy^2 - dz^2 \equiv \eta_{\mu\nu} dx^\mu dx^\nu \tag{1}$$

where t is a time coordinate, x, y, and z are spatial coordinates, τ is called the proper time, and c is the speed of light. Greek superscripts denote the 4 components of space and time.

In terms of 4-velocity $U^\mu \equiv dx^\mu/d\tau$, the invariant interval (1) implies

$$\eta_{\mu\nu} U^\mu U^\nu = c^2 \tag{2}$$

This equation implies

$$\eta_{\mu\nu} U^\mu \frac{dU^\nu}{d\tau} = 0 \tag{3}$$

It's a general rule of motion in spacetime – we haven't done any physics yet – that the 4-velocity and the 4-acceleration are orthogonal vectors.

Consider a spaceship moving in one direction. In the rest frame of the moving spaceship, where the coordinate time is the proper time, $U^\mu_{ship} = (c, 0, 0, 0)$, and $U^2 = c^2$ in all frames, consistent with equation (2).

Consider now the simple case of constant acceleration in the x direction. One viable trajectory to the stars would be to accelerate at 1 g half way, and decelerate at 1 g the other half way; thereby, maintaining artifical gravity for the astronauts. From (3) we deduce that in the rest frame of the spaceship, $(dU^\mu/d\tau)_{ship} = (0, a, 0, 0)$, where

a is the acceleration or effective gravity measured in the frame of the spaceship. It follows that $(dU/d\tau)^2 = -a^2$ in all frames.

Therefore we obtain the two equations in two unknowns $t(\tau)$ and $x(\tau)$:

$$c^2 = \eta_{\mu\nu} U^\mu U^\nu = c^2 \left(\frac{dt}{d\tau} \right)^2 - \left(\frac{dx}{d\tau} \right)^2 \tag{4}$$

$$-a^2 = \eta_{\mu\nu} \frac{dU^\mu}{d\tau} \frac{dU^\nu}{d\tau} = c^2 \left(\frac{d^2t}{d\tau^2} \right)^2 - \left(\frac{d^2x}{d\tau^2} \right)^2 \tag{5}$$

The solutions to this pair of equations are:

$$t(\tau) = \frac{c}{a} \sinh \left(\frac{a\tau}{c} \right) \tag{6}$$

$$x(\tau) = \frac{c^2}{a} \cosh \left(\frac{a\tau}{c} \right) \tag{7}$$

These simple equations tell us how time and distance pass for a ship under constant acceleration. The parameter τ is the time coordinate on board the ship. And we haven't even done any physics!

Equation (6) tells us that for acceleration a at 1 g, and onboard elapsed time τ of 5 years, 69 years would pass on earth, far longer than a typical space program lifecycle. Yet that would scarely allow the astronauts to reach the nearest stars.

Equations (6) and (7) can be combined to demonstrate the limiting speed of light:

$$\frac{dx}{dt} = \frac{at}{\sqrt{1 + a^2t^2/c^2}} \leq c \tag{8}$$

The time-distance problem is that motion in space time introduces severe time dilation effects that completely cut off contact between the earth and any distant explorers. And we haven't even done any physics!

The warp drive solution to the Einstein equations by Alcubierre, and the worm hole solutions to the Einstein equations studied by Kip Thorne, would get around this speed limit. By bending spacetime itself, effective hyper-relativistic speeds can in principle be achieved; but not in practice. Not yet, anyway. Another way around the time-distance problem might involve hyperdimensions. But the time-distance problem is quite profound and fundamental.

Warp Drives and Wormholes: Good News, Bad News

The good news is that general relativity *appears* to allow in principle the traversal of distances faster than light speed, and the solution of the Time-Distance Problem.

From equation (8) of the Time-Distance Problem summary, you might infer that the limiting speed will be the coefficient of the time component in the metric. In flat space, $\eta_{tt} = c^2$. In the curved spacetime around a black hole, the Schwarzschild metric gives the time-time component as

$$g_{tt} = c^2 \left(1 - \frac{2GM}{rc^2}\right)$$

We conclude the speed of light gets smaller as one approaches a star, and note that the limiting speed c need not be the limit everywhere in spacetime. Since mass affects the speed of light, one might hope to control the shape of space and time to overcome the time-distance problem. This is where warp drives and wormholes come in.

The Einstein equations describe black holes, warp drives, and worm holes. They are written:

$$R_{\mu\nu} - \frac{1}{2} g_{\mu\nu} R = \frac{8\pi G}{c^4} T_{\mu\nu} \tag{1}$$

These equations are in the 10 unknowns $g_{\mu\nu}$. The quantities in $R_{\mu\nu}$ and R are second order derivatives of the $g_{\mu\nu}$.

The quantity $T_{\mu\nu}$ is the stress energy tensor, with units of energy density. Some are surprised to learn that there is no formula or prescription for choosing $T_{\mu\nu}$, but there are many standard forms for various situations.

The Newtonian analogue of (1) is

$$\nabla^2 \phi = 4\pi G \rho$$

In either case, a second derivative is related to a mass/energy density, with the coupling constant G. Therefore, curvature of space is quantified by the magnitude of G. The units of the LHS of (1) are $1/l^2$. Therefore (1) gives a curvature scale:

$$L_\rho \sim \sqrt{c^2/G\rho} \tag{2}$$

We may reasonably hope to transcend the light barrier by building a wormhole or bubble of some sort, and (2) allows us to estimate how much mass density is needed for a given size warp or hole. A 15-meter bubble requires a mass density of 1 earth mass per cubic *meter*. This seems far beyond our means. Because the gravitational constant is so small, astronomically large amounts of mass density are needed to curve space appreciably.

If we substitute $\rho \sim M/L^3$, then we recover the Schwarzschild radius of $R_S \sim MG/c^2$. The Scwharzschild radius of the earth is 4 millimeters. Even cobbling together a mass the size of earth could only give you a warp or wormhole big enough to transport a flea.

But if that is not enough to depress you, there is more.

The equation (1) universally describes an attractive force of gravity. Einstein did not anticipate any sign change on the RHS of (1). But to build a workable bubble or wormhole, the mass energy must push out like antigravity, and we hope to somehow insert a minus sign in (1). This is sometimes called negative energy. Standard physics only tells us how a black hole can eat you, but we have no idea how to get one to barf you back out, like Jonah from the whale.

The problem is we have never seen or measured negative energy. Perhaps its best known example is the quantum vacuum, but the measured value of the vacuum energy in cosmology is orders of magnitude smaller than we expect from quantum theory. So we really don't even understand the quantum vacuum, let alone other forms of exotic energy.

Wormholes and warp drives are only achievable with astronomical quantities of something unknown to science.

Maxwellian Gravity

Reference: *Spacetime and Geometry*, by Sean Carroll, 2004, section 7.2

General Relativity (GR) is our theory of gravity, space, and time. The theory has been confirmed experimentally in many different ways. Yet the equations are enormously complex. Specifically, they are non-linear. Unlike the Maxwell equations, there are no systematic techniques to obtain solutions to the Einstein field equations. All solutions – such as the Robertson-Walker metric, the Schwarzschild metric, the Kerr metric, etc – are guessed and then verified. This means there may well be complexity in the field equations that we have not yet discovered.

Therefore, linear solutions have been sought to the equations since Einstein. To linearize GR, one expresses the full spacetime metric $g_{\mu\nu}$ into a perturbation $h_{\mu\nu}$ about the flat space metric $\eta_{\mu\nu}$, such that $g_{\mu\nu} = \eta_{\mu\nu} + h_{\mu\nu}$, $h_{\mu\nu} \ll 1$. This expression is plugged into the equations of GR and terms are only kept to linear order in $h_{\mu\nu}$.

Carroll suggests decomposing the components of $h_{\mu\nu}$ according to their spatial transformation properties. Then $h_{00} \equiv \phi$ transforms as a scalar, and $h_{0i} \equiv \mathbf{A}$ transforms as a vector. The remaining components are the 3x3 matrix h_{ij}. This decomposition is entirely analogous to decomposing the electromagnetic field strength tensor into electric and magnetic field vectors.

For a particle of energy E and velocity $\mathbf{v}$ moving in this gravitational field, its energy equation is (Carroll 7.23)

$$\frac{dE}{dt} = -E\left[\frac{\partial\phi}{\partial t} + 2\mathbf{v}\cdot\nabla\phi - \mathcal{O}(v^2)\right]$$

Now define gravito-electric field $\mathbf{G}$ and gravito-magnetic field $\mathbf{H}$:

$$\mathbf{G} \equiv -\nabla\phi - \frac{\partial\mathbf{A}}{\partial t}$$
$$\mathbf{H} \equiv \nabla\times\mathbf{A}$$

Then the particle spatial momentum $\mathbf{p}$ is described by (Carroll 7.26):

$$\frac{d\mathbf{p}}{dt} = E\left[\mathbf{G} + \mathbf{v}\times\mathbf{H} - \mathcal{O}(\partial h_{ij}/\partial t, v^2)\right]$$

These are clearly very similar to the Lorentz force law of electromagnetism, and one can infer that GR includes magnetic-type gravitational forces. Unlike the Maxwell equations, however, we also have additional, non-linear terms.

Interestingly, Carroll goes on to show how the only components with true degrees of freedom are the spatial components h_{ij}. The suggestive gravito-electric and gravito-magnetic fields are fixed by the stress energy tensor and the h_{ij}. Carroll goes on to choose a particular gauge for the $h_{\mu\nu}$, and to show the h_{ij} is the piece that contains gravitational radiation.

Inertia from Gravity: Insights of Sciama

Reference: *On the Origin of Inertia*, D.W. Sciama, MNRAS, 113, 1953

The fuel problem (see EP Quick Study I) can also be seen as a problem of inertia. If it weren't for inertia, we would not need any fuel to push a spaceship. The resistance to acceleration comes from inertia.

We may expect there to be some link between gravity and inertia, since they have the same mass parameter. While Einstein built General Relavitity on the equivalence of gravitation and inertia, the origin of inertia is still debated. Insight into the origin of inertia came from a simple argument by Sciama. This insight has formed a cornerstone of Woodward's Mach Effect theory.

Sciama quantifies inertia by assuming gravity is a vector field and using the well-known mathematics of electrodynamics to quickly derive its inertial implications. We know, and Sciama knew, that gravity is a tensor field, but it is a reasonable approximation because Sciama's result only requires that gravity be at least as complex as a vector field. Einsteins equations of gravity can be linearized, and they do indeed show a Maxwellian character (see EP Quick Study IV). There are of course the gravito-electric effects one expects for Newtonian gravity, but other gravito-magnetic effects that Newton would not have recognized. These latter effects are more conventionally known as frame dragging.

So Sciama starts with a Maxwellian gravitational 4-vector potential $(\phi, \mathbf{A})$. The scalar potential has the usual mathematical form, but in terms of mass density ρ instead of charge density, and in terms of the gravitational constant G instead of the dielectric constant:

$$\phi = -G \int \frac{\rho}{r} dV$$

. The integral is taken over the whole universe, but we know the universe is undergoing a Hubble expansion of speed $v_H = Hr$, where H is the Hubble parameter. The current value of $H_0 \simeq 70$ km/s per megaparsec. It is presumed no part of the universe receding faster than the speed of light can influence the local scalar field of gravity, so the integral is cut off at a distance $r_H = c/H$. The value of H changes over time, and the horizon distance is the farthest object to have emitted light just now reaching us. The horizon distance depends on the energy content of the universe, but it scales with the instantaneous horizon distance $r_H = c/H \sim c/H_0$. Therefore we can approximate the scalar potential of the universe:

$$\phi \simeq -G \int_0^{r_H} \frac{\rho}{r} 4\pi r^2 dr = -2\pi G \rho_U \left(\frac{c}{H_0}\right)^2$$

where we have approximated the mass density of the universe as a constant ρ_U. This equation already contains a compelling feature. If taken at infinity, the integral would diverge quadratically. This means the inertia here is dominated by matter in the distant universe.

We construct the usual spatial vector potential in terms of a mass current $\mathbf{J}$:

$$\mathbf{A} = -\frac{G}{c^2}\int \frac{\mathbf{J}}{r} dV$$

At this point, Sciama invokes Mach's principle to presume that there is a rest frame for the universe, and in that frame the current must be zero. But for an object in motion with respect to the rest frame of the universe, the universe appears to be in motion and the object at rest. Therefore an apparent current arises in the universe from the motion of the object. In this case, the current of the universe due to the motion $\mathbf{v}$ of the object is $\mathbf{J} = \rho\mathbf{v}$. The gravitational vector potential of the universe is then:

$$\mathbf{A}_U = -\frac{G}{c^2}\int_0^{r_H} \frac{\rho\mathbf{v}}{r} 4\pi r^2 dr = \phi_U \frac{\mathbf{v}}{c^2}$$

Construct the usual Maxwellian gravito-electric force from the potentials:

$$\mathbf{f} = -\nabla\phi_U - \frac{\partial \mathbf{A}_U}{\partial t} = 2\pi G \frac{\rho_U}{H_0^2}\frac{\partial \mathbf{v}}{\partial t}$$

Now the identification of inertia is complete, if the coefficient leading the derivative of the velocity is unity. Remarkably – and unknown in Sciama's time – cosmology tells us it is.

The Friedmann equation is the workhorse of modern cosmology. It relates the expansion of the universe $H(t)$ to curvature κ and energy density $\epsilon(t)$:

$$H^2(t) = \frac{8\pi G}{3c^2}\epsilon(t) - \frac{\kappa c^2}{R_0^2 a^2(t)}$$

For a flat universe, $\kappa = 0$ and the energy density of the universe is the critical density:

$$H^2(t) = \frac{8\pi G}{3c^2}\epsilon_c(t)$$

In fact, modern cosmology tells us that the universe is flat and the equation above relates the Hubble parameter to the energy density of the universe. If we set $\epsilon_c = \rho_U c^2$ with the understanding that ρ_U includes all the gravitating mass-energy in the universe, we find

$$H_0^2 = \frac{8\pi G}{3}\rho_U$$

and therefore

$$\mathbf{f} = \frac{3}{4}\frac{\partial \mathbf{v}}{\partial t}$$

The coefficient is close enough to unity that we would have to revisit our approximation to GR, our integration limit, and our detailed model of the expansion of the universe, to definitively rule out gravity as the origin of inertia. Modern cosmology and the flat universe appears to reinforce the conclusion that inertia can be accounted for by the gravitational influence of the universe.

A closely related result of the flat universe is that the gravitational potential energy of every particle in the universe exactly equals its rest mass energy. That is, $\phi = c^2$. Therefore, the speed of light is set by the gravitational potential of the universe.

Woodward's Mach Equation

This is a summary of Woodward's own derivation of the Mach equation, as given in his book *Making Starships and Stargates*. It is compressed to facilitate comparison and analysis.

Woodward starts with the observation from Sciama, 1953, that gravitational forces from the rest of the universe can account for inertia. The inertial force is per unit mass, like a gravitational field; call it $\mathbf{f}$.

A relativistic description of force involves the proper time derivative of the 4-momentum:

$$F^\mu = \frac{dp^\mu}{d\tau} = \left(\frac{dp^0}{d\tau}, \frac{d\mathbf{p}}{d\tau}\right) \tag{1}$$

This is a 4-vector expression. Greek indices range over the 4 coordinates of space-time. The time component of the 4-vector is noted with a 0 index, and the 3 spatial components are written as a vector in bold-face. The time component of the 4-momentum is the energy. Therefore a 4-vector that corresponds to the inertial force $\mathbf{f}$ per unit mass will have a time-component equal to the work done on the object by the force, per unit mass:

$$\frac{F^\mu}{m} = f^\mu = \left(\frac{1}{m}\frac{dp^0}{d\tau}, \mathbf{f}\right) \tag{2}$$

Woodward elects to investigate the 4-divergence of the relativistic inertial force field:

$$\nabla_\mu f^\mu = \frac{1}{c}\frac{\partial}{\partial t}\left(\frac{1}{m}\frac{dp^0}{d\tau}\right) - \nabla \cdot \mathbf{f} \tag{3}$$

Woodward posits that the divergence (3) of the inertial force must correspond to a field equation. He sets the right hand side equal to some unspecified source $4\pi Q$, as might be expected for such an equation. He converts the particle energy into an energy density E, to conform to the expected units in a field equation. And he considers non-relativistic speeds, so that the proper time derivative becomes a simple time derivative, and the energy density is simply the mass density time the speed of light squared, c^2:

$$\frac{1}{c^2}\frac{\partial}{\partial t}\left(\frac{1}{\rho}\frac{\partial E}{\partial t}\right) - \nabla \cdot \mathbf{f} = 4\pi Q \tag{4}$$

The first term on the left side expands into 2 terms, differing by a minus sign due to the derivative of the inverse mass density. Now Woodward makes 3 simultaneous ansatzes, one for each term of equation (4):

1. The source term is the usual source term of Newtons law of gravity: $Q \to G\rho$, the product of mass density and Newton's gravitational constant

2. The inertial reaction force $\mathbf{f} \to -\nabla\phi(\mathbf{x}, t)$, the gradient of the gravitational potential in Newton's law of gravity

3. The energy density $E \to \rho(\mathbf{x}, t)\phi(\mathbf{x}, t)$. This is the Mach hypothesis: that the energy of a body depends on the gravitational potential. Equivalently, the speed of light squared is the same as the value of the scalar potential, $c^2 \to \phi(\mathbf{x}, t)$.

With these assumptions and a prescription for where to make the substitutions, Woodward calculates his Mach effect equation, which is a modification of Newtons field equation:

$$\nabla^2\phi - \frac{1}{c^2}\frac{\partial^2\phi}{\partial t^2} = 4\pi G\rho + \frac{\phi}{\rho c^2}\frac{\partial^2\rho}{\partial t^2} - \left(\frac{\phi}{\rho c^2}\right)^2\left(\frac{\partial\rho}{\partial t}\right)^2 - \frac{1}{c^4}\left(\frac{\partial\phi}{\partial t}\right)^2 \tag{5}$$

The basic feature of Woodwards equation (5) is time-derivatives of the field acting as a source, and these sources are scale free: they dont involve the gravitational constant. So they are relatively larger than the conventional source term, the first term on the right side. They also have the negative-definite terms that Woodward would suggest for creating warp drives or wormholes.

As Woodward notes, equation (5) does not tell us anything about how the mass time derivatives come about. Naively it would appear to say a change in internal energy of any sort could bring about this effect. But Woodward hearkens back to the original assumption, we could call it Woodwards zeroth ansatz, that inertial reaction forces arise from the rest of the universe resisting the acceleration of a body. If the body is not accelerated, no inertial reaction force is raised.

Woodwards 4th ansatz is that the change in internal energy scales with the acceleration that raises the inertial reaction force. So he then equates the inertial reaction force with the bulk acceleration of the object:

$$\Delta E = m\mathbf{f} \cdot \Delta\mathbf{s} = m\mathbf{a} \cdot \Delta\mathbf{s} \tag{6}$$

The quantity $\Delta\mathbf{s}$ is a parameterization of the work done by the inertial reaction force, with units of length. It is understood that this does *not* correspond to the bulk displacement of the object, but rather, to some internal dissipation. This gives

$$\frac{\partial E}{\partial t} = m\mathbf{a} \cdot \frac{\partial\mathbf{s}}{\partial t} \tag{7}$$

and

$$\frac{\partial^2 E}{\partial t^2} = m\mathbf{a} \cdot \frac{\partial^2\mathbf{s}}{\partial t^2} + \frac{\partial\mathbf{s}}{\partial t} \cdot \left(m\frac{\partial\mathbf{a}}{\partial t} + \mathbf{a}\frac{\partial m}{\partial t}\right) \tag{8}$$

Finally, Woodward hypothesizes that the parameterization of dissipation $\partial \mathbf{s}/\partial t$ must scale with the bulk velocity $\mathbf{v}$, so that $\partial \mathbf{s}/\partial t = \eta \mathbf{v}$. Then, since $\mathbf{a} = \partial \mathbf{v}/\partial t$, Woodward finds (3.7) of his book:

$$\frac{\partial^2 E}{\partial t^2} = \eta m a^2 + \eta \mathbf{v} \cdot \left(m \frac{\partial \mathbf{a}}{\partial t} + \mathbf{a} \frac{\partial m}{\partial t} \right) \tag{9}$$

At successive points in Woodwards development, he drops the second term as much smaller than the first term in the equation above, and also drops the term quadratic in $\partial m/\partial t$ in (5). Adopting these approximations now, and putting all this together, we obtain the approximate equation for the mass fluctuation:

$$\delta m = V \delta \rho = \frac{\eta}{4\pi G} \frac{V a^2}{c^2} = \frac{\eta}{4\pi G} \frac{m a^2}{\rho c^2} \tag{10}$$

which is equation (5.9) from Woodwards book, and where the mass fluctuation is defined in terms of the standard Newtonian expression:

$$\nabla^2 \phi = 4\pi G(\rho + \delta \rho)$$

This is apparently the mass fluctuation that is produced from accelerating objects, and which Woodward would hope to engineer into various designs that time the mass fluctuations with internal constituent motions of the thruster to produce a net impulse.

Note that the gravitational constant enters inversely, which presumably results in very large effects.

Appendix B

Estes Park Prep Kit

The following summaries are to aid preparation for the various sessions of the workshop. They are based on discussions with the presenters and materials they provided.

The summaries are in a dashboard format. They are held to one page, and are binned for theory vs experiment, new physics vs existing physics, and fuel problem vs time-distance problem.

Web links to references are embedded, so it is best to see the online version

Fuel Problem Time-Distance Problem	✔ Theory ✔ Experiment	✔ Existing Physics ✔ New Physics

General

- Lance Williams will lead a short discussion regarding acceptable extensions to existing laws of physics
- George Hathaway will lead a full block discussion on aspects of valid experiments

Issue Summary:

To start the conference, we wanted to spend some time giving an overview of expectations for a valid theory or valid experiment. We have made a lot of progress with the scientific method, and we feel sure we are not going to get to the stars without it. That means repeatable, verifiable experiments; and theories that conform to expectations from modern physics.

Lance will use a short block to present a summary of the aspects of a valid extension to the laws of physics. These aspects are few, but profound. These aspects incorporate the criteria that Robert Dicke used when he set about verifying general relativity versus other possible theories of gravity.

George will lead a discussion on the aspects of a valid experiment, cutting across theories and effects of all types. George is particularly interested in low-thrust experiments, and so this is quite relevant to the Mach Effect and RF cavity thruster sessions to follow.

These two preparatory sessions should lay the groundwork somewhat for the type of scrutiny on theory or experiment to expect in the subsequent sessions, and which will be captured in the proceedings.

✔ Fuel Problem ✔ Time-Distance Problem	✔ Theory ✔ Experiment	✔ Existing Physics New Physics

Mach Effect Thrusters

- Jim Woodward and Heidi Fearn will lead a discussion about theory and experimental efforts regarding a Mach Effect thruster
- Heidi Fearn and José Rodal will lead a discussion regarding Mach Effects interpreted within the Hoyle-Narlikar theory. Heidi will give an overview, and José will discuss a particular application.

Issue Summary:

This is the most well-developed topic of the conference, because there is substantial development in both theory and experiment. Interestingly, it does not invoke any new physics, although experimental validation would be a great discovery. The Mach Effect thrusters exploit an understanding of inertia that lies within the framework of our current understanding of gravity; see the Estes Park Quick Study on Sciama's insight into inertia.

The theory and first experiments were developed by Jim Woodward at Cal State Fullerton. He has been collaborating in recent years with Heidi Fearn at Fullerton, and other groups have performed Mach thruster experiments. Since many of you know Jim Woodward personally, you may have access to his book, Making Starships and Stargates, so that is recommended as an overview of Woodward's theory and experiment. An online resource is here. A digest of Woodward's mathematical theory lifted from Woodward's book is included as Estes Park Quick Study VI, to facilitate analysis of Woodward's theory. One finds that while the derivation is reasonable, an alternative derivation suggests itself within standard techniques of linearized GR.

Woodward maintains that the Mach Effect addresses both the fuel problem and the time-distance problem. The latter is because there are negative-definite source terms in the field equations that are suggestive of the negative energies posited by Kip Thorne's worm hole analysis.

Jim and Heidi will tag-team the discussion of theory and experiment. One objective for the theory part of the session is whether the Mach Effect theory can be more firmly embedded in the techniques of GR. Another objective is to gain a clear understanding of the experimental set up. The implications for a Mach interpretation of other experiments will be discussed.

Heidi Fearn and José Rodal will tag-team discussions on Mach effect applications within the theory of Hoyle and Narlikar from 1964. See this reference and this reference. The Hoyle-Narlikar theory is closely tied to the old Steady-State cosmology of the 1960s. Now, in the age of precision cosmology, the Lambda-Cold-Dark-Matter model is parameterized to 3 or 4 significant figures, and Steady-State cosmologies are no longer considered. But Heidi and José will share some compelling experimental implications of the theory, which they feel addresses some causal aspects of the coupling of inertia to the distant universe. They are particularly intrigued by the concept of Wheeler-Feynman absorber theory and how it applies to inertia.

✔ Fuel Problem Time-Distance Problem	Theory ✔ Experiment	Existing Physics ✔ New Physics

RF Resonant Cavity Thrusters

- Paul March will lead a discussion about experimental efforts at Eagleworks
- Martin Tajmar will lead a discussion about experimental efforts at Dresden
- John Brandenburg will offer a theoretical explanation for the effect

Issue Summary:

These devices purport to provide propellantless thrust by emitting RF waves inside a shaped cavity. By the shaping of the cavity, a net thrust can result from the momentum transfer of the RF waves with the walls of the cavity. These are alternatively called the electromagnetic drive (EM drive) by Roger Shawyer, and the Cannae drive by Guido Fetta.

Any such effect constitutes new physics, because our current understanding is that momentum conservation should not allow such a thing. It is similar to being able to make a spaceship go by pushing on the inside. If confirmed, such effects would revolutionize physics. A compelling, repeatable experiment is needed because conservation of momentum is a cornerstone of physics. The electromagnetic field has never been found to violate conservation of momentum.

Shawyer has released a technical paper online. His theory is based on a misconception regarding his equation (1), the Lorentz force law. The Lorentz law gives the electromagnetic force on charged particles; it does not describe the dynamics of photons or RF waves, which are uncharged. Shawyer's theory, at least, appears unsatisfactory. At this time we must consider this effect an experiment with no accepted theoretical explanation or theoretical estimate of the magnitude of the effect.

John will pick up that gauntlet and offer a theoretical explanation in terms of his GEM theory, a unified theory of gravity and electromagnetism. He has done much work on it over the years; a recent paper is here.

Martin will summarize experimental work done at Dresden, where they have also conducted a wide array of experiments in related areas. See this web site for additional discussion possibilities.

Like at Dresden, Eagleworks has done a wide array of experiments. But Paul will focus at Estes Park on the RF cavity thrust experiments.

A Wikipedia page has appeared on this topic since April, initiated by an IP address in New York. Reputable people have provided inputs, and the experimental efforts of two of our session leaders are described. This page is annotated and well-written, and so is recommended for background review, even though it only includes journalistic sources.

Our objectives in session will be to understand the experiments in a way that allows peers to verify them, and to understand what theoretical modifications are necessary to relinquish conservation of momentum.

✔ Fuel Problem ✔ Time-Distance Problem	✔ Theory Experiment	Existing Physics ✔ New Physics

Kaluza Unification of Gravity and EM

- Lance Williams will lead a discussion about the Kaluza theory as a promising framework to address the fuel and time-distance problems.

Issue Summary:

Lance will present the Kaluza unified theory of gravity and electromagnetism. It was developed in the few years between the publication of GR, and the quantum revolution of Heisenberg and Schroëdinger. It provided a compelling unification of gravity and electromagnetism that accorded with the existing theory in every way. Einsten himself spent several years working on it, and it has formed the basis of subsequent higher-dimensional quantum theories.

The Wikipedia page on Kaluza-Klein theory provides a very good summary of the Kaluza theory. Lance has a recent article that derives the full Kaluza equations for the first time, using tensor algebra software. The Lagrangian is also established.

Essentially, Kaluza found the the equations of GR and EM could be recovered by writing the equations of GR in 5 dimensions. The 15 components of the 5D metric are now accounted for by the 10 components of the 4D metric of GR, the 4 components of the electromagnetic four-vector potential, and an unidentified scalar field. The Einstein equations in 5D produce the 4D Einstein equations, the Maxwell equations, and an equation for the scalar field. Simultaneously, and independently, the 5D geodesic equation produces the 4D geodesic equation and the Lorentz force law of EM. Remarkably, the 5D theory written in vacuum yields the 4D EM stress energy tensor in the Einstein equations: an example of "matter from geometry".

The theory promises a solution to the fuel problem through an adjustable coupling of gravity, and a solution to the time-distance problem through a hyper-dimension. Both of these are through electromagnetic means. So far, no experimental verification has been suggested that would verify the theory. Lance hopes to present one to the group for discussion.

Objectives of the discussion will be to understand the motivation behind the Kaluza theory; and to address experimental ways to validate the theory.

✔ Fuel Problem ✔ Time-Distance Problem	✔ Theory Experiment	Existing Physics ✔ New Physics

Modified Chameleon Density Model

- Tony Robertson will lead a discussion about a propulsion application of the Chameleon Cosmology model

Issue Summary:

The Chameleon Cosmology theory was proposed by Khoury and Weltman in 2004; see this reference and this reference. A useful overview is here. The theory involves a scalar field with a variable coupling to matter, proposed to explain Dark Energy by providing a reduction to gravity. This theory is in the family of scalar field theories whose most famous member is the Brans-Dicke theory of gravity, which augmented GR with a scalar field that depended on the mass density of the universe, and identified that scalar field with the gravitational constant. In this case, the coupling is apparently variable. The Wikipedia page is short, but has additional references and detail on experimental implications.

Tony explores the implications for acceleration. He will discuss the thin-shell aspect of Chameleon Cosmology, and point out connections to the Alcubierre bubble. Finding a means for propellantless propulsion with this framework, Tony will also touch on application to seemingly-unrelated thrust experiments, such as the RF resonant cavity, the Podkletnov superconductor experiments, and the Mach effect experiments.

Objectives of the discussion will be to introduce a new acceleration model based on the Chameleon scalar field theory; to point out similarities to other theories, including the Alcubierre warp bubble; and to explore experimental verification.

Fuel Problem ✔ Time-Distance Problem	Theory Experiment	✔ Existing Physics New Physics

Alternate Concept: Tri-Space Model

- Greg Meholic will lead a discussion on an alternate conceptual viewpoint to thinking about spacetime that could facilitate faster-than-light propulsion

Issue Summary:

This session will be a departure from previous sessions. Instead of discussing a particular experiment, or a particular mathematical theory, Greg will discuss an alternative viewpoint that he calls the Tri-Space Model of the universe. It is inspired by the mathematics of the expression for relativistic energy, $E = m_0 c^2 / \sqrt{1 - v^2/c^2}$, which is a real number for speeds below light, diverges when the speed equals the speed of light, and becomes imaginary for speeds above light.

Greg has applied his model to the origin of inertia. At Estes Park he will discuss how the Tri-Space model relates to the known particles and fields in physics and cosmology, and why it has implications for faster-than-light travel.

Greg would like to share this alternative way of thinking about spacetime and about faster-than-light propulsion, and also to gather your feedback and ideas.

APPENDIX C

Proof that EM Drive Thrust/Power and Q scale as $\sqrt{L}$

José J. A. Rodal[1]
Rodal Consulting
Research Triangle Park, North Carolina

I prove that the thrust force per input power (for all three EM-Drive theories) scales like the square root of any geometrical dimension, for constant resistivity and magnetic permeability of the interior wall of the cavity and for constant geometrical ratios, constant medium properties and for the same mode shape. To maximize the thrust per input power, according to all three theories the most efficient EM-Drive would be as large as possible, this being due to the fact that the quality of factor of resonance Q (all else being equal) scales like the square root of the geometrical dimensions. Small cavity EM-Drives (all else being equal) are predicted to have smaller quality of resonance Q and therefore smaller thrust force/input power.

1. THRUST PER POWER OF EM DRIVE COMPARED TO A PHOTON ROCKET

Here I briefly describe the thrust per power input claimed by various authors for the EM-Drive and its comparison to the one of a photon rocket. I start with the definition of Power $P(t)$ as the time derivative of work W, and therefore equal to the vector dot product of force times velocity,

$$P(t) = \frac{dW}{dt} = \vec{F} \cdot \vec{v} \tag{1}$$

For an ideal photon rocket with a perfectly collimated photon beam, the exhaust velocity (not the spaceship velocity!) is the speed of light c and therefore, $Fc = P_{in}$, where P_{in} is the power input into the exhaust ("power input" here only stands for the power at this late stage, notice that there may be further losses at earlier stages from the power plant, etc.). Therefore, for an ideal photon rocket, the "thrust" force per input power is,

$$\left(\frac{F}{P_{in}}\right)_{\text{photonRocket}} = \frac{1}{c} \tag{2}$$

Furthermore: For rockets exhausting particles-with-mass at speeds much lower than the speed of light, for example ion thrusters, this ratio is $2/v$ instead of $1/c$, where v is the speed of the particle-having-mass (as propellant). Particles-with-mass, unlike photons, need to be accelerated to the exhaust speed. The reason for the factor of 2 is because kinetic energy of a massive low speed particle is $E = (1/2)mv^2$ instead of the energy of a photon $E = mc^2$. Therefore, the efficiency (F/P_{in}) for ion thrusters is much larger than the one for photon rockets since $v \ll c$, and hence $2/v \gg 1/c$ and that is why this type of photon rocket has not seen, and is not envisioned to have, practical use.

Interestingly the "thrust" force per input power for the EM Drive, according to all three different theories (McCulloch, Shawyer and "*Notsosureofit*") can be expressed similarly as:

$$\left(\frac{F}{P_{in}}\right)_{\text{EM-Drive}} = \frac{Q\, g}{c} \tag{3}$$

---

[1] jrodal@alum.mit.edu

where Q is the quality factor of resonance (an inverse measure of damping) and g is a dimensionless factor due to geometry, relative magnetic permeability, relative electric permittivity and mode shape. The specific form of g depends on the specific theory of each author. So, the force per input power for an EM Drive is predicted to be superior to a photon rocket as follows:

$$\left(\frac{F}{P_{in}}\right)_{\text{EM-Drive}} / \left(\frac{F}{P_{in}}\right)_{\text{photonRocket}} = Q\,g \tag{4}$$

In other words, the theoretical outperformance of the EM-Drive is predicted to be due to just the quality of resonance Q and the dimensionless factor g. For the purpose of this discussion I will avoid dealing with the strange consequences of these theories regarding conservation of momentum and conservation of energy issues inherent to the concept of proposing a closed resonant electromagnetic cavity for space propulsion.

2. THE SPECIFIC FORM OF THE FACTOR G FOR DIFFERENT THEORIES

McCulloch [1], has presented a number of simple formulas for the EM-Drive, all having the general form as Eq.(3) above. The simplest of which has the following definition for the dimensionless factor g,

$$g_{McCulloch} = \left(\frac{L}{D_s} - \frac{L}{D_b}\right) \tag{5}$$

where L is the length of the truncated cone, measured perpendicular to the end faces, along the axis of axial symmetry of the cone. D_s is the diameter of the small end of the truncated cone and D_b is the diameter of the big end of the truncated cone. So, it is evident that for this formula from McCulloch, the factor g is a dimensionless factor that only depends on the geometrical ratios L/D_s and L/D_b. It is also obvious that if one scales the EM-Drive geometry, such that the geometrical ratios L/D_s and L/D_b are kept constant, that the dimensionless factor g will remain constant in McCulloch's equation.

Shawyer [2], has presented a formula for the EM-Drive where the dimensionless factor g is defined as follows: $g_{Shawyer} = 2D_f$ where D_f is a dimensionless factor called the *Design Factor* by Shawyer, and where D_f is a function of the diameter-to-length ratios and in addition is also a function of the relative magnetic permeability $\mu_{r_{medium}}$ and the relative electric permittivity $\varepsilon_{r_{medium}}$, as well as the natural frequency of resonance and its associated mode shape (with associated mode shape numbers m, n, p),

$$g_{Shawyer} = g_{Shawyer}\left(\frac{L}{D_s}, \frac{L}{D_b}, \mu_{r_{medium}}, \varepsilon_{r_{medium}}, m, n, p\right) \tag{6}$$

where the diameters of the truncated cone appear explicitly in his formula for the design factor and where the length and the mode shape numbers appear only implicitly because the design factor is dependent on the natural frequency at which resonance with a particular mode shape occurs. It is simple to show that if one scales the EM-Drive geometry such that the geometrical ratios L/D_s and L/D_b, and the medium properties $\mu_{r_{medium}}, \varepsilon_{r_{medium}}$ are kept constant, and the mode shape is kept the same, that the dimensionless factor g will remain constant in Shawyer's equation.

Notsosureofit [3], has presented a more sophisticated formula for the EM-Drive, with explicit dependence on the mode shape, where the dimensionless factor g is defined as follows,

$$g_{Notsosureofit} = \left(\frac{\psi_{mn}^2}{4\pi^3}\right)\left(\frac{c}{f_{mnp}}\right)^3 \frac{1}{L}\left(\frac{1}{D_s^2} - \frac{1}{D_b^2}\right) \tag{7}$$

where $\psi_{mn} = x_{mn}$ (the n^{th} zeros of the cylindrical Bessel function (of the first kind) $J_m(x)$) for transverse magnetic (TM) modes, and $\psi_{mn} = x'_{mn}$ (the n^{th} zeros of the first derivative $J'_m(x)$ of the cylindrical Bessel functions (of the first kind) $J_m(x)$) for transverse electric (TE) modes.

Side note: This link [4], is an excellent source for the numerical values of the n^{th} roots x_{mn} and x'_{mn} of $J_m(x)$ and $J'_m(x)$, respectively, for the following values of m and n: $m < 11$ and $n < 6$.

Therefore, it can be shown that the g factor in *Notsosureofit's* hypothesis is a function of the geometrical ratios, the medium properties and the mode shape of resonance:

$$g_{Notsosureofit} = g_{Notsosureofit}\left(\frac{L}{D_s}, \frac{L}{D_b}, \mu_{r_{medium}}, \varepsilon_{r_{medium}}, m, n, p\right) \tag{8}$$

which is the same form of nondimensional dependence as in Shawyer's $g_{Shawyer}$. Exactly how this is so will be shown in detail in the next section.

3. NATURAL FREQUENCY SCALING

For simplicity, since the truncated cone resonant cavities tested by NASA, Shawyer, Tajmar, and others have all been close to a cylindrical cavity, I will derive the scaling relationship for the natural frequencies of a cylindrical cavity, but this can also be done with the more complicated equations for a truncated conical cavity. For an electromagnetically resonant cylindrical cavity the functions are: the cosine of the longitudinal coordinate z, the cosine of the cylindrical polar angular coordinate ϑ and the cylindrical Bessel functions $J_m(\kappa_{mn}\,\varrho)$ of the cylindrical polar radial coordinate ϱ (where $\kappa_{mn} = \frac{\psi_{mn}}{R}$ is the angular wave number associated with the circular cross-section of the cylinder, which for $p \neq 0$, in other words, for mode shapes with electromagnetic field not constant in the axial direction z, is different from the angular wave number $k_{mnp} = \omega_{mnp}\sqrt{\mu_{r_{medium}}\varepsilon_{r_{medium}}}/c$ for the cylindrical cavity). For an electromagnetically resonant truncated conical cavity instead, the functional dependence is expressed in terms of cosine functions in the azimuthal angle direction ϕ, associated Legendre functions P_n^m in the spherical polar angle (also called zenith angle) direction θ, and spherical Bessel functions $\frac{1}{\sqrt{r}}J_{\pm(n+1/2)}(k_{mnp}r)$ ([5] and [6]). (Here $k_{mnp} = \omega_{mnp}\sqrt{\mu_{r_{medium}}\varepsilon_{r_{medium}}}/c$ is the angular wave number and r is the spherical radial coordinate directed along the generatrix, which for zero spherical polar angle θ coincides with the longitudinal axis z of symmetry of the cone, which is perpendicular to the direction of the radial polar coordinate ϱ for a cylinder. Hence it is important to distinguish between the spherical radial coordinate r and the cylindrical polar radial coordinate ϱ directions: they are very different directions. Also notice that the cylindrical Bessel function $J_m(\kappa_{mn}\,\varrho)$ for the cylinder is only associated with mode shape numbers m and n of the circular cross-sections perpendicular to the longitudinal axis z of the cylinder, and hence independent of mode shape number p, while the spherical Bessel function $\frac{1}{\sqrt{r}}J_{\pm(n+1/2)}(k_{mnp}r)$ for the truncated cone with spherical ends is associated with all mode shape numbers m, n and p of the entire truncated cone, including the trapezium shaped plane sections perpendicular to the azimuthal direction ϕ of the truncated cone).

The reason why all EM-Drive experiments have been performed up to now with EM-Drive geometries close to a cylindrical cavity is because experimenters have tried to follow Shawyer's prescription that, for a given frequency and mode shape, the small diameter of the truncated conical cavity should be larger than the diameter of an open cylindrical waveguide at the cut-off frequency for that mode shape (although the EM-Drive is a closed cavity, and not an open waveguide, and it is known that cut-off does not take place in truncated conical cavities under the same conditions). For practical applications to cavities resonating at the desired mode shapes: TE012 and TE013, this prescription forbids geometries of truncated cones where the small diameter is much different from the big diameter. Therefore it turns out that one can use a mean radius, $R = (D_s + D_b)/4$ to model the truncated cone as a cylindrical cavity, having natural frequencies f_{mnp}

$$f_{mnp} = \frac{c}{R}a_{mnp} \tag{9}$$

angular wave number $k_{mnp} = 2\,\pi\,a_{mnp}\sqrt{\mu_{r_{medium}}\varepsilon_{r_{medium}}}/R$ (radians per unit length), wavelength $\lambda_{mnp} = R/\left(a_{mnp}\sqrt{\mu_{r_{medium}}\varepsilon_{r_{medium}}}\right)$, and where c is the speed of light, R is the previously defined mean radius and where m, n, p are the so called "mode shape numbers" defining the mode shape, where for a cylinder, m is the integer related to the circumferential direction (cylindrical polar angle ϑ direction), n is the integer related to the cylindrical polar radial direction (ϱ direction) and p is the integer related to the longitudinal axial direction (z cylindrical polar axis). From the closed-form solution for an electromagnetically resonant cylindrical cavity (for example Eq.(7.56) of Collin [7], or Eqs.(9.39a) and (9.45) of Balanis [8]) it follows that:

$$a_{mnp} = \sqrt{\frac{(\psi_{mn}/\pi)^2 + (p\,R/L)^2}{4\mu_{r_{medium}}\varepsilon_{r_{medium}}}} \tag{10}$$

It is also trivial to show that since the mean radius is $R = (D_s + D_b)/4$ then the ratio of the mean radius to the length can be expressed in terms of the geometrical ratios $\frac{L}{D_s}$, $\frac{L}{D_b}$:

$$\frac{R}{L} = \frac{1}{4}\left(\frac{D_s}{L} + \frac{D_b}{L}\right) \quad \text{hence} \tag{11}$$
$$a_{mnp} = a_{mnp}\left(\frac{L}{D_s}, \frac{L}{D_b}, \mu_{r_{medium}}, \varepsilon_{r_{medium}}, m, n, p\right)$$

for constant geometrical ratios $\frac{L}{D_s}$, $\frac{L}{D_b}$, constant medium properties $\mu_{r_{medium}}$, $\varepsilon_{r_{medium}}$, and for the same mode shape m, n, p, a_{mnp} will remain constant. Since the frequency scales like $\frac{c}{R}$, and R divided by L, or D_s, or D_b can be expressed in terms of the geometrical ratios $\frac{L}{D_s}$, $\frac{L}{D_b}$, it follows that the frequency f_{mnp} scales like the inverse of any geometrical dimension $\frac{c}{L}$, $\frac{c}{D_s}$ or $\frac{c}{D_b}$ and the geometrical ratios $\frac{L}{D_s}$, $\frac{L}{D_b}$, the medium properties and the mode shape:

$$\begin{aligned} f_{mnp} &= \frac{c}{R} a_{mnp}\left(\frac{L}{D_s}, \frac{L}{D_b}, \mu_{r_{medium}}, \varepsilon_{r_{medium}}, m, n, p\right) \\ &= f_{mnp}\left(\frac{c}{L}, \frac{L}{D_s}, \frac{L}{D_b}, \mu_{r_{medium}}, \varepsilon_{r_{medium}}, m, n, p\right) \\ &= f_{mnp}\left(\frac{c}{D_s}, \frac{L}{D_s}, \frac{L}{D_b}, \mu_{r_{medium}}, \varepsilon_{r_{medium}}, m, n, p\right) \\ &= f_{mnp}\left(\frac{c}{D_b}, \frac{L}{D_s}, \frac{L}{D_b}, \mu_{r_{medium}}, \varepsilon_{r_{medium}}, m, n, p\right) \end{aligned} \tag{12}$$

To illustrate this for *Notsosureofit's* dimensionless factor, substituting Eq. (9) into Eq. (7) it follows that:

$$g_{Notsosureofit} = \left(\frac{\psi_{mn}^2}{4\pi^3}\right)\left(\frac{1}{a_{mnp}}\right)^3 \frac{R}{L}\left(\left(\frac{R}{D_s}\right)^2 - \left(\frac{R}{D_b}\right)^2\right) \tag{13}$$

therefore the dimensionless factor $g_{Notsosureofit}$ depends on the ratio of the mean radius R to the length L and on the square of the ratio of the mean radius R to the diameters D_s and D_b. Since the ratio of the mean radius R to the length L or to the diameters D_s, D_b of the EM-Drive can be expressed in terms of the geometrical ratios $\frac{L}{D_s}$, $\frac{L}{D_b}$:

$$\begin{aligned} \frac{R}{L} &= \frac{1}{4}\left(\frac{D_s}{L} + \frac{D_b}{L}\right) \\ \left(\frac{R}{D_s}\right)^2 &= \frac{1}{16}\left(1 + \frac{\frac{L}{D_s}}{\frac{L}{D_b}}\right)^2 \\ \left(\frac{R}{D_b}\right)^2 &= \frac{1}{16}\left(1 + \frac{\frac{L}{D_b}}{\frac{L}{D_s}}\right)^2 \end{aligned} \tag{14}$$

then it follows that the g factor in *Notsosureofit's* hypothesis is a function of the geometrical ratios, the medium properties and the mode shape of resonance:

$$g_{Notsosureofit} = g_{Notsosureofit}\left(\frac{L}{D_s}, \frac{L}{D_b}, \mu_{r_{medium}}, \varepsilon_{r_{medium}}, m, n, p\right) \tag{15}$$

Therefore for constant geometrical ratios $\frac{L}{D_s}$, $\frac{L}{D_b}$, constant medium properties $\mu_{r_{medium}}$, $\varepsilon_{r_{medium}}$, and for the same mode shape m, n, p, the dimensionless factor g will remain constant. It is trivial to show the same result for Shawyer's design factor, and hence for the dimensionless factor g in Shawyer's expression. So, in general I can state that all theoretical expressions, McCulloch's, Shawyer's and *Notsosureofit's*, are such that the dimensionless factor g will remain constant for constant geometrical ratios $\frac{L}{D_s}$, $\frac{L}{D_b}$, constant medium properties $\mu_{r_{medium}}, \varepsilon_{r_{medium}}$, and for the same mode shape m, n, p.

4. QUALITY OF RESONANCE (Q) SCALING

The quality of resonance factor (Q) is defined as follows:

$$\begin{aligned} Q &\stackrel{\text{def}}{=} 2\pi \frac{\text{EnergyStored}}{\text{EnergyDissipatedPerCycle}} \\ &\stackrel{\text{def}}{=} \omega_{mnp} \frac{\text{EnergyStored}}{\text{PowerLoss}} \end{aligned} \tag{16}$$

where:

$$\begin{aligned} \omega_{mnp} &= \text{resonant angular frequency} \\ &= 2\pi f_{mnp} \\ f_{mnp} &= \text{resonant frequency with mode shape numbers } m, n, p \\ \text{EnergyStored} &= \int \text{ElectromagneticEnergyDensity } dV \\ \text{PowerLoss} &= \frac{\omega_{mnp}\delta}{2} \int \text{ElectromagneticEnergyDensity } dA \\ &= \frac{R_s}{\mu_{wall}} \int \text{ElectromagneticEnergyDensity } dA \\ &= \frac{\rho}{\mu_{wall}\delta} \int \text{ElectromagneticEnergyDensity } dA \\ R_s &= \text{ surface resistance} \\ &= \frac{\rho}{\delta} \\ \rho &= \text{ resistivity of the interior wall of the EM Drive resonant cavity} \\ \mu_{wall} &= \text{ magnetic permeability of the interior wall of EM Drive} \\ &= \mu_0 \mu_{r_{wall}} \\ \delta &= \text{ skin depth (penetration depth of the electromagnetic energy)} \\ V &= \text{ interior volume of EM Drive resonant cavity} \\ A &= \text{ interior surface of EM Drive resonant cavity} \end{aligned}$$

In general, for arbitrary frequencies, the skin depth is:

$$\delta = \sqrt{\frac{2\rho}{\omega\mu_{wall}} \left(\sqrt{1 + (\rho\omega\epsilon_{wall})^2} + \rho\omega\varepsilon_{wall} \right)} \tag{17}$$

where $\varepsilon_{wall} = \varepsilon_0 \varepsilon_{r_{wall}}$ = electric permittivity of the interior wall of the EM-Drive resonant cavity. At angular frequencies ω much below $1/(\rho\varepsilon_{wall})$, for example, in the case of copper, for frequencies much below exahertz (10^9 GHz, the range of hard X-rays and Gamma rays), the skin depth can be expressed as follows,

$$\delta = \sqrt{\frac{2\rho}{\omega\mu_{wall}}} \tag{18}$$

Now, at resonance $\omega = \omega_{mnp}$, using the fact that

$$\text{PowerLoss} = \frac{\omega_{mnp}\delta}{2} \int \text{ElectromagneticEnergyDensity } dA$$

substituting into Eq. (16) definition for the quality factor of resonance, one immediately obtains,

$$Q = \frac{2}{\delta} \frac{\int \text{ Electromagnetic Energy Density } dV}{\int \text{ Electromagnetic Energy Density } dA} \tag{19}$$

Alternatively one can arrive at the same result, using the formula for power loss that depends on the *surface resistance* R_s,

$$\begin{aligned} \text{PowerLoss} &= \frac{R_s}{\mu_{wall}} \int \text{ElectromagneticEnergyDensity } dA \\ &= \frac{\rho}{\mu_{wall}\delta} \int \text{ElectromagneticEnergyDensity } dA \end{aligned}$$

and substituting this into the definition for the quality factor of resonance Eq. (16), one gets,

$$\begin{aligned} Q &= \frac{\omega_{mnp}\mu_{wall}}{R_s} \frac{\int \text{ Electromagnetic Energy Density } dV}{\int \text{ Electromagnetic Energy Density } dA} \\ &= \frac{\omega_{mnp}\mu_{wall}\delta}{\rho} \frac{\int \text{ Electromagnetic Energy Density } dV}{\int \text{ Electromagnetic Energy Density } dA} \end{aligned} \tag{20}$$

and using the fact that at angular frequencies ω much lower than $1/(\rho\varepsilon)$ the angular frequency ω is a function of the square of the skin depth δ,

$$\omega = \frac{2\rho}{\mu_{wall}\delta^2} \tag{21}$$

it is straightforward to show that the quality of resonance Q is:

$$Q = \frac{2}{\delta} \frac{\int \text{ Electromagnetic Energy Density } dV}{\int \text{ Electromagnetic Energy Density } dA} \tag{22}$$

the electromagnetic energy density integrated over the cavity volume, divided by the electromagnetic energy density integrated over the cavity surface area, divided by the skin depth.

Skin depth scaling: At frequencies much below $1/(\rho\varepsilon)$ the skin depth at a resonant frequency f_{mnp} can be expressed as

$$\delta = \sqrt{\frac{\rho}{\mu_{wall}\pi f_{mnp}}} \tag{23}$$

Substituting the expression for frequency Eq. (9), $f_{mnp} = \frac{c}{R} a_{mnp}$, into the above skin depth equation, results in the following expression:

$$\delta = \sqrt{R}\sqrt{\frac{\rho}{\mu_{wall}\,\pi\, c\, a_{mnp}}} \tag{24}$$

Using the previously derived expression for a_{mnp} Eq. 11 and Eq. 14 for the dimensional ratios, one concludes that the skin depth δ scales like the square root of any geometrical dimension, for constant resistivity ρ and magnetic permeability μ_{wall} of the interior wall of the cavity, for constant geometrical ratios $\frac{L}{D_s}$,

$\frac{L}{D_b}$, constant medium properties $\mu_{r_{medium}}, \varepsilon_{r_{medium}}$ and for the same mode shape m, n, p. In other words, for increasing dimensions of the cavity, preserving all geometrical ratios, and keeping medium properties constant and for the same mode shape, the skin depth will increase with the square root of the dimension, while the frequency will decrease, as the inverse of the dimension.

Quality of resonance (Q) scaling: Having determined the scaling law for the skin depth, what now remains to be shown is the scaling for the energy integral ratio in the expression for Q,

$$Q = \frac{2}{\delta}\left(\frac{\int \text{Electromagnetic (EM) Energy Density } dV}{\int \text{ Electromagnetic (EM) Energy Density } dA}\right) \tag{25}$$

The expressions under the integrals are dependent on each mode shape, as the electromagnetic energy distribution depends on mode shape, of course. However, notice that the lowest mode shapes (those with low values of mode shape numbers m, n, p, for example TE012, TE013, TM212) have been of interest in the EM Drive experiments so far. So, for simplification purposes assume that the distribution of the electromagnetic field is of low order, and hence not that much variable throughout the cavity, for low m, n, p number mode shapes (for example m=0, associated with the mode shape numbers TE012 and TE013 used by Shawyer, means a constant distribution in the azimuthal circumferential direction of the cavity). Under this assumption one can (for approximation purposes) take the energy density out of the volume and surface integrals:

$$\begin{aligned}\left(\frac{\int \text{ EM Energy Density } dV}{\int \text{ EM Energy Density } dA}\right) &\sim \left(\frac{\text{EM Energy Density}}{\text{EM Energy Density}}\right)\left(\frac{\int dV}{\int dA}\right) \\ &\sim \frac{\text{InteriorVolume}}{\text{InteriorSurfaceArea}} \\ &\sim \frac{\pi R^2 L}{2\pi R(R+L)} \\ &\sim \frac{R}{2(1+R/L)}\end{aligned} \tag{26}$$

and substituting this and the previously found scaling law for the skin depth, into the expression for the quality of resonance factor Q, leads to:

$$\begin{aligned}Q &= \frac{2}{\delta}\left(\frac{\int \text{ EM Energy Density } dV}{\int \text{ EM Energy Density } dA}\right) \\ &\sim \frac{2}{\sqrt{R}\sqrt{\rho/(\mu_{wall}\,\pi\, c\, a_{mnp})}}\frac{R}{2(1+R/L)} \\ &\sim \sqrt{R}\frac{1}{(1+R/L)}\sqrt{\frac{\mu_{wall}\,\pi\, c\, a_{mnp}}{\rho}} \\ &\sim \sqrt{L}\frac{\sqrt{\frac{D_s}{L}+\frac{D_b}{L}}}{2(1+\frac{1}{4}\left(\frac{D_s}{L}+\frac{D_b}{L}\right))}\sqrt{\frac{\mu_{wall}\,\pi\, c\, a_{mnp}}{\rho}} \\ &\sim \sqrt{D_s}\frac{\sqrt{1+\frac{\frac{L}{D_s}}{\frac{L}{D_b}}}}{2(1+\frac{1}{4}\left(\frac{D_s}{L}+\frac{D_b}{L}\right))}\sqrt{\frac{\mu_{wall}\,\pi\, c\, a_{mnp}}{\rho}} \\ &\sim \sqrt{D_b}\frac{\sqrt{1+\frac{\frac{L}{D_b}}{\frac{L}{D_s}}}}{2(1+\frac{1}{4}\left(\frac{D_s}{L}+\frac{D_b}{L}\right))}\sqrt{\frac{\mu_{wall}\,\pi\, c\, a_{mnp}}{\rho}}\end{aligned} \tag{27}$$

where the dimensionless mode shape factor a_{mnp} is:

$$a_{mnp} = \sqrt{\frac{(\psi_{mn}/\pi)^2 + (p\,R/L)^2}{4\mu_{r_{medium}}\varepsilon_{r_{medium}}}} = \sqrt{\frac{(\psi_{mn}/\pi)^2 + (\frac{p}{4}\,(\frac{D_s}{L} + \frac{D_b}{L}))^2}{4\mu_{r_{medium}}\varepsilon_{r_{medium}}}}$$

Therefore one concludes that the quality of resonance Q scales like the square root of any geometrical dimension L, D_s or D_b, for constant resistivity ρ and magnetic permeability μ_{wall} of the interior wall of the cavity and for constant geometrical ratios $\frac{L}{D_s}$, $\frac{L}{D_b}$, constant medium properties $\mu_{r_{medium}}, \varepsilon_{r_{medium}}$, and for the same mode shape m, n, p. In other words, for increasing dimensions of the cavity, preserving all geometrical ratios, keeping medium properties constant and for the same mode shape, the quality of resonance Q will increase with the square root of the dimension, also the skin depth will increase with the square root of the dimension, while the frequency will decrease, as the inverse of the dimension.

Furthermore, I previously proved that all three theories for the EM Drive (McCulloch, Shawyer and *Notsosureofit*) have expressions for the force/input power proportional to the quality of factor Q times a dimensionless factor g,

$$\left(\frac{F}{P_{in}}\right)_{\text{EM-Drive}} / \left(\frac{F}{P_{in}}\right)_{\text{photonRocket}} = Q\,g$$

$$\left(\frac{F}{P_{in}}\right)_{\text{EM-Drive}} = \frac{Q\,g}{c} \tag{28}$$

and I previously proved that the dimensionless factor g (for all three theories: McCulloch, Shawyer and *Notsosureofit*) remains perfectly constant for constant geometrical ratios, constant medium properties $\mu_{r_{medium}}, \varepsilon_{r_{medium}}$ and for the same mode shape m, n, p. Therefore one concludes that the force per input power (for all three theories: McCulloch, Shawyer and *Notsosureofit*) scales like the square root of any geometrical dimension, for constant resistivity ρ and magnetic permeability μ_{wall} of the interior wall of the cavity and for constant geometrical ratios $\frac{L}{D_s}$, $\frac{L}{D_b}$, constant medium properties $\mu_{r_{medium}}, \varepsilon_{r_{medium}}$ and for the same mode shape m, n, p.

In other words, to maximize the force per input power, according to all three theories: (McCulloch, Shawyer and *Notsosureofit*) the most efficient EM-Drive would be as large as possible, this being due to the fact that the quality of factor of resonance Q (all else being equal) scales like the square root of the geometrical dimensions. Small cavity EM-Drives (all else being equal) are predicted to have smaller quality of resonance Q and therefore smaller thrust force/input power.

It is not clear whether this has been known to EM-Drive experimenters, given the fact that the recent experiments by Prof. Tajmar at TU Dresden, Germany, (under advice from Roger Shawyer according to the report [9]) were performed with a much smaller EM-Drive than previously tested by Shawyer and by NASA [10], and the fact that there are several EM-Drive researchers discussing really tiny EM-Drives (as the group in Aachen, Germany [11]) for use in CubeSats. Such EM Drives are predicted to be less efficient, having lower thrust force/input power, if the claimed thrust is not an experimental artifact.

5. NUMERICAL VERIFICATION ANALYSIS

The scaling law for the EM-Drive discussed in the previous sections is verified numerically using the exact solution for a truncated cone in terms of spherical Bessel and associated Legendre functions, using Wolfram *Mathematica*, and the experimental results from NASA [10].

NASA's truncated cone dimensions and material

$D_b = 11.01$ inch $= 0.279654$ m
$D_s = 6.25$ inch $= 0.15875$ m
$L = 9.00$ inch $= 0.2286$ m
$\rho = 1.71 \times 10^{-8}$ ohm meter (wall material: copper alloy 101)
$\mu_{r\,wall} = 0.999991$

Since the exact solution assumes spherical ends, while NASA's truncated cone experiment has flat ends, the spherical radii r_1 and r_2 are calculated as the mean value of the radii to a) the intersection of the ends with the lateral conical walls and b) the top of the dome. From analysis of the problem and verification using numerical analysis (comparison with COMSOL FEA solutions for a large number of examples) I have determined that this mean value is an excellent approximation to the solution of Maxwell's equations for a truncated cone with flat ends. These input parameters result in the following values (in SI units) for the spherical radii r_1 and r_2:

$r_1 = 0.305316$ m
$r_2 = 0.537845$ m

and for the truncated cone half angle value at the conical wall θ_w (the spherical polar angle measured from the axis of symmetry z of the cone to the conical wall):

$\theta_w = 14.8125$ degrees

Experimental measurement by NASA (for mode shape TE012):

$f_{012} = 2.168$ GHz

Output (exact solution output results for mode shape TE012):

$f_{012} = 2.16467$ GHz
$\delta = 1.41457$ micrometers
$Q = 78,642.4$

Scaled geometry: ten times larger than NASA's geometry

Input

$D_b = 110.1$ inch $= 2.79654$ m
$D_s = 62.5$ inch $= 1.5875$ m
$L = 90.0$ inch $= 2.286$ m
$\rho = 1.71 \times 10^{-8}$ ohm meter (wall material: copper alloy 101)
$\mu_{r\,wall} = 0.999991$

Output (exact solution results for mode shape TE012):

$f_{012} = 0.216467$ GHz
$\delta = 4.43121$ micrometers
$Q = 251,049$

frequency scaling: $(2.16467231443426289^9/2.16467231443426678^8)/10 = 1$
Q scaling: $(78642.44767279371/251049.34868706256)/\sqrt{10} = 0.990599$

Scaled geometry: ten times smaller than NASA's geometry

Input

$D_b = 1.101$ inch $= 0.0279654$ m
$D_s = 0.625$ inch $= 0.015875$ m
$L = 0.900$ inch $= 0.02286$ m

$\rho = 1.71 \times 10^{-8}$ ohm meter (wall material: copper alloy 101)
$\mu_{r\,wall} = 0.999991$

Output (exact solution output results for mode shape TE012):

$f_{012} = 21.6467$ GHz
$\delta = 0.443121$ micrometers
$Q = 25,104.9$

frequency scaling: $(2.16467231443426289^9/2.164672314434267^{10}) * 10 = 1$
Q scaling: $(78642.44767279371/25104.934868706456)/\sqrt{10} = 0.990599$

The following is confirmed: when using the exact solution for resonance of a truncated conical cavity, for constant resistivity and magnetic permeability of the interior wall of the cavity and for constant geometrical ratios, constant medium properties and for the same mode shape (TE012): 1. the frequency scales (exactly) like the inverse of any geometrical dimension, 2. therefore the skin depth scales (exactly) like the square root of any geometrical dimension, 3. the quality of resonance (Q) scales approximately like the square root of any geometrical dimension, within 1% accuracy due to the approximation that the electromagnetic energy density is approximately constant through the interior volume and through the interior surface area of the cavity (this approximation is good for a low mode like TE012 but is expected to gradually degrade with higher mode shape numbers).

References

[1] M. McCullogh, "Can the EM-Drive Be Explained by Quantized Inertia?" Progress in Physics, Volume 11, Issue 1, pp. 78-80, (2015). Available at `http://www.ptep-online.com/index_files/2015/PP-40-15.PDF`

[2] R. Shawyer, "A Theory of Microwave Propulsion for Spacecraft," Theory Paper V 9.4 (2006). Available at `http://www.emdrive.com/theorypaper9-4.pdf`

[3] *Notsosureofit*, Ph.D. in General Relativity, is a physicist in the Boston area, who would like to remain anonymous using this pen name that expresses his views about the experimental claims made about the EM Drive. The mathematical basis for his hypothesis (July 16, 2015) can be accessed at `http://emdrive.wiki/@notsosureofit_Hypothesis`

[4] Accelerator Laboratory of Kyoto University, "Roots of Bessel functions (15 digits)," and "Roots of Derivatives of Bessel functions," numerical values to 15 digits precision of the n^{th} roots x_{mn} and x'_{mn} of the cylindrical Bessel function $J_m(x)$ and its derivative $J'_m(x)$, respectively, for the following values of m and n: $m < 11$ and $n < 6$, (April 10, 2013). Available at `http://wwwal.kuicr.kyoto-u.ac.jp/www/accelerator/a4/besselroot.htmlx`

[5] G. Egan, "Resonant Modes of a Conical Cavity," (August 5, 2014). Available at `http://www.gregegan.net/SCIENCE/Cavity/Cavity.html`

[6] F. Minotti, "Scalar-Tensor Theories and Asymmetric Resonant Cavities," Gravitation and Cosmology, Volume 19, Issue 3, pp. 201-208, (July 2013). Available at `https://arxiv.org/abs/1302.5690`

[7] R. Collin, "*Foundations for Microwave Engineering*," Wiley-IEEE Press, second edition (January 5, 2001).

[8] C. Balanis, "*Advanced Engineering Electromagnetics*," Wiley, second edition (January 24, 2012).

[9] M. Tajmar and G. Fiedler, "Direct Thrust Measurements of an EM Drive and Evaluation of Possible Side-Effects," 51st AIAA/SAE/ASEE Joint Propulsion Conference, AIAA Propulsion and Energy Forum (July 27-29, 2015), Orlando, FL, AIAA 2015-4083. Available at `http://arc.aiaa.org/doi/abs/10.2514/6.2015-4083`

[10] D. Brady, H. White, P. March, J. Lawrence and F. Davies, "Anomalous Thrust Production from an RF Test Device Measured on a Low-Thrust Torsion Pendulum," 50th AIAA/ASME/SAE/ASEE Joint Propulsion Conference, AIAA Propulsion and Energy Forum (July 28-30, 2014), Cleveland, OH, AIAA 2014-4029. Available at `https://ntrs.nasa.gov/search.jsp?R=20140006052`

[11] P. Kocyla, "EMDrive/Satellite, Developing a Small Fuelless Microwave Thruster," (2016). Available at `https://hackaday.io/project/5596-emdrivesatellite`

APPENDIX D

Mach Effect Propulsion, an Exact Electroelasticity Solution

José J. A. Rodal[1]
Rodal Consulting
Research Triangle Park, North Carolina

Mathematical models and numerical results for the Mach Effect Gravitational Assist (MEGA) drive are presented. The MEGA drive is shown to be a Langevin stack where the piezoelectric and electrostrictive effects resulting from an oscillating electric field excitation are used to produce a Mach effect force. An exact electroelasticity solution is obtained for a Langevin (MEGA) piezoelectric/electrostrictive stack. The calculated natural frequency of the Langevin stack compares very well with previously reported MEGA experiments. The calculated direction of the Mach effect force and the optimal tail brass mass are also shown to compare excellently with MEGA experimental data. The reported optimal tail (brass) mass of the MEGA experiments is shown to be an experimental artifact associated with dissipative end fixity. For a MEGA drive free in space there is no optimal mass tail mass, but rather, the Mach effect force increases as a decaying exponential rapidly approaching an asymptotic value for increasing tail mass of the Langevin (MEGA) stack.

CONTENTS

1. PIEZOELECTRICITY, THE LANGEVIN TRANSDUCER AND PZT

First, a short history of piezoelectricity, the invention of the Langevin transducer, and lead (Pb) zirconate titanate (PZT):

- 1880: Pierre and Jacques Curie started research at the École de Physique et Chimie (nowadays École supérieure de physique et de chimie industrielles de la ville de Paris, ESPCI), on crystal electro-elastic properties that led to the discovery of piezoelectricity.
- 1888: Paul Langevin entered ESPCI and helped Pierre Curie with further piezoelectric experiments. Later, he attended Cambridge University and studied in the Cavendish Laboratory under Sir J. J. Thomson. Langevin returned to the Sorbonne and obtained his Ph.D. from Pierre Curie in 1902.

---

[1] jrodal@alum.mit.edu

- 1905: Langevin, aged 34, became Professor and in 1906 succeeded P. Curie (who died instantly in 1906, aged 46, as a consequence of a road accident) as head of the piezoelectric laboratory at ESPCI.

- 1916, 100 years ago (World War I): invention of piezoelectric stack sonar, P. Langevin and C. Chilowsky awarded 1916 French patent 502,913 and 1917 US Patent 1,471,547 for first ultrasonic submarine detector. It described a sandwich stack of thin quartz crystals, 15 mm long, bonded to steel masses. Resonant frequency: 50 kHz. Time taken by the signal to travel to the enemy submarine and echo back to the ship was used to calculate the distance.

- 1940's: (World War II): discovery of ferroelectricity (demonstrating that it could exist in simple oxide materials, and it was not always associated with hydrogen bonding): barium titanate $BaTiO_3$. In 1941, H. Thurnaurer and J. Deaderick filed US Patent 2,429,588 for doping studies of BaO and TiO_2 which produced ceramics with enhanced dielectric permittivity. Later, more precise studies by Wainer and Solomon in the USA (1942), Ogawa and Waku (1944) in Japan and Wul and Goldman (1945) in Russia. von Hippel at MIT (USA) published his WWII work demonstrating ferroelectric switching in $BaTiO_3$ in 1946. US firm Sonotone in 1947 marketed $BaTiO_3$ phonograph pickups.

- 1950's: 1952: invention of lead zirconate titanate (PZT) $Pb[Zr_xTi_{1-x}]O_3$ ($0 \leq x \leq 1$) at Tokyo Institute of Technology by Y. Takagi, G. Shirane and E. Sawaguchi. 1953: E. Sawaguchi published the phase diagram for PZT. 1957: US firm Clevite trademarked the name PZT and developed the formulations for PZT-4, PZT-5, PZT-6, PZT-8, etc. and secured their patents.

Langevin (see Fig. 1 for a photo of Langevin at the 5^{th} Solvay conference) realized that there was a limit as to how thick piezoelectric plates could be made to make effective piezoelectric transducers for underwater acoustic applications (sonar). For this reason, to this date, sonar and ultrasonic-application transducers are often composed of a sandwich stack of piezoelectric plates. The sandwich stack of piezoelectric plates is attached to a tail (or back) mass at the rear, and a head (or front) mass at the front, facing the acoustic medium (for example, water, for a sonar transducer).

The attached masses allow the transducer to match the frequency required for particular applications. (The mechanical natural frequencies of the Langevin stack are dictated by the masses and by the longitudinal stiffness of the stack). This way, the stack is resonant at the desired operating frequency with the mass of the piezoelectric element being a small component of the overall mass. In the original patents by Langevin, the piezoelectric stack is compressed between the two masses by a central bolt, Fig. 3. Other transducers use instead a number of bolts around the outside perimeter of the stack to apply compression. This compressive stress is necessary because the piezoelectric materials often used for these transducers are brittle ceramics formed by a sintering process (the process of compacting ceramic particles and forming a solid mass, by applying pressure and heat, at a temperature below the melting temperature). The resulting ceramic plate is a brittle polycrystalline material, with low fracture toughness, due to the voids created during the forming process and which are present between the sintered ceramic grain boundaries (grains with typical dimensions of 2 micrometers, Fig. 2), that can coalesce into cracks. Therefore these discs easily fracture under low magnitude tensile stress. The purpose of the initial compressive stress on the stack is to ensure that the ceramic discs never experience tension but instead oscillate between greater and lesser levels of compression during ultrasonic vibration. During assembly of the stack under controlled conditions, the bolt(s) is(are) tightened to provide a precise amount of compressive stress (typically 15 to 30 MPa=2,200 to 4,400 psi for hard stacks).

Lead Zirconate Titanate (PZT) is a ceramic that is:

- Ferroelectric: it has spontaneous electric polarization which can be reversed with a large enough electric field.

FIG. 1: Attendees of the 5^{th} Solvay International Conference, *On electron and photons*, Brussels, October 1927, 17 of these 29 participants were or became Nobel Prize winners.(Photo credit: B. Couprie, Institut International de Physique de Solvay)

- Piezoelectric: it displays extremely large (relative to other materials) dielectric and piezoelectric constants when the solution has near equal parts of lead titanate and lead zirconate solution. The piezoelectric PZT plate develops a voltage difference across its two faces when compressed or stretched (with the polarity of the electric field depending on the sign of the strain). This is called the direct piezoelectric effect and it is used for stress or strain sensing applications. This effect is used to measure the dynamic strain, using passive PZT plates, in the Mach effect Langevin stack that has been used in the experiments of Woodward and Fearn at California State University, Fullerton. These passive PZT plates measure the strain through the thickness of the PZT, resulting from the stress transmitted from the other plates in the stack, and hence act essentially as strain gauges. One should be cautious not to interpret the reading from these passive plates as measuring anything but strain, for example as measuring acceleration, because the relationship between the measured strain and the acceleration is very dependent on the equations of motion, specifically the amount of damping and the difference between the excitation frequency and the natural frequency. Scientific piezoelectric accelerometers are restricted to operating at excitation frequencies lower than 3 dB below the first natural frequency (in other words, approximately below $\frac{1}{2}$ of the first natural frequency). This $\frac{1}{2}$ of the first natural frequency limit marks the frequency where the measuring error becomes 30%. If the exciting frequency becomes closer to the natural frequency, the error becomes much larger. The PZT also deforms when an external electric field is applied across its faces in direct linear proportion to the applied electric field. This is called the inverse piezoelectric effect and it is used for actuator applications as in ultrasonic transducers, or as in the active PZT plates in the Mach effect Langevin stack that have been used in the experiments of Woodward and Fearn, to produce the force.

- Electrostrictive: this is a much smaller effect in PZT than the inverse piezoelectric effect. It deforms when an external electric field is applied across its faces, in proportion to the square of the applied electric field. This electrostrictive feature is usually ignored in most PZT applications, but it is essential to produce the Mach effect force in the Langevin stack that has been used in the experiments of Woodward and Fearn.

- Pyroelectric: a PZT plate develops a voltage difference across its two faces when it experiences a temperature change. Therefore, it can be used as a sensor to measure temperature differences.

The above properties have made PZT piezoelectric ceramics the most prominent and useful electroceramics since they were first marketed in 1957 by US firm Clevite, who trademarked the name PZT and developed the formulations for PZT-4, PZT-5, PZT-6, PZT-8, etc., under the scientific leadership of Hans Jaffe (Ph.D. Goettingen, 1934) and Bernard Jaffe [1], and was awarded their patents. The US Navy standardized several of these types of PZT (Navy Types I, II, III, etc., where Navy Type IV is barium titanate instead of lead zirconate titanate) originally developed by Clevite, in a military standard [2]. PZT, besides being brittle, cannot readily withstand contact stresses, wear, high humidity, or aggressive media, therefore a housing is used in many applications. In some Langevin stack designs the metal housing itself (which serves the purpose of protecting the brittle piezoelectric material from fluid attack, etc.) has been used as the pre-stressing spring, instead of using bolts.

For most underwater acoustic applications the front mass usually is made lighter than the back mass, in order to increase the displacement amplitude at the front end, facing the acoustic medium, Fig. 4. For sonar applications the front end is also widened to a larger flat radiation surface at the acoustic end to provide good acoustic matching with the water. The ratio of the back mass to the front mass has a significant effect on the acoustic radiation. The lighter the head mass, compared to the back mass, the greater the velocity of the head mass, and the greater the sonic pressure level generated. In order to decrease the mass of the front mass, the material selected for the head mass should have a low density, while preserving a high ratio of stiffness to mass density, so that the speed of sound in the head mass is relatively high. Aluminum satisfies these conditions and therefore aluminum is commonly used for the head mass.

For applications different than sonar, such as sonochemistry (the application of ultrasound to chemical reactions, using acoustic cavitation) and ultrasonic surgery, ultrasonic cleaning, ultrasonic welding, ultrasonic machining, etc., that require amplification of the displacement amplitude and focusing the oscillatory energy into a spot, the front mass is connected to a long horn (also known as sonotrode, acoustic wave guide, booster, plunger, or ultrasonic probe). Another purpose of the long horn is to prevent tensile stresses on the brittle piezoelectric actuator, resulting for example from dynamic bending moments or dynamic torques at the tip of the horn. These horns can have different cross-sectional profiles in the longitudinal direction: stepped, exponential, conical, catenoidal, or a composite of different profiles. The horn is usually bolted to the front mass. The whole assembly (back mass, stack, front mass and horn) is impedance matched to maximize

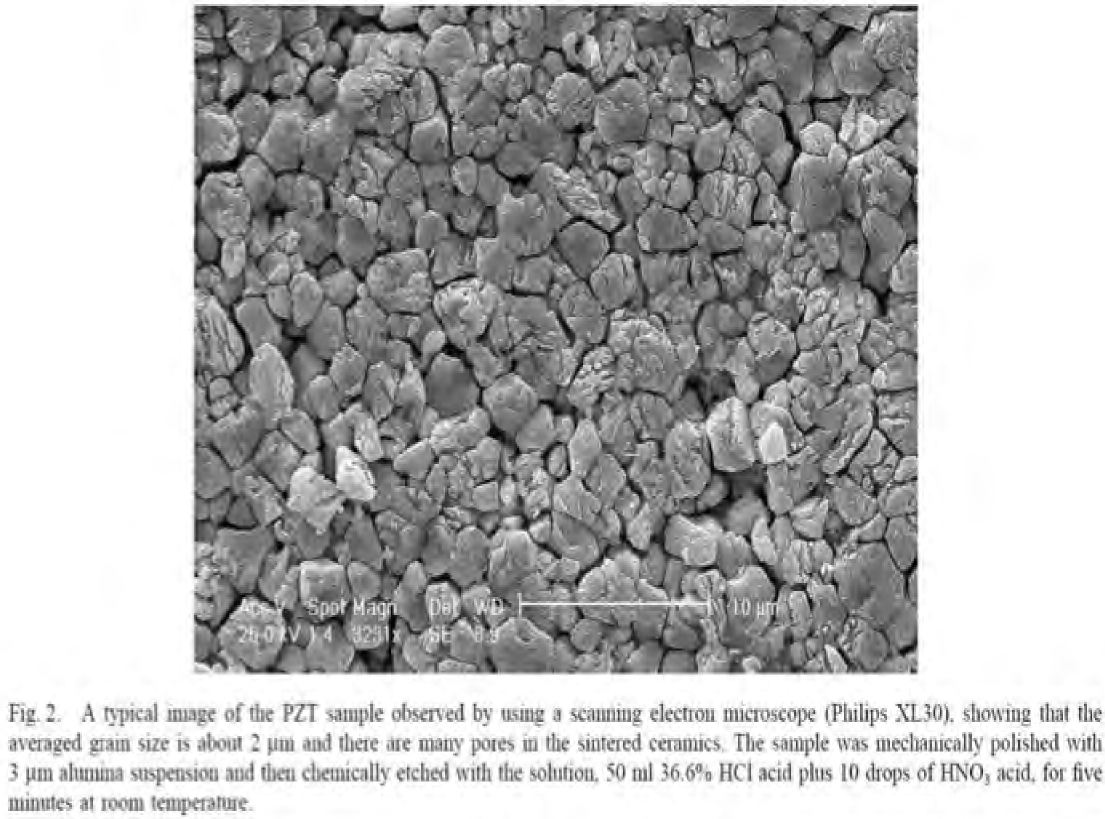

FIG. 2: Scanning electron microscope (SEM) image of lead zirconate titanate (PZT-4, Navy Type I, supplied by Morgan Matroc) grain structure, showing an average grain size of 2 μm and several inter-granular voids. (Image from Fig. 2 of [5])

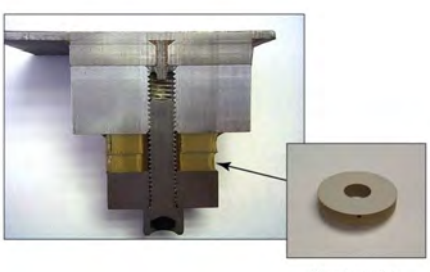

FIG. 3: Langevin Ultrasonic transducer. Piezo disc shown enlarged on the right. (Image from John Fuchs at John's Corner Technical Blog)

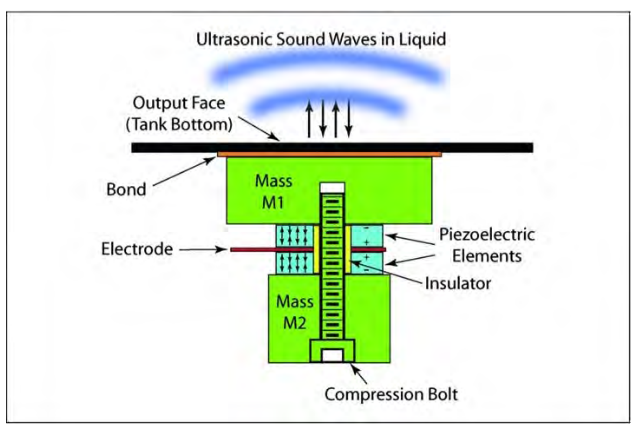

FIG. 4: Langevin Ultrasonic transducer, for underwater acoustic applications. (Image from John Fuchs at John's Corner Technical Blog)

energy transfer to the tip of the horn. The total length of the whole transducer assembly is designed to be an integer multiple of the half wavelength of vibration.

The tail mass is usually considered the least important part when compared with the head mass and the stack. Its main function is to be a counter mass to the head mass to produce a two-mass (the head and the tail masses), 1-spring (the stack) resonant system. To increase the radiated power and bandwidth of the transducer, the mass of the tail mass should be as large as possible. The back mass, due to being the largest mass, has a major influence on the resonant frequency of the transducer. Hence, the material selected for the tail mass must have a high density to satisfy this need with a reasonable volume, and it must have a high stiffness to have a high speed of sound. Therefore, steel is commonly used as the material for the tail mass. For high frequency designs where the volume needs to be small, tungsten is also used. In most ultrasonic applications, the transducer is driven by a continuous sinusoidal wave source tuned to the first natural frequency of the Langevin transducer. Langevin transducers usually work at a frequency range from 20 kHz to 200 kHz.

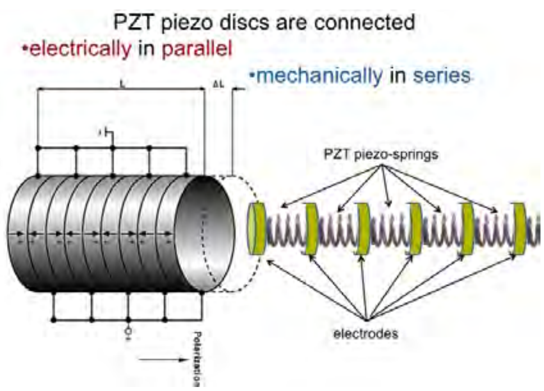

FIG. 5: Langevin piezoelectric stack. Lead zirconate titanate (PZT) discs are connected electrically in parallel and mechanically in series.

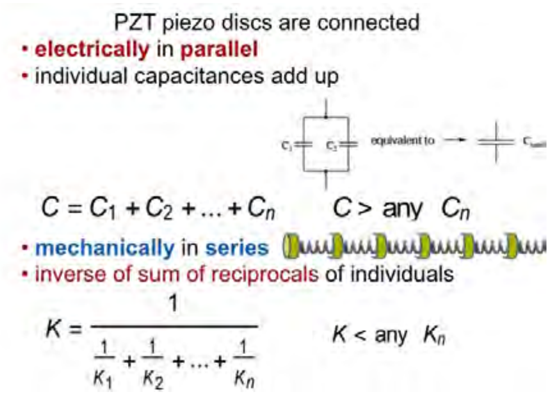

FIG. 6: Capacitors are connected electrically in parallel and springs are connected mechanically in series.

To this date, sonar transducers are often composed of a sandwich stack of piezoelectric discs or plates connected mechanically in series, and electrically in parallel so as to result in the largest displacement for a given level of voltage excitation, Figs. 5 and 6. The piezoelectric plates are placed so that their positively poled faces contact a positive electrode. The negatively poled faces of the plates, including the front and the back masses, are at negative or ground potential and complete the circuit of the piezoelectric stack. The faces of the piezoelectric ceramic elements are sometimes coated with a conductive material (like silver) to enhance this electrical connection to the electrodes. Each piezoelectric plate in the Langevin stack can be idealized as behaving like a spring in the thickness direction of the piezoelectric plate. The stress in the longitudinal direction at the interface of each piezoelectric plate with the electrode and the next piezoelectric plate in the sandwich construction of the stack has to satisfy stress continuity. This means that if the cross-sectional areas of the piezoelectric plates are identical, the transmitted force must be continuous. It is simple to show that if the force is continuous, this implies that the springs representing each piezoelectric plate are connected in series. The effective stiffness of the stack is the inverse of the sum of the reciprocals of the individual stiffness of each piezoelectric plate in the stack. This means that the larger the number of piezoelectric plates, the longer the stack, the lower the effective stiffness of the stack. The simplest equivalent circuit representation of each piezoelectric plate is a capacitor in parallel with a resonant circuit composed of another capacitor, an inductor and a resistance in series. As Monkman et.al. state in page 92 of [6], piezoelectric actuators are basically capacitive elements; this means that current only flows during the charging process (while the actuator is providing motion) and so long as leakage currents and losses can be kept small, force is maintained at the end of the stroke without the need of supplying additional energy. Since the piezoelectric plates are connected electrically in parallel, this means that each of these equivalent circuits is connected in the stack in parallel. Capacitances in parallel add up, therefore the Langevin stack results in an actuator which provides a motion that is a multiple of the number of piezoelectric plate capacitances in the Langevin stack, but whose stiffness decreases as the inverse of the sum of the reciprocals of the individual stiffness of each piezoelectric plate in the stack. Hence if the design goal is to amplify the displacement, the number of plates in the Langevin stack should be maximized while, if the goal is to have the highest stiffness and highest natural frequency, then the lower the number of piezoelectric plates the better, Fig. 6.

Comparing a Langevin piezoelectric stack made with hard PZT piezoelectric plates with an electromagnetic

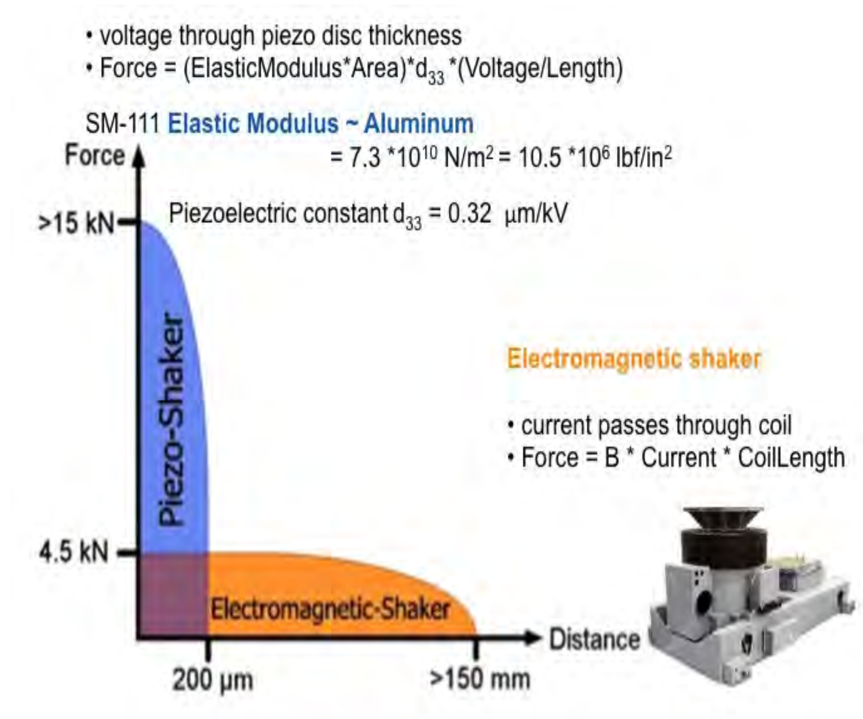

FIG. 7: Piezoelectric Shaker compared with Electromagnetic Shaker. (Images from Piezosystem Jena and from Thermotron Electromagnetic Shakers)

shaker, one notices a significant difference between them. An electromagnetic shaker, Fig. 7, provides a much larger displacement than a hard PZT Langevin stack, but a significantly smaller force. This is because the force provided by the electromagnetic shaker is effectively given by the magnetic field times the current times the coil length. On the other hand the hard PZT Langevin stack provides a much greater force with a much smaller displacement. This is because the hard PZT Langevin stack's force is proportional to the modulus of elasticity of the hard PZT (which is close to the modulus of elasticity of aluminum) times the cross-sectional area of the PZT plates, times the piezoelectric coefficient in the longitudinal direction of the stack, times the electric field (applied voltage to each piezoelectric plate in the stack divided by the thickness of the piezoelectric plate). The force provided by the PZT Langevin stack can be much greater than that of an electromagnetic shaker because it relies on the high modulus of elasticity of the PZT. This is the reason why electromagnetic shakers have to be made very large, much larger than the cross-sectional area of Langevin stacks, to provide similar forces. On the other hand, the piezoelectric stack provides a much smaller displacement because the piezoelectric strain effect in a piezoelectric material like hard PZT is very small (less than 200 micrometer displacement for a typical stack), particularly when compared to an electromagnetic shaker (typically over 100 mm). As Monkman et.al. state in page 92 of [6], piezoelectric actuators are basically capacitive elements whose force is maintained at the end of the stroke without the need of supplying additional energy (ignoring losses), and this is in complete contrast with electromagnetically driven actuators like electromagnetic shakers, where energy must continue to be supplied if the full actuator force is to be maintained.

Lead zirconate titanate (PZT) is the ferroelectric material used in the Langevin ultrasonic transducers tested for the Mach effect in the MEGA (Mach effect Gravity Assist) drive, Figs. 8 and 9. The chemical formula of PZT is Pb$[Zr_xTi_{1-x}]O_3$ (where x is the mole fraction, with possible range $0 \leq x \leq 1$; and best properties typically $0.47 \leq x \leq 0.52$). The piezoelectric properties of PZT ceramics are a result of their molecular structure. The largest piezoelectric effects are observed when the mole fraction of titanium (Ti) and zirconium (Zr) are close to 0.5, in the transitional region between the tetragonal and rhombohedral perovskite crystal phases (perovskite: a type of crystal structure like the one in calcium titanium oxide ($CaTiO_3$), ${}^{XII}A^{2+}\,{}^{VI}B^{4+}X_3^{2-}$ where A and B are two cations (a positively charged ion), with A atoms larger than B atoms, and where X is an anion (a negatively charged ion) that bonds them, with the oxygen anion in the face centers). In the transitional area between the tetragonal and rhombohedral phases there is a significant polarization variation. (A crystalline structure is polarized if the average position of all of its positive ions is not the same as the average position of all of its negative ions.) This transitional area is called the morphotropic phase boundary (MPB). Examining the phase diagram, Figs. 8 and 9, it is apparent that multiple crystalline structures can exist near this boundary.

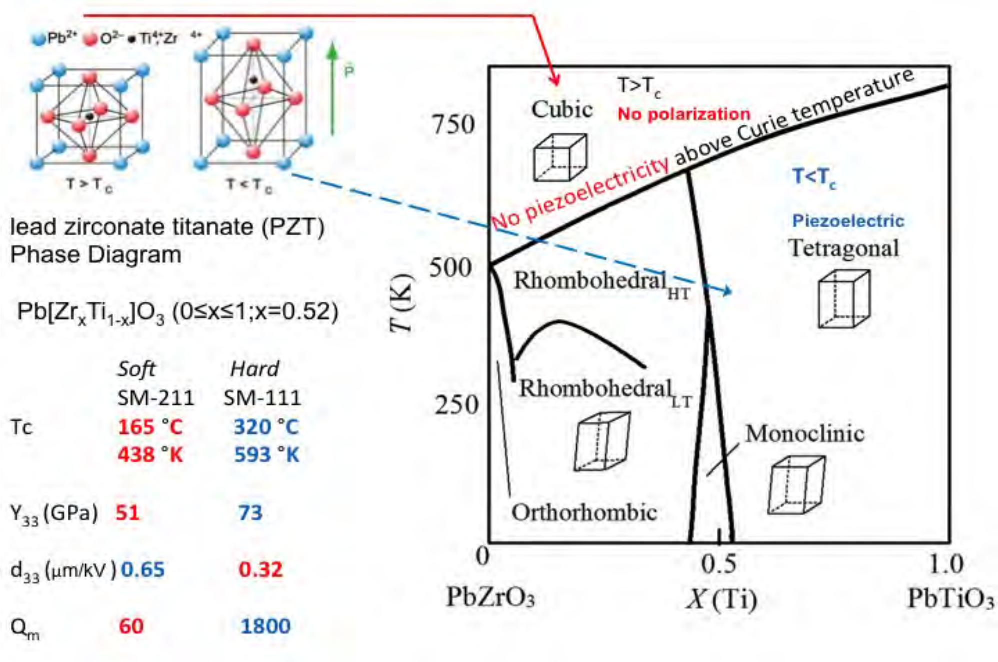

FIG. 8: Phase diagram and properties of lead zirconate titanate (PZT). (Background phase diagram from Fig. 1 of Shindo et.al. [3])

The Curie temperature (Tc) for a ferroelectric material is defined as the transition temperature such that the material is ferroelectric below Tc and dielectric above Tc. Materials in their ferroelectric state (below Tc) are piezoelectric: they have a spontaneous electric polarization as their structures are unsymmetrical. In the ferroelectric state the spontaneous polarization can be reversed by a suitably strong applied electric field in the opposite direction; the polarization is therefore dependent not only on the current electric field but also on its history, yielding a hysteresis loop (when plotting polarization versus electric field). Above Tc, the material's spontaneous electric polarization changes to induced electric polarization. Above Tc the material is in a dielectric state and therefore it has no electric polarization in the absence of an applied electric field. The electric dipoles are unaligned and have no net polarization. Electric susceptibility only occurs above Tc. Above Tc the structure has cubic symmetry: the crystal structure is centrosymmetric and hence there is no dipole moment. In perovskite structures the dipole is created by movement of the central ion in the crystal structure. Below Tc the central ion moves out of the centrosymmetric location and so the charges no longer balance and this results in a net dipole. Once the temperature drops below Tc, the crystal structure becomes tetragonal or rhombohedral resulting in an electric dipole moment. These non-cubic structures have over 14 stable domain configurations at the MPB giving them great flexibility during polarization. The region of the MPB near the Tc favors enhancement of the longitudinal piezoelectric coefficient and longitudinal susceptibility.

Materials in their ferroelectric state (below Tc) can be forced to have their dipoles aligned in a particular direction by a process called poling. The poling process involves aligning the individual dipole moments, so that they point in the same general direction. This is accomplished by exposing the crystal to a constant electric field in the desired direction. Under the electric field, dipoles that are not parallel to the electric field lines experience a torque, and so they are turned to the same direction as the electric field. When the electric field is removed from the material in the ferroelectric state (below Tc), the dipoles remain fairly aligned, and the material is said to be "poled" in that direction. Poling usually is done by heating the material above the Tc, applying the electric field, cooling below the Tc, and finally halting the electric field. The result is a "remanent" polarization as well as a permanent deformation. The piezoelectricity is maintained as long as the material is not de-poled, which can happen for example if the material is exposed to a temperature above Tc, or to an extreme electric field or to high stress conditions. For example, later exposure to a high magnitude electric field causes polarization reversal, leading to the hysteresis loop shown by ferroelectrics.

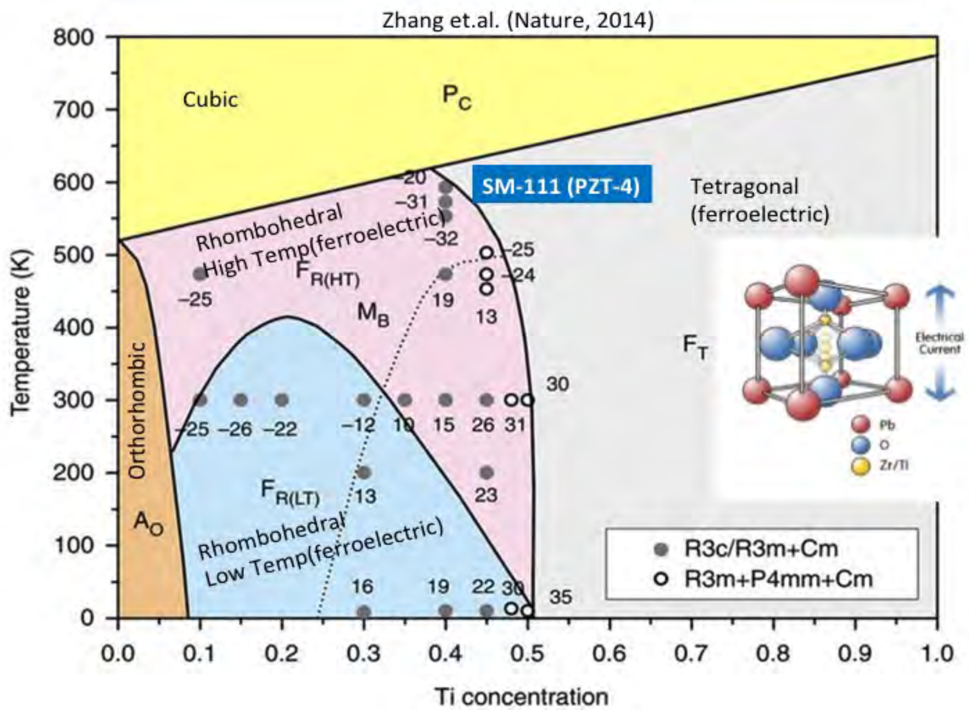

FIG. 9: Phase diagram of lead zirconate titanate (PZT) (Background image from Fig. 7 of Zhang et.al. [4]).

The perovskite structure is very tolerant to element substitution (doping) – therefore the terms "hard doped" and "soft doped" are frequently used. Even small amounts of a dopant (∼1%) may cause large changes in the material properties. Most types of piezoelectric ceramic materials, including PZT, are supplied as doped materials, and can be differentiated based on whether they are "hard doped" or "soft doped," or simply "hard" and "soft" for short. Ferroelectric ceramics like PZT are usually "hard" doped with acceptors, which create oxygen (anion) vacancies, or "soft" doped with donors, which create metal (cation) vacancies and facilitate domain wall motion in the material. Acceptor "hard" doping results in hard PZT while donor "soft" doping results in soft PZT. In general, soft PZT has a higher piezoelectric constant, but larger internal losses, and greater material damping (low quality of resonance Q_m) due to internal friction. Donor dopants are usually lanthanum (La), niobium (Nb), antimony (Sb) or tungsten (W), and are incorporated at a lattice site of lower valency. They increase the dielectric constant (relative electric permittivity up to 3,000), and increase the coupling constant (up to 0.7), but also increase electrical and mechanical losses (decrease the mechanical quality factor of resonance Q_m).

In hard PZT, domain wall motion is pinned by the impurities thereby lowering the losses in the material (increasing quality of resonance Q_m), but this is usually at the expense of a reduced piezoelectric constant. Hard doping ions are usually from the group of transition metals like iron (Fe), manganese (Mn), nickel (Ni) and cobalt (Co), and are incorporated at a lattice site of higher valency. They reduce the dielectric constant, the coupling factor, and reduce the damping (they raise the quality factor of resonance Q_m), while improving aging properties. They also increase the stability of the ceramic with respect to electrical or mechanical (stress) de-polarization. The best performing piezoelectric material used up to now in Mach effect experiments has been a hard doped proprietary modified form of PZT-4 (Navy Type I) ceramic, having the supplier's (Steiner & Martins) trade name "SM-111." Another material from the supplier Steiner & Martins with trade name "SM-211" was tried, with awful results. From the properties given by the supplier one can ascertain that SM-211 is a soft ferroelectric ceramic. Comparing these:

TABLE I: Table of Hard/Soft PZT material properties.

Material PZT type	Steiner & Martins designation	T_c °C	T_c K	Y_{33} (GPa)	d_{33} (μm/kV)	Q_m
Hard	SM-111	320	593	73	0.32	1800
Soft	SM-211	165	438	51	0.65	60

It is clear that the hard PZT has much higher mechanical quality factor of resonance (Q_m), higher Curie temperature (Tc), and higher stiffness (Y_{33}), while the soft material's only redeeming value is a higher value of the piezoelectric coefficient (d_{33}). It is not surprising that the hard PZT gave much higher Mach effect force, due to its much higher quality factor of resonance (Q_m) and higher stiffness (Y_{33}), that more than compensate for the lower value of the piezoelectric coefficient (d_{33}). Also the lower value of Tc for soft PZT is an issue for the application because the PZT gets hotter as it vibrates, and the quality factor of resonance (Q_m) degrades as the temperature gets closer to Tc.

2. THE MEGA LANGEVIN STACK

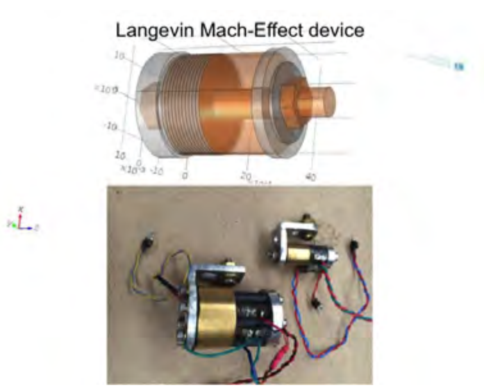

FIG. 10: Top: Drawing of Mach effect device with central bolt as per original Langevin transducer design, Bottom: two different sizes of Mach effect (MEGA) drives shown using a Langevin transducer design. The smaller one has a central bolt, the larger uses 6 concentric bolts equally spaced around the periphery.

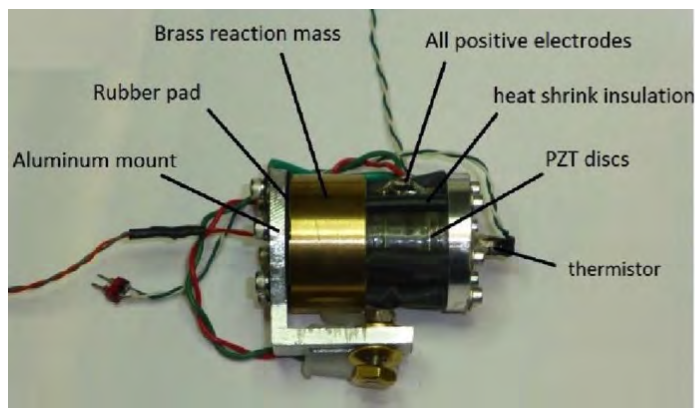

FIG. 11: Parts of the MEGA (Mach effect Gravitational Assist) drive: a Langevin transducer, namely, from right to left: aluminum head mass, PZT stack, brass tail mass, and supported by an aluminum bracket at its tail end.

Looking at the images, Figs. 10 and 11, for the MEGA (Mach effect Gravitational Assist) drive stack, one can see that it is a typical Langevin stack, very similar to the typical Langevin transducers that have been used for decades in many applications: with a small aluminum head mass, a stack of PZT-4 (US Navy Type I) plates, and a tail mass made of brass (instead of more common choices like steel or tungsten) reportedly because it was desired to provide a heat sink for thermal diffusion of heat generated by dissipation in the PZT stack during vibration. It would be better to use a copper tail mass instead of brass for this purpose since copper has 3.5 times thermal conductivity of brass, with practically the same density, as shown in Table 2.

Also of great importance, for the MEGA stack vibrating during tests at the resonant frequency of the stack (typically between 20 to 100 kHz, depending on the length of the stack), what matters for the duration of typical experimental MEGA tests are the material properties governing transient heat conduction: the unsteady state of heat transfer. The material properties involved are: thermal conductivity divided by the heat capacity per unit volume (the product of the heat capacity per unit mass times the mass density), this property is called thermal diffusivity. The thermal diffusivity measures the time rate of heat transfer from the hotter side to the colder side. The higher thermal diffusivity, the faster that heat moves through the material, essentially because the material conducts heat quickly relative to its heat capacity per unit volume. If two materials have the same thermal conductivity, the material with lowest value of heat capacity per unit volume will have the highest thermal diffusivity, because it will transport heat faster in the unsteady state of heat transfer. It is obvious from Table 2, that the present choice of brass for the tail mass is not optimal. All the other materials in Table 2 (including tungsten, which has 2.2 times the mass density) have higher thermal diffusivity. Among this group of metals, silver has the highest thermal conductivity and thermal diffusivity. Copper has 3.4 times greater thermal diffusivity than brass. Hence copper has 3.5 times thermal conductivity and 3.4 times thermal diffusivity of brass and it would make a better choice for tail mass of the MEGA drive to conduct and thermally diffuse the heat generated in the PZT stack, at practically the same mass density. Concerning cost, as of this writing (November 2016) the spot price for silver is 59 US dollars per 100 grams, while copper sells for approximately fifty cents: 0.49 US dollars per 100 grams, and brass sells for 0.29 US dollars per 100 grams.

TABLE II: Table of thermal properties of a few possible metals to use for end mass for the MEGA drive compared with piezoelectric PZT, Butyl rubber pad and epoxy adhesive, properties at room temperature

Material	**Density** kg/m^3	**Heat Cap.** J/(kg K)	**Therm. Cond.** W/(m K)	**Therm. Diff.** m^2/s
PZT-5	7650	350	1.3	0.049×10^{-5}
Unfilled epoxy Bisphenol A	1150	1100	0.17	0.013×10^{-5}
Unfilled Butyl rubber (IIR) pad	920	1950	0.13	0.0072×10^{-5}
Aluminum	2700	900	205	8.44×10^{-5}
Brass	8730	380	109	3.29×10^{-5}
Copper	8960	386	385	11.13×10^{-5}
Gold	19320	126	314	12.90×10^{-5}
Silver	10490	233	406	16.61×10^{-5}
Tungsten	19250	134	173	6.71×10^{-5}

Since the tail mass used for the MEGA drives is only about 100 grams, the cost of copper should not be an issue. Also, there are no experimental concerns with copper's magnetic properties as compared to brass, since the relative magnetic permeability of copper is closer to 1, the value for free space. Copper is slightly diamagnetic, with relative magnetic permeability of 0.999994, compared to high tensile brass CZ114 or HT1 with a relative magnetic permeability of 1.05 (a value higher than several types of stainless steels). From the values shown in Table 2 it is evident that the present choice of aluminum for the head mass is an ideal choice to fulfill the requirement of low mass density, high thermal conductivity, high thermal diffusivity, and speed of sound typical of metals. Fearn et.al. on page 1512 of [9] write "The temperature of the aluminum cap is seen to rise much faster than the brass mass which is also slower to cool," and on page 1513, they write "the temperature rise in the aluminum is on the order of 18 degrees Celsius and that of the brass mass is about 8 degrees," Figs. 12 and 13. This information is consistent with thermal diffusivity of aluminum being 2.56 times higher than thermal diffusivity of brass, and therefore shows that it would be better to use copper or (preferably silver) for the back mass, to rapidly diffuse the temperature internally generated in the piezoelectric stack, instead of the present choice of brass, which has lower thermal diffusivity.

On page 111 of his book [57], Woodward states: "In this case, since vibration getting to the suspension was a background concern, thin rubber pads were added to the system between the brass reaction masses and aluminum mounting brackets." In a private communication, James Woodward stated that the rubber pad thickness is $\frac{1}{16}$ of an inch (1.59 mm) and that the rubber came from a tire's inner tube. The standard type of rubber used for inner tubes is butyl rubber, a synthetic rubber, copolymer of isobutylene with isoprene, with a common technical abbreviation: IIR, which stands for isobutylene isoprene rubber. As shown on Table 2, the thermal conductivity and thermal diffusivity of butyl rubber is very low, so this rubber pad acts as a thermal insulator between the tail (brass) mass and the aluminum mounting bracket.

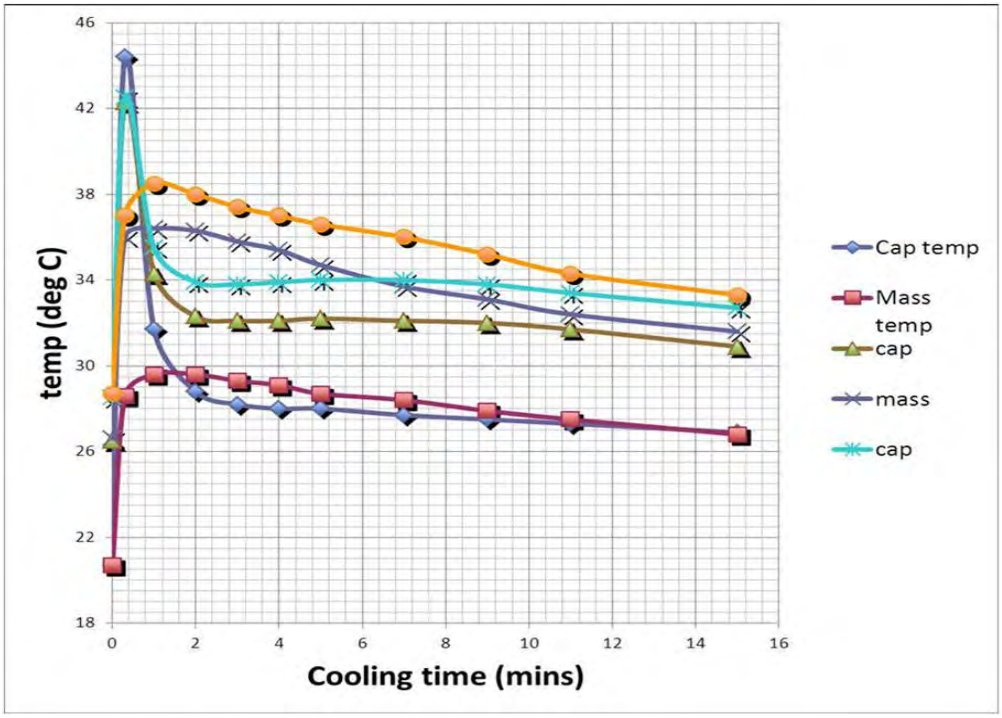

FIG. 12: Temperature (°C) vs. time (min) for a MEGA stack experiment by Fearn and Woodward, during a typical 14 second run, at different locations in the front aluminum mass (star-turquoise, diamond-dark-blue and triangle-green-brown) and tail brass mass (square-red, x-gray and circle-orange), from Fig. 4 of [9].

In the MEGA drive, the Langevin PZT stack is excited by the converse piezoelectric effect where an electric field (an applied voltage difference across the thickness of each PZT plate) induces mechanical strains (under free-ends boundary conditions) or an applied stress (under mechanical constraints, or under dynamic conditions). The direct piezoelectric effect, where the piezoelectric material (PZT) responds to strain by generating an electric voltage, is used in one or more pairs of passive 0.3 mm thick piezoelectric plates in the MEGA drive Langevin stack, for the purpose of dynamic strain measurements.

These passive PZT plates measure the strain, through the thickness of the PZT, resulting from the stress transmitted from the other plates in the stack. They act essentially as strain gauges. One should not interpret the reading from these passive plates as measuring anything but strain, for example as measuring acceleration, particularly for the case of this MEGA Langevin stack operating at an excitation frequency very close to the first natural frequency of the Langevin stack. An accelerometer should be operated, as a measuring instrument, in the so-called flat response region of vibration response (p.58 of Den Hartog [10], p.80 of Scanlan and Rosenbaum [11], and p.62 of Clough and Penzien [12]). Scientific piezoelectric accelerometers are restricted to operating at excitation frequencies lower than 3 dB below the first natural frequency of the vibrating system defining the accelerometer (in other words, approximately below $\frac{1}{2}$ of the first natural frequency).

The first natural frequency of the vibrating system is dictated, of course, by the stiffness and masses composing the accelerometer vibrating system. In the case of the MEGA Langevin stack under free-free conditions, this natural frequency is dictated by both end masses (in Fearn and Woodward's experiments: the front aluminum mass and the back brass mass), the mass of the PZT stack and the stiffness of the PZT stack between the end masses. This limit, restricting the excitation frequency to be below $0.5 f_o$, $\frac{1}{2}$ of the first natural frequency, marks the frequency where the measuring error becomes 30%. (At approximately $0.3 f_o$, $\frac{1}{3}$ of the first natural frequency, the error is 10%, while at approximately $0.2 f_o$, $\frac{1}{5}$ of the first natural frequency, the error is 5%). If the exciting frequency becomes closer to the natural frequency, the error becomes much larger (the measured strain becomes unrepresentative of the acceleration, due to the fact that close to the natural frequency the damping term in the equations of motion starts to dominate the amplitude of the response). For the MEGA drive experiments, Fearn and Woodward purposefully operate the stack at an

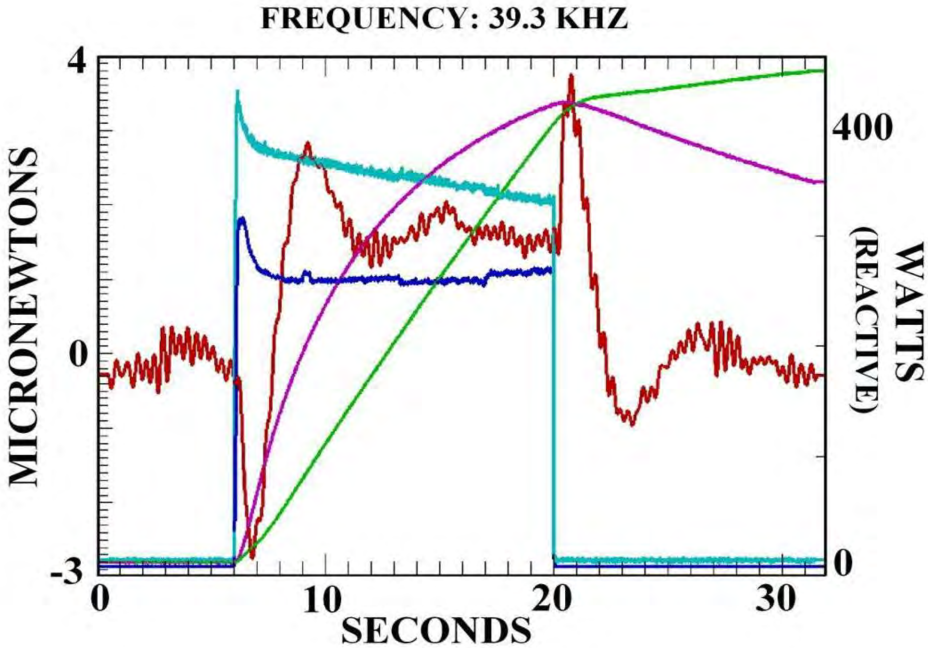

FIG. 13: Force (μN, left vertical) vs. time (sec, bottom horizontal), power (W, right vertical) vs. time (sec) and temperature (not scaled) vs. time (sec) for a MEGA experiment. Power duration: 14 sec. Excitation frequency: 39.3 kHz (*labeled at the top, the upper horizontal axis is not a frequency scale*). Force is indicated with a red trace and power with a dark blue trace. Positive force is directed from the aluminum mass towards the brass mass. Negative force is directed from the brass mass towards the aluminum mass. After the transient (with initial negative peak towards aluminum mass, followed by positive peak towards brass mass) there is a fairly steady force with a magnitude of 2 μN towards the brass mass. This is followed by another transient (first peaking positively towards the brass mass and then negatively towards the aluminum mass). The turquoise trace (labeled in [9] as accelerometer) is from the passive PZT plates that measure strain through their thickness (not acceleration, since the excitation frequency is very close to the natural frequency) and it is not scaled. The green trace is the temperature from thermistor embedded in the back brass mass, while the magenta trace is from thermistor in the front aluminum mass. Temperatures are not to scale, but Fearn et.al. write that "the temperature rise in the aluminum is in the order of 18 deg C, and that of the brass mass is 8 deg C." Image from Fig. 3 of [9].

excitation frequency closer than $\frac{0.75}{Q_m}$ to the natural frequency of the Langevin stack (which has a mechanical-quality-factor-of-resonance (Q_m) equal to 190). Therefore, for the MEGA drive experiments conducted by Fearn and Woodward, the output of the passive PZT plates is unrepresentative of the acceleration, and instead should be interpreted strictly as representing solely the strain through the thickness of the PZT plate.

The PZT presently used for the MEGA drive is supplied by Steiner & Martins Inc. with trade name SM-111, which is a modified PZT-4 (US Navy Type I). It is shaped like a thin circular plate (disc), of 19 mm diameter. The piezoelectric PZT-4 disc is electrically poled through the thickness and it has a silver coating on the surfaces. Stacks have been constructed with 8 discs 2 mm thick and other stacks with 16 discs 1 mm thick. The electrodes are made of brass of the same diameter, 0.05 mm thick, and with holes in them, for the adhesive to penetrate through. The adhesive is a low viscosity liquid bisphenol A based epoxy containing n-butyl glycidil ether. It is supplied by E. V. Roberts with trade name Hexion Epon resin 815C and it is cured with E. V. Roberts Versamid 140 (presently named RF61 Epoxy curing agent), which is a polyamide resin based on dimerized fatty acid and polyamines. The brass electrodes are sanded before applying the adhesive. The stack is compressed under bolt tension and then cured in an oven for 1 hour at 120 °C. Therefore the glass transition temperature (Tg) of the epoxy adhesive used to adhere the electrodes to the piezoelectric material is significantly lower than the Curie temperature (Tc) of the piezoelectric material (320 °C for SM-111 PZT-4). Therefore the glass transition temperature of the adhesive used for present MEGA drive experiments constitutes a lower threshold for the piezoelectric integrity of the MEGA drive.

Instead of using an unfilled epoxy as in the present MEGA stack, it would be better to use a filled adhesive, for several reasons, including increasing thermal conductivity (Table 3) and possibly increasing the electrical conductivity. Also a filled epoxy will have a reduced coefficient of thermal expansion, more compatible with the coefficients of thermal expansion of the electrodes and the piezoelectric plates. Also a polymer adhesive filled with inorganic fillers will have a higher modulus of elasticity closer in stiffness to the stiffness of the electrodes and the piezoelectric plates. Also filled adhesives are stronger, particularly regarding important properties like shear strength, and their properties with respect to temperature drop less precipitously than unfilled adhesives. The thermal conductivity of the unfilled Epon epoxy used for the MEGA stack is only 0.17 W/(mK), which is only 0.04% of thermal conductivity of copper and only 0.08% of thermal conductivity of aluminum, and 11% to 16% of thermal conductivity of PZT, hence the unfilled epoxy adhesive acts as a thermal insulator between the PZT and the copper (or brass). To improve thermal conductivity of the adhesive, fillers like Aluminum Nitride and Boron Nitride are known to raise thermal conductivity to 1.4 to 1.7 W/(mK), depending on the size of the filler and filler content. Therefore, an epoxy filled with Aluminum Nitride or Boron Nitride would match thermal conductivity of PZT, instead of acting as a thermal insulator. Other possible choices are to use an adhesive with higher glass transition temperature. For example Creative Materials 124-41 is a polyimide adhesive with a glass transition temperature exceeding 250 °C. Such an adhesive would provide an upper temperature limit more commensurate with the Curie temperature of SM-111. Also this adhesive is claimed to have a thermal conductivity of 11 W/(mK), which is 69 times more conductive than the presently used unfilled epoxy. Adhesives using micronized silver are claimed to have a thermal conductivity exceeding 7.5 W/(mK), almost 50 times thermal conductivity of the unfilled epoxy presently used for the MEGA drive, such silver-filled adhesives would also have significantly greater electrical conductivity.

TABLE III: Table of thermal conductivity of unfilled and filled adhesives at room temperature, compared with piezoelectric PZT and different metal electrode materials (present MEGA drive experiments use brass electrodes)

Material	**Thermal Conductivity** (W/(m K))
Brass	109
Copper	385
Silver	406
PZT-5	1.3
Unfilled epoxy Bisphenol A	0.17
Aluminum Nitride filled epoxy	1.4 to 1.7
Boron Nitride filled epoxy	1.4 to 1.7
Silver filled epoxy	7.5
Creative Materials 124-41 polyimide	11

The adhesive method of making a piezoelectric stack has a number of disadvantages due to the properties of the adhesive. For example, the adhesive used for the MEGA stack is more than an order of magnitude more compliant than the piezoelectric material, so it lowers the stiffness of the stack. The adhesive used for the MEGA drive is also not electrically or thermally conductive, therefore it acts as a thermal and as an electrical insulator, which is detrimental to the functioning of the stack. Also the adhesive used for the MEGA drive has low fracture toughness, and due to the abrupt change in stiffness between the adhesive and the electrode and the piezoelectric materials being adhered to, it is a source of delamination for fracture mechanics and fatigue. Furthermore, the coefficient of thermal expansion for the adhesive is considerably larger than the coefficient of thermal expansion of the electrodes and of the piezoelectric material, which introduces thermal stresses upon changes in temperature. Finally, the glass transition temperature (Tg) of the adhesive is considerably lower than the Curie temperature (Tc) of the piezoelectric material. This results in a lower upper temperature that the piezoelectric stack can be operated at without losing its integrity. Besides the old fabrication method used for the MEGA drive of stacking (laminating) a plurality of piezoelectric plates by adhering them to the sandwiched electrodes, there is a newer fabrication method called co-sintering. In co-sintering, layers of molded sheets (green sheets) containing an organic binder of piezoelectric ceramic are stacked before sintering and layers of electrodes are sandwiched in between them before sintering, thermally pressing them into an incorporated form, and sintering the whole stack together.

This newer fabrication method can fabricate a compact and higher-performance stack (laminate) element, because the piezoelectric ceramic layers can be formed thinner and because thermal press can obviate a need for use of the adhesive. However, the co-sintering fabrication process becomes technically more complex, since residual stresses between the ceramic and the electrodes have to be considered, and hence the thickness of the electrode is a major consideration in this process. The thickness of the electrode needs to be considered, as well as the thickness and stiffness of the piezoelectric ceramic layers, and the sintering temperature. In US Patent 6114798 by Maruyama et.al [13] the authors discuss such a con-sintering process and state that electrodes thicker than 5 micrometers (0.003 to 0.005 mm), or 10% of the thickness of the electrodes used in the MEGA drive, decrease the value of the quality factor of mechanical resonance Q_m. Based on experiments with piezoelectric stacks made with piezoelectric ceramics having a quality factor of mechanical resonance Q_m value of 1200, the authors conclude that the thickness of the electrode should desirably be as thin as possible within the scope of where electrical conduction can be assured. The authors found best results with higher values of Q_m, between 1400 and 2000, and concluded that Q_m =2000 is the limit value of Q_m for materials available at that time. This is still the case nowadays (2016), as Q_m =2000 is about the upper limit for presently available piezoelectric ceramics. In a later patent [14] Maruyama et.al state that when the electrode thickness is 2 to 3 micrometers (0.002 to 0.003 mm), the current abruptly generated after the start of the polarization process generates sparks that can lead to crack formation in the piezoelectric material. They conclude that the electrode thickness should optimally be 4 to 6 micrometers (0.004 to 0.005 mm) or about 10% of the thickness of the electrodes used in the MEGA drive, because electrodes thinner than that generate sparks.

Fearn et.al. [9] state that six (unified thread standard 4-40) stainless-steel bolts are used between the front aluminum mass and the back brass mass to compress the Langevin piezoelectric stack. The choice of stainless-steel material for these bolts is not optimal, because it is known that the piezoelectric material used for the plates in the MEGA stack for the experiments of Fearn and Woodward, a modified form of PZT-4 (Navy Type I) has a much smaller coefficient of thermal expansion than stainless-steel. For example, Morgan Technical Ceramics (page 8 of [15]) states that the coefficient of thermal expansion in the thickness direction for poled PZT4D is $-0.1 \times 10^{-6} \frac{1}{K}$ in the first heat and $+1.7 \times 10^{-6} \frac{1}{K}$ in subsequent heating, both at 50 °C, and $-6 \times 10^{-6} \frac{1}{K}$ in the first heat and $-1 \times 10^{-6} \frac{1}{K}$ in subsequent heating, both at 100 °C. (The negative sign meaning that PZT4 contracts in the thickness direction upon an increase in temperature). This compares with a coefficient of thermal expansion of $+16.9 \times 10^{-6} \frac{1}{K}$ between 0 °C and 100 °C for stainless steel 304. Therefore, as the MEGA Langevin stack gets heated by internal damping as a result of vibration in the experiments by Fearn and Woodward, the PZT plates will slightly contract, particularly if their temperature exceeds 50 °C, while the stainless steel bolts will expand as a result of the increase in temperature. (Obviously thermal expansion of the brass and aluminum masses located at the ends of the Langevin stack is immaterial to this issue because it is well-known that the stress in the bolt acts between its boundary conditions, which are mainly governed by the first thread the bolt is in contact with. Hence it is the free length of the bolts that matters in this consideration, and thermal expansion of the aluminum and brass mass is immaterial to this). Hence a significant portion of the initial compression may be lost due to internal heat generated from damping during vibration. Thus, the use of stainless-steel bolts is particularly detrimental to their purpose which is to compress the stack. As a significant portion of the compressive stress may be decreased, this will translate into damage to the stack, with a concomitant decrease in modulus of elasticity, hence a decrease in stiffness, and therefore a decrease in the natural frequency of the stack, leading to de-tuning of the MEGA stack as a result of the natural frequency getting away from the excitation frequency. Furthermore this will lead to fatigue damage to the piezoelectric plates as a result of this decrease in compression because of thermal expansion mismatch between the bolts and the PZT plates, and a shortening of the life of the PZT plates. Therefore, it would be a better choice to use bolts with a very small coefficient of thermal expansion, for example invar bolts. For example, Nabeya Bi-tech Kaisha (NBK) [16] supplies hex socket head cap screws with size M3 equivalent to 4-40 bolts, made of super invar with a thermal expansion coefficient of $+0.69 \times 10^{-6} \frac{1}{K}$, a thermal expansion coefficient which is 25 times smaller than the one of stainless steel.

The location of the maximum stress and strain in the PZT stack is a function of the mass distribution in the stack and the boundary conditions. For example, for a symmetric mass distribution, with free-free boundary conditions at the ends, the vibration displacement amplitudes at the two ends are the same, and the vibration displacement node is at the middle of the stack, therefore the maximum stress and strain, and strain energy are located at the middle of the stack. Since internal heat generation is proportional to the strain energy, the resulting heat generation and temperature will also be maximum at the middle of the stack for a symmetric transducer with symmetric, free-free boundary conditions. For piezoelectric materials like PZT it is advisable to limit the amount of stress and strain (because of fracture mechanics and fatigue considerations) and therefore (if no other more important consideration is at play) it is advisable to have a mass distribution that minimizes the maximum stress and strain in the stack. It must also be taken into account that in order to protect the brittle PZT it is advisable not to have the PZT exposed at the end. Therefore many applications have the PZT stack placed near one end, usually around one quarter of the total length of the Langevin transducer (including the length of the end masses).

A more sophisticated (and complicated) approach is to design a transducer that incorporates more than one mode shape, using several piezoelectric stacks instead of just one, with metal masses in between the stacks. One such design is to use two piezoelectric stacks at different positions within the same transducer, independently excited at two different frequencies. The analysis of such stacks is complicated because (deliberately by design or not) such complicated distribution of the piezoelectric materials may excite unwanted bending modes of vibration as well as the desired longitudinal modes of vibration. Bending modes of vibration are particularly harmful because bending involves tension in one of the surfaces of the bent shape, and as previously discussed, tension should be avoided for brittle ceramics like PZT.

To conclude this section, the present design of the MEGA drive could be improved, as it is essentially similar to Langevin's transducer design of 100 years ago. The present choice of brass for the tail mass could be substituted by copper, in order to increase thermal conductivity by a factor of 3.5 times and to increase thermal diffusivity by a factor of 3.4 times. If the cost of silver at 59 US dollars per 100 grams (compared to copper at 0.49 US dollars per 100 grams, and brass at 0.29 US dollars per 100 grams) is not an issue, silver would be an even better choice for the tail mass, since it would improve thermal conductivity by a factor of 3.7 times and the more important (for unsteady heat conduction) thermal diffusivity by a factor of 5 times, as compared to the present choice of brass. Similar, other choices for the electrode should be investigated instead of the present brass electrodes, for example, copper and silver. The present choice of stainless steel for the bolts that apply the necessary compression to the PZT plates is not optimal, because of thermal expansion mismatch with the PZT plates, leading to loss of compression, and hence to damage and decrease of stiffness of the PZT plates, also leading to de-tuning between the excitation frequency and the natural frequency of the MEGA stack. Instead of stainless-steel, a material with a much smaller coefficient of thermal expansion should be used. For example Nabeya Bi-tech Kaisha (NBK) [16] bolts made of super invar with a thermal expansion coefficient 25 times smaller than the one of stainless steel, will better match the coefficient of thermal expansion of the PZT plates in the thickness direction. The present choice of adhesive (unfilled Bisphenol A epoxy) could be substituted by a filled epoxy to raise thermal conductivity (aluminum nitride or boron nitride filled epoxy), and if desired, the electrical conductivity (a silver-filled epoxy) as well. Also a filled adhesive with a higher glass transition temperature (for example a polyimide adhesive like Creative Materials 124-41 with a thermal conductivity of 11 W/(m K) as compared to the present unfilled epoxy 0.17 W/(m K) should also be investigated, because the present adhesive is limiting the upper temperature of the MEGA Drive due to loss of integrity of the adhesive due to its glass transition temperature being significantly lower than the Curie temperature of the PZT. Also co-sintering of the MEGA PZT-electrodes stack should be investigated, as co-sintering would eliminate the adhesive altogether, and involve much thinner electrodes. Finally, but not least, newer piezoelectric materials should be investigated to replace the 64 year old PZT, materials like high-Curie-temperature ferroelectric single-crystal Mn doped PIN-PMN-PT discussed by Zhang et.al. [17].

3. VARIATION OF INERTIAL MASS FROM HOYLE-NARLIKAR'S COSMOLOGY

In [18], Fearn discusses how Hoyle and Narlikar (HN) [19] [20] [21] in the 1960's developed a theory of gravitation which is Machian and uses both retarded and advanced waves to communicate gravitational influence between mass particles (a gravitational version of the absorber theory derived by Wheeler and Feynman for classical electrodynamics). The HN theory reduces to Einstein's theory of gravity in the smooth mass field approximation, with particles having constant rest mass. The theory was ignored by much of the gravitation community since it was developed with Hoyle's static universe in mind. However, it is trivial to drop the static universe condition (by dropping the "C"-field matter creation terms) and then one obtains a non-static theory of gravitation. Hawking in 1965 pointed out a possible flaw in theory. This involved integrating out into the distant future to account for all the advanced waves which might influence the mass of a particle here and now. Hawking used infinity as his upper time limit and showed the integral was divergent. Fearn recently pointed out that when considering HN without the creation "C" field, theory agrees with the observation that the universe is known to be expanding, and accelerating, and hence the upper limit in the advanced wave time integral should not be infinite but should be bounded by the cosmic event horizon. Fearn showed that the advanced integral is in fact finite when the cosmic event horizon is taken into account. Therefore, Hawking's objection is no longer valid and the HN theory becomes a working theory once again. Mach's principle can be summarized by stating that the inertia of a body is determined by the rest of the mass content of the universe. Ciufolini and Wheeler [22] simply stated that "inertia here arises from mass there." The HN inertial interaction is scalar: the inertial mass of a particle is determined by the scalar field contributions from the rest of the particles in the universe. The HN gravitational theory is wider in scope than Einstein's general relativity and it is conformally invariant: if the measured inertial mass of a particle in a given spacetime metric g_{ik} is m, then in a conformal transformation $\Omega^2 g_{ik}$ of this metric, the inertial mass becomes $\frac{m}{\Omega}$. Most interestingly for this article, HN gravitational theory easily accommodates a rest mass that is variable with time. For example Narlikar and Arp [23] consider an inertial mass that varies with epoch t as $m_o(t) = t^2$ to explain the redshift in cosmology and make the same predictions as the standard expanding model, using instead a static model with particle masses that increase quadratically with epoch, instead of the conventional model of an expanding universe with constant masses. Narlikar and Das [24] argue that the excess redshift of high-redshift quasars may be explained as quasars born in galactic explosions and ejected from galactic nuclei and that the observed quasar alignment and redshift bunching can be understood within the framework of the variable mass HN theory, with the particle masses in them increasing quadratically with epoch. In the following, I consider HN without the creation "C" field, such that the HN theory agrees with the observation that the universe is known to be expanding, and where a HN variable mass hypothesis is used to calculate the Woodward Mach effect thruster hypothesis involving mass fluctuations.

Fearn et.al. [25] [26] outline a derivation of the Woodward Mach effect thruster theory based on the HN field equation that Fearn shows to have the same type of mass fluctuation terms. The force equation, used to predict the thrust in the MEGA drive, can be derived from the mass fluctuation. In General Relativity, length, and hence surface and volume, are observer dependent and hence not invariant like mass. This argues for the time derivatives of the mass field to govern the fluctuation in inertial mass, instead of the mass fluctuation being governed by mass density (which is observer dependent due to the observer-dependence of the volume). This distinction is irrelevant for isochoric media (e.g. perfect fluids or idealized elastomers) or for solid media undergoing isochoric (equivoluminal) deformation, but it is important when considering solids like piezoelectric materials that are not isochoric and that undergo non-isochoric deformation. Fearn basically obtains the following equation for the mass density fluctuation (in SI units), after neglecting a number of derivative terms with respect to space (assuming spatial homogeneity of the mass function in a smooth mass field approximation, such that the time derivatives of the mass function are much more significant than any mass transport through the solid medium):

$$\begin{aligned}\Delta\rho &= \frac{1}{G}\left(\frac{1}{m}\frac{\partial^2 m}{\partial t^2} - \left(\frac{1}{m}\frac{\partial m}{\partial t}\right)^2\right) \\ &= \frac{1}{G}\frac{\partial^2 \ln[m]}{\partial t^2}\end{aligned} \tag{1}$$

Which I have expressed directly as the second derivative with respect to time of the natural logarithm of the mass. This can be expressed as a function of the kinetic energy.

A few words about the subtleness of the energy mass equivalence. Léon Brillouin (shown behind Bohr, and next to Heisenberg, at the upper right hand corner of Fig. 1, and whose doctor's thesis committee was composed of Paul Langevin, Marie Curie and Jean Perrin) stated [27], [28], [29]:

"Einstein's relation between mass and energy is universally known. Every scientist writes

$E = mc^2$ ([Brillouin] 1)

but almost everybody forgets to use this relation for potential energy. The founders of Relativity seemed to ignore the question, although they specified that relation ([Brillouin] 1) must apply to all kinds of energy, mechanical, chemical, etc. When it comes to mechanical problems, the formulas usually written contain the mass of kinetic energy, but they keep silent about the mass of potential energy. We must investigate this situation carefully and try to understand what sort of difficulties are raised by such a revision. ... The physical body may be moving in a static field of forces and obtain, at a certain instant of time, an external potential energy U. Everybody assumes the total energy to be represented by the formula

$E_{tot} = mc^2 + U$ ([Brillouin] 3)

where U remains unchanged, despite the motion of the body at velocity v; this fact reveals that one completely ignores any possibility of mass connected with the external potential energy. If this external potential energy had any mass, this mass would somehow be set in motion by the displacement of the physical body, and this moving mass would obtain some kinetic energy. No provision for any such effect can be seen in equation

([Brillouin] 3). We are thus in a strange situation, where the internal potential energy obtains a mass, while the external potential energy does not! The contradistinction is striking and shocking! ”

If external electromagnetic potential energy change needs to be considered, then Brillouin ([27] and [28]) subtracts the potential energy contribution from the total energy:

$$mc^2 = E_{total} - \frac{m_{el}c^2}{\sqrt{1-\frac{v^2}{c^2}}} - U\left(1+\frac{1}{2}\left(\frac{1}{\sqrt{1-\frac{v^2}{c^2}}}-1\right)\right) \tag{2}$$

where m_{el} is the total mass associated with the electric field around a mass density point having rest mass m_o and electric charge distributed uniformly, spherically, around it. In those references, Brillouin gives examples of the external potential energy associated with an external electric field, showing that the external electric field itself carries a mass, and shows how, according to the sign of U, the correction can be positive or negative.

Medina ([30] and [31]) states:

“Unlike the inertia of energy, which is well known, many physicists are not aware of the inertia of pressure (stress). In many cases such an effect is negligible, but for the case of the stress produced by electrostatic interactions, it is comparable to the inertial effects of the electromagnetic fields.”

Electromagnetic energy problems may contain components of the mechanical momentum that are of order $\frac{1}{c^2}$, which are sometimes labeled as “hidden” momentum [32]. Brillouin made the above observation in regards to theory of special relativity (which he called restricted relativity). In general relativity and in HN gravitational theory, this energy is implicit in the fields. The important thing is to account for all terms in the equations of conservation of energy and conservation of momentum. While the attribution of meaning to different types of forces is non-unique, what matters is the actual experimentally measured force [33]. For general unsteady behavior, the body force is due to all terms in the equations of motion, and not just one of them. Henceforth I account for the change from the rest mass m_o to m which accounts for the mass of kinetic energy, and I assume that there is no mass change to the mass particle connected with changes in external potential energy.

The standard definition of relativistic kinetic energy is:

$$\begin{aligned} K &= m_o c^2\left(\frac{1}{\sqrt{1-\frac{v^2}{c^2}}}-1\right) \\ &= mc^2 - m_o c^2 \end{aligned} \tag{3}$$

where m_o is the relativistic rest mass: the mass in the frame in which the velocity is zero, and hence in which the kinetic energy itself is zero. Disregarding time variations of external potential energy, and substituting the expression for the mass m in terms of the kinetic energy Eq. (3) into the expression for the mass fluctuation Eq. (1), one obtains:

$$\begin{aligned} \Delta\rho &= \frac{1}{G}\frac{\partial^2 \ln\left[m_o+\frac{K}{c^2}\right]}{\partial t^2} \\ &= \frac{1}{G}\frac{\partial^2 \ln\left[m_o\left(1+\frac{K}{m_o c^2}\right)\right]}{\partial t^2} \\ &= \frac{1}{G}\left(\frac{\partial^2 \ln\left[m_o\right]}{\partial t^2}+\frac{\partial^2 \ln\left[1+\frac{K}{m_o c^2}\right]}{\partial t^2}\right) \end{aligned} \tag{4}$$

If the speed v of material points is much smaller than the speed of light c, an assumption that is well satisfied for piezoelectric vibration experiments conducted at less than 100 kHz, it is trivial to show that the kinetic energy K is

$$
\begin{aligned}
K &= m_o c^2 \left(\frac{1}{\sqrt{1-\frac{v^2}{c^2}}} - 1 \right) \\
&\approx \frac{1}{2} m_o v^2 \quad \text{for} \quad \frac{v}{c} < 1
\end{aligned}
\tag{5}
$$

and that the natural logarithm expression becomes

$$
\begin{aligned}
\ln\left[1 + \frac{K}{m_o c^2}\right] &\approx \frac{K}{m_o c^2} \quad \text{for} \quad \frac{v}{c} < 1 \\
&\approx \frac{v^2}{2c^2}
\end{aligned}
\tag{6}
$$

and therefore the mass fluctuation, Eq. (4), for speed v of material points much smaller than the speed of light c, becomes:

$$
\begin{aligned}
\Delta\rho &\approx \frac{1}{Gc^2} \left(c^2 \frac{\partial^2 \ln[m_o]}{\partial t^2} + \frac{\partial^2 \left(\frac{K}{m_o}\right)}{\partial t^2} \right) \quad \text{for} \quad \frac{v}{c} < 1 \\
&\approx \frac{1}{2Gc^2} \left(2c^2 \frac{\partial^2 \ln[m_o]}{\partial t^2} + \frac{\partial^2 v^2}{\partial t^2} \right)
\end{aligned}
\tag{7}
$$

Next let us assume the condition that the second derivative with respect to time of the natural logarithm of the rest mass is negligibly small compared to the second derivative with respect to time of the kinetic energy per unit mass:

$$
\begin{aligned}
\Delta\rho &\approx \frac{1}{Gc^2} \frac{\partial^2 \left(\frac{K}{m_o}\right)}{\partial t^2} \quad \text{for} \quad \frac{v}{c} < 1 \quad \text{and} \quad \frac{\partial^2 \ln[m_o]}{\partial t^2} < \frac{\partial^2 \left(\frac{K}{m_o}\right)}{c^2 \partial t^2} \\
&\approx \frac{1}{2Gc^2} \frac{\partial^2 v^2}{\partial t^2}
\end{aligned}
\tag{8}
$$

Therefore one arrives at the conclusion that the inertial mass fluctuation is due to the second derivative with respect to time of the kinetic energy per unit mass, divided by the gravitational constant G and the square of the speed of light. The only assumptions involved in this conclusion have been: 1. Hoyle-Narlikar's theory of gravity (dropping the creation "C" field, assuming spatial homogeneity of the mass function in a smooth mass field approximation, and assuming negligible mass transport within the solid: neglecting the space gradients of mass terms in the mass fluctuation expression), 2. speed of material points negligibly small compared to the speed of light and 3. second derivative with respect to time of the natural logarithm of the rest mass negligibly small compared to the second derivative with respect to time of the kinetic energy per unit mass.

The second derivative with respect to time of the kinetic energy per unit mass, is a function of the square of the acceleration $\frac{\partial v}{\partial t}$, and the product of the velocity v times the time rate of the acceleration $\frac{\partial^2 v}{\partial t^2}$ (the second derivative with respect to time of the velocity) of the mass points, which is also called the jerk, jolt, surge or lurch:

$$
\begin{aligned}
\Delta\rho &\approx \frac{1}{2Gc^2} \frac{\partial^2 v^2}{\partial t^2} \\
&\approx \frac{1}{Gc^2} \left(\left(\frac{\partial v}{\partial t} \right)^2 + v \frac{\partial^2 v}{\partial t^2} \right)
\end{aligned}
\tag{9}
$$

The presence of the jerk $\frac{\partial^2 v}{\partial t^2}$ is significant because it has been shown by Sprott [35] [36] in the field of chaotic dynamics that an equation involving the jerk is equivalent to a system of three first order, ordinary, non-linear differential equations, and such a system is the minimal setting for solutions that can show chaotic behavior. The transient mass fluctuation equation is a nonlinear differential equation involving the jerk, the acceleration and the velocity. Therefore, it is interesting to consider whether the solution of the Machian force due to inertial mass fluctuations (following Fearn's derivation from HN theory) of a piezoelectric/electrostrictive Langevin stack undergoing vibrations may be capable of showing chaotic, complex dynamic behavior. Such chaotic, complex dynamic behavior may result in different dynamic behavior regimes and perhaps it can be exploited to maximize the response if properly engineered.

4. THE MEGA DRIVE MODEL: 2 UNEQUAL MASSES CONNECTED BY A VISCOELASTIC PIEZOELECTRIC/ELECTROSTRICTIVE STACK

Next, I model the MEGA drive as a dynamic system composed of two unequal, lumped, end masses (the front, aluminum, mass and the tail, brass, mass) connected by a linearly viscoelastic piezoelectric/electrostrictive stack. Therefore the two coupled differential equations can be visualized as modeling a 2-mass dynamic system connected by a spring and a dashpot (the spring stiffness and the dashpot's damping given by the viscoelastic piezoelectric/electrostricitve stack and the stiffness of the bolts providing initial compression), undergoing piezoelectric and electrostrictive excitations. The boundary conditions are modeled as free-free, as if the MEGA drive would be vibrating in space. It is critical to take damping into account in addition to considering unequal end masses. To calculate the maximum amplitude of a vibrating system it is imperative to consider non-zero damping because for zero damping, the response will have infinite amplitude at resonance, which is an unphysical result. All piezoelectric dynamic systems obey the second law of thermodynamics, and hence have non-zero damping.

The strain excitation is composed of piezoelectric and electrostriction excitation components, Fig. 15. The piezoelectric strain excitation is proportional to the piezoelectric coefficient d_{33} in the thickness direction of the PZT plates, and proportional to the electric field E_{33} in the thickness direction (voltage differential divided by the thickness of the plate). The electrostrictive strain excitation is proportional to the electrostriction coefficient M_{33} in the thickness direction of the PZT plates, and proportional to the square of the electric field $(E_{33})^2$ in the thickness direction (voltage differential divided by the thickness of the plate). The voltage excitation $V_o \cos(\omega t)$ is assumed to be proportional to a cosine function $\cos(\omega t)$ of time t and angular frequency ω oscillating with zero to peak voltage amplitude V_o. The piezoelectric and electrostrictive force excitations are proportional only to the stiffness of the piezoelectric stack, since the bolts provide no piezoelectric or electrostrictive excitation. By contrast, for the dynamic equations of motion, the stiffness is given by the stiffness of the PZT stack plus the stiffness of the bolts providing initial compression to the stack. The piezoelectric/electrostrictive equations are formulated based on the results of theory for segmented electromechanical stacks developed by Gordon E. Martin [37] at the U.S. Navy Electronics Laboratory, San Diego, California, in the early 1960's. The exact solution to the coupled differential equations of motion for the dynamic system of two unequal masses with damping and stiffness, excited by piezoelectricity and electrostriction, can be decomposed into a piezoelectric solution for the displacement of each end mass, with an in-phase and an out-of-phase component, for a total of 4 terms; and an electrostrictive solution for the displacement of each end mass, with an in-phase and an out-of-phase component, for a total of an additional 4 terms; so the solution has 8 such terms. Piezoelectric resonance occurs when the voltage excitation frequency ω equals the first natural frequency of the MEGA drive ω_o. Calculating the first natural frequency, using the following properties:

length of PZT stack = 0.018288 m
thickness of PZT plates = 2×10^{-3} m
thickness of brass electrode = 5×10^{-5} m
thickness of epoxy adhesive = 5×10^{-6} m
outer diameter of PZT stack = 0.019 m
outer diameter of bolts = 0.002845 m
screw head diameter = 0.00452 m
screw head length = 0.00277 m
number of outside bolts = 6
mass of PZT stack = 0.046 kg
mass of aluminum (head end) = 0.010 kg
mass density of steel bolts = 7850 kg/m^3
mass density of PZT SM-111 = 7900 kg/m^3
mass density of aluminum = 2720 kg/m^3

mass density of brass = 8525 kg/m^3
Poisson's ratio of PZT stack (radial strain to longitudinal strain ratio) = 0.4375
modulus of elasticity of PZT "SM-111" plates (Y_{33}, stress and strain both in thickness direction "3") = 7.3×10^{10} Pa
modulus of elasticity of brass electrodes =10×10^{10} Pa
modulus of elasticity of unfilled epoxy Bisphenol A =0.2×10^{10} Pa
modulus of elasticity of stainless steel bolts =19×10^{10} Pa

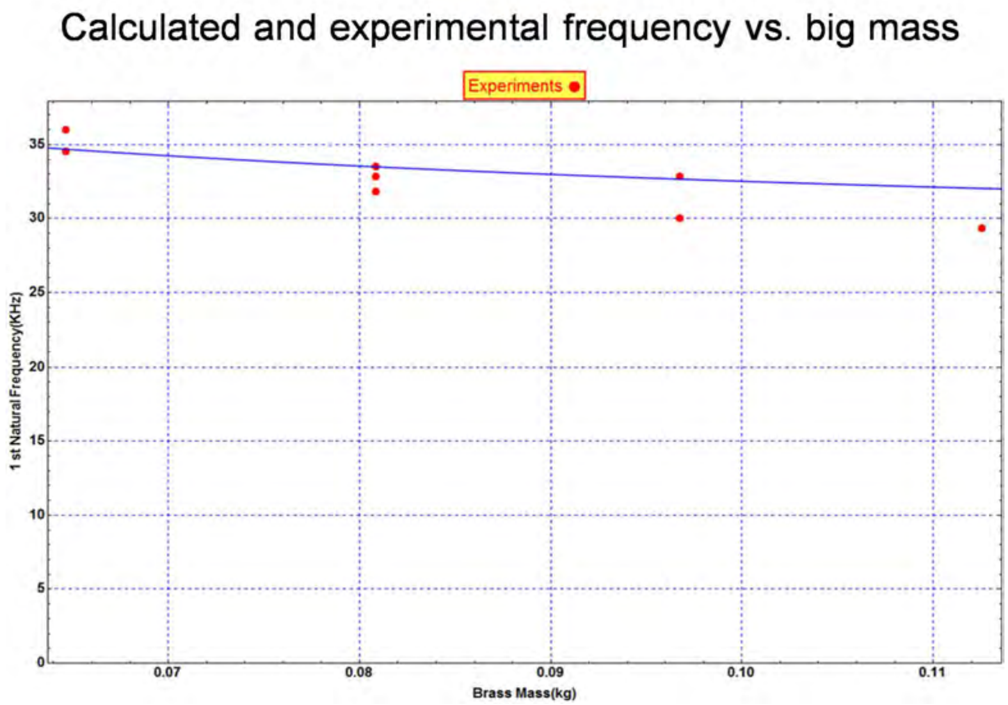

FIG. 14: Calculated (blue line) and measured (red dots) natural frequency vs. mass of brass tail end

one can see, Fig. 14, that the calculated natural frequency falls within the experimentally measured values. The modulus of elasticity in the thickness direction (Y_{33}) of PZT is known to be a complicated nonlinear function of frequency, temperature, voltage, initial compressive stress, fatigue life, and electromechanical history, including polarization history. The calculated values of natural frequency are based on the book value of the modulus of elasticity provided by the supplier (Steiner & Martins), who does not specify the values of these variables during the testing of the PZT that resulted in those book values. Furthermore, the piezoelectric stack is a composite where several layers (PZT plates, brass electrodes and adhesive layers) are sandwiched together by hand, where the adhesive has a modulus of elasticity much lower than the one of the PZT. Also, the actual stack is a continuum with a very large number of material points, rather than a simple 2-mass lumped system connected with a viscoelastic spring and dashpot as in the numerical model, and it is known that the actual natural frequency of such a continuum will be different than the one calculated in this simplified numerical model. Considering all the above factors, the comparison between the calculated and the measured natural frequency is very reasonable, particularly considering the unknown electromechanical state of the piezoelectric stack, and the level of damage (a more damaged stack will have a lower stiffness and hence a lower natural frequency, Fig. 19), at the time of the natural frequency measurements.

Electrostrictive resonance occurs when the electrostriction voltage excitation frequency 2ω equals the first natural frequency of the MEGA drive ω_o, this happens at $2\omega = \omega_o$, or equivalently at $\omega = \frac{1}{2}\omega_o$, so the electrostrictive resonance occurs at the $\frac{1}{2}$ subharmonic of the first natural frequency.

5. THE MACH EFFECT FORCE: ANALYSIS OF INPUT VARIABLES

The Mach effect force on the center of mass is calculated as the product of the total mass times the acceleration of the center of mass [38]. The acceleration of the center of mass contains terms (due to Mach effect inertial mass fluctuations) of the form of the product of the time derivative of the mass fluctuation times the velocity, and of the form of the product of the second time derivative of the mass fluctuation times the displacement, as well as square terms of the previously mentioned expressions. As a result of these multiplications, trigonometric expressions due to the product of harmonic terms at frequency ω (due to piezoelectric excitation) multiplying harmonic terms at frequency 2ω (due to electrostrictive excitation) occur, such as:
$(\sin(\omega t))^2 \cos(2\omega t)$
$(\cos(\omega t))^2 \cos(2\omega t)$
$\cos(\omega t) \sin(\omega t) \sin(2\omega t)$.
Expressions such as these give constant uniaxial force terms. Such terms comprise a single term with frequency 2ω due to electrostriction times two terms with frequency ω due to the piezoelectric effect. Some terms contain all factors that are completely in-phase (with the excitation frequency) and other terms contain a mixture of out-of-phase and in-phase factors. No term consists entirely of out-of-phase (with the excitation frequency) factors. Mass fractions occur implicitly in these expressions. There are also more complicated terms that result due to the square terms of the derivatives, such terms are composed of the product of five factors that can be in-phase or out-of-phase. In such terms, the electrostrictive effect factors occur from the first power up to the third power, while the piezoelectric factors occur from the first power up to the fourth power. There is a total of $20 + 269 = 289$ such terms that contribute to the Mach effect force. In the interest of saving space these 289 terms are not shown explicitly in this article, but it is remarked that the solution is an exact analytical solution, that is solved using Wolfram *Mathematica*.

The Mach effect force can then be calculated, using the input variables previously discussed in section 4, which were used to calculate the fundamental natural frequency, and also using these additional properties:
G (gravitational constant)$= 6.67408\times10^{-11}$ N m^2/kg^2
c (speed of light in vacuum) $= 2.99792458\times10^8$ m/s
d_{33} (piezoelectric constant: strain due to electric field, both in thickness direction “3”)
$= 320\times10^{-12}$ m/V
M_{33} (electrostrictive constant: strain due to (electric field)^2, both in thickness direction “3”)
$= 13.5\times10^{-18}$ m^2/V^2
V_o (voltage excitation, constant term) = 200 V
Q_m (quality factor of resonance due to mechanical dissipation) = 190
mass of brass (tail end) = 0.0809 kg
outer diameter of brass mass = 0.02819 m
outer diameter of aluminum mass = 0.02819 m
aluminum bracket mount mass = 0.007 kg
Mach effect coupling factor on piezoelectric and electrostrictive excitations = 0.006

Both the modulus of elasticity (Y_{33}) and the piezoelectric constant (d_{33}), in the thickness direction of the PZT plates, for plates poled through the thickness, are obtained from the values published in the website of the supplier of the piezoelectric material plates “SM-111,” Steiner & Martins [39]. Also, from Steiner & Martins [39] published values, the piezoelectric Poisson’s ratio is taken to be the ratio $-d_{31}/d_{33} = -(-140/320) = 0.4375$ of the value of the piezoelectric constant d_{31} (the piezoelectric strain in the radial direction of the circular plates due to electric field applied in the thickness direction) to the piezoelectric constant d_{33} (the piezoelectric strain in the thickness direction of the plates due to electric field applied in the thickness direction). In other words, the piezoelectric strain in the radial direction of the circular plates due to electric field applied in the thickness direction, equals the negative of the piezoelectric Poisson’s ratio times the piezoelectric constant d_{33}.

The value for the electrostrictive constant M_{33} for hard PZT is difficult to get, because electrostrictive strains are much smaller than piezoelectric strains, Fig. 15, in hard-doped PZT materials like (Steiner & Martins) “SM-111.” Steiner & Martins does not report any electrostriction values. Reviewing the literature, I conclude that the electrostrictive coefficient (giving the strain due to the (electric field)^2, both in thickness direction “3”) for PZT-4 “SM-111” (Navy Type I) used for the MEGA experiments has a value $M_{33}=$ 13.5×10^{-18} m^2/V^2. I base this conclusion on the following experimental support (here and in the following I adopt the subscript “3” for the thickness direction for M_{33} and for Q_{33} in agreement with IEEE convention, while the authors in their articles use the “1” convention for the crystallographic axis, the important point being that I am referring to the diagonal tensor components due to uniaxial electrostriction and not to the off-diagonal shear properties):

1. Haun et.al. [40] present electrostrictive data for a number of PZT compositions, including, most interestingly (Haun et.al. show this value in a chart vs. temperature showing little temperature dependence):

1a. tetragonal PZT 40/60 (40% antiferroelectric lead zirconate $PbZrO_3$, 60% ferroelectric lead titanate $PbTiO_3$), $Q_{33} = 0.1$ m^4/C^2

1b. tetragonal PZT 50/50 (50% $PbZrO_3$, 50% $PbTiO_3$), Q_{33} =0.0966 m^4/C^2

Although Steiner & Martins does not disclose their "SM-111" formulation, one can reasonably ascertain from its properties that it must have a tetragonal structure, with a composition between these two. (This follows from the fact that the Curie Temperature is known to depend heavily on composition and that the Curie Temperature for SM-111 is 320 °C). The fourth order electrostriction tensor component M_{33} and the fourth order electrostriction tensor component Q_{33} (where the IEEE notation convention is used for the fourth order tensor component indices) are related to each other through the value of the electric permittivity of the material. One can derive this relationship as follows: the second order strain tensor component S_{33} and the electric field vector component E_3, are related through the following electrostrictive constitutive equation (e.g. pages 73 and 79 of Burfoot and Taylor [45]):

$$S_{33} = M_{33} E_3 E_3 \tag{10}$$

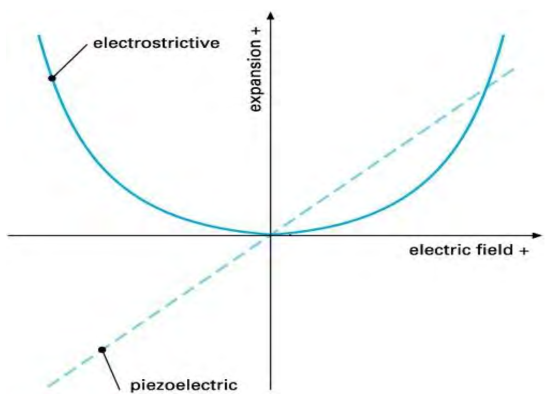

FIG. 15: Comparison of piezoelectric and electrostrictive strains vs. electric field. (Image from PI USA (Physik Instrumente))

Electrostriction is an electromechanical effect that is always present, to some extent, in all dielectric materials, whether isotropic or anisotropic. This is unlike the piezoelectric effect which cannot exist in isotropic dielectrics, Fig. 15. A piezoelectric effect can exist only in special anisotropic dielectrics, that are not centro-symmetric, where the electric vector field $\boldsymbol{E}$ creates in anisotropic materials a polarization vector field $\boldsymbol{P}$ that points, in general, not parallel to the electric field $\boldsymbol{E}$, and hence for a piezoelectric material, the permittivity and susceptibility are second-order tensors with non-zero off-diagonal components. Crystals are anisotropic materials composed of atoms, ions or molecules that have long range periodic order in three dimensions. Crystals may be grouped into 7 crystal systems which may be characterized in terms of axes of symmetry: cubic, tetragonal, othorhombic, rhombohedral (or trigonal), hexagonal, monoclinic and triclinic. Each of these systems is subdivided into a number of crystal classes. There are 32 crystal classes corresponding to 32 crystallographic point groups. All piezoelectric coefficients disappear when a crystal has a center of symmetry. This eliminates 11 crystal classes. In addition, the piezoelectric coefficients become zero in crystal class 29 because of holoaxial symmetry (a crystal class with axial symmetry such that all the possible axis of symmetry are present but that has no planes of symmetry). Thus, as Voigt showed [46], of the 32 crystal classes, only 20 of these, all non-centrosymmetric, can exhibit direct piezoelectricity, and 10 of these are polar crystals which show a spontaneous polarization without mechanical stress. Electrostriction causes elongation (extensional strain) in the direction of the electric field, in response proportional to the square of the electric field $\boldsymbol{E}$ [44]. Thus, an electostrictive actuator's movement is independent of the electric field

TABLE IV: Comparison between piezoelectric and electrostrictive effects

Property	**Piezoelectricity**	**Electrostriction**
Material direction dependence	Anisotropic, non-centro-symmetric	All dielectrics
Strain's electric field dependence	Linear	Mostly Quadratic
AC strain for zero DC bias	Elongation ($\boldsymbol{E}$+) & Contraction($\boldsymbol{E}$-)	Elongation
Strain's voltage polarity dependence	Dependent	Independent
Inverse effect	Yes	No
Electric poling required	No(natural), Yes(engineered material)	No
Actuators or sensors	Both	Mostly actuators
Property	**Hard PZT**	**PMN-PT**
Electric poling required	Yes	No
Electric-field-dependent phase fragility	Smaller	Greater
Strain vs. electric field hysteresis	Larger	Smaller
Tangent d_{33}	Lower	Higher
Tangent d_{33} DC bias dependence	Much smaller	Much greater
Linear stroke	Larger	Smaller
Electric permittivity ϵ_{r33}	Lower	Higher
Coupling coefficient k_{33}	Lower	Higher
Mechanical quality factor of resonance Q_m	Higher	Lower
Curie temperature Tc	Higher	Lower
Tc transition	Sharp, well-defined	Gradual transition over wide range
Single crystal	No	Yes
Cost	Lower	Higher

polarity. The directions orthogonal to the applied electric field contract in proportion to the Poisson's ratio of the material. Electrostriction, unlike piezoelectricity, has no inverse (a strain or stress cannot produce an electric field as a result of inverse electrostriction). Thus, while the piezoelectric effect has been used either for actuators, where an electric field causes strain, or for sensors, where an applied stress generates an electric field, the electrostrictive effect can mostly be used for actuators. Both electrostrictive and piezoelectric actuators are basically capacitive elements [6]. Current only flows during the charging process (while the actuator is providing motion) and so long as leakage currents and losses can be kept small, force is maintained at the end of the stroke without the need of supplying additional energy. Electrostrictive actuators usually have lower (strain vs. electric field) hysteresis than piezoelectric actuators. For most dielectrics, including PZT, the electrostrictive effect is too small to be used for actuator purposes. Relaxor ferroelectrics with extremely high electric permittivity, and having a very gradual transition Curie temperature range, display a more complex strain-electric field response, with an approximately linear range (approximately constant tangent d_{33}) over a narrow range of electric field that can be exploited for actuator purposes using a DC bias. Examples of such relaxor ferroelectrics are lead-magnesium-niobate $Pb(Mg_{\frac{1}{3}}Nb_{\frac{2}{3}})O_3$ (PMN) and lead magnesium niobate - lead titanate $Pb(Mg_{\frac{1}{3}}Nb_{\frac{2}{3}})O_3$-$PbTiO_3$ (PMN-PT). These electrostrictive relaxor ferroelectrics can produce larger stresses than piezoelectric actuators of similar size, and have larger values of the coupling coefficient k_{33}. Such electrostrictive actuators are ideal candidates for precision optical positioning systems. However, electrostrictive actuators have the drawbacks of a more limited stroke than piezoelectric actuators (because of their limited range of approximately linear strain vs. electric field behavior, under a direct current bias), temperature dependence (because interesting electrostrictive properties occur near phase transition temperatures), lower mechanical quality of resonance Q_m than hard PZT (also because interesting electrostrictive properties occur near phase transition temperatures, that are associated with higher dissipation) and higher cost than PZT materials. PMN-PT are single crystals, and hence do not have the grain boundaries and inter-grain voids typical of sintered PZT, but, on the other hand, PMN-PT exhibit temperature-dependent and electric-field-dependent phase fragility as well as low fracture toughness, yielding to progressive degradation of polarization, electric permittivity ϵ_{r33}, and tangent d_{33}. Thus, there are several engineering trade-offs to make between electrostrictive and piezoelectric actuators, for example the available force vs. the length of the stroke, Q_m, temperature limitation, phase fragility, etc.

The polarization vector $\boldsymbol{P}$ is a field (due to the electric dipole moment per unit volume of the dielectric material, and having units of charge per unit area) that only arises from the electric dipoles bound within the material, while the electric field $\boldsymbol{E}$ (with units of force per unit charge, or volts per unit length) is induced by all charges: external and internal to the material. The electric field $\boldsymbol{E}$ polarizes a dielectric material by inducing new dipole moments and/or changing the magnitude and orientation of pre-existing dipole moments. This deforms (alters the dimensions of) the dielectric solid by moving electrons and nuclei to new equilibrium positions. An electric field can remove a center of charge symmetry by creating a polar axis. The area inside the hysteresis loop in the polarization $\boldsymbol{P}$ vs. electric field $\boldsymbol{E}$ coordinate space has units of stress (force per unit area), or equivalently energy (force times length), per unit volume. Therefore the area inside the polarization vs. electric field hysteresis loop has the physical meaning of energy density loss (due to internal dissipation). The second order strain tensor component S_{33} and the polarization vector component P_3, are related through this electrostrictive constitutive equation (e.g. pages 73 and 79 of Burfoot and Taylor [45]):

$$S_{33} = Q_{33} P_3 P_3 \tag{11}$$

The polarization vector component P_3 and the electric field vector component E_3 are related to each other, in the linear range by (e.g. Eq. (6.4.2) of Haus and Melcher [47], or Eq. (4.36) of Jackson [48], or Eq. (4.30) of Griffiths [49]) the following constitutive equation:

$$\begin{aligned} P_3 &= (\epsilon - \epsilon_o) E_3 \\ &= \epsilon_o (\epsilon_r - 1) E_3 \\ &= \epsilon_o \chi_e E_3 \end{aligned} \tag{12}$$

where, for anisotropic electric susceptibility, the electric susceptibility $\chi_e = \epsilon_r - 1$ (dimensionless, since it expresses the ratio of the bound charge density to the free charge density) and the relative electric permittivity ϵ_r are second order tensors. Piezoelectric materials, for example PZT used in the MEGA drive experiments, have anisotropic electric susceptibility, therefore the electric susceptibility, and the relative electric permittivity in the above equation should be taken to be the value of the anisotropic tensor component coaxial with the thickness direction 3:

$$\begin{aligned} P_3 &= (\epsilon_{33} - \epsilon_o) E_3 \\ &= \epsilon_o (\epsilon_{r33} - 1) E_3 \\ &= \epsilon_o \chi_{e33} E_3 \end{aligned} \tag{13}$$

One can visualize this anisotropic susceptibility by imagining the electron's binding within the crystal as a mechanical system whereby the electron charge distribution is connected to the positively charged nucleus by springs in three orthogonal directions, whereby for an anisotropic crystal, the springs have different stiffness in different directions. (Also, it can be shown by energy considerations (page 30 and chapter 6 of Panofsky and Phillips [50]), that the anisotropic susceptibility tensor must be symmetric and hence it should be possible to express the anisotropic relationship between the polarization and the electric field vectors in terms of principal directions by a set of only three eigenvalues, and hence there are at least three directions in which the polarization and the electric field vectors are parallel in the anisotropic case.) The polarizability starts to saturate at high values of the electric field, depending on the material initial properties, the material electromechanical history and most importantly on the temperature (particularly when the temperature is close to a phase transition temperature or to the Curie temperature). Therefore at high values of the electric field, this saturation must be modeled with a nonlinear susceptibility model, which leads, in that case, to a very nonlinear relationship between the constitutive material properties M_{33} and Q_{33}. Newnham et.al. [51] point out that the polarization related electrostrictive material tensor $\boldsymbol{Q}$ components better describe the electrostrictive strain behavior, than the electric field related electrostrictive material tensor $\boldsymbol{M}$ components, in the nonlinear regime of electric field $\boldsymbol{E}$ vs. polarization field $\boldsymbol{P}$, in which the strain ceases to be a quadratic function of the electric field $\boldsymbol{E}$.

Assuming that the electric field is low enough below saturation and hence that the linear relationship, Eq. (13), between the polarization vector component P_3 and the electric field vector component E_3 is valid, substituting Eq. (13) into Eq. (11), one obtains:

$$S_{33} = Q_{33}(\epsilon_{33} - \epsilon_o)^2 E_3 E_3 \tag{14}$$

and equating the expressions for the strain component, from Eqs. (10) and (14), one obtains the following relationship between M_{33} and Q_{33}, valid in the linear range of susceptibility, below saturation:

$$\begin{aligned} M_{33} &= Q_{33}(\epsilon_{33} - \epsilon_o)^2 \\ &= Q_{33}(\epsilon_o(\epsilon_{r33} - 1))^2 \\ &= Q_{33}(\epsilon_o \chi_{e33})^2 \end{aligned} \tag{15}$$

where $\epsilon_o = 8.854187817 \times 10^{-12}$ F/m (notice that the units F/m can equivalently be expressed as C/(mV) which is useful for this conversion) is the value of the vacuum permittivity, also known as the permittivity of free space, and as the electric constant. Using the relative electric permittivity value reported for SM-111 in the website of Steiner & Martins [39]: $\epsilon_r = 1400$, and the above-mentioned values in cases 1a and 1b for Q_{33} I obtain the following values for M_{33} using Eq. 15:

1a. for PZT 40/60 (40% $PbZrO_3$, 60% $PbTiO_3$): $M_{33} = 15.34 \times 10^{-18}$ m^2/V^2

1b. for PZT 50/50 (50% $PbZrO_3$, 50% $PbTiO_3$): $M_{33} = 14.82 \times 10^{-18}$ m^2/V^2

2. Li and Rao [41] report the following values

2a. $M_{33} = 2.5 \times 10^{-18}$ m^2/V^2 for PZT-7A from 0% to 80% volume fraction PZT ceramic embedded in P(VDF-TrFE) polymer.

2b. $M_{33} = 2.5 \times 10^{-18}$ m^2/V^2 for PZT-5 at 0% volume fraction PZT ceramic embedded in P(VDF-TrFE) polymer to $M_{33} = 8 \times 10^{-18}$ m^2/V^2 at 90% volume fraction PZT ceramic embedded in P(VDF-TrFE) polymer.

2c. $M_{33} = 2.5 \times 10^{-18}$ m^2/V^2 for PZT-5H at 0% volume fraction PZT ceramic embedded in P(VDF-TrFE) polymer to $M_{33} = 13.5 \times 10^{-18}$ m^2/V^2 at 95% volume fraction PZT ceramic embedded in P(VDF-TrFE) polymer.

Taking the value for the composite having 95% volume fraction PZT-5H ceramic as representative of 100% PZT-5H (assuming that 95% is already over the percolation threshold), one obtains $M_{33} = 13.5 \times 10^{-18}$ m^2/V^2

3. As an extreme upper value comparison, a different type of ferroelectric known for its high electrostrictive material properties, a relaxor ferroelectric, is lead-magnesium-niobate (PMN). Lee et.al. [42] report a value: $Q_{33} = 0.0115$ m^4/C^2. Swartz et.al [43], report a high value of $\epsilon_r = 18{,}000$ for PMN. Using these values for ϵ_r and Q_{33}, I obtain the following value for M_{33} for PMN using Eq. 15:

$M_{33} = 292 \times 10^{-18}$ m^2/V^2

To obtain a value of $M_{33} = 13.5 \times 10^{-18}$ m^2/V^2, similar to the PZT value, a lower value of the relative electric permittivity would be required: $\epsilon_r = 3{,}870$, for $Q_{33} = 0.0115$ m^4/C^2. Thus, the higher value of M_{33} $= 292 \times 10^{-18}$ m^2/V^2 for PMN is shown to be due mainly to the very high value of $\epsilon_r = 18{,}000$ for PMN.

Thus, from the above data in points 1 through 3, the value of M_{33} for PZT materials like (Steiner & Martins) "SM-111" can be reasonably ascertained to be between $M_{33} = 13.5 \times 10^{-18}$ m^2/V^2 and $M_{33} = 15.34 \times 10^{-18}$ m^2/V^2.

As previously stated, the constant term in the voltage excitation is taken to be $V_o = 200$ V, and the thickness of the PZT plates $= 2 \times 10^{-3}$ m, therefore the electric field vector component in the thickness direction is $E_3 = \frac{200}{0.002} \frac{V}{m} = 1 \frac{kV}{cm}$. To assess whether this magnitude of electric field is high enough to result in significant nonlinear effects, one can compare this magnitude of electric field with the magnitude of electric fields responsible for signficant hysteresis in the strain vs. electric field plane.

As shown in Fig. 16 (from Fig. 2 of Zhang et.al. [52]), the magnitude of the applied electric field in this example of MEGA drive experiments, 1 kV/cm, is 20 times smaller than the electric field that results in significant nonlinearity (strain vs. electric-field hysteresis due to piezoelectric internal damping losses) for PZT-4.

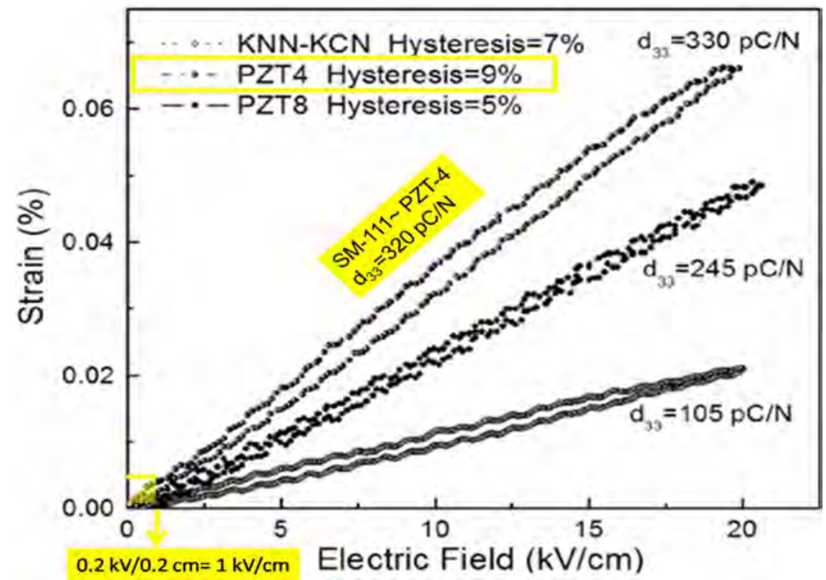

FIG. 16: Hysteresis, strain vs. electric field, for several piezoelectric materials, PZT-4 is the upper curve (from Fig. 2 of Zhang, Lim, Lee and Shrout, [52])

Fig. 17 (from Fig. 1 of Zhang et.al. [52]), shows the polarization hysteresis, plotted with coordinate axes: polarization field vs electric field, for three different piezoelectric materials, including PZT-4. All measured at an electric field of 40 kV/cm and frequency of 1 Hz.

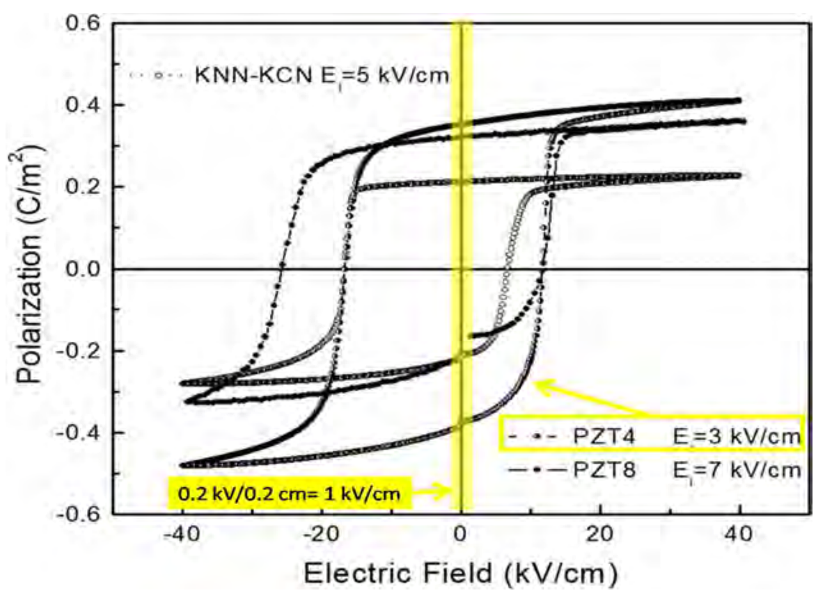

FIG. 17: Hysteresis, polarization vs. electric field, for several piezoelectric materials, PZT-4 has the largest hysteresis (from Fig. 1 of Zhang, Lim, Lee and Shrout, [52])

Hard PZT ceramics such as PZT-4 (Navy Type I) are doped with impurities that introduce an internal bias field, which is made evident by a lateral shifting along the electric field axis of hysteresis loops (described in the polarization vs. electric field domain). This internal field has been attributed to the introduction of acceptor impurity-oxygen vacancy complexes. This internal field increases the coercive field and allows the material to be driven with a higher electric field amplitude. The horizontal (electric field) offset in Fig. 17 is the result of building up of the internal bias field E_i (3 kV/cm for PZT-4). It is evident that PZT-4 has a larger hysteresis than the other two materials, at this high level (40 kV/cm) of electric field magnitude, but it is also evident that the electric field magnitude used for these MEGA experiments (1 kV/cm) is 40 times smaller than for the example shown in Fig. 17 (and also smaller by a factor of 3 than the internal bias field used in this example). Of course, care should be taken in MEGA drive experiments to perform experiments at identical electric field magnitude, rather than identical voltage excitation magnitude. For example, if the same voltage excitation were used for PZT plates 1 mm thick instead of 2 mm thick, the electric field would be twice as large in the stack with the thinner plates, and hence closer to the region of nonlinearity.

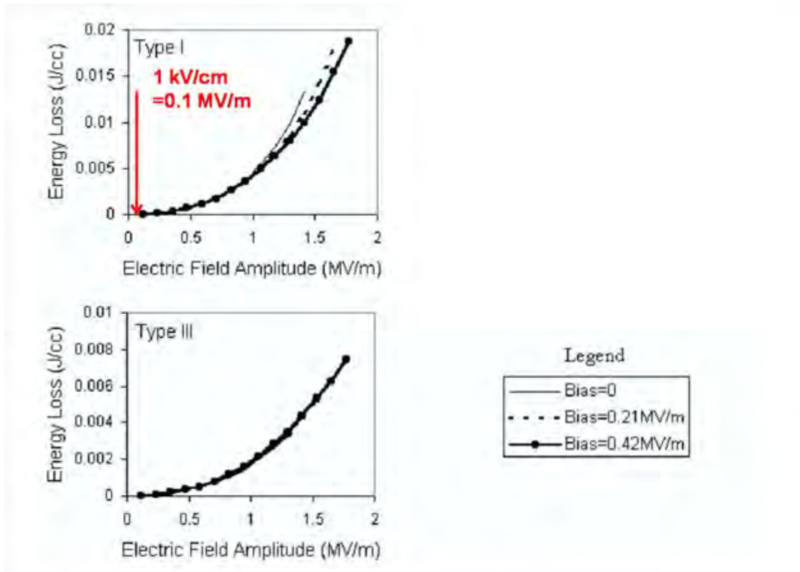

FIG. 18: Energy density loss vs. electric field amplitude for Navy Type I (PZT-4) and Navy Type III (PZT-8), calculated from hysteresis (polarization vs. electric field), for different values of externally applied DC bias (0.21 MV/m = 2.1 kV/cm)(from Fig. 5 of Waechter et.al. [53])

Waechter et.al. [53] report energy density loss data, calculated from integration of (polarization vs. electric field) hysteresis loop data, Fig. 18, for Navy Type I (PZT-4) and Navy Type III (PZT-8) hard-doped PZT materials used in sonar transducers. It is evident from these data that the magnitude of the applied electric field, 1 kV/cm = 0.1 MV/m, in this example of MEGA drive experiments using a modified form (SM-111 from Steiner & Martins) of PZT-4, is very small compared with the amplitude of electric field required for significant energy density loss. Therefore, independently confirming that this magnitude of applied electric field, 1 kV/cm = 0.1 MV/m, should be safely within the approximately linear, small loss range.

The maximum permissible electric field in a sonar transducer involves the choice of a suitable safety margin. Often, the safety margin is determined by the electric field amplitude that would produce excessive internal losses and therefore excessive heating of the material. The previously presented data shows that the magnitude of the applied electric field, 1 kV/cm = 0.1 MV/m, in this example of MEGA drive experiments using a modified form (SM-111 from Steiner & Martins) of PZT-4 is safely within the margin of approximately linear, small hysteretic loss behavior. However, a lower electric field limit is dictated based on long-term reliability (fatigue and fracture toughness) considerations. Fig. 19 shows the impedance vs. frequency spectra vs. stress cycle for Navy Type I (PZT-4) and Navy Type III (PZT-8) experimental data from Waechter et.al. [53], where the piezoelectric samples were excited by a 2 Hz sine wave with peak amplitude of 31.5 kV/cm. This electric field is substantially higher than the coercive field of these materials (the coercive field is the electric field necessary to bring the polarization in the material to zero, typical values are $E_c \approx$14 kV/cm at room temperature to $E_c \approx$10 kV/cm at 100 °C for PZT-4). The samples were indented with a Vickers diamond pyramid indenter, using a load of 20 N, applied for a period of 10 sec. This indentation process typically caused cracks of 200 to 300 μm length emanating from the corners of the indenter. For all the material specimens tested, the impedance spectra were shifted to lower frequencies and decreased in magnitude with increasing numbers of cycles. Non-indented samples of Navy Type III (PZT-8) samples that were exposed to the same electric field exhibited only minimal change in the impedance spectra for 5,000 cycles. Non-indented Navy Type I (PZT-4) samples were also more robust than the indented samples, but still showed significant change with as few as 100 cycles. Navy Type I (PZT-4) was the least robust material

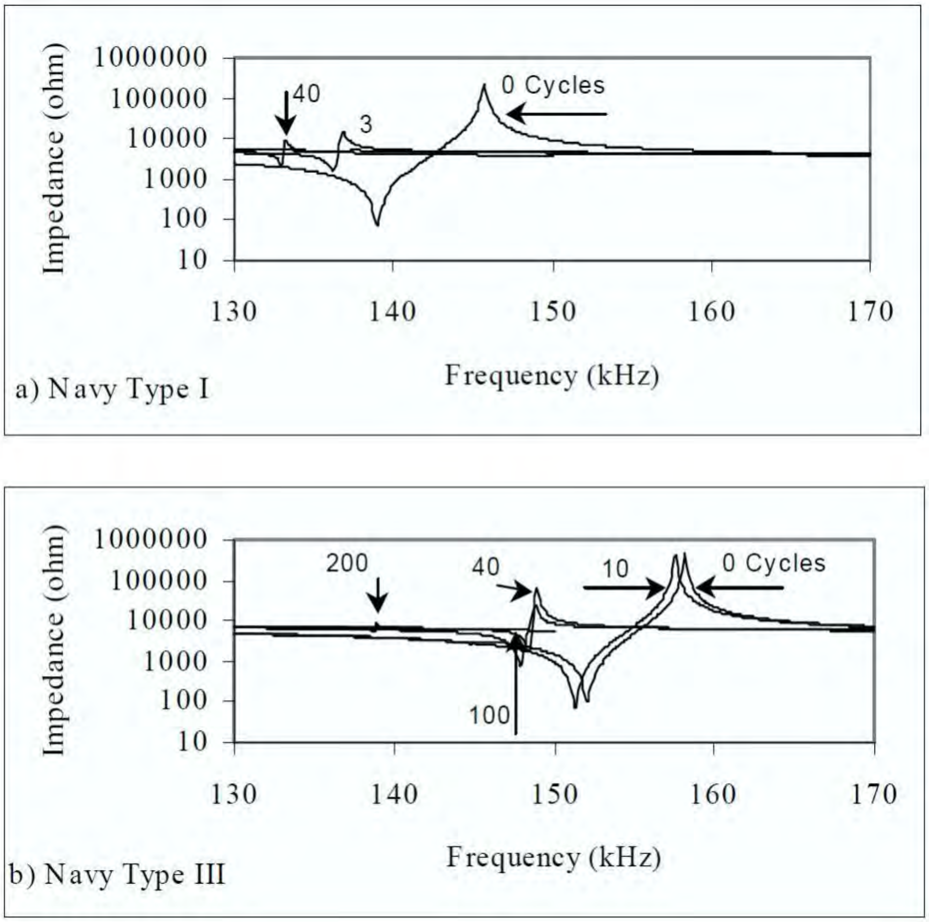

FIG. 19: Impedance vs. frequency spectra vs. stress cycle at 31.5 kV/cm for Navy Type I (PZT-4) and Navy Type III (PZT-8) (from Fig. 6 of Waechter et.al. [53])

tested: it showed the largest resonant frequency shift and the largest impedance peak reduction, with the fewest number of stress cycles.

Impedance vs. frequency spectra measurements of the MEGA drive stack, using non-indented plates made of SM-111 piezoelectric material from Steiner & Martins, measured with a Stanford Research Systems SR-780 dynamic signal analyzer, at California State University, Fullerton, by Heidi Fearn in the summer of 2016, at much lower electric field strength, at frequencies between 22 and 30 kHz, showed similar behavior: the impedance spectra were shifted to lower frequencies and decreased in magnitude with increasing numbers of cycles. It is necessary to perform a rigorous analysis of this cyclic behavior of SM-111 piezoelectric material from Steiner & Martins used in the MEGA drive, in order to characterize the natural frequency dependence on the cyclic stress history, and to assess its fatigue resistance and the appropriate limit of the electric field that should be applied to this material. More robust materials, like Navy Type III, (PZT-8) should also be assessed.

Jones and Lindberg [54] state that for Navy Type III (PZT-8) piezoelectric ceramics, an electric field limit of 10 V/mm = 0.1 kV/cm (determined on a root mean square basis) has been chosen as an industry standard based on considerations of both reliability and acceptable losses. This reliability limit is 10 times smaller than the electric field used for the MEGA experiments and for this numerical example. Since Navy Type III (PZT-8) is a hard-doped PZT with fairly similar properties as the modified Navy Type I (PZT-4) material (with trade name SM-111 from supplier Steiner & Martins) used for the MEGA experiments, and as shown by Waechter et.al. [53] Navy Type III (PZT-8) has significantly greater fracture toughness than Navy Type I (PZT-4), one would expect that the electric field limit for Navy Type I (PZT-4) should be smaller than 0.1 kV/cm and hence this indicates that the 1 kV/cm applied to the MEGA experiments is already more than 10 times higher than the industry standard based on considerations of reliability.

The mechanical quality factor of resonance Q_m (an inverse measure of mechanical damping, energy dissipation) is known to be a complicated nonlinear function of frequency, temperature, electromechanical history (including fatigue) and electric field. Furthermore, the quality factor of resonance for a stack composed of a number of piezoelectric plates will be affected by the energy dissipation occurring at the adhesive interfaces between the piezoelectric plates and the electrodes. Therefore if one knows empirically the value of the quality factor of resonance (which can be obtained empirically from the width of the resonance bandwidth) one is better off using this empirical value, instead of using book values for just the piezoelectric plates. The supplier of the piezoelectric material with tradename “SM-111,” (a modified form of PZT-4, Navy Type I) used in the MEGA drive experiments, Steiner & Martins, gives a value of Q_m=1800 in its website [39]. However, an, empirical determination of the value of the mechanical quality factor of resonance Q_m, based on the frequency response, gives a value 10 times smaller: Q_m=190, probably due to the dissipation occurring at the adhesive interfaces. It should also be taken into account that the supplier does not provide any information on the experimental test conditions under which the reported values were measured. The value Q_m=190 was determined as follows:

1. The peak amplitude response at the resonant frequency f_o was determined.
2. A horizontal line was constructed at the position $\frac{peak\ amplitude}{\sqrt{2}}$ ($\sqrt{2}$ is used because the measured response is proportional to the square root of the power). This is equivalent to constructing the horizontal line at the position: peak response minus $10\log_{10}[(\frac{1}{\sqrt{2}})^2]$=3.0103 dB.
3. The two frequencies f_1 and f_2 at which the constructed horizontal line cuts the amplitude vs. frequency response curve were determined.
4. The mechanical quality factor of resonance was then determined empirically as $Q_m = \frac{f_o}{f_2-f_1}$.

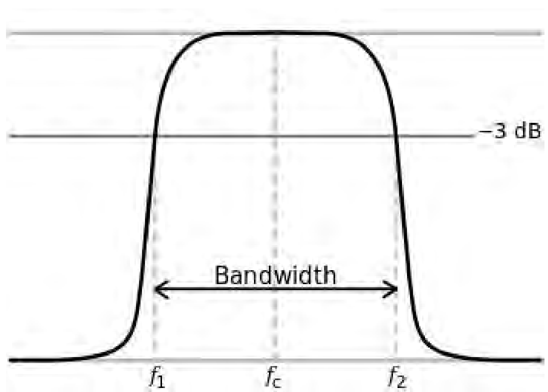

FIG. 20: Empirical calculation of mechanical quality factor of resonance Q_m based on half-power bandwidth (Image from Wikipedia/Wikimedia Commons, author Henrikb4)

(In cases in which the resonant frequency f_o is difficult to determine precisely, it can be approximated, assuming central symmetry, by the central frequency as $f_o \approx f_c = \frac{f_2+f_1}{2}$, f_c shown in Fig. 20). The difference between the two frequencies f_1 and f_2 at which the constructed horizontal line cuts the amplitude vs. frequency response curve, is known as the half-power bandwidth. Half-power bandwidth is an arbitrary measure that has been adopted by convention to empirically define the mechanical quality factor of resonance from experimental results. This arbitrary measure was adopted by convention by the electrical engineering community to determine the damping ratio from the frequencies for which the power input is half the input at resonance, or, equivalently from the frequencies at which the response is reduced from the peak response by $\frac{peak\ amplitude}{\sqrt{2}}$. The half-power bandwidth was determined to be $f_2 - f_1 = 0.2$ kHz. Using a resonant frequency of 38 kHz, then $Q_m = \frac{f_o}{f_2-f_1} = \frac{38}{0.2} = 190$, while using a resonant frequency of 30 kHz gives $Q_m = \frac{f_o}{f_2-f_1} = \frac{30}{0.2} = 150$.

Finally, concerning the input variables for this analysis, it is noted that in order to match the experimental results it is necessary to introduce a factor of 0.6% multiplying the piezoelectric coefficient d_{33} and the electrostrictive coefficient M_{33}. This factor is about 100 times smaller than any coupling coefficient one could expect based for electromechanical coupling reasons. As of the time of this writing, the reason for this factor remains to be explained.

6. THE MACH EFFECT FORCE: OUTPUT ANALYSIS

Having described and analyzed the input variables necessary to calculate the Mach effect force, I now proceed to discuss and analyze the results from such calculations. The first results to be discussed are for a MEGA Langevin stack freely floating in space, completely free from any constraints. In contrast, the MEGA Langevin stack measurements by Fearn and Woodward have been conducted with a MEGA Langevin stack that is constrained away from the center of mass, being held at the tail (brass) end. Preliminary analysis for a MEGA Langevin stack with damping force constraints is discussed later in this section.

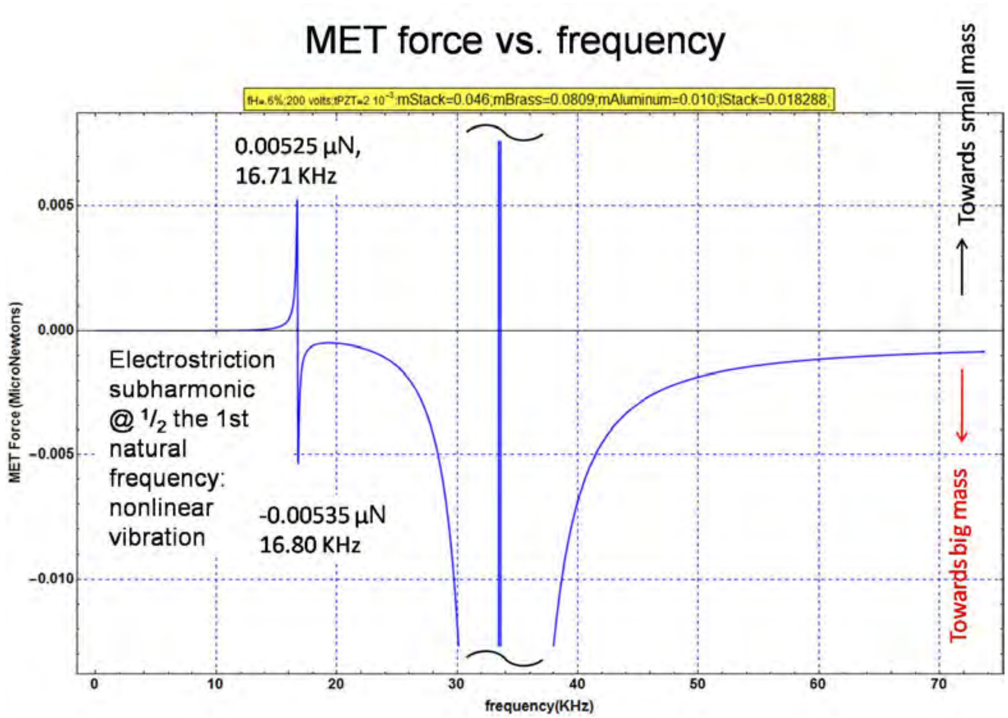

FIG. 21: Mach effect force vs. frequency, detailing the subharmonic resonance due to electrostriction, for brass mass (tail end) = 0.0809 kg

Fig. 21 shows the Mach effect force, in microNewtons (μN), vs. the vibration frequency, in kiloHertz (kHz), zooming-in for a close-up view in detail of the subharmonic resonant frequency due to the electrostrictive effect, occurring at $\frac{1}{2}$ the first natural frequency. This subharmonic response takes place due to the nonlinear excitation proportional to the square of the electric field, when the electrostrictive voltage excitation frequency 2ω equals the first natural frequency of the MEGA drive ω_o. This happens at $2\omega = \omega_o$, or equivalently at $\omega = \frac{1}{2}\omega_o$. As shown in Fig. 21, there is a subharmonic peak at the lower resonant frequency of 16.714 kHz, with a Mach effect force magnitude of only 5.25 nanoNewtons, directed towards the front (aluminum) small mass, immediately followed by a slightly higher subharmonic resonant frequency of 16.802 kHz, oriented in the opposite direction, with a Mach effect force magnitude of only 5.35 nanoNewtons, directed towards the tail (brass) big mass. It is interesting that the response is slightly asymmetric: with a 2% higher amplitude force directed towards the tail (brass) mass, at a 0.53% higher frequency. The amplitude of the response due to the piezoelectric effect is so much larger than this subharmonic response due to the electrostrictive effect that the fundamental natural frequency response needs to be shown cut-off, in this detailed view.

Fig. 22 shows the Mach effect force, in μN, vs. the vibration frequency, in kHz, zooming-in for a close-up view in detail of the fundamental resonant frequency due to the piezoelectric effect. The resonant frequency occurs at 33.514 kHz, with a peak magnitude of 21.576 μN, directed towards the front (aluminum) small mass. This is over 4,000 times greater amplitude than the electrostrictive response amplitude, which shows that the electrostrictive response of hard ferroelectric ceramic materials like PZT-4, Navy Type I, is indeed very small in comparison with the piezoelectric effect response at this amplitude of the electric field (1 kV/cm), and therefore, often times neglected. It is noteworthy that the amplitude vs. frequency approach

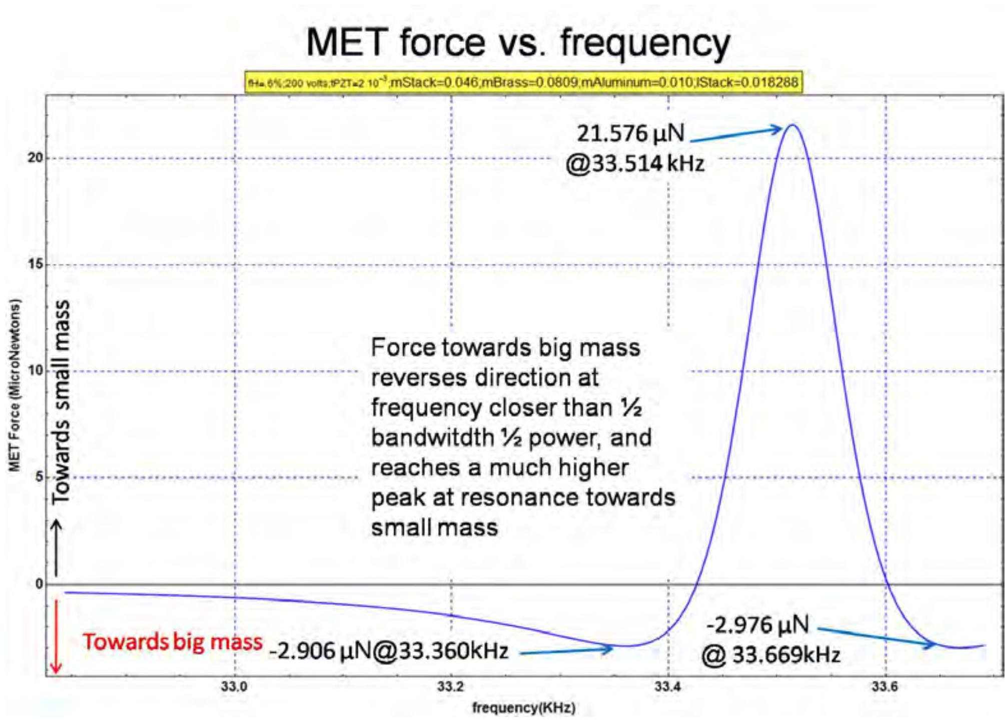

FIG. 22: Mach effect force vs. frequency, detailing the first natural frequency due to piezoelectricity, for brass mass (tail end) = 0.0809 kg

to this resonant frequency response is not monotonic. Rather as the resonant frequency is approached from lower, or higher frequencies, that are more than 0.26% away from the resonant frequency peak, it is observed that the response is actually directed in the opposite direction, towards the tail (brass) big mass, and that as the resonant frequency is approached, the amplitude of the Mach effect towards the tail (brass) big mass increases in amplitude until it reaches 2.906 μN directed towards the tail (brass) big mass at 33.360 kHz when approaching from lower frequencies towards higher frequencies. And it reaches 2.976 μN directed towards the tail (brass) big mass at 33.669 kHz when approaching from higher frequencies towards smaller frequencies. This frequency ratio, between the local peak amplitude response directed towards the tail (brass) big mass (at 33.360 and 33.669 kHz) and the central peak amplitude resonant response (at 33.514 kHz) directed towards the front (aluminum) small mass is due to the mechanical quality factor of resonance, which is assumed, as previously discussed, $Q_m = 190 = \frac{1}{0.53\%}$. The local peak amplitude responses, directed towards the tail (brass) big mass, occur at frequencies that are $(33.514 - 33.360)/33.514 = (33.669 - 33.514)/33.514 = 0.46\% = \frac{1}{1.15 Q_m} = \frac{1}{1.15 \times 190} \approx \frac{1}{Q_m}$ from the central resonant frequency. The Mach effect force transitions from being directed towards the tail (brass) mass to being directed towards the front (aluminum) mass by going through zero at a frequency ratio $(\frac{f - f_o}{f_o})$ that is $\pm\frac{1}{2Q_m}$ away from the peak natural frequency response. Thus, the frequency ratio $(\frac{f - f_o}{f_o})$ between the peak natural frequency Mach effect force (directed towards the front (aluminum) mass) and the frequencies at which the Mach effect is zero is $\frac{1}{2Q_m}$, and the distance between the frequencies at which the Mach effect is zero and the local peak responses directed towards the tail (brass) mass is also $\frac{1}{2Q_m}$. The frequency bandwidth between the lower frequency and upper frequency peak responses due to the electrostrictive effect are also separated by a similar factor $(\pm\frac{0.53\%}{2} = \pm 0.26\% = \pm\frac{1}{2Q_m})$. It can be shown that the transient vibration response of the MEGA Langevin stack is also governed by a decaying exponential having the same factor $\frac{1}{2Q_m}$. The (dimensionless) damping ratio ζ (the ratio of the actual damping to the critical value of damping at which the dynamic system does not overshoot its starting position, does not make a single oscillation and returns to equilibrium in the minimum amount of time) is related to the mechanical quality factor of resonance Q_m by $\zeta = \frac{1}{2Q_m}$. Thus the reason for the appearance of the factor $\frac{1}{2Q_m}$ in the dynamic response of the Mach effect force for the vibrating MEGA Langevin stack is easy to understand: the response is governed by the damping ratio ζ. Since the mechanical quality factor of

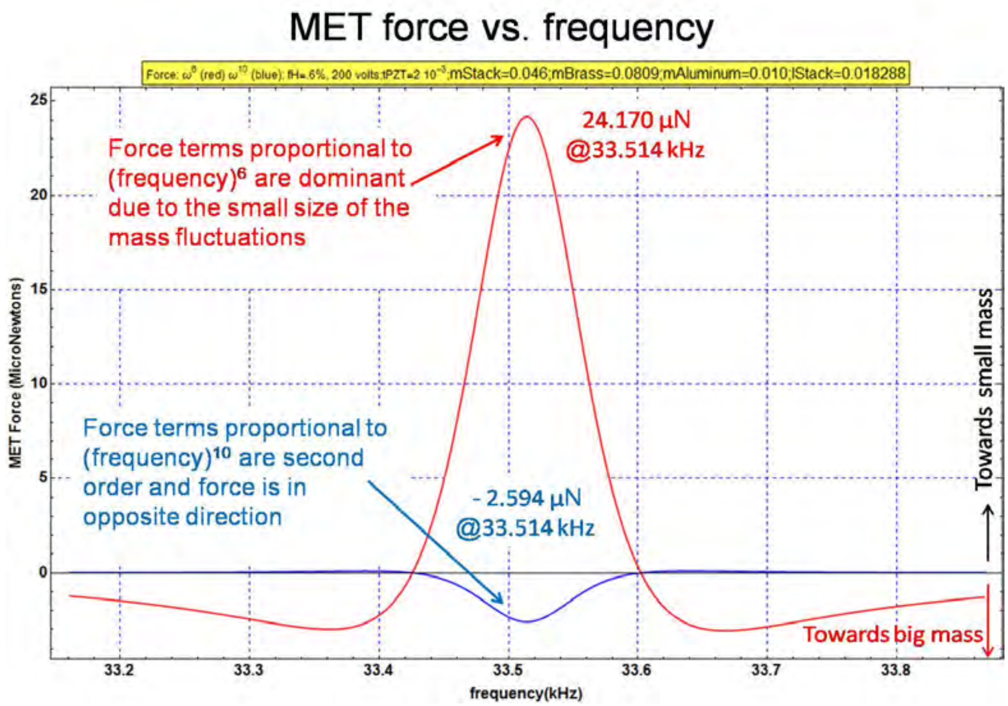

FIG. 23: Mach effect force vs. frequency, showing the first natural frequency due to piezoelectricity, for brass mass (tail end) = 0.0809 kg. In this plot, the Mach effect force is shown to be composed of two terms: a main component proportional to the sixth power of the frequency and a second order term proportional to the tenth power of the frequency.

resonance Q_m is an inverse measure of damping ζ, it governs the amplitude of resonant response. Since the MEGA drive experiments by Fearn and Woodward [26] have been performed with a manual operator chasing the natural frequency, and no frequency control algorithm has been used, it is suspected that the response that they have measured up to now is not the global peak natural frequency response, but rather the significantly lower amplitude local peak directed towards the tail (brass) big mass. Notice that there is a factor of 7.4 (=21.576/2.906) times greater response at the natural frequency, but that it is necessary to have equipment that can lock on this frequency with a bandwidth much smaller than $\pm\frac{1}{2Q_m} = \pm\frac{1}{2\times 190} = \pm 0.26\%$ in order to reach the main resonant peak. This is difficult to do because as the MEGA Langevin stack vibrates, heat gets internally dissipated inside the PZT discs, which raises the temperature, which changes the dimensions of the stack, as well as the piezoelectric and electrostrictive responses, which are all temperature dependent, hence the natural frequency changes during operation and the natural frequency needs to be chased within this small bandwidth. To have the highest Mach effect forces, it is better to have higher quality factor of resonance, but the higher the quality factor of resonance, the smaller the bandwidth at which this peak natural frequency response will be located, hence the higher the quality factor of resonance, the more difficult it is to be at peak resonance and to stay at peak resonance.

Fig. 23 is a plot of the Mach effect force vs. frequency, showing the first natural frequency due to piezoelectricity, for brass mass (tail end) = 0.0809 kg, where the Mach effect force is shown to be composed of two terms: a main component proportional to the sixth power of the frequency and a second order term proportional to the tenth power of the frequency. As was discussed in section 5, the Mach effect force on the center of mass is calculated as the product of the total mass times the acceleration of the center of mass. The acceleration of the center of mass contains terms (due to Mach effect inertial mass fluctuations) of the form of the product of the time derivative of the mass fluctuation times the velocity, and of the form of the product of the second time derivative of the mass fluctuation times the displacement, as well as square terms of the previously mentioned expressions. The term due to the product of the time derivative of the mass fluctuation times the velocity, and due to the product of the second time derivative of the mass fluctuation times the displacement is proportional to the angular frequency to the sixth power, divided by the product of the gravitational constant times the square of the speed of light. The second term, due to the product of the difference of the displacements, times the square of the difference between the mass fluctuations, is proportional to the angular frequency to the tenth power, divided by the square of the product of the gravitational constant times the square of the speed of light. This is a higher order term, which for small mass fluctuations, should be second order. This is confirmed by these numerical experiments, as Fig. 23 shows that the term proportional to the frequency to the tenth power is an order of magnitude smaller than the term proportional to the frequency to the sixth power. The term proportional to the frequency to the sixth power is dominant. It is also interesting that the direction of the force is in opposite direction for both terms, and both of them cross at the same frequencies at which the Mach effect force is zero.

Fig. 24 is a three-dimensional plot showing the Mach effect force (μN), in the vertical axis, vs. (brass) mass (kg) of tail end, in the horizontal axis, vs. frequency (kHz) in the cross axis. The spikes in the plot are numerical artifacts of the plotting resolution due to the very narrow frequency bandwidth $\pm\frac{1}{2Q_m} = \pm\frac{1}{2\times190} = \pm0.26\%$ associated with the first natural frequency Mach effect force response directed towards the front (aluminum) mass, that make it numerically taxing to plot such a small bandwidth (smaller than 0.0026×33.514 kHz=0.087 kHz=87 Hz) smoothly over an axis scale spanning 40 kHz ($\pm\frac{0.087}{40} = \pm0.22\%$). In reality the curve should be smooth. Looking at the behavior of the curve along the frequency axis, one can see that the bandwidth around the natural frequency response is very narrow, as expected from the small amount of damping associated with the relatively high value ($Q_m = 190$) of mechanical quality factor of resonance. The positive direction of the vertical axis represents a force towards the front (aluminum) small mass, and the negative direction a force towards the tail (brass) big mass. In this view it is apparent that the amplitude of the Mach effect force diminishes rapidly for a (brass) tail mass smaller than 0.1 kg, and that for a higher (brass) mass than 0.1 kg (of the tail end) the Mach effect force approaches an asymptote in value. In contrast, Fearn and Woodward's experimental results [55] for a held device (not freely floating in space) show the Mach effect force reaching an optimum value below 0.1 kg; more on this later. For a MEGA Langevin stack that is perfectly symmetric about its center of mass, the Mach effect force is zero. This is the reason for the abrupt decrease in Mach effect force for small values of the brass mass. Also observe that the point at which the Mach effect force diminishes rapidly for a (brass) mass (kg) of tail end a little smaller than 0.1 kg is accompanied by a significant increase in the natural frequency.

Fig. 25 is a close-up view of Fig. 24, looking at the Mach effect force (μN), in the vertical axis vs. (brass) mass (kg) of tail end variation from 0 to 0.12 kg instead of 0 to 1 kg. The plot is still a three-dimensional plot of these variables vs. frequency (kHz) in the cross axis. Again, the spikes in the plot are numerical artifacts of the plotting resolution due to the very narrow frequency bandwidth associated with the Mach effect force response at the first natural frequency. This close-up view makes it more apparent that the Mach effect force rapidly changes from a value of zero for a (brass) mass of tail end similar to the (aluminum) mass of the head end (0.010 kg), up to the point at which the brass mass nears 0.060 kg. The Mach effect force variation is smaller for larger values of the brass mass. The plot shows that if the brass mass is less than the aluminum mass, the Mach effect force (associated with an excitation frequency equal to the first natural frequency) is predicted to switch direction.

Figs. 26 and 27 are flipped views of Figs. 24 and 25, respectively, with viewing emphasis on the force directed towards the (brass) mass tail end, instead of the force directed towards the (aluminum) mass front end. The plots are still three-dimensional plots of the Mach effect force (μN), in the vertical axis, vs. (brass) mass (kg) of tail end, in the horizontal axis, vs. frequency (kHz) in the cross axis. Again, the spikes in the plots directed toward the bottom of the plots are numerical artifacts of the plotting resolution due to the very narrow frequency bandwidth. It is evident from the picture that as previously discussed, as the resonant frequency is approached from lower, or higher frequencies, that are more than 0.26% away from the resonant frequency peak, it is observed that the response is actually directed towards the (brass) mass at the tail end, as observed in experiments. And that as the resonant frequency is approached, the amplitude of the Mach effect towards the tail (brass) big mass increases in amplitude until it reaches its local peak (2.57 μN directed towards the tail (brass) big mass at 33.42 kHz when approaching from lower frequencies towards higher frequencies). As previously discussed, the Mach effect force suddenly reverses direction as the frequency gets closer to the resonant frequency peak, and this happens over a very small bandwidth $\pm\frac{1}{2Q_m} = \pm\frac{1}{2\times190} = \pm0.26\%$ centered on the natural frequency. It is also observed that the Mach effect force, as the resonant frequency is approached from lower or higher frequencies that are more than 0.26% away from the resonant frequency peak, is much smoother (it does not present the plotting artifact looking like spikes that occur at the global peak of the fundamental natural frequency).

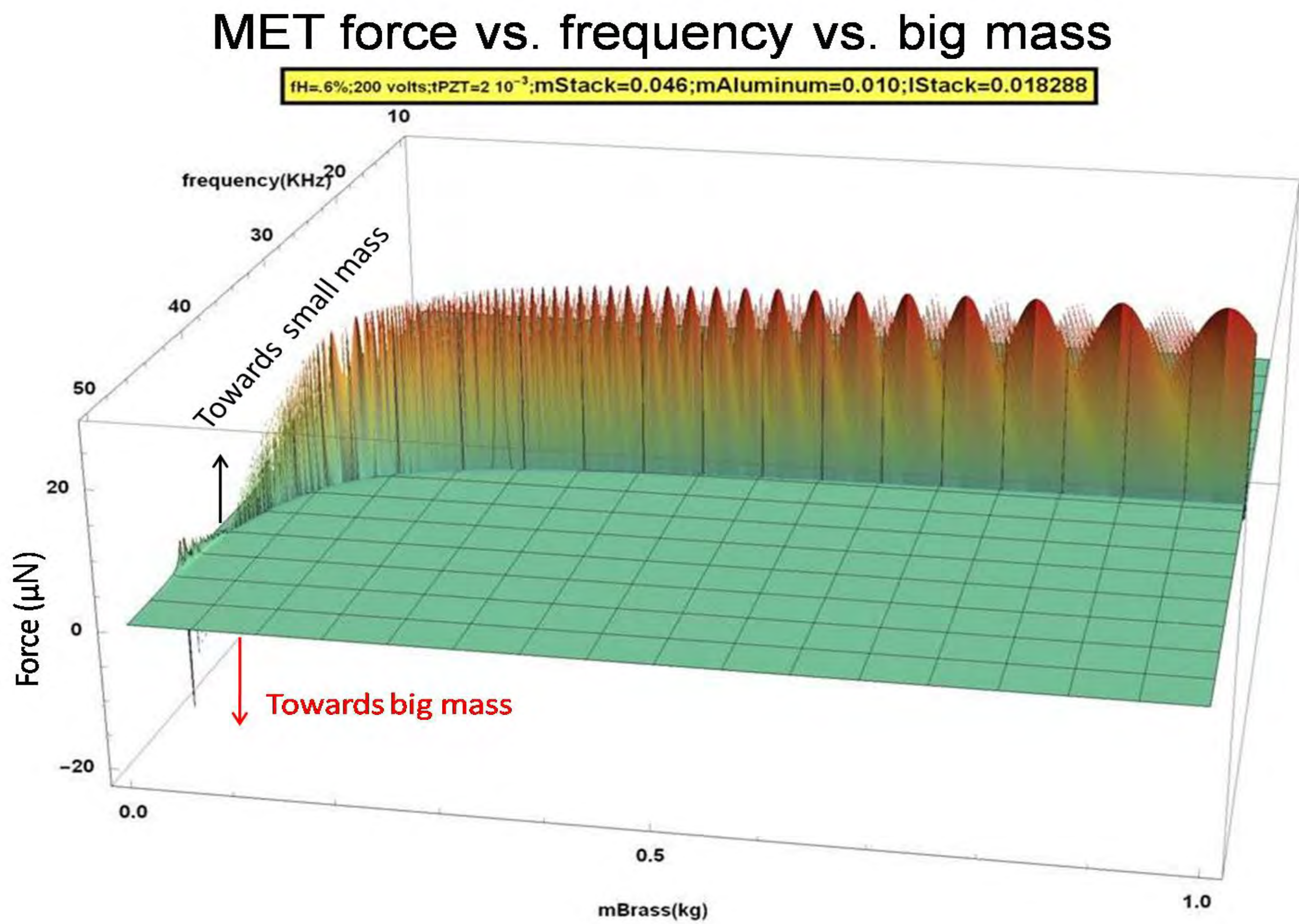

FIG. 24: 3D Plot of Mach effect force (μN) vs. frequency (kHz) vs. (brass) mass (kg) of tail end. MEGA Langevin stack modeled as floating free in space.

It is much smoother because the derivative of the Mach effect force with respect to frequency is much smaller. Therefore one has to be very careful about statements regarding the dependence of the Mach effect force on frequency, like “the force depends on frequency to the sixth power” or “the force depends on frequency to the second power,” as the force’s dependence on frequency is a function of how far away from the resonant frequency the force is calculated at. Again, since the MEGA drive experiments by Fearn and Woodward [26] have been performed with a manual operator chasing the natural frequency, and no frequency control algorithm has been used, it is suspected that the response that they have measured up to now is not the force with global peak natural frequency response shown in Fig. 24, but rather the significantly lower amplitude force directed towards the tail (brass) big mass shown in Fig. 26. There is a factor of 7.4 times greater response at the natural frequency shown in Fig. 24, but in order to reach it, it is necessary to have equipment that can lock on this frequency with a bandwidth much smaller than $\pm\frac{1}{2Q_m} = \pm\frac{1}{2\times 190} = \pm 0.26\%$.

This is very difficult to do because as the MEGA Langevin stack vibrates, heat gets internally dissipated inside the PZT discs, which raises the temperature, which changes the dimensions of the stack, as well as the piezoelectric and electrostrictive responses, which are all temperature dependent, hence the natural frequency changes during operation and the natural frequency needs to be chased within this small bandwidth.

Fig. 28 is a plot of the first natural frequency vs. (brass) mass (kg) of tail end. As one can see from this plot, as the brass mass increases, the natural frequency decreases, from 44 kHz for zero brass mass to 29 kHz for brass mass=0.3 kg. The natural frequency decreases as the brass mass increases because the natural frequency is inversely proportional to the square root of the reduced mass $m = \frac{m_1 m_2}{m_1 + m_2}$.

Fig. 29 shows the behavior of the Mach effect force vs. (brass) mass (kg) of tail end for a MEGA Langevin stack in space. Each curve is for a constant value of the ratio of excitation frequency to the first natural frequency. Each curve is calculated at a different value of this ratio. The purpose of this plot is to understand the experimental results when the excitation frequency does not match exactly the natural frequency. Recall that the natural frequency is a property of the physical system (regardless of excitation frequency) that is set by the material and geometrical properties of the system. The excitation frequency may not match the natural frequency for a number of reasons, due to inaccuracies of the electronics as well as due to the fact that the natural frequency changes with temperature, and the temperature changes during the test due to transient internal heating. Also the natural frequency changes cycle to cycle due to electromechanical history of the piezoelectric material, and due to the possible growth of internal damage due to micro-cracks and coalescence of internal voids. To understand these curves, we must take into account that as one varies the brass mass, keeping everything else constant, the natural frequency will change as well, due to the fact that the natural frequency is a function of the brass mass. The natural frequency is proportional to the square root of the inverse of the reduced mass $\frac{1}{m} = \frac{1}{m_1} + \frac{1}{m_2}$, so that as one mass (for example the brass mass m_2) is reduced, the natural frequency increases, and vice-versa, as one mass (for example the brass mass m_2) is increased, the natural frequency decreases (up to the point at which the larger mass m_2 becomes so large that its inverse $\frac{1}{m_2}$ is negligible in comparison with the inverse of the smaller mass $\frac{1}{m_1}$). In Fig. 29 the Mach effect force vs. (brass) mass (kg) of tail end (up to 0.12 kg), is shown for $f = f_o(1 - \frac{1}{NQ_m})$ for N=$\frac{1}{2}$,1,$\frac{4}{3}$,2,3,4 and ∞. Since Q_m=190, this means that this plot is for the ratio of excitation frequency to the first natural frequency $\frac{f}{f_o} = (1 - \frac{1}{N190}) = 98.95\%, 99.47\%, 99.61\%, 99.74\%, 99.82\%, 99.87\%$, and 100%. Or, in other words, Fig. 29 shows the calculated behavior for the Mach effect force for different values of the brass mass, where all experiments are conducted such that the excitation frequency is $\frac{1}{NQ_m} = \frac{1}{N190}$ less than the natural frequency (and where the natural frequency decreases as the brass mass increases).

For comparison, consider the experimental data in the “Conclusions” section of page 105 of Fearn et.al.’s [55] article, where they state:

“In addition, it was determined that an optimal brass reaction mass is necessary to give maximal thrust. Several different brass reaction masses 64.7g, 80.9g, 96.8g, 112.6g and 128.3g were tried. We found that for this PZT stack, the preferred brass reaction mass 80.9g. The data is not displayed here since for a different device one would have to run this kind of test again. But it is clearly something that would be worthwhile to optimize the thrust for a given device.”

(The arXiv version of this article [56] also gives the lengths of the brass masses: 0.5, 0.625, 0.75, 0.875 and 1.0 inch, respectively). Unfortunately, the measured force vs. brass mass for brass masses of 64.7g, 80.9g, 96.8g, 112.6g and 128.3g is not shown in [55], and one cannot ascertain from this what was the actual dependence of force vs. brass mass in the experiments.

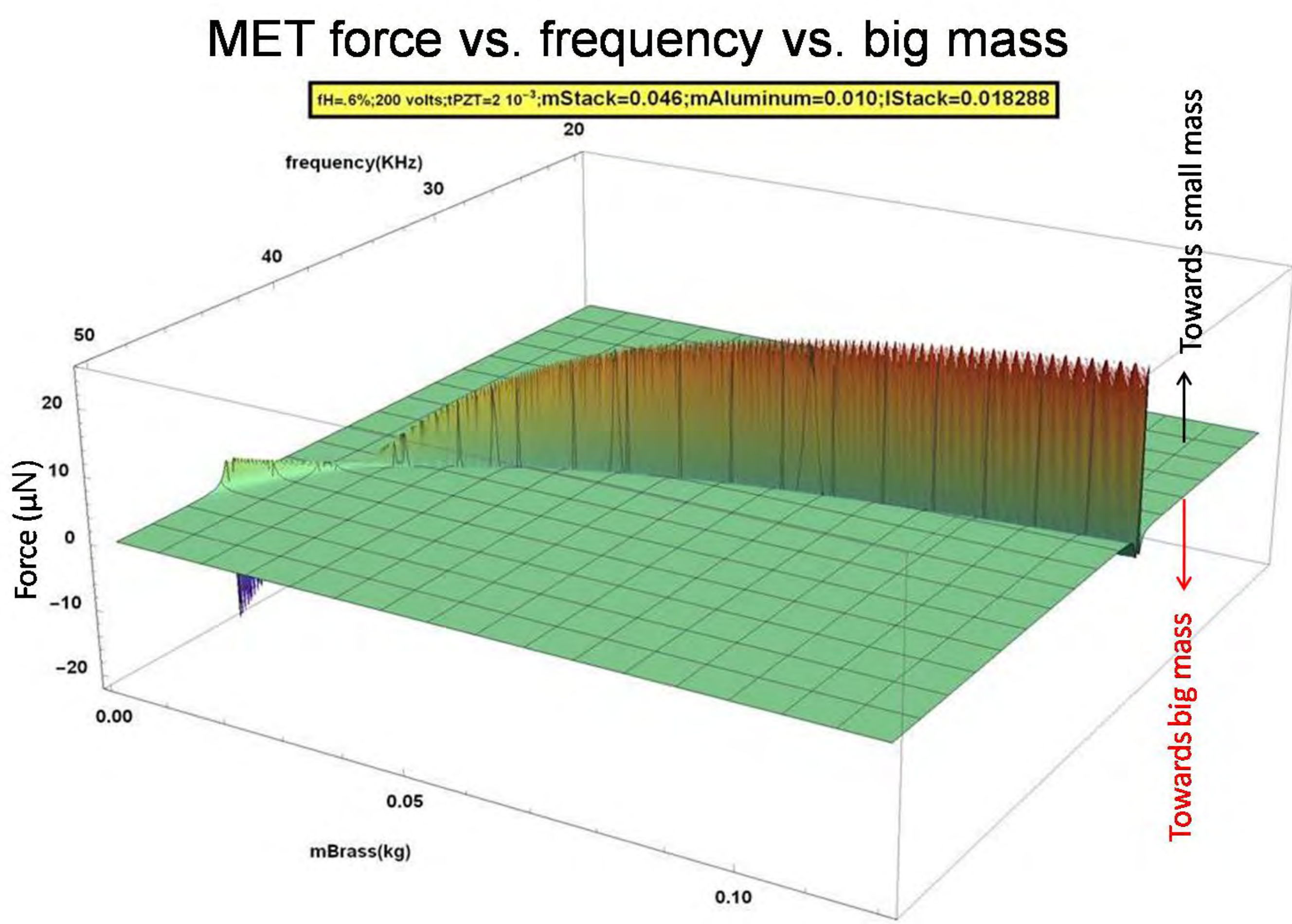

FIG. 25: 3D Plot of Mach effect force (μN) vs. frequency (kHz) vs. (brass) mass (kg) of tail end. Detail close-up of (brass) tail mass lower than 0.1 kg. MEGA Langevin stack modeled as floating free in space.

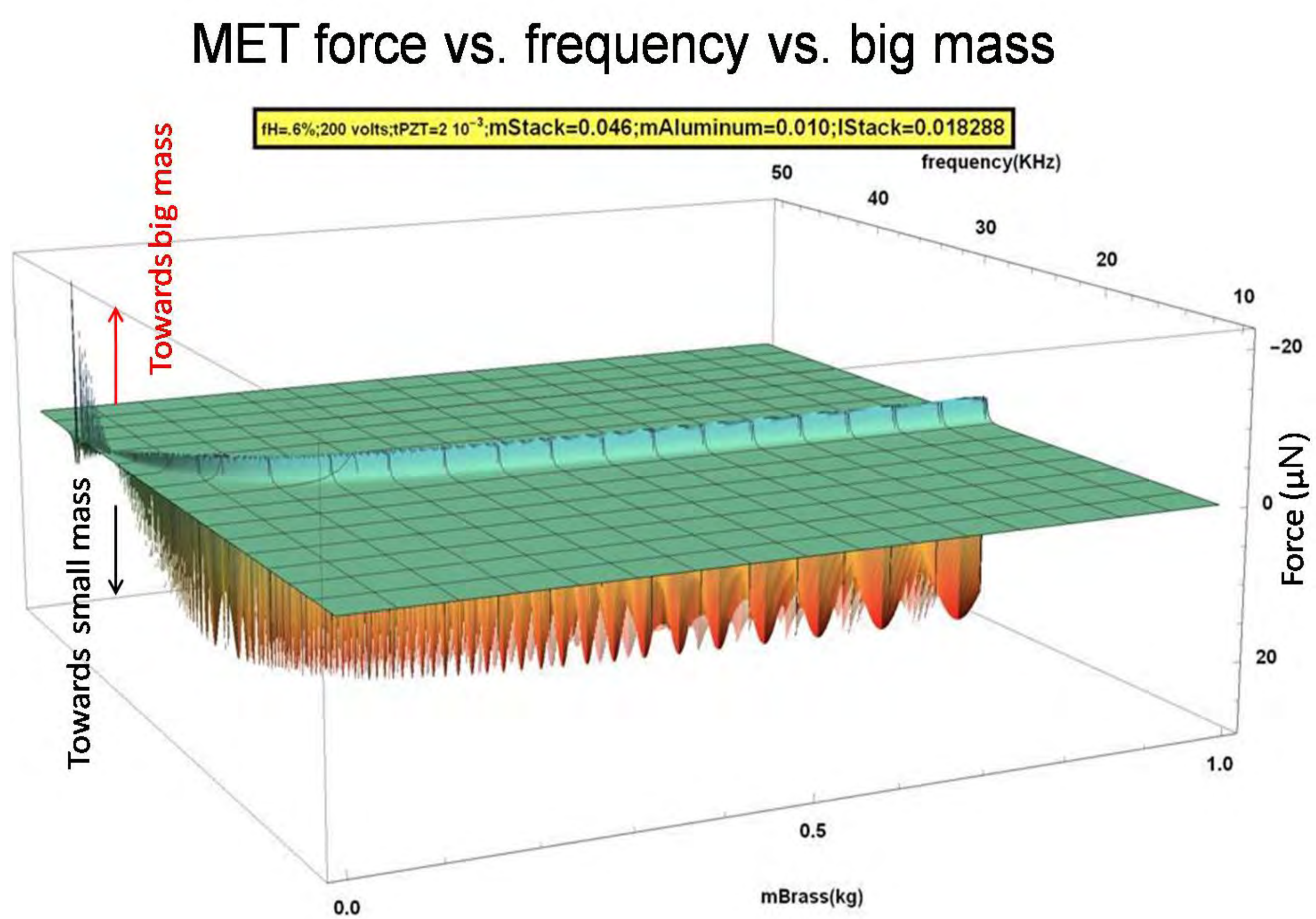

FIG. 26: 3D Plot of Mach effect force (μN) vs. frequency (kHz) vs. (brass) mass (kg) of tail end. View of force directed towards the (brass) mass tail end. MEGA Langevin stack modeled as floating free in space.

However, it looks like there is a discrepancy between the calculated results for a MEGA drive in space, free of any end constraints, for which there is no optimal mass except at an infinity brass mass: as the greater the brass mass, the greater the Mach effect force and the experimental results obtained with the MEGA drive supported at the back of the brass mass in the experiments by Fearn et.al.'s [55], where the optimal mass is reported to be 80.9g. The calculated curves in Fig. 29 show the Mach effect force grows rapidly with brass mass initially up to about 60 grams, in what looks like an exponential decay curve, with the Mach effect force growth exponentially decaying towards an asymptote. The value of the Mach effect force asymptote is different depending on the excitation frequency (depending on how far the excitation frequency is from the natural frequency). The calculations show practically the same results for an excitation frequency $f = f_o(1 - \frac{1}{NQ_m})$ with N=1 and N=$\frac{4}{3}$, indicating that the maximum response directed towards the tail (brass) mass occurs when the excitation frequency is between those two values, at approximately N$\approx \frac{7}{6}$, $f \approx f_o(1 - \frac{6}{7Q_m})$, which for $Q_m = 190$ is $f \approx f_o(1 - \frac{6}{7\times190})$ or a ratio between the excitation frequency to natural frequency of $\frac{f}{f_o} \approx 99.55\%$, at an excitation frequency approximately 0.45% lower than the natural frequency peak.

One may ask, what happens to the Mach effect force if one wants to attach the MEGA drive to a much larger mass, like a large spacecraft? What is the effect on the Mach effect force, in the limit as the tail mass goes to infinity? Fig. 30 shows the asymptotic behavior of the Mach effect force vs. (brass) mass (kg) of tail end for a MEGA Langevin stack in space. Fig. 30 shows that the Mach effect force grows rapidly as the brass mass increases towards 60 grams and that it rapidly converges towards an asymptotic value for a brass mass of less than 2 kg. It is evident that, to maximize the Mach effect force when using the MEGA drive in space, one should attach it to the most massive part of the spacecraft, preferably at its center of mass, and that the attachment should be as stiff as possible. The spacecraft's mass does not need to be too massive to provide an optimal mass for this size of MEGA stack, since an attachment mass equal or greater to 2 kg works practically as optimally as any greater mass. Of course, this conclusion is for one MEGA Langevin stack of these dimensions, if there is a multiple number of MEGA Langevin stacks, the needed mass of the spacecraft would need to be correspondingly more massive to provide near optimum force.

A preliminary numerical investigation appears to reveal that the optimal mass of 80 grams, discussed on page 105 of Fearn et.al.'s [55] article, is an experimental artifact (there would not be such an optimal brass mass if the MEGA Langevin stack were free in space) due to holding the MEGA Langevin stack behind the brass mass with a rubber pad (page 111 of Woodward's [57] book) between the brass mass and an aluminum bracket that holds the device on the arm of a torque pendulum. Thus, in Fearn and Woodward's experiment, the Mach effect device is not held at its center of mass, but it is held behind the more massive end: behind the tail brass mass, with a rubber pad that provides damping at the tail end of the device. A preliminary numerical investigation was carried out modeling the stack as being supported by a bracket with negligible bending stiffness compared to the uniaxial stiffness of the MEGA Langevin stack, and with the damping force taking place at the ends of the stack, as a first approximation of the situation where the damping provided by the rubber pad between the tail (brass) mass and the aluminum bracket is much greater than the internal damping in the PZT stack (thus providing one possible explanation of the experimentally measured mechanical quality factor of resonance being only Q_m=190 instead of the book value Q_m=1800 reported by Steiner & Martins for their modified PZT-4 material SM-111).

The following figures show the Mach effect force as a function of frequency and the mass of the tail (brass) mass for a MEGA Langevin stack with damping at the ends, where the damping force is due to a rubber pad between the end mass and a holding bracket. Figs. 31, 32 and 33 cover the same parameters as Figs. 24, 25 and 26, respectively, did for the MEGA Langevin stack floating in space.

Fig. 34 is a plot of the Mach effect force vs. (brass) mass (kg) of tail end for a MEGA Langevin stack with damping at the ends, where the damping force is due to a rubber pad between the end mass and a holding bracket. Each curve is for a constant value of the ratio of excitation frequency to the first natural frequency. Each curve is calculated at a different value of this ratio. The purpose of this plot is to understand the experimental results when the excitation frequency does not match exactly the natural frequency.

For a ratio of excitation frequency to natural frequency equal to $\frac{f}{f_o} = (1 - \frac{1}{0.5\times190}) = 98.95\%$, the maximum Mach effect force under such conditions is 0.457 μN, and it is directed in the direction from the aluminum mass towards the brass mass, and this maximum amplitude Mach effect force occurs for a brass mass equal to 0.206 kg, at a natural frequency of $f_o = 30.19$ kHz, and excitation frequency of 29.87 kHz. For $\frac{f}{f_o} = (1 - \frac{1}{190}) = 99.47\%$ the maximum Mach effect force is 1.43 μN, and it is directed in the direction from the aluminum mass towards the brass mass, and this maximum amplitude Mach effect force occurs for a brass mass equal to 0.106 kg, at a natural frequency of $f_o = 31.87$ kHz, and excitation frequency of 31.70 kHz.

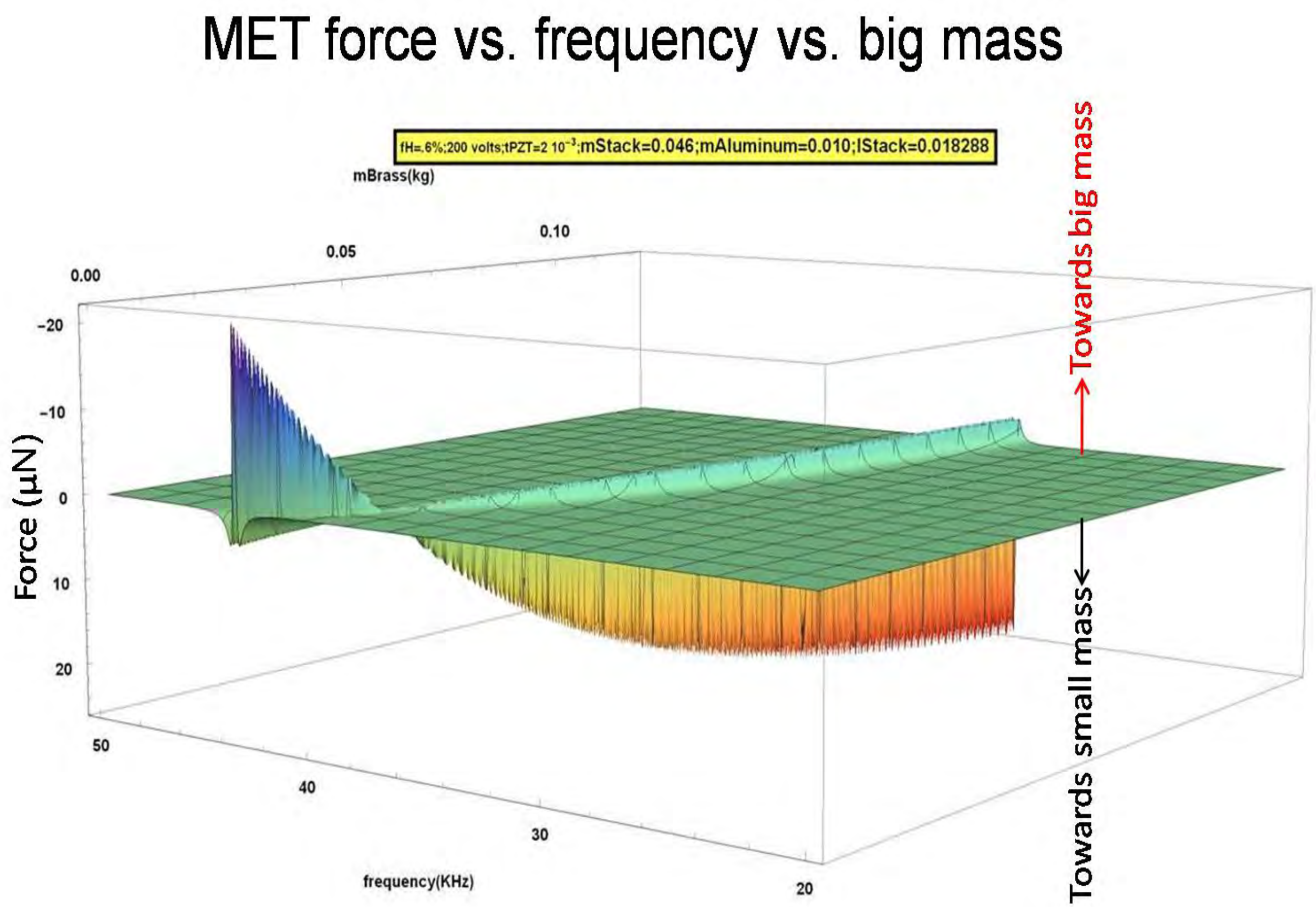

FIG. 27: 3D Plot of Mach effect force (μN) vs. frequency (kHz) vs. (brass) mass (kg) of tail end. View of force directed towards the (brass) mass tail end. MEGA Langevin stack modeled as floating free in space.

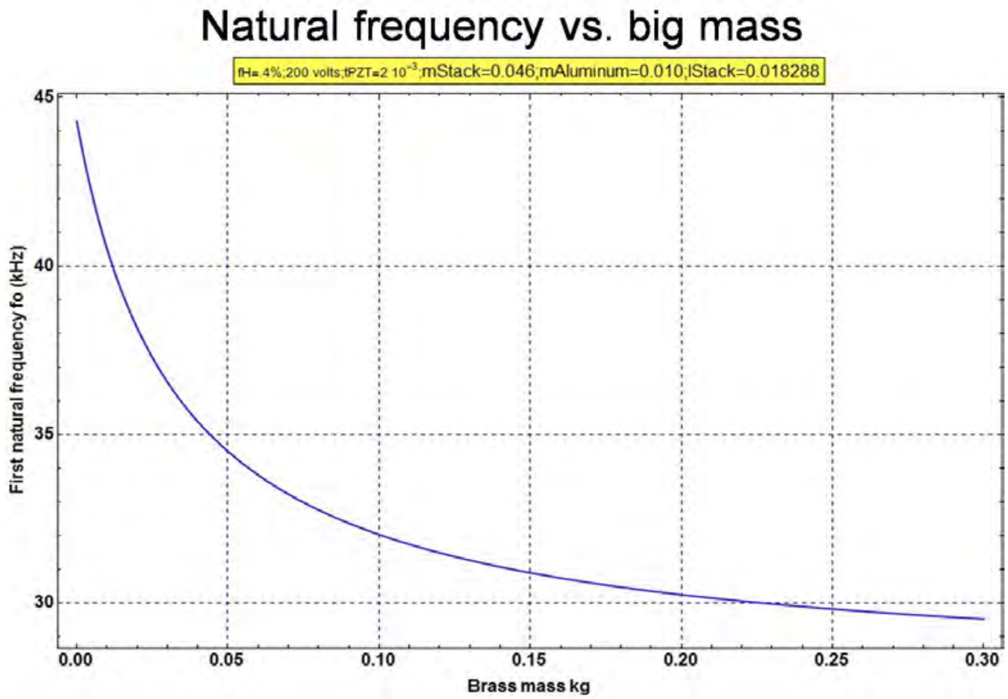

FIG. 28: First natural frequency vs. (brass) mass (kg) of tail end

For $\frac{f}{f_o} = (1 - \frac{0.75}{190}) = 99.61\%$ the maximum Mach effect force is 2.03 μN, and it is directed in the direction from the aluminum mass towards the brass mass, and this maximum amplitude Mach effect force occurs for a brass mass equal to 0.083 kg, at a natural frequency of $f_o = 32.63$ kHz, and excitation frequency of 32.50 kHz.

For $\frac{f}{f_o} = (1 - \frac{1}{2\times190}) = 99.74\%$ the maximum Mach effect force is 2.58 μN, and it is directed in the direction from the aluminum mass towards the brass mass, and this maximum amplitude Mach effect force occurs for a brass mass equal to 0.061 kg, at a natural frequency of $f_o = 33.76$ kHz, and excitation frequency of 33.67 kHz. For $\frac{f}{f_o} = (1 - \frac{1}{3\times190}) = 99.83\%$ the maximum Mach effect force is 1.59 μN, and it is directed in the direction from the aluminum mass towards the brass mass, and this maximum amplitude Mach effect force occurs for a brass mass equal to 0.106 kg, at a natural frequency of $f_o = 35.22$ kHz, and excitation frequency of 35.15 kHz.

If the excitation frequency exactly matches the natural frequency, the (global) maximum Mach effect force is 17.16 μN, and it is directed in the direction from the brass mass towards the aluminum mass, and this maximum amplitude Mach effect force occurs for a brass mass equal to 0.083 kg, at an excitation frequency exactly matching the natural frequency of $f_o = 32.64$ kHz.

These calculations are summarized in Table V. For comparison, consider the experimental data in the “Conclusions” section of page 105 of Fearn et.al.’s [55] article. It is encouraging that the experiments show the optimal mass to be 81 grams, since this agrees very well with the calculations, (given the sparsity of the experimental data, at increments of 16 grams, or 20% of the optimal mass) within 2% of the optimal mass of 83 grams calculated for the maximum calculated Mach effect force of 17 μN when the excitation is exactly identical to the natural frequency and with the optimal mass of 83 grams when the excitation frequency is $\frac{0.75}{Q_m}$=0.395% smaller than the natural frequency, giving a calculated Mach effect force of 2 μN. As previously discussed, the MEGA drive experiments by Fearn and Woodward [26] have been performed with a manual operator chasing the natural frequency, and no frequency control algorithm has been used. Therefore it is suspected that the response that they have measured up to now is not the global peak natural frequency response predicted to be 17 μN directed towards the head aluminum mass, but rather the significantly lower amplitude local peak of 2 μN directed towards the tail (brass) big mass. Indeed, the net forces measured by Fearn and Woodward [26] have all been directed towards the tail brass mass. Thus, it is strongly suspected that, on the average they have managed their excitation frequency to be only within $\frac{0.75}{Q_m}$=0.395% of the

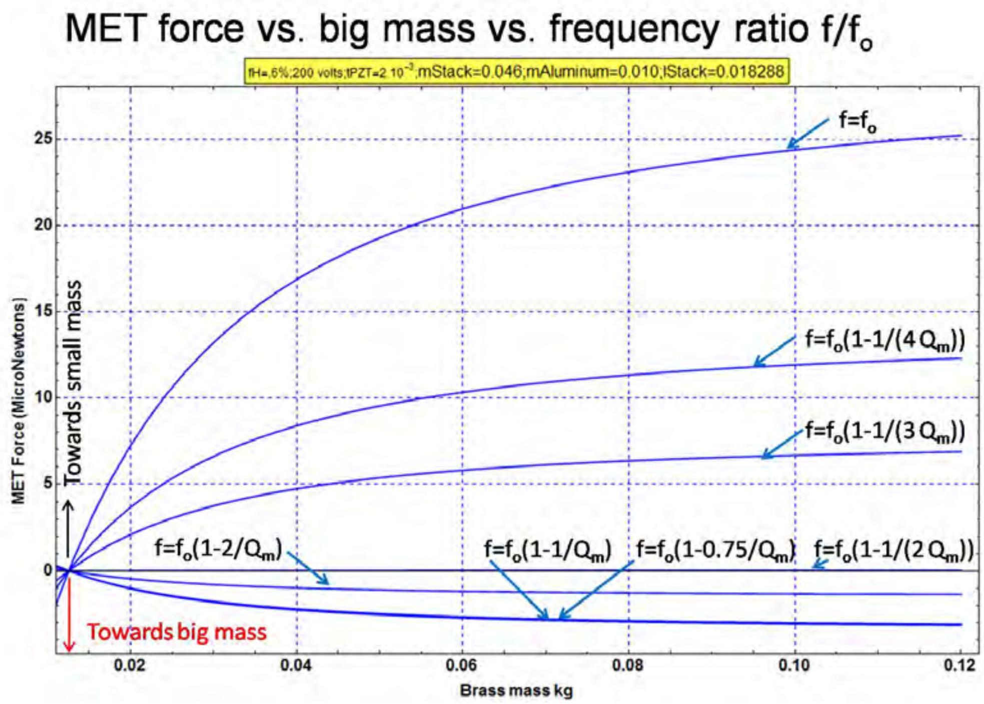

FIG. 29: Mach effect force vs. (brass) mass (kg) of tail end (up to 0.12 kg), for excitation frequency f to natural frequency f_o ratio of $f = f_o(1 - \frac{1}{NQ_m})$ for N=$\frac{1}{2}$,1,$\frac{4}{3}$,2,3,4 and ∞. MEGA Langevin stack modeled as floating free in space.

natural frequency.

TABLE V: Optimal brass mass at which maximum Mach effect force occurs for different values of the excitation frequency to natural frequency ratio $\frac{f}{f_o}$. MEGA Langevin stack modeled as being held at the ends with a bracket much more compliant than the stack and held by a damping force at the ends.

frequency ratio $\frac{f_o - f}{f_o}$	$\frac{1}{NQ_m}$	**Opt. brass mass (kg)**	**Max. Mach force (μN)**	**Force towards**	**Optimal** f**(kHz)**	**Optimal** f_o**(kHz)**
1.053%	$\frac{1}{0.5Q_m}$	0.206	-0.4571	brass	29.874	30.192
0.526%	$\frac{1}{Q_m}$	0.106	-1.427	brass	31.701	31.869
0.395%	$\frac{0.75}{Q_m}$	0.0831	-2.031	brass	32.503	32.631
0.263%	$\frac{1}{2Q_m}$	0.0606	-2.575	brass	33.669	33.758
0.175%	$\frac{1}{3Q_m}$	0.0417	-1.588	brass	35.153	35.215
0	0	0.0830	17.16	aluminum	32.637	32.637

It is important to understand that this "optimal tail mass" is not a fixed characteristic of a stack and the head mass. First of all, the existence of such an "optimal tail mass" is entirely dependent on the boundary conditions. There is no optimal mass for the tail end of a MEGA Langevin stack floating in space, in which case the greater the tail end mass the greater the force, and it reaches an asymptote fairly quickly with practically no difference for tail end masses greater than 2 kg. The existence of an optimal tail (brass) mass is due to fixing the tail end and providing damping forces with a damper that is held at a fixed point in space. Under a fixed-end condition there is a different optimal tail mass depending on how far the excitation frequency is from the natural frequency. For example, one cannot really distribute at this Estes Advanced Propulsion Workshop to testing groups an "optimal brass mass" for the stack. Because there is no such

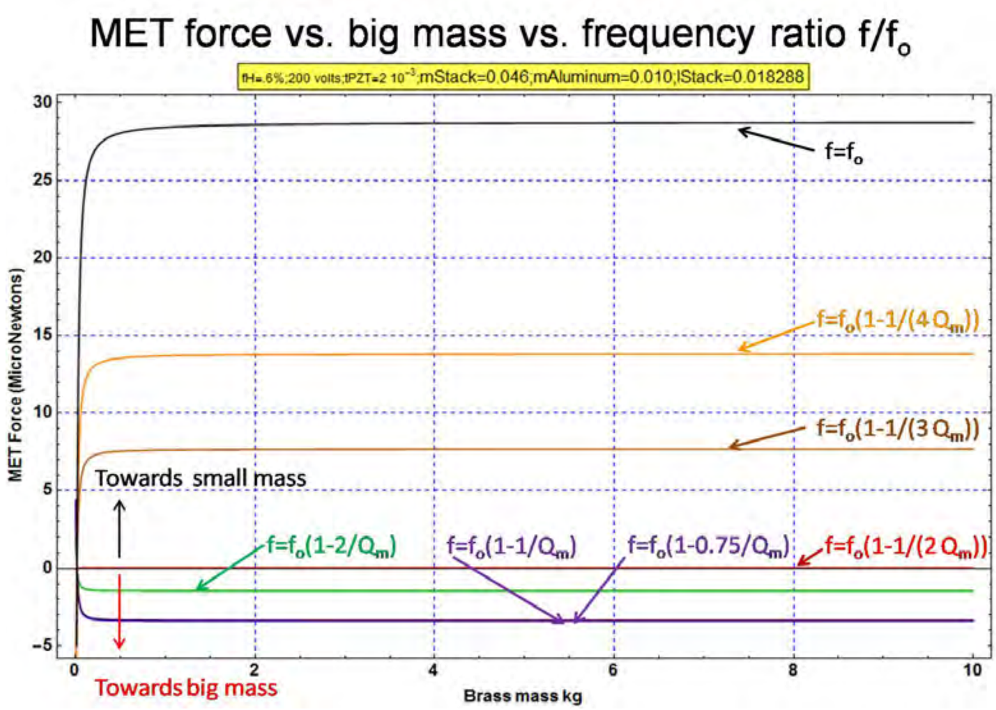

FIG. 30: Mach effect force vs. (brass) mass (kg) of tail end, for different values of the excitation frequency to natural frequency ratio $\frac{f}{f_o}$, showing the asymptotic behavior of the Mach effect force for infinite mass of the brass tail end of the stack (as would happen if the Langevin stack was attached to a very massive and rigid spacecraft in space).

optimal tail mass in general, as the optimal tail mass is a function not just of the head mass, and the material and geometry of the stack, but it is also a function of the stress and electrical history of the stack's material (since the electromechanical properties are history dependent, and the material is subject to internal damage, which affects several properties, including its natural frequency). Not just that, but the optimal tail mass is also a function of how far the excitation frequency is from the natural frequency. Therefore, even in the unlikely case that several groups were testing the same identical stack's material, with identical material history, and geometry, the optimal tail mass would be different if they tested with a different ratio of excitation frequency to natural frequency. For excitation frequencies that are further away than $\frac{1}{2Q_m}$ from the natural frequency, the larger the ratio between the excitation frequency to the natural frequency, the larger the "optimal tail mass" will be. If the excitation frequency is 1% away from the natural frequency, the optimal tail brass mass is twice as large as for a difference of 0.5%.

Fig. 35 is a plot, under a fixed-end condition constraint, of the Mach effect force vs. (brass) mass (kg) of tail end, for different values of the excitation frequency to natural frequency ratio $\frac{f}{f_o}$, showing the asymptotic behavior of the Mach effect force for infinite mass of the brass tail end of the stack. One sees that the Mach effect force decreases, from its optimal value, but that it is still finite for infinite tail mass. For example, for excitation frequency identical to the natural frequency (27.82 kHz for any value of excitation frequency because the brass mass is asymptotically infinite in this example) the Mach effect force is half (8.51 μN) of the value (17.16 μN) for the optimal mass. With an excitation frequency of $\frac{1}{2Q_m}$=0.263% less than the resonant frequency, the asymptotic limit for infinite tail brass mass gives a Mach effect force close to zero, while, using the optimal mass, it gives a local maximum for the Mach effect force. And using an excitation frequency of $\frac{1}{0.5Q_m}$= 1.053% less than the resonant frequency, the asymptotic limit for infinite tail brass mass gives a Mach effect force practically identical (94% or 0.43 μN) to the Mach effect force (0.46 μN) using an optimal tail mass for that difference between the excitation frequency and the natural frequency. This is all summarized in Table 6.

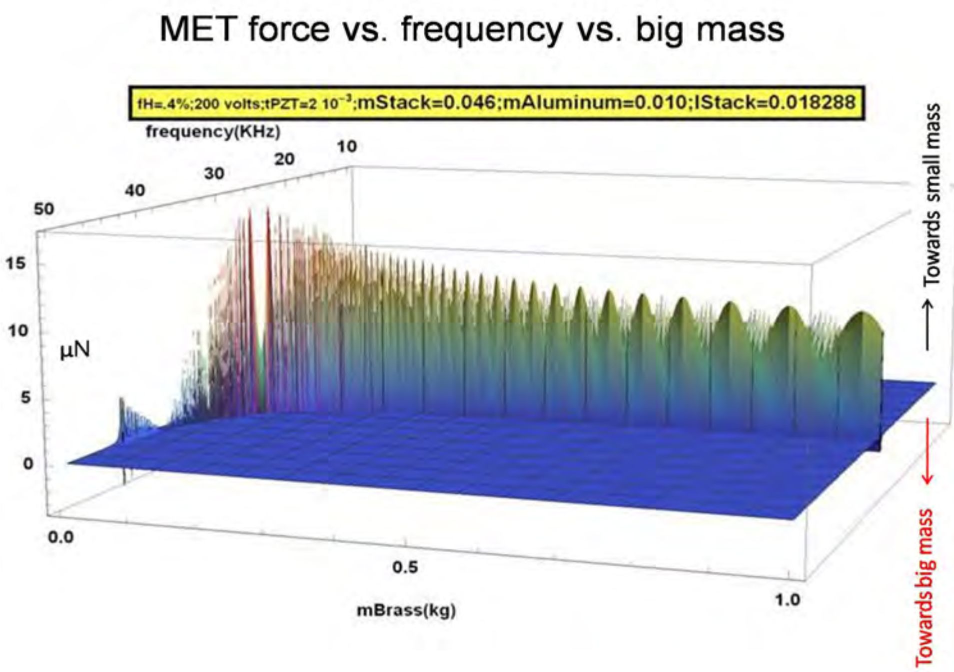

FIG. 31: 3D Plot of Mach effect force (μN) vs. frequency (kHz) vs. (brass) mass (kg) of tail end. MEGA Langevin stack modeled as being held at the ends with a bracket much more compliant than the stack and held by a damping force at the ends.

TABLE VI: Mach effect force for infinite brass mass for different values of the excitation frequency to natural frequency ratio $\frac{f}{f_o}$. MEGA Langevin stack modeled as being held at the ends with a bracket much more compliant than the stack and held by a damping force at the ends.

frequency ratio $\frac{f-f_o}{f_o}$	$\frac{1}{NQ_m}$	m_∞**Mach force** (μ**N**)	**Force towards**	$m_\infty f$**(kHz)**	$m_\infty f_o$**(kHz)**
1.053%	$\frac{1}{0.5Q_m}$	-0.43	brass	27.53	27.82
0.526%	$\frac{1}{Q_m}$	-1.01	brass	27.68	27.82
0.263%	$\frac{1}{2Q_m}$	0.009	aluminum	27.75	27.82
0	0	8.51	aluminum	27.82	27.82

7.CONCLUSIONS

It is evident from the images, Figs. 10 and 11, for the MEGA (Mach effect Gravitational Assist) drive stack tested by Fearn and Woodward and its description [25], [26] and [55], that it is a conventional Langevin stack, similar to the typical Langevin transducers that have been used for decades in many applications since Langevin invented it in 1916: with a small aluminum head mass, and a piezoelectric stack composed of modified PZT-4 (US Navy Type I) plates (a material similar to those marketed by US firm Clevite in 1957). The one unconventional choice is the use of a tail mass made of brass, reportedly because it was desired to provide a heat sink for thermal diffusion of heat generated by dissipation in the PZT stack during vibration. The present choice of brass for the tail mass is not optimal: the brass could be substituted by copper, in order to increase thermal conductivity by a factor of 3.5 times and to increase thermal diffusivity by a factor of 3.4 times. If the cost of silver at 59 US dollars per 100 grams (compared to copper at 0.49 US dollars per 100 grams, and brass at 0.29 US dollars per 100 grams) is not an issue, silver would be an even better choice for the tail mass, since it would improve thermal conductivity by a factor of 3.7 times and the more important (for unsteady heat conduction) thermal diffusivity by a factor of 5 times, as compared to the present choice of brass. Other choices for the electrode should be investigated instead of the present

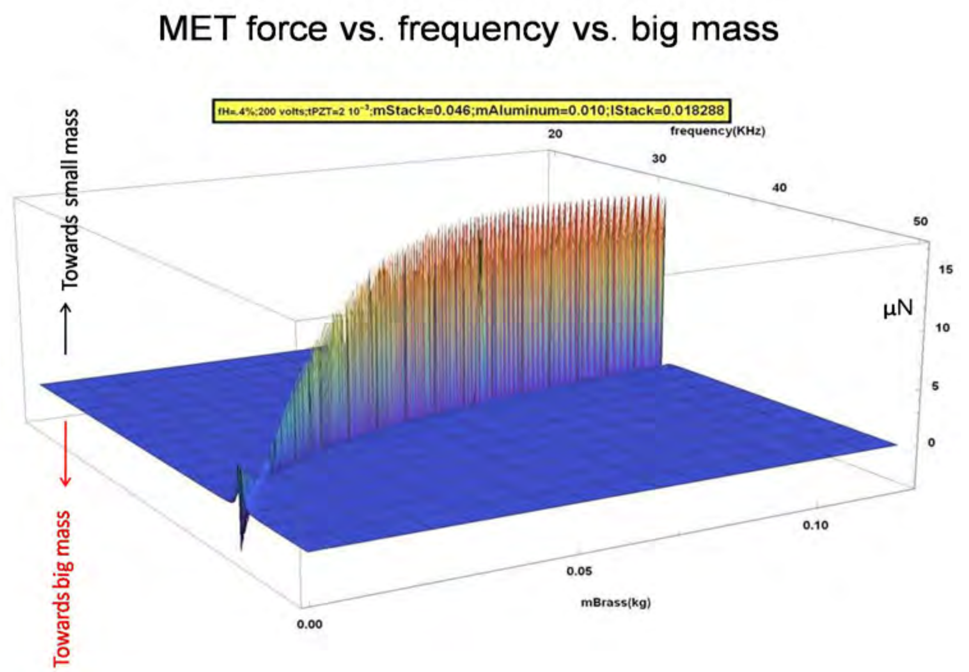

FIG. 32: 3D Plot of Mach effect force (μN) vs. frequency (kHz) vs. (brass) mass (kg) of tail end. Detail close-up of (brass) tail mass lower than 0.1 kg. MEGA Langevin stack modeled as being held at the ends with a bracket much more compliant than the stack and held by a damping force at the ends.

brass electrodes, for example, copper and silver.

The present choice of stainless steel for the bolts that apply the necessary compression to the PZT plates is not optimal, because of thermal expansion mismatch with the PZT plates, leading to loss of compression, and hence to damage and decrease of stiffness of the PZT plates. Worst of all, this thermal expansion mismatch also leads to de-tuning between the excitation frequency and the natural frequency of the MEGA stack, and hence to a substantial decrease in the Mach effect force. This is confirmed by the experimental data of Fearn et.al.[9] displayed in Fig. 13, where the turquoise trace is the output from one or more pairs of 0.3 mm thick passive PZT plates in the MEGA Langevin stack. The direct piezoelectric effect, where the piezoelectric material (PZT) responds to strain by generating an electric voltage, is used in one or more pairs of passive 0.3 mm thick piezoelectric plates in the MEGA drive Langevin stack. They measure the strain, through the thickness of the PZT, resulting from the stress transmitted from the other plates in the stack. They act essentially as strain gauges. Scientific piezoelectric accelerometers are restricted to operating at excitation frequencies lower than 3 dB below the first natural frequency (in other words, approximately below $\frac{1}{2}$ of the first natural frequency). This limit, restricting the excitation frequency to be below $0.5 f_o$, $\frac{1}{2}$ of the first natural frequency, marks the frequency where the measuring error becomes 30%. (At approximately $0.3 f_o$, $\frac{1}{3}$ of the first natural frequency, the error is 10%, while at approximately $0.2 f_o$, $\frac{1}{5}$ of the first natural frequency, the error is 5%). If the exciting frequency becomes closer to the natural frequency, the error becomes much larger (the measured strain becomes unrepresentative of the acceleration, due to the fact that close to the natural frequency the damping term in the equations of motion starts to dominate the amplitude of the response). For the MEGA drive experiments, Fearn and Woodward purposefully operate the stack at an excitation frequency closer than $\frac{0.75}{Q_m}$ to the natural frequency of the Langevin stack (which has a mechanical-quality-factor-of-resonance (Q_m) equal to 190). Therefore, for the MEGA drive experiments conducted by Fearn and Woodward, the output of the passive PZT plates is unrepresentative of the acceleration, and instead should be interpreted strictly as representing solely the strain through the thickness of the PZT plate. Therefore the turquoise trace in Fig. 13 shows the strain vs. time in the MEGA PZT passive plates. As one can see, the strain steadily decreases at a steady slope with time (after a short initial faster nonlinear decay). The compressive strain decreases with time as the temperature in the stack increases, and this is a natural result of loss of compressive stress as the stainless steel bolts expand with temperature with a much higher coefficient of thermal expansion than the one of the PZT plates. Instead of stainless-steel, a material

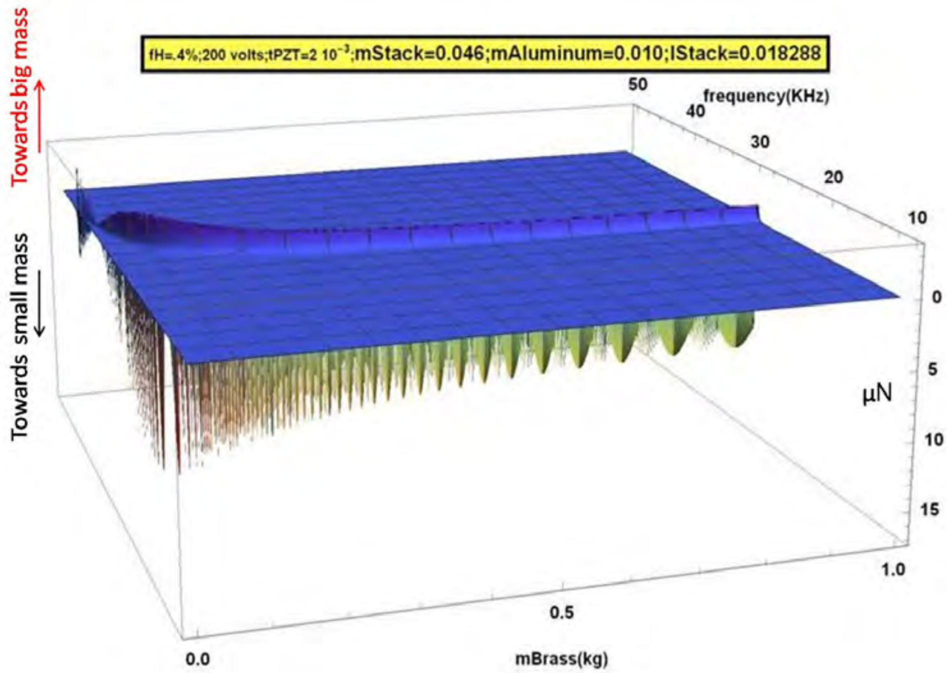

FIG. 33: 3D Plot of Mach effect force (μN) vs. frequency (kHz) vs. (brass) mass (kg) of tail end. View of force directed towards the (brass) mass tail end. MEGA Langevin stack modeled as being held at the ends with a bracket much more compliant than the stack and held by a damping force at the ends.

with a much smaller coefficient of thermal expansion should be used. For example Nabeya Bi-tech Kaisha (NBK) [16] bolts made of super invar with a thermal expansion coefficient 25 times smaller than the one of stainless steel, will better match the coefficient of thermal expansion of the PZT plates in their thickness direction.

The present choice of adhesive (unfilled Bisphenol A epoxy) could be substituted by a filled epoxy to raise thermal conductivity (aluminum nitride or boron nitride filled epoxy) to a similar value as PZT, and if desired, the electrical conductivity (a silver-filled epoxy) as well. Also a filled adhesive with a higher glass transition temperature (for example a polyimide adhesive like Creative Materials 124-41 with a thermal conductivity of 11 W/(m K) as compared to the present unfilled epoxy 0.17 W/(m K) should also be investigated, because the present adhesive is limiting the upper temperature of the MEGA Drive due to loss of integrity of the adhesive due to its glass transition temperature being significantly lower than the Curie temperature of the PZT. Also co-sintering of the MEGA PZT-electrodes stack should be investigated, as co-sintering would eliminate the adhesive altogether, and involve much thinner electrodes. Newer piezoelectric materials should be investigated to replace the 64 year old PZT, materials like high-Curie-temperature ferroelectric single-crystal Mn doped PIN-PMN-PT discussed by Zhang et.al. [17].

Fearn et.al. [25] [26] outline a derivation of the Woodward Mach effect thruster theory based on the Hoyle-Narlikar field equation that Fearn shows to have the same type of mass fluctuation terms. The force equation, used to predict the thrust in the MEGA drive, can be derived from the mass fluctuation. In General Relativity, length, and hence surface and volume, are observer dependent and hence not invariant like mass. This argues for the time derivatives of the mass field to govern the fluctuation in inertial mass, instead of the mass fluctuation being governed by mass density (which is observer dependent due to the observer-dependence of the volume) as done for example in other derivations. This distinction is irrelevant for isochoric media (e.g. perfect fluids or idealized elastomers) or for solid media undergoing isochoric (equivoluminal) deformation, but it may be relevant when considering solids like piezoelectric materials that are not isochoric and that undergo non-isochoric deformation. I show that the inertial mass fluctuation is due to the second derivative with respect to time of the kinetic energy per unit mass, divided by the gravitational constant G and the square of the speed of light. The only assumptions involved in this conclusion have been: 1. Hoyle-Narlikar's theory of gravity (dropping the creation "C" field, and neglecting the gradients of mass terms, assuming spatial homogeneity of the mass function in a smooth mass field approximation), 2. speed

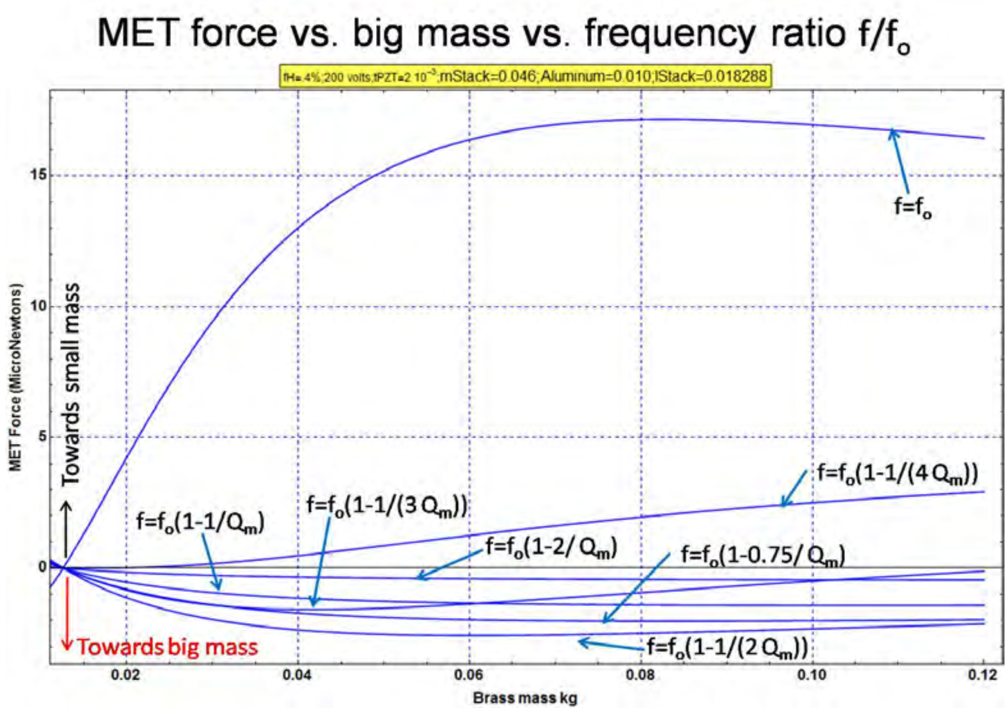

FIG. 34: Mach effect force vs. (brass) mass (kg) of tail end (up to 0.12 kg), for excitation frequency f to natural frequency f_o ratio of $f = f_o(1 - \frac{1}{NQ_m})$ for N=$\frac{1}{2}$,1,$\frac{4}{3}$,2,3,4 and ∞. MEGA Langevin stack modeled as being held at the ends with a bracket much more compliant than the stack and held by a damping force at the ends.

of material points negligibly small compared to the speed of light and 3. second derivative with respect to time of the natural logarithm of the rest mass negligibly small compared to the second derivative with respect to time of the kinetic energy per unit mass. The second derivative with respect to time of the kinetic energy per unit mass is a function of the square of the acceleration $\frac{\partial v}{\partial t}$, and the product of the velocity v times the time rate of the acceleration $\frac{\partial^2 v}{\partial t^2}$ (the second derivative with respect to time of the velocity) of the mass points, which is also called the "jerk." The presence of the jerk $\frac{\partial^2 v}{\partial t^2}$ is significant because it has been shown by Sprott [35] [36] in the field of chaotic dynamics that an equation involving the jerk is the minimal setting for solutions that can show chaotic behavior. It is interesting to consider whether the solution of the Machian force due to inertial mass fluctuations (a system of coupled nonlinear differential equations involving the jerk, the acceleration and the velocity) of a piezoelectric/electrostrictive Langevin stack undergoing vibrations may be capable of showing chaotic, complex dynamic behavior. Such chaotic, complex dynamic behavior may result in different dynamic behavior regimes and perhaps it can be exploited to maximize the response if properly engineered.

I modeled two different conditions. In the first and main condition, the MEGA drive is in space, free of any boundary fixity constraints (modeling the MEGA drive as rigidly attached, at the tail end of the Langevin stack, to the spacecraft's center of mass, with the spacecraft considered a rigid body). In the second condition, I modeled the MEGA drive in the Woodward and Fearn experiments as being held at the ends with a bracket much more compliant than the stack and held by a damping force at the ends. I modeled the MEGA drive as a dynamic system composed of two unequal, lumped, end masses (the front mass and the tail mass) connected by a viscoelastic piezoelectric/electrostrictive stack. Obviously, to calculate the maximum amplitude of a vibrating system it is imperative to consider non-zero damping because for zero damping, the response will have infinite amplitude at resonance, which is an unphysical result. The exact solution to the coupled differential equations of motion for the dynamic system of two unequal masses with damping and stiffness, excited by piezoelectricity and electrostriction, can be decomposed into a piezoelectric solution for the displacement of each end mass, with an in-phase and an out-of-phase component, for a total of 4 terms; and an electrostrictive solution for the displacement of each end mass, with an in-phase and an out-of-phase component, for a total of an additional 4 terms; so the solution has 8 such terms. Piezoelectric resonance occurs when the voltage excitation frequency ω equals the first natural frequency of the MEGA

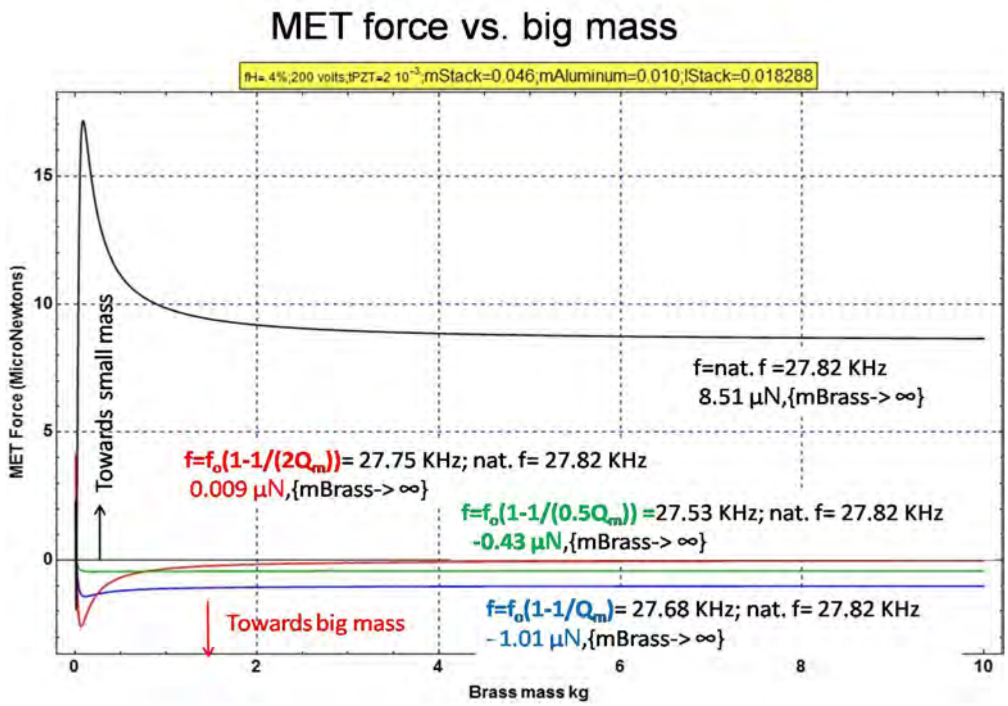

FIG. 35: Mach effect force vs. (brass) mass (kg) of tail end, for different values of the excitation frequency to natural frequency ratio $\frac{f}{f_o}$, showing the asymptotic behavior of the Mach effect force for infinite mass of the brass tail end of the stack. MEGA Langevin stack modeled as being held at the ends with a bracket much more compliant than the stack and held by a damping force at the ends.

drive ω_o. One can see, Fig. 14, that the calculated natural frequency falls within the experimentally measured values. The calculated values of natural frequency are based on the book value of the modulus of elasticity provided by the supplier, who does not specify the values of these variables during the testing of the PZT that resulted in those book values. Furthermore, the piezoelectric stack is a composite where several layers (PZT plates, brass electrodes and adhesive layers) are sandwiched together by hand, where the adhesive has a modulus of elasticity much lower than the one of the PZT. Also, the actual stack is a continuum with a very large number of material points, rather than a simple 2-mass lumped system connected with a viscoelastic spring and dashpot as in the numerical model, and it is known that the actual natural frequency of such a continuum will be different than the one calculated in this simplified numerical model. Considering all the above factors, the comparison between the calculated and the measured natural frequency is very reasonable, particularly considering the unknown electromechanical state of the piezoelectric stack, and the level of damage (a more damaged stack will have a lower stiffness and hence a lower natural frequency, Fig. 19), at the time of the natural frequency measurements.

The Mach effect force on the center of mass is calculated as the product of the total mass times the acceleration of the center of mass [38]. The acceleration of the center of mass contains terms (due to Mach effect inertial mass fluctuations) of the form of the product of the time derivative of the mass fluctuation times the velocity, and of the form of the product of the second time derivative of the mass fluctuation times the displacement, as well as square terms of the previously mentioned expressions. As a result of these multiplications, trigonometric expressions due to the product of harmonic terms at frequency ω (due to piezoelectric excitation) multiplying harmonic terms at frequency 2ω (due to electrostrictive excitation) occur, that give constant uniaxial force terms. There is a total of 289 such terms that contribute to the Mach effect force. The solution is an exact analytical solution, that is solved using Wolfram *Mathematica*.

A fundamental difference between the exact solution discussed in this article and previous efforts by Fearn and Woodward [25], [26], [55] at calculating the Mach effect force is that I have taken into account that the problem is one of vibration and hence that damping (or the inverse measure, the mechanical quality of resonance) and stiffness of the stack have a most important role in the value of the Mach effect force. The previous solutions by Fearn and Woodward [25], [26], [55] did not involve important material properties like the mechanical quality of resonance or the modulus of elasticity. Note that Fearn and Woodward [25], [26], [55] use *dimensional* ad-hoc factors in their Mach effect force calculation. One can readily extract this information from their unconventional definitions of their piezoelectric constant K_p and their electrostrictive constant K_e, where Fearn and Woodward define their constitutive equations in terms of the strain to voltage ratio, instead of the strain to electric field ratio. They define the piezoelectric strain as $\epsilon_{p33} = K_p V_3$ instead of the proper constitutive relationship $\epsilon_{p33} = d_{33} E_3 = d_{33} \frac{V_3}{l_{plate}}$, where l_{plate} is the thickness of the piezoelectric plates, and the electric field in the thickness direction E_3 is assumed constant through the thickness of the plate. Therefore $K_p = \frac{d_{33}}{l_{plate}}$. Similarly, Fearn and Woodward use an unconventional definition of the electrostrictive constant K_e, in terms of the strain to voltage ratio, instead of the strain to electric field ratio. They define the electrostrictive strain as $\epsilon_{e33} = K_e (V_3)^2$ instead of the proper constitutive relationship $\epsilon_{e33} = M_{33} (E_3)^2 = M_{33} (\frac{V_3}{l_{plate}})^2$. Therefore $K_e = \frac{M_{33}}{l_{plate}^2}$. In Fearn and Woodward's experimental example, the thickness of the plates l_{plate} is taken as 0.002 m, therefore their piezoelectric constant is $K_p = \frac{d_{33}}{0.002} = \frac{d_{33}}{0.2\%}$ and their electrostrictive constant is $K_e = \frac{M_{33}}{0.002^2} = \frac{M_{33}}{0.04\%}$. The thickness of the PZT plate (0.002 m for their PZT plate thickness example) appears as an extraneous factor in these material constants, due to the unconventional choice of constitutive parameters. Then, for the piezoelectric constant K_p, they take the book value of $d_{33} = 320 \times 10^{-12}$ m/V from Steiner & Martins SM-111, to be the value of K_p (and in doing so, they disregard the different units of d_{33} (m/V) and K_p (1/V)). Therefore they set the magnitude of $K_p = 320 \times 10^{-12}$ (1/V), but since their definition for K_p was $K_p = \frac{d_{33}}{0.002} = \frac{d_{33}}{0.2\%}$, in doing so they effectively set $d_{33} = 0.2\% \times 320 \times 10^{-12}$ m/V instead of the correct book value for d_{33}, which amounts to using an ad-hoc constant of 0.2% multiplying the book value of the Steiner & Martins SM-111 piezoelectric constant d_{33}. The reason for the appearance of these extraneous length dimensional factors is that Fearn and Woodward define their constitutive equations in terms of the strain to voltage ratio, instead of the strain to electric field ratio. The proper field variable in piezoelectric and electrostrictive constitutive relations should be the electric field instead of the voltage. Fearn and Woodward [26] state $N f_p \approx l_o$ and therefore that their *dimensional* coupling factor is $f_p \approx \frac{l_o}{N} \approx l_{plate}$ where N is the number of PZT plates and l_o is the length of the stack, and therefore that their coupling factor is the thickness of each plate ($l_{plate} = 0.002$ m in their example), but I find this justification for the coupling factor unconvincing, based on a) correct dimensions of the constitutive variables (the constitutive variables should be formulated in terms of the electric field instead of the voltage), b) the well-established constitutive equations of theory of electroelasticity and c) the thorough analysis of a Langevin stack by Martin [37] at the U.S. Navy Electronics Laboratory, San Diego, California, in the early 1960's.

Concerning the input variables for this analysis, it is noted that in order to match the magnitude of the experimentally measured Mach effect force, using book values for the material constants it is also necessary in my analysis to introduce an ad-hoc *non-dimensional* factor of 0.6% multiplying the piezoelectric coefficient d_{33} and the electrostrictive coefficient M_{33}, when modeling the MEGA Langevin stack free in space. Preliminary modeling of the MEGA Langevin stack restrained at the ends by a damping force needs an ad-hoc *non-dimensional* factor of 0.4% multiplying the piezoelectric coefficient d_{33} and the electrostrictive coefficient M_{33} to match the magnitude of the experimentally measured Mach effect force, when using book values for the material constants. This *non-dimensional* factor is about 100 times smaller than the coupling coefficient one would expect based on electromechanical coupling. Since the total Mach effect force is comprised of the multiplication of three force excitation factors, (one factor with frequency 2ω due to the electrostrictive excitation force times two factors with frequency ω due to the piezoelectric excitation force) the total *non-dimensional* coupling factor for the Mach effect force (multiplying the reduced mass times the excitation frequency to the sixth power, divided by the product of the gravitation constant G times the square of the speed of light) is of the order of $(10^{-2})^3 = 10^{-6}$.

The reason for the need of this coupling factor (10^{-2} on the excitation force) based on book values of material properties (needed to match the experimental results on this study and, as shown above, also used in previous papers by Fearn and Woodward) remains to be fully explored. Following is a consideration of different possible explanations:

- Arguable validity of the Mach effect propulsion hypothesis for our Universe. If the argument were made that it is physically invalid, one would need to otherwise explain: a) the physical nature of the net unidirectional force that has been measured by Woodward and Fearn, as well in other replication experiments independently conducted by N. Buldrini at Forschungs- und Technologietransfer in Austria, G. Hathaway in Canada and by M. Tajmar at TU Dresden in Germany (described in other articles in this workshop proceedings), b) the fact that experimental measurements with a symmetric Langevin stack (with equal tail and head masses) result in no measured net unidirectional force, c) reported experimental measurements of the force scaling like the fourth power of the exciting voltage, and therefore (for uniform thickness of the piezoelectric plates in the Langevin stack) like the fourth power of the exciting electric field (the Mach effect force is predicted to be proportional to the fourth power of the electric field because it is due to the product of the second power of the piezoelectric strain excitation times the first power of the electrostrictive strain excitation), and d) the success of the present calculations to correctly predict the experimental measurements for the direction of the Mach effect net force as well as accurately predicting the experimentally measured optimal mass of the tail brass end, that maximizes this Mach effect force.

- The effect of neglecting the gradients of mass terms appearing in the full derivation of the mass fluctuation based on Hoyle-Narlikar theory. Such mass transport might take place for example due to electric gradients, and due to coupling with temperature gradients. This may be particularly relevant at the interface of the electrodes with the piezoelectric (PZT) plates, due to migration of metallic species (e.g. copper) from the electrode into the dielectric.

- The effect of neglecting a number of mass fluctuation (time differential) terms in the derivation, assuming they were too small. Most important among these neglected terms are the derivatives of mass with respect to time terms that would multiply the velocity in the equations of motion, as for low damping materials (high mechanical quality factor of resonance) these mass fluctuation terms may not be negligible.

- Fluctuations in internal energy that have been disregarded in the analysis. The analysis considers only the mass fluctuations due to kinetic energy. I also take the position that external potential energy terms (see the previous discussion regarding the analysis of Brillouin, Medina and others regarding hidden momentum terms) that such external energy and momentum carried by the fields is automatically taken into account in the Hoyle Narlikar theory of gravitation through the energy-stress tensor, physically through advanced-retarded waves, and that they do not need to be incorporated as extra mass terms.

- The Mach effect mass fluctuations, rather than affecting the whole mass density of an object, as assumed in this analysis, may mainly affect the bonds that hold the mass particles together, as when a solid is deformed, the strain affects mainly the bonds between the particles.

- Material properties: modulus of elasticity Y_{33} and masses: it is unlikely that the discrepancy is due to either the modulus of elasticity or the mass values because the calculated natural frequency is very close to the measured natural frequency and because the optimal brass mass is accurately calculated.

- Material nonlinearity: strain vs. electric field hysteresis. As shown in Fig. 16 (from Fig. 2 of Zhang et.al. [52]), the magnitude of the applied electric field in this example of MEGA drive experiments, 1 kV/cm, is 20 times smaller than the electric field that results in significant nonlinearity (strain vs. electric-field hysteresis due to piezoelectric internal damping losses) for PZT-4. Hence, the data shows that strain vs. electric field nonlinearity is unlikely to be the reason for the ad-hoc factor needed to be used in these calculations.

- Material nonlinearity: polarization vs. electric field hysteresis nonlinearity. Fig. 17 shows that PZT-4 has a larger hysteresis than the other two materials, at the high level (40 kV/cm) of electric field magnitude used in the experiments plotted in that figure. The electric field magnitude used for the MEGA experiments (1 kV/cm) is 40 times smaller than for the example shown in Fig. 17 (and also smaller by a factor of 3 than the internal bias field used in this example). Of course, care should be taken in MEGA drive experiments to perform experiments at identical electric field magnitudes, rather than identical voltage excitation magnitudes. For example, if the same voltage excitation were used for PZT plates 1 mm thick instead of 2 mm thick, the electric field would be twice as large in the stack with the thinner plates, and hence closer to the region of nonlinearity. Waechter et.al. [53] report energy density loss data, calculated from integration of (polarization vs. electric field) hysteresis loop data, Fig. 18, for Navy Type I (PZT-4) and Navy Type III (PZT-8) hard-doped PZT materials used in sonar transducers. It is evident from these data that the magnitude of the applied electric field, 1 kV/cm = 0.1 MV/m, in this example of MEGA drive experiments using a modified form (SM-111 from Steiner & Martins) of PZT-4, is very small compared with the amplitude of electric field required for significant energy density loss. Therefore, independently confirming that this magnitude of applied electric field, 1 kV/cm = 0.1 MV/m, should be safely within the approximately linear, small loss range. Therefore, the data shows that polarization vs. electric field nonlinearity is unlikely to be the reason for the ad-hoc factor needed to be used in these calculations.

- Thermal effects. As shown in Figs. 12 and 13 (from Figs. 3 and 4 of [9]) the transient temperature peak measured in the front aluminum mass was reported as 18 °C above initial temperature, and the transient temperature peak measured in the back brass mass was reported as 8 °C (which is consistent with the aluminum mass having 2.56 times higher thermal diffusivity than the brass mass, and therefore being able to more rapidly diffuse the temperature generated in the PZT stack). Also, the maximum transient temperature measured in the aluminum was 45 °C. This temperature is much lower than the Curie temperature of 320 °C for the modified PZT-4 material used in the stack (SM-111 from Steiner & Martins), even allowing for the fact that the transient temperature inside the PZT must have reached a higher temperature than the temperature measured at the end metal masses. Furthermore, the mechanical quality factor of resonance Q_m for PZT-4 is fairly constant from room temperature to at least 150 °C (page 11 of [15]), a temperature much higher than the measured temperatures in the MEGA stack experiments of Fearn et.al. [9]. Similarly, Hooker, on page 19 Fig. 10 of [58], shows that the effective electro-mechanical coupling coefficients of PZT-4 only begin to have a gentle drop-off after 150 °C. Also (polarization vs. electric field) hysteresis data for PZT-4 show appreciable changes only for temperatures exceeding 125 °C. Therefore, the temperatures measured by Fearn et.al. [9] do not indicate that the MEGA stack reached temperatures high enough to appreciably influence the material properties. Fig. 13 shows that the temperatures in the aluminum and brass masses were still increasing at the end of the 14 second run of the MEGA stack, because the internally generated heat exceeded the heat being transiently conducted in both the aluminum and the brass masses. Therefore, the maximum temperature that a MEGA stack will reach under the present design is a function of the time duration of the run. The shorter the run, the lower the temperature. The longer the run, the higher the temperature. Besides using a back mass with significantly higher thermal diffusivity (copper, or preferably silver instead of the present inferior choice of brass), active cooling may be required. Therefore, under the present design of the MEGA drive, care has to be exercised regarding temperature effects, because with the present design (relying only on passive cooling and using a material like brass that has lower thermal diffusivity than copper or silver) the stack may reach temperatures that will affect material properties if run long enough. I would recommend that more detailed temperature measurements are made to further characterize the transient temperatures throughout the stack during a test, and that a detailed numerical model of the MEGA stack, as well as of thermal expansion changes (including viscoelastic compression set of the PZT stack) are carried out.

- Material properties: since the ad-hoc factor multiplies the piezoelectric constant d_{33} and the electrostrictive constant M_{33}, the book values taken for these material constants are prime suspects for the need to adopt an ad-hoc multiplying factor. Perhaps the tested materials have values substantially lower than book values, either due to damage (due to micro cracks, and voids between grains) and/or electroelastic history. The piezoelectric constant d_{33} and the electrostrictive constant M_{33} of the actual stack should be measured, for example, using strain gauges. For example, the book value (from the supplier, Steiner & Martins) of the mechanical quality factor of resonance Q_m is 1800, but the measured value for the actual stack used for the MEGA experiments is only 190, which shows a severe degradation of the actual mechanical quality factor of resonance Q_m compared to the book value. If these calculations had been carried out using the book value of mechanical quality factor of resonance Q_m instead of the actual value, there would have been a huge discrepancy between calculated and actual magnitudes of response, as the amplitude of resonant response near the natural frequency is very dependent on the magnitude of the mechanical quality factor of resonance Q_m.

- The electric field limit used in MEGA experiments is 10 times higher than industry standard based on reliability. Jones and Lindberg [54] state that for Navy Type III (PZT-8) piezoelectric ceramics, an electric field limit of 10 V/mm = 0.1 kV/cm (determined on a root mean square basis) has been chosen as an industry standard based on considerations of both reliability and acceptable losses. This reliability limit is 10 times smaller than the electric field used for the MEGA experiments and for this numerical example. Since Navy Type III (PZT-8) is a hard-doped PZT with fairly similar properties as the modified Navy Type I (PZT-4) material (with trade name SM-111 from supplier Steiner & Martins) used for the MEGA experiments, and as shown by Waechter et.al. [53] Navy Type III (PZT-8) has significantly greater fracture toughness than Navy Type I (PZT-4), one would expect that the electric field limit for Navy Type I (PZT-4) should be smaller than 0.1 kV/cm and hence this indicates that the 1 kV/cm applied to the MEGA experiments is already more than 10 times higher than the industry standard based on considerations of reliability. This is another prime suspect reason for the need to apply an ad-hoc multiplying factor on the book values of the piezoelectric and electrostrictive constants. The importance of the fracture mechanics and fatigue reliability limit has been known for a long time. For example, W. Mason (head of Mechanics Research at Bell Labs), pointed out in 1958 (p. 157 of [59]) that:

"For dynamic conditions, the amount of strain can be increased by the buildup of vibrations as a function of time. Here the limitation is either the strength of the material, the heat produced by the electrical input to the transducer, or the Q of the transducer with its associated load.... For relatively high Q systems, it is usually the breaking or fatiguing strength of the transducer material or associated vibrating parts that provides the limitation.... The third limitation, that of heating, is generally worse for a magnetostrictive transducer than for a piezoelectric or electrostrictive transducer, and usually requires auxiliary cooling to overcome it."

It is clear that several of the effects discussed above cannot be responsible for the piezoelectric and electrostrictive coupling factor of 10^{-2} needed to match the experimental results. For example, material nonlinearity due to strain vs. electric field hysteresis, or due to polarization vs. electric field hysteresis cannot be responsible because the strains and electric field values in Woodward and Fearn's experiments are significantly lower than the values needed for material nonlinearity. On page 261 of his book [57], Woodward states: "More difficult than the forgoing theoretical activities is investigation of the way in which Mach effects are generated. That is, the detailed examination of how changes in the internal energies of materials take place, and how that relates to the production of Mach effects should be examined. Although it is clear that internal energy is stored in the interatomic bonds of the dielectric materials in the capacitors involved in the experiments described in Chaps. 4 and 5, it is not clear how that process produces the Mach effects predicted, or where exactly the mass fluctuations take place." Also, on page 100 of [55] Fearn and Woodward state "Capacitors store energy in the electric field between the plates or, as in this case, in the electric polarization of the dielectric medium by ion core displacements. The condition that the capacitor rest mass vary in time is met as the ions in the lattice are accelerated by the changing external electric field. If the amplitude of the proper energy density variation and its first and second time derivatives are large enough, a small (10^{-11} Kg) mass fluctuation should ensue. That mass fluctuation, δm_o, is given by Eqn.(8) above. Note that the assumption that all of the power delivered to the capacitors ends up as a proper energy density fluctuation is an optimistic assumption. Some of this energy is likely stored in the gravitational field, and some will dissipate as heat. Nonetheless, it is arguably a reasonable place to start."

Yes, indeed, if the Woodward mass fluctuation propulsion hypothesis is real, the most plausible explanation for the small value of the coupling factor seems to be that the mass fluctuations do not take place uniformly over the entire piezoelectric-electrostrictive material mass, but most significantly take place only over a small proportion of its total inertial mass. However, why the coupling factor on the piezoelectric and electrostrictive forces should be 10^{-2} or the coupling factor on the total Mach effect force should be 10^{-6} is unclear, as for example the electron-to-proton (dimensionless) mass ratio is 5.446×10^{-4}. Another reason to back this view, that the Mach effect mass fluctuations take place only over a small proportion of its total inertial mass, is shown in Fig. 23. This figure shows that the Mach effect force is composed of two terms: a main component proportional to the sixth power of the frequency and a second order term proportional to the tenth power of the frequency. The term proportional to the tenth power of the frequency is negligible compared to the main component proportional to the sixth power of the frequency, as long as the inertial mass fluctuations are negligibly small. Using a coupling factor on the piezoelectric and electrostrictive forces of 0.6% results in the term proportional to the tenth power of the frequency being negligible, as shown in Fig. 23. However, increasing the magnitude of this coupling factor results in greater mass fluctuations and this term proportional to the tenth power of the frequency becomes dominant, which is unphysical and unintuitive. In other words, if there were no need for a coupling factor on the piezoelectric and electrostrictive forces of 0.6%, the mass fluctuations would be orders of magnitude larger, the Mach effect force would be orders of magnitude larger, and it would be governed mainly by the tenth power of the frequency, with unphysical results. Such forces would have already been measured in countless experiments, man-made and natural phenomena. If the mass fluctuations were orders of magnitude larger this would also be in contradiction with this mathematical analysis, since the mathematical derivation was conducted under the assumption of small mass fluctuations.

Focusing now on the calculated Mach effect force results, a very small amplitude subharmonic response Mach effect force is calculated to take place due to the electrostrictive effect: a nonlinear excitation proportional to the square of the electric field, when the electrostrictive voltage excitation frequency 2ω equals the first natural frequency of the MEGA drive ω_o, this happens at one half the first piezoelectric natural frequency: $\omega = \frac{1}{2}\omega_o$. As shown in Fig. 21, there is a subharmonic peak at the lower resonant frequency of 16.714 kHz (16.74 kHz for damping force with restrained end), with a Mach effect force magnitude of only

5.25 nanoNewtons (2.38 nanoNewtons for damping force with restrained end), directed towards the front (aluminum) small mass, immediately followed by a slightly higher subharmonic resonant frequency of 16.802 kHz (16.78 kHz for damping force with restrained end), oriented in the opposite direction (towards the tail (brass) big mass), with a Mach effect force magnitude of only 5.35 nanoNewtons (2.78 nanoNewtons for damping force with restrained end). The magnitude of the Mach effect force at the first piezoelectric natural frequency is 4,000 times (7,000 times for damping force with restrained end) larger than this subharmonic electrostrictive response, because the value of the piezoelectric constant d_{33} (strain linearly proportional to the electric field) is 24 million times greater than the value of the electrostrictive material constant M_{33} (strain due to the square of the electric field), and the electric field (1 kV/cm) is not high enough to fully compensate for this difference, Fig. 15.

As the first fundamental frequency due to piezoelectricity is approached from lower, or higher frequencies, that are more than $\frac{1}{2Q_m} = \frac{1}{2\times190} = 0.26\%$ ($\frac{1}{3Q_m} = \frac{1}{3\times190} = 0.17\%$ for damping force with restrained end) away from the resonant frequency peak, it is observed that the response is actually directed towards the tail (brass) big mass, and that as the resonant frequency is approached from below, the amplitude of the Mach effect towards the tail (brass) big mass increases in amplitude until it reaches 2.906 μN (2.57 μN for damping force with restrained end) directed towards the tail (brass) big mass at 33.360 kHz (33.42 kHz for damping force with restrained end) when approaching from lower frequencies towards higher frequencies. The mechanical quality factor of resonance is an inverse measure of damping, and hence governs the amplitude of resonant response. Since the MEGA drive experiments by Fearn and Woodward [26] have been performed with a manual operator chasing the natural frequency, and no frequency control algorithm has been used, it is suspected that the response that they have measured up to now is not the global peak natural frequency response, but rather the significantly lower amplitude local peak directed towards the tail (brass) big mass. Notice that there is a factor of 7.4 (6.5 times for damping force with restrained end) greater absolute magnitude response at the natural frequency, but that it is necessary to have equipment that can lock on this frequency with a bandwidth much smaller than $\pm\frac{1}{2Q_m} = \pm\frac{1}{2\times190} = \pm0.26\%$ ($\pm\frac{1}{3Q_m} = \pm\frac{1}{3\times190} = \pm0.17\%$ for damping force with restrained end). This is very difficult to do because as the MEGA Langevin stack vibrates, heat gets internally dissipated inside the PZT discs, which raises the temperature, which changes the dimensions of the stack, as well as the piezoelectric and electrostrictive responses, which are all temperature dependent, hence the natural frequency changes during operation and the natural frequency needs to be chased within this small bandwidth. To have the highest Mach effect forces, it is better to have higher quality factor of resonance, but the higher the quality factor of resonance, the smaller the bandwidth at which this peak natural frequency response will be located, hence the higher the quality factor of resonance, the more difficult it is to be at peak resonance and to stay at peak resonance.

Fearn et.al. [55] tested the MEGA drive with several different brass tail masses: 65 g, 81 g, 97 g, 113 g and 128 g, while keeping everything else, the PZT stack and the aluminum head mass, constant. They found that for this PZT stack, the optimal brass tail mass was 81 grams. This experimental finding by Fearn et.al. agrees very well with my preliminary calculations of the effect of the tail brass mass based on my exact electroelasticity solution of the Mach effect force modeling the MEGA drive as being held at the ends with a damping force. An optimal mass of 83 grams is calculated for the maximum calculated Mach effect force of 17 μN when the excitation is exactly identical to the natural frequency. Also an optimal mass of 83 grams is calculated for an excitation frequency $\frac{0.75}{Q_m}$=0.395% smaller than the natural frequency, giving a calculated Mach effect force of 2 μN. As previously discussed, the MEGA drive experiments by Fearn and Woodward [26] have been performed with a manual operator chasing the natural frequency, and no frequency control algorithm has been used. Therefore it is suspected that the response that they have measured up to now is not the global peak natural frequency response predicted to be 17 μN directed towards the head aluminum mass, but rather the significantly lower amplitude local peak of 2 μN directed towards the tail (brass) big mass. Indeed, the forces measured by Fearn and Woodward [26] have all been directed towards the tail brass mass. Thus, it is strongly suspected that, on the average they have managed their excitation frequency to be only within $\frac{0.75}{Q_m}$=0.395% of the natural frequency.

The optimal tail mass is a function not just of the head mass, and the material and geometry of the stack, but it is also a function of the stress and electrical history of the stack's material. It is important to understand that this "optimal tail mass" is not a fixed characteristic of a stack and the head mass, but it is an experimental artifact due to the end fixity conditions in the experiments run by Fearn and Woodward. A MEGA drive in space does not have an optimal tail mass. For a MEGA drive in space, the greater the tail mass the better, with diminishing returns as the tail mass gets larger, see Fig. 30. For the experiments run by Fearn and Woodward, with end fixity at the tail end, there is a different optimal tail mass that depends on how far the excitation frequency is from the natural frequency. For excitation frequencies that are further away than $\frac{1}{3Q_m}$ from the natural frequency, the larger the difference between the excitation frequency from the natural frequency, the larger the "optimal tail mass" will be. If the excitation frequency is 1% away from the natural frequency, the optimal tail brass mass is twice as large as for a difference of 0.5%.

What happens to the Mach effect force if one attaches the MEGA drive to a much larger mass, like a large spacecraft? Fig. 30 is a plot of the Mach effect force vs. (brass) mass (kg) of tail end, for different values of the excitation frequency to natural frequency ratio $\frac{f}{f_o}$, showing the asymptotic behavior of the Mach effect force for infinite mass of the brass tail end of the stack (as would happen if the Langevin stack was attached to a very massive and rigid spacecraft). For the modeled response of the Mach effect force when one attaches the MEGA drive to a much larger mass, for the experiments run by Fearn and Woodward, with end fixity, see Fig. 35 summarized in Table 6.

References

[1] B. Jaffe, W. Cook and H. Jaffe, "*Piezoelectric Ceramics*," Academic Press (1971).

[2] "Military Standard, Piezoelectric Ceramic Material and Measurement Guidelines for Sonar Transducers," MIL-STD-1376B(SH), Document Date 24 February 1995, US Naval Sea Systems Command, Department of the Navy, Arlington, VA. (This US Military standard describes six types of piezoelectric ceramic materials utilized to manufacture sonar transducers for the US Naval service. The 1376B standard was cancelled in 1999, among many defense standards that were cancelled as a result of the 1994 memo by US Secretary of Defense William Perry that prohibited the use of most defense standards without a waiver. This action was motivated by criticism that standards imposed unnecessary restrictions, increased cost to contractors, impeded the incorporation of the latest technology, and that if an enemy discovers a drawback in a standardized system, the system's uniformity leaves it vulnerable to total incapacitation rather than a limited compromise. The US Navy Types of piezoelectric ceramic materials, created as guidelines specifically for sonar transducer design, survive today as industry standards, used by manufacturers to classify their PZT materials and referenced by scientists and engineers working in a broad range of industries.) http://quicksearch.dla.mil/qsDocDetails.aspx?ident_number=116168

[3] Y. Shindo and F. Narita, "Piezomechanics in PZT Stack Actuators for Cryogenic Fuel Injectors," Chapter 24 of "*Smart Actuation and Sensing Systems - Recent Advances and Future Challenges*," edited by G. Berselli, R. Vertechy and G. Vassura, ISBN 978-953-51-0798-9 (October 17, 2012). http://www.intechopen.com/books/smart-actuation-and-sensing-systems-recent-advances-and-future-challenges/piezomechanics-in-pzt-stack-actuators-for-cryogenic-fuel-injectors

[4] N. Zhang, H. Yokota, A. Glazer, Z. Ren, D. Keen, D. Keeble, P. Thomas and Z. Ye, "The Missing Boundary in the Phase Diagram of $PbZr_{1-x}Ti_xO_3$," Nature Communications, 5 (2014). http://www.nature.com/articles/ncomms6231

[5] T. Zhang, T. Wang and M. Zhao, "Failure Behavior and Failure Criterion of Conductive Cracks (Deep Notches) in Thermally Depoled PZT-4 Ceramics," Acta Materialia, Volume 51, Issue 16, (2003), pp. 4881-4895.

[6] G. Monkman, S. Hesse, R. Steinmann and H. Schunk, "*Robot Grippers,*" Wiley-VCH (December 15, 2006).

[7] E. Lierke, W. Littmann, T. Morita and T. Hemsel, "Various Aspects of the Placement of a Piezoelectric Material in Composite Actuators, Motors, and Transducers," Journal of the Korean Physical Society, Volume 57, No. 4, (October 2010), pp. 933-937. http://www.ems.k.u-tokyo.ac.jp/morita/Papers/51_tobias.pdf

[8] A. Mathieson, A. Cardoni, N. Cerisola and M. Lucas, "The Influence of Piezoceramic Stack Location on Nonlinear Behavior of Langevin Transducers," IEEE Transactions on Ultrasonics, Ferroelectrics, and Frequency Control, Jun. 2013, Volume 60, Issue 6, (2013), pp. 1126-1133.

[9] H. Fearn, A. Zachar, K. Wanser and J. F. Woodward, "Theory of a Mach Effect Thruster I," Journal of Modern Physics, Volume 6, (2015), pp. 1510-1525. https://physics.fullerton.edu/~heidi/JMP-MachII.pdf. http://file.scirp.org/pdf/JMP_2015091711084670.pdf

[10] J. Den Hartog, "*Mechanical Vibrations,*" 4th edition, McGraw-Hill (1956).

[11] R. Scanlan and R. Rosenbaum, "*Aircraft Vibration and Flutter,*" Dover (1968).

[12] R. Clough and J. Penzien, "*Dynamics of Structures,*" McGraw-Hill (1975).

[13] Y. Maruyama, N. Kojima, T. Ezaki and T. Yamakawa, US Patent 6114798 A, "Stacked Element and Vibration Drive Device," publication date: Sep. 5, 2000, filing date: Mar. 25, 1997, priority date: Mar. 25, 1996.

[14] Y. Maruyama, N. Kojima, T. Ezaki and T. Yamakawa, US Patent 6951048 B2, "Method for Producing a Stacked Piezoelectric Element," publication date: Oct. 4, 2005, filing date: Nov. 5, 2003, priority date: Feb. 17, 1998.

[15] D. Berlincourt, H. Krueger and C. Near, "Properties of Morgan Electro Ceramic Ceramics," Technical Publication TP-226 Properties of Piezoelectricity Ceramics. http://www.morgantechnicalceramics.com/media/1885/tp226.pdf

[16] NBK Hex Socket Head Cap Screws - Super Invar. https://www.nbk1560.com/en-US/products/specialscrew/nedzicom/specialmaterialscrew/SNSIV/

[17] S. Zhang, F. Li, N. Sherlock, J. Luo, H. Lee, R. Xia, R. Meyer, W. Hackenberger and T. Shrout, "Recent Developments on High Curie Temperature PIN-PMN-PT Ferroelectric Crystals," Journal of Crystal Growth, Volume 318, Issue 1, (March 2011), pp. 846-850. https://www.researchgate.net/publication/51073215_Recent_developments_on_high_Curie_temperature_PIN-PMN-PT_ferroelectric_crystals

[18] H. Fearn, "Mach's Principle, Action at a Distance and Cosmology," Journal of Modern Physics, Volume 6, Issue 3, (February 2015). https://physics.fullerton.edu/~heidi/JMP-Mach0.pdf

[19] F. Hoyle and J. V. Narlikar, "A New Theory of Gravitation," Proc. Roy. Soc. Lon., Volume A282, Issue 191 (1964).

[20] F. Hoyle and J. V. Narlikar, "On the Gravitational Influence of Direct Particle Fields," Proc. Roy. Soc. Lon., Volume A282, Issue 184 (1964). See also "A Conformal Theory of Gravitation," Proc. Roy. Soc. Lon. Volume A294, Issue 138 (1966).

[21] F. Hoyle and J. V. Narlikar, "*Action at a Distance in Physics and Cosmology,*" W. H. Freeman and Company, San Francisco (1974).

[22] I. Ciufolini and J. Wheeler, "*Gravitation and Inertia*," Princeton University Press (1995).

[23] J. Narlikar and H. Arp, "Time Dilation in the Supernova Light Curve and the Variable Mass Hypothesis," The Astrophysical Journal, Volume 482, (June 20, 1997), pp. L119-L120. ftp://ftp.lal.in2p3.fr/pub/flower/bibliographie/cosmology/narkilar-arp-1997.pdf

[24] J. Narlikar and P. Das, "Anomalous Redshifts of Quasi-Stellar Objects," The Astrophysical Journal, Part 1, Volume 240, (September 1, 1980), pp. 401-414. http://repository.iucaa.in:8080/jspui/bitstream/11007/1523/1/105A_1980.PDF

[25] H. Fearn, J. F. Woodward and N. van Rossum, "New Theoretical Results for the Mach Effect Thruster," 51st AIAA/SAE/ASEE Joint Propulsion Conference, AIAA Propulsion and Energy Forum (July 27-29, 2015), Orlando, FL, (AIAA 2015-4082). http://arc.aiaa.org/doi/abs/10.2514/6.2015-4082.

[26] H. Fearn, N. van Rossum, K. Wanser and J. F. Woodward, "Theory of a Mach Effect Thruster II," Journal of Modern Physics, Volume 6, (2015), pp. 1868-1880. https://physics.fullerton.edu/~heidi/JMP-MachII.pdf

[27] L. Brillouin, "The Actual Mass of Potential Energy, a Correction to Classical Relativity," Proceedings of the National Academy of Sciences, USA, Volume 53, Issue 3, (March 15, 1965), pp. 475-482. https://www.ncbi.nlm.nih.gov/pmc/articles/PMC336961/pdf/pnas00155-0003.pdf

[28] L. Brillouin, "The Actual Mass of Potential Energy, II," Proceedings of the National Academy of Sciences, USA, Volume 53, Issue 6, (June, 1965), pp. 1280-1284. https://www.ncbi.nlm.nih.gov/pmc/articles/PMC219831/pdf/pnas00158-0114.pdf

[29] L. Brillouin, "*Relativity Reexamined*," Academic Press (1970).

[30] R. Medina, "The Inertia of Stress," American Journal of Physics, Volume 74, (2006), pp. 1036-1040. https://arxiv.org/pdf/physics/0609144.pdf

[31] R. Medina, "Radiation Reaction of a Classical Quasi-Rigid Extended Particle," Journal of Physics A: Mathematical and General, Volume 39, (2006), pp. 3801-3816. http://citeseerx.ist.psu.edu/viewdoc/download?doi=10.1.1.205.7077&rep=rep1&type=pdf

[32] K. McDonald, "Stress and Momentum in a Capacitor that Moves with Constant Velocity." http://citeseerx.ist.psu.edu/viewdoc/download?doi=10.1.1.412.5459&rep=rep1&type=pdf

[33] P. Penfield and H. Haus, "*Electrodynamics of Moving Media*," The MIT Press (August 15, 1967).

[34] C. Leibovitz, "Rest Mass in Special Relativity," American Journal of Physics, Volume 37, Issue 8, (August 1969), pp. 834-835. http://cleibovitz.upwize.com/physics/

[35] J. Sprott, "Some Simple Chaotic Jerk Functions," American Journal of Physics, Volume 65, Issue 6, (June 1997), pp. 537-543.

[36] J. Sprott, "*Chaos and Time-Series Analysis*," Oxford University Press (2003).

[37] G. Martin, "On the Theory of Segmented Electromechanical Systems," The Journal of the Acoustical Society of America, Volume 36, Issue 7, (July 1964), pp. 1366-1370.

[38] K. Wanser, "Center of Mass Acceleration of an Isolated System of Two Particles with Time Variable Masses Interacting with Each Other via Newton's Third Law Internal Forces: Mach Effect Thrust 1," Journal of Space Exploration, Volume 2, Issue 2, (2013), pp. 121-130.

[39] Steiner & Martins, Inc., "Piezo Material Properties." https://www.steminc.com/piezo/PZ_property.asp.

[40] M. Haun, Z. Zhuang, E. Furman, S. Jang and L. Cross, "Electrostrictive Properties of the Lead Zirconate Titanate Solid-Solution System," Journal of the American Ceramic Society, Volume 72, Issue 7, (July 1989), pp.1140-1144.

[41] J. Li and N. Rao, "Dramatically Enhanced Effective Electrostriction in Ferroelectric Polymeric Composites," Applied Physics Letters, Volume 81, Issue 10, (September 2002), pp. 1860-1862.

[42] S. Lee, R. Monteiro, R. Feigelson, H. Lee, M. Lee and S. Park, "Growth and Electrostrictive Properties of $Pb(Mg_{1/3}Nb_{2/3})O_3$ Crystals," Applied Physics Letters, Volume 74, Issue 7, (February 1999), pp. 1030-1032.

[43] S. Swartz, T. Shrout, W. Schulze and L. Cross, "Dielectric Properties of Lead-Magnesium Niobate Ceramics," Journal of the American Ceramic Society, Volume 67, Issue 5, (May 1984), pp. 311-314.

[44] A. von Hippel, "*Dielectrics and Waves*," John Wiley & Sons (1954).

[45] J. Burfoot and G. Taylor, "*Polar Dielectrics and their Applications*," University of California Press, Berkeley and Los Angeles, (June 1979).

[46] W. Voigt, "*Lehrbuch der Kristallphysik*," Teubner, Leipzig, 1910; Springer Fachmedien Wiesbaden (1966).

[47] H. Haus and J. Melcher, "*Electromagnetic Fields and Energy*," Prentice Hall, (September,1989).

[48] J. Jackson, "*Classical Electrodynamics*," Third Edition, John Wiley & Sons (August, 1998).

[49] D. Griffiths, "*Introduction to Electrodynamics*," Fourth Edition, Pearson (October, 2012).

[50] W. Panofsky and M. Phillips, "*Classical Electricity and Magnetism*," Second Edition, Addison-Wesley Publishing Company, (1962).

[51] R. Newnham, V. Sundar, R. Yimnirun, J. Su and Q. Zhang, "Electrostriction: Nonlinear Electromechanical Coupling in Solid Dielectrics," The Journal of Physical Chemistry B, Volume 101, Issue 48, (1997), pp. 10141-10150.

[52] S. Zhang, J. Lim, H. Lee, T. Shrout, "Characterization of Hard Piezoelectric Lead-Free Ceramics," IEEE Transactions on Ultrasonics Ferroelectrics and Frequency Control, Volume 56, Issue 8, pp. 1523-1527, (September, 2009).

[53] D. Waechter, S. Prasad, R. Blacow and B. Yan, "Internally Biased PZT Materials for High-Power Sonar Transducers," Proceedings of the 11th CF/DRDC International Meeting on Naval Applications of Materials Technology, Dartmouth, Nova Scotia, Canada, (June 7th-9th, 2005). `http://sensortechcanada.com/wp-content/uploads/2014/08/2005-06-Internally-Biased-PZT-Materials-for-High-Power-Sonar-Transducers.pdf`

[54] D. Jones and J. Lindberg, "Recent Transduction Developments in Canada and the United States," Proceedings of the Institute of Acoustics (Institute of Acoustics, St. Albans, Herts, UK), Volume 17, Part 3, (1995), pp. 15-33.

[55] H. Fearn and J. Woodward, "Experimental Null Test of a Mach Effect Thruster," Journal of Space Exploration, Volume 2, Issue 2, (2013), pp. 98-105. `https://physics.fullerton.edu/~heidi/JSE13.pdf`

[56] H. Fearn and J. Woodward, "Experimental Null Test of a Mach Effect Thruster," arXiv:1301.6178, (Jan 25, 2013), pp. 1-10. `https://arxiv.org/abs/1301.6178`

[57] J. Woodward, "*Making Starships and Stargates: The Science of Interstellar Transport and Absurdly Benign Wormholes*," Springer 2013 edition (December 15, 2012).

[58] M. Hooker, "Properties of PZT-Based Piezoelectric Ceramics Between -150 and 250 °C," NASA/CR-1998-208708, prepared for Langley Research Center under Contract NAS1-96014, Lockheed Martin Engineering & Sciences Co., Hampton, Virginia, (September, 1998). `https://ntrs.nasa.gov/archive/nasa/casi.ntrs.nasa.gov/19980236888.pdf`

[59] W. Mason, "*Physical Acoustics and the Properties of Solids*," D. van Nostrand Company, (1958).